UNIVERSITY OF Southampton

University of Southampton Research Repository
ePrints Soton

Copyright © and Moral Rights for this thesis are retained by the author and/or other copyright owners. A copy can be downloaded for personal non-commercial research or study, without prior permission or charge. This thesis cannot be reproduced or quoted extensively from without first obtaining permission in writing from the copyright holder/s. The content must not be changed in any way or sold commercially in any format or medium without the formal permission of the copyright holders.

When referring to this work, full bibliographic details including the author, title, awarding institution and date of the thesis must be given e.g.

AUTHOR (year of submission) "Full thesis title", University of Southampton, name of the University School or Department, PhD Thesis, pagination

http://eprints.soton.ac.uk

UNIVERSITY OF SOUTHAMPTON

FACULTY OF SOCIAL AND HUMAN SCIENCES

Geography and Environment

Testing peatland carbon responses to late Holocene climate change in eastern North America

by

Helen Mackay

Thesis for the degree of Doctor of Philosophy

June 2015

UNIVERSITY OF SOUTHAMPTON

ABSTRACT

FACULTY OF SOCIAL AND HUMAN SCIENCES

Geography and Environment

Thesis for the degree of Doctor of Philosophy

TESTING PEATLAND CARBON RESPONSES TO LATE HOLOCENE CLIMATE CHANGE IN EASTERN NORTH AMERICA

Helen Mackay

Peatlands are an important component of the global carbon (C) cycle. Peak C accumulation rates (CAR) are associated with higher net primary productivity (NPP) and warmer climates. However, warmer conditions could force peatlands close to the moisture limit of development to cross a critical threshold where decay processes exceed NPP gain. The sensitivity of the peatland C stores in regions proximal to such bioclimatic boundaries must be characterised to assess their likely contribution to the global C cycle under projected future climate warming. This thesis investigates the relationship between climate and CAR over the last 2000 years using four peatlands located towards the southern limit of peat growth in eastern North America.

Chronologies were developed using tephra and radiocarbon measurements to determine loss-on-ignition inferred carbon accumulation histories. The Alaskan White River Ash eastern lobe (AD 847 ± 1) was detected at all study sites and four previously unidentified cryptotephras of Russian, Japanese, Mexican and Pacific Northwestern origin were detected in Nova Scotia.

Investigations into the relationship between CAR and climate reveal that multi-decadal to centennial CAR fluctuations are related to changes in the summer moisture balance, whilst temperature changes become increasingly important over multi-centennial timescales. The most prominent decrease in CAR over the last 2000 years coincided with drier conditions associated with the Medieval Climate Anomaly (MCA). This suggests that the southern moisture limit of peat growth moved northwards during the MCA, suppressing C sequestration in southern sites. Therefore, whilst projected future climate warming may increase peat CAR in more northern regions, peatlands proximal to the southern moisture limit of peat growth may experience a reduction in their C sequestration rates and act as a positive feedback to climate warming.

Table of Contents

Table of Contents i
List of Tables vii
List of Figures xi
DECLARATION OF AUTHORSHIP xxv
Acknowledgements xxvii
Definitions and Abbreviations xxix
Chapter 1 Introduction 1

1.1 Context and project rationale 1
1.2 Research aim and objectives 3
1.3 Thesis structure 4

Chapter 2 Literature review 7

2.1 Peat accumulation 7
2.2 Carbon accumulation 8

1.1.1 Climatic control: role of temperature and precipitation 10
2.2.1 External disturbances: fire and nutrient loading 13
2.2.2 Internal self-regulating mechanisms 14
2.2.3 Influence of vegetation 14

2.3 Estimating peatland carbon stores 15

2.3.1 Carbon accumulation rates 16

2.4 Peatlands as environmental archives 17

2.4.1 Peatland-climate link 18
2.4.2 Controls of peatland water table depth 19
2.4.3 Water table depth controls: climate system oscillations 20
2.4.4 Reliability of peatland climate records 22

2.5 Peatland climate proxies 24

2.5.1 Plant macrofossils 25
2.5.2 Testate amoebae 28
2.5.3 Peat humification 31

2.6 Peat chronology 33
2.6.1 Radiocarbon dating 33
2.6.1 Tephra 37
2.7 Climate variability 43
2.7.1 External climate forcing mechanisms 45
2.7.2 Internal climate forcing mechanisms 47
2.8 Late Holocene climate change 55
2.8.1 Medieval Climate Anomaly 55
2.8.2 Little Ice Age 56
2.8.3 MCA-LIA transition 57
2.9 Climate of last 2000 years from eastern North America 59
2.9.1 Northeastern Canada (Quebec, Labrador and Nunavut) .. 59
2.9.2 Newfoundland 60
2.9.3 Nova Scotia 60
2.9.4 North-eastern US (Maine-New Jersey) 61
2.10 Hypotheses generated from the literature review 63

Chapter 3 Methods 65

3.1 Introduction 65
3.2 Sample collection 65
3.3 Sample preparation 66
3.4 Laboratory methods 66
3.4.1 Plant macrofossil analysis 67
3.4.2 Testate amoebae analysis 68
3.4.3 Carbon content 69
3.4.4 Cryptotephra analysis 71
3.4.5 Radiocarbon measurements 74
3.5 Statistical analysis of palaeoecological data 75
3.5.1 Detrended correspondence analysis 75
3.5.2 Non-metric Multidimensional Scaling 77
3.5.3 Dupont Hydrological Index for plant macrofossils 78

3.5.4 Transfer functions 83
3.5.5 Palaeoecological statistical approaches adopted within this thesis 85

Chapter 4 Study sites 89

4.1 Introduction 89
4.2 Site selection 89
4.3 Location and description of study sites 90
4.4 Modeled climate data 90
4.4.1 Climatic trends across the study transect 91
4.5 Saco Heath, Maine 96
4.6 Villagedale Bog, Nova Scotia 98
4.7 Framboise Bog, Nova Scotia 101
4.8 Jeffrey's Bog, Newfoundland 104

Chapter 5 Chronology 107

5.1 Bayesian age-depth models 107
5.1.1 Age-depth model of Jeffrey's Bog (JRB12) 108
5.1.2 Age-depth model of Framboise Bog (FBB12) 110
5.1.3 Age-depth model of Villagedale Bog (VDB12) 112
5.1.4 Age-depth model of Saco Heath (SCH10) 114
5.2 Crypto-tephrostratigraphies 116
5.2.1 Abstract 117
5.2.2 Introduction 117
5.2.3 Methods 119
5.2.4 Results and discussion 121
5.2.5 Conclusions 134

Chapter 6 Palaeoecological evidence of environmental change 137

6.1 Introduction 137
6.2 Formation of an eastern North American DHI for plant macrofossils 138

6.2.1 Process of DHI formation 138
6.3 Jeffrey's Bog 143
6.3.1 Plant macrofossils 143
6.3.2 Testate amoebae 155
6.3.3 Full JRB12 palaeoecological comparison 173
6.4 Framboise Bog 175
6.4.1 Plant macrofossils 175
6.4.2 Testate amoebae 186
6.4.3 Full FBB12 palaeoecological comparison 202
6.5 Villagedale Bog 204
6.5.1 VDB12 plant macrofossils 204
6.5.2 VDB12 testate amoebae 218
6.5.3 Full VDB12 palaeoecological comparison 233
6.6 Saco Heath 234
6.6.1 Plant macrofossils 234
6.6.1 Testate amoebae 249
Full SCH10 paleoecology comparison 263
Chapter 7 Carbon accumulation 265
7.1 Testing the sensitivity of C histories to inferred C content 265
7.2 C accumulation histories 267
7.2.1 Bulk density and inferred C content 267
7.2.2 CAR 269
7.2.3 Cumulative C 270
7.2.4 CAR over different temporal resolutions 271
Chapter 8 Discussion 277
8.1 Reconstructed peatland environmental change: considerations 278
8.1.1 Proxy sensitivity to environmental change 279

8.1.2 Constraining ecological environmental preferences and preservation issues 283
8.2 Late Holocene environmental change in eastern North America 284
8.2.1 Characterisation of late Holocene environmental change across the eastern coast of North America 288
8.2.2 Comparing proxy records with climate drivers 299
8.3 Tephra isochrons: testing the synchroneity of environmental change 305
8.3.1 Utilising the White River Ash (WRA): transatlantic comparisons of environmental change 305
8.3.2 Mount St Helens isochron 313
8.4 Late Holocene peat carbon accumulation in eastern North America 316
8.4.1 Spatial patterns of peat C accumulation 317
8.4.2 Temporal patterns of peat accumulation over the last 2000 years 324
8.4.3 Constraining the contribution of peat C accumulation drivers over the last 2000 years 330
8.4.4 Assessment of the C store vulnerability in peatlands at the southern limit of peat growth 343
Chapter 9 Conclusions 345
9.1 Main findings 345
9.1.1 Development of robust stratigraphic chronologies in eastern North America 345
9.1.2 Late Holocene climate change in eastern North America 346
9.1.3 Late Holocene carbon accumulation rates in eastern North America 346
9.1.4 Controls on late Holocene carbon accumulation rates in eastern North America 347

9.2 Recommendations for future research 348

Appendices 353

Appendix A 355

Appendix B 369

Appendix C 377

C.1 Similarity coefficient tables 377

C.2 Correlations by similarity coefficient (SC) 377

List of References 381

List of Tables

Table 3.1 Comparison of sample sizes and resolution for methods used within this study. 67

Table 3.2 DHI index values applied in each revised index. 82

Table 4.1 Summary of the climatic parameters from 1901 to 2010 95

Table 5.1 JRB12 radiocarbon data 109

Table 5.2 FBB12 radiocarbon data 111

Table 5.3 VDB12 radiocarbon data 113

Table 5.4 SCH10 radiocarbon data 115

Table 5.5 Means and standard deviations of glass compositions from cryptotephra layer. All data are normalised. n = number of analyses 123

Table 5.6 Means and standard deviations of single-grain glass compositions from reference material of potential correlatives. 124

Table 6.1 Allocated indicator values and corresponding habitat type for each species or aggregated groups based on results from Figures 6.1 – 6.4. 142

Table 6.2 JRB12 plant macrofossil assemblage description 145

Table 6.3 JRB12 testate amoebae assemblage data description 158

Table 6.4 Pearson Correlation Coefficents for the JRB testate amoebae transfer function model reconstructions 170

Table 6.5 FBB12 plant macrofossil assemblage description 178

Table 6.6 FBB12 testate amoebae assemblage descriptions 189

Table 6.7 Table of Pearson correlation coefficients between transfer function models. All significant at the $P < 0.001$ level 200

Table 6.8 Description of VDB12 plant macrofossil assemblage. 207

Table 6.9 VDB12 plant macrofossil DCA statistics 210

Table 6.10 Description of VDB testate amoebae assemblage 220

Table 6.11 Description of SCH10 plant macrofossil assemblage 236

Table 6.12 Axis one eigenvalues and gradient lengths for different DCA conditions .. 244

Table 6.13 SCH10 description of testate amoebae assemblage data 252

Table 7.1 Comparison of C accumulation rates and cumulative C when %C is altered. Updated values have been obtained using the published % C values from proximal sites (Charman *et al.*, submitted)..... 266

Table 8.1 Summary of main reconstructed water table changes distinguished by dominant changes which broadly correspond with named climatic periods over the last 2000 years. Each period is described from north (JRB12; top) to south (SCH10; bottom). 290

Table 8.2 Summary of peatland responses reconstructed within this study that are associated with the MCA and LIA 298

Table 8.3 Pearson correlation coefficients: relationship between climatic variables and total amount of cumulative C from AD 1901 to 2001.The sensitivity of the correlations is tested within the age-depth model uncertainty using the 2σ age range. Bold indicate significant relationships. 321

Table.8.4 WTD change associated with the MCA 326

Table 8.5 Pearson correlation coefficients between CAR and Viau *et al*. (2006) temperature reconstructions over 100-year intervals. 330

Table 8.6 Pearson correlation coefficients between carbon accumulation and reconstructed WTD by site on multidecadal timescales..... 333

Table 8.7 Pearson correlation coefficients between groups of vegetation and CAR by site at a multidecadal timescale. Significant correlations in bold ($p = <0.05$) with * denoting $p = < 0.01$. 337

Table 8.8 Multivariate modelling to account for carbon accumulation rates on multidecadal timescales. Bold indicate significant relationships. 341

Table 8.9 Multivariate modelling to account for carbon accumulation rates on centennial timescales. Bold indicates significant relationships..... 342

List of Figures

Figure 1.1 Peat carbon sequestration was an important driver of carbon dioxide (CO_2) change reduction during the last 7000 years. 1

Figure 2.1 Conceptual model of controls over growth and carbon accumulation in northern peatlands (Yu *et al*., 2009).....9

Figure 2.2 Conceptual model linking climate warming with peatland C sequestration (Loisel and Yu, 2013a). The arrows represent processes and boxes indicate consequences. 12

Figure 2.3 Global peat distribution (from Jackson and Charman (2010); based on Charman (2002) and Lappalainen (1996). Main areas of peatland occurrence expressed as proportion of the landscape covered. 16

Figure 2.4 Characteristic species habitats of a European ombrotrophic peatland (Rydin and Jeglum, 2006)..... 26

Figure 2.5 Comparison of biological proxies (A, top) and humification (B, bottom) relationships with climate (Yeloff and Mauquoy, 2006) 32

Figure 2.6 The process of ^{14}C incorporation into the environment..... 34

Figure 2.7 Continental-scale climatic change over the last 2000 years 44

Figure 2.8 Global correlations between a positive NAO and precipitation and temperature. Conditions in north-eastern North America are opposite to those in the western Europe and south-eastern North America (NASA, 2011). 49

Figure 2.9 Observed temperature patterns for December 2010-February 2011 (left). Patterns that would be expected based only on the relative strength and frequency of the negative NAO phases that occurred (right). 50

Figure 2.10 Ocean-atmosphere conditions in the tropical Pacific during normal conditions (top); El Niño conditions (middle) and La Niña conditions (bottom) (NOAA, last accessed 23/05/2014) 54

Figure 2.11 North American temperature anomalies between MCA and LIA transition. The temperature difference between the MCA and the LIA was smaller in Newfoundland and northern Nova Scotia than southern Nova Scotia and Maine (Sawada *et al*., 2004). 58

Figure 2.12 Example of a holistic approach to MCA-LIA driving mechanisms (based on the findings from Section 2.8)..... 58

Figure 2.13 Regional palaeoenvironmental synthesis over the 2300 cal yr BP in eastern North America separated by region based on findings from literature (Section 2.9). 62

Figure 4.1 Location of Ph.D. study sites in context of other relevant peatland studies 90

Figure 4.2 ANUSPIN modelled average monthly temperature by site 92

Figure 4.3 ANUSPIN modelled average monthly precipitation by site 93

Figure 4.4 ANUSPIN modelled average monthly available moisture by site 94

Figure 4.5 Aerial photograph of SCH10 (Google Earth, imagery date 19/9/2013). White star indicates coring location. 96

Figure 4.6 ANUSPIN modelled average annual precipitation (blue) and potential evapotranspiration (green) by month for SCH10 97

Figure 4.7 Aerial photography of VDB12 from Map Library, Service Nova Scotia and Municipal Relations (2010). White star indicates coring location. 98

Figure 4.8 Section of core (100 – 150 cm) obtained from a lawn habitat. *Sphagnum*-dominated peat with obvious stratigraphic changes in the degree of humification (as represented by colour change). 99

Figure 4.9 Surface characteristcis of VDB12 at the coring location. Peatland is dry and with abundant shrubs and patches of *Cladonia* (white areas). Wetter lawn conditions are restricted to the center of the peatland. 100

Figure 4.10 ANUSPIN modelled rates of precipiation and potential evapotranspiration (1901-2010) for VDB12 100

Figure 4.11 Aerial photography of FBB12 from Map Library, Service Nova Scotia and Municipal Relations (2008). White star indicates coring location. 101

Figure 4.12 Section of FBB12 core (50- 100 cm) obtained from a lawn habitat. *Sphagnum* dominated peat with obvious alternating stratigraphic changes in the degree of humification (as represented by colour changes). 102

Figure 4.13 Surface characteristics of FBB12 at the coring location. Large pool systems are common, divided by areas of *Eriophorum* and patches of *Cladonia*. The peatland is surrounded by dense woodland. 103

Figure 4.14 ANUSPIN modelled rates of precipiation and potential evapotranspiration (1901-2010) for FBB12 103

Figure 4.15 Aerial photograph of JRB12 (Google Earth, imagery date 17/7/2013). White star indicates coring location. 105

Figure 4.16 *Sphagnum* dominated core section (100-150 cm) with obvious stratigraphic changes in the degree of humification (as represented by colour changes). 105

Figure 4.17 Surface characteristics of JRB12 at the coring location. Pool present in the centre of the peatland with varying hummock topography. 106

Figure 4.18 ANUSPIN modelled rates of precipiation and potential evapotranspiration (1901-2010) for JRB12. 106

Figure 5.1 JRB12 Bayesian age-depth model 109

Figure 5.2 FBB12 Bayesian age-depth model 111

Figure 5.3 VDB12 Bayesian age-depth model 113

Figure 5.4 SCH10 Bayesian age-depth model 115

Figure 5.5 The location of study sites Saco Heath (SCH10), Villagedale Bog (VDB12), Framboise Bog (FBB12) and Jeffrey's Bog (JRB12) in relation to the previous Newfoundland record from Nordan's Pond Bog (Pyne-O'Donnell *et al*., 2012). 119

Figure 5.6 Tephrostratigraphies from the four study sites 122

Figure 5.7 Harker diagrams comparing the major element glass compositions of MSH-Wn, MSH-We and JRB12-71. JRB12-71's composition mirrors the geochemical trend seen in MSH-We..... 125

Figure 5.8 Selected major element glass geochemical plots of proximal White River Ash (east and north lobe) and correlated cryptotephras. Most samples tend to cluster with the main WRAe geochemical population of ~73-74.5 SiO2 wt%..... 126

Figure 5.9 Major and minor element glass compositions of proximal lapilli and distal ash from Mount St Helens layer T and the potential correlative FBB12-31..... 127

Figure 5.10 Geochemical plots of FBB12-162 in comparison with tephra from the Tarumai (Ta) and Komagatake (Ko) volcanoes of Hokkaido. 129

Figure 5.11 Major-element glass compositions of: A-C- Ksudach 1 from visible ash deposits collected in Kamchatka plotted with VDB12-176; D-F- Glass analyses from crushed lapilli of P1 from Volcán Ceboruco plotted with VDB12-90. 131

Figure 5.12 Major-element glass compositions of VDB12-41 and SCB12-42. 132

Figure 5.13 Eastern North American cryptotephra lattice: sites from this study and Nordan's Pond Bog (Pyne-O'Donnell *et al*., 2012)..... 136

Figure 6.1 Distribution of *Sphagnum* (S.) species across microtopographical habitats. Full species names: *S. papillosum, S. magellanicum, S. rubellum, S. capillifolium, S. flavicomens, S. fuscum, S. tenellum, S. cuspidatum, S. pulchrum.* 140

Figure 6.2 Distribution of selected species across microtopographical habitats. Full species names: *Kalmia angustifolia, Empetrum nigrum*, *Rhododendron groenlandicum, Chamaedaphne calyculata, Kalmia polifolia, Picea*, *Andromeda polifolia*, *Juniperus communis.* 140

Figure 6.3 Distribution of selected species across microtopographical habitats. Full species names: *Odontoschisma sphagni, Drosera rotundifolia, Drosera*

intermedia, Sarracenia purpurea, Rubus chamaemorus, Cladonia, Nymphaea, Dicranum species, *Lycopodium* 141

Figure 6.4 Distribution of aggregate vegetation components across microtopographical habitats. Full names: *S.* section (sect.*) Sphagnum*, *S*. sect. *Acutifolia*, *S*. sect. *Cupsidata*, Ericaceae undiff., *Vaccinnium* spp. undiff.*, Eriophorum* spp. undiff. monocots undiff. 141

Figure 6.5 JRB12 macrofossil assemblage diagram plotted against depth with secondary age axis. 144

Figure 6.6 JRB12 variability by aggregate groups of the major peat forming components as determined by the residuals from LOESS smoothing. 147

Figure 6.7 JRB12 plant macrofossil DCA axis one (x-axis) and two (y-axis) species scores coloured by similar vegetation types..... 148

Figure 6.8 JRB12 plant macrofossil DCA axis one (x-axis) and two (y-axis) sample scores coloured by the zones allocated in the assemblage diagram..... 149

Figure 6.9 A: JRB12 macrofossil DCA axis one scores (lower values indicate wetter conditions); B: Variability of DCA axis one scores as determined by the residuals from LOESS smoothing: sampling proportion = 0.103 (equivalent to n=6) and 1 polynomial degree applied. 150

Figure 6.10 JRB12 plant macrofossil nMDS results. A: sample scores, B: species scores, C: nMDS model results, D: normalised nMDS and DCA axis one score reconstructions; lower y-axis values indicate wetter conditions. 151

Figure 6.11 JRB12 plant macrofossil DHI reconstructions: the updated full index; the index derived by Daley and Barber (2012); the updated index excluding UOM; and the updated index excluding roots. Lower y-axis values indicate wetter conditions..... 153

Figure 6.12 JRB12 plant macrofossil normalised data transformations using DCA and nMDS axis one scores and DHI derived from the updated index and the Daley and Barber (2012) index. Lower y-axis values indicate wetter conditions. 155

Figure 6.13 JRB12 testate amoebae assemblage diagram plotted against depth with a secondary age axis. 157

Figure 6.14 Variability of the four most abundant testate amoebae taxa. 159

Figure 6.15 JRB12 testate amoebae ecological measures. 161

Figure 6.16 JRB12 testate amoebae DCA axis one (x-axis) and axis two (y-axis) species scores. 163

Figure 6.17 JRB testate amoebae DCA sample scores. Colours represent zones allocated in CONISS analysis (see **Error! Reference source not found.**) 164

Figure 6.18 JRB12 testate amoebae DCA environmental reconstruction and associated variability 165

Figure 6.19 JRB12 testate amoebae nMDS results. 166

Figure 6.20 JRB12 Testate amoebae reconstructed depth to the peatland water table based on the WA.inv.tol (green) and WA.inv (blue) transfer function models of Amesbury *et al*. (2013) 168

Figure 6.21 JRB12 Testate amoebae reconstructed depth to the peatland water table based on the WA.cla.tol (green) and WA.cla (blue) transfer function models of Lamarre *et al*. (2013). 169

Figure 6.22 Variability of the Amesbury *et al*. models (upper) and Lamarre *et al*. models (lower) using the residuals from LOESS smoothing. A sampling proportion of 0.103 (equivalent to n=6) and 1 polynomial degree were applied. 170

Figure 6.23 JRB12 testate amoebae transfer function reconstructions using ATLANTIC.NA WA.inv.tol (upper) and QUEBEC WA.cla (lower). Grey lines indicate standard error of prediction. Lower y-axis values indicate wetter conditions 171

Figure 6.24 JRB12 testate amoebae normalised data transformation. Lower y-axis values indicate wetter conditions. 173

Figure 6.25 JRB12 normalised comparison of ecohydrological reconstructions blue shaded areas indicate coherent trends towards wetter conditions and red shaded areas indicate trends towards drier conditions. 174

Figure 6.26 FBB12 macrofossil assemblage diagram plotted against depth with secondary age axis. 177

Figure 6.27 Variability of the FBB12 major peat forming components plotted against depth, with a secondary age axis..... 179

Figure 6.28 FBB12 plant macrofossil species DCA axis one (x-axis) and two (y-axis) scores. 180

Figure 6.29 FBB12 plant macrofossil DCA sample scores coloured by zones allocated in stratigraphic diagram (Figure 7.1-1) 181

Figure 6.30 A: FBB12 plant macrofossil DCA axis one scores and B. Variability of the DCA axis one scores obtained using the residuals from LOESS smoothing: sampling proportion = 0.09 (equivalent to n=6) and 1 polynomial degree applied. 182

Figure 6.31 FBB12 plant macrofossil assemblage nMDS results. 183

Figure 6.32 FBB12 plant macrofossil DHI reconstructions 185

Figure 6.33 FBB12 plant macrofossil DCA, nMDS and DHI normalised comparisons of reconstructed environmental change. 186

Figure 6.34 FBB12 testate amoebae assemblage diagram plotted against depth with a secondary age axis. 188

Figure 6.35 Variability of the four most abundant testate amoebae taxa..... 191

Figure 6.36 FBB12 testate amoebae ecological measures. 192

Figure 6.37 FBB12 testate amoebae DCA axis one (x-axis) and two (y-axis) species scores Red symbols represent species with drier WTD preferences and blue symbols represent species with wetter water table depth preferences. Colours (and thus dry or wet preferences) have been assigned based on the training sets of Amesbury *et al*., (2013) and Lamarre *et al*., (2013)..... 194

Figure 6.38 Alternative FBB12 testate amoebae DCA with rare species omitted. Red symbols represent species with drier WTD preferences and blue symbols represent species with wetter water table depth preferences. Colours (and

thus dry or wet preferences) have been assigned based on the training sets of Amesbury *et al*., (2013) and Lamarre *et al*., (2013). 194

Figure 6.39 FBB12 testate amoebae DCA axis one (x-axis) and two (y-axis) sample scores coloured by zones allocated by CONISS (see Figure 6.34) 195

Figure 6.40 A: DCA Axis one scores for each sample representing changes in hydrological conditions down core. Lower values indicate wetter conditions. B: variability of the DCA axis one scores using the residuals from LOESS smoothing. A sampling proportion of 0.09 (equivalent to n=6 in the higher resolution sampling period) and 1 polynomial degree were applied. 195

Figure 6.41 FBB12 testate amoebae nMDS results 197

Figure 6.42 Upper and lower estimates of FBB12 testate amoebae reconstructions using ATLANTIC.NA WA.inv.tol and WA.inv models. Red bands indicate periods of diverging trends. Lower y-axis values indicate wetter conditions. 199

Figure 6.43 Upper and Lower estimates of FBB12 transfer function reconstructions from QUEBEC WA.inv.tol and WA.inv, red bands indicate periods of diverging trends. Lower y-axis values indicate wetter conditions 199

Figure 6.44 FBB12 testate amoebae transfer function reconstructions variability based on the residuals from LOESS smoothing. 200

Figure 6.45 FBB12 testate amoebae normalised data transformation comparison. Lower y-axis values indicate wetter conditions. 201

Figure 6.46 FBB12 normalised ecohydrological reconstructions 203

Figure 6.47 VDB12 macrofossil assemblage diagram plotted against depth with secondary age axis. 206

Figure 6.48 VDB12 variability of the major peat forming components plotted against depth, with a secondary age axis. 208

Figure 6.49 VDB12 plant macrofossil species DCA axis one (x-axis) and two (y-axis) distributions. 210

Figure 6.50 Alternative VDB12 plant macrofossil species DCA axis one (x-axis) and two (y-axis) distributions. 211

Figure 6.51 VDB12 plant macrofossil sample DCA axis one (x) and two (y) scores. Zone colourations correspond with the CONISS-based zonation of the assemblage diagram (Figure 6.47). 212

Figure 6.52 A: VDB12 DCA axis one scores (lower y-axis values indicate wetter conditions) and B: variability reported using the residuals from LOESS smoothing: sampling proportion = 0.12 (equivalent to n=6) and 1 polynomial degree applied 213

Figure 6.53 VDB12 plant macrofossil nMDS results. 214

Figure 6.54 VDB12 plant macrofossil DHI reconstructions using the Daley and Barber (2012) index and three obtained from the updated index: full, excluding UOM and excluding roots. Lower y-axis values indicate wetter conditions. 216

Figure 6.55 VDB plant macrofossil normalised data transformations. Lower y-axis values indicate wetter conditions. 217

Figure 6.56 VDB12 testate amoebae assemblage diagram plotted against depth with a secondary age axis. 219

Figure 6.57 VDB12 variability of the four main testate amoebae taxa determined using the residuals from LOESS smoothing: sampling proportion = 0.12 (equivalent to n=6) and 1 polynomial degree applied 222

Figure 6.58 VDB12 testate amoebae ecological measures. 223

Figure 6.59 VDB12 testate amoebae DCA species axis one (x-axis) and two (y-axis) scores. 225

Figure 6.60 VDB12 testate amoebae DCA axis one scores from the original DCA with rare species downweighted and the DCA conducted with the rare (<10%) species removed. Environmental interpretations would be the same in both reconstructions. Lower y-axis values indicate wetter conditions. 225

Figure 6.61 VDB12 testate amoebae DCA axis one (x-axis) and two (y-axis) sample scores coloured by zones allocated by CONISS analysis. 226

Figure 6.62 VDB12 testate amoebae nMDS results 227

Figure 6.63 Upper and lower estimates of VDB12 water table depth obtained from the ATLANTIC.NA WA.inv.tol and WA.inv models from Amesbury *et al.* (2012). Red bands indicate divergences in the direction of change between the two models. 228

Figure 6.64 Upper and lower estimates of VDB12 water table depth obtained from the QUEBEC WA.cla.tol and WA.cla models from Lamarre *et al*. (2013). Red bands indicate divergences in the direction of change between the two models. 229

Figure 6.65 Variability of models using residuals from LOESS with a sampling proportion of 0.12 (equivalent to n=6) and 1 polynomial degree. 230

Figure 6.66 VDB12 testate amoebae transfer function reconstructions (black lines) with sample errors (grey lines) 231

Figure 6.67 VDB12 testate amoebae normalised reconstructions. Lower y-axis values indicate wetter conditions. 232

Figure 6.68 VDB12 ecohydrological reconstruction..... 233

Figure 6.69 SCH10 macrofossil assemblage diagram plotted against depth with secondary age axis. 235

Figure 6.70 SCH10 variability of the major peat forming components plotted against depth, with a secondary age axis. 237

Figure 6.71 SCH10 DCA axis one (x) and two (y) species distribution. 238

Figure 6.72 Alternative SCH10 plant macrofossil DCA, colours follow key in Figure 6.71. 243

Figure 6.73 SCH10 DCA axis one (x) and two (y) sample distributions, samples coloured by zones allocated during CONISS analysis (see Figure 6.69) 244

Figure 6.74 SCH10 plant macrofossil nMDS results. 245

Figure 6.75 SCH10 plant macrofossil data transformed using DHI. Lower y-axis values indicate wetter conditions. 247

Figure 6.76 SCH10 plant macrofossil DCA axis one scores and DHI normalised. Lower y-axis values indicate wetter conditions..... 249

Figure 6.77 SCH10 testate amoebae assemblage diagram plotted against depth with a secondary age axis. 251

Figure 6.78 SCH10 variability of the four most dominant testate amoebae species plotted against depth, with a secondary age axis. 253

Figure 6.79 SCH10 testate amoebae ecological measures. 254

Figure 6.80 SCH10 testate amoebae DCA axis one (x-axis) and two (y-axis) scores. 256

Figure 6.81 SCH10 testate amoebae DCA axis one (x-axis) and axis two (y-axis) sample scores. Samples are coloured by zones corresponding allocated from the CONISS cluster analysis (see Figure 6.77). 256

Figure 6.82 SCH10 testate amoebae nMDS results. 257

Figure 6.83 Upper and lower estimates of SCH10 water table depth obtained from the ATLANTIC.NA WA.inv.tol and WA.inv models from Amesbury *et al.* (2012). Red bands indicate divergences in the direction of change between the two models. 258

Figure 6.84 Upper and lower estimates of SCH10 water table depth obtained from the QUEBEC WA.cla.tol and WA.cla models from Lamarre *et al.* (2012). Red bands indicate divergences in the direction of change between the two models 260

Figure 6.85 Variability of models using residuals from LOESS with a sampling proportion of 0.12 (equivalent to n=6) and 1 polynomial degree, before normalisation..... 260

Figure 6.86 SCH10 testate amoebae transfer function reconstructions (black lines) with sample errors (grey lines) 261

Figure 6.87 SCH10 testate amoebae normalised water table reconstructions obtained from DCA and transfer functions. Lower y-axis values indicate wetter conditions. 263

Figure 6.88 SCH10 normalised palaeo-ecohydrological reconstructions with fire indicated in grey box. 264

Figure 7.1 Bulk density, inferred C and CAR by site over the last 2000 years. Sites arranged from north (JRB12; top) to south (SCH10, bottom). Scales of the y-axes are optimised on a site-by-site basis; therefore, the y-axis scales differ between sites. 268

Figure 7.2 Carbon accumulation rates by site (arranged from north (JRB12; top) to south (SCH10; bottom) over last 2000 years. 270

Figure 7.3 Cumulative C by site over the last 2000 years. Key arranged from north (JRB12) to south (SCH10). 271

Figure 7.4 Mean C accumulation rates: 100-year intervals with key arranged from north (JRB12) to south (SCH10) 272

Figure 7.5 Mean variability of C accumulation rates in 100-year intervals. Key arranged from north (JRB12) to south (SCH10)..... 273

Figure 7.6 Mean C accumulation rates: 200-year intervals with key arranged from north (JRB12) to south (SCH10) 274

Figure 7.7 Mean variability of C accumulation rates in 200-year segments. Key arranged from north (JRB12) to south (SCH10) 275

Figure 7.8 Mean C accumulation rates: 500-year intervals with key arranged from north (JRB12) to south (SCH10) 276

Figure 7.9 Mean C accumulation rates: 500-year intervals with key arranged from north (JRB12) to south (SCH10) 276

Figure 8.1 Plant macrofossil DHI reconstructions (left column) with standard error presented and testate amoebae transfer function reconstructions (Amesbury *et al*., 2013 in solid line; Lamarre *et al*., 2013 in dashed line; right column) with transfer function error of prediction presented. Sites arranged from northeast (JRB12, top) to southwest (SCH10; bottom). Lower y-axis values indicate wetter conditions. 281

Figure 8.2 Modelled relationship between modern mire plants (a) and testate amoebae (b) species and the current mean water table depth at each measurement plot in Kontolanrahka Bog based on Generalised Additive Models from Väliranta *et al*. (2012). Wet species generally show narrower tolerances than drier species. 282

Figure 8.3 Example of scarcity of late Holocene palaeoenvironmental reconstructions in eastern North America with adequate chronological control using NOAA's palaeoclimate database interactive map (last accessed 01/05/2015). 286

Figure 8.4 Summary of reconstructed temperature and precipitation trends over the 2300 cal yr BP in eastern North America by region (obtained from synthesis of regional records, Section 2.9). 287

Figure 8.5 The four peatland environmental reconstructions obtained using plant macrofossils (lighter solid line) and testate amoebae reconstructed environmental change using Amesbury *et al*., (2013) training set (darker solid line) and Lamarre *et al*., (2013) training set (darker dashed line). 289

Figure 8.6 Proximal reconstructed peatland water table depths from other published studies (black) and this study (coloured) separated by geographical region. Lower y-axis values indicate wetter conditions whilst higher y-axis values indicate drier conditions. 291

Figure 8.7 Testate amoebae water table reconstructions (using Amesbury *et al*., 2013 training set) for JRB12 (top) and FBB12 (bottom) presented with chronological uncertainty derived from Bacon age-depth Bayesian modelling. Darker narrower periods indicate increased chronological control. Lower y-axis values indicate wetter conditions. 294

Figure 8.8 Summary of the main reconstructed water table conditions (pink represents dry and purple represents wet) with directional shifts in wetness indicated by arrows. Sites arranged from northeast (JRB12; top) to southwest (SCH10; bottom). 298

Figure 8.9 Palaeoenvironmental records obtained from around the North Atlantic region: more western North Atlantic regions in left panel, more eastern regions in right panel. 300

Figure 8.10 Reconstructed characteristics of climatic drivers (left panel) and reconstructed peatland WTD obtained within this study (right panel). 302

Figure 8.11 Transatlantic comparison of environmental reconstructions at the time of the WRA. 312

Figure 8.12 Peatland environmental change at the deposition time of the MSH We tephra. Top: records from Nordan's Pond Bog (Newfoundland; Hughes *et al*. 2006; Daley *et al*. 2010); middle: JRB12 (southwestern Newfoundland; this study); lower: FBB12 (Nova Scotia; this study). Lower y-axis values indicate wetter/colder conditions. 314

Figure 8.13 Testate amoebae water table reconstructions (using Amesbury *et al*., 2013 training set) for JRB12 (top), FBB12 (second top), VDB12 (second from bottom) and SCH10 (bottom) presented with chronological uncertainties derived from Bacon age-depth modelling. Darker narrower periods indicate increased chronological control 315

Figure 8.14 Pollen-inferred summer temperatures for Northern Quebec and Southeastern US (adapted from Viau *et al*., 2006). 322

Figure 8.15 CAR and cumulative carbon content over the last 2000 year by site. Sites have been presented north (JRB12) – south (SCH10). 323

Figure 8.16 CAR (in black) and testate amoebae reconstructed water table depths using the (Amesbury *et al*. (2013) transfer function (in blue) and the (Lamarre *et al*. (2013) transfer function (in purple). 328

Figure 8.17 CAR by site over the last 2000 years with modelled chronological uncertainties (using Bacon (Blaauw and Christen, 2011) package in R (R Core Development Team, 2014) 329

DECLARATION OF AUTHORSHIP

I, Helen Mackay,

declare that this thesis entitled "*Testing the peatland carbon responses to late Holocene climate change in eastern North America*" and the work presented in it is my own and has been generated by me as the result of my own original research.

I confirm that:

1. This work was done wholly or mainly while in candidature for a research degree at this University;
2. Where any part of this thesis has previously been submitted for a degree or any other qualification at this University or any other institution, this has been clearly stated;
3. Where I have consulted the published work of others, this is always clearly attributed;
4. Where I have quoted from the work of others, the source is always given. With the exception of such quotations, this thesis is entirely my own work;
5. I have acknowledged all main sources of help;
6. Where the thesis is based on work done by myself jointly with others, I have made clear exactly what was done by others and what I have contributed myself;
7. None of this work has been published before submission.

Signed: .....

Date: 09 June 2015

Acknowledgements

Firstly I would like to thank my supervisors, Paul Hughes and Pete Langdon, for all their support and guidance throughout my PhD. I am grateful for the trust that they placed in me to explore new ideas and develop this project. I would also like to thank Kim, Alan, Min, Charlotte, John, Ellie, Tom, Pete, Cath, Thierry and all others that I have worked with within Geography and Environment who have made the last few years so enjoyable. A special thanks is extended to Hayley Essex for all of her support within the PLUS lab.

This research has been primarily funded by Geography and Environment at the University of Southampton, who provided the scholarship and many additional funds for fieldwork and training courses, for which I am very grateful. NERC also provided financial assistance, facilitating the radiocarbon measurements and time on the tephra probe, and the QRA provided fieldwork and conference travel funds.

The development of the core chronologies benefited from the support of the tephra-community, including: Alison MacLeod (Royal Holloway, University of London), Siwan Davies and Anna Bourne and their lab (Swansea University) and Mike Hall (University of Edinburgh) assisted with the isolation and preparation of the tephra shards; Chris Hayward (University of Edinburgh) provided fantastic support for the EPMA (along with many DVD's and CD's making the long nights much more enjoyable!) and Britta Jensen, Sean Pyne-O'Donnell, Gill Plunkett (Queen's University Belfast) and Duane Froese (University of Alberta) assisted with data analysis and correlations. I am especially grateful to Britta who has dedicated a lot of time to this project and acted as a great mentor throughout. Thanks also to Mark Garnett and the team at the NERC ^{14}C laboratory for their advice and for an enjoyable time during the lab visit to East Kilbride.

This PhD has benefited from many discussions other 'bogtrotters' (Gunnar Mallon (who also provided invaluable help with fieldwork), Matt Amesbury, Nicole Sanderson, Gabriel Magnan, Tom Roland, and Emma Rice). I am especially to Matt Amesbury (University of Exeter) and Gabriel Magnan (L'Université du Québec à Montréal; UQAM) who promptly applied their testate amoebae transfer functions to my data and provided subsequent assistance. Michelle Garneau (UQAM) has also provided a great amount of support and encouragement throughout this project.

My PhD training experience benefited greatly from the time that I spent within Birmingham University's Molecular Climatology group: thanks to James Bendle, Heiko Moossen and Rike Wittkopp for welcoming me into their lab and providing me with such excellent training. My time in Birmingham University was facilitated by the provision of free accommodation, food and taxi services from my grandparents so I am very grateful to them for that and for their unwavering support. Thanks also to the Laws for their continued support throughout the PhD, especially to Robert for his emergency IT help.

I would like to thank Daniel Law for his constant support, encouragement and understanding throughout this process. He has been through every up and down of my PhD with me and indulged extensive late night peat discussions and tireless proofreading.

Finally, I would like to dedicate this thesis to my mum who always encouraged and believed in me, showing me that it is possible to achieve anything with enough enthusiasm and hard work. She supported me in every way possible throughout this PhD, from trailing the peatlands of the New Forest identifying mosses, to keeping me up-to-date with news clippings on anything peat-related. I could not have got to this stage without her.

Definitions and Abbreviations

σ	Standard Deviation
δ	Delta
^{14}C	Carbon-14 (radiocarbon)
^{210}Pb	Lead-210 (radioisotope)
^{18}O	Oxygen-18 (stable isotope)
^{13}C	Carbon-13 (stable isotope)
AMO	Atlantic Meridional Oscillation
AMOC	Atlantic Meridional Overturning Circulation
ANOVA	Analysis of Variance
C	Carbon
C-IT	Chironomid-inferred temperature
ca.	*circa*
cal yr BP	Calibrated years before present
CAR	Carbon Accumulation Rate
CH_4	Methane
CO_2	Carbon Dioxide
CONISS	Constrained Instrumental Sum of Squares Analysis
DACP	Dark Ages Cool Period
DCA	Detrended Correspondence Analysis
DFA	Discriminant Function Analysis
DHI	Dupont Hydroclimatic Index
DWT	Depth to Water Table
ENSO	El Niño Southern Oscillation
EPMA	Electron Probe Micro-Analyser
FBB12	Framboise Bog 2012 core
GDGT	Glycerol Dialkyl Glycerol Tetraethers
GGD0	Growing degree day above zero °C
GICC05	Greenland Ice Core Chronology 2005
IPCC	International Panel on Climate Change
JRB12	Jeffrey's Bog 2012 core
KSI	Ksudach 1 tephra
LIA	Little Ice Age
LOESS	Local Weighted Scatterpoint Smoothing
LORCA	Long Term Average Rate of Carbon Accumulation
MCA	Medieval Climate Anomaly
MCMC	Markov chain Monte Carlo
monocot.	monocotyledon
MSH	Mount St Helens
N_2	Nitrogen
NADW	North Atlantic Deep Water
NAO	North Atlantic Oscillation
NASA	North American Space Agency
NCB	Net Carbon Balance

NERC	Natural Environment Research council
NGRIP	North Greenland Icecore Project
nMDS	Non-Metric Multidimensional Scaling
NOAA	National Oceanic and Atmospheric Administration
NPP	Net Primary productivity
P-E	Precipitation - Evaporation
PAR	Photosynthetically Active Radiation
PCA	Principle component analysis
PDO	Pacific Decadal Oscillation
RWP	Roman Warm Period
S. sect.	*Sphagnum* section
SCH10	Saco Heath 2010 core
SCP	Spheroidal Carbonaceous Particle
SDI	Shannon Diversity Index
SST	Sea surface temperatures
THC	Thermohaline Circulation
UNFCCC	United Nations Framework Convention on Climate Change
UOM	Unidentifiable organic matter
VDB12	Villagedale Bog 2012 core
WRA	White River Ash
WTD	Water Table Depth
yr	Years

Chapter 1: Introduction

1.1 Context and project rationale

Ombrotrophic (rain-fed) peatlands are important palaeoclimate archives since their growth is closely coupled to atmospheric moisture conditions and signals of past environmental change are well preserved within the acidic, waterlogged conditions. Peatlands have played an important role in the global carbon (C) cycle throughout the Holocene (Yu, 2011; Figure 1.1) and currently sequester a third of the Earth's soil carbon (Gorham 1991; Turunen *et al.*, 2002) and contribute *ca.* 10% of the total methane flux to the atmosphere (Smith *et al.*, 2004). Understanding these systems is of increasing interest owing to their high carbon content, their extensive distribution and the uncertain fate of peatland-atmospheric carbon (C) exchange in a changing climate.

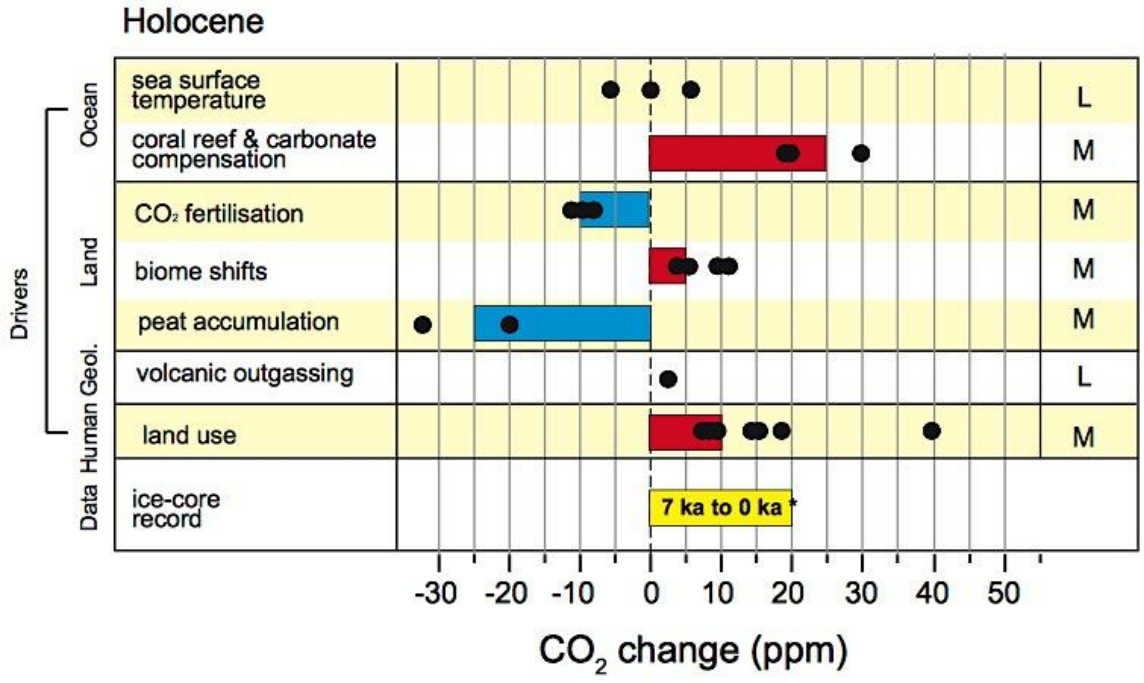

Figure 1.1 Peat carbon sequestration was an important driver of carbon dioxide (CO_2) change reduction during the last 7000 years. Black circles represent individual model-based estimates for individual mechanisms whilst solid bars represent estimated based on expert judgement. Confidence intervals for each driver are indicated in the right column (M: medium; L: low). Presented within the International Panel for Climate Change (IPCC) AR5 report (Ciais *et al.*, 2013).

Peak C accumulation rates (CAR) are associated with higher net primary productivity (NPP) and warmer climates; therefore, it is likely that C sequestration in northern peatlands will increase with predicted future temperature rises and possibly act as a negative feedback to climate change (Charman *et al*., 2013; Yu, 2011; Section 2.2). However, warmer conditions could force peatlands close to the moisture limit of development to cross a critical threshold, where decay processes exceed NPP gain, and become net sources of C release. This thesis contributes to the understanding of peatland sensitivity to climate change, with the aim of characterising the relationship between late Holocene peatland hydrological conditions and C accumulation across a climate gradient in eastern North America that extends to the current southern moisture limit of peat growth.

Many peatlands in eastern North America remain in pristine conditions preserving undisturbed records of peat growth and past environmental conditions. Palaeo-records of peatland water table depths represent the prevailing balance between precipitation and evapotranspiration (Charman *et al*., 2009; Section 2.52). Valuable long-term climatic contexts have been provided by many water table depth (WTD) reconstructions, primarily from peatlands located in Northwestern Europe (Charman *et al*., 2006). Until recently, the eastern coast of North America was largely neglected in terms of palaeo-peatland studies. However, recent work by Hughes *et al*. (2006), Nichols *et al.* (2012) and others have shown the peatlands to be responsive to past climatic changes (influenced by their proximity to the North Atlantic's Gulf Stream and Labrador Current). Therefore, the eastern seaboard of North America is an ideal location to explore interactions between climate and peatland C.

The most prominent Northern Hemisphere climate change during the last 2000 years was the transition from the warmer Medieval Climate Anomaly (MCA: *ca*. 950-1250 AD) to the cooler Little Ice Age (LIA: *ca.* 1400-1700 AD; Jansen *et al*., 2007; Mann *et al*., 2008; 2009); however, the timing, spatial extent and climatic drivers of these periods remain poorly constrained (Section 2.8). Eastern North American climatic reconstructions with a temporal focus on the late Holocene are sparse (Section 2.9); therefore, the peatland water table reconstructions obtained within this thesis seek to enhance the characterisation and understanding of MCA-LIA climate change in this region.

Projections of future climate change in Maine, Nova Scotia and Newfoundland suggest that by 2050, summer precipitation will decrease by up to 15% and annual temperatures will increase by 2–3 °C (Bruce, 2011); therefore, the peatland moisture availability in the study region will decrease. The MCA presents the opportunity to characterise past C accumulation responses of peatlands and could be used as an analogue for future C responses to climate change. The MCA-LIA transition was associated with a *ca*. 7-10 ppmv decline in atmospheric carbon dioxide (CO_2) (Ahn *et al*., 2012). The full cause of this decrease is unknown and the role of peatlands is still to be deduced. Within this thesis, the relationship between climate change and C accumulation will be determined through comparisons of records of past C accumulation rates and reconstructed peatland environmental changes. These data will then be used to infer possible peatland C responses to future climatic change in the study region.

1.2 Research aim and objectives

The primary aim of this thesis is to characterise the relationship between late Holocene peatland hydrological conditions and C accumulation rates (CAR) across a climate gradient in eastern North America. This aim will be addressed through four main objectives:

1. Robust core chronologies will be developed using radiocarbon measurements and tephra to enhance spatial and temporal comparisons of reconstructed climatic and CAR changes (Chapter 5).
2. Peatland water table reconstructions will be obtained from four sites across Maine, Nova Scotia and Newfoundland to improve the characterisation of late Holocene climate change in eastern North America (Chapter 6).
3. Late Holocene carbon accumulation rates will be reconstructed using inferred carbon contents and age-depth models to investigate temporal and spatial variations in C sequestrations (Chapter 7).
4. The extent to which late Holocene peatland carbon accumulation rates fluctuate with vegetation patterns, climatic conditions and disturbance events will be assessed (Chapter 8).

To address the first objective, tephra (volcanic ash) horizons have been characterised within each study site and, alongside radiocarbon measurements, the timings of the identified eruptions form the basis of Bayesian age-depth models. Prior to this study, only one tephrostratigraphic record had been obtained from the study region (Pyne-O'Donnell *et al*., 2012); therefore, the tephrostratigraphic results presented within this thesis form the foundations of a late Holocene tephra framework for eastern North America. Late Holocene climatic records have been obtained from each of the study sites using water table depth reconstructions inferred from plant macrofossil and testate amoebae assemblages, addressing the second objective. The third objective will provide estimates of carbon accumulation rates over the last 2000 years and will facilitate the testing of relationships between carbon accumulation, water table depth reconstructions and physical peat characteristics in an attempt to isolate dominant drivers of peat accumulation in eastern North America, addressing objective four. Specific hypotheses related to these aims will be generated following a review of the relevant literature (outlined in Section 2.10) and will be tested within this thesis.

1.3 Thesis structure

Chapter 1 has outlined the rationale for the research and provided context for the main aim and objectives of the thesis.

Chapter 2 reviews the relevant published literature concerning peatland carbon accumulation, peat-based palaeoclimatology and late Holocene climate change. Specific hypotheses are generated from the synthesis of the existing literature and will be tested within this thesis to address the overall aim.

Chapter 3 outlines the methodologies employed during fieldwork, laboratory analysis and statistical data processing.

Chapter 4 provides detailed information on each of the study sites and compares modelled historical climatic conditions.

Chapter 5 presents the age-depth models developed using radiocarbon measurements and tephrostratigrahies for each of the sites. The development of the eastern North American cryptotephra framework is also presented in the format of a manuscript for submission to *Quaternary Science Reviews*.

Chapter 6 reports the modern observed relationships between the water table depth and vegetation assemblages and uses the data to construct an updated hydrological index for eastern North American peatlands. The plant macrofossil and testate amoebae assemblage data are then presented on a site-by-site basis and converted into water table reconstructions using different statistical techniques, the performance of which are assessed.

Chapter 7 presents the carbon accumulation histories of the peatlands

Chapter 8 presents a detailed discussion of all results, which can be distinguished into two main sections: characteristics of late Holocene climatic change and environmental controls on carbon accumulation rates.

In order to characterise late Holocene climate change, the performance of the palaeoenvironmental reconstructions are assessed, outlining considerations for the inference of climatic conditions. The climate reconstructions are then compared across the four sites and with records from proximal previously published studies to characterise late Holocene climatic change in eastern North America. The likely mechanisms of climate change are discussed and an investigation into the synchroneity of climate change is facilitated using tephra as temporal pinning-points between the records.

Modern environmental controls on the carbon accumulation at each of the study sites are assessed using modelled data based on instrumental measurements. Spatial and temporal changes in carbon accumulation rates are assessed and the persistence of the modern water table depth-CAR relationships over the last 2000 years then tested using the environmental reconstructions obtained within this thesis and other published studies.

Chapter 9 summarises the conclusions that may be drawn from this study and provides suggestions for the future direction of this research.

Chapter 2: Literature review

2.1 Peat accumulation

Peatlands are acidic and largely anoxic ecosystems characterised by a continuous accumulation of partly decomposed organic matter (Gore, 1983). Whilst accumulation rates vary, ombrotrophic (rain-fed) bogs in oceanic regions grow approximately 1mm yr^{-1} (Barber *et al.*, 1994). The peat organic matter originates from the plant litter of *Sphagnum* moss and vascular plants, which are tolerant of the harsh conditions. The peatland vertical structure was historically categorised into two functional layers based on hydrological and decay characteristics: the acrotelm and catotelm (Ivanov, 1953; Overbeck, 1975; Ingram, 1982; Clymo, 1984). The boundary between the layers occurs at the average depth of the minimum summer water table (Ivanov, 1981). Generally, the shallow surface acrotelm is characterised by an oscillating water table, aerobic bacteria, a live matrix of plants, and is the principal location of matter and energy exchange. The underlying catotelm is characterised by permanent waterlogging, low hydraulic conductivity, poor microbial activity, and less abrupt stratigraphic variations in physical properties than the acrotelm.

Whilst this diplotelmic model provides a basic description of the heterogeneity of the peat structure, its usefulness has been queried (e.g. Belyea & Baird, 2006). In a comprehensive assessment of the model Morris *et al*. (2011a) concluded that definitions used are not consistently applied, the model has not been comprehensively tested and it overlooks the complexity of internal peatland dynamics by assuming that changes can be represented by a single discrete boundary. More flexible models could incorporate the ecohydrological complexity by representing the peatland as continuous hydrological, biogeochemical and ecological gradients in a continuum boundary approach (Belyea & Baird, 2006; Frolking *et al.*, 2010). Alternatively, multiple asynchronous boundaries that describe the peat properties and processes could be applied (Morris *et al.*, 2011a). Further work on this categorisation is required; however, this is outside the scope of this thesis. For simplicity, the subsequent sections will use the definitions of acrotelm

and catotelm as described above, accompanied by ecohydrological descriptions when appropriate.

The formation of peat is influenced by geological, geomorphological, ecological, climatic and anthropogenic controls and subsequent development is determined by feedbacks between plant ecology, soil biogeochemistry and ground and soil water hydrology (Belyea, 2009; Eppinga *et al*., 2009). Peatland expansion occurs due to the positive balance between net primary production and peat decomposition rates (Clymo, 1984). Plant litter deposited within the acrotelm is buried under the weight of younger material, which eventually causes the disintegration of plant structures. The associated decrease in pore spaces restricts hydraulic conductivity and, with continued precipitation input, may result in a rise of the water table and the addition of more organic matter to the catotelm (Clymo *et al*., 1998). As the catotelm enlarges, so does the amount of anaerobic decay, which is about a thousand times slower than aerobic decay (Clymo, 1984). Eventually, on Holocene timescales, anaerobic decay matches the annual deposition of litter at the surface, thus limiting the overall depth of peat that can accumulate in a given bioclimatic region (Clymo, 1984).

2.2 Carbon accumulation

Carbon (C) is fixed by the photosynthesis of surface vegetation that use atmospheric carbon dioxide (CO_2). This may be stored within the peat organic matter, respired through aerobic decay or lost as methane (CH_4) (Clymo *et al*., 1998). The rate of C accumulation is dictated by the balance between productivity and decay, which is controlled by a combination of prior and current climatic conditions, internal self-regulating mechanisms and ecosystem disturbance events such as fire or drainage (Figure 2.1). These controls influence the vegetation composition, peat structural characteristics and microbial activity, which also contribute to the productivity-decay balance. Parent material, regional climate and topography are overriding carbon accumulation controls since they determine the timing of peat formation and therefore long term rates of decay.

Average Holocene C accumulation rates in northern peatlands are estimated at 18.6 g C m^{-2} yr^{-1} (Yu *et al*., 2009), with annual peatland uptake of CO_2

estimated between 0.076-0.088 Gt C yr^{-1} (Gorham, 1991; Yu, 2011 respectively) and CH_4 release of *ca.* 0.004 Pg C yr^{-1} (Frolking *et al.*, 2010). The sensitive peatland C flux requires a detailed understanding of factors influencing CO_2 fixation and release, and CH_4 production and consumption (Gorham, 1991). Progress has been made in terms of estimating C stocks and assessing peatland feedback responses; however, a better understanding of the magnitude of climate feedback effects and of the full complexities of these ecosystems is required to help improve peat-C-climate model predictions (Belyea & Baird, 2006; discussed in Sections 3.2.1 - 3.2.3). Sections 2.2 and 2.3 of this literature review investigate the influences on C accumulation rates and assess the way in which C content can be calculated. C controls on different peatland types are highly variable; therefore, this literature review focuses on factors relating to ombrotrophic peatlands which have been selected for analyses within this thesis owing to their direct coupling between climate and peatland moisture balance (Barber, 1981; Section 3.5.1).

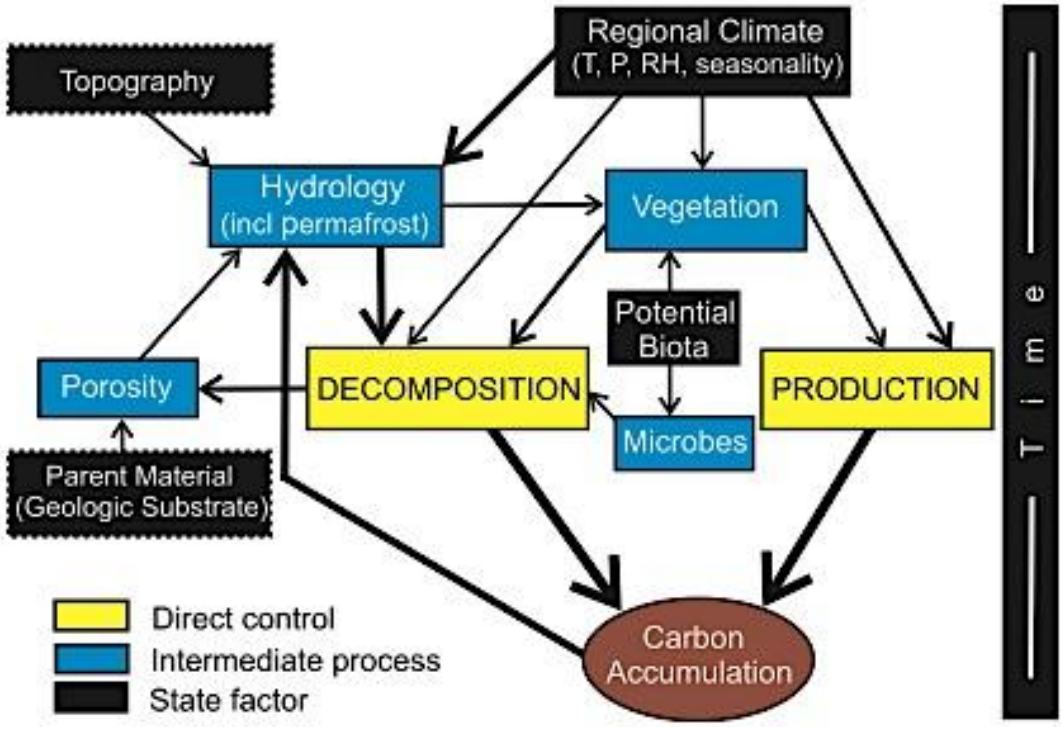

Figure 2.1 Conceptual model of controls over growth and carbon accumulation in northern peatlands (Yu *et al.*, 2009). The thickness of the arrows indicates the relative importance of the controls. T, temperature; P, precipitation; RH, relative humidity.

1.1.1 Climatic control: role of temperature and precipitation

Peatlands expanded monotonically throughout the Holocene influenced by regional rates of deglaciation and associated climate controls (Kuhry and Turunen, 2006). A study of Patagonian peatlands demonstrated that the overall C accumulation rates were mainly influenced by the characteristics of peat formation (Loisel and Yu, 2013a). The rate of initiation affects the overall rates of C accumulation by influencing residence time of the organic matter in the peat column and therefore the overall degree of decomposition. More recent peat has higher apparent accumulation rates since there has been less time for decay to occur (Yu *et al*., 2009).

Regional climate determines peatland moisture conditions over time (Barber *et al*., 1994; Chambers & Charman, 2004; Section 2.4), which affects the peatland C flux by influencing the potential for aerobic and anaerobic decay, the vegetation type and productivity. The peatland C response to future warming is uncertain since higher temperatures would increase productivity and carbon sequestration but would also increase decay. This balance between productivity and decay will determine whether peatlands are a net sink or source of C (Charman *et al*., 2013).

Early investigations into climatic controls on C accumulation rates (CAR) found that the number of degree-days and mean annual air temperature dominated (Clymo *et al*., 1998). Warmer conditions increase the growing season length, suggesting that productivity is a more important long-term control on C accumulation than decomposition (Beilman *et al*., 2009; Charman *et al*., 2013; Jones and Yu, 2010; Loisel and Yu, 2012). In oceanic settings, the amount of available moisture would be expected to influence C accumulation characteristics since precipitation is assumed to be the main climatic driver of water table height (Charman *et al*., 2009; Section 2.4.2) and would influence the potential for aerobic decay by controlling the depth of the acrotelm. Field studies and laboratory experiments characterising the effect of lower water tables on CAR have reported conflicting results that vary over different timescales, depending on the balance of production and decomposition (e.g. Laiho, 2006; Laiho and Prescott, 2004; Minkkinen *et al*., 1999; Moore *et al*., 2002; Alm *et al*., 1999). Furthermore, studies into long-term carbon accumulation histories have found no significant correlation with

precipitation (e.g. Charman *et al*., 2013; Beilman *et al*., 2008). This thesis continues the investigation into the influence of changes in the water table depth on carbon accumulation rates over the last 2000 years in eastern North America.

The control of productivity and temperature on CAR is primarily expressed through growing season length (Lund *et al*., 2010) which, in combination with available light, influences the amount of photosynthetically active radiation (PAR) and controls photosynthetic C fixation (Charman *et al*., 2013; Loisel and Yu, 2012). In a study of northern peatlands over the last millennia, PAR was identified as the main C accumulation rate control and explained a third of the data variation (Charman *et al*., 2013). Future climate warming may therefore encourage peatlands to act as a negative feedback mechanism to climate change: warmer temperatures could increase the peatland C sink through their control on NPP (Charman *et al*., 2013; Figure 2.2) by extending the growing season length and bringing forward the time of snow melt (Moore *et al*., 2006). However, enhanced C accumulation may only occur if evaporative demand does not exceed precipitation (Cai and Yu, 2011; Jones and Yu, 2010). Regional C accumulation histories are required to test the robustness of this feedback mechanism over time and space. This thesis will investigate carbon accumulation histories over the past 2000 years across the eastern seaboard of North America to establish the main climatic driver of carbon accumulation in this oceanic region and to determine whether this remains constant over time and space. It is hypothesised that C accumulation will be greater in the southern sites owing to increased net primary production (NPP) under warmer temperatures (Hypothesis two; Section 2.10) and that temperature will be a more dominant CAR control than precipitation.

The sensitivity of peatlands at the current climatic limit of peat growth are of particular concern since climate change could inhibit peat expansion and carbon accumulation whilst promoting C release and thus contract the current geographical range (Charman *et al*., 2013). To address this concern, the sites selected within this thesis extend to the current southern limit of peat growth on the eastern seaboard for North America. Changes in peatland moisture balances and carbon accumulation across a southwest – northeast transect from Maine, Nova Scotia and Newfoundland will be compared to identify differences in the sensitivities of the sites. It is hypothesised that sites closer

to the southern limit of eastern North American peat growth will be more sensitive to hydrological variability and will contain more fluctuating carbon accumulation rates than sites in the north (Hypothesis four; Section 2.10).

On decadal-centennial timescales, some individual peatland reconstructions attribute the dominant C accumulation control to hydrologically induced decomposition (Dorrepaal *et al*., 2009; Ise *et al*., 2008) with temperature often reported as a secondary influence (e.g. Klein *et al*., 2013). Additionally, instrumented studies, often measuring gas flux, have demonstrated that water table depth influences the C balance on annual timescales (Bubier *et al*., 2007; Pelletier *et al*., 2011): for example, late summer droughts are detrimental to growing season length and production and therefore reduce C accumulation (Aurela *et al*., 2007; Lund *et al*., 2012). Despite the possibility of different C accumulation rate controls on different timescales, few studies have investigated decadal-centennial controls and feedback mechanisms on regional scales. This thesis will contribute towards this understanding by testing the relationship between the peatland C accumulation and ecohydrological changes on various centennial timescales across Maine, Nova Scotia and Newfoundland.

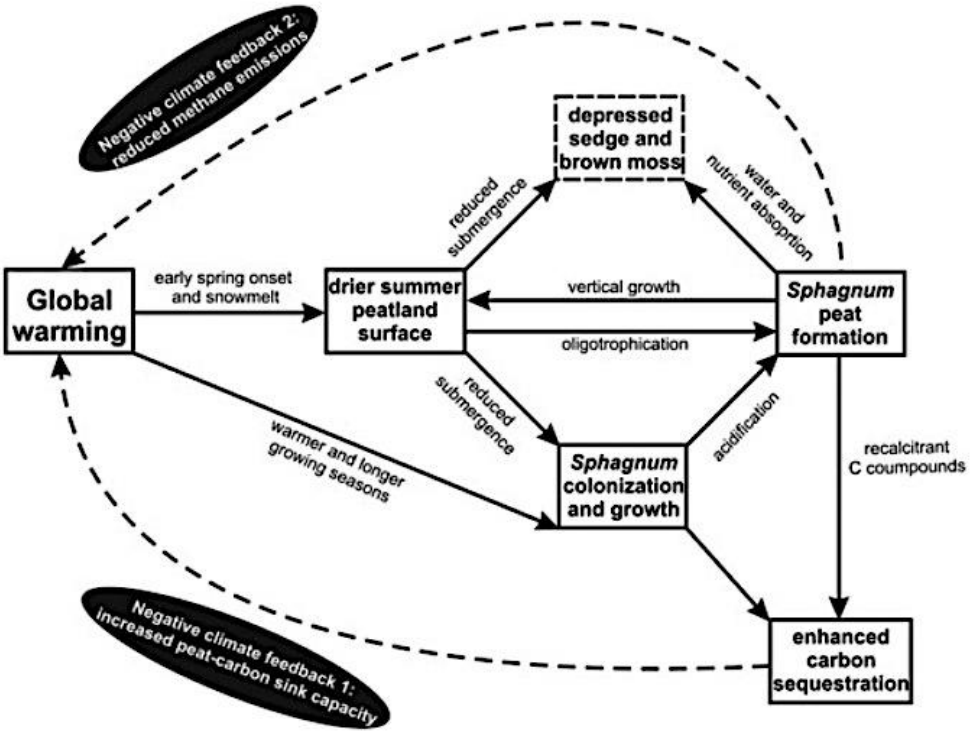

Figure 2.2 Conceptual model linking climate warming with peatland C sequestration (Loisel and Yu, 2013a). The arrows represent processes and boxes indicate consequences.

2.2.1 External disturbances: fire and nutrient loading

Future climate scenarios indicate that peatlands will be increasingly exposed to disturbances such as fire, droughts and drainage (e.g. Bergeron *et al.*, 2010; Flannigan *et al.*, 2005). Such disturbances may result in a reduction in CAR and the release of previously stored C, which are exacerbated by the delay in recovery of peat growth (Wieder *et al.*, 2009). Furthermore, fires can influence carbon accumulation by altering the vegetation assemblage to different species after fire-induced colonisation of exposed peat (Pitkanen *et al.*, 1999). Fires can release several hundreds of years worth of accumulated carbon in a single event (Turetsky *et al.*, 2011). Therefore, whilst a previous study has found no apparent relationship between C accumulation and fires on millennial timescales in Canada (van Bellen *et al.*, 2012), on shorter time scales fires can have huge impacts on peatland C balances. Future induced droughts by climate change may increase the number of peatland fires if the surface becomes drier with increased shrub vegetation that is susceptible to burning (Higuera *et al.*, 2009).

The addition of nutrients can also alter C accumulation by changing the vegetation, which determines the potential for peat decomposition and the amount of C provided. Plants contain variable proportions of labile material depending on their cellulose and lignin content: *Sphagnum* is more decay resistant than vascular plants since its recalcitrant tissue and release of phenolic compounds (Freeman *et al.*, 2001) limit microbial breakdown (van Breemen, 1995). Typically 50% of preserved peatland biomass is *Sphagnum* (Rydin and Jeglum, 2006); therefore, its abundance influences the capacity for C accumulation (discussed further in Section 2.2.3).

Moderate to large depositions of tephra on peatlands proximal to volcanic areas reduce C accumulation (Hughes *et al.*, 2013). This is likely triggered by the phosphorus and potassium content of the ash (De Vleeschouwer *et al.*, 2008) and enhanced by the thermal effects associated with the change in vegetation and shard cover, promoting microbial activity. Increases in atmospheric levels of nitrogen (N_2) have been also been shown promote peatland C loss by enhancing microbial decomposition through a combination of improving litter quality and by removing microbial metabolic N_2 constraints (Bragazza *et al.*, 2004).

2.2.2 Internal self-regulating mechanisms

Complex ecohydrological feedbacks may disconnect the peatland ecosystem from climatic influences through self-regulating mechanisms (Belyea & Baird, 2006; Belyea, 2007, 2009; Swindles *et al.*, 2012a). Additionally, the timing and magnitude of peatland water table depth response to climate change is often influenced by antecedent conditions (Yu *et al.*, 2009). Therefore, changes in C accumulation are forced by a combination of external and internal factors.

Peatland microforms influence long-term C fluxes (Baird *et al.*, 2009): wet hollows release more CH_4 and accumulate more slowly than drier lawns and hummocks (Waddington and Roulet, 1996), which act as stronger C sinks whilst emitting CO_2 (Laine *et al.*, 2009). These surface features have different rates of formation, and such difference is accentuated with time (Belyea and Clymo, 2001; Eppinga *et al.*, 2009). Non-linear self-regulated feedbacks may control the formation of these surface features independently of climate (Eppinga *et al.*, 2009; Rietkerk *et al.*, 2004); however, the microforms can also be initiated or amplified by climate change (Walker and Walker, 1961). Dynamics within the climate system must, therefore, influence peat growth and C sequestration over large temporal and spatial scales (Clymo *et al.*, 1998; Yu *et al.*, 2010).

2.2.3 Influence of vegetation

Peatland vegetation assemblages, determined by the height of the water table and internal self-regulating processes (Loisel and Yu, 2013b; Section 2.2.2) as well as external disturbances such as increased N_2 deposition or tephra loading (e.g. Hughes *et al.*, 2013; Section 2.2.1), form the basis of the preserved substrate and determine the decomposability of the peat. Changes in major vegetation types can significantly influence CAR (e.g. Loisel and Yu, 2012; van Bellen *et al.*, 2011); however, few studies have fully characterised the role of plant type on CAR. *Sphagnum* has a lower bulk density, contains less C and has a higher C:N_2 ratio than vascular plants. If hydrological conditions allow for rapid peat burial, there is the potential for vascular plants to have higher accumulation rates (Loisel *et al.*, 2014). However, the recalcitrant polymers of *Sphagnum* are more resistant to decay; thus

Sphagnum-dominated assemblages have a greater capacity for enhanced C accumulation over longer time scales than assemblages dominated by vascular plants (e.g. Malmer *et al*., 2003). Within *Sphagnum* species, differential decay occurs as species with wet preferences tend to decay faster than those associated with dry conditions (van Bellen *et al*., 2012).

2.3 Estimating peatland carbon stores

Estimates of peatland C content vary due to the difficulty of estimating their spatial extent and basin depth. Land cover estimates cannot be achieved by remote sensing due to the diversity in vegetation cover, therefore temporally and spatially restrictive exploration and mapping techniques are required. Best estimates suggest that peat covers *ca*. 2.5-3.5% of the global land surface (Figure 2.3) and accounts for one third of all soil C (Lappalainen, 1996; Joosten,and Clarke, 2002), making it the most spatially efficient terrestrial carbon store.

Early peatland C content estimates combined C content from bulk density measurements and peat area to calculate the total carbon content per unit area (Armentano and Menges, 1986). Subsequent approaches included peat depth to determine the C content by volume. Gorham (1991) estimated global peat C content as 455 Gt (Gorham, 1991) and this values remains the most widely cited value. Uncertainties in calculations of peatland C originate from their sensitivity to peat depth and bulk densities, which are difficult to measure (Turunen *et al*., 2002). Commonly, half of the peat bulk density is assumed to be C; however, this ignores fluctuations driven by changes in decomposition and vegetation types. Measured C content ranges between 46.6% (Charman *et al*., 2013) and 51.8% (Yu *et al*., 2009); therefore, this seemingly small difference may generate considerable variations in estimates of peat C stocks when scaled to a global level.

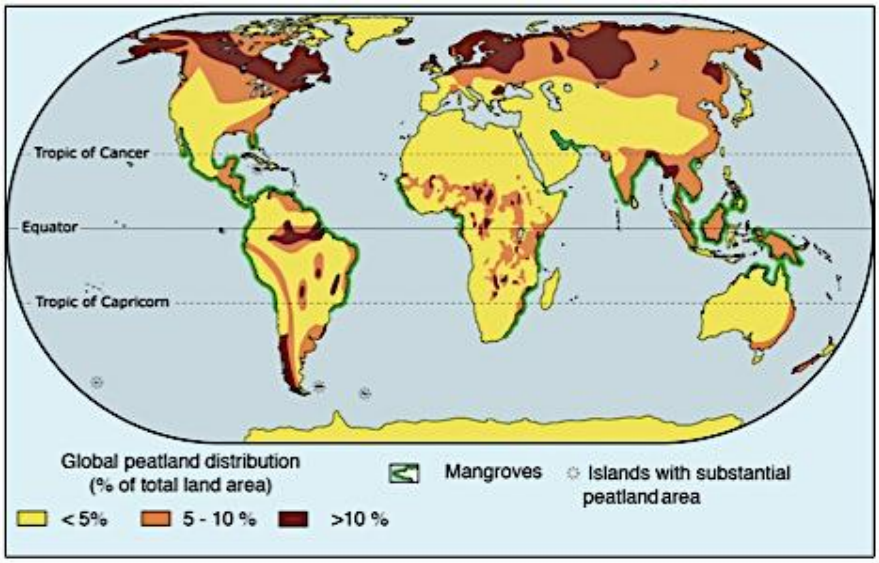

Figure 2.3 Global peat distribution (from Jackson and Charman (2010); based on Charman (2002) and Lappalainen (1996). Main areas of peatland occurrence expressed as proportion of the landscape covered.

2.3.1 Carbon accumulation rates

The long-term apparent rate of C accumulation (LORCA: Tolonen and Turunen, 1996) characterises C accumulation per unit area over time. The C dynamics of many peatlands can be quickly characterised using this method, which requires the basal peatland date to indicate the time of formation and the bulk density inferred C content. This approach has been updated to calculate the changes in carbon content over smaller distinct time intervals by including multiple peat ages (CAR; Yu *et al.*, 2009a). The rates of C accumulation calculated using these methods are termed 'apparent' since they are a direct measure of peat carbon remaining between two core depths at the point of measurement and do not account for C loss through decomposition.

C losses may be modelled alongside peat addition rates to calculate the net carbon balance (NCB; e.g. Yu (2011). Models of peat decay and accumulation vary in their assumptions surrounding autogenic processes of long term decay (Clymo, 1984; Clymo *et al.*, 1998) and ecosystem maturity (e.g. Yu *et al.*, 2003). Under the simplified assumption that no autogenic processes occur, the decay rate coefficient in the linear decay model can be calculated using linear regression (Clymo *et al.*, 1998; Yu *et al.*, 2001). Other models

that consider autogenic processes calculate the decay rate coefficient using minimisation (e.g. by Newton-Raphson and bisection methods), which determines an optimal estimate from a systematic set of alternative values (e.g. Belyea and Baird, 2006).

The application of these long-term decay models facilitates the direct comparison of more recent and past C accumulation rates and becomes increasingly important as the age of the peat deposit (and therefore time for decomposition processes to occur) increases. The NCB approach is based on two main assumptions, the constant rate of peat addition and the catotelm decay coefficient, which vary over time and cannot be directly measured. Current understandings of both terms are based on simplistic assumptions that require further revision. This study investigates the influence of peatland hydrological changes on late Holocene C accumulation and the assumption of fixed peat addition rates and decay rates within the NCB approach contradicts the expectation that hydrological change will alter both terms over time. Therefore, it is deemed appropriate to estimate C accumulation histories using CAR rather than NCB within this study. This approach is supported by the findings of a recent study that compared CAR and NCB estimates using a process-based peatland-C and water-cycle model over the last 8500 years: CAR approximately behaved as a running mean of NCB throughout the majority of the record (Frolking *et al.*, 2014). CAR was shown to be elevated relative to NCB over the last 500 years, owing to partial decomposition in the more recently deposited peat (Frolking *et al.*, 2014). Therefore, when comparing more recent CAR with CAR obtained from earlier in the peat record, such decomposition driven elevated levels of CAR must be considered.

2.4 Peatlands as environmental archives

Evidence of climatically forced changes contained within peat stratigraphies were first hypothesised by Blytt (1876) and later confirmed by Sernander (1908), proposing that the degree of peat humification was associated with the amount of available moisture: less humified peat represented wetter/cooler conditions restricting decay, and more humified peat represented warmer/drier times enhancing decay. These findings led to the development of the Blytt-Sernander scheme for Northwest Europe that,

although later shown to be overgeneralised and imprecise, was the first climatostratigraphic division of the Holocene.

Despite such an early recognition of a peatland-climate link, the use of peatlands as a climate archive was hindered by the misconceived concept of internal peat growth originating from Osvald's (1923) theory of cyclic regeneration. Therefore, it was not until 1970s that changes within the peat stratigraphy were again suggested to be of a climatic origin when consistent changes in the degree of peat humification and protozoa communities were identified (Aaby, 1976). The peatland-climate link was firmly established by Barber (1981), using detailed analyses of plant macrofossils in the cut peatland of Bolton Fell Moss, UK. The exposures provided the opportunity to explore the nature of the stratigraphic changes over large areas and, once dated, to conclude that they were not cyclic, but rather coincided with the climatic indices of Lamb (1977).

2.4.1 Peatland-climate link

Ombrotrophic peatlands have a particularly close link to atmospheric moisture conditions since all inputs are atmospherically derived and they are not affected by surface run-off or local groundwater influences. In these environments, the prevailing balance between precipitation and evapotranspiration (effective precipitation) determines the position of the water table, which can be reconstructed based on three main assumptions:

1. Peatland biological, physical and chemical characteristics respond to changes in the water table, which are climatically forced.
2. The acidic, waterlogged conditions preserve the fossil remains and these are representative of conditions at the time of peat deposition.
3. Robust reliable core chronologies can be constructed (Chambers *et al.*, 2012).

The widespread geographical distribution and their ease of sampling enhances the usefulness of peatlands as records of climate change.

The traditional proxy methods commonly used to reconstruct water table depths (WTD) are plant macrofossil analysis (Barber *et al.*, 2004; Mauquoy & van Geel, 2007), which reconstructs changes in vegetation assemblages; testate amoebae analysis (Charman *et al.*, 2000), which reconstructs changes

in protozoan communities; and peat humification analysis (Blackford & Chambers, 1993), which measures the degree of peat decomposition. These methods are reviewed in Section 2.5, along with their application in this study.

2.4.2 Controls of peatland water table depth

The balance between precipitation and evaporation is reflected in the peatland water table depth (WTD) and is determined by a combination of temperature, precipitation, humidity and wind speed. Therefore, WTD reconstructions (also known as bog surface wetness) represent a mixed climate signal. The isolation of parameters, such as temperature and precipitation, from the overall signal is required to provide a greater understanding of the climate system. Attempts to constrain the dominant decadal-millennial-scale climate forcing factors have compared reconstructed WTD with instrumental data and other well established independent climate proxies (discussed below; for a full review see Charman *et al*., 2009). The complexity of distinguishing between the direct influences of temperature and precipitation is driven by the variety of conditions that can result in a particular WTD. This problem is compounded by variations in the relationship between precipitation and temperature over time and space (Schoning *et al*., 2005).

Relative to precipitation, temperature exhibits more consistent spatial and temporal patterns. Barber *et al*. (2000), therefore, hypothesised that temperature drives consistent changes evident in hydrologically separated peatlands, as supported by other studies recording spatially consistent hydrological changes (e.g. Hughes *et al*., 2000; Barber and Charman, 2003). The comparison of a proximal mid-late Holocene chironomid-based temperature reconstruction from a lake and WTD record from a bog revealed synchronous changes (within dating errors), suggesting the dominant role of July temperatures on WTD over centennial timescales (Barber and Langdon, 2007). However, simulated surface responses to temperature and precipitation suggest that a large temperature change would be required to achieve the reconstructed changes in WTD and the magnitude of mid-late Holocene temperature changes in isolation would not have been sufficient (Charman, 2007).

The isolation of a dominant climatic WTD driver is limited by the negative correlation that exists between instrumental summer temperature and precipitation records (Charman *et al*., 2009) indicating that both parameters drive WTD changes in same direction. However, despite such complications, comparisons with instrumental meteorological data extending over the last 200 years indicate that precipitation plays a more dominant role on WTD than temperature in oceanic settings (Charman *et al*., 2004). More specifically, the climate parameter most highly correlated with WTD is the annual precipitation-evapotranspiration (P-E) deficit (the sum of P-E for all months where precipitation is less than evapotranspiration; Charman, 2007). This acknowledges the importance of seasonality and periods of limited precipitation. The seasonal influence on the palaeo-peatland record may be enhanced since rates of primary productivity are comparatively higher in summer than winter. These findings indicate that over centennial timescales, changes in WTD reconstructions are primarily driven by precipitation and reinforced by temperature, which are negatively correlated (Charman *et al*., 2009; Booth, 2010). Comparisons with instrumental records since AD 1775 suggest that the relative control of temperature and precipitation on the peatland moisture balance varies between oceanic and continental settings with a greater, but still subsidiary role, of temperature in continental areas (Charman *et al*., 2004; Charman, 2007). These relationships may also vary with time.

2.4.3 Water table depth controls: climate system oscillations

The control of the summer moisture deficit on WTD (Charman *et al*., 2009) indicates that aspects of the climate system that influence summer conditions will be the overriding drivers of WTD. Peatland records from eastern North America and northwest Europe have demonstrated concurrent changes in WTD (Barber and Charman, 2003; Hughes *et al*., 2006); therefore, a common climatic driver has been postulated. In these locations the Atlantic Multidecadal Oscillation (AMO: Section 2.7.2.2) influences summer conditions (Sutton and Hodson, 2005; Denton and Broecker, 2008) and may drive the WTD patterns (Charman *et al*., 2009). Other possible drivers of change in terrestrial moisture balance may include the North Atlantic Oscillation (NAO;

Section 2.7.2.1) and the Atlantic Meridional Overturning Circulation (AMOC; Section 2.7.2.3).

The North Atlantic has been extensively investigated as the driving source of climatic change; however, attention is now increasingly focusing on change originating in the Pacific Ocean. Consistent WTD changes in peatland records from Argentina (Chambers *et al*., 2007) and Europe (Mauquoy *et al*., 2008) have been detected, suggesting the role of wider teleconnections with a common distal control (Charman *et al*., 2009). Such forces are likely to include the El Niño-Southern Oscillation (ENSO) and the Pacific Decadal Oscillation (PDO) as discussed in Sections 2.7.2.4 – 2.7.2.5.

The identification of specific climatic controls on WTD requires robust core chronologies to facilitate the precise correlation of records. The use of tephras as pinning-points in time provides great potential for cross-core and cross-location correlation (Turney *et al*., 1997; Langdon and Barber, 2004, 2005) as discussed in Section 2.6.1. The potential to obtain tephrostratigraphies from coastal regions of eastern North America has recently been revealed (Pyne-O'Donnell *et al*., 2012; Section 2.6.1.1). Additionally, since peatlands in this region extend towards the geographical limit of peat growth, they are likely sensitive to climate change. The responsiveness of the peatlands to climate change and the ability to precisely temporally link sites using tephrostratigraphies makes eastern North American an ideal location to address the projects main aim: to reconstruct changes in the peatland moisture balance and carbon accumulation rates to better understand the relationship between them, and may also indicate the dominate WTD control. To address this aim, four sites from Maine, Nova Scotia and Newfoundland have been selected (Section 4.3).

An additional approach that can be applied to regional records is to compare large-scale climatic changes by 'stacking and tuning' records (Charman *et al*., 2006). Whilst this reduces site-specific biases, changes are assumed to be synchronous and any leads and lags in the data sets will be lost. The current climate conditions across Maine, Nova Scotia and Newfoundland vary (Section 4.4.1); therefore, differences in environmental responses may be expected, violating the assumption of climatic synchroneity. Tuning and stacking is not an appropriate approach for this study.

2.4.4 Reliability of peatland climate records

Comparisons of WTD and instrumental records have successfully demonstrated the peatland-climate link (e.g. Amesbury *et al.*, 2011; Charman *et al.*, 2006); however, the debate surrounding the reliability of single core climatic reconstructions has been revived, focusing on the role of autogenic versus allogenic processes. Internal influences associated with the process of peat accumulation require peatlands to be viewed as complex adaptive systems (e.g. Belyea and Baird, 2006; Morris *et al.*, 2011b). Ecohydrological feedback mechanisms can alter WTD independently of climate, potentially partially disconnecting WTD from external influences (Swindles *et al.*, 2012a). An example of this was provided using a long-term peatland development model (from Morris *et al.*, 2011b): apparent drying after a wet shift could be triggered in response to increased peat accumulation since the rate of peatland surface rise exceeded the rate of WTD rise (Swindles *et al.*, 2012a). Early peatland hydrological studies stated that wet-shifts were the most suitable focus for peatland moisture balance reconstructions and that dry-shifts may not be reliable (Barber, 1993, 1981) More recently, studies have focused on drying trends (e.g. Booth, 2010). Therefore, to obtain robust climate reconstructions, the role of internal peatland dynamics and ecohydrological feedbacks must be considered when evaluating perceived hydrological changes (Belyea & Baird, 2006; Frolking *et al.*, 2010; Morris *et al.*, 2011b; Swindles *et al.*, 2012a).

Early peatland studies used hand-cut peat exposures to reveal consistent changes within the stratigraphy (Barber, 1981; Walker and Walker, 1961), suggesting that numerous locations across the site would be representative of the peatland as a whole. Subsequent conservation measures preventing peat cutting and the desire to investigate undisturbed sites meant that such uniformity within a site could no longer be visually ensured (Barber *et al.*, 1994). Whilst laterally consistent shifts in the stratigraphy were confirmed by this approach, the relative influence of autogenic and allogeneic forced variability could not be deduced. This variability was tested using ten short cores from two adjacent peatlands in northern England (Barber *et al.*, 1998). Variations in plant macrofossil assemblages between stratigraphies were minimal with some 'ecological noise' (less than surface vegetation would imply) and changes were largely contemporaneous. The detection of

synchronous changes in WTD between sites suggests that these could be attributed to climatic forcings rather than independently acting autogenic processes. It was therefore concluded that, if coring locations were carefully and suitably selected to obtain the most sensitive record, a single core could be representative of the peatland and the surrounding climate change.

The reliability of a single core has also been rigorously tested by comparing cores from the peatland centre and edge, based on the hypothesis that autogenic differences would be accentuated in these locations (Hendon *et al.*, 2001). However, similar WTD records were obtained during the late Holocene, concluding that robust reconstructions could be obtained from single cores for this time period. Despite these findings, it is prudent to note that different cores from the same site may contain differences in climatic sensitivity (Charman *et al.*, 1999). Such differences, attributed to variations in microtopography, were reduced over the last 1500 years and diminished over the last 1000 years possibly driven by the maturity of the investigated peatland investigated, which reduced local hydrological influences (Charman *et al.*, 1999).

Broadly synchronous changes (as limited by chronological controls) between sites are attributed to climatic changes (e.g. Mauquoy & Barber, 1999; Barber *et al.*, 2000; Hendon *et al.*, 2001; Barber *et a*l., 2003, 2004; Loisel & Garneau, 2010). Comparisons of regional records facilitates the distinction of changes that are likely allogenic and those which are internally driven. Some variations may be expected between sites owing to variations in regional and local climatic manifestations and site-specific sensitivity (Blackford, 2000). WTD-climate responses may also be non-linear, therefore, any changes in reconstructed WTD must be fully characterised and evaluated.

Single cores from a number of regional sites have been selected for analysis in this thesis. This will facilitate the distinction between allogenic and autogenic changes whilst focusing on characterising the regional climate change.

2.5 Peatland climate proxies

Confidence in reconstructed environmental change and processes requires a multi-proxy approach whereby detailed comparisons can validate consistent trends between records, whilst highlighting periods of uncertainty (Charman *et al*., 1999). In peatland studies three main techniques are commonly applied to reconstruct the peatland moisture balance: plant macrofossils, testate amoebae and humification analyses. Different sensitivities and response characteristics of proxies cause reconstructions to deviate (Booth and Jackson, 2003). Such controlling influences will be discussed in Sections 2.5.1-2.5.2.

One approach to interpret the varying results between individual proxy reconstructions is to combine them in a composite record. This method had been shown to improve climate reconstructions (e.g. Langdon *et al*., 2003; Blundell & Barber, 2005); however, it ignores any complicating issues with the individual proxies, which vary over time. Additionally, it overlooks the possibility of different climatic controls or seasonal effects on the different proxies that could reveal information on peatland functioning. A further critique of the combination approach is that it requires the removal of the quantitative aspect of the testate amoebae reconstruction to be comparable with the other semi-quantitative or qualitative techniques (Brown, 2006).

An alternative approach is to combine the different proxies in a single transfer function accounting for differences in their responses (Mitchell *et al*., 2013). Whilst single proxy reconstructions must still be thoroughly investigated to ensure results are ecologically sensible. This method, which combines testate amoebae, bryophytes and vascular plants, has been shown to outperform single-proxy transfer functions (Mitchell *et al*., 2013). Despite promising results, the use of a single transfer function for multiple proxies violates a basic transfer function assumption: that the components must be responding to a single environmental gradient. Different proxies will be responding to different forcings; therefore, the exact gradient that is being reconstructed is uncertain (s*ensu* Juggins, 2013; Section 3.5.4). Combination approaches will therefore not be applied in this thesis.

2.5.1 Plant macrofossils

Plant macrofossils are any plant fragment with a median size of 0.5 mm - 2 mm that is visible by the naked eye (Birks, 2007). In the peatland context, macrofossils are dominated by leaves, branches, roots and seeds of *Sphagnum* mosses, Ericaceous species and Monocotyledons (monocots) growing *in situ*. The identification and quantitative estimates of the plants can be used to infer past surface vegetation assemblages. These are integral to understand the peatland systems since they are the source of the decomposed peat organic matter; they characterise the peatland surface features (microtopography) and they influence the amount of stored C.

Each plant has an optimum set of environmental conditions for growth (Figure 2.4), under which they will thrive and obtain a competitive advantage over other species (Rydin and Jeglum, 2006). The different habitat preferences of different species are visible on the peatland surface through the microtopographical dry-wet gradient from hummocks, lawns and pools (Malmer, 1988; McMullen *et al.*, 2004). When the WTD changes, it may exceed the existing plant community's threshold of tolerance and will be replaced with a new community that is more adapted to the altered WTD (McMullen *et al.*, 2004). This Phasic Theory of bog growth was proposed by (Barber, 1981) based on his pivotal application of plant macrofossil analyses in an English peatland. Many studies have since exploited this relationship between plants and environmental conditions to reconstruct peatland WTD (e.g. Barber, 1994; Barber *et al.*, 1998b; Hughes *et al.*, 2000; Barber *et al.*, 2003; Langdon *et al.*, 2003; Hughes *et al.*, 2006; Swindles *et al.*, 2007; Mauquoy *et al.*, 2008; Amesbury *et al.*, 2011; Daley & Barber, 2012; Swindles *et al.*, 2012).

Several methods are used to determine the abundance of macrofossils: the simplest and quickest are ordinal value techniques, e.g. 1 representing rare and 5 abundant (Walker and Walker, 1961) and the most detailed converts estimates of absolute number of species as concentrations (Booth *et al.*, 2004) or influx (Daniels and Eddy, 1990). A commonly used intermediate method is termed the quadrat and leaf count macrofossil analysis (Barber *et al.*, 1994). This method provides estimates of the percentages of major peat components and ordinal values for smaller components such as the number of seeds and charcoal. This facilitates more analyses than would be possible

using the more time-consuming methods, whilst providing a sufficient degree of detail, therefore, this will be the method applied in this thesis (Section 3.4.1).

Abundance data obtained from the quadrat and leaf count method is readily converted into peatland moisture balance reconstructions using weight average ordination (e.g. Dupont Index; Dupont, 1986), ordination techniques e.g. detrended correspondence analysis (DCA; e.g. Barber *et al.*, 1994) and Principal Components Analysis (PCA; Mauquoy *et al.*, 2010) and/or non-metric Multidimensional Scaling (nMDS; e.g. Daley and Barber, 2012). A comparison of these statistical measurements by Daley and Barber (2012) found that weighted averaging techniques work as well or better than ordination analyses and non-metric multidimensional scaling. An alternative approach is to use modern training sets to build transfer functions for vegetation-WTD measurement, resulting in quantitative WTD reconstructions (Valiranta *et al.*, 2007). This approach is not widely applied owing to: the lack of developed transfer functions, the time taken to compile sufficient surface samples, the large range of WTD preferences of some species and the factors other than WTD that can influence vegetation preferences.

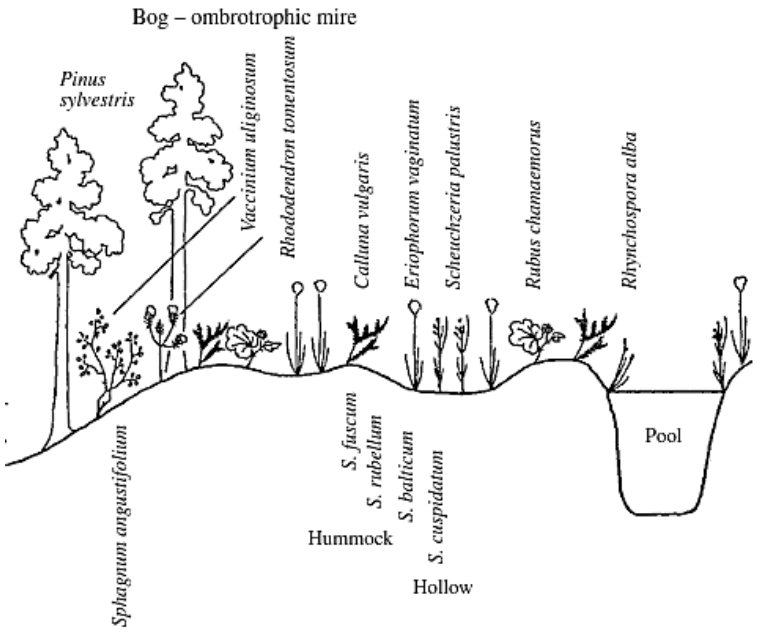

Figure 2.4 Characteristic species habitats of a European ombrotrophic peatland (Rydin and Jeglum, 2006).

2.5.1.1 Limitations and considerations

Plant macrofossil analysis relies on the plant fragments resisting decay so they can be visually recognisable. This is assisted by the acidic, anoxic peatland conditions that promote preservation and facilitates identification to a high taxonomic level. Despite such preservation, the peat increasingly contains a less comprehensive representation of surface vegetation as decay progresses (Clymo, 1984), which is exacerbated by differential decay rates between species that may result in differences between the sub-fossil assemblage composition remaining in the identified peat subsample and the original surface vegetation composition. When characterising the macrofossil assemblage it is prudent to note the section of the plant that has been identified since roots penetrate downwards and are more modern than the time slice investigated. Since roots may inhabit waterlogged conditions during growth, they are often resistant to decay and may be over represented in the fossil record (Brown, 2006). Conversely, lichens are often, but not always (e.g. *Cetraria islandica* was present in a Newfoundland record (Hughes *et al*., 2006)), absent from the macrofossil record but are abundant on dry surface areas.

The possible level of plant macrofossil identification is determined by the degree of decomposition and can be complicated by subtle differences between taxa. For example, members of S*phagnum* sect. *Acutifolia* have different water table depth preferences but are often not identified to species level (Daniels and Eddy, 1990). If these species are not identified then climatic complacency is added to the water table reconstruction. Additionally, peat that is dominated by *Sphagnum fuscum* or by monocots with little change in *Sphagnum* species, creates an ambiguous record of WTD change owing to their large water table tolerances (Chiverrell, 2001; Hughes *et al*., 2000).

Plant communities have a non-linear response to changes in the WTD (Barber *et al*., 2003). These threshold responses often result in complacency in the vegetation community response to small and/or short-lived WTD changes (e.g. Hughes *et al*., 2006). Changes in macrofossil reconstructions may therefore lag behind other proxy records (e.g. Blundell and Barber, 2005). The sensitivity of the macrofossil record is improved when a range of species is present (Barber *et al*., 1994), especially wet species since they have a narrow

ecological tolerance and a quicker response time than drier plants (Rydin, 1985; Valiranta *et al*., 2007).

Influences other than climate may force changes in vegetation assemblages. *Sphagnum austinii* (formerly *Sphagnum imbricatum*) provides an example of this since the UK palaeorecord shows local decline and extinction, possibly caused by competition (Mauquoy and Barber, 1999) and loss of genetic diversity (Langdon and Barber, 2005), perhaps exacerbated by climate. More recently its decline has also been attributed to agricultural land use intensity (Hughes *et al*., 2007) and general human disturbances (McClymont *et al*., 2008). The addition of moderate to high quantities of tephra also acts as an external driver of plant community change, shifting plant communities from *Sphagnum* to Monocotyledon dominance on multi-decadal to multi-centennial timescales (Hughes *et al*., 2013).

2.5.2 Testate amoebae

Testate amoebae (Protozoa: Rhizopoda) are unicellular polyphyletic organisms that construct taxonomically-distinctive, well-preserved shells (tests) to enclose their cytoplasm (Tolonen, 1986). They are abundant in peat where their community compositions change rapidly, primarily in response to surface moisture conditions (Warner and Charman, 1994; Woodland *et al*., 1998; Payne *et al*., 2006; Charman and Blundell, 2007; Booth, 2008; Mitchell *et al*., 2008); thus representing mean annual WTD (e.g. Tolonen *et al*., 1992; Woodland *et al*., 1998; Bobrov *et al*., 1999; Mitchell *et al*., 1999). Their sensitivity to changes in hydrological conditions arises from their biological dependency on the host substrate's water film (Tolonen 1986; Charman, 2001; Wilmshurst *et al*., 2003). For comprehensive testate amoebae reviews see Charman *et al*. (2000), Warner (1990) and Tolonen (1986).

Tests are usually between 20-250 µm with characteristic sizes, shapes and textures that are used to identify to species level. Since they reproduce asexually a 'morphospecies' approach is required for some species (Charman, 2001) highlighting some taxonomic and ecological uncertainties. Their suitability as a WTD proxy is enforced by their fast reproductive rates of 10-27 generations per year (Charman, 2001) and high species diversity (*ca*. fifteen per $4cm^3$ sample; Woodland *et al*., 1998). The preparation of testate

amoebae follows the methods outlined by (Charman, 2000; Hendon *et al*., 2001). Traditionally, 150 tests were counted from each sample. However, whilst this total is required to identify all taxa and estimate relative abundance of rare taxa (Wall *et al*., 2009) a count of 100 has been shown to be sufficient for characterising WTD changes in most samples (Payne and Mitchell, 2009).

2.5.2.1 Quantitative reconstructions

Other peatland hydrological proxies are limited by difficulties with scaling indices (Charman *et al*., 1999), whereas testate amoebae can produce quantitative palaeohydrological reconstructions using transfer functions (Charman, 2001). Many transfer functions have been developed for different regions such as the UK (Woodland *et al*., 1998), Poland (Lamentowicz and Mitchell, 2005), Europe (Charman *et al*., 2007), China (Qin *et al*., 2013); Alaska (Payne *et al*., 2006), America (Booth, 2008) and eastern North America (Charman *et al*., 1999; Booth, 2008; Amesbury *et al*., 2013; Lamarre *et al*., 2003). Confidence in the application of these transfer functions has been demonstrated through the detection of coherent regional patterns of water table reconstructions (Hendon *et al*., 2001; Lamarre *et al*., 2013), correlations with recent instrumental climatic records (Schoning *et al*., 2005; Charman *et al*., 2006; Charman, 2007; Booth, 2010), multiproxy studies from the same peat cores (e.g. Nichols *et al*., 2006; Lamentowicz *et al*., 2010) and long term observed water table measurements (Lamentowicz *et al*., 2008). A detailed discussion of transfer functions is provided in Section 3.5.4.

2.5.2.2 Testate amoebae limitations and considerations

Quantitative testate amoebae reconstructions may be limited by the preferential decay of tests. Tests can be proteinaceous, siliceous or calcareous with mixtures of mineral grains, fungal hyphae and diatoms (Charman *et al*., 2004). Comparisons of modern and fossil communities have demonstrated preservation differences (Wilmshurst *et al*., 2003). Those with siliceous plates ('idiosomes') are susceptible to degradation (Tolonen, 1986; Mitchell *et al*., 2008) although resistance within genera varies (e.g. *Assulina* and *Nebela*: Wilmshurst *et al*., 2003). Some transfer functions respond to this by excluding the idiosomes e.g. *Euglypha* species (Swindles and Roe, 2007); however, other studies have shown that the inclusion of poorly persevered

species does not affect water table reconstructions since the transfer functions are sufficiently robust (Mitchell *et al.*, 2008; Swindles *et al.*, 2009).

Testate amoebae are also associated with taxonomic limitations since intra-species variations may influence identification (Mitchell *et al.*, 2008). Morphospecies are determined by size, composition and morphology of the tests; however, such differences may be gradual and induce a degree of subjectivity in division and identifications between taxa (Charman, 2001). Species may adapt to their surroundings, generating morphological variation both within and between populations depending on biotic and abiotic factors (Schönborn, 1992; Wanner, 1999). Whilst further taxonomic assessments are required to ensure that species definitions are sufficient and robust (Charman, 2001), consistent identification within individual studies and between regionally comparable studies facilitates the extraction of palaeoenvironmental information from testate amoebae assemblage data (Mitchell *et al.*, 2008).

The main consideration when applying testate amoebae transfer functions is that, whilst the community compositions may primarily respond to moisture conditions, other abiotic factors, such as pH (e.g. Booth and Jackson, 2003; Booth *et al.*, 2004), may influence the assemblage. Transfer functions rely on changes in species composition being attributed to one environmental variable. If this is not the case then the transfer function will not be coherent (Juggins, 2013). Many studies have shown that the testate amoebae compositions are primarily controlled by moisture, with a secondary influence of pH (Charman and Warner, 1992; Tolonen *et al.*, 1994; Charman and Warner, 1997; Bobrov *et al.*, 1999; Booth, 2002; Mitchell *et al.*, 2000; Booth, 2008; Markel and Booth, 2010). Whilst the influence of pH may be associated with increased sampling of minerotrophic conditions (Payne *et al.*, 2006), the appropriateness of the transfer functions applied for the specific study sites must be assessed. Other concerns surrounding transfer functions include their spatial autocorrelation (Telford and Birks, 2005, 2009), clustered training set design (Juggins, 2013) and uneven sampling of environmental gradients (Telford and Birks, 2011), which can lead to over-optimistic performance statistics. These issues are statistically addressed in newly developed transfer functions (e.g. Amesbury *et al.*, 2013; Lamarre *et al.*, 2013). Whilst this provides increased confidence in the validity of this

technique, modern surface sample training sets must be further improved by focusing on species that have poor modern analogues (e.g. *Difflugia pulex*; Lamarre *et al.*, 2013) and by achieving a better understanding of the vertical distributions of testate habitats (e.g. Mieczan, 2009; Mitchell and Gilbert, 2004).

2.5.3 Peat humification

Peat humification analysis is commonly applied alongside plant macrofossil and testate amoebae as a proxy for WTD reconstructions. However, its appropriateness as a climate indicator has been queried. The height of the water table dictates the length of time that the organic matter spends in the acrotelm being subjected to faster aerobic decomposition. Lower water tables result in a longer residence time of the organic matter in the acrotelm thus increasing the degree of decomposition (Charman *et al.*, 2007). Humification describes decompositional changes in the chemical state of the peat (Aaby, 1976; Clymo, 1984) commonly determined in peatland palaeo-studies through an alkali extraction and colorimetric measurement of dark humic acids (Aaby, 1976; Clymo, 1984).

Changes in humification can indicate wet and dry shifts but it is a qualitative technique that cannot reconstruct absolute WTD (reviewed by Yeloff & Mauquoy, 2006). Humification records often deviate from the plant macrofossil and testate amoebae reconstructions. Four main factors may contribute to this (Figure 2.5):

1. The hydrological signal can be dominated by plant species-specific susceptibility to decay (*sensu* Overbeck, 1947; Aaby, and Tauber, 1975; Chambers *et al.*, 1997; Caseldine *et al.*, 2000; Yeloff and Mauquoy, 2006; Hughes *et al.*, 2012);
2. The degree of humification relates to the amount of oxygen (as well as availability of nitrogen and phosphorus; (Clymo, 1991) which is controlled by WTD (Yeloff and Mauquoy, 2006) making it a secondary response to climate;
3. Secondary decay may occur during a fluctuating water table (Tipping, 1995), overprinting the original signal;

4. Humification is not uniform with time limiting its utility downcore and in surface samples (Yeloff and Mauquoy, 2006).

The diagenetic signal of increased humification with time can be removed by using linear regression (Yeloff and Mauquoy, 2006; Blundell *et al.*, 2008) and species specific k-values, based on their absorption qualities (Blundell and Barber, 2005; Hughes *et al.*, 2013) can partially account for the species signal. However, it has been suggested that the degree of peat humification is a function of local characteristics influenced by external forcings (Blackford and Chambers, 1993; Chambers and Blackford, 2001; Chambers *et al.*, 1997; Payne and Blackford, 2008; Hughes *et al.*, 2012).

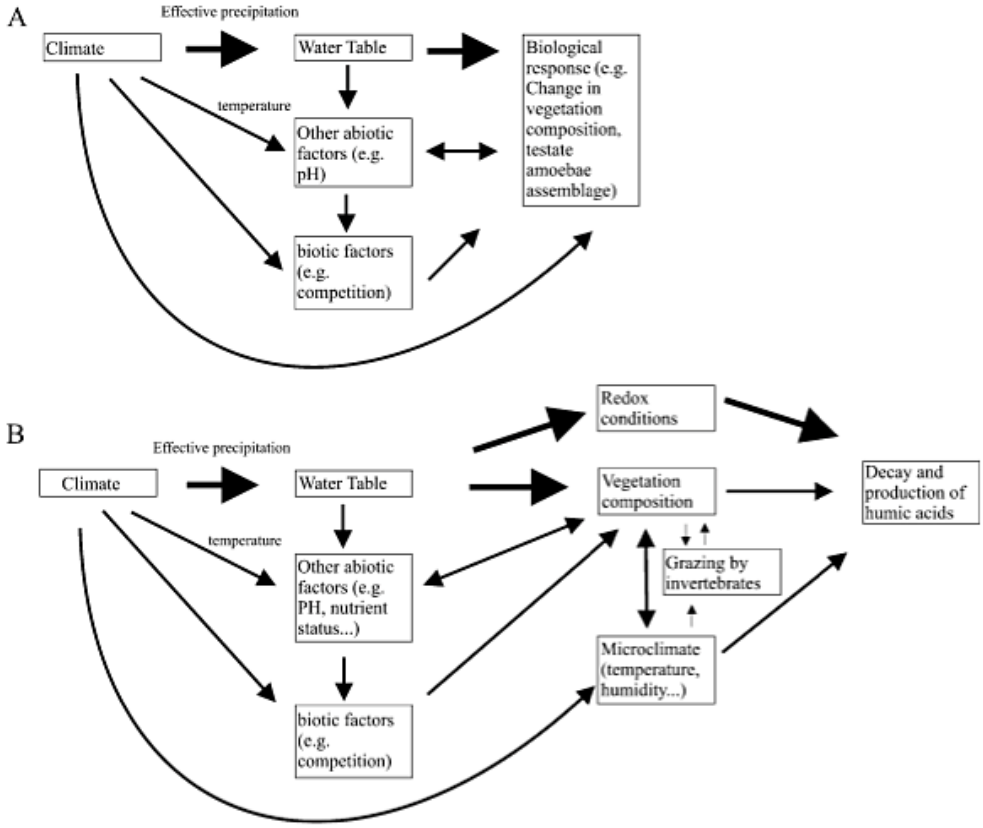

Figure 2.5 Comparison of biological proxies (A, top) and humification (B, bottom) relationships with climate (Yeloff and Mauquoy, 2006)

Interestingly, the standard humification method in peat-based palaeoecological studies is a poor measure of decomposition when compared with other available techniques (Biester *et al.*, 2013). It is unclear what compounds are measured in the alkali extraction method (Caseldine *et al.*,

2000; Morgan *et al*., 2005) and the impact of decomposition on the formation of these compounds is poorly constrained. Humification results are therefore suggested to be a chemically poor definition of mass loss during mineralisation (Biester *et al*., 2013). Improved measures of decomposition can be achieved by using a combination of C/N; pyrolysis and Fourier Transform infrared spectroscopy (Biester *et al*., 2013). However these approaches do not eliminate the complicating species effect since they are also influenced by both hydrological conditions and vegetation type.

Despite reservations surrounding the use of humification, reconstructions have correlated with other terrestrial proxies and external forces on centennial timescales (Blackford and Chambers, 1995), proving their utility in certain circumstances. It is especially appropriate when the vegetation composition is stable (Biester *et al*., 2013) or dominated by *Sphagnum* (Yeloff and Mauquoy, 2006), thereby minimising the species signal. Humification reconstructions appear to be particularly sensitive in very wet conditions (Hughes *et al*., 2012) and can be more sensitive than testate amoebae in some circumstances (Charman *et al*., 1999; Booth and Jackson, 2003). Whilst the underlying mechanisms are unclear, humification analysis can yield useful information when used in combination with plant macrofossils and testate amoebae (Baker *et al*., 1999; Gunnarson *et al*., 2003; Hughes *et al*., 2006). However, owing to the aforementioned uncertainties surrounding the origin of the peat humification signal, this approach will not be used to reconstruct the peatland moisture balance within this thesis. Rather, efforts will focus on increasing plant macrofossil and testate amoebae sampling resolution across all study sites.

2.6 Peat chronology

2.6.1 Radiocarbon dating

The most widely used dating method for environmental and archaeological samples on Holocene timescales is radiocarbon (^{14}C) dating. This technique utilises ^{14}C, the cosmogenic isotope, which forms during the reaction between secondary neutrons (produced by cosmic rays) and atoms of nitrogen (Libby *et al*., 1949). ^{14}C (t½: 5730 years) is dispersed throughout the atmosphere and $^{14}CO_2$ is transferred into soils and biota through photosynthesis, which stops

upon death (Figure 2.6). The time since deposition can therefore be calculated using the ^{14}C content in the biosphere at present (measured as 95% of ^{14}C activity of the standard Oxalic Acid 1 (with 'present' taken as the 1950s value; Stuiver and Polach, 1977) and the concentration of ^{14}C in the sample. 1950 represents year 0 BP by radiocarbon convention since the first radiocarbon dates were calculated and corrected for radioactive decay at the end of 1949 (Struiver and Polach, 1977).

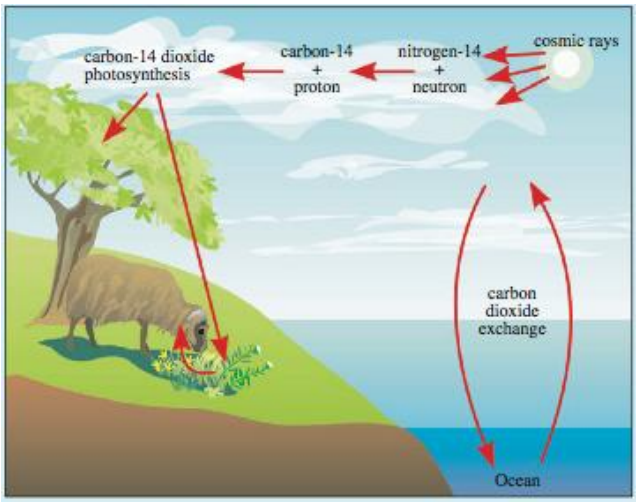

Figure 2.6 The process of ^{14}C incorporation into the environment. ^{14}C is formed in the upper atmosphere when the neutrons produced from cosmic rays collide with ^{14}N nuclei. ^{14}C enters sedimentary archives through photosynthesis (from Charman *et al.*, 1999)

The range of ^{14}C dating is limited by its half-life and atmospheric concentration: it can be theoretically extended to 40,000 years BP (although this range is limited by the calibration stage, Section 2.6.1.2) but is problematic in recent materials since fossil fuel consumption and nuclear weapons testing altered the atmospheric ^{14}C concentrations (e.g. Charman and Garnett, 2005). Originally, ages were obtained by bulk techniques using large sample sizes (5-10 g C); however, accelerator mass spectrometers (AMS) revolutionised ^{14}C dating by facilitating the analysis of sample sizes 1000 times smaller than bulk methods (Charman, 2002).

2.6.1.1 Peat sample requirements

The potential for obtaining robust peatland ^{14}C chronologies is facilitated by its high carbon content and *in situ* plant material, high in ^{14}C, that

corresponds to surface accumulation at the point of decomposition. Traditionally, bulk peat samples were used; however, the presence of rootlets may yield ages 100-200 years too old, possibly because of the reuse of 'old' carbon from fungi (Charman, 2002). Contrasting evidence has since suggested that bulk dates can yield ages contemporaneous with pure *Sphagnum* samples (Kilian *et al.*, 1995) and produce well constrained chronologies; however, aboveground leaves of species specific samples, e.g. *Sphagnum* stems, are preferred to avoid a 'mixed' ^{14}C source. The removal of any rootlets, fungi, and foreign material can be achieved by washing and macrofossil selection under a stereomicroscope.

2.6.1.2 Calibration and age modelling

Cosmic ray production varies by geomagnetic and solar modulation, changes in the carbon cycle and human influences; therefore, ^{14}C years are not the same as calendar years (De Vries, 1958; Reimer *et al.*, 2009). ^{14}C measurements must be calibrated against the known atmospheric variations in ^{14}C to obtain meaningful age-depth models. Known variations are obtained by dating material of absolute dates and known ^{14}C values such as tree rings, corals and annually laminated sediments. The most widely used series of calibration curves have been developed by the IntCal group and were recently extended to 13900 cal yr BP (Blaauw *et al.*, 2004).

^{14}C years are converted to calendar ages by calibrating individual dates or by wiggle matching a series of uncalibrated dates. This creates uncertainties that are often asymmetrical and multi-peaked. Therefore, age ranges generated by calibration indicate the best possible approximation of the samples calendar age (Reimer *et al.*, 2013). Time periods contain variable degrees of calibrated uncertainty owing to fluctuations in the calibration curve. Multiple possible calendar ages are provided during periods of nearly constant ^{14}C production (creating plateaus) or when concentrations rapidly fluctuate (creating wiggles). Treating the years individually may result in inaccurate and imprecise age estimates since it cannot account for contamination or characterise a multimodal probability distribution (Blaauw, 2010). The wiggle-match approach uses the non-linear relationship between ^{14}C dates and calendar ages to fit a sequence of closely spaced, uncalibrated measurements to the calibration curve (van Geel and Mook, 1989; Kilian *et al.*, 1995; Blaauw

et al., 2003). This approach may be appropriate in places where the calibration curve contains pronounced wiggles such as during the Little Ice Age (Mauquoy *et al.*, 2002) and provides age estimates for the sediment sections between dated levels.

A limitation to the wiggle-match approach is that different models can be produced depending on accumulation rate assumptions which influence assigned ages. Linear interpolations can be applied (Bennett, 1994), however, they lack sufficient complexity. Improved approaches can apply linear accumulation over distinct time periods (Mauquoy *et al.*, 2002, Blaauw and Christen, 2005), concave curves to account for the continuing decomposition of organic matter in peat (Yu *et al.*, 2001), or convex curves based on the slowing of accumulation rates when peatlands near their height limit (Yu *et al.*, 2001). It may be difficult to confidently apply these accumulation rate assumptions to specific settings, hence, wiggle-matching is now less commonly used.

The use of Bayesian statistics is an alternative approach to age-depth modelling, which combines ^{14}C ages with prior information on stratigraphy, accumulation rates and other variables (Blaauw and Christen, 2005; Ramsey, 2008). It assumes that the true calendar age will never be known but that an age-depth curve can be applied thousands to millions of times through the unknown points to obtain a reliable approximation of the true accumulation history with known uncertainty. This can be achieved using the OxCal ^{14}C calibration programme and its Poisson Sequence, which simulates the accumulation of depositions through random small increments. Alternatively, Bacon (Blaauw and Christen, 2011) a dating calibration package of R (R Development Team, 2014) performs comparable procedures to OxCal but can account for limitations on accumulation rates and its variability.

Ages applied to sample depths are uncertain owing to the calibration process, the selected age-depth model and its accumulation rate assumptions. An advantage of using Bacon rather than OxCal is its function to plot proxy data on a grey-scale age-depth model (Blaauw *et al.*, 2007) to acknowledge the chronological uncertainty. If specific point dates (displayed without visible age ranges) are required for plotting data then the weighted mean or mode of the age distribution may be most appropriate (Blaauw, 2010).

2.6.1 Tephra

Tephrochronology, the attribution of dates to volcanic ash layers upon the identification of their parent eruption, provides a robust way to determine the age of sedimentary archives. Each horizon has a unique chemical signal, which matches the parent eruption. If the date of the parent eruption is well constrained then tephrochronology can yield high precision ages (Hunt and Hill, 1993). Eruption durations are often shorter than the temporal resolution achievable from sedimentary archives (commonly hours to days but rarely long than 2 years) and shards are transported and deposited rapidly. Ash layers also act as time-parallel markers (isochrons) when present in more than one sedimentary sequence. This application, known as tephrostratigraphy, creates 'pinning-points' in time to further facilitate palaeoenvironmental comparisons across sites and regions (e.g. van den Bogaard *et al*., 2002; Langdon and Barber, 2004). Isochrons also present the rare opportunity of temporally linking archives to a common fix-point even if the actual eruption age is unknown.

2.6.1.1 Cryptotephra

Advances in the field of tephrochronology have led to the investigation of non-visible cryptotephras (*sensu* Lowe & Hunt, 2001) horizons of shards (<125 μm) present in sediment more distal to the volcanic origins. This revolutionary advance allows for the detection of previously unidentified eruptions and provides the opportunity to obtain precise chronologies in areas previously considered to be outside the scope of this technique (reviewed by Lowe, 2011).

The wealth of cryptotephras in eastern North American is emerging: Pyne-O'Donnell *et al*. (2012) published the region's first Holocene record from Nordan's Pond Bog, Newfoundland, which contained seven distinct correlated isochrons from up to *ca*. 7000 km away in Alaska and the Cascades. One of the largest eruptions detected at Nordan's Pond Bog was the White River Ash (WRA eastern lobe; Pyne-O'Donnell *et al*., 2012). The WRAe originated from Mount Bona-Churchill, Alaska, and was recently correlated to the European cryptotephra "AD860B" (Jensen *et al*., 2014a), which has been dated by the Greenland Ice Core Chronology to AD 847 ± 1 (Coulter *et al*., 2012). The Mount Bona-Churchill region was also active *ca*. 1890 cal yr BP (north lobe;

Lerbekmo *et al.*, 1975) and possibly *ca.* 300 cal yr BP (Lena tephra; Payne and Blackford, 2008). Other correlated eruptions reaching Newfoundland include Mount St Helens, Newberry Pumice, Mount Augustine, Aniakchak, East Lake and Mazama.

The possibility of tephras arriving in eastern North America from other source regions cannot be precluded. Satellite imagery from the 2010 Icelandic Eyjafjallajökull eruption showed that ash reached the eastern seaboard of Canada and Kamchatkan tephra has been found in Greenland ice cores (Davies *et al.*, 2010) suggesting the presence of such far-travelled ash in the terrestrial records of eastern North America. Mexican source regions are also a possibility owing to the frequency of eruptions and their relative proximity. This thesis investigates the presence of tephra from these additional source regions as well as other North American eruptions to provide the temporal accuracy to address the overall aim of the thesis (Section 1.2). The presence of tephra pinning-points will enhance the degree of confidence with which climatic changes and alterations in the carbon balance can be compared across the transect of sites.

2.6.1.2 Methods of detection and extraction

Tephrochronology relies on shards being identified, quantified, extracted, geochemically characterised and correlated with a constrained parent eruption. Different approaches to these methods have been adopted depending on tephra characteristics and sediment types; therefore, this section focuses on such issues relating to peat.

To quantify the amount of tephra present in sedimentary archives, shards are generally extracted from the cores in a known volume or weight and counted under polarized microscopic conditions to facilitate within and between core comparisons. The most efficient method follows Pilcher and Hall (1992), which ashes the peat at 5 cm intervals before refining to 1cm at periods of interest. Samples are commonly mounted in Canada Balsam, however, distinguishing between shards and phytoliths can be difficult in this medium, thus glycerol can also be used. This method is efficient in highly organic ombrotrophic peat.

Tephras are most commonly identified using the measured ratios of major and minor elements (Dugmore *et al*., 1992). Identification, therefore, relies on the stability of shard chemistry, which must not be altered in the preparation stages (Dugmore *et al*., 1992; Pollard *et al*., 2003). Samples cannot be ashed (Pilcher and Hall, 1992; Dugmore and Newton, 1995; Hall and Pilcher, 2002). Two main low-temperature methods are currently used to concentrate shards: acid digestion and floatation. The chosen extraction method will be determined by the location, sediment type and shard characteristics.

The extraction of tephra was traditionally completed through acid digestion (Persson, 1971; Dugmore, 1989; Hall and Pilcher, 2002; Swindles *et al*., 2010); however, the vulnerability of shards to chemical alteration during this technique was suggested by Dugmore *et al*. (1992) and Blockley *et al*. (2005), depending on the severity of the acid used, length of digestion and the type of tephra shards. Harsh acidic or basic digestion stages required for lake sediments are of particular concern. These stages are not required when working with peats. Despite the demonstration of rhyolitic shard chemical stability in the peatland context (Dugmore *et al*., 1992; Roland *et al*., 2015), some peatland studies, particularly those concerned with very small shards in new areas, still avoid this method to eliminate any possibility of deterioration (e.g. Pyne-O'Donnell *et al*., 2012).

The alternative method, density separation, was developed in response to the chemical stability concerns (Turney *et al*., 1998; Blockley *et al*., 2005) and uses heavy liquid to extract the shards. Its effectiveness in identifying previously unknown horizons of low shard concentrations has been demonstrated (Blockley *et al*., 2005). This method was, however, designed for tephra extraction from minerogenic lake sediments (Blockley *et al*., 2005; Turney *et al*., 1997) and is less effective in peat since shards are trapped within the organic rich matrix. A modified method involving stirring and additional cleaning floats is therefore required to extract sufficient shard numbers for chemical analyses (Pyne-O'Donnell, pers comm). The density separation technique will be used in this thesis to echo the one existing record from the region (Pyne-O'Donnell *et al*., 2012), which will be used for comparisons.

2.6.1.3 Geochemical analyses and eruption correlations

Tephras are chemically typed using an electron probe micro-analyser (EPMA) which requires the shards to mounted in epoxy resin, which is ground and polished so that they are exposed on the surface, and carbon coated (Froggatt, 1992; Hall and Hayward, 2014). The EPMA focuses a beam of electrons into the sample generating X-rays of particular energies and wavelengths. These relate directly to individual elements, and recorded intensities are an accurate and precise measure of specific element abundance (Shane, 2000; Coulter *et al*., 2010). The beam size is integral to the success of the analysis owing to the small available surface area of the cryptotephras. Previously, defocused beams were used to prevent the loss of the mobile oxides NaO and K_2O and the associated exaggeration of SiO_2 and Al_2O_3 (Froggatt, 1983; Suzuki, 1996; Hunt and Hill, 1996; Hunt and Hill, 2001; Davies *et al*., 2008; Coulter *et al*., 2010). The pivotal development of reliable 5 µm and 3 µm beam sizes (Hayward, 2011) has increased the number of small shards that can be analysed. Tephras in this study are likely to have small available surface areas so the recent advances that have led to reduction in beam size now facilitate the analysis of the very small far-travelled shards.

2.6.1.4 Data treatment: normalisation and dataset compilation

The total oxide weight per cent of a sample should equate to 100 and any difference may be thought to represent magmatic water content (Froggatt, 1992). Normalisation is often applied to remove this dilution effect (Shane, 2000) and facilitate more direct comparisons of oxides. Normalisation is contested in some circumstances since the difference can also be attributed to elements that are not measured, those that have become mobile during the analysis or effects of spectrometer drift (Hunt and Hill, 1993; Pollard *et al*., 2006). Rigorous experimental conditions have been tested to ensure no such drift or loss of volatile oxides occurs during analysis (Hayward, 2012).

Water can account for 7-8% of rhyolitic glass; however, often any totals less than 95% are often discounted on the assumption that additional factors contribute to the deficit (Froggatt, 1992; Hunt and Hill, 1993). A 95% cut off point is arbitrary with no geological basis (Pollard *et al*., 2006). Rhyolitic shards will only no longer be vitric when water exceeds 9-10%; therefore

totals above 90% must be not be rejected based on their totals alone (WoldeGabriel *et al*., 2005) but rather in combination with standard deviations. At least fifteen shard analyses are required to establish whether the tephra population is likely homogeneous and can thus represent the average composition of the melt phase (Shane, 2000).

The geochemistry of tephras originating within the same volcanic source region is similar and hinders correlations between shards and parent eruptions. Furthermore, the chemistry of cryptotephra shards may only represent a segment of the full eruption trend, which can complicate correlations depending on the scope of available reference databases. Many statistical approaches have been applied to assist with eruption correlations; however, a firm match will require a combination of these alongside stratigraphical information. The real utility of these statistical techniques lies in their ability to disprove rather than confirm matches since there is always the risk of false correlations (*sensu* Pollard *et al*., 2006, 2008). They cannot be used as a substitution for graphical inspections, since correlations are limited by the available data (Hayward, 2011). The statistical tests should be viewed as valuable screening methods on which to base further investigations (Newton *et al*., 2007).

Similarity coefficients of variation provide a simple, efficient statistical test of tephra correlation by comparing the averages of each of the major oxides between two ash populations and indicating an overall measurement of similarity. This approach is limited by the subjective nature of what values constitute a correlation: generally, 0.95 is assumed to represent close correlation, 0.90-0.94 represent a different tephra from the same source region and less that 0.90 indicates no correlation (Borchardt *et al*., 1972; Riehle, 1985; Beget *et al*., 1992). This technique is further limited by the use of averages that ignores the data structure, the equal weighting of all oxides despite the range of accepted variation differing and the omission of potentially minor oxides (those with a maximum value of less than 0.4% are excluded; Riehle, 1985). Despite these issues, similarity coefficients are a powerful screening tool when used alongside bi-plots, due to the speed with which they can be used to characterise large datasets.

Other statistical approaches include Students t-test (Keenan, 2003); cluster analysis; Discriminant Function Analysis (DFA - Borchardt *et al*., 1972) and Principal Component Analysis (PCA - e.g. Pollard *et al*., 2006). The latter two approaches consider all data points individually, which has an advantage over the methods that simply consider the mean. They are, however, more time intensive and may still produce spurious results owing to the complex nature of cryptotephra data.

2.6.1.5 Complications

2.6.1.5.1 Shard distributions

Tephra has the potential to provide unparalleled temporal precision but inconsistent shard distributions, post-depositional movement and non-discrete horizons can act as limiting factors. Under such conditions, tephra may represent a 'passage of time' rather than a 'confirmed moment in time' (*sensu* Dugmore *et al*., 2004).

The presence of cryptotephra shards is often spatially variable, with unpredictable shard concentrations even at local scales (Davies *et al*., 2010b). This arises from a combination of initial ash plume behaviour and atmospheric features influencing the distal plume distribution, such as atmospheric wind strength and direction. The prevailing weather conditions at the point of depositions are an important tephra distribution control: for example, increased wind strength encourages discontinuous deposition, and rainfall through the ash cloud encourages the deposition of shards and locally thickened tephra deposits (Kobayashi *et al*., 2005).

Tephra distributions within sites vary, as confirmed by the fine-scale horizontal variability evident in imaging studies (Caseldine *et al*., 1999; Dugmore and Newton, 1992). The movement of shards may be controlled by internal factors such as water table fluctuations, peat density, plant growth and root channels and influenced by shard characteristics such as size and volume. Experiments to characterise the vertical distributions of shards found movement ranging from 6 cm in 2 years using experimental plots (Payne *et al*., 2005); to 15cm over 6 years (Payne *et al*., 2005); to 30 cm (Payne and Gehrels, 2010). Shard movement is related to density and position of the peat surface rather than a simple relationship with wetness (Payne and Gehrels,

2010). The downward spread of tephra is attributed to shards sinking, whereas upward movement is associated with plant growth and water table variability. Despite movement in shards, the majority remain at the surface and it is unlikely that a whole peak would move (Payne and Gehrels, 2010). Additionally, peat compaction over time limits broad distributions in Holocene records.

2.6.1.5.2 Correlations

Matching the chemical signature of a tephra with that from another eruption, within an appropriate stratigraphic context, underpins the use of tephra for correlative purposes and age transfers. Tephra matches are limited by the available information and comprehensiveness of databases used. Therefore, the role of updating and contributing to such data databases (e.g. Tephrabase; Newton *et al.*, 2007) is vital. Miscorrelations arise if there are indistinguishable chemical signatures, ambiguous reworking of tephra or multiple chemical fingerprints arising from magmatic changes (Payne *et al.*, 2005).

2.7 Climate variability

Full reviews of late Holocene climate change can be found in Mayewski *et al.* (2004), Wanner *et al.* (2008), Mann *et al.* (2008) and PAGES 2k Consortium, (2013). These sources indicate that the last 2000 years was characterised by a cooling trend until the 20th century anthropogenic warming (Figure 2.7). Within this cooling trend, the highest global temperatures before anthropogenic warming occurred between AD 830-1100 (PAGES 2k Consortium, 2013) and this period is termed the Medieval Climate Anomaly (MCA: Section 2.8.1). During the MCA there was a period of regionally cooler, fluctuating conditions between AD 1050-1150 which coincides with the Oort minimum of solar activity (Wanner *et al.*, 2008). The coldest period of the last 2000 years occurred between AD 1300-1850 (Wanner *et al.*, 2008) during the Little Ice Age (LIA: Section 2.8.2) with cooling culminating around AD 1600 and 1800 (Wanner *et al.*, 2008). The MCA and LIA were the most prominent episodes of change during the last 2000 years, however, they were not globally synchronous and their spatial extent remains unclear.

This thesis investigates changes associated with the MCA and LIA (Sections 2.8.1 - 2.8.3), therefore the aim of this section is to provide context for the origin and manifestation of these climatic change. The subsequent Sections (2.7.1 - 2.7.2) explore possible drivers of climatic change and other contributing influences before specifically discussing their roles on the MCA and LIA associated climatic changes. The final section (2.9) reviews the available literature that identifies climatic change from the eastern North American study region over the last 2000 years to provide sufficient background climatic context for the MCA and LIA, whilst also identifying any other consistent environmental fluctuations.

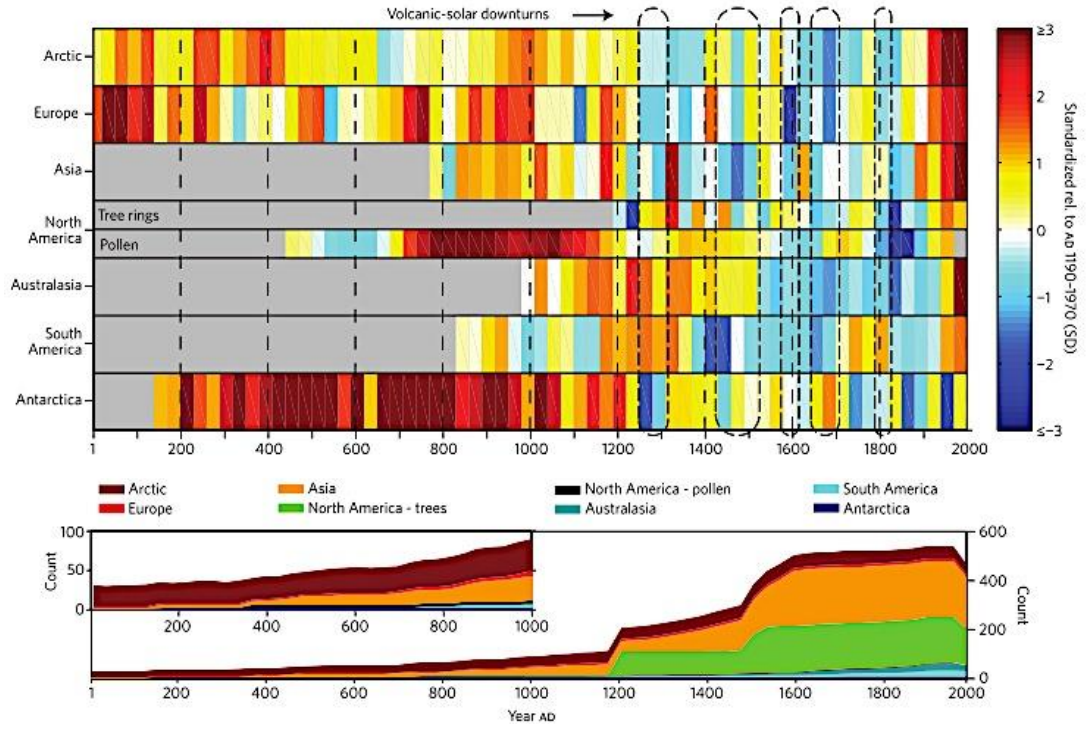

Figure 2.7 Continental-scale climatic change over the last 2000 years 30-year-mean temperatures by region standardised to have the same mean (0) and standard deviation (1) over the period of (AD 1190-1970). The North American record includes tree-ring-based and pollen-based reconstructions that indicate warmer conditions around AD 800-1100 and cooler episodes around AD 1600-1700 and AD 1800. Dashed outlines represent times of pronounced volcanic and solar negative forcing since AD 850. The lower panel shows the number of individual proxies by region and highlights the lack of records before *ca*. 1200 AD compared with more recent times (PAGES 2K Consortium, 2013).

2.7.1 External climate forcing mechanisms

2.7.1.1 Orbital variations

There are three main celestial controlled variations in the earth's orbit with associated solar insolation changes: eccentricity, obliquity and precession of the equinoxes. The periodicities and timings of these influences can be calculated using Milankovitch's theory (1941) making them unique in the sense that they are the only climate forcing mechanisms that can be accurately predicted. The eccentricity is a measure of the departure of the elliptical orbit from circularity, which varies with the dominant periodicities of 100 ka and 400 ka, based mainly on interactions with the gravitational field of Jupiter and Saturn. Mean annual temperature is altered since insolation marginally decreases with increased eccentricity (Roedel, 1994) and differences between seasonal temperatures are more pronounced. These changes have been expressed as a steady marginal decrease on insolation throughout the Holocene.

The two shorter cycles of 23 ka and 40 ka are respectively attributed to the periodicity of the precession of the equinoxes (describing the time of year that the earth is furthest from the sun) and the obliquity cycle, referring to changes in tilt of the angle of the earth's axis between 21.5˚ and 24.5 ° (the larger the tilt, the stronger the contrast between summer and winter insolation). Precessional forcing shifted the perihelion (the closest approach of the earth to the sun) from summer towards winter. It now occurs in January making the northern hemisphere winters slightly milder than 11 ka BP when it existed in July, reducing seasonality. The axial tilt was slightly increased at the beginning of the Holocene and decreased towards the present creating more similarities between summer and winter insolation.

The combined effect of the precession cycle and change of tilt, with a smaller influence from changes in eccentricity, forced high Northern Hemisphere summer insolation to increase into the beginning of the Holocene (Davis and Brewer, 2011). This peaked around 10 ka BP and decreased towards the present, especially over the last 2 ka when summer insolation reduced by *ca*. 6 Wm^{-2} (Berger *et al*., 1991).

2.7.1.2 Solar variations

Sunspots are dark hot areas on the surface of the sun, which originate from changes in magnetic activity. These vary in quasi-periodic cycles, of 11 years (known as the Schwabe cycle) and the associated 22 years (Hale cycle; Lean and Rind, 1998). The Schwabe cycle is a response to increased magnetic field strength generated by the differential rotation of the sun's convection zone that partially blocks energy flow and creates sunspots. When the magnetic field of the sun reverses, Hale cycles are generated. Whilst sunspot generation is understood, the mechanisms behind solar driven climate change are debated. It is suggested that atmospheric circulation is influenced by changes in ozone production caused by solar forced alterations in ultra violet (UV) radiation and amplified solar radiation due to increased solar winds (Shindell *et al.*, 2001; Haigh *et al.*, 2010).

Observational records have characterised our understanding of solar variations (e.g. Struiver, 1961; Suess, 1965; Bray, 1971), however reconstructing changes in solar radiation beyond instrumental times presents a challenge. Since periods of high solar irradiance are accompanied by stronger solar winds (resulting in a reduction of cosmogenic rays and cosmogenic nuclide production (Masarik *et al.*, 1999; Bradley, 2003), cosmogenic isotopes, namely ^{14}C from tree rings (Struiver *et al.*, 1998) and ^{10}Be (Finkel, 1997) and ^{36}Cl (Baumgartner, 1998) from ice cores, can be used to reconstruct long-term changes in solar activity. Comparisons of cosmogenic isotope data and records of environmental change demonstrate a correlation between climate change and solar variations: e.g. from lake-level rises and glacier dynamics in the Alps (Magny, 1993); ^{18}O changes in GISP2 record over the last millennium (Stuiver *et al.*, 1995); temperature and moisture changes of an Alaskan lakes (Hu *et al.*, 2003) and 9 of 11 wet-shifts recorded in a Dutch bog (Berger *et al.*, 1991). However, the confidence with which solar forcing can be attributed as a climatic driver is limited by the chronological precision and the variation in cosmogenic isotopes (Chambers and Blackford, 2001) since ^{14}C can be affected by deep-ocean circulation and the amount of precipitation determines values of ^{10}Be (Maslin and Thomas, 2003).

Since solar forcing provides the Earth System with energy, radiation changes must influence climate; therefore, the main debate surrounding solar variation may be less focused on 'if' it affects climate but rather on 'to what extent' and 'what other feedback mechanisms are involved'. Solar variability influences climate on multi-decadal to centennial timescales by triggering the onset of change which is sustained and globally amplified through positive feedback mechanisms within internal climate system drivers (Section 2.7.2; Ammann *et al.*, 2007). Due to the regional characteristics of internal climatic drivers (Section 2.7.2), periods of climatic change that appear hemispherically or globally synchronous are often attributed to solar change (e.g. Hu *et al.*, 2003). It is, however, unlikely that solar variability alone could force the magnitude and duration of late Holocene change (Schurer *et al.*, 2014) since the magnitude of solar fluctuations was small (Kelly and Wigley, 1990, 1992).

2.7.1.3 Volcanic forcing

The ejected material from large explosive volcanic eruptions scatters solar radiation, reducing the overall amount that reaches the Earth's surface (Lockwood, 2001). The forcing potential of an eruption depends on the volume of material ejected, height of ejection, latitude of volcano, prevailing stratospheric circulation and amount of sulphur dioxide emitted (Lockwood, 2001). Volcanically driven climate change may persist for 1 to 4 years after eruption (Baillie, 1995; Stuiver *et al.*, 1995; Lockwood, 2001), owing to the short atmospheric retention time of volcanic particles. Change can be sustained on decadal to centennial timescales by a more frequent cluster of eruptions (Bradley, 2003) or by involving internal ocean-atmosphere feedbacks (Miller, 2012). Over the last 2000 years, volcanic eruptions have been too small or free of long-term trends to force climate alterations (IPCC, 2013); however, they do have the potential to exacerbate the late-Holocene climatic cooling trend.

2.7.2 Internal climate forcing mechanisms

Changes within the ocean and atmosphere may be triggered by external forcing (Heiri *et al.*, 2004) or simply be a product of their own 'random' variability (Rind and Overpeck, 1993). This stochastic influence hinders the identification of their driving mechanisms and limits predictions of their

future behaviour and interactions. Atmospheric and surface ocean responses to change occur within days to years, whereas it takes decades to centuries for the deep ocean to respond (Maslin and Thomas, 2003). Therefore, the ocean is considered the 'memory' of the climatic system and is the likely driver of long-term climatic change.

2.7.2.1 The North Atlantic Oscillation

The North Atlantic Oscillation (NAO; Walker, 1924) is a dominant mode of climate variability that, in its positive state, expresses the tendency for winter atmospheric pressures to be low near Iceland when they are high in the subtropics near the Azores (Walker and Bliss, 1932). Pressure differences between these two areas influence the intensity and location of the North Atlantic jet stream and storm tracks, altering the transport of atmospheric moisture and determining the relative strength of the westerly winds (Hurrell, 1995). The positive phase invokes a strong Atlantic Meridional Overturning Circulation (AMOC; Section 02.7.2.3), bringing mild, moist air across northern Europe and eastern North America whilst delivering cold, dry conditions to Greenland and southern Europe. Conversely, during the negative phase, high atmospheric pressures near Iceland and low pressures near the Azores weakens westerly winds, reducing heat loss over the Labrador Sea (Dickson *et al.*, 1996) thus weakening the AMOC, delivering cold dry conditions to eastern North America and northern Europe whilst mild, most air to Greenland. During strong prolonged phases, climatic variations can extend to central Russia, north-central Siberia and the equatorial regions (Hurrell, 1995).

From observational records, the NAO-associated climatic conditions of this study region are opposite to those of the British Isles and more southern regions of eastern North America: when western Europe experiences warmer wetter conditions in a positive NAO, Newfoundland, Nova Scotia and parts of Maine are cooler (Figure 2.8). Additionally, areas to the north of the transect experience a greater temperature decrease under positive NAO conditions that those to the south.

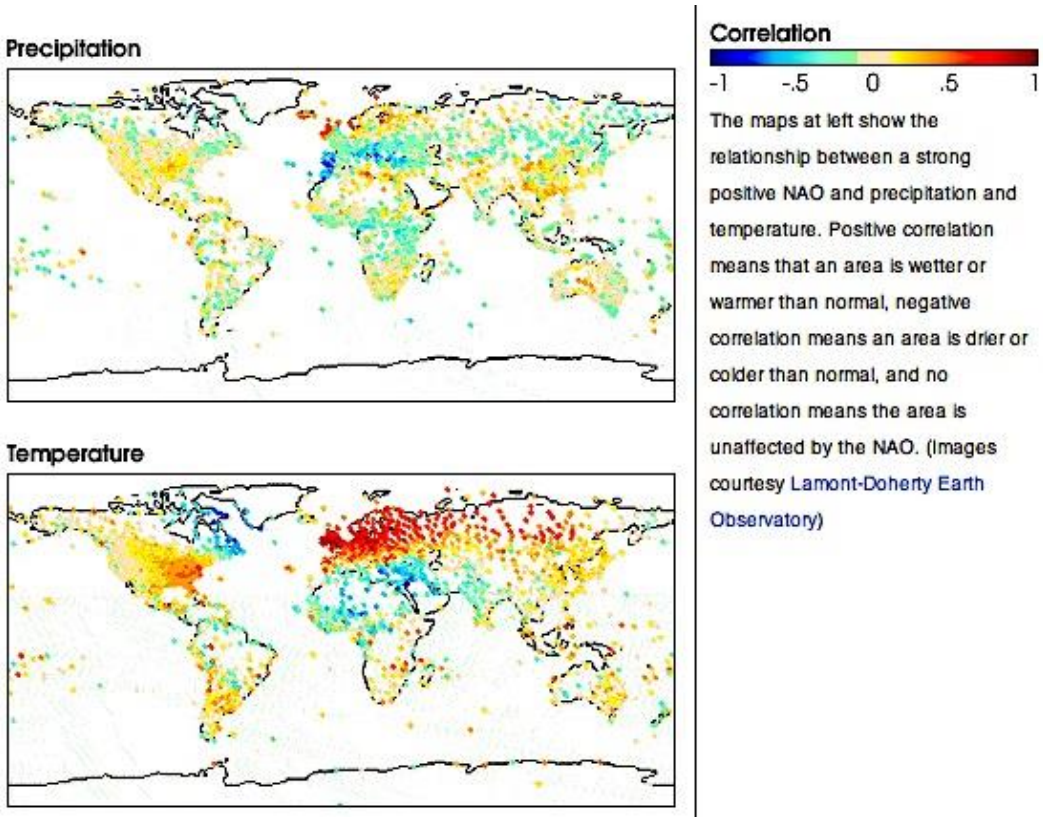

Figure 2.8 Global correlations between a positive NAO and precipitation and temperature. Conditions in north-eastern North America are opposite to those in the western Europe and south-eastern North America (NASA, 2011).

Phases in the NAO have been recorded since the 1870s using normalised, time-average pressure differences termed 'NAO index' (Rogers, 1984; Hurrell, 1995). Fluctuations occur on annual to decadal timescales with the greatest amplitude and spatial extent occurring in winter (e.g. Wallace, 1996). Summer manifestations of the NAO are smaller and more spatially confined than those of winter, and they have been identified as the major driver for precipitation in parts of Europe and eastern North America (Hurrell, 1995). During the winter of 2010-2011, the general pattern of observed temperature change could largely be attributed to expected NAO conditions (from instrumental records; Figure 2.9). The magnitude of expected temperature anomaly change was less than observed change, demonstrating the reliance of interactions with other climatic forces. The temperature anomalies over the study region of this thesis vary from *ca.* 2.5 °C in the north to *ca.* 0 °C in the south. This suggests that there will be a north-south divide in the environmental response

to NAO associated climate change across the study transect over the last 2000 years.

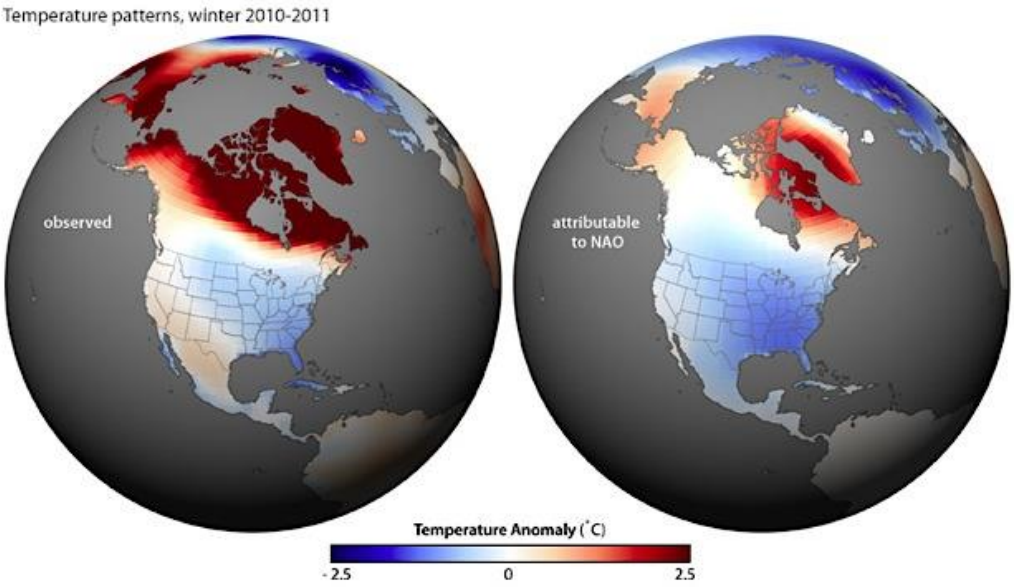

Figure 2.9 Observed temperature patterns for December 2010-February 2011 (left). Patterns that would be expected based only on the relative strength and frequency of the negative NAO phases that occurred (right).
Temperature anomalies are based on the 1961-1990 average and expected conditions are based on monthly summer temperature anomalies and NAO index from 1961; NOAA (CSI; 2011).

Multidecadal NAO reconstructions have been developed using tree-ring-based drought records from Morocco (southern node of NAO dipole) and speleothem-based precipitation proxy from Scotland (northern node of NAO dipole) for the last 947 years (Folland *et al.*, 2009). These reconstructions, combined with other records indicate a persistent positive NAO phase during the MCA and weaker NAO conditions during the LIA (Trouet *et al.*, 2009). Therefore, during the positive NAO conditions of the MCA, a north – south divide in the peatland response to climate change across the transect is likely (Hypothesis 1; Section 2.10).

The driving mechanisms of the NAO remain unclear although it is likely forced by a combination of oceanic and atmospheric influences with the primary forcing mechanism suggested to be internal to the atmosphere in the form of eddy-mean flow interactions of storm tracks (Trouet *et al.*, 2009). Secondary drivers of atmospheric origin are thought to include stratosphere-troposphere

interactions and forcings in the tropics. Oceanic mechanisms may involve the ocean's mixed layers since, on seasonal timescales, the ocean's mixed layer is in thermal equilibrium with atmospheric forcing and when the SST varies, heat exchange at the atmosphere-ocean interface is reduced (Barsugli and Battisti, 1998). Ocean gyres may also influence the NAO since they have internal oscillatory modes of variability affecting SST, compressing atmospheric heat transport (Bjerknes, 1964). The persistence of the NAO and its selective memory for winter conditions suggest that the ocean interior must contribute to the characteristics of the NAO. An investigation into the frequency of shifts in the NAO, using GCMs and ice core data, found that the dominant frequency varied over the last 350 years from *ca.* 15 years to *ca.* 90 years (Marshall *et al.*, 2001); therefore, the potentially stochastic element hinders the attribution of the exact combination atmospheric or oceanic influences (Timmerman *et al.*, 1998).

2.7.2.2 Atlantic Multidecadal Oscillation

Observations from the North Atlantic Ocean over the last 150 years have revealed alternating cold and warm phases with a quasi-periodic cycle of 65-80 years (Schlesinger and Ramankutty, 1994; Enfield *et al.*, 2001) termed the Atlantic Multidecadal Oscillation (AMO: Kerr, 2000). SST anomalies between these recurring periods are most pronounced east of Newfoundland and can persist for 20-40 years (Sutton and Hodson, 2005). Since the predominant signal of the AMO is expressed in the North Atlantic, the main driver is thought to be the Thermohaline Circulation (THC) (Delworth and Mann, 2000; Knight *et al.*, 2006) perhaps varying in a response to a stochastic surface flux force (Delworth and Greatbatch, 2000).

Climatic variations of the AMO are characterised by changes in summer rainfall (Delworth and Mann, 2000; Knight *et al.*, 2006) affecting certain areas of North America (Sutton and Hodson, 2005), western Europe, the Sahel, India and northeastern Brazil (Folland *et al.*, 2001; Sutton and Hodson, 2005). The AMO is correlated with the hurricane activity index and is attributed as the cause of the approximate doubling of hurricanes since 1995 (Goldenberg *et al.*, 2001). Whilst the modern physical expression of the AMO is reasonably well constrained, its long-term nature is unclear. Several studies have detected AMO imprints in proxy data (e.g. Gray, 2004; Mann *et al.*, 2009;

Seager *et al.*, 2009; Wang *et al.*, 2011; Chylek *et al.*, 2012) but different periodicities and durations have been identified e.g. 65-80 year quasi-cycles (Schlesinger and Ramankutty, 1994), 60-110 year periodicities (Delworth and Mann, 2000), or 70-120 years over the last 1400 years from modelled periodicities (Knight, 2005).

The AMO and the NAO have a non-stationary relationship (Section 02.7.2.1): SST positively correlate with the NAO index during negative AMO, but a weak correlation exists when the AMO is positive. Therefore, it is suggested that the AMO and NAO are manifestations of the same climate system phenomena expressed differently for the atmosphere and ocean (Enfield *et al.*, 2001). Alternatively, the AMO may be a response to the atmospheric changes in SST arising from the Thermohaline Circulation (THC) and NAO (Timmerman *et al.*, 1998) or it may be a dampened oscillatory ocean mode, which is excited by atmospheric anomalies (Frankcombe *et al.*, 2010).

2.7.2.3 Atlantic Meridional Overturning Circulation

The Atlantic Meridional Overturning Circulation (AMOC) is responsible for *ca.* 25% of the ocean-atmosphere poleward heat transport above 25°N (Bryden and Imawaki, 2001). Warm, saline surface waters move across the North Atlantic into the Nordic seas collecting water from proximal subpolar and subtropical gyres (Thornalley *et al.*, 2009). The waters cool in the north and sink, returning south as a major component of the North Atlantic Deep Water (NADW; Bryden and Imawaki, 2001). The AMOC is thought to have slowed by 30% between 1957-2005 (Thornalley *et al.*, 2009) and, whilst the probability of greenhouse gas emissions triggering complete future shutdown during the 21st century is less than 10%, it is very likely that the AMOC will weaken by 11% - 34% over the 21st century (IPCC, 2013).

Three features relating to the homogeneity of the ocean water control the stability of the AMOC: the density structure of the Atlantic Ocean, small-scale mixing and surface momentum and buoyancy flux (IPCC, 2013). These features are influenced by the THC and wind-driven overturning (Longworth *et al.*, 2005); however, the driving mechanisms behind these forces are uncertain. Some explanations look to the ocean itself, postulating that density anomalies in regions of deep-water formation are sufficient to act as the sole driver of the AMOC (e.g. Delworth *et al.*, 1993; Jungclaus *et al.*, 2005).

Others suggest that AMOC is an internal ocean mode stochastically excited by the atmosphere (e.g. Frankcombe *et al*., 2010), that it is stratospherically driven (Manzini *et al*., 2012; Reichler *et al*., 2012) or that it is a coupled ocean-atmosphere mode involving the NAO (e.g. Timmermann *et al*., 1998) or AMO (Hurrell *et al*., 2006).

2.7.2.4 El Niño Southern Oscillation (ENSO)

The Southern Oscillation is a seesaw trend in energy exchange between the eastern and western Pacific, most likely triggered by stochastic forcing and involving ocean-atmosphere feedbacks (Bjerknes, 1969; Kessler, 2002; Wang *et al*., 2012). ENSO controls warming on interannual timescales in the tropical Pacific Ocean. It disturbs the Walker circulation (Rasmusson and Carpenter, 1982) as well as the Hadley cell thus extending its influence across the Northern and Southern hemispheres. The opposite (or arguably neutral (Bryden *et al*., 2005)) phase of the Southern Oscillation is termed La Niña (Philander, 1990; Figure 2.10).

Detailed reviews by Wang *et al*. (2012) and Sheinbaum (2003) outline ENSO mechanisms and manifestations. El Niño periods are characterised by a positive SST anomaly in the equatorial eastern Pacific that weakens trade winds and thus oceanic circulation, reinforcing the SST anomalies. When El Niño periods peak, a negative feedback mechanism involving equatorial heat discharge and/or equatorial winds in the western Pacific is required to terminate continued growth. ENSO alters rainfall, westerly winds, ocean currents and sea surface temperatures. The main expression is observed through amplified variations in summer precipitation (e.g. Hu and Feng, 2001): for example, during strong La Niña years, eastern North America is drier than average conditions (Oglesby *et al*., 2012).

Instrumental records of ENSO extend back 150 years, which is too brief to confidently characterise the oscillation (Wittenberg, 2009); however, fluctuations on a timescale of 2-7 years have been detected (Wang *et al*., 2012) attributing ENSO as the largest source of inter-annual variability in the global climate system (McPhaden *et al*., 2006). Extending the records of ENSO behaviour beyond instrumental records is hindered by other embedded climate signals and the internal noise of the ENSO signal. Attempts to reconstruct an ENSO record from proxies have been hindered by a lack of

proxy agreement owing to dating difficulties on decadal time scales and varied spatial manifestations (Ashok *et al*., 2007). Despite this, modelled experiments have suggested that strong, persistent La Niña conditions occurred around 1000 years ago, contributing to the MCA expression (Mann *et al*., 2009: Section 2.8).

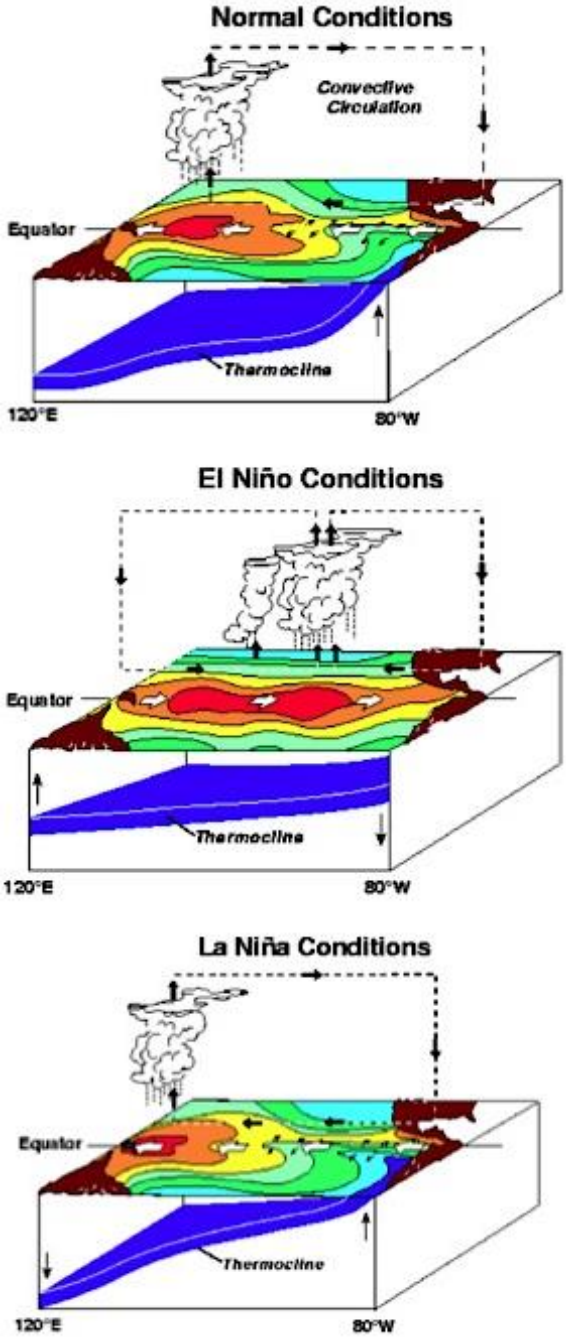

Figure 2.10 Ocean-atmosphere conditions in the tropical Pacific during normal conditions (top); El Niño conditions (middle) and La Niña conditions (bottom) (NOAA, last accessed 23/05/2014)

2.7.2.5 Pacific Decadal Oscillation

The Pacific Decadal Oscillation (PDO) is a mode of decadal climate variability manifesting in the North Pacific and extending into the Atlantic regions through ocean-atmosphere interactions (Newman *et al.*, 2003) and/or stochastic drivers (Pierce *et al.*, 2001). The regional and global patterns of PDO and ENSO (Section 2.7.2.4 – 2.7.2.5) are similar but the links between the oscillations remain unclear. It is suggested that the PDO modulates ENSO (Oglesby *et al.*, 2012; Wang *et al.*, 2012), or that the PDO is dependent on ENSO (Newman *et al.*, 2003); or that they are superimposed on each other and not independent climate modes (Goodrich and Walker, 2011). Therefore, whilst there is much to understand about ENSO and the PDO, it is clear that the oscillations modify climate on sub-decadal and decadal timescales (Shabber *et al.*, 1997; Mantua and Hare, 2002).

2.8 Late Holocene climate change

2.8.1 Medieval Climate Anomaly

The North Atlantic region experienced warmer conditions between AD 900-1350, initially termed the Medieval Warm Epoch (Lamb, 1965). During this period the British Isles received increased precipitation (Lamb, 1965), droughts persisted through parts of western North America (Cook *et al.*, 2010; Oglesby *et al.*, 2012) and southern Europe (Proctor *et al.*, 2000), and SST in the North Atlantic Ocean was 1°C warmer than present day (Feng *et al.*, 2008). Since climatic conditions were temporally and spatially heterogeneous (Hughes and Diaz, 1994; Bradley, 2000, 2003; Folland *et al.*, 2009) this period is now more commonly referred to as the Medieval Climate Anomaly (MCA). The MCA provides the most suitable baseline conditions for future climatic warming since the climatic boundary conditions were similar to those of the present day and it represents a natural period of warming, arguably without large-scale anthropogenic influence.

The pattern of MCA climatic change suggests that conditions were caused by changes in Pacific and Atlantic SST, which forced large-scale changes in oceanic and atmospheric circulation patterns as comprehensively summarised in Mann *et al.* (2009), Trouet *et al.* (2009), Graham *et al.* (2010), Oglesby *et*

al. (2012). Such changes may have been exacerbated by a persistent positive phase of the AMOC, driven by changes in the NAO, AMO and ENSO (Cobb *et al*., 2003; Graham *et al*., 2007; Seager *et al*., 2007; Feng *et al*., 2008; Conroy *et al*., 2009; Mann *et al*., 2009; Trouet *et al*., 2009). Whilst alterations in the circulation patterns likely drove the climatic changes, the persistence of the MCA may have been influenced by volcanism and changes in solar irradiance (Mann *et al*., 2008) but this remains unclear (Diaz *et al*., 2011).

2.8.2 Little Ice Age

The Little Ice Age (LIA) originally described the northern hemisphere Neoglacial period of glacier regrowth (Matthes, 1939, p.520); however, the term was later applied to the period between AD 1430-1850 when the northern hemisphere was cooler than the preceding periods (Lamb, 1965). The precise timing of the LIA remains contentious: the duration is traditionally defined as AD 1550-1850 (Jones and Bradley, 1992) although significant cooling may have occurred as early as AD 1250 and lasted until *ca*. AD 1920 in Scandinavia (Grove and Switsur, 1994). More recently, Grove (2004) suggested that the climate anomaly began in AD 1200-1300, culminating in AD 1500-1800, whilst Wanner *et al.* (2008) placed its duration from AD 1350 to 1850.

The lack of consensus surrounding the LIA timings stems from its regional and temporal variability. The LIA was not a long synchronous cold period (Jones and Bradley, 1992) but rather contained two (Bradley and Jones, 1995; Dahl-Jensen, 1998) or three major periods of glacier advance separated by moderate retreat (Wanner *et al*., 2000). This may contribute to subjective impressions of the date of onset, duration and termination depending on whether peak extreme conditions are considered or the cold spell in its entirety. These issues have made the LIA a somewhat contentious term (Jones and Bradley, 1992; Ogilvie and Jónsson, 2001; Jones and Mann, 2004) and it has been suggested that it would be more appropriately referred to as 'Little Ice Age**s**' (Grove, 2004) or 'Little Ice Age type events' (Diaz *et al*., 2011). Despite such concerns, for simplicity, the period predominantly remains referred to as the Little Ice Age.

LIA climatic conditions were recorded by instrumental data (Central England Temperature Series, Manley, 1974) and documentary sources (written/photos/sketches; Lamb, 1977) and are also contained in palaeoenvironmental records such as peat cores (reviewed by Barber *et al.*, 2004); lake levels (Magny, 2004); lake sediment proxies (e.g. chironomids; Langdon *et al.*, 2011); tree rings (Briffa *et al.*, 1992) and ice cores (Johnsen *et al.*, 2001; Figure 2.11). Many LIA records have been obtained from the North Atlantic region (e.g. Bradley, 2000) and they indicate that the LIA was asynchronous across the North Atlantic region, first visible on the eastern coast of North America (D'Arrigo *et al.*, 2006; Cronin *et al.*, 2010). Despite the proposed earlier North American onset, the most pronounced LIA conditions occurred earlier in Europe around AD 1600 rather than in AD 1800 in North America (D'Arrigo *et al.*, 2006; Cronin *et al.*, 2010).

2.8.3 MCA-LIA transition

The driving forces of the MCA-LIA transition are subject to extensive debate. It is largely considered to involve ocean-atmosphere interactions, since the dominant signal surrounds the North Atlantic, with staggered manifestations of difference timings and magnitude. Specifically, the NAO is thought to be an influential factor since the anti-correlated patterns of NAO driven precipitation could account for its asynchronous nature (Matthews and Briffa, 2005) and its multi-decadal fluctuations are typical of the NAO (Nesje and Dahl, 2003).

Solar variability has been postulated as the trigger of the MCA-LIA transition due to the concurrent timing of changes in sunspot activities and climatic change (Lean and Rind, 1998; Ammann *et al.*, 2007): the solar medieval maximum existed from AD 1100-1250 before moving to the Maunder minimum in AD 1645-1715 (Struiver, 1961; Eddy, 1976). The asynchronous nature of the MCA-LIA transition, however, suggests that solar forcing could not have directly driven the LIA in isolation (Cronin *et al.*, 2003). Rather, the likelihood of solar amplification of internal drivers such as the NAO (Cronin *et al.*, 2010), AMO (Cronin *et al.*, 2010), AMOC (Moffa-Sánchez *et al.*, 2014), and/or ENSO (Shindell *et al.*, 2001) have been proposed. The frequency and magnitude of volcanic eruptions increased around AD 1250 (Crowley, 2000; Crowley *et al.*, 2003; Ammann *et al.*, 2007; Gao *et al.*, 2008) and, combined with land-use changes (Ruddiman, 2007), may have contributed to the

magnitude of change. The palaeoenvironmental evidence and model simulations (e.g. Rasmussen *et al.*, 2007) suggest the drivers of the LIA can only be identified through a holistic approach. Such approach is suggested in Figure 2.12.

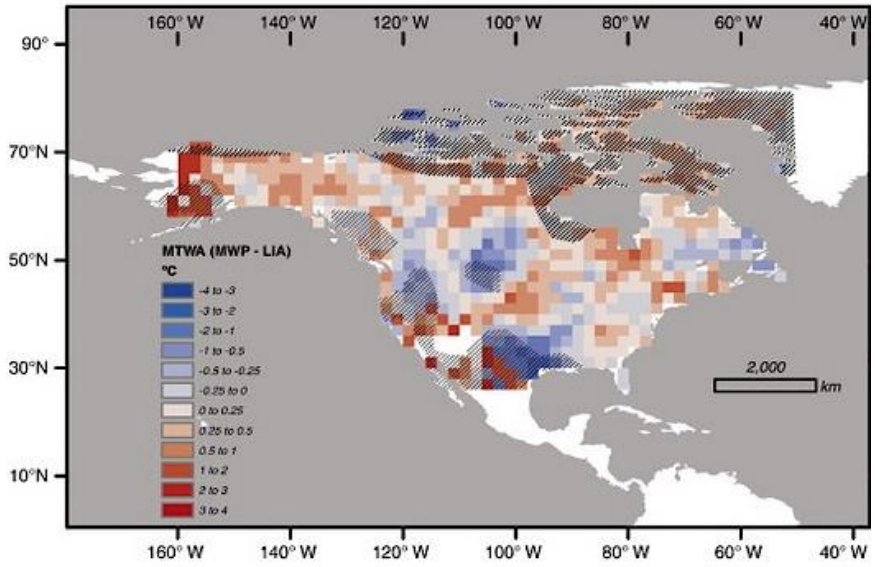

Figure 2.11 North American temperature anomalies between MCA and LIA transition. The temperature difference between the MCA and the LIA was smaller in Newfoundland and northern Nova Scotia than southern Nova Scotia and Maine (Sawada *et al.*, 2004).

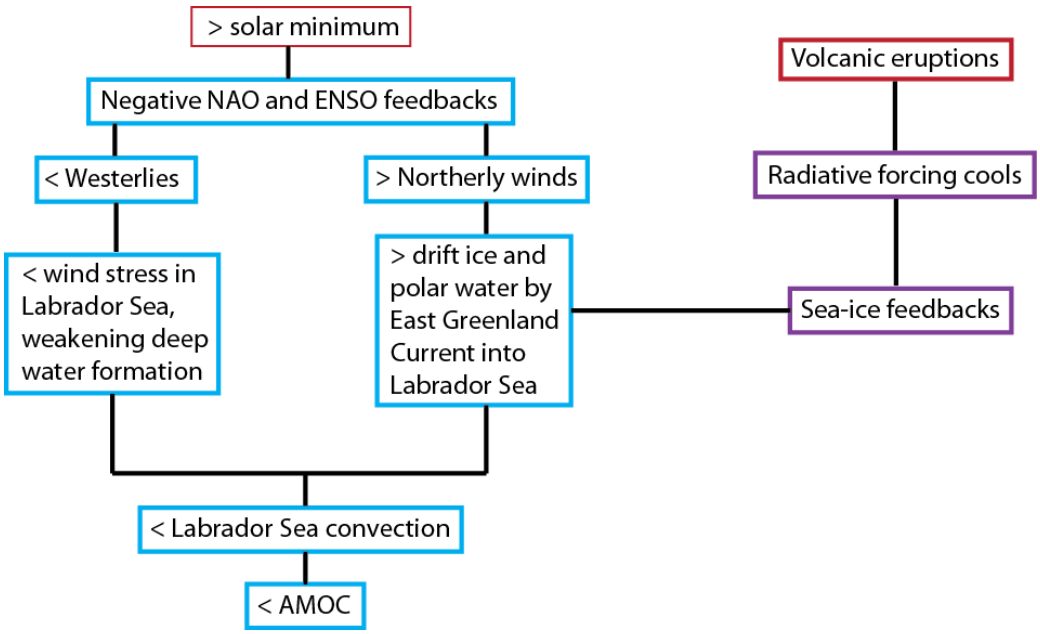

Figure 2.12 Example of a holistic approach to MCA-LIA driving mechanisms (based on the findings from Section 2.8)

2.9 Climate of last 2000 years from eastern North America

Whilst there is a paucity of late Holocene climate records from eastern North America, the existing records from the eastern US coast to Labrador and Nunavut are summarised in the subsequent sections and in Figure 2.13. At times the available reconstructions suggest contradictory climatic conditions and, since there are often only a few records for each region, it is unclear whether they reflect regional climate variation or whether such differences are associated with limitations in the proxy reconstructions or the study site sensitivities.

2.9.1 Northeastern Canada (Quebec, Labrador and Nunavut)

Compared with other regions of eastern North America, late Holocene climate change in Quebec and Labrador is fairly well characterised. The peak of the neoglacial cooling occurred at *ca.* 1800 cal yr BP, indicated by dry peatland conditions (Magnan and Garneau, 2014) and regional pollen data suggest a temperature decrease of -0.5 °C *ca.* 1700 cal yr BP (Viau and Gajewski, 2009). Peatlands were wetter after *ca.* 1600 cal yr BP (Magnan and Garneau, 2014), corresponding to warmer SST in Gulf of St Lawrence (Dhahri, 2010).

The warm wet conditions of the MCA likely occurred no earlier than *ca.* 1100 cal yr BP in north eastern Canada (Payette and Delwaide, 2004; Viau *et al.*, 2012). Quebec conditions were humid and stable around 1000 cal yr BP (Khider *et al.*, 2011; Yan *et al.*, 2011) which agree with records from sand dunes (Filion, 1984), regional pollen (Viau and Gajewski, 2009), peatland water tables (Magnan and Garneau, 2014) and a flooding event (Payette and Delwaide, 2004). Pollen records from lake sediments suggested that conditions in Labrador were more humid around 1000 cal yr BP (Roy *et al.*, 2011) and temperature increased (+ 0.26°C) around 1100 cal yr BP (Viau and Gajewski, 2009) as well as further north in Southampton Island (Rolland *et al.*, 2009).

The LIA is largely reported as a cool, dry period in Quebec. Peatland records indicate dry conditions around 600 cal yr BP (Magnan and Garneau, 2014) encouraging palsa aggradation from 600-140 cal yr BP (Loisel and Garneau,

2010) and 350 cal yr BP (Payette and Delwaide, 2004). Similarly, sparse vegetation and low diversity occurs from 440 -140 cal yr BP (Lemieux *et al.*, 2011). Regional temperature reconstructions suggest a cooling of 0.5 °C *ca.* 500 cal yr BP from Labrador (Viau and Gajewski, 2009) and Southampton Island temperatures cooled *ca.* 590-250 cal yr BP (Rolland *et al.,* 2009). Persistent LIA onset, therefore, perhaps occurred *ca*. 600-500 cal yr BP, although cold advances and associated dry conditions have been recorded at 770, 400 and 140 cal yr BP in Quebec (van Bellen *et al.*, 2011). Most sites from northern Quebec demonstrate a rise in water table over the 20th century (Loisel and Garneau, 2010; van Bellen *et al.*, 2011).

2.9.2 Newfoundland

A peatland from northeastern Newfoundland demonstrated wet phases at 2050, 1700, 600 and 200 cal yr BP (Hughes *et al.*, 2006). Chironomid temperature reconstructions from northwestern Newfoundland identified a cooling trend around 2200 cal yr BP, a brief warm oscillation prior to 1500 cal yr BP and a peak in summer temperatures 1100-1000 cal yr BP (echoed by marine warming at 1500-1100 cal yr BP (Renouf and Bell, 2009)) before declining to present day levels by around 500 cal yr BP (Rosenberg *et al.*, 2004). Marine records from the Bay of Islands on the west of Newfoundland indicate a warming period *ca.* 2000-1800 cal yr BP and cooler conditions *ca.* 800 cal yr BP (Levac, 2003), whilst the east coast show warming at 1700 cal yr BP until 1500-1100 cal yr BP and cool conditions 400-300 cal yr BP (Solignac *et al.*, 2011).

2.9.3 Nova Scotia

Increased precipitation and decreased air temperatures were reconstructed using pollen records from lake sediments between 3500-700 cal yr BP in Nova Scotia (Lennox *et al.*, 2010). Other palaeoclimatic records with increased resolution indicate that drying occurred *ca*. 1700 cal yr BP and *ca*. 1000 cal yr BP in southern Nova Scotia (Spooner *et al.*, 2014), whilst wet conditions occurred around *ca.* 850 – 600 cal yr BP in southwestern Nova Scotia (Neil *et al.*, 2014). Marine reconstructions from the nearby Laurentian Fan suggest that summer and winter SST were decreasing around 2300 and 1100 cal yr BP (Balestra *et al.*, 2013). Similarly, no MCA warming was detected in a core from

Emerald Basin in Nova Scotian coastal waters (Keigwin *et al*., 2003). Elsewhere, waters around the Laurentian Slope were 3 °C warmer at 900-750 cal yr BP during the MCA and 1.5-2.5 °C colder *ca.* 750 cal yr BP at onset of LIA (Marchitto and Demenocal, 2003).

2.9.4 North-eastern US (Maine-New Jersey)

Between 2000-1500 cal yr BP, Maine peatlands were wetter than the preceding 500 years (Nichols *et al*., 2006), corroborated by a lake-level rise *ca*. 2100 cal yr BP (Parris *et al*., 2010). Further south, a drying trend was reconstructed from a Massachusetts lake record between 2200-1800 cal yr BP (Oswald and Foster, 2011) and drought events were detected in peatlands in Michigan between 1900-1600 cal yr BP, extending across the Great Lakes to Minnesota (Booth *et al*., 2006). Temperature reconstructions in Maine indicated cooler conditions *ca*. 1650 cal yr BP (Rhodes and Davis, 1995); however, this contradicts pollen reconstructions from (Gajewski, 1988).

A clear MCA signal is not obvious from this region. Between 1700-1000 cal yr BP, Maine WTD reconstructions suggest a drying trend (Nichols *et al*., 2006), which occurred around 1300 and 1200-800 cal yr BP in Massachusetts lakes (Oswald and Foster, 2011); however, lake levels rose *ca.* 1400 cal yr BP (Parris *et al*., 2010). Dry conditions were reconstructed *ca.* 1350 – 750 cal yr BP from marine sediments obtained from Chesapeake Bay (Cronin *et al*., 2010) and warmer temperatures were reconstructed *ca.* 1350 - 1000 cal yr BP in Chesapeake Bay (Cronin *et al*., 2010). Reconstructions from the Gulf of Maine suggest there was less seasonality *ca.* 900 cal yr BP than during the LIA (*ca.* 600 cal yr BP (Wanamaker *et al*., 2011). Temperatures were cooler in the LIA around 200-500 cal yr BP (Gajewski, 1988) and possibly drier since concurrent fires were detected in three Maine sites at 550 cal yr BP (Clifford and Booth, 2013).

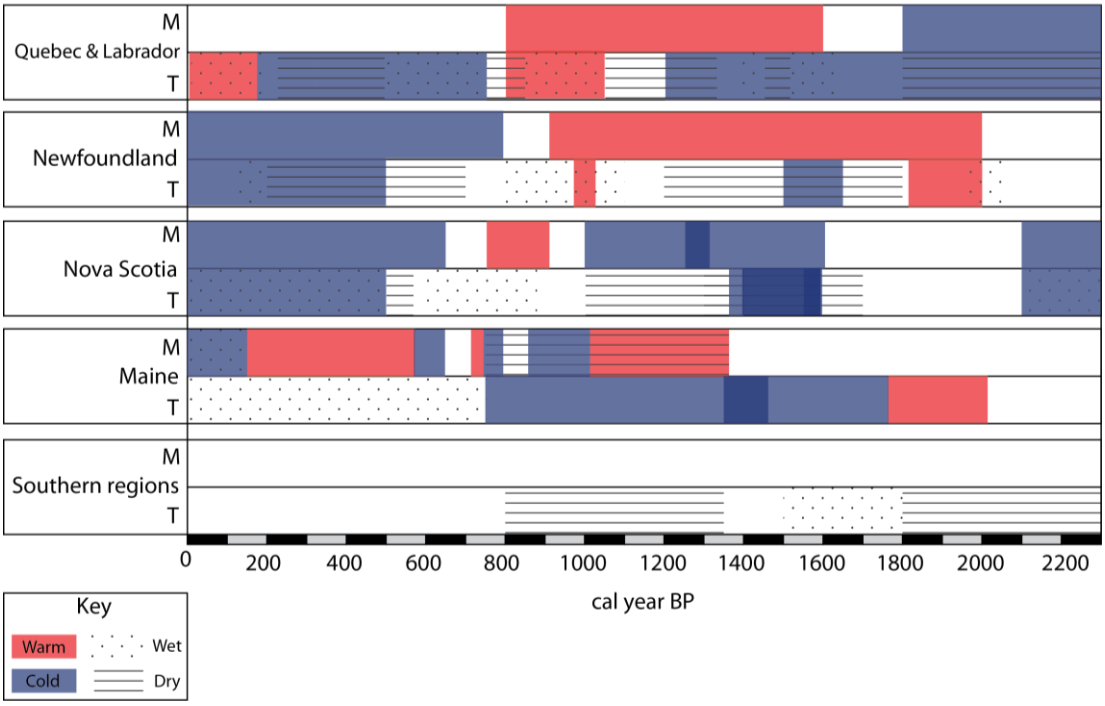

Figure 2.13 Regional palaeoenvironmental synthesis over the 2300 cal yr BP in eastern North America separated by region based on findings from literature (Section 2.9).
M = records obtained from marine sediments, T = records obtained from terrestrial records. Red represents warm conditions and blue represents cold conditions whilst dots indicate wet conditions and stripes indicate dry conditions.

2.10 Hypotheses generated from the literature review

The primary aim of this thesis (as outlined in Section 1.2) is to characterise the relationship between late Holocene peatland hydrological conditions and C accumulation rates (CAR) across a climate gradient in eastern North America. Towards addressing this aim, four main hypotheses have been generated from the synthesis of the relevant literature presented within this chapter and will be tested throughout the thesis:

Conclusion from literature review: During the MCA (LIA), the NAO, AMOC and ENSO were in persistent positive (negative) phases (Section 2.8). Based on modern observations and proxy reconstructions, the combination of these climate forces likely generated a less pronounced response to the MCA-LIA climatic transition in the north of the transect than the south.	**Hypothesis 1:** There will be a north-south divide in the peatland responses to MCA-LIA climate change: the influence of the NAO, AMOC and ENSO will maintain more similar peatland moisture balances across the MCA-LIA transition in the north than the south of the transect.
Conclusion from literature review: Peatland carbon (C) accumulation rates are primarily influenced by net primary productivity (NPP) with a lesser control of decomposition (Section 2.2).	**Hypothesis 2:** C accumulation over the last 2000 years will be greater in the southern sites than the northern sites owing to increased NPP influenced by average warmer temperatures.
Conclusion from literature review: The amount of photosynthetically active radiation (PAR) is determined by growing season length and available light, and is the main control on NPP and C accumulation (Section 2.2.1).	**Hypothesis 3:** Carbon accumulation rates will be increased during the warmer MCA period with higher NPP relative to colder LIA period with reduced NPP and increased cloudiness.
Conclusion from literature review: Peatlands close to the current moisture limit of peat growth will be particularly sensitive to changes in the moisture balance, with more uncertainty surrounding their C accumulation responses (Section 2.2).	**Hypothesis 4:** Sites close to the southern moisture limit of eastern North American peat growth are sensitive to disturbances (such as fire and droughts); therefore, they will be more vulnerable to episodic C loss.

Chapter 3: Methods

3.1 Introduction

This chapter gives an overview of the field, laboratory and statistical methods used within this thesis. The combination of analytical techniques has been selected following conclusions obtained from the review of existing literature (Chapter 2).

3.2 Sample collection

The optimum coring location on each peatland was inferred to be in the deepest area on a lawn microtope with an abundance of *Sphagnum* and obvious stratigraphic changes, such as fluctuating pool layers, indicating the potential for a more sensitive record of environmental change (Barber *et al*., 1998). Stratigraphic investigations of the previously unstudied peatlands were completed to locate the optimum coring locations: transects of cores were obtained across the longest axis of each peatland using a 50 x 5 cm Russian pattern corer. The maximum depth of the peat at each site was recorded and the depths of any changes in stratigraphy were measured and described using the Troels-Smith (1955) method of sediment classification. Three of the sites (SCH10, VDB12, FBB12) had been investigated (but not used) for prior projects, whilst JRB12 was a previously uninvestigated site. Details of each specific coring location can be found in Chapter 4.

Master cores were taken in 2012 proximal to the optimum assessment core site using a 50 x 11 cm Russian pattern corer with the exception of SCH10 which was obtained by NERC-PRECIP members in 2010 using a smaller 30 x 11 cm Russian pattern corer. The decision to obtain a continuous record, rather than use overlapping cores, followed the protocol of the NERC-PRECIP project: PRECIP has a similar regional focus to this thesis, therefore, similar protocols were followed when possible to facilitate future result comparisons and syntheses studies.

Once the cores were obtained, they were placed in prepared plastic guttering that had been cut to size with rounded edges to avoid ripping the core wrapping. Core depths were labelled on the outside of the guttering and a

layer of cling film covered the inside, before fully wrapping the cores in cling film and placing them in labelled carbon stable plastic bags sealed using electrical tape. The cores were kept cool and as horizontal as possible until they could be permanently stored in a cold store at a constant temperature of 4 ˚C to minimise further biological activity.

3.3 Sample preparation

All subsamples used in this study were obtained from the peat cores using individually cleaned stainless steel sampling tools in a clean environment to prevent any contamination. This was essential for the chronological techniques. During coring, there is the possibility that some peat may be dragged down across the core sections; however, evidence of this is clear in the lab as any such material will be exposed on the core surface. To eliminate this source of contamination, the surface of the core was removed with a scalpel and a spatula. Subsamples for each of the proxy techniques were obtained from within the core (sample sizes outlined in Table 3.1). This was achieved using very fine scissors that could cut through roots and other tough material. Cores were returned to the cold store to be kept at 4 ˚C when not in use and all samples that were not immediately analysed were also stored under these conditions.

3.4 Laboratory methods

This study uses methods that can be broadly separated into three main categories: biostratigraphic techniques (plant macrofossil and testate amoebae analysis), physical techniques (bulk density and carbon content) and chronological techniques (tephra and radiocarbon dating). The biostratigraphic techniques will indicate changes in the ecology and thus the wider environmental conditions of the peatland surface, whilst the carbon dynamics will be determined by the physical techniques. Chronological methods will determine the ages of the peat, facilitating comparisons of environmental conditions across the sites and other published studies.

Undertaking these approaches requires large amounts of sample material; therefore, efforts focused on minimising sample size where possible whilst ensuring optimal results. Such efficient use of core material was achieved by

halving the sample sizes used in the analysis of plant macrofossils and testate amoebae as recommended by Amesbury *et al*. (2011) who demonstrated that this did not alter the interpretation of results. The sample sizes used for each method and sampling resolutions are outline in Table 3.1.

Table 3.1 Comparison of sample sizes and resolution for methods used within this study.

Proxy method	Sample size	Resolution
Plant macrofossils	2 cm^3	Initially 4 cm then increased to represent every 40 years when chronological information obtained
Testate amoebae	1 cm^3	Initially 4 cm then increased to represent every 40 years when chronological information obtained
Bulk density & inferred C	2 cm^3	Contiguous 1 cm
Tephra (rangefinders)	2 cm^3	5 cm contiguous samples; refined to 1 cm where tephras present
Tephra (geochemistry)	6+ cm^3	Where tephras present
Radiocarbon	4+ cm^3	Where ages were allocated in NERC ^{14}C application

3.4.1 Plant macrofossil analysis

The plant macrofossils were analysed using the Quadrat and Leaf Count (QLC) technique (Barber *et al.*, 2003), modified by using 2 cm^3 of peat per sample (Amesbury *et al.*, 2011; discussed above). The samples were washed through a 125 μm sieve to disaggregate the plant remains and remove any fine particles that would obscure identification without damaging the plants. A standard volume of water (2.5 l) was used, thus ensuring that the resultant unidentifiable organic matter content is comparable between samples. The samples were transferred using deionised water into Sterilin tubes ready for analysis.

The sample was decanted into a clear plastic trough with a little deionised water added to ensure that the sample covered the entire trough surface in a single layer. The trough was shaken to further disaggregate the sample into the individual components and, if the sample was particularly cohesive,

forceps were used to tease the plant material apart. The trough was placed under a low powered stereo-zoomed microscope and inspected at 10x magnification. Fifteen different random locations within the trough were analysed, with plant remains estimated as percentages of each view using a 10x10 square grid graticule. The percentage of empty space was recorded and each scan percentage was corrected to account for this before an average of the fifteen scans was taken as the final sample result (Mauquoy *et al*., 2010).

Identifications were made using reference literature (Grosse-Brauckmann, 1972; Lévesque, 1988; Daniels and Eddy, 1990; Smith, 2004; Mauquoy and van Geel, 2006) and type material collected from the field. The individual components of each species were recorded separately to aid interpretation of the macrofossil record: for example stems are a contemporary component of the sample, whereas roots grow downward and thus may represent a younger vegetation assemblage. It is also useful to know the abundance of *Sphagnum* stems per sample since this can help guide the sampling strategy for radiocarbon dating. Fruits, seeds, charcoal, charred remains, mites and insect remains were recorded on a 5 point scale of abundance where 1 = rare, 2 = occasional, 3 = frequent, 4 = common and 5 = abundant. If samples contained epidermal tissues of monocotyledon species, these were mounted in water on microscope slides and identified to species level using 100 – 400x magnification.

To determine the proportion of *Sphagnum* species present, 100 *Sphagnum* leaves were randomly selected, mounted on a slide in Aqua-Mount and identified using 200 - 400x magnification. If the concentration of *Sphagnum* leaves were very low then the maximum feasible number of leaves was identified. Identifications were made using Daniels and Eddy (1990); McMullen (2000); Bastien and Garneau (1997) and reference samples collected in the field. *Sphagnum* counts were later adjusted as percentage of total identifiable *Sphagnum* from the QLC.

3.4.2 Testate amoebae analysis

The preparation of testate amoebae samples followed a modified version of the method outlined by Hendon and Charman, (1997); Charman *et al*. (2000);

Booth *et al*. (2010). Samples were placed in a 250 ml beaker with 100 ml of deionised water and a *Lycopodium* spore tablet in order to calculate the testate amoebae concentration. The beakers were placed on a hot plate to simmer for 10 minutes, disaggregating the peat assisted by occasional stirring. Samples were then individually washed through a stack of two sieves (coarse, 300 μm and fine, 10 μm) to remove large plant remains and fine detritus. The material that remained in the 10 μm sieve was retained for analysis and the rest discarded. Samples were washed into a centrifuge tube with deionised water and centrifuged at 3000 rotations per minute (rpm) for 5 minutes. The supernatant was decanted and the process repeated. Samples were finally washed into labelled, stoppered vials and stored in deionised water.

The samples were mixed in the vials and mounted on slides using a 9:1 deionised water: glycerol mixture to prevent sample evaporation and minimise the known hydration effect of glycerol on the tests. Testate amoebae were identified using the guides of Charman *et al*. (2000) and Booth *et al*. (2012). Samples were scanned under 100x magnification and 400x magnification was used for identification of each test, noting the morphology, size, colour and texture.

At least 100 individual tests were counted in each sample. Whilst 150 tests are required to capture the rare taxa (Charman, 1999), results using 100 tests have demonstrated that the main faunal components of the assemblages are still represented (Payne and Mitchell, 2009). Counts of 100 are sufficient to provide robust environmental reconstructions within this study. Counts of tests as low as 50 have been used for statistical analysis when preservation is poor or there are low concentrations of taxa (e.g. Swindles *et al*., 2007); however, this was not required in this study.

3.4.3 Carbon content

Peat carbon (C) content can be quantified using measures of bulk density and total C content. Whilst C content can be directly measured, approximately 50% of the organic matter density is assumed to be C in peat (Turunen *et al*., 2002). This latter approach has been applied in many recent studies (e.g. Charman *et al*., 2013; Loisel and Yu, 2013) and is advantageous owing to the

speed of processing and reduced analytical costs. A full overview of bulk density and total C analysis can be found in Chambers *et al*. (2011).

3.4.3.1 Bulk density

Clean, dry crucibles were weighed using a microbalance and a 2 cm^3 subsample of peat was measured using a volumetric sampler and added to a crucible. Care was taken not to compress peat in the volumetric sampler to ensure that a standard volume is used for each sample. The crucible was reweighed and the weight of the crucible and the sample was recorded. Crucibles were placed in an oven at 100 ˚C over night to completely dry the samples. The crucibles were then cooled to room temperature in a desiccator and the dry weight of peat was recorded. The bulk density is determined using the following equation:

$$\textit{Bulk density } (g/cm^3) = \textit{dry weight } (g) / \textit{fresh sample volume } (cm^3) \qquad (3.1)$$

3.4.3.2 Organic matter content

To measure the organic matter content, the samples of dried peat were placed in a muffle furnace at 550 ˚C for 4 hours. The crucibles were cooled to room temperature in a desiccator and the weight of the ashed peat was measured. The organic matter content was determined using the following equation:

$$\textit{Organic matter content } (g) = (\textit{dry weight} - \textit{weight after ashing}) / \textit{dry weight} \qquad (3.2)$$

The density of the organic matter could then be calculated, based on Equations 3.1 and 3.2, using the following equation:

$$\textit{Organic matter density } (g/cm^3) = \textit{bulk density x organic matter content} \qquad (3.3)$$

3.4.3.3 Peat C content

The C content of the peat sample is obtained assuming that the C content of organic matter is 50%:

$$\textit{C content } (g/cm^3) = \textit{density of organic matter } (g/cm^3) \times 0.5 \qquad (3.4)$$

Whilst the percentage C content of organic matter does vary by location and peat type, 50% is assumed to be a good estimate (discussed in Section 2.3) and will be applied in this study.

Owing to the speed and ease of this method, any samples that appeared to be outliers were repeated. Carbon accumulation rates (CAR) then were calculated by dividing the C mass in each 1-cm-thick peat layer (g cm^{-3}) by the deposition time of the each layer (yr cm^{-1}; obtained from the core chronologies (Chapter 5) reported over an area of 1 m^2.

3.4.4 Cryptotephra analysis

3.4.4.1 Detection of tephra

The detection of tephra in peat cores follows the method outlined by Pilcher and Hall (1992). The method used in this study has been slightly modified to follow the same protocol as was used in the one existing regional tephra record (Pyne-O'Donnell *et al*., 2012). This was deemed important since the two data sets will be compared directly. Contiguous samples of 5 x 1 x 1 cm^3 were extracted across the entire length of the cores. Each sample was placed in a lidded crucible and ashed in a muffle furnace at 600 ˚C for six hours. Once the samples had cooled, three drops of 10% hydrochloric acid (HCl) were added to cover the resultant ash. Crucibles were topped up with deionised water and samples were sieved using a 10 μm sized mesh to remove any fine particles that will obscure the identification of tephra shards. The sample retained in the 10 μm sieve was washed into centrifuge tubes using deionised water. The samples were placed in the centrifuge at 3000 rpm for 10 minutes with the brake off to concentrate the tephra at the bottom of the tubes.

To prepare the samples for microscopy, slides were placed on a hot plate at a low heat. Tephra samples were pipetted onto the slides, allowing the water to evaporate whilst leaving the ash dispersed across the slide. A layer of glycerol was applied and the sample was sealed with a coverslip. The slides were counted using a transmitted light microscope at 100x – 400x magnification in transects. Plane-polarised light assisted with distinguishing between tephra and other minerogenic material. Every shard was counted and the tephra concentration was calculated per 5 cm^3 of peat. A description of the shape, colour and vesicularity of the shards was noted.

Once the outline tephra stratigraphy had been determined, the tephra counts were repeated at 1 cm resolution where tephra horizons were located. Whilst the utility of identifying tephra to 0.5 cm resolution has been demonstrated (Amesbury, 2008), 1 cm resolution was selected for this study since large volumes of peat would be required to geochemically characterise any unknown tephra horizons with low peak tephra concentrations.

3.4.4.2 Extraction of tephra

Tephra shards from the 1 cm resolution peak horizons were extracted from the peat core for geochemical analysis using a modified version of the floatation method outlined by Blockley *et al*. (2005). Samples of *ca*. 4 cm^3 of peat were gently sieved with deionised water over 125 μm and 10 μm mesh sizes to remove large plant material and fine detritus. The sample retained on the 10 μm sieve was washed into a centrifuge tube with deionised water and was placed in the centrifuge at 3000 rpm and the brake on for 5 minutes. The supernatant was carefully decanted to leave the peat sample concentrated at the bottom of the tube.

A cleaning float removed the organics from the samples: 4 ml of sodium polytungstate (SPT) at a specific gravity of 1.95 was added to the sample and mixed using a vortex mixer. The samples were placed in the centrifuge for 15 minutes with the brake off. Since shards can remain trapped in the peat matrix, the sample was then mixed again to release all shards into the SPT before being placed in the centrifuge again at the same settings for 15 minutes. The supernatant was decanted into a beaker and the organics were removed from the SPT by sequential filtration using grade one and grade five filter papers. Some organic material remained in the samples, therefore, the cleaning float process was repeated until it was completely removed.

To isolate the tephra shards, an extraction float required the addition of 6 ml of SPT at a specific gravity of 2.55 to each sample. The samples were placed in the centrifuge for 15 minutes at the same settings (acceleration 3000 rpm, brake off). Once centrifuged, half of the sample (*ca*. 3 ml) was decanted into a correspondingly labelled extraction centrifuge tube. The original tubes were then returned to the centrifuge for a further 15 minutes at the same settings to ensure all shards were extracted. The remaining sample was decanted into

the corresponding extraction tube (now containing the full 6 ml of SPT and the tephra shards).

The extraction tubes were filled with deionised water and centrifuged for 5 minutes with the brake on. This lowered the SPT density so that the shards would be concentrated at the bottom of the tubes. The supernatant was decanted into a second set of filters to recycle the extraction SPT. This was repeated at least three times to ensure that the centrifuge tubes and tephra shards were free of SPT.

3.4.4.3 Geochemical analysis of tephra shards

Shards were mounted in epoxy resin stubs for geochemical characterisation by electron probe microanalyser (EPMA). Samples were transferred from the extraction tubes into plastic pots using pipettes and, once dry, were sent to the University of Edinburgh to be mounted on stubs.

The preparation of stubs followed the method outlined in Hall and Hayward (2014): Buehler Epo-Thin resin was mixed with hardener in a 9:1 ratio. One drop of the mixture was placed into a 26 mm diameter plastic ring mould on top of a silicone rubber sheet and evenly spread out using a spatula. Tephra shards were individually placed on the resin with their orientation arranged to maximise the surface area exposed at the final polished surface. The resin was cured overnight in a pressure vessel to remove air bubbles. Approximately 4 g of resin mixture was added by pipette to create the appropriate depth required for the stub and this was left to cure for 72 hrs. Samples were labelled using a diamond engraving tool.

Tephra shards were exposed on the surface through careful grinding and polishing. Grinding was completed using 800, 1200 and 2500 grit silicon carbide paper and water in a figure of eight motion. Frequent checks of the tephra shards were made under a binocular microscope. The surface was then polished with 6 μm, 1 μm and 0.25 μm diamond paste and frequent visual checks were employed until the surface was well polished and flat. Samples were ultrasonicated in AnalaR petroleum spirit for 10 minutes to remove all oil-based abrasive residues.

The stubs were carbon coated at the University of Edinburgh and a line of carbon paste was added to improve conductivity. Analyses were conducted on

the Cameca SX100 electron probe micro analyser with accelerating voltage of 15 keV at the School of Geosciences, University of Edinburgh. Rhyolitic (Lipari, ID 3506) and basaltic (BCR2g) secondary standards were used to test analytical consistency. A focused 3 μm beam diameter was used and is described in Hayward (2012). This beam size was used because shard sizes were typically very small (*ca*. 25-102.5 μm) with many vesicles

3.4.5 Radiocarbon measurements

Thirty-six AMS radiocarbon measurements were applied across the four study sites. Five samples were distributed through the last 1000 years of SCH10 as part of NERC project NE/I012915/1 and a basal date was obtained from SCH10 through the NERC-PRECIP project. A two-part application was submitted to the NERC ^{14}C Steering Committee for the remainder of the dates (thirty measurements) and these were fully funded. The first rangefinder application requested basal dates for the cores and aimed to locate the 2000-year limit of interest to guide sampling resolutions for the environmental proxies. The follow-up radiocarbon application was guided by results from plant macrofossil and testate amoebae analysis, with measurements obtained at periods of interest and where required to obtain robust estimates of CAR.

At each sample layer, 2 cm^3 of peat was washed through a 125 μm sieve with deionised water and then transferred into a cleaned plastic trough. Samples were inspected under a low powered stereo-zoom microscope at 10x magnification. *Sphagnum* stems were selected since they are guaranteed to be growing in situ and thus representative of the age of the peat sample. Stems were picked into a fresh petri dish and cleaned in deionised water removing rootlets, unidentifiable organic matter (UOM) and obvious fungal material using forceps. The cleaned stems were then picked into a new clean petri dish to be rinsed before transfer to a stoppered glass vial. This process was repeated until at least 200 mg of *Sphagnum* stems were individually extracted. The basal samples did not contain any *Sphagnum* stems; therefore, brown moss material was preferentially used. If no above ground plant material was present, bulk peat was analysed.

The samples were sent to the NERC Radiocarbon Lab in East Kilbride, Scotland to be pre-treated and processed into graphite for analysis at the SUERC AMS

facility. The resultant radiocarbon measurements were calibrated in the R package "Bacon" (Blaauw and Christen, 2011), and this package was also used to construct Bayesian age-depth models (Chapter 5).

3.5 Statistical analysis of palaeoecological data

Environmentally driven changes in palaeoecological assemblages can be visually identified from stratigraphic diagrams using ecological knowledge. However, the effectiveness of this technique is limited by the size of the datasets. The palaeoecological information must therefore be condensed into numerical representations of change using data transformation techniques, including: detrended correspondence analysis (DCA; Section 3.5.1); non-metric multidimensional scaling (NMDS; Section 3.5.2); Dupont Hydrological Index (DHI; Section 3.5.3) and transfer functions (Section 3.5.4). All four statistical methods are critiqued in the subsequent sections and their application within this study are outlined in Section 3.5.5.

3.5.1 Detrended correspondence analysis

DCA, developed by Hill and Gauch (1980), is an ordination technique that uses two-way weighted averages in a Gaussian unimodal response model to extract patterns from large datasets based on species composition using Chi-square distance measures (for full a review see ter Braak (1995). Eigen analysis separates the data along ordination axes, or 'Eigenvectors', which are scaled in standard deviation (SD) units. Each axis can be usually interpreted as a different, independent environmental gradient to which the species composition responds. In a unimodal response model, a change of one SD unit represents a 50% change in composition and complete species turnover occurs over four SD units (ter Braak, 1987). Therefore, species at opposing ends of the axes have the least similar environmental preferences and samples differentiated by more than four SD tend to have no taxa in common. Each axis is assigned Eigen values that indicate the amount of data variation that they can explain (Kent and Coker, 1992): axis one accounts for the most data variation and Eigen values close to or greater than 0.5 indicates that a good separation of the species along the axis has occurred (ter Braak, 1995).

Within DCA, the data are passively plotted without using information on environmental variables; therefore, the drivers behind the data distribution must be inferred. Whilst this introduces a degree of subjectivity, the dominant environmental driver of plant variability in undisturbed ombrotrophic peatlands is usually the height of the water table (Section 2.4.2). This can be confirmed through comparisons of the first and second DCA axes and visual inspections of the raw vegetation assemblage data informed by ecological knowledge. If it is concluded that water table depth is driving the variation in the dataset, sample scores (based on the species scores) can then be plotted to represent surface hydrological changes.

DCA can be skewed by rare species or samples that are very different from others (known as crossed gradients; Kovach, 1995). The technique places such components towards the extremes of the axes, damping the separation of other species that are forced to cluster in the middle to the axis. Therefore, it is often necessary downweight or remove rare species. Usually crossed gradients occur when another driver, such as ecological succession, replaces the climatic influence as a dominant driver. An example of this is the UK extinction of *Sphagnum austinii* and the replacement with *Sphagnum magellanicum* or *Sphagnum papillosum* (Daley and Barber, 2012). Therefore, whilst scores of species in the middle of the ordination may indicate that the species is genuinely located in the centre of the underlying gradient, the positioning may also be generated by the cross gradient effect, a ubiquitous species or indicate the taxon's lack of relationship to the factor explained by the axis.

DCA was designed to address the "arch effect" in correspondence analysis (CA), which is generated when the first ecological gradient is much longer than the second. Under such conditions, CA 'constructs' the second gradient as a quadratic function of the first, leading to spurious curvature and shrinking at the ends of the ordination. To correct for this, DCA uses a combination of detrending, rescaling and downweighting of rare species; however, these approaches may be viewed as 'tricks' rather than robust statistical methods (Steve Juggins, pers. comm.). Therefore, whilst DCA is an essential data-screening tool to assess the clarity with which specific environmental drivers can be assigned to the dataset; other techniques, such as multidimensional dimensional scaling (MDS), may be considered more

statistically robust for obtaining indirect environmental reconstructions from species data. Despite the statistical reservations associated with DCA, numerous examples of effective DCA peatland plant macrofossil reconstructions exist (e.g. Barber *et al.,* 1994; Charman *et al.,* 1999; Barber *et al.,* 2000; Barber *et al*., 2003; Barber *et al*., 2004; Langdon and Barber, 2005; Hughes *et al*., 2006; Swindles *et al*., 2007b; Amesbury *et al*., 2011, 2012; Daley and Baber 2012; Valiranta al., 2012; Magnan *et al*., 2014; Roland *et al*., 2014) and the most appropriate transformation technique will ultimately be dictated by the characteristics of the individual datasets.

3.5.2 Non-metric Multidimensional Scaling

nMDS (Minchin, 1987; Virtanen *et al*., 2006) is similar to DCA since it passively plots the species dissimilarities onto an ordinal space and then requires interpretation of the environmental control on the ordinal axes and sample scores. However, there are two main differences between statistical approaches: the distance measure used in nMDS can be specified, whilst DCA is limited to Chi-square. Unlike DCA, which is based on a unimodal species response to environmental gradients, the replacement of inter-sample distance with ranks makes nMDS less sensitive to non-linear relationships and discontinuous disturbances.

Within nMDS, the specification of the number of dimensions (or axes) for the solution is required along with an appropriate distance metric to calculate a distance matrix (Minchin, 1987). The Bray and Curtis dissimilarity matrix is commonly applied in ecological studies (Legendre and Legendre, 1998) and can be employed within nMDS. A measure of 'stress' within the nMDS model is calculated, which compares the differences between rank order of distances in the data and rank order of distances in the ordination. Samples can then be moved to minimise the stress in an iterative process. The order of dimensions is arbitrary and does not reflect relative importance for explaining data variation. Therefore, a Principal Component Analysis (PCA) is required to rotate the results and attribute the axis with the most variance as axis one.

There is no overwhelming consensus as to whether DCA or nMDS is the better method of unconstrained ordination (Ruokolainen and Salo, 2006); however, McCune and Grace (2002) state that nMDS is the most generally effective

ordination method for ecological community data. Studies using different types of data with differing gradient lengths and distance or similarity methods have come to opposing conclusions: Hill and Gauch (1980) showed that results from DCA were more easily interpretable and Bakus (2007) found DCA results to be more realistic. Conversely, Minchin (1987) found nMDS to be more robust and Gauch *et al*. (1981) obtained better results using NMDS for some datasets. Therefore, to determine the optimal ordination method for each study, both DCA and nMDS should be completed and results compared using ecological considerations.

3.5.3 Dupont Hydrological Index for plant macrofossils

DHI uses weighted averaging whereby each plant category is assigned a weighed indicator value based on its hydrological niche. The name 'Dupont' Hydrological Index is in recognition of the first application by Dupont (1986) who desired a semi-quantitative method to obtain a single curve that could summarise peatland hydrological fluctuations. Based on the demonstrated unimodal response of species to environmental gradients (Whittaker, 1956), Dupont represented the optimum condition for the growth of each species by indicator values. The vegetation components were classified into 6 groups and assigned an individual optimum moisture value in a scale from 1 to 8: 1 representing wet and 8 representing dry (Table 3.2). These indicator values were based purely on the ecological knowledge of the preferred niches across the peatland surface. The following equation could then be applied to obtain weighted average ordinations (DHI scores) for each sample:

$$x_0 = \frac{\sum_k Y_k u_k}{\sum_k Y_k} \qquad 3.5$$

where: x = Dupont hydrological index; x_0 = value of x for a given sample; Y_k = abundance of the k^{th} species; u_k = indicator value of the k^{th} species (following ter Braak and Barendregt, 1986).

Many peat-based palaeoenvironmental studies have applied DHI (e.g. Mauquoy, 1997; Barber *et al*., 2003; Daley, 2007; Swindles *et al*., 2007a,b; Amesbury, 2008; Daley and Barber, 2012; Roland *et al*., 2014). The index has evolved from Dupont's original form since more vegetation categories are included (Table 3.2). The DHI was firstly modified by Stoneman (1993) who attempted to increase the objectivity of indicator values by creating seven zones to representing particular microenvironments ranging from pools (1) to hummock tops (7). This was a subtle difference that still focused on hydrological changes but enables the plant group to be ordered based on an optimal microtopographical feature for growth. The original Dupont index omitted positions 7 and 4 to emphasis the difference between both Ericaceae and *Sphagnum* hummock builders and the wetter *Sphagnum* species (Dupont, 1986). This omission was removed by Stoneman (1993) and has remained absent from the scale in subsequent revisions. The next substantial revision of the index was completed by Mauquoy (1997) when it returned to an 8-point scale based on species water table depth preferences rather than microtopography. Further extensions and alterations of the DHI have remained in this approach and the most recent version was outlined by Daley and Barber (2012). Alterations of the indicator values applied in different 'DHI' are outlined in Table 3.2.

A comparative study demonstrated that the DHI-inferred plant macrofossil results correlated more closely with independent proxy data from the same core than DCA (Section 3.5.1) or nMDS (Section 3.5.3), advocating its use in studies of past peatland environmental change (Daley and Barber, 2012). One of the main advantages of using DHI, compared with ordination techniques, is that problems with rare species and small gradients are minimised. Additionally, when using the DHI there is a certainty that hydrological conditions are being represented, whereas the species ordination may be a mix of environmental variables (Mauquoy *et al*., 2008), thus reducing the certainty with which reconstructions of water table fluctuations can be made. A comparison of ordination and weighted averaging-based results can therefore be used to identify hydrologically driven periods (when both records agree) and periods when other drivers may predominantly influence the floral and faunal assemblage (when records diverge).

Despite the demonstrated utility of the current DHI in peat-based studies, there is scope for revising the indicator scores (*sensu* Daley and Barber, 2012) and refining the method. The indicator scores are attributed based on broad ecological knowledge; however, they have never been explicitly based on field measurements of species distributions and water table depths and are therefore subjective (Barber *et al*., 2000, 2004). Although the direction of change indicated through the DHI may be sensible, the magnitude of change is meaningless since the differences in indicator values are not directly related to real differences in water table depth tolerances. This emphasises the need for the selection of optimum indicator scores and caution required when interpreting the results.

The current approach, based on ecological knowledge alone, is likely effective when species have a narrow, well-defined niches towards the end of the water table depth range. For example, *Sphagnum cuspidatum* is a robust indicator of pool or pool edge environments that cannot survive under drier conditions; therefore, it is sensibly attributed an indicator value of 1, representing wet conditions. Generally, hollow species have narrower ranges than hummock species (Andrus, 1983) and may therefore be more suited to this scale. However, for species with wide niches that can be present on a range of microtopographical habitats, the lack of basis on empirical studies is cause for concern. For example, *Eriophorum vaginatum* is commonly assigned an indicator value of 7, towards the dry end of the DHI scale, since it can grow on drier lawns and hummocks (e.g. Ratcliffe and Walker, 1958). However, other field observations have recorded this species in shallow pools (Osvald, 1923; Barber, 1981) and alongside *Sphagnum* (Meade, 1992). Clearly, as others such as Okland (1990) and McMullen (2000), have observed *Eriophorum vaginatum* has a broad niche and it is therefore perhaps misguided to assign poorly constrained species such a high, indicator value. The overlapping niches are problematic since they violate the species packing model (whereby species occupy separate niches), a requirement of weighted averaging techniques (ter Braak, 1995).

Identifying plant macrofossils to species level in palaeo-peat samples can be hindered by decomposition. Often, this results in plants being grouped by family or even clade, rather than species. Assigning a whole family a universal indicator value may reduce the effectiveness of the overall DHI since the

individual species of the larger group occupy very different locations on the microtopographical gradient. Such complications are demonstrated through the example of the clade monocotyledons (monocots), which has been assigned drier indicator values of 6 and 7 in different studies. Within monocots, species have very distinct habitats: e.g. *Rhynchospora alba* thrive in low lawns and pool edges (e.g. Godwin, 1956; Backeus, 1985); therefore, they are representative of high water tables and are usually assigned an indicator value of 3. *Eriophorum angustifolium* often accompanies *Rhynchospora alba* in wet hollows (Philips, 1954); however, it can also grow on hummocks (Ratcliffe and Walker, 1958; Madden and Doyle, 1990). Despite tolerance of drier conditions than *Rhynchospora alba, Eriophorum angustifolium* is usually assigned the same wetter indicator value of 2.

Another monocot. species, *Eriophorum vaginatum*, can be found in hummocks and drier lawns (Ratcliffe and Walker, 1958), although it has been found waterlogged with *Sphagnum* (Meade, 1992). It is generally assumed to be ubiquitous and to thrive under fluctuating water table heights (Okland, 1990; Hammond *et al* 1990; McMullen, 2000). *Eriophorum vaginatum*, assigned indicator value of 6, is a common component of the macrofossil assemblages, and has been suggested to be over represented owing to its high preservation rates (Hughes and Barber, 2004). Monocots undiff. are allocated the indicator value of 6, perhaps owing to the influence of *E. vaginatum*; however this may be a biased representation of the clade. Arguably, a lower indicator value would be more appropriate for *Eriophorum vaginatum* and thus the monocot. clade as a whole.

The index relies on components having unimodal responses to environmental gradients; therefore, the current indicator values cannot represent components with bimodal distributions, such as UOM. UOM usually represents drier conditions owing to enhanced decomposition (hence the usual indicator value of 8). It can also represent the presence of algal mud that forms in pools. If the UOM did originate from wet conditions (corresponding to an indicator value of around 1), then the assignment of the indicator value 8 would skew the sample scores. Perhaps to prevent this, a filtering stage could be included within the index which, if the other constituent components represented pool conditions, would alter the UOM index to 1 rather than 8.

Table 3.2 DHI index values applied in each revised index. UOM = unidentifiable organic matter; undiff. =undifferentiated; monocot. = monocotyledons; S = *Sphagnum*

	Dupont (1986)	**Stoneman (1993)**	**Mauquoy (1997)**	**Mauquoy (2008)**	**Daley and Barber (2012)**	*Mallon (2012)*
UOM		7		8	8	
Algal mud					1	
Ericaceae undiff.		7		8		8
Ericaceae roots	8		8		8	
***Betula* wood**					8	
Andromeda polifolia						6
Calluna vulgaris			8		8	8
Empetrum nigrum						6
Erica tetralix			8		8	8
Vaccinium Oxycoccos						4
Monocot. undiff.		6	6	7	7	
Eriophorum angustifolium			2	2	2	2
Eriophorum vaginatum			6	7	7	6
Rhynchospora alba			2	3	3	3
Hypnum jut.						6
Trichophorum cespitosum				6	6	6
Aula palustre			8	5	6	6
***Polytrichum* spp.**			8		8	
Brown moss undiff.					6	6
Drepanocladus fluitans				2		
S.* sect. *Acutifolia	6	5		5	6	6
S. imbricatum	5	4		4	4	5
S. magellanicum	3	4	4	4	3	3
S. papillosum	2	4	3	3	3	4
S. fuscum						3
S.* sect. *Cuspidata	1	2	1	1	1	1
Cuspidatum						1
S. pulchrum						2
S. subsecunda		1				

A further concern with the current method is that roots are assigned the same value as other components from the same species. Roots can penetrate long distances downwards; therefore, they may not be contemporaneous of the sample in question. Therefore, it has been suggested that root categories should be omitted from the index (Mallon, 2012).

3.5.4 Transfer functions

Transfer functions produce quantitative reconstructions of environmental conditions from fossil assemblages assuming that the observed modern relationship between the organisms and environmental variables has remained constant. Training sets measure the current environmental parameters of interest and the corresponding taxa assemblage. The statistical relationships between the environment and the biological entity are used to develop the transfer function. Such an approach has been used for many different palaeoecological parameters, although in the peatland context it is most commonly applied to testate amoebae data in order to reconstruct water table depth. A plant macrofossil transfer function has been developed to reconstruct water table depth from peatlands in Finland and Estonia (Väliranta *et al.*, 2012); however, the design and construction of an appropriate plant macrofossil transfer function for this study is beyond the aims of this thesis.

The quality of the training set determines the overall effectiveness of the transfer function. Species environmental preferences must be well characterised and must be able to reliably predict modern responses before it can reconstruct past records. An ideal training set would sample the full gradient of environmental conditions at as many sites as possible over a prolonged period of time (Booth, 2008). This is often not possible and many training sets are based on single point measurements. Single point measurements are problematic since the current surface assemblages of testate amoebae represent years of accumulation (Booth, 2008). Furthermore, water table conditions at the point of sampling may not be generally representative of the season or year. Training sets have also been critiqued for small geographical sampling range (Booth, 2008), leading to spatial autocorrelation and over optimistic performance statistics (Telford and Birks, 2005, 2009; Payne *et al.*, 2011).

Linear or unimodal statistical models of the ecological and environmental responses can be used for transfer function development: e.g. partial least squares regression (linear), weighted average (WA) regression, weighted average tolerance down weighted, weighted average partial least squares regression and modern analogue techniques. The performance of these models is assessed throughout the transfer function development using the r^2 and the root mean square error of prediction. Whilst WA techniques are often selected owing to their statistical performances, empirical predictive power and robustness to spatial autocorrelation (Telford and Birks, 2005), recent results from simulations suggest that the WA techniques used in transfer functions are prone to the influence of secondary variables and may produce both spurious trends and values (S. Juggins, pers. comm.).

3.5.4.1 North American testate amoebae transfer functions

Four transfer functions have been developed for eastern North America (Charman and Warner, 1997; Booth, 2008; Amesbury *et al*., 2013; Lamarre *et al*., 2013). The recently developed transfer functions for eastern North America and northeastern North America (Amesbury *et al*., 2013 and Lamarre *et al*., 2013 respectively) are the most directly applicable transfer functions to this study. Whilst the location of the oceanic sites incorporated within the Amesbury *et al.* (2013) transfer function is more directly applicable to this study, a better coverage of modern analogues is contained within the Lamarre *et al*. (2013) transfer function.

Both the Amesbury *et al*. (2013) and Lamarre *et al*. (2013) transfer functions have been subjected to rigorous statistical testing to address areas of concern surrounding transfer function spatial autocorrelation, clustered sampling design and uneven sampling gradients (Telford and Birks, 2009, 2011; Payne *et al*. 2012). The optimal model within the Amesbury *et al*. (2013) transfer function was inverse weighted averaging with tolerance down weighting (WA.inv.tol; RMSEP: 5.66; R^2: 0.87) whilst the most consistent model within Lamarre *et al*. (2013) was the classical weighted averaging with tolerance down weighting (WA.cla.tol; RMSEP: 5.65; R^2: 0.82). Comparisons between the two transfer functions reveal similar trends but lower amplitude of variation is produced when using the Lamarre *et al*. (2013) transfer function.

The species with the most contrasting hydrological preferences within the transfer functions of Amesbury *et al*. (2013) and Lamarre *et al*. (2013) are *Difflugia pulex* (*D. pulex*) and *Hyalosphenia subflava (H. subflava).* Both *D. pulex* and *H. subflava* are commonly assigned as indicators of dry peatland conditions; however, both species have weak modern analogues (e.g. Charman *et al*., 2007; Booth, 2008; Mitchell *et al*., 2008; Turner *et al*., 2013). Recent studies have consistently found *H. subflava* to be one of the driest indicators whilst characteristics of *D. pulex* are more complex. Training sets from Europe and eastern North America found *D. pulex* to thrive in intermediate to very dry conditions (Charman *et al*., 2007; Booth 2008; Lamarre *et al*. 2013; Turner *et al.,* 2013). The training set developed for the study region (Amesbury *et al* 2013) located *D. pulex* in an intermediate to wet position of the water table gradient whilst acknowledging that the distribution was poorly captured. Whilst the representation of *D. pulex* and another complex taxa (e.g. *H. subflava)* is improved in the regionally similar Lamarre *et al*. (2013) transfer function, the ecology of these species remains uncertain (Mitchell *et al.,* 2008) and may be characteristic of sites with highly variable environmental conditions (Sullivan and Booth, 2011). Palaeorecords containing these species must, therefore, be interpreted with caution.

A combination of factors may account for the poor modern analogues of *D. pulex*: firstly, it has a potentially low vertical growing position on *Sphagnum* stems and may be missed in some surface sample collections (Booth, 2008). Secondly, there may be issues with possible genetic diversity (e.g. Gomaa *et al*., 2012) that are not as yet acknowledged or understood (Amesbury *et al*., 2013). Thirdly, it may have a complex response to water table depth by either thriving in more abrupt hydrological fluctuations (Sullivan and Booth, 2011) or by responding to secondary gradients.

3.5.5 Palaeoecological statistical approaches adopted within this thesis

The palaeoecological assemblage data have been separated into zones of similar floral or faunal characteristics using results from Constrained Incremental Sum of Squares (CONISS), a cluster analysis function within TILIA (Gordon and Birks, 1972; Bennett, 1996). All CONISS analyses were stratigraphically constrained with the data square root transformed to

stabilise variance. The zone boundary locations allocated by CONISS were then checked against the assemblage data to ensure that they were placed at the point of the largest percentage change in the majority of taxa. If the zone boundary was not at the point of largest change then the boundary was adjusted to reflect this and the adjustments have been clearly noted within the text.

DCA was conducted on both the plant macrofossil and testate amoebae data within the program CANOCO for Windows v. 4.5.2 (ter Braak, 1987; ter Braak and Smilauer, 1998), completed in segments with non-linear rescaling and rare species downweighted. The results of DCA are presented as bi-plots of axes one and two species and sample scores to identify whether the controlling environmental gradient is WTD. This will not only determine the feasibility of producing down-core DCA environmental reconstructions (*sensu* Barber *et al*., 1994) but also will indicate the clarity of the floral and faunal hydrological relationships, thus justifying the use subsequent use of DHI (plant macrofossils) and transfer functions (testate amoebae). nMDS was conducted in R (R Development Team, 2014) and the solutions have been rotated using PCA to represent variability and to facilitate comparisons with DCA results.

Following confirmation from the DCA and the nMDS that the vegetation is likely responding to water table depth, the European-based DHI (Daley and Barber, 2012) was applied to the plant macrofossil data, attributing all assemblage changes to hydrological fluctuations. Since the existing DHI omits some North American peatland species, a trial eastern North America plant macrofossil DHI has been constructed within this study. However, the construction of this eastern North American index is purely exploratory, to assess the performance of a regionally specific index, and is based on a very limited number of sites (n=2) from a limited geographical range (Newfoundland) in relation to the overall study transect. Final DHI reconstructions from each site were therefore still obtained using the established Daley and Barber (2012) index, whilst the performance of the restricted updated DHI was tested throughout. Two secondary reconstructions using the updated index were completed to assess the climatic inferences obtained when excluding UOM and roots. Environmental inferences from the Daley and Barber derived DHI were compared with results from the DCA and

nMDS. Divergences between records may indicate periods that are not characterised by hydrological induced changes.

DHI is not completed on testate amoebae data since the existing transfer functions are essentially a more advanced version of weighted averaging techniques. Upon confirmation from the DCA and nMDS that the dominant driver of testate amoebae assemblage change is WTD, transfer functions can be applied to the data. Conversion of testate amoebae data to WTD estimates were completed by M. J. Amesbury, University of Exeter, using the Amesbury *et al*. (2013) transfer function models and G. Magnan, Université du Québec à Montréal, using the Lamarre *et al*. (2013) transfer function models. For simplicity, reconstructions obtained from Amesbury *et al*. (2013) will be referred to as 'ATLANTIC.NA' and Lamarre *et al*. (2013) reconstructions will be referred to as 'QUEBEC'. Reconstructions from both transfer functions have sample-specific errors of prediction generated though 1000 bootstrap cycles. Both transfer functions use weighted average regression. The ATLANTIC.NA models use an inverse approach to the regression (WA.inv) whilst the QUEBEC model adopts a classical approach (WA.cla). Species with large water table tolerances may be downweighted within the model reconstructions compared with species with small water table tolerances, which are better indicators of the reconstructed habitat. The effectiveness of such downweighting is assessed within each transfer function by comparing reconstructions obtained from the WA models and those from the WA.tol models.

Comparisons of the plant macrofossil and testate amoebae reconstructions were aided by normalisation, which places the variables on the same axis scale. Normalisation is conducted using the following equation:

$$z = \frac{X - \mu}{\sigma} \qquad 3.6$$

where: z = normalised value, X = raw value, μ = mean of all X, σ = standard deviation of X.

Unless otherwise stated, all palaeoecological correlations were tested using Pearson Correlation Coefficients and all differences are investigated using Mann-Whitney Rank Sum Tests.

Chapter 4: Study sites

4.1 Introduction

This chapter describes the requirements for, and thus the rationale behind, the study site selection. The climate of the study region is outlined using modelled climate data (Section 4.4) and a detailed description of each site is provided (Sections 4.5 - 4.8).

4.2 Site selection

This thesis reconstructs late Holocene variations in the moisture balance and associated carbon dynamics across Maine, Nova Scotia and Newfoundland. The region is proximal to three main oceanic areas that influence climate: the North Atlantic Ocean, the Gulf of Maine and the Gulf of Saint Lawrence. The North Atlantic's Gulf Stream and the shallow Gulf of Maine have a warming effect on temperatures in the south, whilst the North Atlantic's Labrador Current and the Gulf of Saint Lawrence generate cooler conditions in the north. These temperature patterns are also assisted by the influence of three main air masses: tropical maritime, polar continental and polar maritime. Extreme regional precipitation events are delivered by the dominant regional storms termed 'nor'easters' which originate from the US in the spring, summer and winter.

Study sites across this region were selected based on the following criteria:

1. Sites must complement the transect of relevant existing peatlands records (the NERC-PRECIP project, unpublished; Hughes *et al.*, 2006)
2. They must be less than 200 m above sea level to minimise the influence of orographic climate variations (*sensu* Haslam, 1987)
3. Peatlands must be ombrotrophic to ensure a direct relationship between climate and water table depth changes (Section 2.4)
4. Based on average accumulation rates (Section 2.1), they must have at least 2.5 m of ombrotrophic peat to ensure the preservation of a 2000 year old climatic record
5. Sites must not, historically or currently, show signs of anthropogenic disturbance (aside from minor peripheral quad bike tracks)

6. The final transect of sites must span a modern climate gradient.

4.3 Location and description of study sites

Saco Heath (SCH10); Villagedale Bog (VDB12); Framboise Bog (FBB12) and Jeffrey's Bog (JRB12) were selected as the study sites (Figure 4.1). These peatlands are located on a southwest to northeast transect across Maine, Nova Scotia and Newfoundland. Historical modelled climate conditions are compared across the sites in Section 4.4 and site specific rationale and descriptions are provided in Sections 4.5 - 4.8.

Figure 4.1 Location of Ph.D. study sites in context of other relevant peatland studies

4.4 Modeled climate data

North American elevation-dependent spatial climate models (McKenney *et al.*, 2011) were used to assess the historical climate conditions of each site. The models use data from meteorological stations (see McKenney *et al.*, 2006) for maps of station locations) and were generated using thin-plate smoothing splines in the ANUSPIN climate modeling software (Hutchinson, 2004) for the period 1901 to 2010. Site-specific data of direct climatic variables (such as

temperature and precipitation) were generated and then applied to the programs ANUCLIM (Houlder *et al*., 2000) and SEEDGROW (Mackey *et al*., 1996) to infer a range of bioclimatic variables, such as growing degree-days, which influence vegetation distributions.

The predictive power of the ANUSPIN model is ultimately limited by the quality of weather station data available: northern sites had few proximal stations until *ca.* 1960s; therefore early climate estimates are less robust than the southern study sites (McKenney *et al*., 2006). An assessment of the model's bias and accuracy highlighted its strong predictive capacity since resultant errors were similar to the initial instrument measurement error (Hutchinson *et al*., 2009). Temperature is more reliably estimated than precipitation with the respective average absolute errors of *ca*. 1 to 1.5 °C compared with 20 - 40% (McKenney *et al*., 2006).

4.4.1 Climatic trends across the study transect

Annual trends of average monthly temperatures from 1901 to 2010 are similar across all sites with average temperatures generally decreasing with increasing latitude and longitude (Figure 4.2; Table 4.1). The most southerly site (SCH10) experiences the largest annual temperature range, with summer temperatures *ca.* 4 °C higher than other sites. VDB12 has the mildest winters, *ca.* 3 °C higher than the other sites. The growing season begins earliest in the year at SCH10, whilst it is most extended at VDB12, reflecting the less extreme temperature range at this site. This may be of importance when considering peatland surface conditions at VDB12 since climatic conditions over a larger proportion of the year will contribute to the vegetation assemblage compared with the other sites.

Modelled average precipitation data show less consistent patterns among sites than temperature: June levels of precipitation are comparable across all four sites; however, the trends diverge during the winter and spring months, particularly in March and April (Figure 4.3; Table 4.1). The overall annual precipitation patterns of VDB12 and FBB12 are similar with peak rainfall occurring in November and decreasing until July (excluding a small fluctuation to wetter conditions in March). SCH10 receives the lowest average annual rainfall and follows a similar annual average precipitation trend to those of

VDB12 and FBB12; however, the driest period occurs later in August and the spring increase in precipitation is larger. Since winter rainfall is low at SCH10, the peatland water table may be lower at the start of the growing season than the more northerly sites. Precipitation trends at JRB12 differ from the other sites since the driest month occurs earlier in April and the summer is generally wetter. From 1971 to 2000, JRB12 had greater snow cover than all other sites: the amount of snow that remained on the ground between October to April was double that of FBB12 and almost an order of magnitude higher than VDB12 and SCH10 (Table 4.1). The additional snow cover could have an insulating effect on the peatland (e.g. Zhang, 2005).

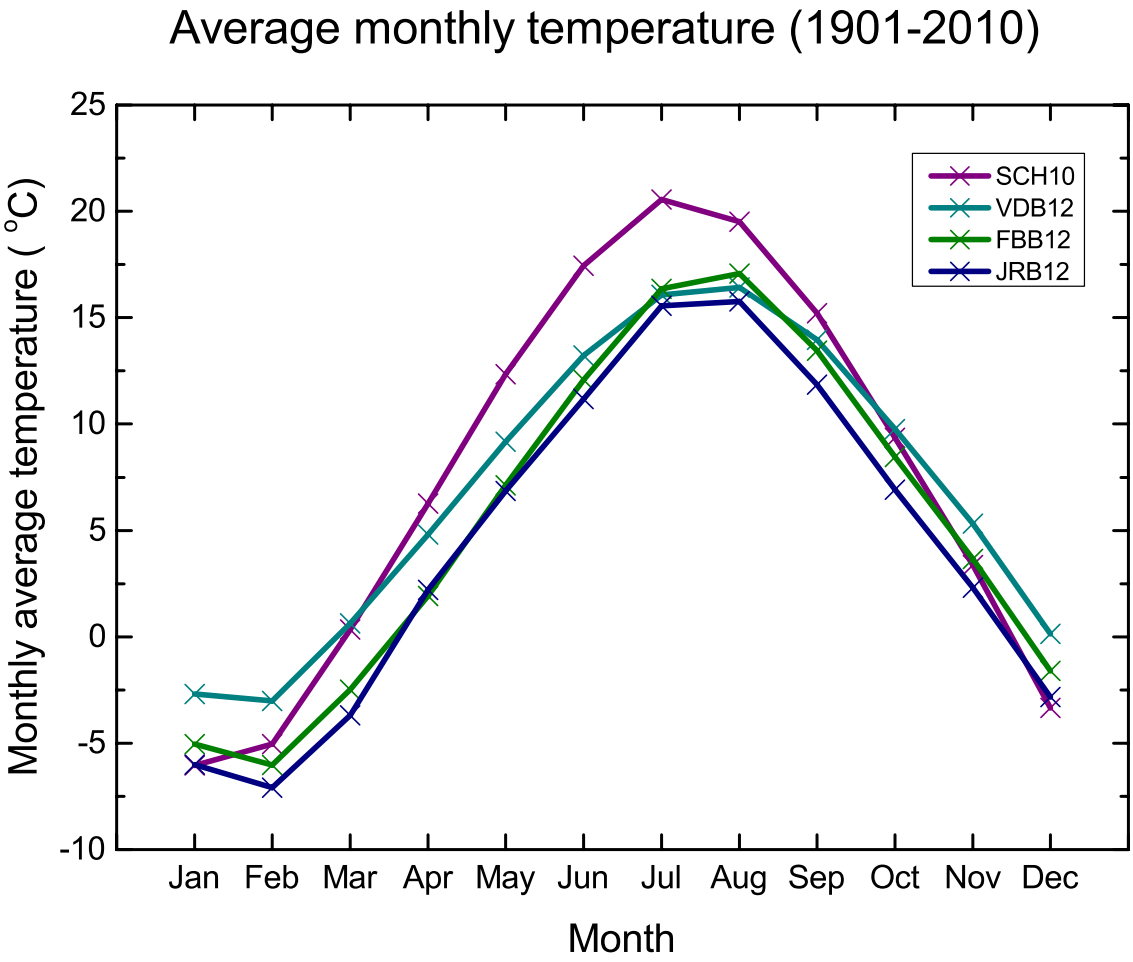

Figure 4.2 ANUSPIN modelled average monthly temperature by site

The monthly climate moisture index (*sensu* Hogg, 1997) was calculated by subtracting modelled potential evapotranspiration from precipitation. This indicates the amount of available moisture (or effective precipitation) at each

site, which controls the height of the peatland water tables (Charman *et al.*, 2009). The summer moisture deficit is attributed as the main driver of surface peatland conditions (Charman *et al.*, 2004, 2007); however, it is also useful to note antecedent conditions that may influence the rate and extent of water table change at each site.

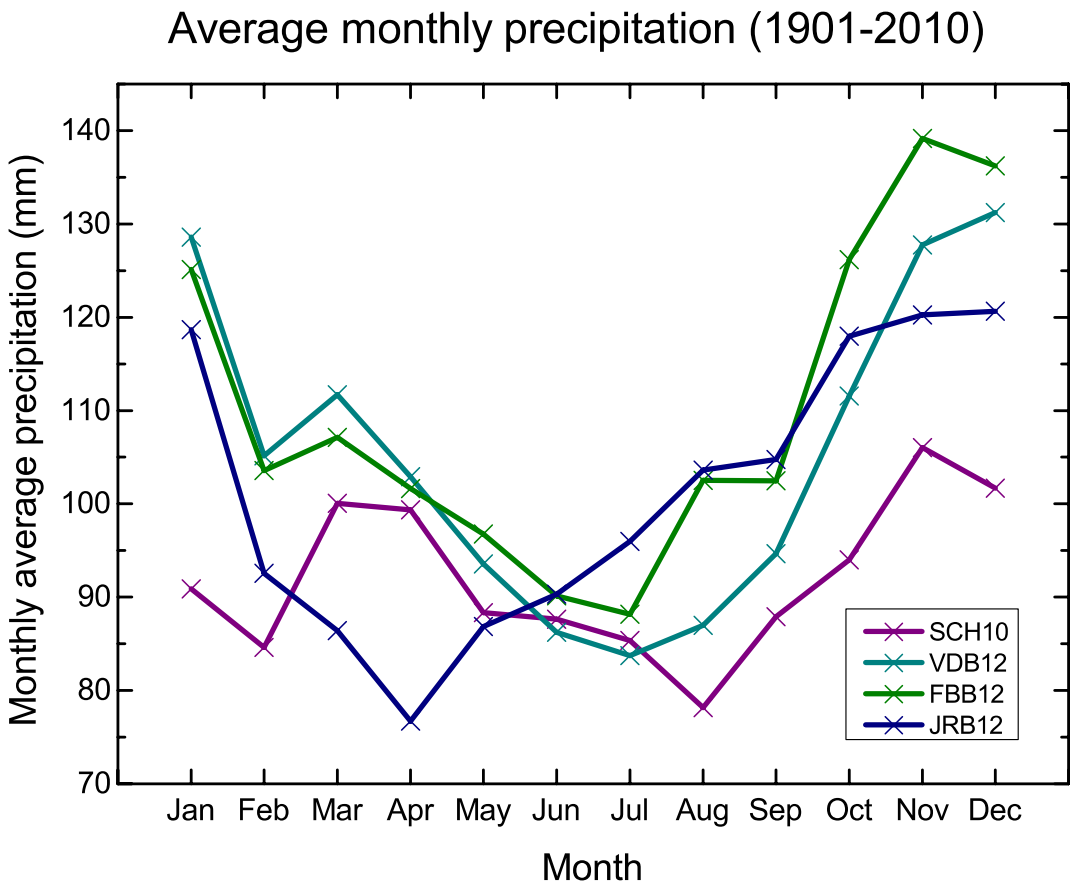

Figure 4.3 ANUSPIN modelled average monthly precipitation by site

Average available summer moisture increases with increasing latitude and longitude (Figure 4.4; Table 4.1). SCH10 is the only site to experience a summer moisture deficit, although all sites experience a reduction in summer available moisture that will lower water tables relative to the preceding months. Spring, autumn and winter averages of effective precipitation increase with increasing latitude and longitude across the three most southern sites.

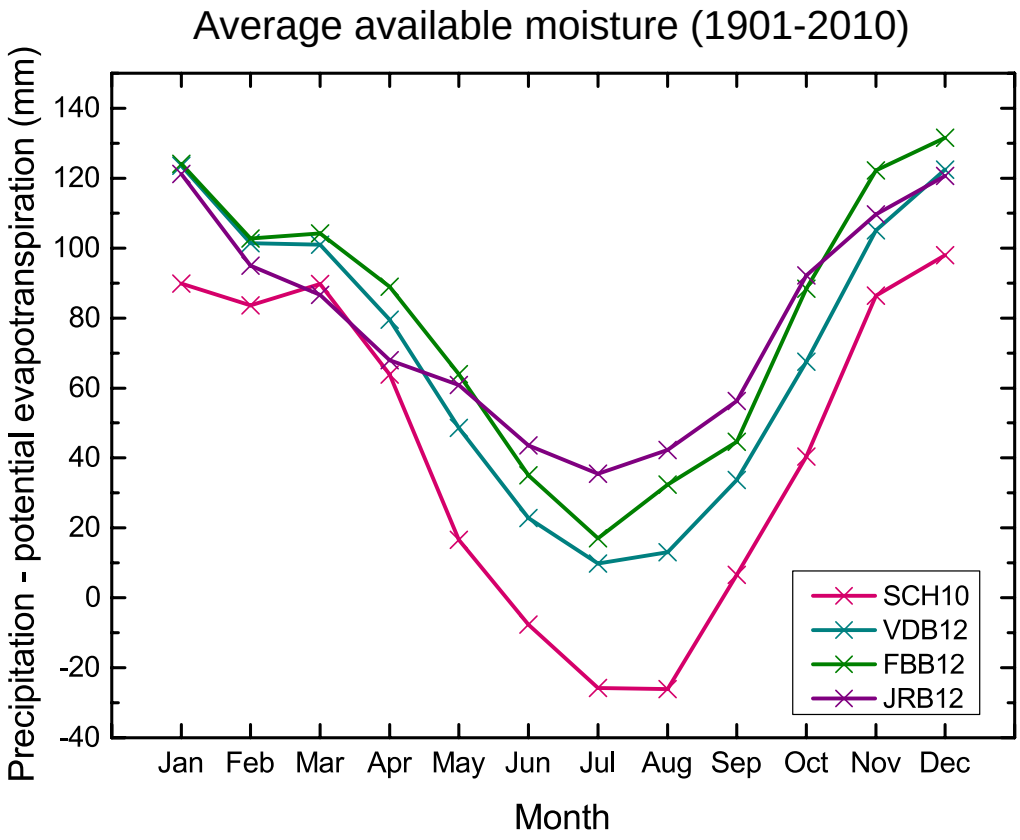

Figure 4.4 ANUSPIN modelled average monthly available moisture by site

Table 4.1 Summary of the climatic parameters from 1901 to 2010 Unless denoted with * which represents 1971-2000 or ^ which represents 1961-1990.

Climate variable	SCH10	VDB12	FBB12	JRB12
Average annual precipitation (mm)	1104	1264	1319	1215
Driest month (mm)	August (78.2)	July (83.8)	July (88.2)	April (76.7)
Wettest month (mm)	November (106)	December (131.2)	November (139.2)	December (120.6)
Average annual temperature (˚C)	7.49	6.98	5.41	4.42
Warmest month (˚C)	July (20.6)	August (16.4)	August (17.1)	August (15.8)
Coolest month (˚C)	January (-6.1)	February (-3)	February (-6)	February (-7.1)
Average summer (JJA) available moisture (mm)	-19.8	15.2	28.1	40.4
Start of growing season	Mid April	Late April	May	May
Length of growing season (days)	211	226	202	195
Snow depth Oct to Apr* (cm)	2.03	2.07	9.64	18.31
Solar radiation (JJA; (min/m^2/day)	20.3	19.9	19	18.4
Average daily sun hours ^	4.92	4.94	4.78	4.07

4.5 Saco Heath, Maine

Saco Heath is located in York, Maine, northeastern USA (43°33'05'' N; 70°2'03"W), at the current southern most limit of domed boreal peat growth. The peatland is located 44 m above sea level and its longest axis currently spans *ca.* 2 km (Figure 4.5). The formation of the peatland occurred during the infilling of two adjacent ponds. The Nature Conservancy protects the peatland as a 'Focus Area of Statewide Ecological Significance' owing to the presence of the rare Atlantic White Cedar and Pitch Pine Bog and the endangered Hessel's hairstreak butterfly. A boardwalk has been constructed through the site; however, the peatland is suitably undisturbed at the coring location. Members of NERC-PRECIP obtained the main research core (SCH10; 3.7 m long).

Figure 4.5 Aerial photograph of SCH10 (Google Earth, imagery date 19/9/2013). White star indicates coring location.

The current peatland vegetation community includes *Rhododendron groenlandicum, Kalmia angustifolia, Kalmia polifolia, Chamaedaphne calyculata, Gaylussacia dumosa* and *Sphagnum* section *Acutifolia.* The average annual temperature of the site is 7.49 ˚C and the average annual precipitation is 1104 mm (Section 4.4; Table 4.1). High potential evapotranspiration and low precipitation occurs during the months of June – August generating a summer water deficit that peaks at -26 mm (Figure 4.6).

Although these dry conditions will lower the water table and have implications for physical and biological functioning, spring conditions are wet (available moisture is comparable to the more northern sites; 866 mm), which may delay the peatland's responsiveness to the deficit.

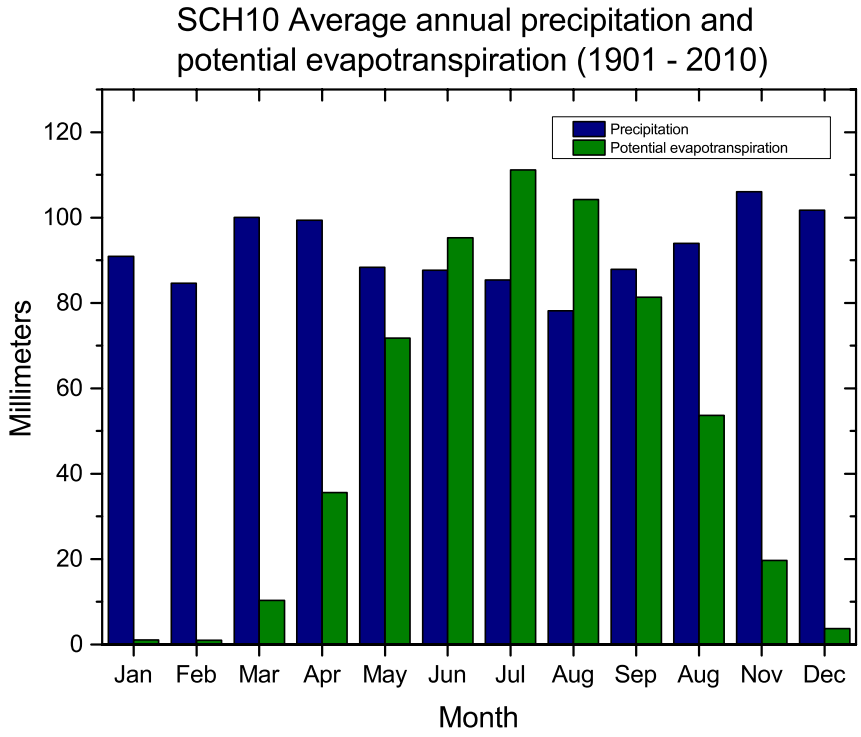

Figure 4.6 ANUSPIN modelled average annual precipitation (blue) and potential evapotranspiration (green) by month for SCH10

There is one identified published study from Saco Heath by Clifford and Booth (2013). Within this published study, testate amoebae and charcoal records were obtained from a core at the edge of the peatland to investigate the relationship between drought and fire history. A large visible charcoal band was located alongside a missing section of peat *ca.* 1500 - 580 years BP, suggesting that the peatland burned during a drought period. The study also concluded that fires occurred in the absence of droughts after the period of European land clearances *ca.* 150 cal yr BP. The SCH10 core used in this thesis was taken from a more central location than the published study; therefore, it is possible that the fire had a reduced direct effect on the peat stratigraphy in the more open region of the bog. The effect of the fire is discussed further in Section 6.6.

4.6 Villagedale Bog, Nova Scotia

Villagedale Bog is located in western Shelburne Country on the south shore of Nova Scotia, 8 m above sea level and 1 km from the coast (Figure 4.7). The longest axis of the peatland is 1.5 km, with spruce and pine trees fringing the peatland edge. The site is remote with no evidence of disturbance aside from a few peripheral quad bike tracks.

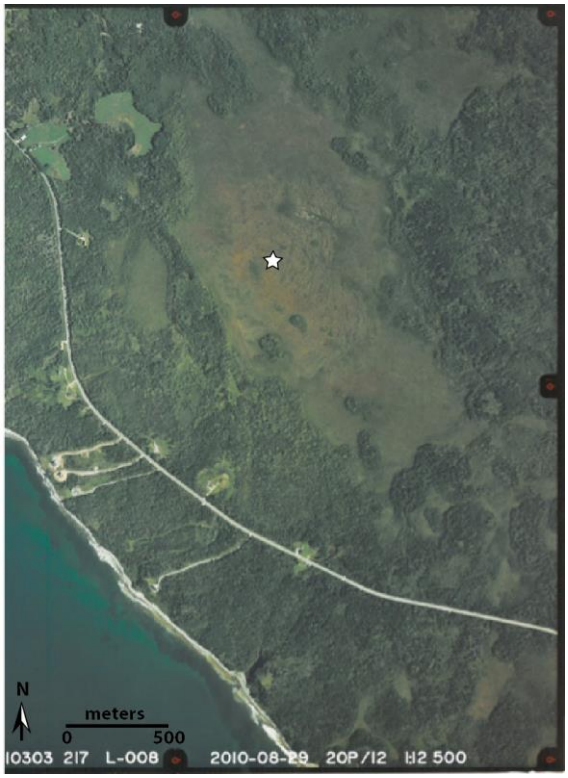

Figure 4.7 Aerial photography of VDB12 from Map Library, Service Nova Scotia and Municipal Relations (2010). White star indicates coring location.

The lawn core (Figure 4.8) was obtained in May 2012 at 43˚31'09" N; 65˚31'54" W following the guidance of stratigraphic transects completed by members of the Palaeoenvironmental Laboratory at the University of Southampton in 2008. Current surface vegetation includes: *Sarracenia purpurea*, *Myrica gale*, *Rhododendron groenlandicum*, *Larix laricina*, *Cladonia* spp*, Lycopodium* spp*, Eriophorum* spp and *Sphagnum* sect. *Acutifolia* (Figure 4.9). Therefore, the vegetation indicates that VDB12 a fairly dry site with small pools restricted to its centre. There is no known published information about Villagedale Bog.

Figure 4.8 Section of core (100 – 150 cm) obtained from a lawn habitat. *Sphagnum*-dominated peat with obvious stratigraphic changes in the degree of humification (as represented by colour change).

The ANUSPIN modelled average annual temperature of the site is 6.98 ˚C and, on average, 1264 mm of precipitation is received annually (Section 4.4.1; Table 4.1). Whilst there is no period of moisture deficit, the available moisture does decrease in the summer with the lowest values of 10 mm occurring in July. The precipitation reduction and potential evapotranspiration increase (Figure 4.10) will lower the water table over the summer relative to the wet conditions at the start of the growing season.

Figure 4.9 Surface characteristcis of VDB12 at the coring location. Peatland is dry and with abundant shrubs and patches of *Cladonia* (white areas). Wetter lawn conditions are restricted to the center of the peatland.

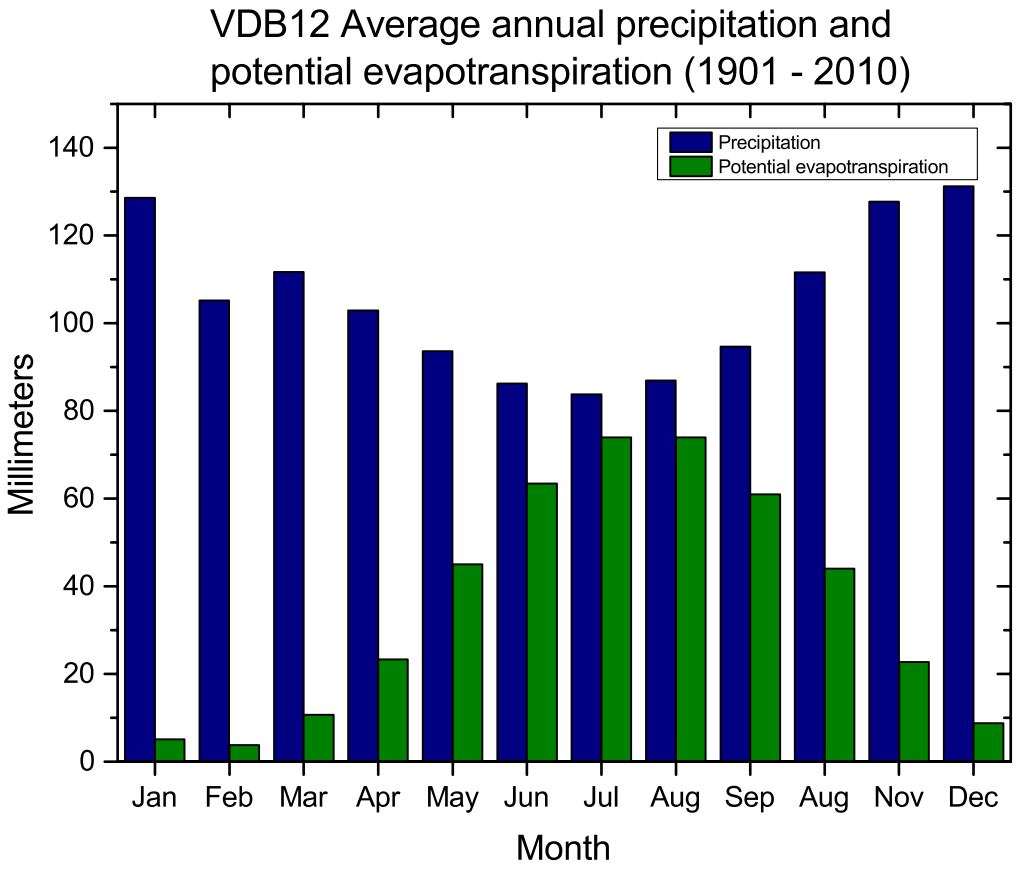

Figure 4.10 ANUSPIN modelled rates of precipiation and potential evapotranspiration (1901-2010) for VDB12

4.7 Framboise Bog, Nova Scotia

Framboise Bog (FBB12) is plateau peatland located in Richmond Country in the northeast of Nova Scotia. At an elevation of 90 m, FBB12 is the most upland peatland in the transect of sites. The longest axis of the peatland is *ca*. 0.75 km, surrounded by dense woodland with no evidence of disturbance (Figure 4.11). The site has a large pool complex on the main dome with a secondary smaller peatland extending from the northeastern edge.

Figure 4.11 Aerial photography of FBB12 from Map Library, Service Nova Scotia and Municipal Relations (2008). White star indicates coring location.

The lawn core (Figure 4.12) was obtained in May 2012 at 45˚43'14 N; 60˚33'09" W following the guidance of previous investigations completed by members of the NERC-PRECIP group in 2010. This site was not used within the NERC-PRECIP project as at 370 cm deep, it was deemed too shallow to contain a full Holocene record. Current vegetation includes *Vaccinium oxycoccos, Vaccinium macrocarpon, Ondontoshizma, Cephalozia comnivens, Eriophorum* species, *Cladonia* spp, *Sphagnum* sect. *Acutifolia* and sect. *Cuspidatum* (Figure 4.13). No previous studies of this site have been identified.

Figure 4.12 Section of FBB12 core (50- 100 cm) obtained from a lawn habitat. *Sphagnum* dominated peat with obvious alternating stratigraphic changes in the degree of humification (as represented by colour changes).

The ANUSPIN modelled average annual temperature at Framboise Bog is 6.85 ˚C and the average annual amount of precipitation received is 1539 mm (Section 4.4.1; Table 4.1), making it the wettest location in the transect of sites. Precipitation always exceeds potential evapotranspiration (Figure 4.14); therefore, there is no water deficit. Minimum levels of available moisture briefly occur in July with a difference of 17 mm.

Figure 4.13 Surface characteristics of FBB12 at the coring location. Large pool systems are common, divided by areas of *Eriophorum* and patches of *Cladonia*. The peatland is surrounded by dense woodland.

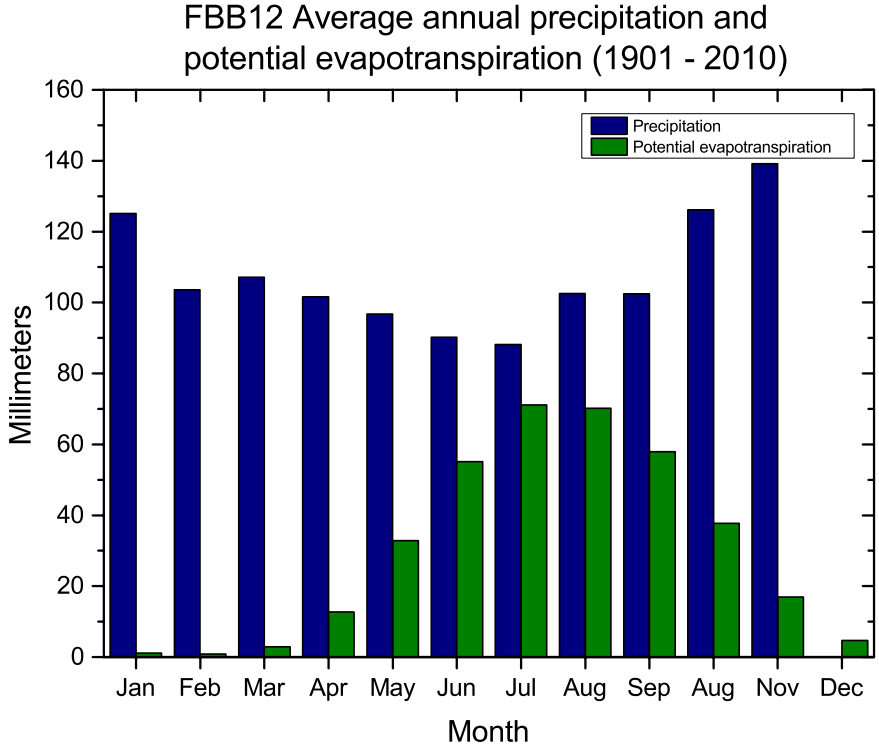

Figure 4.14 ANUSPIN modelled rates of precipiation and potential evapotranspiration (1901-2010) for FBB12

4.8 Jeffrey's Bog, Newfoundland

Access to the interior of Newfoundland is limited by the existing road network; therefore, possible site locations of plateau peatlands are restricted to the northern peninsula, the north east of the main island and the south west. Two peatland records have been obtained from Newfoundland: Nordan's Pond Bog (Hughes *et al.*, 2006) on the north east of the main island, and Burnt Village Bog (NERC-PRECIP) in the northern peninsula (Figure 4.1). Therefore, a core was obtained from the southwest coast of the island to complement the distributions of existing records.

Two peatlands were initially investigated, located close to the southwest shore of Newfoundland (47° 50' 31" N; 59° 09' 36" W and 47° 49' 24" N 59° 42' 40" W). These sites met aerial photographic requirements; however, they were less than 1 m deep. The third peatland to be investigated, named Jeffrey's Bog, was 3.7 m deep and therefore met the requirements of this study (outlined in Section 4.2).

Jeffrey's Bog (JRBB12) is located in Stephenville on the southwest coast of Newfoundland at an elevation of 37 m, 2.7 km from the shore. It is a plateau bog and the length of the longest axis is *ca*. 0.75 km. The peatland is surrounded by small forested areas to the north, east and west; however, the full peatland complex extends to the south, increasing its exposure relative to the other sites (Figure 4.15). It is a fairly dry site with small pools in the centre of the plateau.

The lawn peat core (Figure 4.16) was obtained in May 2012 at 48°12'46" N; 58°49'06" W. Current common surface vegetation includes *Kalmia angustifolia*, *Kalmia polifolia*, *Vaccinium oxycoccos*, *Rhododendron groenlandicum, Cladonia spp*, *Eriophorum* species, *Sphagnum* sect. *Sphagnum* and sect. *Acutifolia* (Figure 4.17). No previous studies of this site have been identified.

The ANUSPIN modelled average annual temperature at Jeffrey's bog is 6.03 °C and annual precipitation rate is 1065 mm, making it the coldest, driest location in the transect (Section 4.4.1; Table 4.1). There is no modelled average water deficit at Jeffrey's Bog and this site has the largest average

summer difference between precipitation and evapotranspiration (Figure 4.18) of all peatlands with a minimum difference of 40 mm in July.

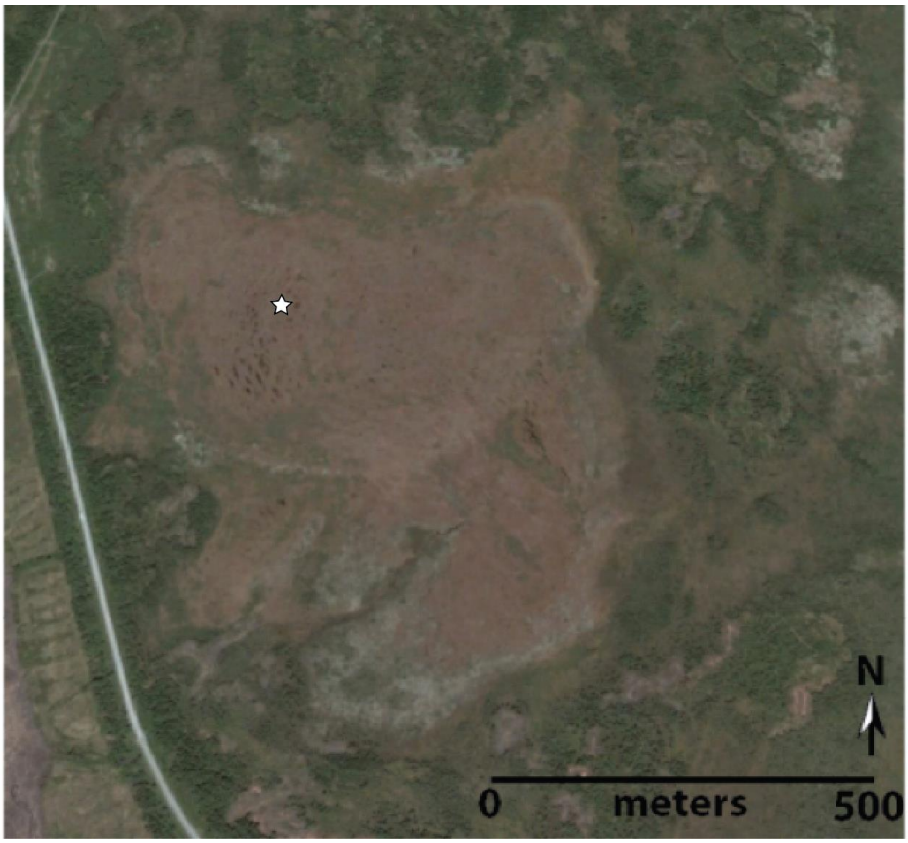

Figure 4.15 Aerial photograph of JRB12 (Google Earth, imagery date 17/7/2013). White star indicates coring location.

Figure 4.16 *Sphagnum* dominated core section (100-150 cm) with obvious stratigraphic changes in the degree of humification (as represented by colour changes).

Figure 4.17 Surface characteristics of JRB12 at the coring location. Pool present in the centre of the peatland with varying hummock topography.

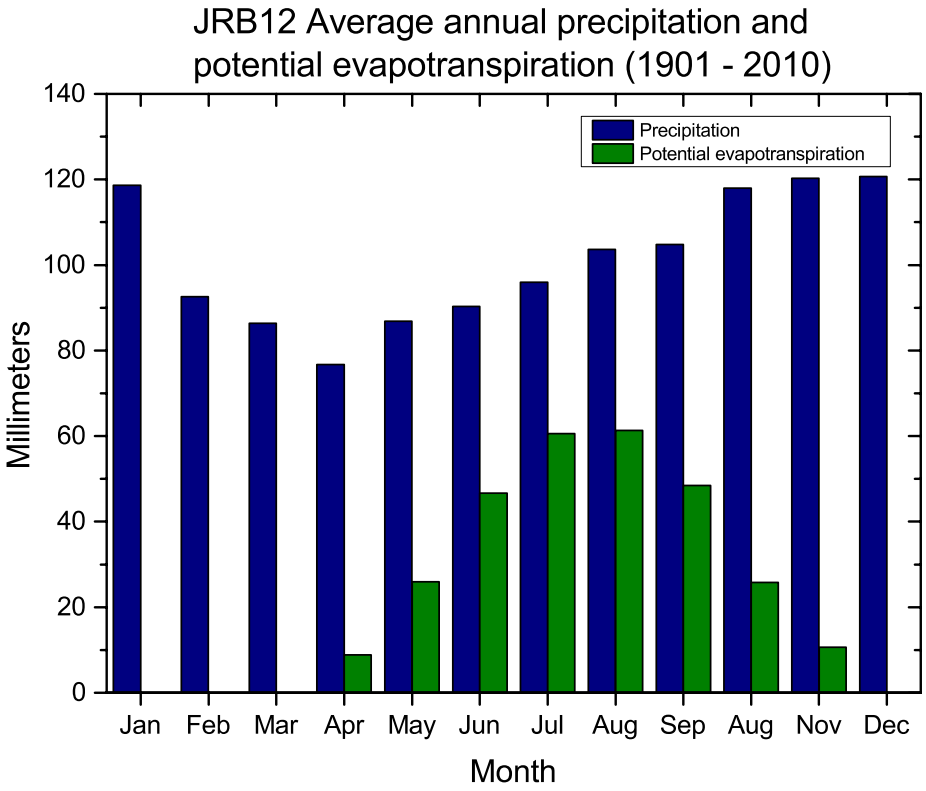

Figure 4.18 ANUSPIN modelled rates of precipiation and potential evapotranspiration (1901-2010) for JRB12.

Chapter 5: Chronology

5.1 Bayesian age-depth models

The age-depth models used within this thesis have been produced in 'Bacon', an open-source R package using Bayesian statistics to reconstruct accumulation histories for sedimentary archives (Blaauw and Christen, 2011). Bacon divides the core into vertical sections for which it estimates sedimentation times based on millions of Markov Chain Monte Carol (MCMC) iterations. The resultant age-depth models are therefore based on realistic sedimentation rates. The Bayesian approach of considering the stratigraphic ordering of the data whilst accounting for the radiocarbon age error distributions generates age-depth models with smaller uncertainties than those generated by classical age-depth modelling programs such as 'CLAM' (Blaauw, 2010). The self-adjusting MCMC algorithm of Bacon (Christen and Fox, 2010) is advantageous in comparison with other available Bayesian programs such as 'OXCAL' (Ramsey, 2008) and BChron (Haslett and Parnell, 2008), which require tuning and are more parameterised.

Chronologies are based on definitive tephra correlations (White River Ash eastern lobe (WRAe) and Mount St Helens Set W (MSH; Section 5.2)) and the results of 36 radiocarbon measurements obtained from successful NERC rangefinder and full radiocarbon applications (October, 2013 and April, 2014); the NERC MILLIPEAT project (NERC NE/1012915/1 and the NERC PRECIP project (NE/G020272/1; Figure 5.1 – 5.4).

The basal dates of the cores reveal that peat accumulation began during the Early Holocene at FBB12 (*ca.* 10126 cal yr BP), during the Mid Holocene at SCH10 and VDB12 (*ca.* 4826 and 6003 cal yr BP respectively), and during the Late Holocene at JRB12 (*ca.* 3393 cal yr BP). Efforts were made to obtain cores from similar aged peatlands by substituting depth for time to minimise stratigraphic changes associated with peat development; however, the accumulation rates of the study sites varied. JRB12, the youngest peatland was ombrotrophic during the last 2000 years of interest; therefore, developmental influences should be secondary to climatic control.

5.1.1 Age-depth model of Jeffrey's Bog (JRB12)

The chronology of JRB12 has been developed using nine calibrated radiocarbon measurements, the WRAe tephra and Mount St Helen's (Set W) tephra (Section 5.2). All ages fell in stratigraphical sequence with no age reversals or statistical outliers present (Figure 5.1; Table 5.1). The JRB12 Bayesian age-depth model indicates generally consistent peat accumulation across the majority of the 2000-year period of interest. The average peat accumulation rate was 8.7 yr cm^{-1} between 1700 - 0 cal yr BP and this decreased to 15.2 yr cm^{-1} between 2000 - 1720 cal yr BP. The reduced accumulation rate in the older peat is influenced by the radiocarbon measurement obtained from a depth of 232 cm, which has a calibrated age range predominantly older than the range suitable for the Bayesian age-depth model. There is insufficient evidence to reject the validity of this measurement: sufficient C content was extracted from the submitted sample (41.6 % by weight) to produce a robust radiocarbon measurement; the sample was composed of reliable above-ground *Sphagnum* stems growing *in-situ;* and the average accumulation rate of the period is within the *ca.* 10-20 yr cm^{-1} accumulation range typical of oceanic ombrotrophic peatland. The calibrated age range obtained from the radiocarbon measurement at 232 cm was therefore retained within the final JRB12 Bayesian age-depth model.

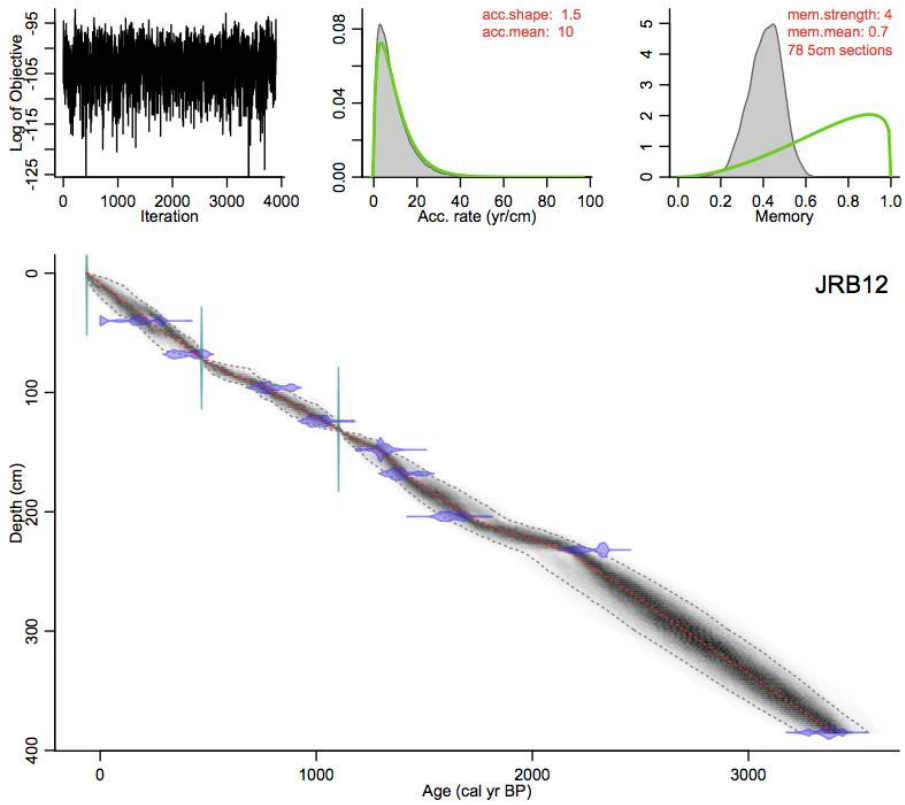

Figure 5.1 JRB12 Bayesian age-depth model
The accumulation rate of over the last 2000 years is the most consistent of all cores within this study. Calibrated ^{14}C dates are represented by transparent blue markers. Tephra horizons and the peatland surface are represented by transparent green markers. Darker grey lines on the age-depth model indicate more likely ages. Grey stippled lines show the 95% confidence intervals and the red curve represent the single 'best' model based on the weighted mean age for each depth.

Table 5.1 JRB12 radiocarbon data

Sample ID	Material	Depth (cm)	^{14}C uncalibrated age (BP)	$\delta^{13}C$ VPDB ‰ ± 0.1	2σ calibrated range (cal yr BP)	Weighted mean (cal yr BP)
SUERC55618	*Sphagnum*	40	193 ± 37	-26.7	135-305	224
SUERC55619	*Sphagnum*	68	365 ± 38	-27.4	343-513	453
SUERC55620	*Sphagnum*	96	873 ± 35	-28.2	686-876	762
SUERC55623	*Sphagnum*	124	1098 ± 35	-27.2	941-1131	1020
SUERC55624	*Sphagnum*	148	1384 ± 37	-28.4	1170-1344	1269
SUERC51073	*Sphagnum*	168	1496 ± 36	-28.8	1313-1545	1430
SUERC55625	*Sphagnum*	204	1715 ± 37	-27.5	1589-1855	1712
SUERC51077	*Sphagnum*	232	2276 ± 35	-28.2	2025-2335	2190
SUERC51078	Brown moss	385	3146 ± 37	-29.5	3252-3571	3401

5.1.2 Age-depth model of Framboise Bog (FBB12)

The chronology of FBB12 has been developed using eight calibrated radiocarbon measurements and the WRAe tephra (Section 5.2). All ages fell in stratigraphical sequence and no age reversals or statistical outliers were present (Figure 5.2; Table 5.2). The accumulation rate of FBB12 is variable throughout the last 2000 years. The average peat accumulation rate was 36 yr cm^{-1} between 2000 – 1700 cal years BP, before increasing to an average of 16.7 yr cm^{-1} between 1655 – 1000 cal yr BP. The slowest period of FBB12 peat growth occurred between 960 – 550 cal yr BP with an average accumulation rate of 44 yr cm^{-1}. This may reflect a period of overall peat growth rate reduction or it may mask a hiatus within peat accumulation; however, it not possible to distinguish between these two possibilities from the resolution of the available radiocarbon measurements. Peat accumulation rates increase to 14 yr cm^{-1} between 545 – 280 cal yr BP and 9.9 yr cm^{-1} between 280 – 0 cal yr BP.

The accumulation rate change between 2000 – 1000 cal yr BP is predominantly influenced by the radiocarbon measurement at 104 cm. Whilst the outer calibrated age limit of this measurement is compatible with the Bayesian age-depth model, the calibrated age range is predominantly younger than may be expected. This radiocarbon measurement at 104 cm was obtained from material containing 15% by weight C content, the smallest sample size measured within this thesis. Whilst the small sample size may be contributing to the younger than excepted age distribution, the calibrated age range of 104 cm is not a statistical outlier and the variation in accumulation rate in question is characteristic of the generally fluctuating peat growth of FBB12. Therefore, there is insufficient evidence to support the omission of the 104 cm radiocarbon measurement from the final Bayesian age-depth model.

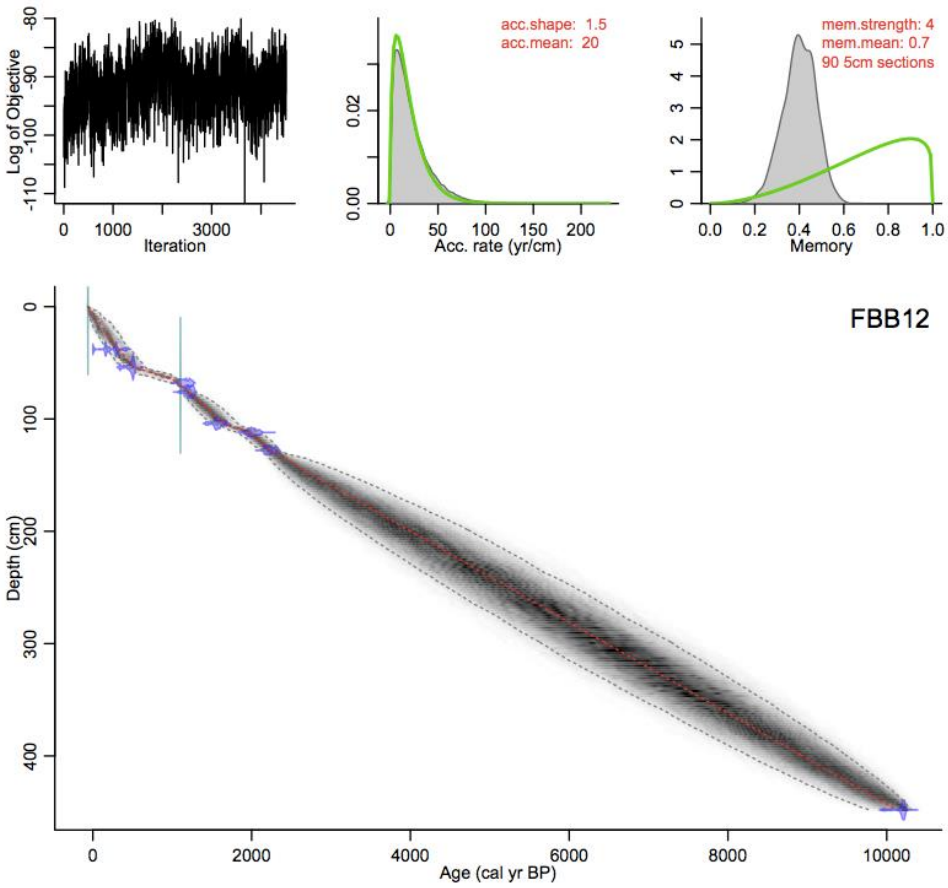

Figure 5.2 FBB12 Bayesian age-depth model
Modelled accumulation rates vary over the last 2000 years. Calibrated ^{14}C dates are represented by transparent blue markers. Tephra horizons and the peatland surface are represented by transparent green markers. Darker grey lines on the age-depth model indicate more likely ages. Grey stippled lines show the 95% confidence intervals and the red curve represent the single 'best' model based on the weighted mean age for each depth.

Table 5.2 FBB12 radiocarbon data

Sample ID	Material	Depth (cm)	^{14}C uncalibrated age (BP)	$\delta^{13}C$ VPDB ‰ ± 0.1	2σ calibrated range (cal yr BP)	Weighted mean (cal yr BP)
SUERC55610	*Sphagnum*	38	231 ± 37	-25.6	190-438	324
SUERC55613	*Sphagnum*	54	441 ± 37	n/a	446-640	522
SUERC55614	*Sphagnum*	68	1228 ± 35	-26.5	969-1185	1085
SUERC55615	*Sphagnum*	76	1280 ± 35	-26.1	1119-1290	1225
SUERC51071	*Sphagnum*	104	1662 ± 37	n/a	1456-1776	1609
SUERC55616	*Sphagnum*	112	2045 ± 37	-26.3	1819-2067	1951
SUERC51072	*Sphagnum*	128	2232 ± 38	25.2	2074 - 2336	2220
SUERC51073	*Bulk Peat*	448	9026 ± 41	25.9	9773 - 10312	10126

5.1.3 Age-depth model of Villagedale Bog (VDB12)

The chronology of VDB12 has been developed using eight calibrated radiocarbon measurements and the WRAe tephra (Section 5.2). All ages fell in stratigraphical sequence with no age reversals or statistical outliers present (Figure 5.3; Table 5.3). The Bayesian age-depth model reveals consistent peat accumulation across the depth of VDB12. Average accumulation rates were typical of oceanic ombrotrophic peatlands: the fastest peat accumulation occurred between *ca.* 1570 – 1100 and 390 – 0 cal yr BP (8.6 and 9.2 yr cm^{-1} respectively), whilst peat accumulated around 14.1 yr cm^{-1} between *ca.* 1090 - 400 cal yr BP and 16.1 yr cm^{-1} between 2000 - 1580 cal yr BP.

The radiocarbon measurements obtained from 152 cm and 132 cm have overlapping 2σ calibrated age ranges suggesting that the 20 cm of peat accumulation occurred within a smaller than expected amount of time, assuming average ombrotrophic peat accumulation rates. Both samples contained sufficient amounts of C (40% and 63% C content by weight, respectively); therefore, small sample sizes cannot be attributed as a limiting factor in the quality of radiocarbon measurements. The calibrated age range of the sample obtained from 152 cm appears to be younger than expected when all of the other chronological information incorporated within the Bayesian model is considered. Whilst this presents the possibility that some modern carbon has been incorporated into the sample during the processing stages prior to the radiocarbon measurement, the calibrated age range does encompass realistic natural fluctuations in peat accumulation rates and it has not been identified by the model an a statistical outlier. Therefore, there is insufficient evidence to omit the 152 cm radiocarbon measurement from the final Bayesian age-depth model.

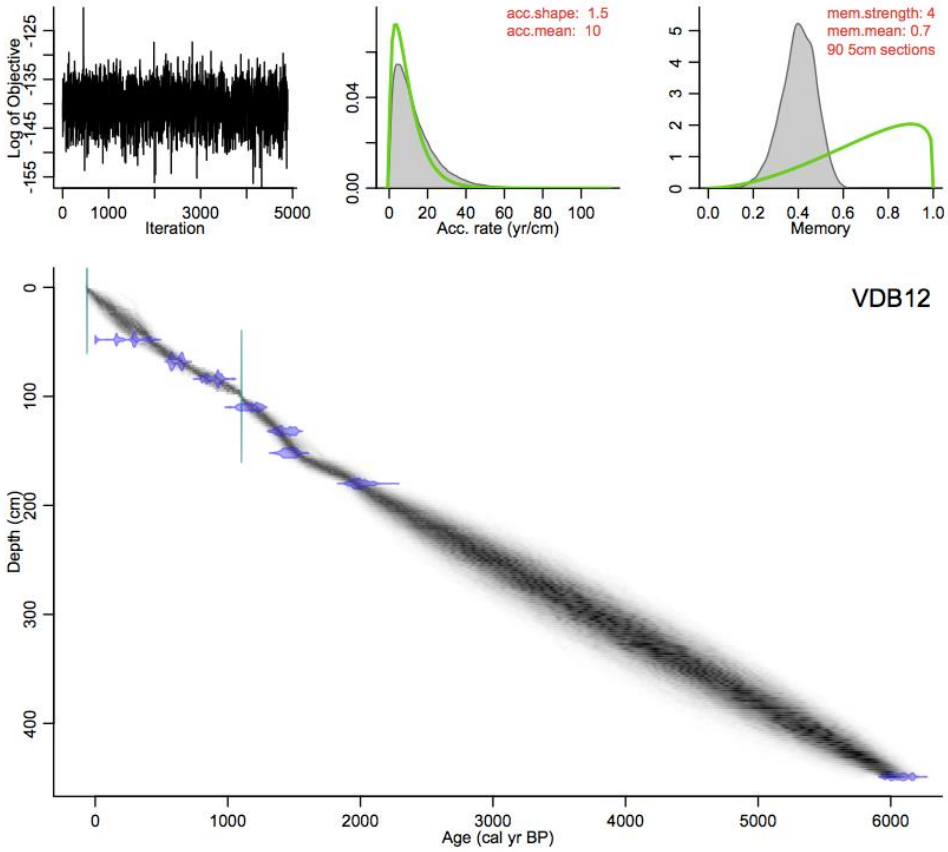

Figure 5.3 VDB12 Bayesian age-depth model
Modelled accumulation rates are generally consistent over the last 2000 years. Calibrated ^{14}C dates are represented by transparent blue markers. Tephra horizons and the peatland surface are represented by transparent green markers. Darker grey lines on the age-depth model indicate more likely ages. Grey stippled lines show the 95% confidence intervals and the red curve represent the single 'best' model based on the weighted mean age for each depth.

Table 5.3 VDB12 radiocarbon data

Sample ID	Material	Depth (cm)	^{14}C uncalibrated age (BP)	$\delta^{13}C$ VPDB ‰ ± 0.1	2σ calibrated range (cal yr BP)	Weighted mean (cal yr BP)
SUERC51063	*Sphagnum*	48	243 ± 37	-24.7	272-476	379
SUERC51066	*Sphagnum*	68	655 ± 37	-23.7	539-687	618
SUERC51067	*Sphagnum*	84	997 ± 35	-26.6	757-959	857
SUERC55608	*Sphagnum*	110	1234 ± 37	-28.1	1056-1261	1158
SUERC51068	*Sphagnum*	132	1529 ± 38	-27.8	1310-1541	1428
SUERC55609	*Sphagnum*	152	1572 ± 37	-28.3	1449-1687	1539
SUERC51069	*Sphagnum*	180	2034 ± 36	-28.6	1831-2120	1977
SUERC56131	Bulk peat	449	5278 ± 40	-25.8	5744-6177	6004

5.1.4 Age-depth model of Saco Heath (SCH10)

The chronology of SCH10 has been developed using ten calibrated radiocarbon measurements and the WRAe tephra (Section 5.2). All ages fell in stratigraphical sequence with no age reversals or statistical outliers present (Figure 5.4; Table 5.4). All calibrated radiocarbon age ranges have been incorporated within the final Bayesian age-depth model.

The most striking feature of the SCH10 Bayesian age-depth model is the hiatus in peat growth *ca*. 950 – 650 cal yr BP. The hiatus within SCH10 has been defined by the placement of radiocarbon measurements, which were guided by the presence of a fire event reported in published results from a core that had been obtained from the edge of Saco Heath (Clifford and Booth, 2012). The SCH10 macrofossil assemblage supports the hypothesis that the hiatus in the more central coring location used within this thesis originated from a fire owing to the presence of charcoal and the sequence of vegetation succession (Section 6.6.1).

The modelled average peat accumulation rate between *ca*. 2000 - 1510 cal yr BP was 16.4 yr $cm^{-1,}$ which is within the typical accumulation range of oceanic peatlands. The average accumulation rate increased to 7.74 yr cm^{-1} between *ca.* 1500 – 0 cal yr BP with the exception of the aforementioned hiatus.

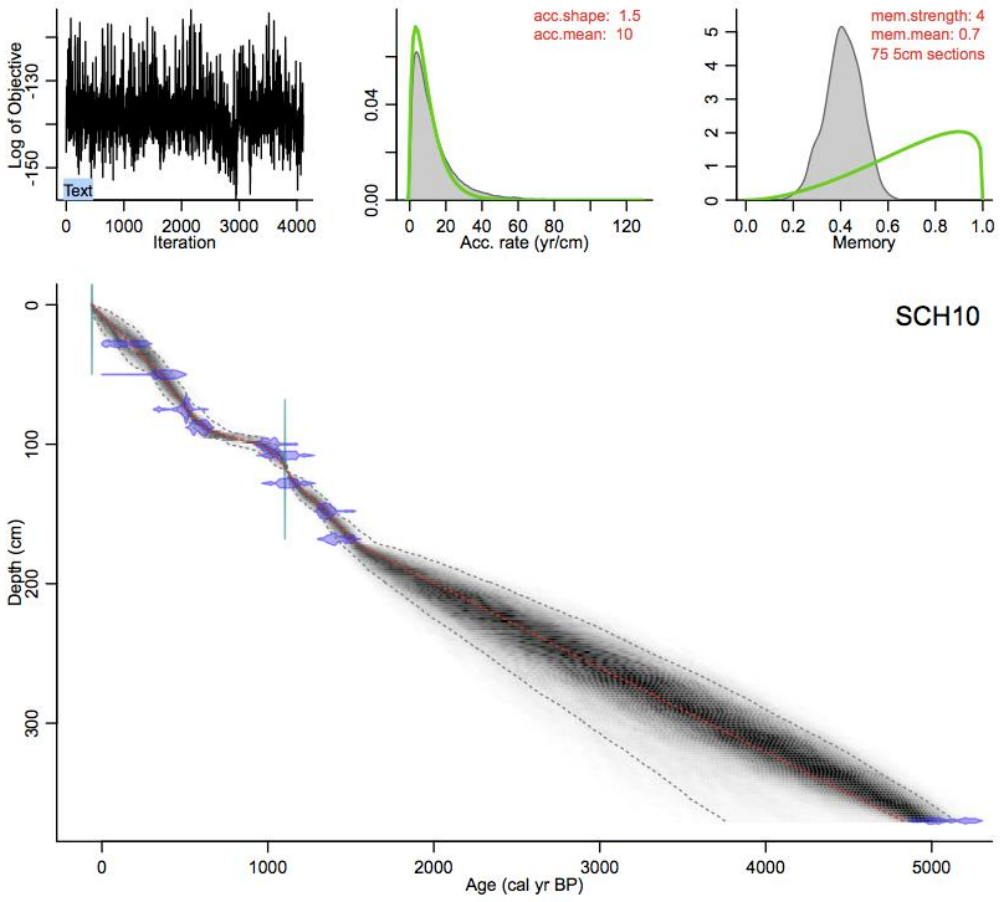

Figure 5.4 SCH10 Bayesian age-depth model
Modelled accumulation rates vary over the last 2000 years. Calibrated ^{14}C dates are represented by transparent blue markers. Tephra horizons and the peatland surface are represented by transparent green markers. Darker grey lines on the age-depth model indicate more likely ages. Grey stippled lines show the 95% confidence intervals and the red curve represent the single 'best' model based on the weighted mean age for each depth.

Table 5.4 SCH10 radiocarbon data

Sample ID	Material	Depth (cm)	^{14}C uncalibrated age (BP)	$\delta^{13}C$ VPDB ‰ ± 0.1	2σ calibrated range (cal yr BP)	Weighted mean (cal yr BP)
SUERC46930	*Sphagnum*	28	130 ± 37	-31.6	61-267	166
SUERC46931	*Sphagnum*	50	326 ± 37	-28.8	292-434	354
SUERC46932	*Sphagnum*	75	449 ± 37	-27.5	457-565	512
SUERC51060	*Sphagnum*	88	588 ± 37	-27.9	560-674	623
SUERC46936	*Sphagnum*	100	1096 ± 35	-28.7	792-1037	951
SUERC51061	*Sphagnum*	108	1175 ± 41	-28.9	949-1117	1033
SUERC46937	*Sphagnum*	128	1199 ± 37	-28.3	1080-1262	1168
SUERC55607	*Sphagnum*	148	1462 ± 35	-29.3	1288-1410	1347
SUERC51062	*Sphagnum*	168	1525 ± 37	-29.1	1376-1670	1495
SUERC32443	Bulk peat	370	4442 ± 38	-27.5	3742-5152	4828

5.2 Crypto-tephrostratigraphies

The tephrostratigraphic data, containing the aforementioned WRAe and MSH correlations, are presented below in the manuscript format for submission to *Quaternary Science Reviews* entitled *'A mid to late Holocene cryptotephra framework from eastern North America'*. The paper confirms the prevalence of Alaskan and Pacific Northwestern tephras in eastern North America whilst identifying others that may originate from new source regions. The age-depth models within the manuscript differ from those in Figure 5.1 – 5.4 since they omit all tephras to allow for ash correlations to be supported by independent chronologies. Whilst the WRAe and MSH tephras are included in the final chronologies (Figure 5.1 – 5.4) the new potential tephras have been omitted since the age uncertainties are greater than the chronological uncertainty generated by the radiocarbon age-depth models.

Authorship list: Helen Mackay, Paul D.M. Hughes, Britta, J.L. Jensen, Pete G. Langdon, Sean D.F. Pyne-O'Donnell, Gill Plunkett, Duane G. Froese, Sarah Coulter, James E. Gardner

Author contributions: Helen Mackay, Paul Hughes and Pete Langdon (University of Southampton) conceived and designed the study. Helen Mackay performed the research, analysed the cryptotephra with guidance from Sean Pyne-O'Donnell (Queen's University Belfast) and wrote the paper with editorial input from the co-authors. North American and Mexican proximal tephra analyses were performed by Britta Jensen (University of Alberta) on reference material provided by Duane Froese (University of Alberta) and James Gardner (The University of Texas at Austin; respectively). Kamchatkan analyses were performed by Gill Plunkett (Queen's University Belfast) and Sarah Coulter (Omagh Minerals Ltd). Data analysis were completed by Helen Mackay under the guidance of Britta Jensen.

Keywords: Tephra; Cryptotephra; Volcanic ash; Peatlands; Late Holocene; North America

5.2.1 Abstract

Holocene cryptotephras of Alaskan and Pacific Northwestern origin have recently been detected *ca.* 7,000 km away on the east coast of North America. This study extends the emerging North American tephrochronological framework by reporting seventeen cryptotephra horizons from four new peatlands. All detected tephras were deposited during the late Holocene, with no horizons present in the peat sediment between *ca.* 3000 - 5000 years ago. The prevalence of the Alaskan White River Ash eastern lobe (AD 847 ±1) is confirmed across the eastern seaboard from Newfoundland to Maine and a regional depositional pattern from Mount St Helens Set W (AD 1479-1482) is presented. The first occurrences of four additional cryptotephras in eastern North America are described, three of which may originate from source regions in Mexico, Russia and Japan. The possibility of such tephras reaching eastern North America presents the opportunity to link palaeo-archives from the tropics and eastern Asia with those from the western Atlantic seaboard, aiding inter-regional comparisons of proxy-climatic records.

5.2.2 Introduction

Precise palaeoclimatic comparisons between sites and regions are essential for understanding Earth systems and past climate dynamics. However, inter-site correlation is often limited by poor chronological control. Tephrochronology provides an age-equivalent dating method by using volcanic ash layers with unique geochemical signatures as time-specific marker horizons (isochrons) to connect and synchronise archives (e.g. Lowe, 2011; Alloway *et al*., 2013). These isochrons are used to create high-resolution records of palaeoenvironmental or archaeological events (e.g. Hall *et al*., 1993; Plunkett and Swindles, 2008; Lowe *et al*., 2012; Lane *et al*., 2013a, b). An air-fall ash layer from a volcanic eruption can be regarded as having been deposited instantaneously in geological time and can thus adopt the eruption's age wherever it is found as a primary, unworked horizon. If the eruption history is unknown or poorly constrained then archives can still be correlated if the same tephra horizons are present and these fixed tie-points can be used to create a common timescale (Lowe, 2011).

Investigations of far-travelled microscopic volcanic glass shards (cryptotephra – with dimensions <~125 μm; *sensu* Lowe & Hunt, 2001) in sediments allow for the detection of previously unrecognised ash horizons and sometimes unknown eruptions. These cryptotephras provide the opportunity to obtain precise chronologies in areas that were thought to be outside the range of tephrochronology, thus greatly expanding the dating framework and increasing the number of regions that can be linked together. Cryptotephra studies originally focused on Icelandic tephras in Western Europe, but the potential for North American cryptotephra studies is rapidly emerging (Payne *et al*., 2008; Pyne-O'Donnell *et al*., 2012).

The first crypto-tephrostratigraphy for the eastern seaboard of North America in Newfoundland was recently developed from one peatland, Nordan's Pond Bog (Pyne-O'Donnell *et al*., 2012). Seven tephras in this *ca*. 9,000-yr-long sequence were correlated to sources in Alaska and the Cascade Range, four of which occurred during the late Holocene: tephra from Mount St Helens (MSH) set W, AD 1479-1482 (Yamaguchi *et al*., 1985; Fiacco *et al*., 1993; Yamaguchi and Hoblitt, 1995); White River Ash, eastern lobe (WRAe), ~AD 847 ± 1 (Jensen *et al*., 2014a); Newberry Pumice *ca*. 1460 cal yr BP (Kuehn and Foit, 2006); and Aniakchak, Greenland Ice Core Chronology 2005 (GICC05) age of 3590 ± 1 BP (Coulter *et al*., 2012). A fifth late Holocene tephra was tentatively correlated with Mount Augustine G, *ca*. 2100 cal yr BP (Tappen *et al*., 2009). However, subsequent geochemical comparisons with reference materials suggest that although this tephra shares characteristics with material sourced from Augustine, it is unlikely to be Augustine G (Kristi Wallace, pers. comm.). All correlated tephras in Nordan's Pond Bog were of North American origin but the detection of horizons from other source regions cannot be precluded. Ash from the 2010 eruption of Eyjafjallajökull, Iceland, approached Newfoundland (Davies *et al*., 2010) and tephra from Changbaishan, China, has been identified in Greenland ice cores (Sun *et al*., 2013); therefore, sources even further afield cannot be discounted.

This study builds on the existing eastern seaboard record by contributing four new peatland tephrostratigraphies from the region. Peatlands are ideal archives for preserving tephrostratigraphies since cryptotephra horizons are often present in discrete layers that have been subjected to minimal post-depositional movement (Dugmore & Newton, 1992; Dugmore *et al*., 1996;

Payne *et al.*, 2005). The findings extend the known regional spatial distribution of previously identified tephras, add several newly characterised tephras and demonstrate the increased potential of this technique in obtaining late Holocene high-precision chronologies. The major and minor element chemistry of several newly characterised tephras in this study reveals potential for delivery of tephra from more distal and previously unconsidered source regions to eastern North America.

5.2.3 Methods

The study sites, Saco Heath (SCH10: 43˚33'05" N; 70˚2'03" W), Villagedale Bog (VDB12: 43˚31'09" N; 65˚31'54" W), Framboise Bog (FBB12: 45˚43'14: N; 60˚33'09" W) and Jeffrey's Bog (JRB12: 48˚12'46" N; 58˚49'06" W) are ombrotrophic plateau bogs located along a south-west to north-east transect across Maine, Nova Scotia, and Newfoundland (Figure 5.5). The cores were sampled from the centre of each bog using an 11-cm-diameter Russian pattern corer, following a full stratigraphic investigation based on the Troels-Smith (1955) system.

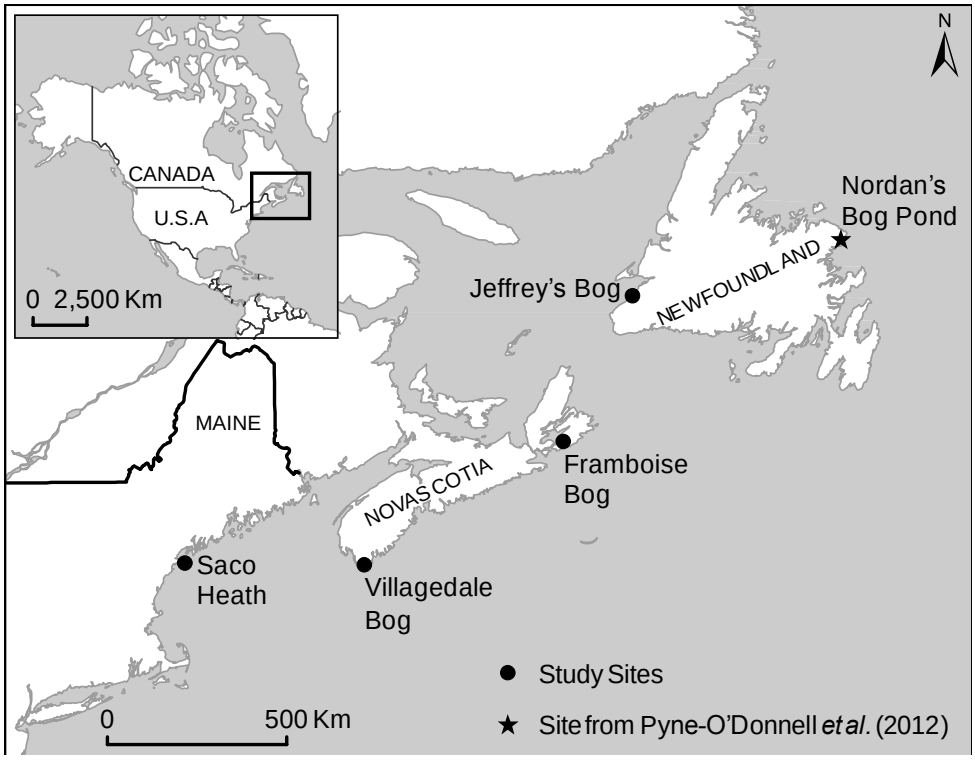

Figure 5.5 The location of study sites Saco Heath (SCH10), Villagedale Bog (VDB12), Framboise Bog (FBB12) and Jeffrey's Bog (JRB12) in relation to the previous Newfoundland record from Nordan's Pond Bog (Pyne-O'Donnell *et al.*, 2012).

The stratigraphic position and shard concentration of cryptotephra horizons were established by the standard method of ashing the peat at 5 cm contiguous intervals (Pilcher and Hall, 1992). The ashed residues were mounted in glycerol and counted under a high power microscope. Guided by these counts, the locations of cryptotephra layers were refined to 1 cm resolution (Pilcher and Hall, 1992). Glass shards for electron probe microanalyses were extracted from the peat matrix using the heavy liquid flotation method (Blockley *et al.*, 2005), modified with additional cleaning floats and gentle stirring to improve shard extraction yields. The flotation method was chosen to avoid any possible chemical alteration that may arise from the alternative acid digestion technique (Blockley *et al.*, 2005). Whilst other peat studies have obtained consistent results using acid digestion (e.g. Roland *et al.*, 2015), flotation was deemed an important precaution since the shards were small with a high surface to volume ratio, characteristics which may make shards prone to chemical alteration (Dugmore *et al.*, 1992; Blockley *et al.*, 2005). Extracted shards were mounted in an epoxy resin and exposed at the surface by careful grinding and polishing.

Major and minor element compositions of single glass shards of unknown cryptotephra horizons were determined by electron probe microanalysis (EPMA) with wavelength dispersive spectrometry (WDS-EPMA) at the Tephra Analytical Unit, University of Edinburgh, using a 3 μm beam (Appendix A). This beam size was used because shard sizes were typically very small (25-102.5 μm) with many vesicles (Hayward, 2012). Ksudach 1 (KS1) proximal tephras were analysed at the University of Edinburgh using the same parameters and at Queen's University Belfast (analytical set up outlined in Appendix B). All Mount St. Helen's, Jala Pumice and White River Ash glass analyses were analysed at the University of Alberta on a JEOL 8900 using a 10 μm beam, 6 nA current, and 15 keV voltage. Analyses at all laboratories use a similar suite of minerals and glass for calibration, and a Lipari obsidian as a secondary standard to track the quality of calibration and assure repeatable analyses (e.g. Kuehn *et al.*, 2011). Therefore, the datasets are comparable amoung laboratories. All results are normalised to 100% on a water and volatile free basis (e.g. Froggatt, 1983; Lowe, 2011) to further assist comparisons. Correlations were identified by searching the University of Alberta tephra database, the Queen's University Belfast dataset, and

published literature. Potential correlations to the unknown cryptotephra layers were visually examined using biplots of selected elements, with correlation strengths indicated by similarity coefficients (Borchardt *et al.*, 1972; Appendix C).

Age-depth models were constructed using ^{14}C measurements on *Sphagnum* stems with the exception of the basal dates, which were obtained from bulk peat or brown mosses (Table 5.1 - Table 5.4). ^{14}C measurements were converted to calendar age distributions using the IntCal13 calibration curve (Reimer *et al.*, 2013) and the weighted averages of the date range distribution (2σ) are referred to throughout. Bayesian age-depth models were constructed using the R package BACON (Blaauw and Christen, 2011) assuming piece-wise linear accumulation (Figure 5.1 – 5.4).

5.2.4 Results and discussion

Seventeen discrete cryptotephra horizons were detected among the four peat cores (Figure 5.6), with all isolated horizons lying within the upper 2 m of peat. Low background shard concentrations are present throughout the cores (average shards/5cm^3: SCH10=1; VDB12=3.5; FBB12=2.6; JRB12=3). Each crypto-tephrostratigraphy is dominated by one eruption occurring at 118 cm, 100 cm, 70 cm and 131 cm from the westernmost to easternmost sites, respectively. The glass compositions are rhyolitic, with some dacitic shards present in SCH10-42 and VDB12-42. Each peak appears to represent a geochemically discrete tephra, with the exception of SCH10-42, which consists of two populations. As described below, nine cryptotephra horizons correlate with known eruptions, five have possible correlations (FBB12-31, FBB12-162, VDB12-90, VDB12-53, VDB12-176) and three do not correlate with known late Holocene eruptions from North America, Iceland, Mexico, Kamchatka or Japan (SCH10-42, SCH10-57, VDB12-42; Table 5.5; Table 5.6). All potential correlations are supported by core chronologies, major element geochemistry and shard morphology where reference material was available; however, definitive correlations require the categorisation of more proximal reference material and the addition trace element geochemistry.

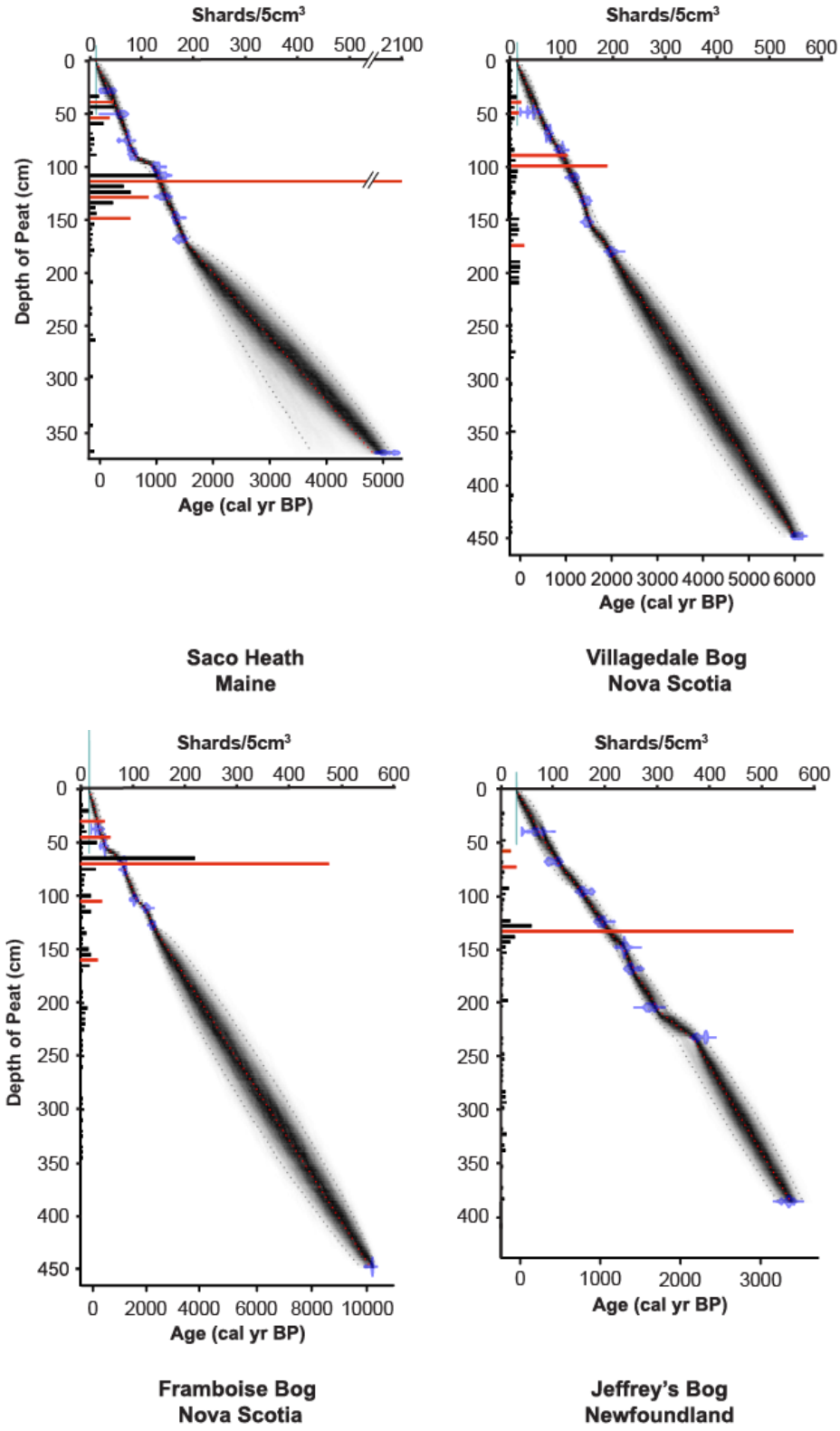

Figure 5.6 Tephrostratigraphies from the four study sites. Shard concentrations are rhyolitic shards/5cm³ and layers extracted for EPMA analyses are highlighted in red. The preliminary radiocarbon age-depth models indicate results from Markov Chain Monte Carlo iterations completed in Bacon. The darker areas represent the most likely age ranges.

Table 5.5 Means and standard deviations of glass compositions from cryptotephra layer. All data are normalised. n = number of analyses

Sample		SiO_2	TiO_2	Al_2O_3	FeOt	MnO	MgO	CaO	Na_2O	K_2O	H_2O diff	n
SCH10-42	**Mean**	70.12	0.46	15.63	2.89	0.07	0.82	3.07	5.07	1.86	0.78	6
Pop. 1	**StDev**	1.74	0.05	1.21	0.23	0.01	0.16	0.40	0.32	0.14	2.16	
SCH10-42	**Mean**	75.89	0.27	13.19	1.44	0.04	0.18	1.22	4.20	3.57	3.04	3
Pop. 2	**StDev**	1.62	0.24	1.93	0.59	0.01	0.08	0.66	0.37	0.17	1.86	
SCH10-57	**Mean**	70.74	0.39	14.94	2.73	0.11	0.65	2.75	4.80	2.88	1.21	4
	StDev	0.41	0.01	0.18	0.14	0.02	0.02	0.16	0.29	0.07	1.65	
SCH10-118	**Mean**	74.06	0.19	14.22	1.54	0.05	0.40	1.93	4.35	3.27	3.51	26
	StDev	0.51	0.02	0.48	0.16	0.01	0.04	0.11	0.19	0.09	1.81	
SCH10-131	**Mean**	74.06	0.18	14.44	1.45	0.05	0.37	1.87	4.35	3.23	2.87	15
	StDev	0.84	0.03	0.56	0.20	0.01	0.06	0.17	0.21	0.12	1.87	
SCH10-150	**Mean**	73.79	0.20	14.70	1.54	0.05	0.39	1.89	4.29	3.15	2.56	13
	StDev	0.23	0.01	0.40	0.12	0.01	0.02	0.08	0.20	0.07	1.94	
VDB12-42	**Mean**	70.44	0.48	15.26	2.96	0.06	0.80	3.13	5.03	1.83	2.31	11
	StDev	0.58	0.04	0.24	0.34	0.01	0.19	0.18	0.29	0.16	1.31	
VDB12-53	**Mean**	75.67	0.38	12.72	2.26	0.06	0.33	2.60	3.85	2.12	0.50	2
	StDev	0.65	0.01	0.34	0.07	0.01	0.03	0.72	0.26	0.08	0.67	
VDB12-90	**Mean**	71.64	0.26	15.46	1.94	0.10	0.37	1.36	5.37	3.49	2.25	23
	StDev	0.50	0.02	0.37	0.12	0.01	0.04	0.11	0.22	0.11	1.39	
VDB12-100	**Mean**	74.38	0.17	14.26	1.42	0.04	0.35	1.81	4.27	3.30	3.05	15
	StDev	0.95	0.03	0.61	0.19	0.00	0.08	0.18	0.25	0.15	1.89	
VDB12-176	**Mean**	73.76	0.36	13.96	2.64	0.12	0.49	2.23	5.03	1.40	2.16	9
	StDev	0.63	0.03	0.62	0.34	0.01	0.08	0.16	0.22	0.07	2.15	
FBB12-31	**Mean**	72.52	0.37	14.62	2.37	0.05	0.61	2.47	4.81	2.17	2.72	12
	StDev	1.63	0.07	0.77	0.37	0.01	0.16	0.45	0.24	0.20	2.57	
FBB12-47	**Mean**	76.58	0.21	12.95	1.53	0.03	0.25	1.45	4.44	2.55	2.37	2
	StDev	0.23	0.01	0.07	0.07	0.00	0.02	0.14	0.22	0.15	0.28	
FBB12-70	**Mean**	74.90	0.17	13.76	1.47	0.04	0.34	1.84	4.22	3.24	4.14	23
	StDev	0.97	0.06	0.71	0.34	0.01	0.10	0.29	0.32	0.38	1.44	
FBB12-105	**Mean**	74.84	0.19	14.08	1.44	0.04	0.35	1.79	4.18	3.10	2.50	14
	StDev	0.79	0.03	0.55	0.20	0.01	0.06	0.24	0.37	0.30	2.25	
FBB12-162	**Mean**	76.72	0.34	11.86	2.21	0.06	0.44	2.40	3.64	2.34	3.10	5
	StDev	0.34	0.03	0.24	0.07	0.01	0.02	0.19	0.16	0.04	1.61	
JRB12-71	**Mean**	76.29	0.22	13.29	1.45	0.03	0.23	1.39	4.55	2.55	1.55	18
	StDev	0.79	0.02	0.66	0.11	0.01	0.04	0.23	0.27	0.15	1.66	
JRB12-131	**Mean**	74.32	0.19	14.25	1.49	0.05	0.36	1.87	4.20	3.28	2.56	27
	StDev	0.49	0.03	0.38	0.13	0.01	0.05	0.14	0.18	0.10	1.91	

Table 5.6 Means and standard deviations of single-grain glass compositions from reference material of potential correlatives. All data are normalised, n = number of analyses. Data sources: MSH-Wn and MSH-We: Pyne-O'Donnell *et al*. (2012) and Jensen *et al*. (2014b); MSH Layer T: Jensen *et al*. (2014b) and this study; Ceboruco P1 and Ksudach KS1: this study; Tarumai Ta-c2: Nanayama *et al*. (2003); WRAe: Pyne-O'Donnell *et al*. (2012) and Jensen *et al*. (2014a); WRAn: Jensen *et al*. (2007).

Sample		SiO_2	TiO_2	Al_2O_3	FeOt	MnO	MgO	CaO	Na_2O	K_2O	Cl	H_2O diff	n
MSH-Wn	**Mean**	74.83	0.19	14.32	1.61	0.04	0.30	1.70	4.63	2.32	0.08	2.75	83
	StDev	0.42	0.03	0.44	0.10	0.03	0.03	0.08	0.25	0.11	0.03	2.45	
MSH-We	**Mean**	75.89	0.25	13.51	1.50	0.04	0.26	1.44	4.50	2.50	0.10	2.61	66
	StDev	0.50	0.04	0.27	0.08	0.03	0.03	0.12	0.19	0.09	0.03	1.94	
MSH	**Mean**	70.80	0.44	15.69	2.88	0.06	0.72	2.89	4.69	1.93	0.12	1.80	62
Layer T	**StDev**	1.52	0.08	0.73	0.43	0.03	0.17	0.54	0.31	0.21	0.04	1.78	
Ceboruco	**Mean**	71.44	0.28	15.94	1.96	0.09	0.34	1.34	5.13	3.39	0.102	1.89	25
P1	**StDev**	0.21	0.05	0.14	0.07	0.03	0.03	0.04	0.16	0.09	0.03	1.05	
Ksudach	**Mean**	73.32	0.40	13.97	2.67	0.16	0.45	2.22	5.22	1.35	0.17	2.54	28
KS1	**StDev**	1.14	0.09	0.75	0.53	0.06	0.14	0.31	0.53	0.10	0.02	1.38	
Tarumai	**Mean**	76.47	0.34	11.94	2.15	0.04	0.46	2.27	3.97	2.36	-	2.20	15
Ta-c2	**StDev**	0.82	0.04	0.22	0.29	0.02	0.14	0.26	0.08	0.12	-	1.04	
WRA east	**Mean**	73.89	0.21	14.49	1.52	0.05	0.36	1.83	4.13	3.19	0.34	2.73	107
(WRAe)	**StDev**	0.63	0.04	0.32	0.20	0.02	0.07	0.18	0.16	0.17	0.04	1.48	
WRA north	**Mean**	73.96	0.21	14.41	1.61	0.06	0.33	1.77	4.10	3.23	0.32	2.69	50
(WRAn)	**StDev**	1.16	0.07	0.53	0.25	0.03	0.08	0.30	0.18	0.15	0.05	1.54	

5.2.4.1 Correlated eruptions

Mount St Helens (MSH): JRB12-71 (AD 1404 - 1578) most likely correlates to the MSH set W eruptions of AD 1479 (MSH-Wn) to 1482 (MSH-We) (Fig. 3). The tephra is characterised by colourless pumiceous shards, similar to proximal samples of Mount St. Helens W. Distinguishing between the dominant ash layers from this set, Wn (which extended north-eastwards) and We (which extended eastwards), is difficult because of the chemical similarities and short time interval between these ash layers (*ca*. 2 to 3 years; Yamaguchi, 1985; Fiacco *et al*., 1993; Mullineaux, 1996). However, when plotting JRB12-71 with proximal data from both eruptions, this tephra demonstrates a clear affinity with the We layer (Figure 5.7). This is consistent with conclusions from Nordan's Pond Bog (Pyne-O'Donnell *et al*., 2012). The MSH ash is restricted to

the northern study site, a pattern that could either be indicative of a patchy tephra fall-out distribution (e.g. Davies *et al.*, 2010) or it may show that the southernmost limit of detectable cryptotephra deposition for this eruption lies close to Newfoundland. Analyses from further sites will be required to distinguish between these two possibilities.

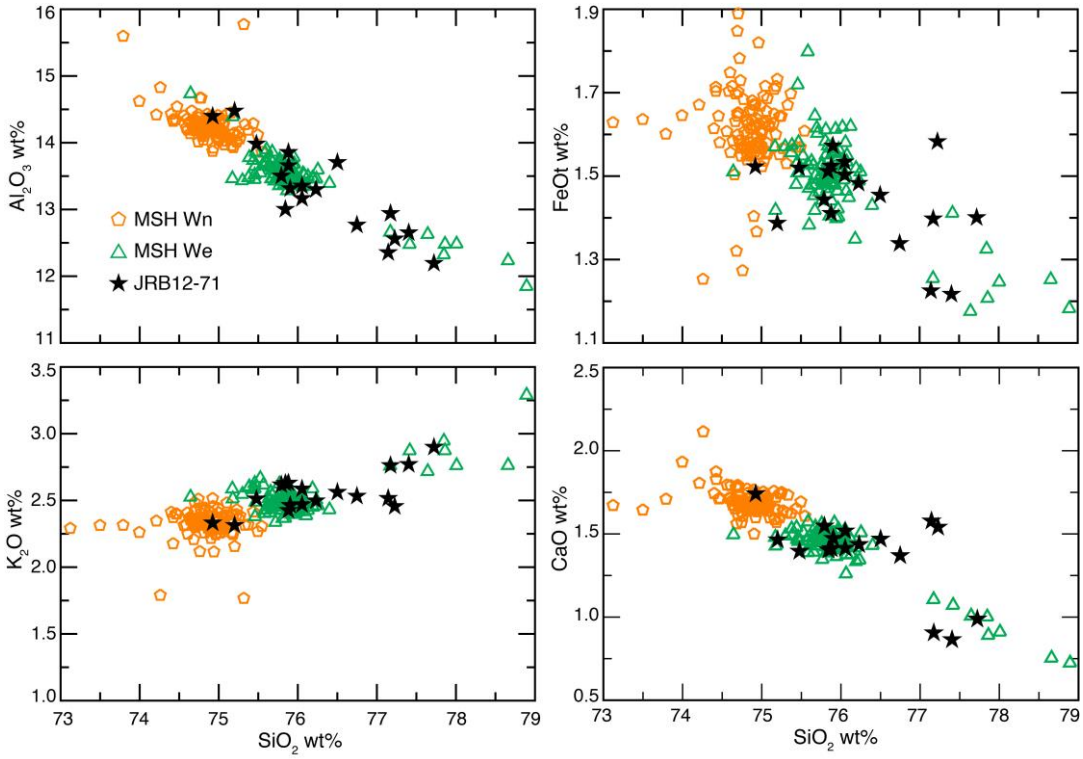

Figure 5.7 Harker diagrams comparing the major element glass compositions of MSH-Wn, MSH-We and JRB12-71. JRB12-71's composition mirrors the geochemical trend seen in MSH-We.

The White River Ash (WRA): all four sites contain horizons of highly pumiceous shards that correlate with the eastern lobe of the WRA (WRAe) from Mount Bona-Churchill, Alaska (Jensen *et al.*, 2014a; Figure 5.8). This tephra has been recently correlated to the European cryptotephra, "AD860B" (Jensen *et al.*, 2014a) which has been dated by the Greenland Ice Core Chronology (GICC05) to AD 847 ± 1 (Coulter *et al.*, 2012). All core chronologies within this study (based on modelled ^{14}C measurements) provide age estimates that encompass this date. The detection of this cryptotephra at all four sites builds on the previous identification of the WRA in Newfoundland (Pyne-O'Donnell *et al.*, 2012) and shows its prevalence across the eastern seaboard of North America. The largest WRA horizon is located in Maine

(SCH10-118), with an order of magnitude more shards (2120 shards/5cm^3) than the closest study site Villagedale Bog, Nova Scotia. Whilst local or regionally specific conditions may contribute to this pattern of tephra deposition, the observed distribution suggests that the southernmost limit of this ash has not been yet been located. This presents the opportunity to extend the tephra distribution map in North America and connect archives across greater distances.

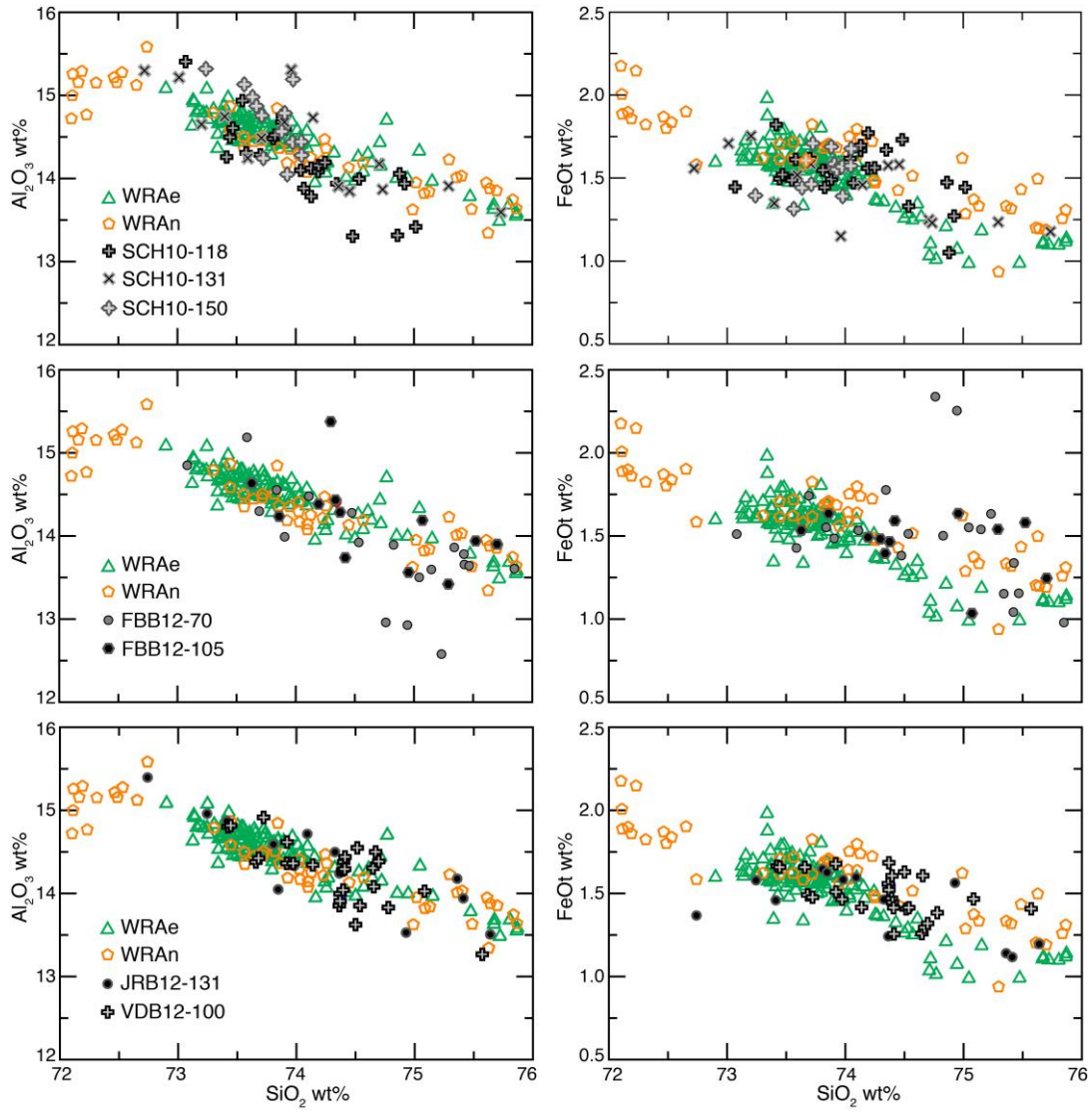

Figure 5.8 Selected major element glass geochemical plots of proximal White River Ash (east and north lobe) and correlated cryptotephras. Most samples tend to cluster with the main WRAe geochemical population of ~73-74.5 SiO2 wt%.

5.2.4.2 Potential correlations

The following potential correlations are based on major-element geochemistry, age data, and glass morphology where reference material was available. Additional access to proximal reference materials and/or data, and trace-element geochemistry could help confirm these correlations.

FBB12-31 (AD 1565 - 1830): Major and minor element geochemistry of FBB12-31 match well with data collected on both proximal and more distal reference samples of MSH Layer T (Figure 5.9). This tephra was deposited in AD 1799-1800 (Yamaguchi, 1983) and is associated with the Mount St. Helens Goat Rocks eruptive period (Mullineaux, 1996). Layer T formed a narrow lobe limited to the northeast of the volcano and although thickness and grain-size rapidly decrease away from source, it has been reported as a visible unit up to 500 km from the source (Mullineaux, 1996). The glass morphology (pumiceous shards with the occasional bubble-walled shards) and the 2σ modelled age range of FBB12-31 confirm the similarity of this horizon to layer T. The correlation is also supported by the lack of other Mount St. Helens eruptions that fall into the required age range (e.g. MSH set X, ash bed Z or set W) with this specific composition (Mullineaux, 1996; Jensen *et al.*, unpublished data).

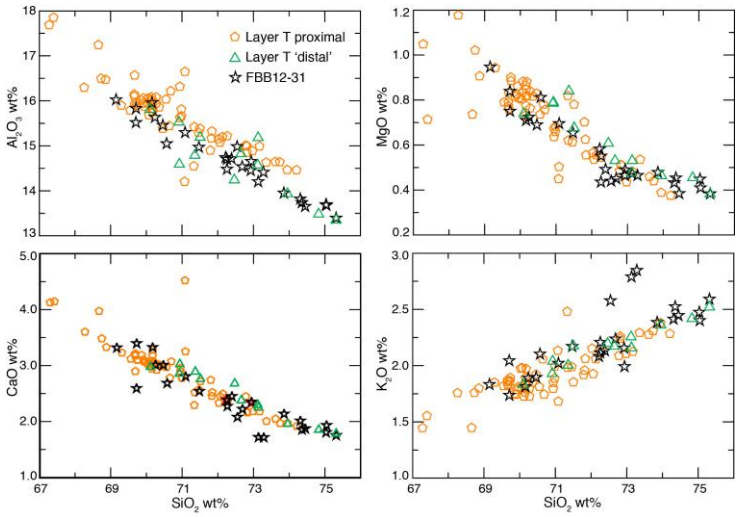

Figure 5.9 Major and minor element glass compositions of proximal lapilli and distal ash from Mount St Helens layer T and the potential correlative FBB12-31.
The proximal data comprise multiple samples that represent the entire event; the distal sample is a visible ash deposit several hundred kilometres distant in NE Washington State.

FBB12-162 (3604 – 2643 cal yr BP): this layer is characterised by pumiceous shards. Only seven analyses were successfully collected, of which two appear to be potentially unrelated to the main population. The remaining analyses characterise a high-SiO_2 rhyolite (~76-77 wt%) that has relatively low Al_2O_3, but high FeO_t and CaO for this SiO_2 concentration in comparison with available glass compositional data from Alaska, Cascades, Iceland and Kamchatka in this age range. Comparisons with Japanese glass chemistries (Nanayama *et al.*, 2003; Hughes *et al.*, 2013) indicate that Hokkaido is a possible source region for this tephra (Figure 5.10). Biplots of K_2O and TiO_2 concentrations have proved useful for distinguishing between Hokkaido regional volcanoes (Tokui, 1989; Furukawa *et al.*, 1997**;** Aoki and Machida, 2006); however, comparisons between the FBB12-162 and proximal ash is limited both by the number of cryptotephra shards analysed from FBB12 and the lack of published individual proximal shard chemistries. FBB12-162 has greater geochemical similarities with the proximal ash from Tarumai than that from Komagatake. This potential correlation is supported by the age of the Tarumai tephra Ta-c2 (3000-2000 cal yr BP; Sato, 1971; Nanayama *et al.*, 2003) that is comparable to the modelled age of FBB12-162. However, the lack of reference data precludes the firm correlation with Tarumai. The geochemical characteristics of two shards from VDB12-53 also show similarities with Japanese tephra (Figure 6); however, the number of successfully typed shards and the exhaustion of core material prevent a firm correlation.

VDB12-176 (2055 – 1771 cal yr BP): this horizon is characterised by pumiceous, sometimes blocky shards. The glass composition of this unknown tephra is strikingly similar to Ksudach 1 from the eastern volcanic front of the Kamchatka Peninsula (KS1; Figure 5.11. A-C; Kyle *et al.*, 2011). Ksudach is a large shield volcano with five overlapping calderas (Volynets *et al.*, 1999). The eruption of KS1 in *ca.* 1800 cal yr BP was Kamchatka's second largest Holocene eruption (Braitseva *et al.*, 1997) containing three proximal fall units of white or yellow pumice, density current deposits and a fall unit of grey pumice (Braitseva *et al.*, 1996; Andrews *et al.*, 2007). Initially, ash was deposited to the north but during the early phases of the eruption it travelled eastward, until the final stages when it shifted westward (Melekestsev *et al.*, 1996). Fall units can be identified over 1000 km from the source covering an

area of 2-3 million km^2 (Braitseva *et al.*, 1996). Glass morphology, composition and similar age estimates strongly support this correlation.

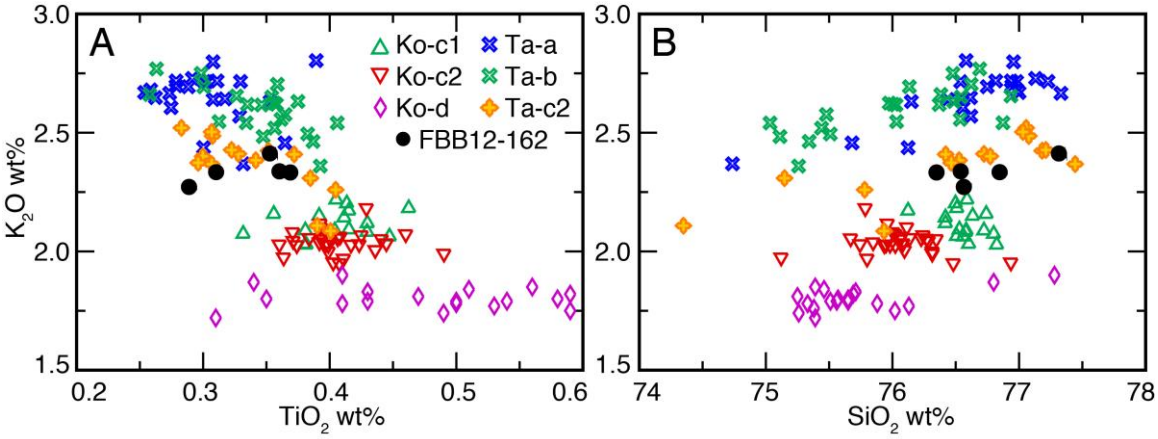

Figure 5.10 Geochemical plots of FBB12-162 in comparison with tephra from the Tarumai (Ta) and Komagatake (Ko) volcanoes of Hokkaido. Single grain analyses of the historic eruptions Ko-c1, c2 and Ta-a,b,c2 are from Nanayama *et al.* (2003) and Ko-d data are from Hughes *et al.* (2013). Traditionally, Ko and Ta tephra are separated from each other on a K_2O and TiO_2 biplot, FBB12-162 plots in the field defined by Ta. B- Plotting K_2O vs. SiO_2 also shows more clearly that FBB12-162 plots more closely with Ta-c, which in terms of age is the most likely correlative. Dates of eruptions: Ta-a: AD 1739 (Yamada, 1958); Ta-b: AD 1667 (Yamada, 1958); Ta-c2: 2000-3000 cal yr BP (Sato, 1971); Ko-c1: AD 1856 (Yamada, 1958); Ko-c2: AD 1694 (Yamada, 1958; Furukawa *et al.*, 1997).

VDB12-90 (AD 889 – 1130): the geochemistry in this horizon does not match any known eruptions of this age from Alaska, the Cascade Range, Kamchatka (V. Ponomareva, pers. comm., 2014), Iceland (Tephrabase, Newton *et al.*, 1997) or Japan. However, examination of published geochemical data available from Mexican sources showed that the chemistry closely resembled the main Plinian fall deposit (P1) of the Jala Pumice, which was deposited by the caldera-forming eruption of Volcán Ceboruco, AD 990-1020 (Chertkoff and Gardner, 2004; Gardner and Tait, 2000). Volcán Ceboruco is located *ca.* 4400 km from the peatland in southeastern Nova Scotia, making the distance of ash transport *ca.* 800 km less than that between Mount Bona-Churchill (WRAe) and VDB12. Re-analysis of lapilli from the upper part of the P1 proximal deposit, collected at Locality 18 in Figure 1 of Gardner and Tait (2000), confirm that VDB12-90 and P1 chemistry share striking similarities (Figure 5.11. D-F). The geochemical data are supported by the VDB12 core

chronology. Therefore, it seems likely that VDB12-90 represents a distal deposit of the Jala Pumice from Volcán Ceboruco.

The potential for eastward dispersion of ash from Volcán Ceboruco was demonstrated using the UK Met Office's Numerical Atmospheric-dispersion Modelling Environment (NAME; Jones *et al.*, 2007). To test the variability in ash transport directions, a large (up to 30 km in plume height) ten-day constant eruption of Volcán Ceboruco was assumed and a small random meteorological sample (current 10 days of meteorology) was used to track the particle dispersion through the modeled lower atmosphere. Whilst the AD 990-1020 eruption of Volcán Ceboruco may have been smaller than the modelled eruption and likely occurred during different meteorological conditions than those of today, the modelling results reveal the potential for the main ash plume to extend eastwards into Africa whilst a secondary plume splits from the main plume over the North Atlantic Ocean, extending northeastwards across Nova Scotia and Quebec (Claire Witham, pers. comm.). Tephra transportation from Mexico to Nova Scotia may also occur when anticyclonic advection merges with a strongly meridional polar jet stream, as modeled using weather and climate observations from NASA's MERRA dataset (NASA, 2012). Furthermore, there are precedents for Mexican tephras reaching the North Atlantic region, as ash from the *ca.* AD 1250 – 1400 (Palais *et al.*, 1992) and AD 1982 (Zielinski *et al.*, 1997) eruptions of El Chichón have been detected in the Summit region of Greenland.

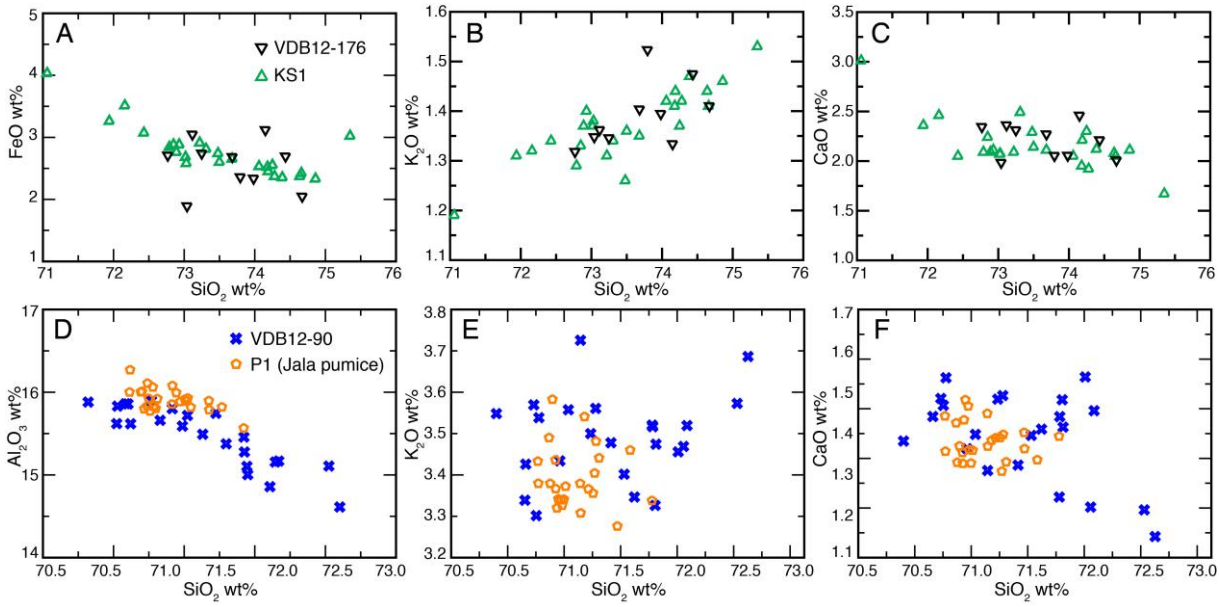

Figure 5.11 Major-element glass compositions of: A-C- Ksudach 1 from visible ash deposits collected in Kamchatka plotted with VDB12-176; D-F- Glass analyses from crushed lapilli of P1 from Volcán Ceboruco plotted with VDB12-90.
All oxides with the exception of Al_2O_3 are virtually identical. The slight offset seen between the two samples with Al_2O_3 is likely the result of calibration differences, Lipari standard data bracketing VDB12-90 shows lower than average Al_2O_3 wt% values, while standard data bracketing P1 analyses were higher than average.

5.2.4.3 Unidentified tephra horizon

VDB12-42 (AD 1517 - 1750): the shard morphology of this horizon is dominated by pumiceous shards, accompanied by occasional brown coloured shards. Although this rhyo-dacitic tephra falls within the compositional range of known Icelandic and Aleutian tephra, and shares similar glass morphological characteristics with them, it has not been correlated and has been provisionally termed here as the 'Villagedale tephra'. The calibrated ^{14}C age of SCH10-42 (AD 1572 - 1762) and geochemical similarity to VDB12-42 (Figure 5.12) suggest that they might be the same tephra, although more analyses are required to clarify this relationship.

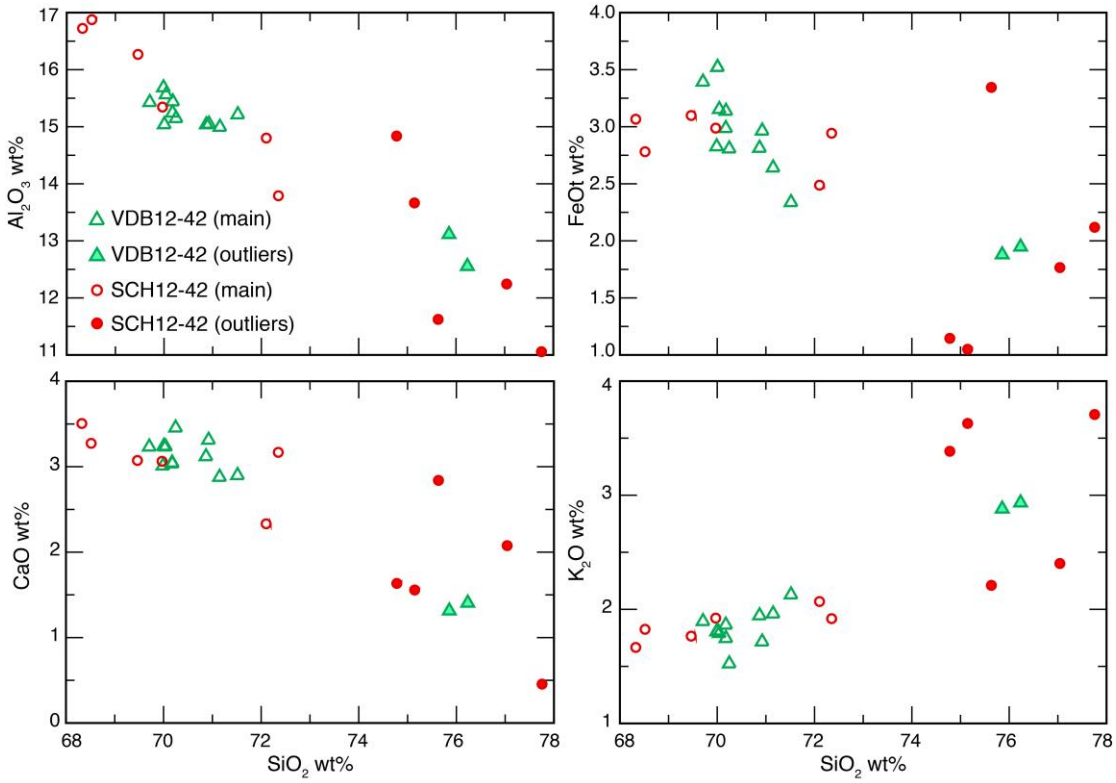

Figure 5.12 Major-element glass compositions of VDB12-41 and SCB12-42. Comparable ages and glass compositions between the lower SiO_2 wt% population of the tephras suggest a potential correlation. The higher SiO_2 wt% values (>74 wt%) are quite scattered and probably largely represent shards that may be from different eruptions.

5.2.4.4 Multiple within-core White River Ash horizons

One caveat related to the use of isochrons is demonstrated in the stratigraphy of SCH10 and FBB12, which register multiple discrete horizons of the WRA tephra. The overlapping geochemistry, representing a single volcanic centre, complicates both the assignment of an age within stratigraphies and the degree of precision when correlating with other records. Therefore, under these conditions the isochron may represent a 'passage in time' rather than a 'moment in time' (*sensu* Dugmore *et al.*, 2004). SCH10 contains three horizons that are distinct at both 5 cm and 1 cm resolutions and FBB12 contains two horizons that are separated by 35 cm of peat accumulation with low or zero background shard counts (Figure 5.6). Since the upper WRA tephra horizons of SCH10-118 and FBB12-70 are an order of magnitude larger than the other within-core WRA horizons, they have been assumed to be the main WRAe eruption.

Two main factors may have contributed to the multiple WRA horizons: firstly, there may be several eruption events/stages from the same volcanic centre (Preece *et al.*, 2014) and secondly, post-depositional movement of the shards may have occurred. Although atmospheric conditions also influence site-specific delivery of ash layers (since circulation and localised precipitation patterns can result in intermittent shard deposition; Dugmore and Newton, 1997; Davies *et al.*, 2010; Pyne-O'Donnell, 2011; Payne *et al.*, 2013), delayed atmospheric transport of shards cannot explain this multiple peak feature. Peat accumulation rates in oceanic settings are usually around 10 yr/cm, whereas the maximum atmospheric retention time of ash clouds is in the order of 1 to 2 years (Zielinski *et al.*, 1994; Fiacco *et al.*, 1994; Cole-Dai *et al.*, 2000; Robock, 2002; Cole-Dai *et al.*, 2009).

Multiple eruptions are a possible explanation for the observed SCH10 and FBB12 pattern since two eruptions from Mount Churchill have been reported around the time period of interest: the prominent eastern lobe (AD 847 ± 1; Jensen *et al.*, 2014a) and the smaller northern lobe (*ca.* 1560-1680 cal yr BP; Froese *et al.*, 2005). This hypothesis cannot be fully tested since the dataset is limited by the low initial shard concentrations and the exhaustion of sample material, thus preventing further analysis of any subtle geochemical differences between the two Mount Bona-Churchill layers. The ^{14}C-modelled age of FBB12-105 is *ca.* 1673 cal yr BP and there is distinct stratigraphic separation of the two FBB12 WRA layers with low tephra concentrations in-between; therefore, a multiple-eruption explanation is possible. However, the ^{14}C-modelled age of tephra deposition at SCH10-150 is *ca.* 1363 cal yr BP; therefore, it is unlikely that this WRA layer originated from the northern lobe of the WRA.

Owing to the age discrepancies between SCH10-150 and the known WRA eruptions, the pattern of tephra horizons within this core is unlikely to represent multiple eruptions. Post-depositional movement of tephra may therefore be responsible. Field experiments have demonstrated the potential for limited vertical tephra movement, especially in smaller shards; however, Payne *et al.*, (2005) argue that there is no evidence for significant movement of whole tephra horizons. Mechanisms of post-depositional movement of tephra are related to peat moisture, density and porosity (Payne and Gehrels, 2010). Therefore, whilst water table fluctuations may have contributed to

downward vertical tephra transport, the distance of transport that is required to explain the observed tephra horizon patterns have not been confirmed by field experiments (Payne *et al*., 2005).

The most feasible explanation for downward post-depositional shard movement is the presence of root channels, which have been attributed to providing pathways for shards to be deposited downwards in lake sediments (e.g. Davies *et al*., 2005; 2007); therefore, similar processes may be occurring on the peatlands. The macrofossil composition of JRB12 is consistently dominated by *Sphagnum* (*ca*. 75-85%) and similar *Sphagnum* abundance values are evident throughout VDB12 (except between 68-84 cm which registers an increase in Ericaceae and monocotyledon plant remains; Section 6.5.1). These moss-dominated conditions would limit the translocation of tephra shards, and this is indicated by the lack of multiple ash layers in the tephrostratigraphies of these sites. In contrast, SCH10 registers fluctuating phases of Ericaceae dominance (*ca.* 50%), one period of which occurs after the WRA deposition between 88–108 cm (Section 6.6.1). The increase of such shrub species with penetrating roots enhances the possibility of post-depositional tephra movement. The considerable concentrations of tephra shards in the upper two WRA-type horizons in SCH10 may exacerbate any post-depositional movement of shards and may also explain why the apparent movement is greater here than at the other study sites.

5.2.5 Conclusions

This study has expanded the known geographical range of cryptotephra deposition in eastern North America and has revealed more ash layers, from more varied source regions, than previously identified. This not only increases the potential chronological control provided by the tephras, but also increases the geographical areas with which palaeoenvironmental records can be synchronised. The potential of linking palaeoenvironmental records across the tropics and the mid- to high latitudes presents exciting opportunities to explore changes in interregional atmospheric and oceanographic circulation patterns.

The White River Ash (eastern lobe) from Mount Bona Churchill is confirmed as a dominant isochron and the scope for its spatial extension across the eastern

seaboard of North American has been presented. The recent correlation of the WRAe to the "AD860B" ash found in Greenland and northern Europe (Jensen *et al.*, 2014a) and the extended eastern North America distribution of the WRAe presented in this study highlights the importance of this tephra as an intercontinental temporal link between environmental archives. Future palaeoenvironmental studies may therefore utilise the extended WRAe distribution to investigate reconstructed climate change associated with the Medieval Climate Anomaly (MCA; AD 900 - 1350) in eastern North America. Comparisons of such reconstructions with records from Greenland and western Europe may identify potential MCA climatic drivers, such as changes in the strength of the Gulf Stream and Labrador Current, enhancing our understanding of the climate system during the MCA as a partial-analogue for future climate warming.

The deposition of the WRAe in Newfoundland also coincides with a time of regional archaeological change: the L'Anse aux Meadows area was intermittently occupied by the Middle Dorsets before the settlement of the Recent Indians (*ca.* AD 670 – 990; Davis *et al.*, 1988; Wallace, 2003). Following the departure of the Recent Indians, a temporary Norse settlement was constructed *ca.* AD 990 - 1050 (Wallace, 1991), documenting the first European presence in North America. Whilst the current study sites do not extend into northern Newfoundland, the potential for a more northerly WRAe distribution is presented. Future research may therefore focus on identifying the WRAe in archaeological and environmental archives from Newfoundland's Great Northern Peninsula with the aim of refining regional settlement chronologies and establishing the extent to which climatic change was responsible for regional population changes.

The possibility of Mexican and East Asian tephras reaching the eastern seaboard of North America provides an exciting prospect for expanding the region's tephra framework. Data from additional sites, the improved availability of proximal geochemical reference data and the incorporation of trace element data will facilitate the characterisation of tephra distributions from these source regions. Two further cryptotephras have been located in eastern North America: Mount St Helens layer T and the newly identified Villagedale tephra; however, more data are required to confirm and constrain these layers. This lack of comparative data will likely be the limiting factor in

future cryptotephra studies; therefore, investigating proximal ashes and enhancing the content and availability of comparative databases is essential for extending tephra frameworks (*sensu* Kuehn *et al.*, 2013).

This study highlights the caution required when interpreting multiple tephra horizons from the same eruption centre for use as isochrons. With appropriate caution, the prevalence of cryptotephra layers found in eastern North America facilitates the construction of a regional tephra lattice (Figure 5.13), which will expand as more records are developed and the region's true tephrochronological wealth is uncovered.

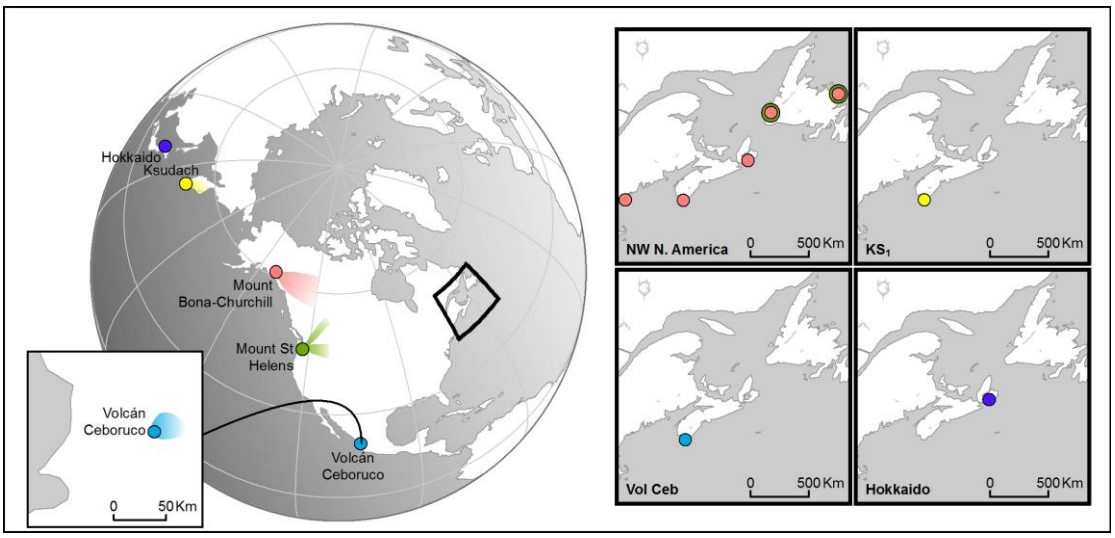

Figure 5.13 Eastern North American cryptotephra lattice: sites from this study and Nordan's Pond Bog (Pyne-O'Donnell *et al.*, 2012)

Chapter 6: Palaeoecological evidence of environmental change

6.1 Introduction

The plant macrofossil and testate amoebae data obtained across all four study sites are presented within this chapter. The chapter begins by outlining the results from field vegetation and water table measurements, which are used to construct a trial eastern North American specific plant macrofossil hydrological index. The plant macrofossil and testate amoebae data are then presented on a site-by-site basis, following the laboratory protocols outlined in Sections 3.4.1 and 3.4.2. A combination of transformation techniques have been applied to the palaeoecological data as outlined in Section 3.5.5: plant macrofossils are transformed using detrended correspondence analysis (DCA), non-metric multidimensional scaling (nMDS) and the Dupont Hydrological Indices (DHI) whilst DCA, nMDS and transfer functions are used to transform the testate amoebae assemblages (Section 3.5). The plant macrofossil and testate amoebae data are primarily plotted against depth, with a secondary age axis. The final palaeohydrological reconstructions obtained for each site are plotted against time with a secondary depth axis, to facilitate the between-site comparisons presented in Chapter 8.

The updated North American DHI results using the plant macrofossil data will be compared with the existing DHI (Daley and Barber, 2012; referered to as 'Daley and Barber') to assess the performance of a more regionally specific index and the effect of excluding roots and unidentifiable organic matter (UOM) within the updated index. Since the North American updated DHI is a preliminary trial version (based on a small number of field measurements), the Daley and Barber derived DHI will be used as the final macrofossil reconstruction in each site, from which the environmental inferences are obtained.

The performances of the two regionally appropriate testate amoebae transfer functions (Amesbury *et al.*, 2013; Lamarre *et al.*, 2013; Section 3.5) will be compared. Within each transfer function, the sensitivity of the reconstructions to species with large water table depth tolerances will be assessed through

the comparisons of models that employ downweighting (indicated by '.tol') and those which do not.

6.2 Formation of an eastern North American DHI for plant macrofossils

Several studies have obtained robust, comparable results from the vegetation assemblage data using the current DHI (Daley and Barber, 2012); however, there are many areas for improvement within this index as outlined in Section 3.5.3. Whilst this study does not attempt a complete overhaul of the method, it generates a trial version of an eastern North American DHI to assess the need for regionally specific indices. The following measures are adopted in the new updated index:

1. Indicator values are altered to follow the early work of Stoneman (1993) whereby values will relate to areas on the microtopographical gradient rather than relative wetness. These areas are defined by water table depth and plant groups will be assigned preferences based on water table depth data collected from two sites in Newfoundland, general field observations and existing literature.
2. Sample scores are computed with and without roots to assess their influence on environmental interpretations.
3. Sample scores are computed with and without UOM. Trend deviations may indicate periods when UOM was not a feature of increased decomposition during dry conditions

6.2.1 Process of DHI formation

Water table depth (WTD) measurements and associated vegetation communities were recorded from two peatlands in western Newfoundland: Jeffrey's Bog (this study; Section 4.3) and neighbouring Fichelle's Bog. Transects were outlined across hummock – hollow gradients and at each sample point along the transect the following information was recorded: the depth to water table; the most abundant taxa; the names of all species present within a 5 x 5 cm grid and the type of microform that the species inhabited.

The WTD measurements and associated species were ranked from highest to lowest water table levels and were grouped into 7 categories (pool, pool edge, wet lawn, lawn, high lawn, hummock and high hummock) based on assigned microtopography in the field and assisted by natural breaks in data. The characteristic WTD associated with each microform did vary between the two peatlands; therefore, characteristic WTD of microforms and vegetation obtained from existing literature (e.g. Andrus *et al*., 1983; Rydin and McDonald, 1985; Van der Molen and Hoekstra, 1988; Bragazza, 1997) were used to confirm that the assigned values were ecologically sensible. Each category was then assigned a value from 1 to 7, from pool (wet) to high hummock (dry).

The frequency of the presence of each species across each of the microtopographical indexed groups was calculated and the group with the highest frequency of each species was allocated as the indicator value (Figure 6.1 – Figure 6.4). If a species was present in equal frequencies across two habitats then the mean of the two indicator values was applied. The allocated values were then cross-referenced with the information collected in the field regarding the most abundant species in each habitat. If the species showed non-unimodal distributions or were poorly characterised with sparse observations then the indicator value was altered based on WTD measurements from existing studies (e.g. Andrus *et al*., 1983; Rydin and McDonald, 1985; Van der Molen and Hoekstra, 1988; Bragazza, 1997). Aggregate components, such as monocotyledons (monocots) and *Sphagnum* sections, required index values since there is often not enough information preserved within the palaeo-macrofossil samples to identify each fragment to species level, thus leaving some components undifferentiated (undiff.). Since the aggregate components showed non-parametric distributions and the numbers of occurrences of each species within the aggregate groups were not constant, the median indicator value was selected. The final allocated indicator values for each of the aggregate groups are outlined in Table 6.1.

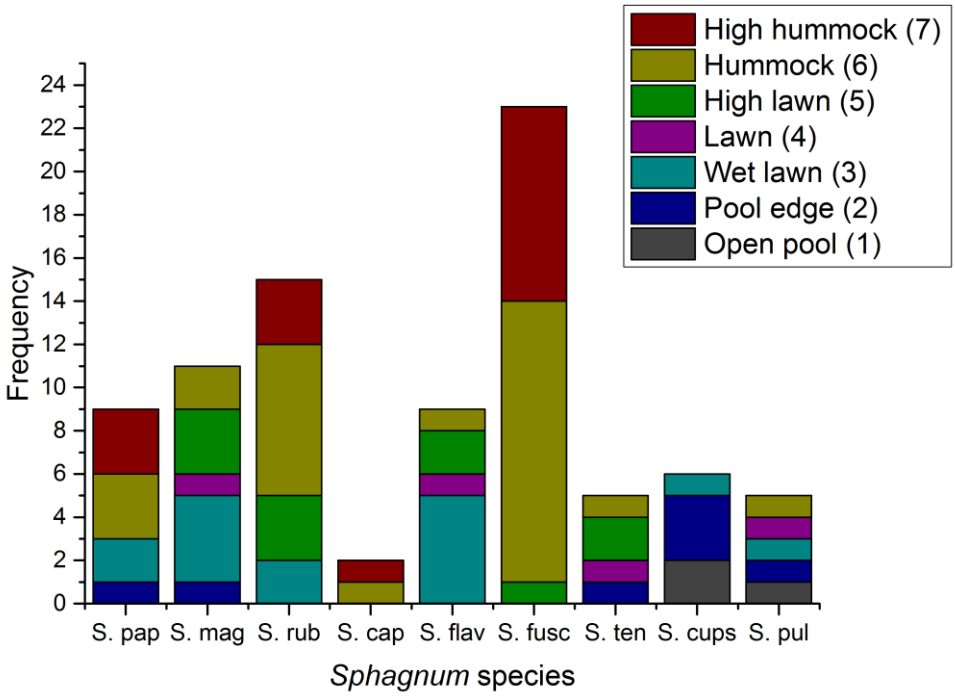

Figure 6.1 Distribution of *Sphagnum* (S.) species across microtopographical habitats. Full species names: *S. papillosum, S. magellanicum, S. rubellum, S. capillifolium, S. flavicomens, S. fuscum, S. tenellum, S. cuspidatum, S. pulchrum.*

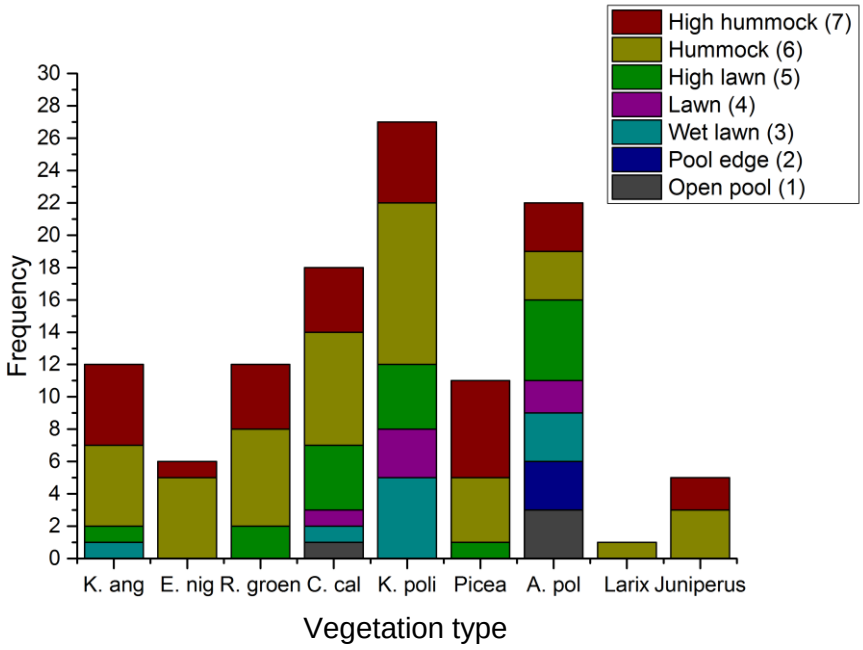

Figure 6.2 Distribution of selected species across microtopographical habitats. Full species names: *Kalmia angustifolia, Empetrum nigrum*, *Rhododendron groenlandicum, Chamaedaphne calyculata, Kalmia polifolia, Picea*, *Andromeda polifolia*, *Juniperus communis.*

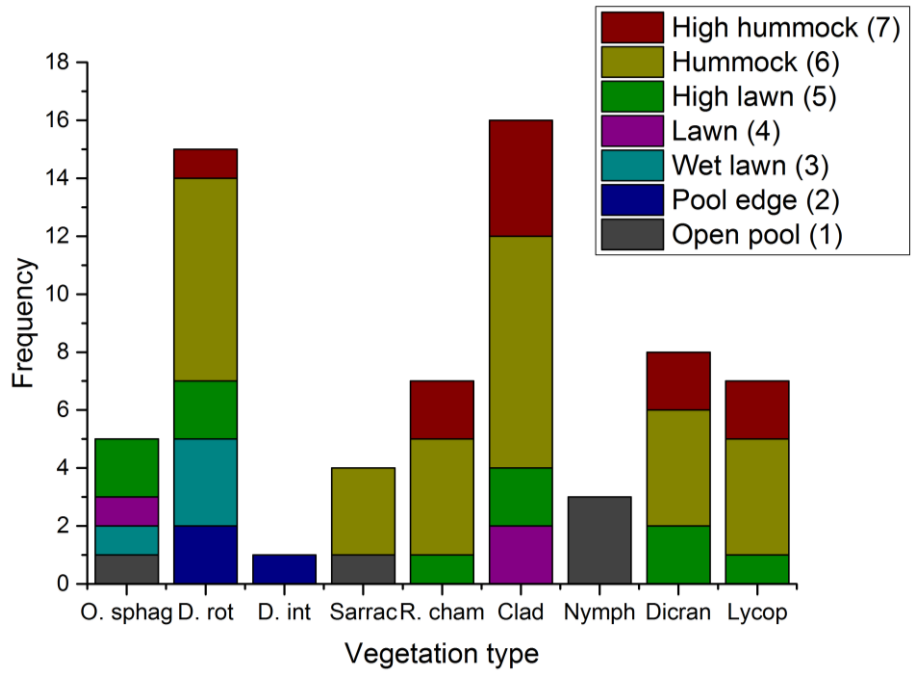

Figure 6.3 Distribution of selected species across microtopographical habitats. Full species names: *Odontoschisma sphagni, Drosera rotundifolia, Drosera intermedia, Sarracenia purpurea, Rubus chamaemorus, Cladonia, Nymphaea, Dicranum* species, *Lycopodium*

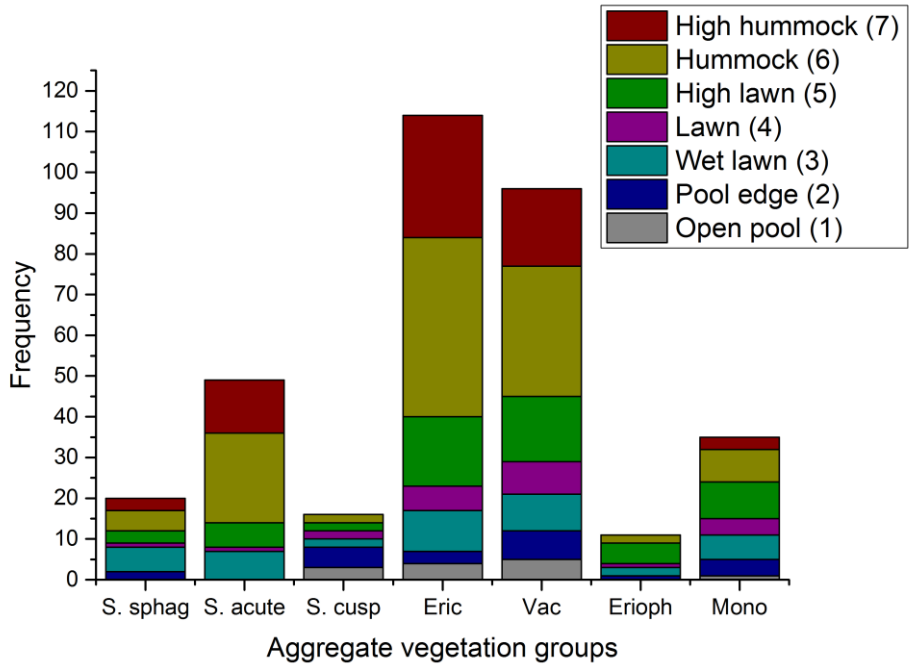

Figure 6.4 Distribution of aggregate vegetation components across microtopographical habitats. Full names: *S.* section (sect.) *Sphagnum*, *S.* sect. *Acutifolia*, *S.* sect. *Cupsidata*, Ericaceae undiff., *Vaccinnium* spp. undiff., *Eriophorum* spp. undiff. monocots undiff.

Table 6.1 Allocated indicator values and corresponding habitat type for each species or aggregated groups based on results from Figures 6.1 – 6.4.

Vegetation	Indicator value	Habitat	Notes
S. papillosum	4	Lawn	Gaps in data
S. magellanicum	5	High Lawn	Bimodal and data gaps
S. rubellum	6	Lower hummock	
S. capillifolium	6	Lower hummock	
S. flavicomens	3	Low lawn	
S. fuscum	6	Lower hummock	
S. cuspidatum	2	Pool edge	
S. pulchrum	2.5	Pool - lawn	
K. angustifolia	6.5	Mid-hummock	
E. nigrum	6	Lower hummock	
R. groenlandicum	6	Lower hummock	
C. calyculata	6	Lower hummock	
K. polifolia	6	Lower hummock	
Picea	7	High hummock	
A. polifolia	5	High lawn	Wide range
Larix	6	Lower hummock	One sample
Juniperus comm.	6	Lower hummock	
V. angustifolium	6	Lower hummock	
V. macrocarpon	3	Low lawn	Wide range
V. oxycoccos	6	Lower hummock	Wide range
R. alba	2	Pool edge	
S. cespitosum	6	Lower hummock	Ubiquitous
E. spissum	3	Low lawn	
E. virginicum	5	High lawn	
O. sphagni	5	High lawn	Gaps in data
D. rotundifolia	6	Lower hummock	Wide range
D. intermedia	6	Lower hummock	One sample
S. purpurea	6	Lower hummock	Few samples
R. chamaemorus	6	Lower hummock	
Cladonia	6	Lower hummock	
Nymphaea	1	Pool	
Dicranum	6	Lower hummock	
Lycopodium	6	Lower hummock	
Aggregate components			
S.* sect. *Sphagnum	4.5	Mid-lawn	
S.* sect. *Acutifolia	6	Lower hummock	
S.* sect. *Cuspidata	2.5	Pool - lawn	
Ericaceae undiff.	6	Lower hummock	
***Vaccinium* undiff.**	4.5	Mid lawn	
Monocot. undiff.	4	Lawn	
***Eriophorum* undiff.**	4	Lawn	

6.3 Jeffrey's Bog

6.3.1 Plant macrofossils

The Jeffrey's Bog (JRB12) macrofossil data were separated into six zones of similar vegetation assemblages (Figure 6.5; Table 6.2). An overview of more subtle variations in the vegetation data is provided in Table 6.1. In broad terms, the assemblage data can be separated into two sections:

1. zones JRB12-a and –b: highly fluctuating conditions with large changes in *Sphagnum* concentrations largely driven by UOM and ericaceous remains and;

2. zones JRB12-c to -f: consistently high abundances of *Sphagnum* with less frequent and less pronounced variability (interrupted by an abrupt disturbance at the end of zone JRB-e).

The main peat forming vegetation in JRB12 is *Sphagnum* section *Acutifolia*, which commonly accounts for *ca.* >60% of the record. *S.* sect. *Acutifolia* dominance can effectively dampen the recording of environmental variability, leading to a complacent macrofossil record (e.g. Hughes *et al*., 2006). Such complacency may be present in zone JRB12-c, a sustained *Sphagnum* dominated zone with minimal inputs from *S.* sect. *Sphagnum* (except from an abrupt *S. austinii* peak to *ca*. 20% at 92 cm) and *S.* sect. *Cuspidata* (sporadic abrupt *S. pulchrum* inputs of 10-20%). The main change in zone JRB12-c occurs around 120 cm when *S. flavicomens* increases to 40% and *S. pulchrum* increases to 20%. Other zones have an improved diversity of *Sphagnum* taxa: *S. magellanicum* and *S. papillosum* are present in JRB12-a, -d and -e and *S. pulchrum* is sporadically present in zones JRB12-d-f.

The macrofossil assemblage suggests that JRB12 has been a *Sphagnum*-rich environment throughout the majority of the record. There is little evidence of sustained pronounced wet conditions since key indicators are either absent (e.g. *S. cuspidatum*) or sporadically present in low concentrations (e.g. *Rhynchospora alba*). During the prominent macrofossil variations in JRB12-a and –b when ericaceous and monocot. inputs increase, the vegetation generally remains *Sphagnum*- dominated owing to the critical role of UOM. The dry alterations in zones JRB12-a and –b are shorter lived than the wet

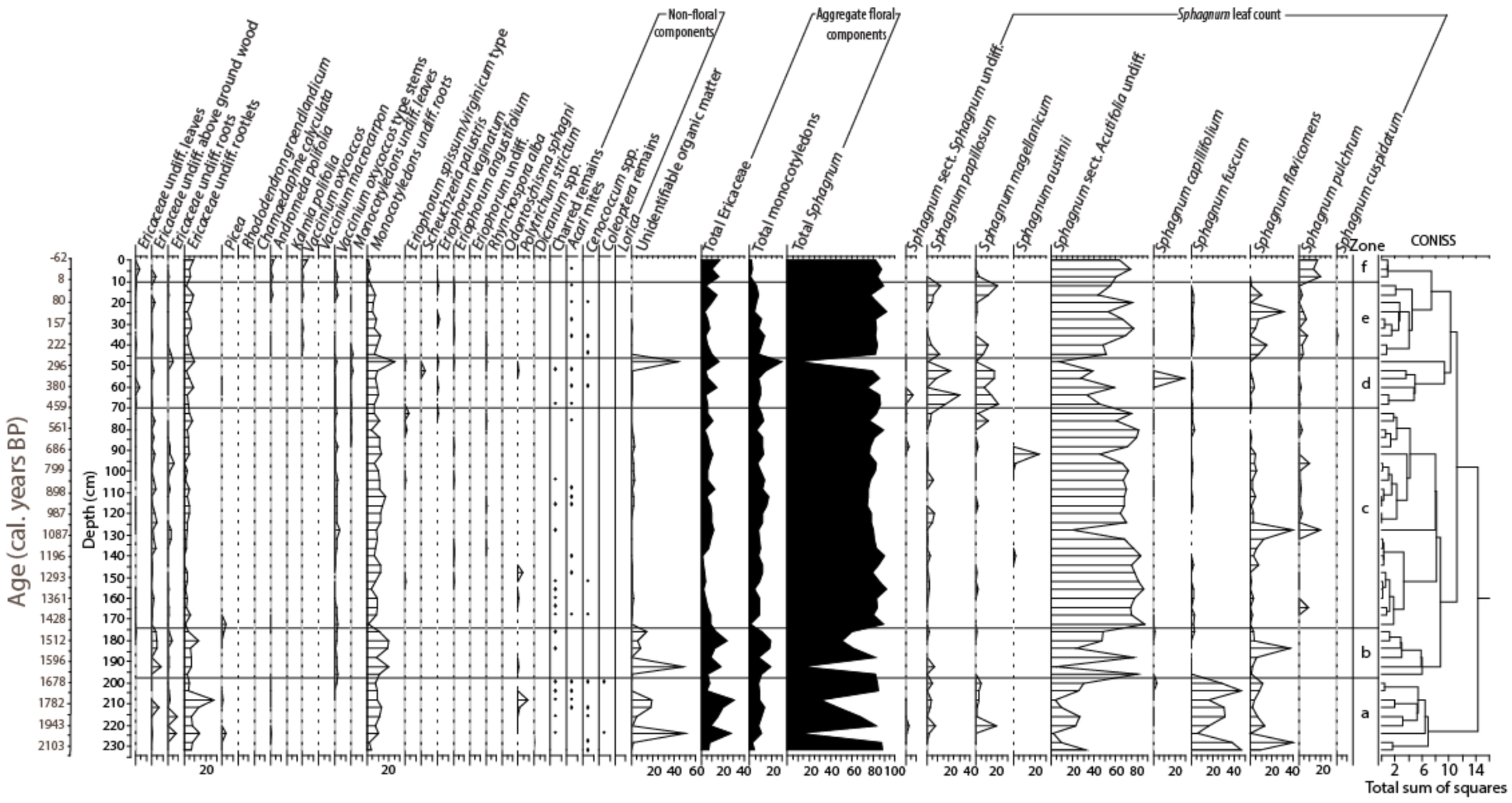

Figure 6.5 JRB12 macrofossil assemblage diagram plotted against depth with secondary age axis.

Peat components displayed with depth bars are derived from averaged quadrat counts (n=15) under low-power magnification (x10). Peat components displayed in solid black denote aggregates of different components. Individual *Sphagnum* leaf counts are also displayed with depth bars as proportion of aggregate *Sphagnum* based on random selection of 100 leaves identified at high magnification (x400). All data are presented as percentages with the exception of presence/absence data, which are displayed as black dots. Zones were assigned after CONISS cluster analysis.

Table 6.2 JRB12 plant macrofossil assemblage description

Zone	Depth (cm)	Vegetation assemblage description	Age (cal yr BP)
JRB12-f	0 - 10	***S.* sect *Acutifolia* dominated peat with presence of *S. pulchrum***. Total monocots are reduced and a slight increase in Ericaceae occurs.	-62 - 8
JRB12-e	10 - 46	**Consistently elevated total *Sphagnum* (dominated by *S.* sect. *Acutifolia*).** Total *Sphagnum* is initially dominated by *S.* sect *Acutifolia* with substantial contributions from *S. papillosum*, S. *magellanicum* and *S. flavicomens* with some *S. pulchrum*. *S.* sect. *Sphagnum* are absent from 36cm to 28cm when *S. flavicomens* increases and *S.* sect. *Acutifolia* slightly decreases. *S.* sect *Sphagnum* increases coincide with the presence of *Rhynchospora alba*, *Andromeda polifolia* and *Kalmia polifolia.* Little–no UOM, total Ericaceae fluctuates *ca.* 10% and monocots subtly decrease towards the end of the zone.	8 - 271
JRB12-d	46 - 70	***S.* sect *Acutifolia* and *S.* sect *Sphagnum* co-dominance**. *S. papillosum* and *S. magellanicum* experience two periods of increase and, when they are decreased, *Picea* is present and *S.* sect. *Acutifolia* increases. There is an abrupt increase in *S. capillifolium* at 56 cm but the majority of *S.* sect. *Acutifolia* is undiff. Total *Sphagnum* dominates with the exception of 48 cm when UOM increases to *ca*. 45%, coinciding with an increase in monocots. *Polytrichum strictum* is present ahead of the UOM increase and *Rhynchospora alba* follows.	271 - 459
JRB12-c	70 - 174	**Sustained zone of increased stability owing to consistent dominance of *S.* sect. *Acutifolia* (*ca.* 80%).** Identifiable *S.* sect. *Acutifolia* is persistently *S. fuscum*, with lower sporadic inputs from *S. capillifolium* and an increase in *S. flavicomens* from 144 cm to 88 cm (*ca*. 10%), abruptly peaking at 128 cm (*ca*. 40%). This peak coincides with an increase in *S. pulchrum* (*ca.* 15%) and the presence of *Rhynchospora alba*. Consistently low inputs from *S.* sect. *Sphagnum* (with the exception of 92 cm when *S. austinii* abruptly increases to *ca*. 20%) although concentrations increase towards the end of the zone. UOM is reduced to background concentrations and fairly consistent fluctuations of total Ericaceae (although a subtle decrease in total Ericaceae occurs from 172 cm to 132 cm) and total monocotyledons occur throughout.	459 - 1462
JRB12-b	174 - 198	**Fluctuating conditions within an increasing total *Sphagnum* trend.** Total monocots are more variable than zone JRB12-a, changing in phase with total Ericaceae and UOM. Initial abrupt increase in UOM at 192 cm (*ca*. 50%) then concentrations varied around 10% for the remainder of the zone. Total *Sphagnum* is dominated by *S.* sect. *Acutifolia* undiff. with an abrupt increase in *S. flavicomens* to *ca*. 35% at 184 cm. Identifiable remains of Ericaceae are *Vaccinium oxycoccos* type with a small input of *Picea* at the end of the zone.	1462 - 1661
JRB12-a	198 - 232	**Highly fluctuating conditions, alternating between *Sphagnum* dominance and UOM and Ericaceae co-dominance.** Total *Sphagnum* is dominated by *S.* sect. *Acutifolia*: mainly *S. fuscum* although *S. flavicomens* initially co-dominates before reducing from 224 cm to the end of the zone. *S.* sect. *Sphagnum* species are present from 224 cm, peaking at 220 cm with 10% *S. papillosum* and 20% *S. magellanicum* before returning to background concentrations throughout the remainder of the zone. Identifiable remains of *Picea* and *Andromeda polifolia* during periods of increased Ericaceae, with *Vaccinium oxycoccos* type present at the end of the zone. *Polytrichum strictum* is generally present in background concentrations, temporarily peaking to 10% at 208 cm.	1661 - 2135

shifts and the return to wet conditions is more abrupt than the original drying.

There are frequent occurrences of insect and non-biological remains within the JRB12 macrofossil record. *Acari* mites are sporadically present with the exception of zone JRB12-b. The highest concentration of mites occurs at the beginning of JRB12-c, coinciding with more stable *Sphagnum*-rich conditions. Around thirty species of mites, with different hydrological preferences, have been previously identified in Canadian bogs (Smith, 1987). Mites were not identified to species level in this study and the bulk mite presence most likely represents a combination of species, which may vary throughout the core. Therefore, *Acari* mites cannot be used to infer environmental conditions in this study. *Cenococcum* species (fungal fruiting bodies) represent enhanced microbial activity associated with aeration (Ferdinandsen and Winge, 1925). These are sporadically present throughout the core, although they are absent for the majority of JRB12-c, during the stable *Sphagnum*-rich conditions. Charred remains are more frequently present in the early stages of the record, indicative of proximal burning events.

Changes in the variability of the major aggregate vegetation components were determined by plotting the residuals generated from Locally Weighted Scatterplot Smoothing (LOESS; Figure 6.6). Of the four components, total *Sphagnum* and UOM contain larger residuals, indicating their dominant role in driving changes in variation. Total *Sphagnum*, total Ericaceae and UOM have increased variability from *ca.* 232 –180 cm, whilst this is less clear in the total monocots. The central section of the record is more stable before an abrupt period of destabilisation is evident *ca*. 60 – 40 cm in the total *Sphagnum*, total monocotyledons and UOM.

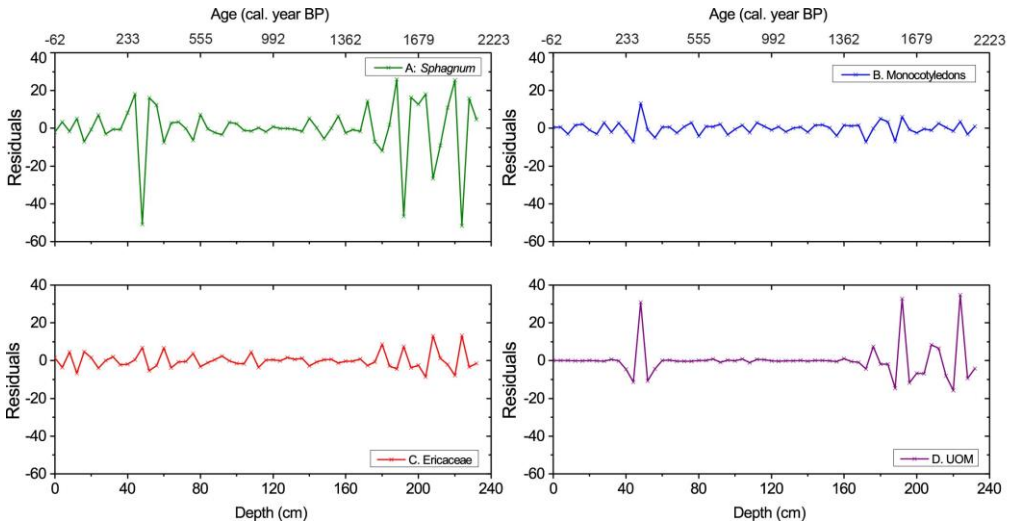

Figure 6.6 JRB12 variability by aggregate groups of the major peat forming components as determined by the residuals from LOESS smoothing.
Sampling proportion = 0.103 (equivalent to n=6) and 1 polynomial degree applied. The y-axes (residuals) scales are consistent between components for comparative purposes.

6.3.1.1 Statistical treatment of JRB12 macrofossil data: DCA

The eigenvalue of the first DCA axis is 0.378, and the gradient length is 2.19, demonstrating that a unimodal response model is appropriate for the ordination of the plant macrofossils within this core.

Visual interpretations of the species distributions across axis one indicate that WTD is a likely driver of vegetation change (Figure 6.7). UOM is located at the positive end of axis one and is indicative of increased decomposition during lower WTD periods. *Picea* and *Polytrichum strictum* are located alongside UOM, supporting the indication of dry conditions. Species towards the negative end of axis one support the presence of a hydrological gradient: *Vaccinium oxycoccos* type and *S. pulchrum* thrive in wetter conditions and *S. cuspidatum is* a key wet indicator. *Rhynchospora alba* is also indicative of wet conditions; however, it has been centrally ordinated. This ordination location can likely be explained by the rarity of the species, which hinders the DCA effectively capturing its environmental preferences.

The aggregate groups of vegetation support water table changes as the major assemblage driver: Ericaceae undiff. is the most positively (dry) located group along the first DCA axis, with monocot. undiff. less positive and the majority

of *Sphagnum* components located towards the negative (wetter) end of the axis. Therefore, the ordination of the main vegetation components across a hydrological gradient supports the use of the axis one scores to reconstruct hydrological driven changes in the vegetation assemblage.

To further test the hydrological influence on the vegetation assemblage and identify periods of similarity within the record, the DCA sample scores were plotted against the first and second DCA axes (Figure 6.8). The majority of the samples are tightly clustered towards the negative end of the axis, which may be indicative of a crossed-gradient within the main axis. The cluster is predominately composed of samples originating from JRB12-c, -e and –f; demonstrating the similarities of these zones. JRB12-a, -b and -d are different from the other zones, with samples being more positively located along axis one. Samples from JRB12-a are dispersed along axis one but are generally the most positive, indicating drier conditions. This spread of JRB12-a samples would be expected based on the macrofossil assemblage diagram since it was a period of high frequency variation. The most positive samples include 224 cm, 192 cm 48 cm, which coincide with a reduction in *Sphagnum* and increase in UOM.

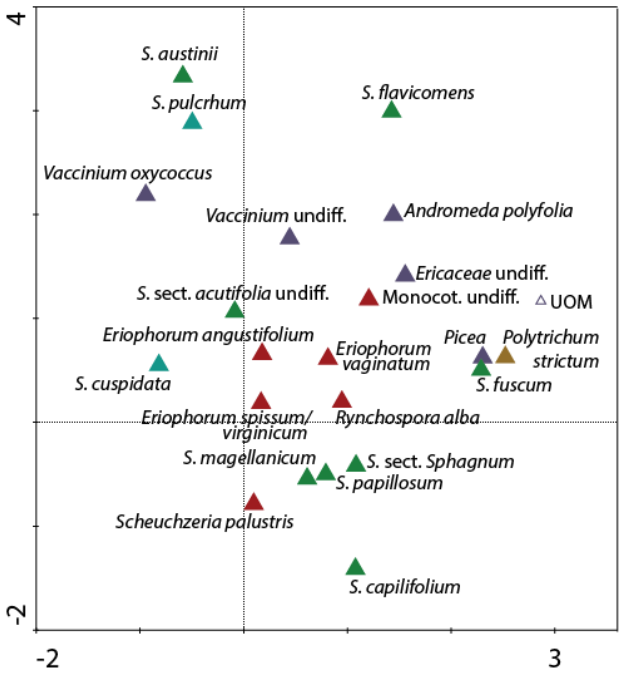

Figure 6.7 JRB12 plant macrofossil DCA axis one (x-axis) and two (y-axis) species scores coloured by similar vegetation types. Purple: Ericaceae; red: monocots and sedges; yellow: brown moss; green: *S.* sect. *Sphagnum* and *S.* sect. *Acutifolia*; blue: *S.* sect. *Cuspidatum*; no fill: UOM.

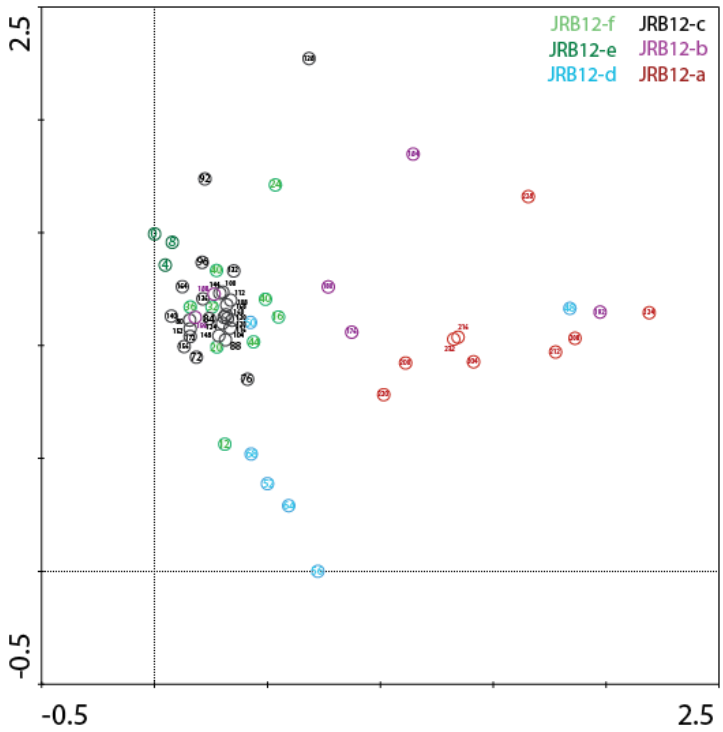

Figure 6.8 JRB12 plant macrofossil DCA axis one (x-axis) and two (y-axis) sample scores coloured by the zones allocated in the assemblage diagram

The driver behind the second DCA axis is unclear: samples 128 cm (zone JRB12-d) and 56 cm (Zone JRB12-c) are positioned towards the opposite ends of the axis and both samples contain increases in *S. flavicomens*. There are two tephra horizons in JRB12: the largest occurs at 131 cm and the other occurs at 71 cm. Therefore, tephra deposition may be influencing axis two of the DCA. Moderate-high tephra loading alters the nutrient content and structure of peat and can shift vegetation communities from being *Sphagnum* to monocot. dominated (e.g. Hughes *et al*. (2013); Payne and Blackford, (2008)). However, an investigation into the effect of distal-tephras in an Alaskan peatland revealed inconsistent peatland vegetation responses to tephra deposition (Payne and Blackford, 2008). Whilst UOM and *Sphagnum* abundance increases coincide with some tephra horizons in the Alaskan peat, these changes do not occur in JRB12. From 128 cm to 108 cm in JRB12, there is a subtle increasing trend in monocot. concentrations and a change in *Sphagnum* type; however, this is not conclusive evidence of a tephra loading driven change since similar trends occur elsewhere (e.g. 184 cm) in the absence of tephra.

The DCA reveals initially high-frequency water table fluctuations, reflecting the enhanced variability detected in the early zones of the assemblage diagram (Figure 6.9). These generally occur within a decreasing trend, suggesting that the peatland became wetter to 172 cm. The wet conditions were more stable until 140 cm when the water table lowered. The peatland was then more stable until a further stepwise drying trend began around 80 cm, culminating in pronounced abrupt dry conditions at 48 cm. The water table then rose and the peatland became increasingly wet to the peat surface. These trends are consistent with early conclusions made from the assemblage diagram, although more subtle alterations within zones JRB12-c and -d are present in the DCA axis one scores.

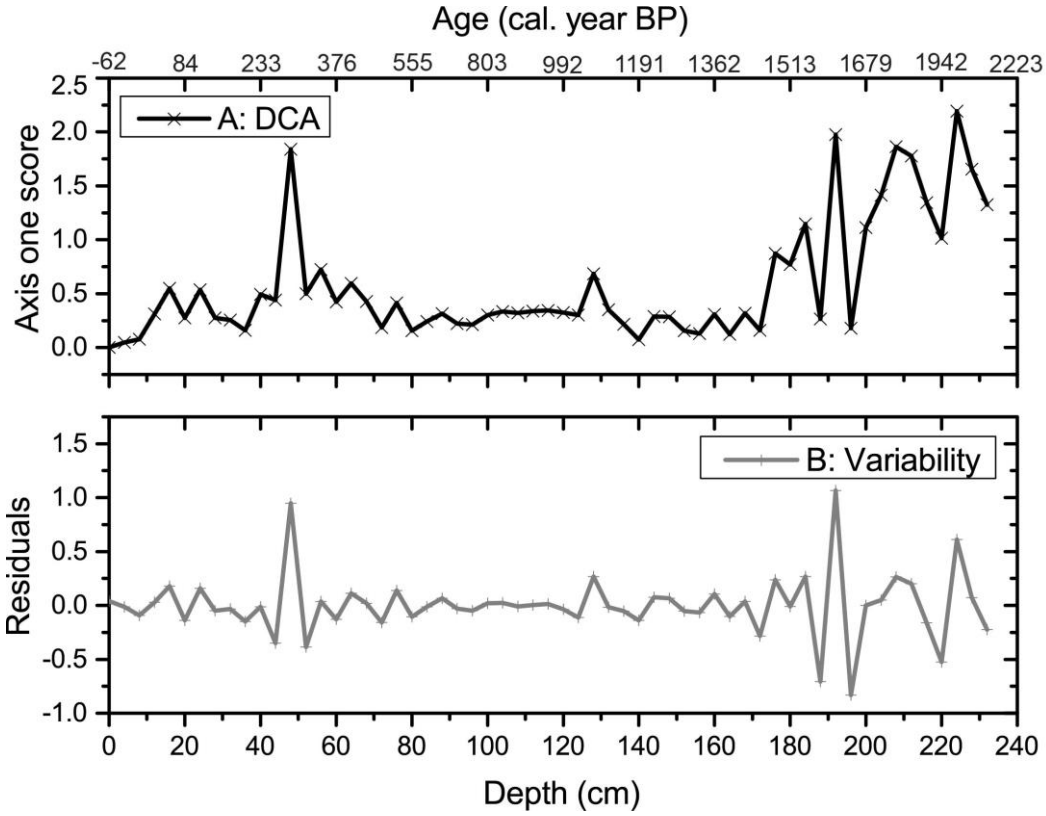

Figure 6.9 A: JRB12 macrofossil DCA axis one scores (lower values indicate wetter conditions); B: Variability of DCA axis one scores as determined by the residuals from LOESS smoothing: sampling proportion = 0.103 (equivalent to n=6) and 1 polynomial degree applied.

6.3.1.2 Statistical treatment of JRB12 macrofossil data: nMDS

The stress value of the nMDS is a measure of the departure from monotonicity in the model and thus provides a measure of the model performance. The nMDS model for the JRB12 macrofossil assemblage had a stress of 0.12,

which suggests that the results of the model can be used with careful interpretation (Figure 6.10).

The nMDS species distribution are similar to the results from the DCA: UOM, *P. strictum*, *Picea* and *S. fuscum* are scaled towards the positive end of axis one, whilst *V. oxycoccos* and *S. pulchrum* are scaled towards the negative end of the axis (Figure 6.10B). The similarity between the DCA and nMDS is also reflected in the similar sample scores: the DCA and nMDS down core reconstructions are positively correlated ($r = 0.98$, $p < 0.001$; Figure 6.10D). Although the magnitude of response within the nMDS and DCA reconstructions vary at points, the direction of change throughout the records is similar. Therefore, the same major climatic interpretations would be extracted from the ordination and multidimensional scaling methods.

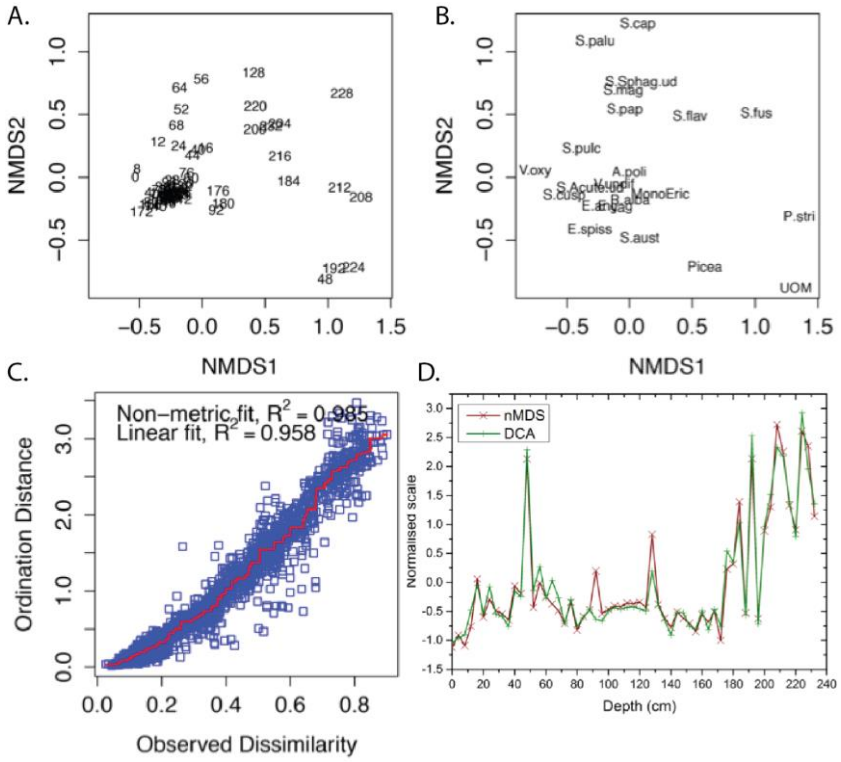

Figure 6.10 JRB12 plant macrofossil nMDS results. A: sample scores, B: species scores, C: nMDS model results, D: normalised nMDS and DCA axis one score reconstructions; lower y-axis values indicate wetter conditions.

6.3.1.3 Statistical treatment of JRB12 macrofossil data: DHI

Based on the results from the DCA and nMDS, which indicated that WTD is the likely driver of vegetation assemblage change (Sections 6.3.1.1 – 6.3.1.2), the

DHI were applied to the JRB12 plant macrofossil assemblage (Figure 6.11). This approach is supported by the conclusions from the DCA and the nMDS, which indicated that WTD is likely the main driver of vegetation change. The medians of the three updated DHI reconstructions (full, excluding UOM and excluding roots) are statistically significantly different (one-way ANOVA H = 14.614, DF = 2, p <0.001). Despite the differences in absolute values, generated by the amplitude of change increasing when the roots are excluded from the index, the indices have statistically significant relationships: the index without roots is more similar to the full index (r = 0.974, p <0.001) than the index without UOM (r = 0.907, p <0.001). Therefore, the hydrological trends between the updated indices are similar.

The index that excludes UOM deviates from the other reconstructions at 192 cm, 48 cm and, to a lesser extent, at 216 cm. Such departures from trend may indicate that the UOM at these depths is associated with algal pool mud rather than dry enhanced decomposition. Alternatively, it may indicate that a driver other than hydrological change generated the increase in UOM. The driver could be a disturbance event or it could represent an increase in a species that is more susceptible to decomposition, such as *Cladonia*.

It is unlikely that algal mud has been mistaken for UOM at 216 cm and 192 cm since the reliable pool indicators, S*. cuspidatum* and *Rhynchospora alba,* are absent. Fires could generate a similar vegetation pattern; however, at these depths charcoal was absent and charred remains were sparse. The wet indicator *Rhynchospora alba* is present around 48 cm. Therefore, whist the presence of algal mud at this depth is possible, such conditions were not observed in the field at the time of coring.

There is a statistically significant difference between the medians of the Daley and Barber derived reconstruction and the full updated reconstruction (U = 689, T = 2580, p = < 0.001); however, they display a significant relationship (r = 0.491, p <0.001), as evident in visual trends which are largely in agreement. The reconstructions do diverge at certain points, particularly between 200 cm and 172 cm. For example, at 188 cm the Daley and Barber derived index increases to 180 cm then gradually decreases, whereas the opposite is true in the full updated index. The assemblage diagram reveals that 180 cm coincided with a *S. flavicomens* increase. This species is not included in the

Daley and Barber (2012) DHI and, whilst weakly characterised in the updated index (Figure 6.1), it could be contributing to the differences in trends.

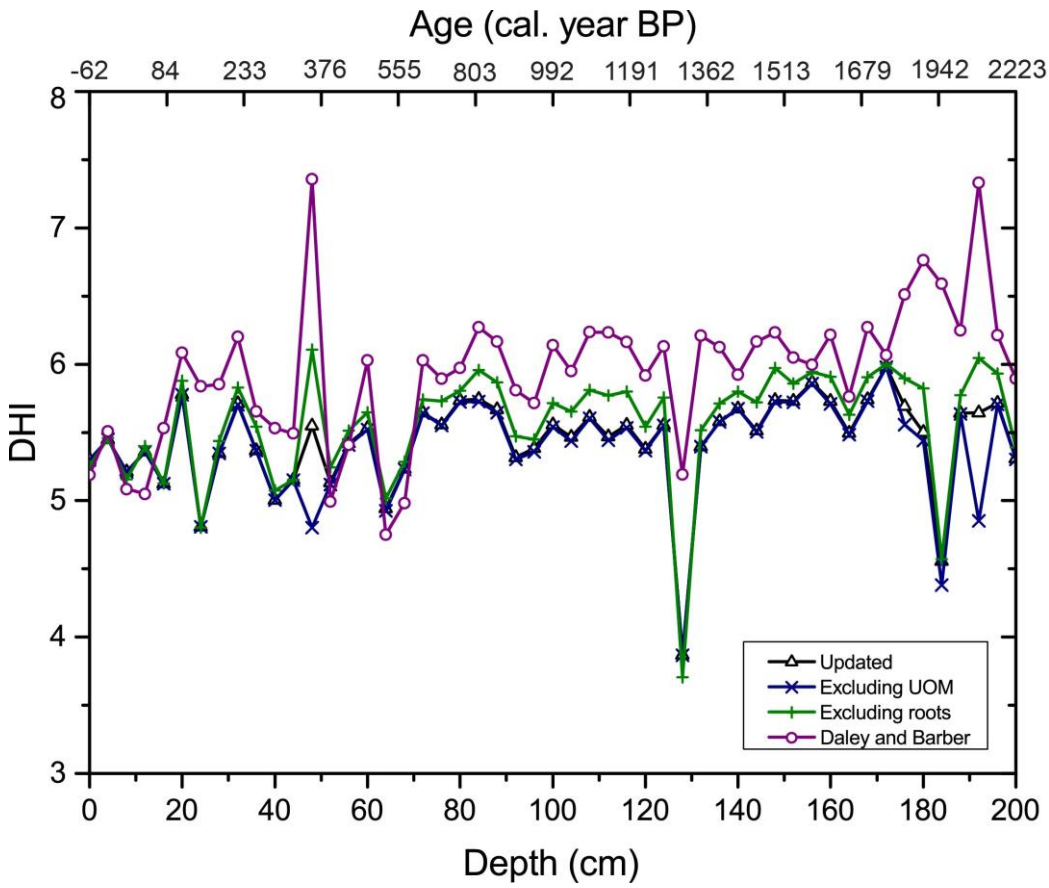

Figure 6.11 JRB12 plant macrofossil DHI reconstructions: the updated full index; the index derived by Daley and Barber (2012); the updated index excluding UOM; and the updated index excluding roots. Lower y-axis values indicate wetter conditions.

6.3.1.4 JRB12 macrofossil hydrological reconstructions

Owing to the similarities between the DCA and nMDS axis one scores (Section 6.3.1.4), it is appropriate to use the DCA axis one reconstructions to represent both methods during statistical comparisons with the DHI indices. The medians of the DCA axis one scores are significantly different from the Daley and Barber derived DHI reconstructed values ($U = 0$, $T = 1770$, $p < 0.001$). However, the DCA trends are more similar to the Daley and Barber derived index ($r = 0.594$, $p < 0.001$), than with the full index ($r = -0.0602$, $p = 0.650$), which has no significant relationship with the DCA reconstruction.

Trends between the different transformation methods are similar until 128 cm, when the DCA increases and the DHI indices decrease (Figure 6.12). This was not a period of divergence between the updated index and the index without UOM; therefore, it is unlikely to have been related to a non-hydrological influence. The assemblage diagram indicates that this divergence coincides with an increase in *S. flavicomens* and, to a lesser extent, *S. pulchrum*. The DCA reconstruction is, therefore, dominated by the higher *S. flavicomens* species score rather than the influence of *S. pulchrum*, whereas the DHI records are more sensitive to the lower scores of *S. pulchrum* and *S. cuspidatum*. Whilst the presence of *S. pulchrum* is indicative of a move towards wetter conditions, it is likely not on the scale that is suggested by updated index. The DHI updated index deviates from both the Daley and Barber derived index and the DCA at 228 cm, 184 cm and 24 cm, each time showing a wet rather than dry change. These depths coincide with *S. flavicomens* peaks, indicating that the hydrological preferences of this taxon may not have been suitably captured in the new index.

These findings indicate that the Daley and Barber index provides a clearer representation of hydrological change in JRB12 than the updated North American index. Through the comparisons of the DHI, DCA and nMDS reconstructions, it is clear that the departure of trends in the index without UOM (at 216 cm, 192 cm and 48 cm), and the associated possibility of non-climate drivers, must be considered when making hydrological comparisons between proxies and sites.

The hydrological reconstructions obtained from the DCA, nMDS and the Daley and Barber derived DHI indicate a fluctuating wetting trend to 176 cm before less fluctuating, more sustained wet conditions. The peatland temporarily becomes drier from 72 cm to 48 cm before the water table rises towards the living surface peat.

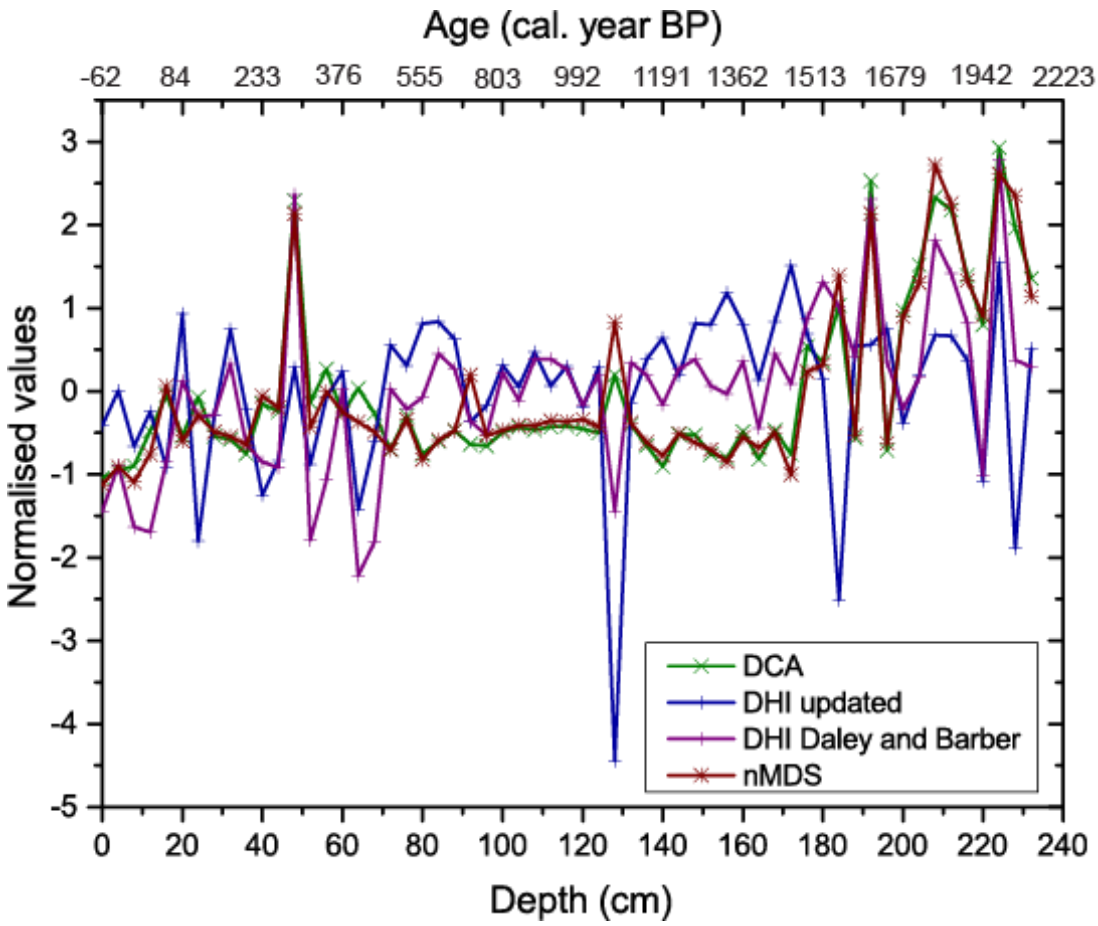

Figure 6.12 JRB12 plant macrofossil normalised data transformations using DCA and nMDS axis one scores and DHI derived from the updated index and the Daley and Barber (2012) index. Lower y-axis values indicate wetter conditions.

6.3.2 Testate amoebae

The testate amoebae data were allocated into eight zones of similar faunal assemblages (Figure 6.13; Table 6.3). The most abundant taxa on JRB12 is *Archerella flavum* which, on average, accounts for 44% of the total assemblage but commonly fluctuates around 70% in the middle section of the core (JRB12-d to –f). *Arcella discoides* and *Hyalosphenia subflava* also provide substantial contributions to the total assemblage: *A. discoides* accounts for *ca.* 20% of the assemblage in zones JRB12-a to –e, and *H. subflava* accounts for *ca*. 30% of the assemblage in JRB12-a to -c.

A. flavum and *A. discoides* are indicators of wet conditions, with *A. flavum* shown to thrive in stable conditions (Charman *et al*., 2007; Amesbury *et al*., 2013; Lamarre *et al*., 2013; Turner *et al*., 2013). *H. subflava* is indicative of dry conditions (*ibid*); therefore, it is encouraging that *H. subflava* is generally

in antiphase with *A. flavum* and to a lesser extent *A. discoides* during zones JRB12-a to -c. Based on the trends of these dominant taxa, the record can be broadly distinguished into three main sections:

1. zones JRB12-a to -c: variable *A. flavum*, high *A. discoides* and *H. subflava* indicating fluctuating conditions;
2. zones JRB12-d to -e: consistently higher *A. flavum*, contribution from *A. discoides* but *H. subflava* input reduced, indicating a wetter more stable period;
3. zones JRB12-f to -h: reduction in *A. flavum*, *A. discoides* and *H. subflava*; increased number of other species contributing to the record thus overall hydrological trends are unclear.

The wet indicator *Amphitrema wrightianum* accounts for *ca.* 10% of the assemblage in zones JRB12-f and -g, suggesting that WTD may have risen in the third section after the wet but more stable conditions of section two. However, *Difflugia pulex*, a dry-intermediate indicator, appeared in abrupt pulses of high concentrations throughout zones JRB12-f to -h after reduced concentrations in section two, perhaps indicating that section three experienced more pronounced fluctuating conditions than section two.

The lack of key dry indicators such as *Trigonopyxis minuta, Centropyxis ecornis* and *Trigonopyxis arcula* suggests that the peatland was a fairly wet habitat throughout the record. Cladocera (water fleas), Chironomidae (non-biting midges) and Platyhelminth (flatworm) egg cocoons are present in the early zones of the core, but are absent throughout the remainder of the core. These organisms require habitats of standing water; therefore, it is possible that the early conditions were wetter than elsewhere in the core. It is interesting to note that *Acari* mites, which consume *chironomids* (Smith 1987), were detected at similar depths in the macrofossil assemblage.

Changes in the variability of the most abundant taxa (*A. flavum, A. discoides, D. pulex* and *H. subflava*) were assessed by plotting the residuals generated from LOESS smoothing (Figure 6.14). Between *ca.* 200 cm and 180 cm, there is an increase in the abundance and variation of *A. flavum, A. discoides* and *H. subflava*. The taxa are then more stable until *ca*. 130 cm when *A. flavum, A.*.

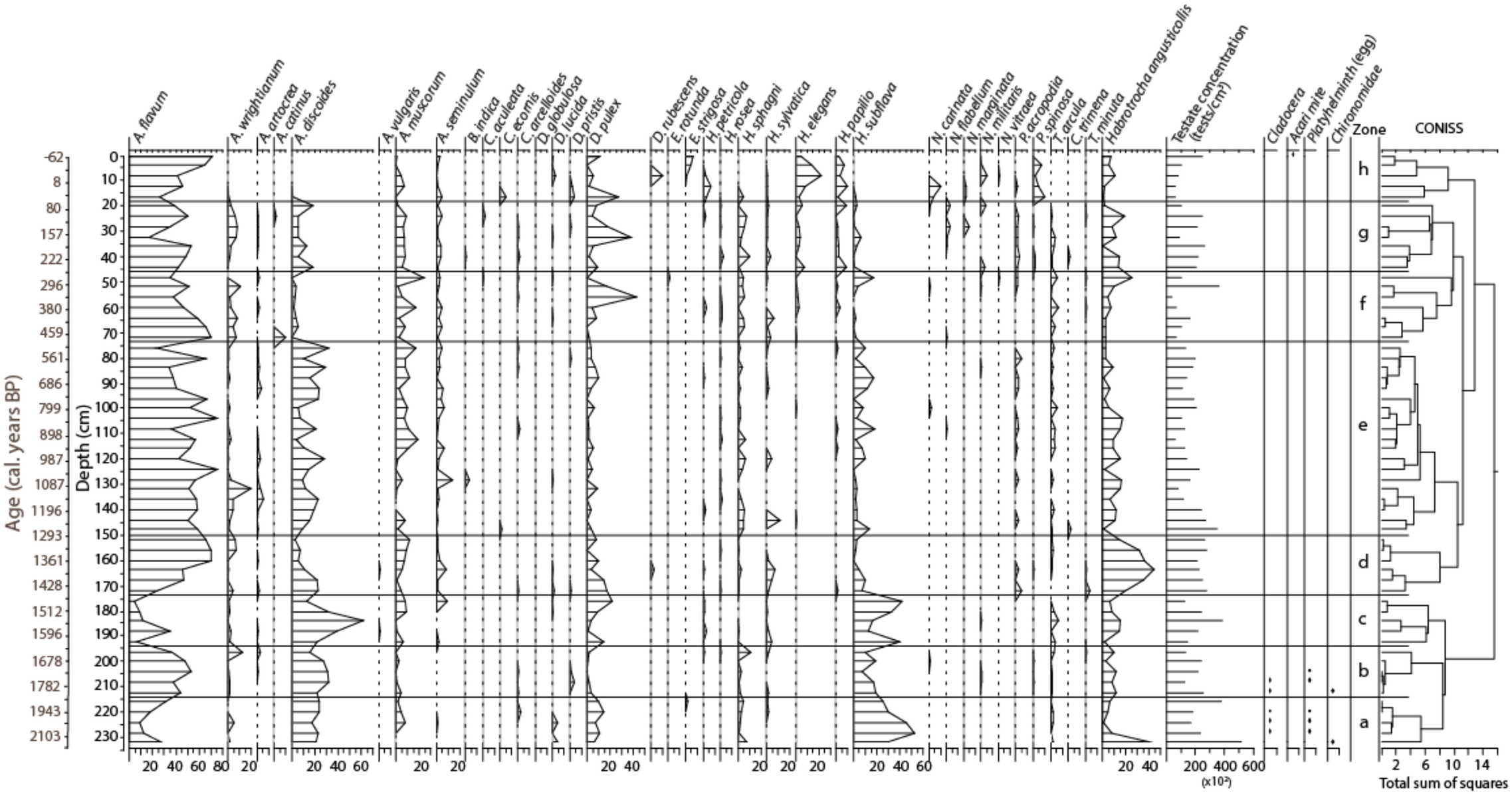

Figure 6.13 JRB12 testate amoebae assemblage diagram plotted against depth with a secondary age axis.

All data are percentages of the 100 tests identified at each sample level. Assemblage data are displayed as depth bars, concentrations of tests per sample are represented by the line graph and the presence of non-testate fauna is indicated by the black dots. Zones have been allocated based on the results of the CONISS cluster analysis.

Table 6.3 JRB12 testate amoebae assemblage data description

Zone	Depth (cm)	Vegetation assemblage description	Age (cal yr BP)
JRB12-h	0 - 18	**Increase in *A. flavum* from *ca.* 25% to 70%.** *A. muscorum* is present in the first half of the zone then is absent whilst D. pulex decreases to the surface. *Hyalosphenia papilio* is present in its highest core concentration (*ca.* 10%) with similar levels of *Placocista spinosa.*	-62 - 64
JRB12-g	18 - 46	***A. flavum* fluctuates around 50% with an abrupt, temporary decrease half way through the zone.** *D. pulex* increases during the abrupt decrease in *A. flavum* to *ca.* 40% then decreases again. *A. discoides* and *A. wrightianum* increase during the first half of the zone before decreasing. Concentrations of *A. muscorum* are stable *ca.* 10%. Many other species are present in background concentrations e.g. *H. sphagni*, *Hyalosphenia elegans, Phryganella acropodia*, *T. arcula.*	64 - 271
JRB12-f	46 - 74	***A. flavum* decreases from *ca.* 70% to 40% and there is a staggered increase in *A. muscorum* reaching *ca.* 20%.** *D. pulex* increases in the first half of the zone reaching *ca.* 40% before decreasing. *A. wrightianum* represents around 10% of the assemblage but becomes absent at end of zone. *A. discoides* decreases to background concentrations along with *Assulina seminulum* and *T. arcula.*	271 - 495
JRB12-e	74 - 150	**Dominance of *A. flavum* which fluctuates in a subtle decreasing trend from *ca.* 40-60%.** *A. flavum* changes ahead of *A. discoides*, which fluctuates around 10-25%. H subflava is present in background concentrations until the second half of zone when it fluctuates around 15 %. *A. wrightianum* initially increases to 20% then is present in background concentrations, accompanied by low levels of *D. pulex* and *T. arcula*.	495 - 1293
JRB12-d	150 -174	***A. flavum* increases from 20% reaching *ca.* 70% by the end of the zone**. *A. muscorum* also increases but only reaches *ca.* 10%. *A. discoide*s, *D. pulex* and H. *subflava* decrease.	1293 - 1462
JRB12-c	174- 194	***A. discoides* increases towards *ca.* 65% in the middle of the zone before decreasing to *ca.* 15%.** *A. flavum* increases ahead of *A. discoides* reaching *ca.* 35% before decreasing throughout the remainder of the zone to *ca.* 5% (lowest core abundance). *D. pulex* and *H. subflava* initially decrease then increase towards the end of zone, with opposing trends in *A. flavum and A discoides. H subflava* is more dominant, reaching *ca.* 45% and a similar trend is evident in *A. muscorum.*	1462 - 1628
JRB12-b	194- 214	**The first half of the zone is dominated by *A. flavum* (*ca.* 50%)** which then decreases. *A. discoides* subtly increases then decreases accounting for *ca.* 30% of the assemblage whilst *H. subflava* fluctuates around 20%. *Amphitrema wrightianum, Heleopera sphagni, A. muscorum* and *T. arcula* are present in background concentrations although the former two species increase to 15% towards the end of the zone.	1628 - 1847
JRB12-a	214 -232	**Initially dominated by *H. subflava* (*ca.* 50%), which decreases throughout the zone as *A. flavum* increases**. Stable abundances of *A. discoides* (*ca.* 20%) and *D. pulex* (*ca.* 10%). *Assulina muscorum* is present throughout the second half of the zone in low abundances accompanied by background levels of other species (e.g. *Trigonopyxis arcula, Heleopera sylvatica* and *Cyclopyxis arcelloides* type).	1847 - 2135

discoides and *H. subflava* increase to *ca*. 70 cm. The high abundances of *D. pulex* and *A. flavum* then alternate between stable and more variable conditions until the surface, whilst *A. discoides* and *H. subflava* are more stable but in reduced abundance.

The concentration of individual tests increases from the depth of the core towards the surface (r=-0.431, p <0.01; Figure 6.15). This increasing trend may be influenced by preservation, assisted by the long term wetting trend identified by the macrofossils that would limit decomposition. The most consistent run of concentrations occurs between 172 cm and 140 cm, whilst test concentrations peaks at 56 cm, fluctuating towards the surface

An average of eleven testate amoebae were identified per sample, however, the species richness increased towards the surface (r=-0.458, p <0.001; Figure 6.15). Excursions to increased species richness (n=17) occurred between 172 cm and 164 cm. The increasing trend in the number of species is particularly clear between 140 cm and 28 cm, before decreasing towards the live peat. This trend is likely influenced by long-term preservation issues (Wilmshurst *et al*., 2003) assisted by the gradually wetting conditions: drier species have large WTD tolerances, therefore, could occupy wetter conditions alongside the species preferring the wetter habitats.

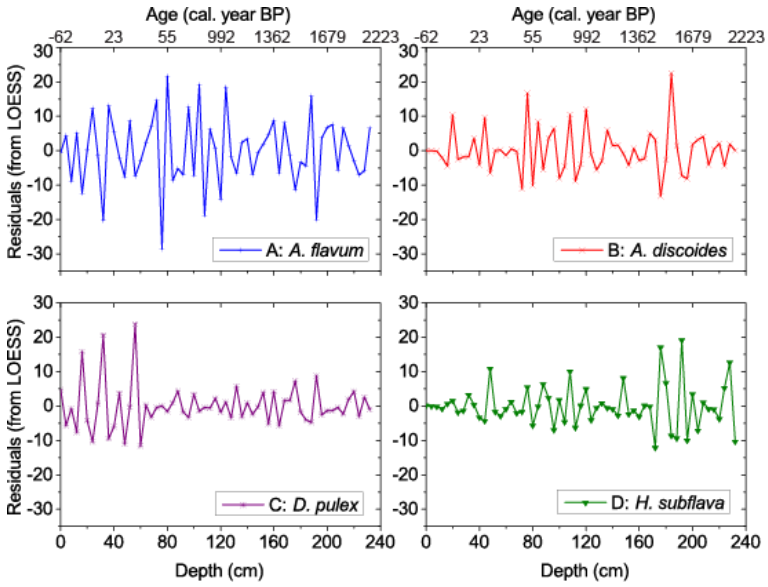

Figure 6.14 Variability of the four most abundant testate amoebae taxa. A: *A. flavum*; B: *A. discoides*; C. *D. pulex*; D*: H. subflava* are plotted using the residuals from LOESS smoothing. A sampling proportion of 0.103 (equivalent to n=6) and 1 polynomial degree were applied.

The Shannon Diversity Index (SDI; Shannon, 1948) considers the relative proportion of species in a population (Equation 6.1) and is often referred to as a measure of the communities 'health' (i.e. stability): values usually lie between 1.5 and 3.5 (Margalef, 1972) with 0.5 to 1.5 representing stressful conditions for the community and over 2.5 representing stable conditions when there is an equitable distribution of species (Patterson and Kumar, 2000). SDI values from published testate amoebae studies rarely exceed 2.5 (Tsyganov *et al.*, 2011); however, changes in the SDI throughout the cores will still provide a useful indication of balance of the population, despite the smaller range.

$$\text{Shannon Index (H)} = -\sum_{i=1}^{s} p_i \ln p_i \qquad (6.1)$$

where p is the proportion (n/N) of individuals of one particular species (n) divided by the total number of individuals (N), s is the number of species.

Whilst other diversity indices exist (e.g. the Simpson Index), the log transformation of the species abundance data in the SDI is an advantageous approach since it reduces the weight of the most abundant taxa (Sageman and Bina, 1997). The SDI provides a useful guide to the degree of dominance within the testate amoebae population; however, it is prudent to note that the assemblage data within this thesis likely violates two of the main SDI assumptions: that the individuals originate from an infinitely large community (Pielou, 1975), and that all species are represented within the sample (Peet, 1974). Therefore, results should be cautiously interpreted.

The majority of JRB12 SDI values indicate that the community is in constant transition. The lowest SDI occurs at 124 cm and the community is highly fluctuating but often stressed between 128 cm and 96 cm. This may be indicative of a particular period of disturbance within the assemblage. Conversely, it may be influenced by the dominance of *A. flavum* and *A. discoides* (as reflected in the species evenness index), indicating unbalanced conditions at these points of low SDI. The SDI then increases towards the peat surface as species richness and species evenness also increase.

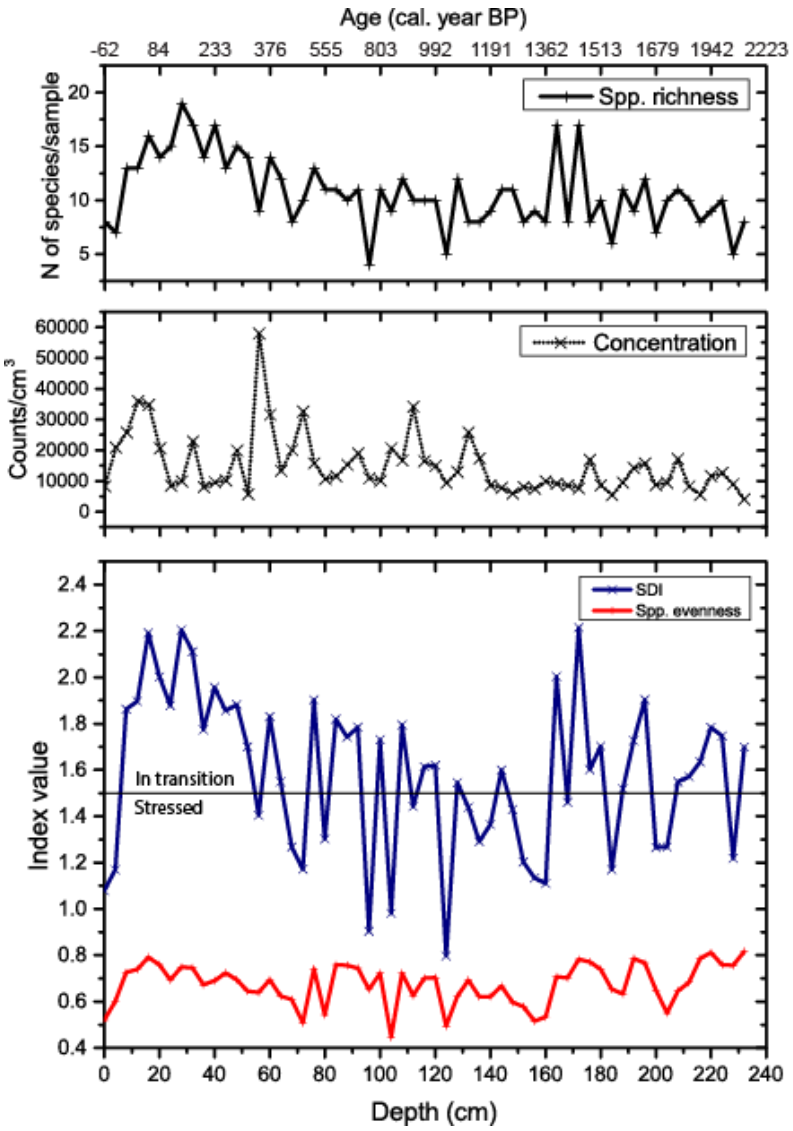

Figure 6.15 JRB12 testate amoebae ecological measures. A: Species richness (number of species per sample); B: Concentrations of individuals (counts per cm^3 of peat; determined used L*ycopodiu*m counts); C: Shannon Diversity index (calculated using the number of species per sample and the total number of species in the core; insert equation); D: Species evenness (indicates the relative abundance of species, calculated using the SDI and the natural log of species with zero = no evenness and 1 = evenness).

6.3.2.1 Statistical treatment of JRB12 testate amoebae data: DCA

The eigenvalue of the DCA is 0.30 and the gradient length is 2.489, indicating that a unimodal response model is appropriate for the ordination of the testate amoebae within this core. The species ordination along axis one is indicative of a water table gradient (Figure 6.16). Species with dry preferences, such as *T. arcula, Arcella artocrea, Bullinularia indica,* and *T. minuta,* are located to the positive end of axis one, whilst species with wetter

preferences such as *Nebela marginata, Heleopera petricola* and *P. spinosa* are located towards the opposite, negative end of the gradient.

The relative distributions of two of the major species, *A. flavum* (wetter) and *H. subflava* (drier), are also in support of a hydrological driver. However, a third major species, *A. discoides*, is in disagreement since it would be expected to be located towards the wetter end of the axis. Similarly, the wet indicator *A. Wrightianum* is located towards the positive, dry end of axis one. This taxon is common throughout the record; therefore, the ordination location may distort water table inferences obtained using the DCA axis one scores. The assemblage diagram reveals that *A. wrightianum* often appears after high concentrations of *A. flavum*. These taxa have overlapping water table tolerances, with *A. wrightianum* extending to wetter conditions than *A. flavum*. Therefore, the trend from *A. flavum* to *A. wrightianum* most likely indicates further wetting conditions rather than the drier conditions inferred from the DCA.

Other species which have unexpected ordination locations include *Hyalosphenia elegans, Euglypha strigosa* and *Centropyxis ecornis* which are situated towards the negative (wet) end of axis one but usually thrive in drier conditions. These species are rare or increase in concentration towards the surface of JRB12; therefore, perhaps the full distribution characteristics of these species have not have been captured within the DCA. Despite these discrepancies, it is unlikely that these taxa are prominent enough to limit the effectiveness of the hydrological reconstructions inferred from the DCA axis one scores.

The effect of rare taxa and the surface zone on the species distributions across axis one were assessed by repeating the DCA with different parameters: firstly, samples from zone JRB12-h were excluded (eigenvalue 0.255; gradient length: 2.041) and secondly, the rare species were excluded rather than simply downweighted (eigenvalue: 0.278; gradient length: 2.259). The eigenvalues of the alternative DCA are lower than the original full DCA and the positions of the major and problematic species experience little change along axis one. Therefore, it is appropriate to use the original DCA results to infer hydrological changes in the JRB12 testate amoebae assemblage.

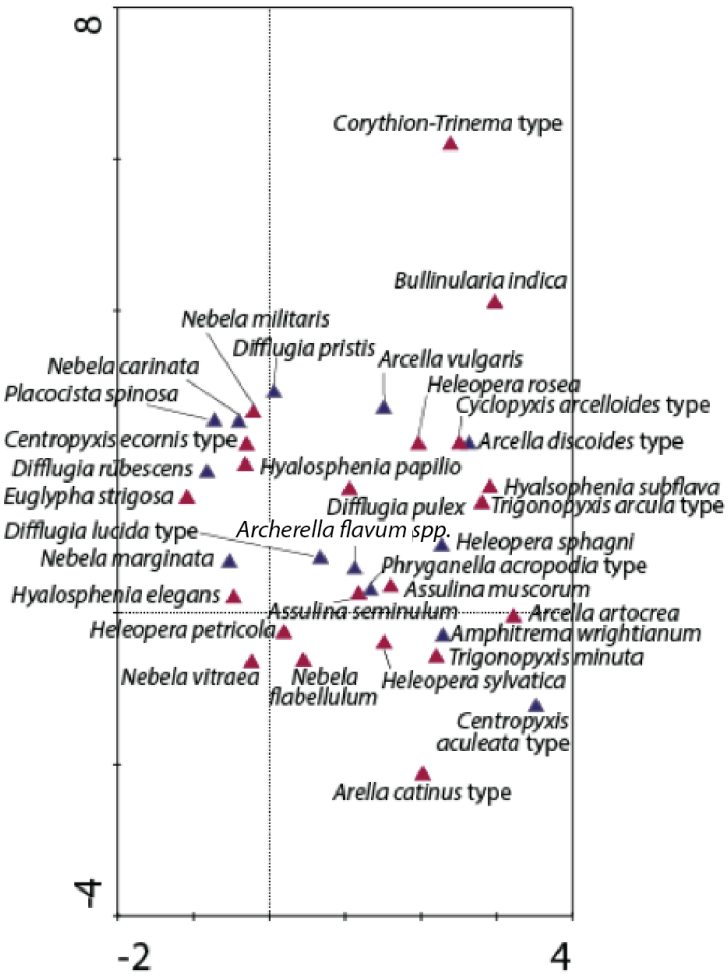

Figure 6.16 JRB12 testate amoebae DCA axis one (x-axis) and axis two (y-axis) species scores.
Red symbols represent species with drier WTD preferences and blue symbols represent species with wetter water table depth preferences. Colours (and thus dry or wet preferences) have been assigned based on the training sets of Amesbury *et al.*, (2013) and Lamarre *et al.*, (2013).

The ecological assessment outlined above concludes that the DCA scores can be used as a guide to general trends in water table variations. However, owing to the ordination location of *A. wrightianum* and *A. discoides*, the axis one scores have potential to be complacent to some wet shifts. During periods of moderate *A. wrightianum* abundances (e.g. the boundary between JRB12-d and -e and throughout JRB12-f and –g) or dominance of *A. discoides* (e.g. JRB12-a to –c), water table changes must be interpreted cautiously.

The JRB12 testate amoebae sample scores can be presented against the first and second axes to identify assemblage similarities within the record (Figure 6.17). The majority of samples are clustered towards the positive (drier) end

of axis one. Within this clustering, there is little evidence of clear zonal separation along axis one, which may be a result of fluctuating hydrological conditions. Samples from the surface zones (JRB12-g and -h) are located towards the negative (wetter) end of axis one and are disconnected from the other zones, which may suggest that taphonomy is influencing the ordination. JRB12-f is generally the most negatively ordinated zone located along axis two; however, the driver behind this axis is unclear.

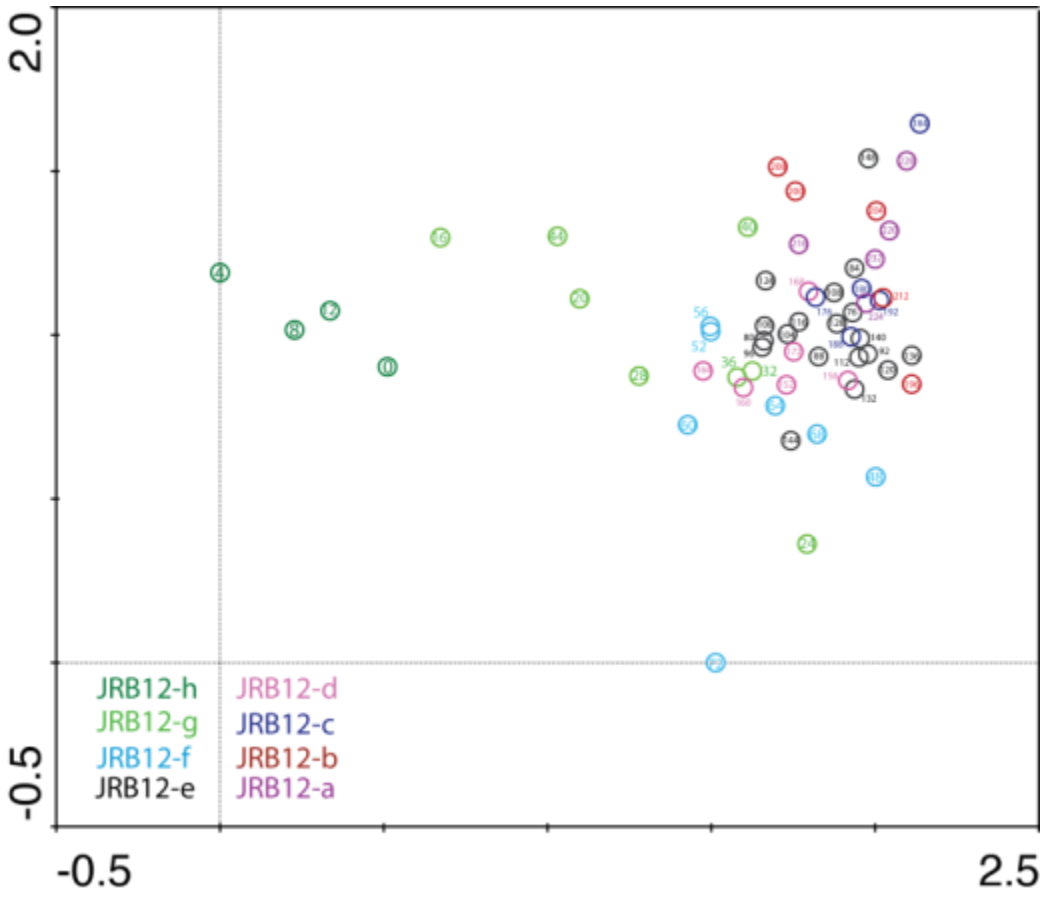

Figure 6.17 JRB testate amoebae DCA sample scores. Colours represent zones allocated in CONISS analysis (see **Error! Reference source not found.**)

The DCA axis one scores reveal a decreasing trend throughout the record, which is indicative of the peatland becoming wetter (Figure 6.18). This is similar to the hydrological reconstructions obtained from the macrofossil data (Figure 6.12). Within the wetting trend, there is an abrupt change to drier conditions between 192 cm and 176 cm. The end of this increase coincides with the abrupt increase in species richness and thus SDI (Figure 6.15).

Following a change to wetter conditions, the water table fluctuated from *ca.* 124 cm - 72 cm before a stepwise decrease to the living peat. This period of fluctuation is related to the pronounced increase in variability of the major species (Figure 6.14). The DCA indicates an accentuated wetting trend from 32 cm to 8 cm in the active layers of peat. This leads a reduction in species richness (which occurs from 28 cm to the surface), a reduction in testate amoebae test concentration (from 12 cm) and coincides with the peak SDI (32 cm; Figure 6.15). Whilst, at this resolution, it is difficult to disentangle the living peat processes from the overall hydrological signal, it could be hypothesised that the reduction in species richness is hydrologically driven, whereas the decrease in test concentration may reflect the zone of living testate amoebae that have not yet been subjected to the compression (hence concentration) processes that occur during accumulation.

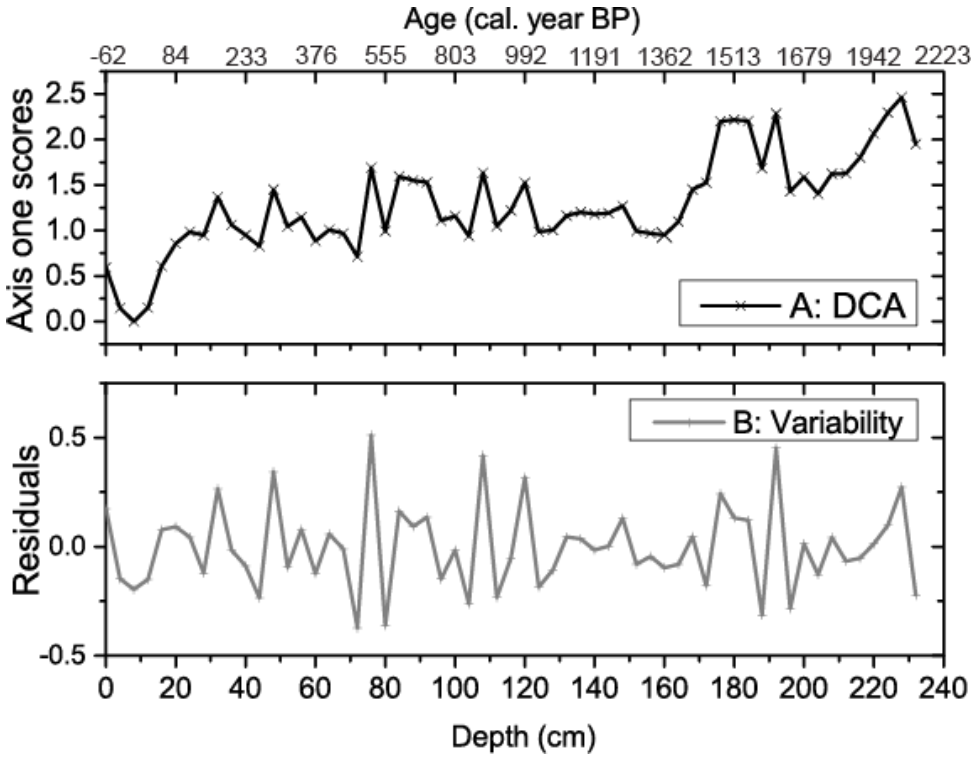

Figure 6.18 JRB12 testate amoebae DCA environmental reconstruction and associated variability.
A: DCA axis one scores reconstructing hydrological change (lower y-axis values indicate wetter conditions); B: Variability of the DCA axis one scores using the residuals from LOESS smoothing. A sampling proportion of 0.103 (equivalent to n=6) and 1 polynomial degree were applied.

6.3.2.2 Statistical treatment of JRB12 testate amoebae data: nMDS

nMDS was conducted on the JRB12 testate amoebae data to confirm and evaluate results obtained from the DCA (Section 6.3.2.1). The nMDS model had a stress of 0.13, which indicates that the results from the model can be carefully interpreted (Figure 6.19).

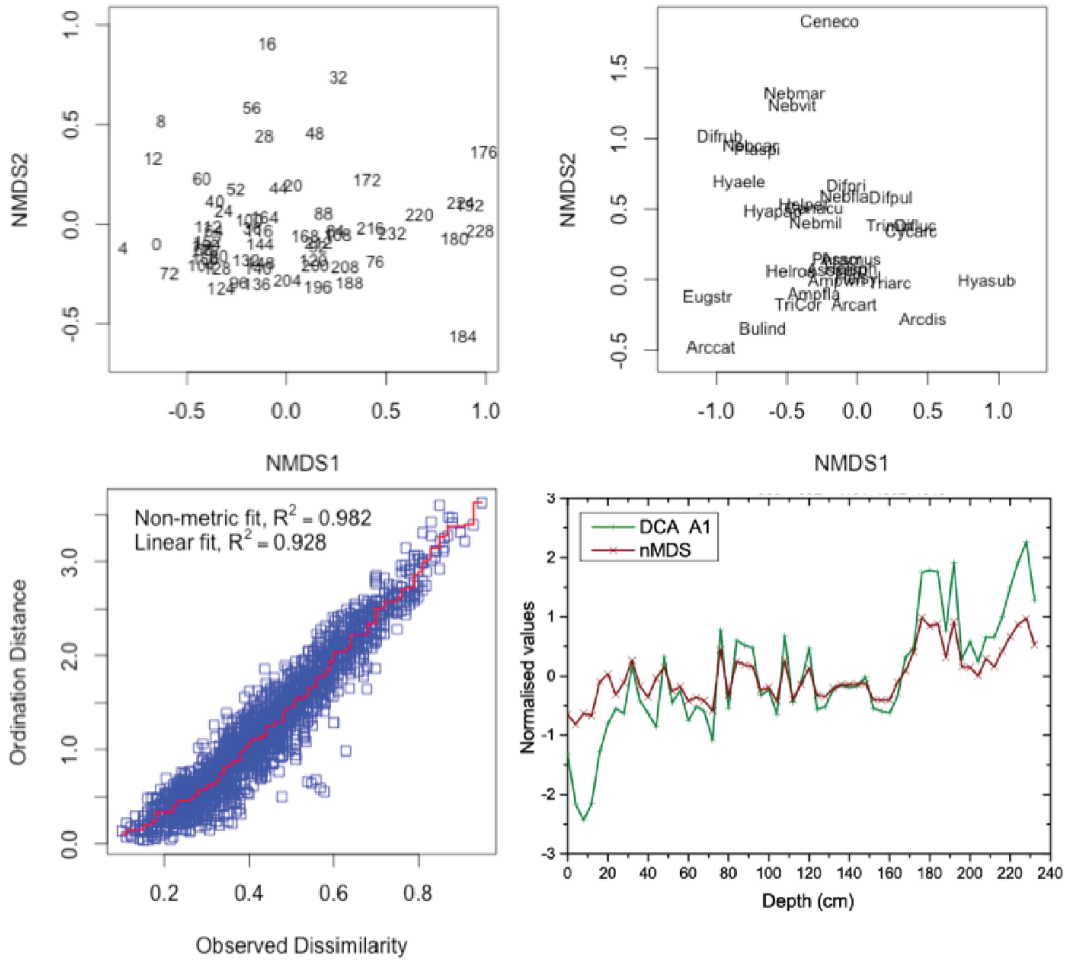

Figure 6.19 JRB12 testate amoebae nMDS results.
A: sample scores, B: species scores, C: nMDS model results, D: normalised nMDS and DCA axis one score reconstructions (lower y-axis values indicate wetter conditions).

The species distributions across the primary nMDS axis are similar to the results of the primary DCA axis: *H. subflava* and *A. discoides* are located towards the positive end of the axis whist *H. elegans* and *Difflugia rubescens* are located towards the negative end of the axis (Figure 6.19B). This suggests that the same underlying environmental variable and associated response from the testate amoebae have been detected using both the DCA and the nMDS. The scaling of the two problematic species (*A. wrightianum* and *A.*

discoides) identified in the DCA axis one results has been slightly refined towards ecological expectations within the nMDS. However, their ordination locations within the nMDS are still indicative of drier conditions than would be expected based on the training sets from Amesbury *et al*. (2013) and Lamarre *et al*. (2013). The downcore reconstructions using the nMDS and DCA axis one scores are similar ($r = 0.94$, $p < 0.001$); therefore, the reconstructed trends would lead to similar climatic interpretations (Figure 6.19D).

6.3.2.3 Statistical treatment of JRB12 testate amoebae data: transfer functions

A comparison of the ATLANTIC.NA transfer function models results using the JRB12 testate amoebae data indicate that there is a statistically significant difference between the medians of the model which downweights species with large water table tolerance (WA.inv.tol) and the model which weights all taxa equally (WA.inv; $U = 1369$, $T = 3139$, $p = 0.046$). The WA.inv reconstruction has a 16.5% greater error than WA.inv.tol. Greater amplitude of change is evident in the WA.inv model compared with the WA.inv.tol; however, there is a significant relationship between the direction of change been the two models ($r = 0.839$, $p < 0.001$; Figure 6.20). Whilst the small differences (e.g. around 40 cm) would not alter the environmental inferences, the reconstructions exhibit opposing trends around 164 cm (highlighted in red; Figure 6.20): the WA.inv.tol-based reconstruction decreases to 164 cm then increases, whilst the WA.inv reconstruction increases then decreases over the same depth interval.

The median values of the QUEBEC WA.cla.tol and WA.cla model reconstructions are also significantly different from one another ($U = 1241$, $T = 3011$, $p = 0.007$). The models show a significant positive relationship ($r = 0.749$, $p < 0.001$; Figure 6.21); however, this correlation is weaker than the correlation between the two ATLANTIC.NA models. The WA.cla model contains greater amplitudes of change compared with WA.cla.tol; however, the error of prediction is similar between the two models: WA.cla reconstruction error is 0.6% greater than WA.cla.tol. Whilst there is agreement in the direction of change between the two models, there are more prominent periods of trend disagreement compared with the in ATLANTIC.NA reconstructions (highlighted in red; Figure 6.21). Despite the presence of these trend

discrepancies between models, they are within a common error range; therefore, it is unlikely that they will alter final environmental inferences.

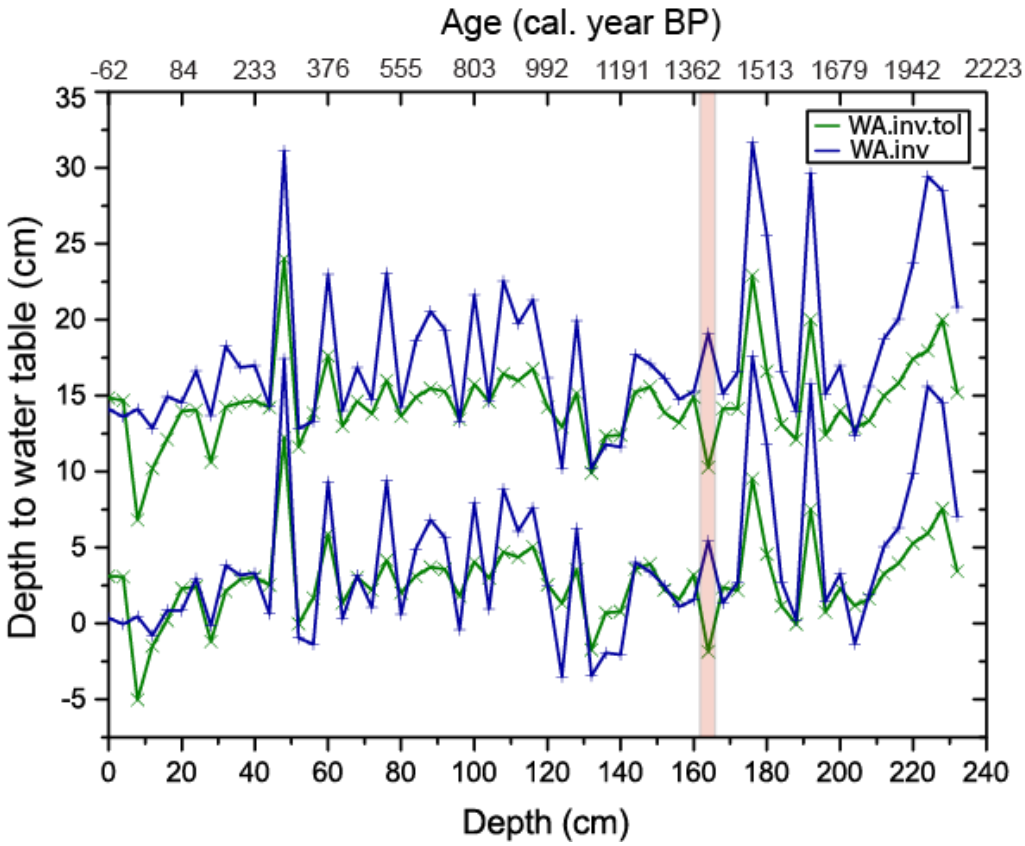

Figure 6.20 JRB12 Testate amoebae reconstructed depth to the peatland water table based on the WA.inv.tol (green) and WA.inv (blue) transfer function models of Amesbury *et al*. (2013). Both upper and lower estimates of depth to the water table are shown for each model. Red sections represent periods of conflicting trends between models. Lower y-axis values indicate wetter conditions.

In both transfer functions, the variability is generally smaller when the species with large water table preferences are downweighted (WA.tol models) than when all species are weighted equally (WA models). The main exception occurs towards the surface of the records when WA.tol variation is larger, perhaps influenced by the decrease in species richness (Figure 6.22). Both transfer functions exhibit increased variation between 192 cm and 172 cm, increased stability from 172 cm to 60 cm and a return to increased variability to 42 cm.

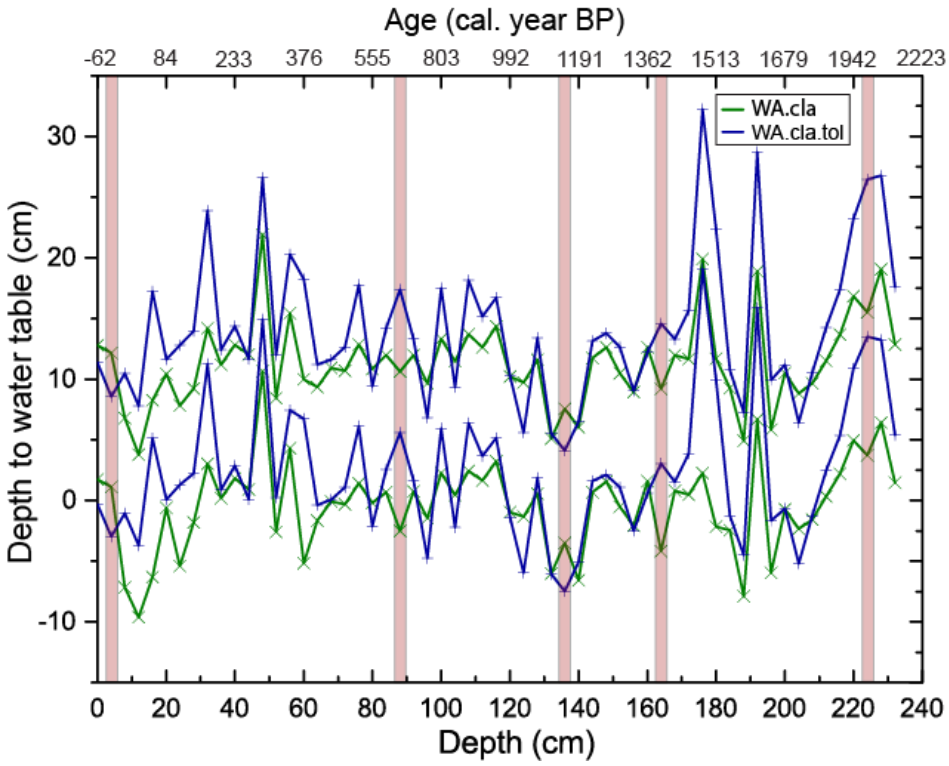

Figure 6.21 JRB12 Testate amoebae reconstructed depth to the peatland water table based on the WA.cla.tol (green) and WA.cla (blue) transfer function models of Lamarre *et al*. (2013). Both upper and lower estimates of depth to the water table are shown for each model. Red sections represent periods of conflicting trends between the models. Lower y-axis values indicate wetter conditions.

The correlation coefficients reveal that there is a significant relationship between all model results from both transfer functions (Table 6.4). Within transfer functions, there is more similarity between the ATLANTIC.NA models than between the QUEBEC models. It may be hypothesised that the similarities would be greater within rather than between transfer functions since the same training set is used; however, the ATLANTIC.NA WA.inv and QUEBEC WA.cla are the most similar. It is interesting to note that the models shown to have the best performance statistics from each transfer function (i.e. ATLANTIC.NA WA.inv.tol; Amesbury *et al*. (2013) and QUEBEC WA.cla.tol; Lamarre *et al*. (2013) have the least similarity. The degree of similarity does not reflect the model performances and should not guide the final model reconstruction selection since this would result in a circular argument. Rather the most robust reconstructions should be obtained using the best performing models of each transfer function. In the instance of JRB12, the best performing models have the added advantage of presenting the least

similar reconstructions: this could be viewed as the safest option for inferences since they cover a wider range of likely water table positions.

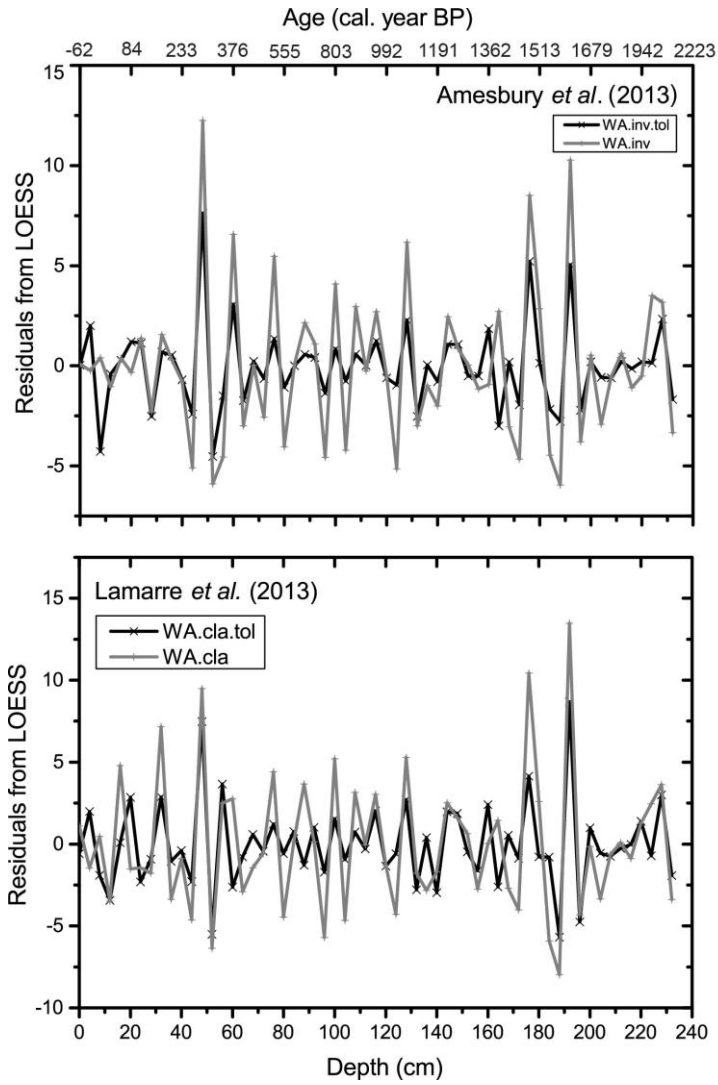

Figure 6.22 Variability of the Amesbury *et al*. models (upper) and Lamarre *et al*. models (lower) using the residuals from LOESS smoothing. A sampling proportion of 0.103 (equivalent to n=6) and 1 polynomial degree were applied.

Table 6.4 Pearson Correlation Coefficents for the JRB testate amoebae transfer function model reconstructions

	ATLANTIC.NA WA.inv	**QUEBEC WA.cla.tol**	**QUEBEC. WA.cla**
ATLANTIC.NA WA.inv.tol	r = **0.839** p < 0.001	r = 0.833 p <0.001	r = 0.752 p < 0.01
ATLANTIC.NA WA.inv		r = 0.703 p < 0.001	**r = 0.897** p < 0.001
QUEBEC WA.inv.tol			r = 0.749 p < 0.001

General trends between the ATLANTIC.NA and QUEBEC transfer function reconstructions are similar: the water table is lower, but more variable, deeper in the core before rising and becoming more stable in wetter conditions until *ca.* 52 cm when it becomes wetter towards the surface peat (Figure 6.23).

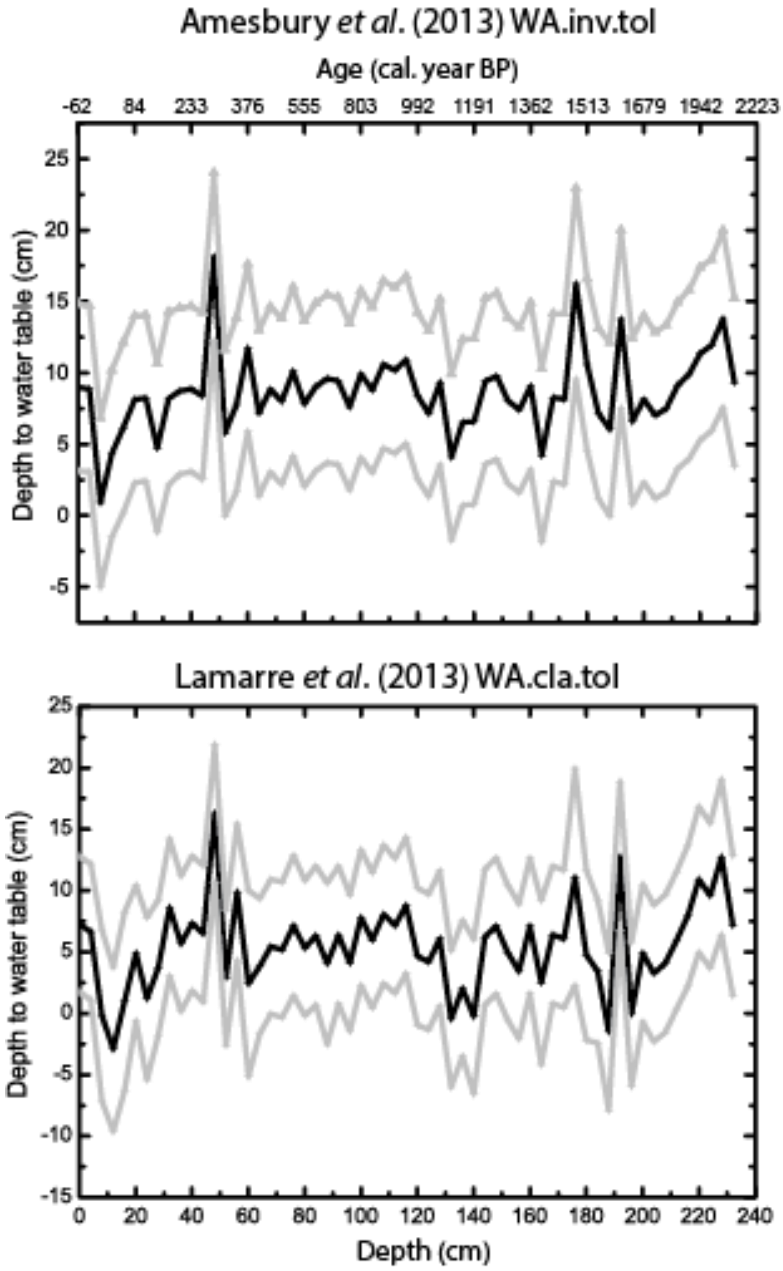

Figure 6.23 JRB12 testate amoebae transfer function reconstructions using ATLANTIC.NA WA.inv.tol (upper) and QUEBEC WA.cla (lower). Grey lines indicate standard error of prediction. Lower y-axis values indicate wetter conditions

6.3.2.4 JRB12 testate amoebae hydrological reconstructions

The testate amoebae transfer function reconstructions, DCA axis one scores and nMDS axis one scores have been normalised to facilitate comparisons between reconstructions (Figure 6.24). Owing to the similarities between the DCA and nMDS scores (Section 6.3.2.2), the DCA can represent both techniques within statistical comparisons with the transfer functions. The DCA has a significant relationship with both the ATLANTIC.NA and QUEBEC reconstructions; however, slightly greater similarities exist between the DCA and ATLANTIC.NA reconstruction ($r = 0.553$, $p < 0.001$) than between the DCA and QUEBEC reconstruction ($r = 0.465$, $p < 0.001$). Whilst the broad trends contained within all reconstructions are similar, differences occur at 184 cm, where the DCA and nMDS increase before the transfer functions, and around 144 cm where the DCA and nMDS do not experience the decrease that appears in both transfer function reconstructions. These deviations may indicate periods when the ecological response is unclear or influenced by secondary gradients.

Based on a combination of the DCA and nMDS axis one scores and the ATLANTIC.NA and QUEBEC transfer function reconstructions, it can be proposed that the peatland initially became wetter to 196 cm before drying to 176 cm. The peatland became wetter to *ca*. 160 cm and then more gently fluctuated around more stable conditions until *ca.* 64 cm when an abrupt stepwise drying occurred to 44 cm. The peatland then became wetter towards the living peat surface.

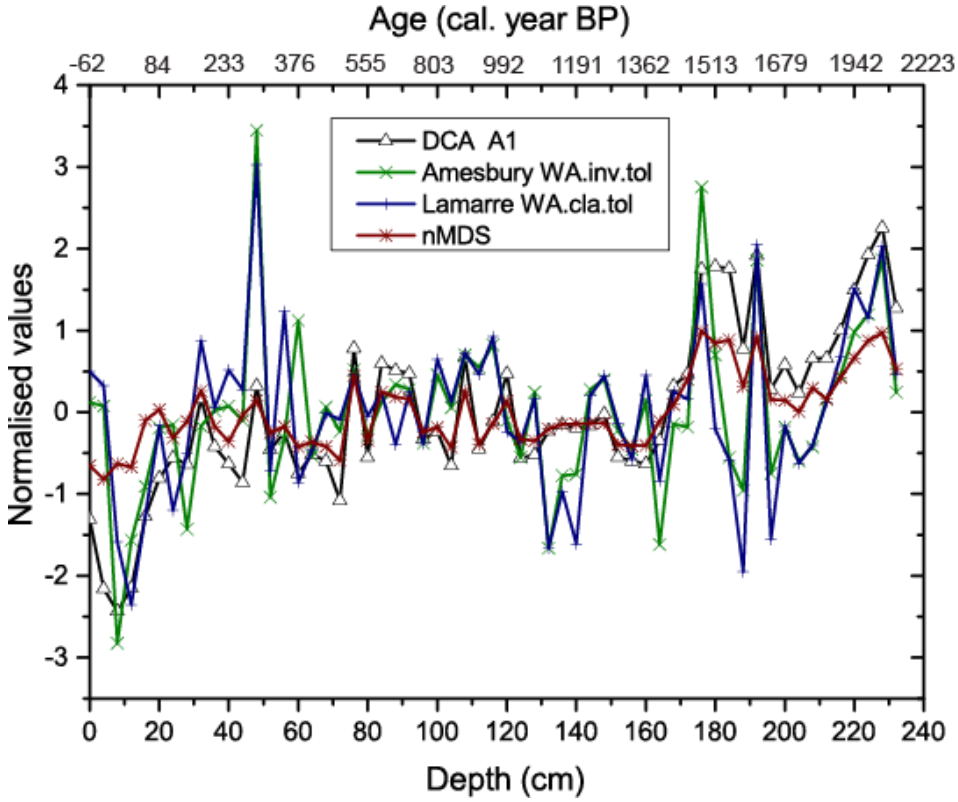

Figure 6.24 JRB12 testate amoebae normalised data transformation. Lower y-axis values indicate wetter conditions.

6.3.3 Full JRB12 palaeoecological comparison

The final testate amoebae water table reconstructions are represented by the QUEBEC WA.cla.tol and ATLANTIC.NA WA.inv.tol reconstructions and the plant macrofossil water table reconstructions are represented by the Daley and Barber derived DHI (Figure 6.25). Samples that show deviations between the ordination and weighted averaging transformation techniques are highlighted using red boxes since they are not confidently representing hydrological conditions.

The trends between the plant macrofossils and the testate amoebae are similar throughout, indicating that WTD is likely the dominant driver of change within both proxies. The main difference between the plants and the testate amoebae records are the response time and the relative size of change. At the start of the record the testate amoebae indicate a wetting record followed by a drying trend before the plant macrofossils, which reveal smaller scale changes. The macrofossils then indicate a wetting trend *ca.* 1600 cal yr BP ahead of the testate amoebae. The testate amoebae respond

ahead of macrofossils into a warming or drying trend *ca.* 1100 cal yr BP; however, the macrofossils then show a wetter period to *ca.* 500 cal yr BP. The broad scale hydrological trends appear to indicate an overall two stage wetting, initially to *ca.* 1100 cal yr BP, then again from *ca.* 950 cal yr BP to the living peat

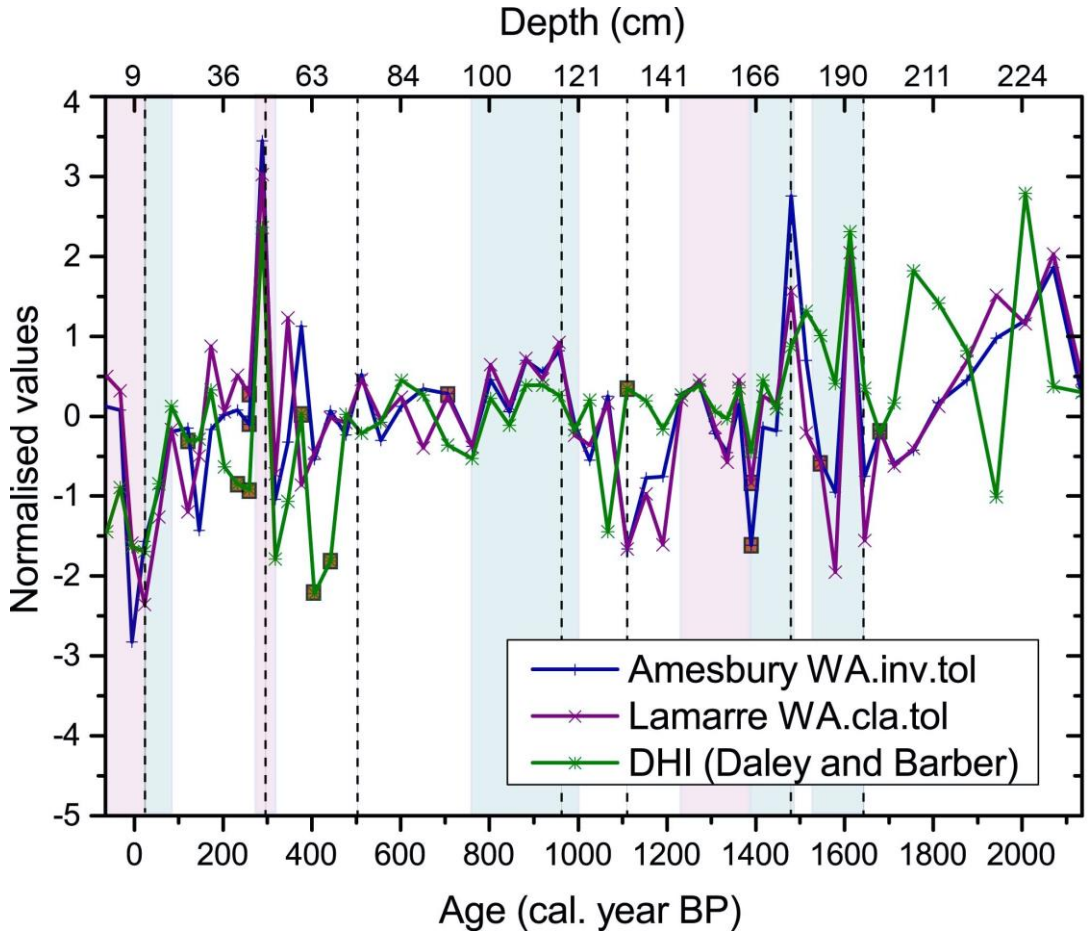

Figure 6.25 JRB12 normalised comparison of ecohydrological reconstructions blue shaded areas indicate coherent trends towards wetter conditions and red shaded areas indicate trends towards drier conditions.
Any white areas indicate periods where trends in the proxies disagree or are unclear. Dashed lines separate periods of similar hydrological conditions. Samples that are likely driven by factors other than hydrological conditions (as identified by differences in ordination and weighted averaging-based techniques) are highlighted by red boxes around individual points along with any divergences in the transfer function trends. Lower y-axis values indicate wetter conditions

.

6.4 Framboise Bog

6.4.1 Plant macrofossils

The Framboise Bog (FBB12) macrofossil record has been separated into eight zones of similar vegetation assemblage. These were guided by results from CONISS analysis, although the placement of the boundaries between FBB12-a, -b, and –c were moved down by one sample to capture the point of the largest difference in concentrations (Figure 6.26; Table 6.5). The outline FBB12 macrofossil and testate amoebae analysis were completed at 4 cm resolution to 200 cm, based on expected accumulation rates. However, rangefinder ^{14}C dates indicated that the peatland was accumulating at roughly half the expected speed with 132 cm indicating the end of the 2000-year period of interest. To compare the palaeoecological record with the other sites in this study, it was desirable to increase the sampling resolution at this site so that all sites were similar over time rather than depth. Therefore, the sampling resolution was increased to 2cm between 132 – 0 cm and remained at 4 cm between 196 - 136 cm.

The full variation by zone is summarised in Table 6.5; however, the vegetation assemblage can be broadly separated into three main sections:

1. zones FBB12-a to -d: gradual but pronounced changes in total *Sphagnum*, Ericaceae and monocots;
2. zone FBB12-e: more variable conditions, with total *Sphagnum* abruptly fluctuating although generally low with an overall subtle increase in UOM;
3. Zones FBB12-f to -i: increasing trend in total *Sphagnum* to more sustained higher concentrations towards the surface.

It is likely that section two was fairly dry, inferred from the reduced *Sphagnum* abundance, possibly containing a further subtle drying trend from 130 cm to 60 cm. The increase in total *Sphagnum* in section three indicates a wetting trend, which culminates at the surface, as indicated by increased concentrations of *S. cuspidatum* and *S. pulchrum*.

Sphagnum sect. *Acutifolia* is the main peat-forming component accounting for 70 % of the total assemblage in the *Sphagnum* dominated zones FBB12-d,

-g, -h and -i. The dominance of *S.* sect. *Acutifolia* is superseded by a dominance of *S.* sect. *Cuspidata* at FBB12-i. Throughout the highly fluctuating zone of FBB12-e, *S.* sect. *Acutifolia* still contributes; however, at points of low *Sphagnum* (often less than *ca*. 20%), monocots dominate (*ca*. 50-60%) accompanied by considerable ericaceous inputs. Frequent *Sphagnum* concentrations of *ca*. 20% are lower than would be expected for a classic plateau peatland and may have contributed to the slow accumulation rates.

UOM input is low throughout the record with the exception of certain samples in zones FBB12-a, -e and -f. This highest UOM concentration is 40%, which coincides with the lowest *Sphagnum* input of <10% around 70-60 cm. The increase in UOM reinforces the likelihood of drier conditions; however, large contributions could also originate from disturbance events. Charred remains are frequently present throughout the record (concentrated in FBB12-a and -e) and an abrupt spike in charcoal occurs during FBB12-e. However, whilst the charcoal and charred remains are indicative of proximal burring events, there is no evidence from the age-depth model, or the vegetation patterns in the macrofossil record, to suggest fire disturbance around the coring location.

A comparison of the major aggregate vegetation components reveals that total *Sphagnum* and total monocots contain more variation than total Ericaceae and UOM (Figure 6.27). Focusing on the higher resolution sampling period (0 - 132 cm), total *Sphagnum* contains high variability until 72 cm, whilst a similar elevated variability continues until *ca.* 36cm in the total monocots. The stability of total Ericaceae increases around 132 cm then decreases to a constant level throughout the remainder of the record. UOM is stable from 176 cm to *ca*. 124 cm where it experiences a trend of increasing variability, culminating *ca*. 60 – 70 cm. Periods of increased stability are visible in all components between *ca*. 56 - 42 cm and *ca*. 28 cm to the peat surface.

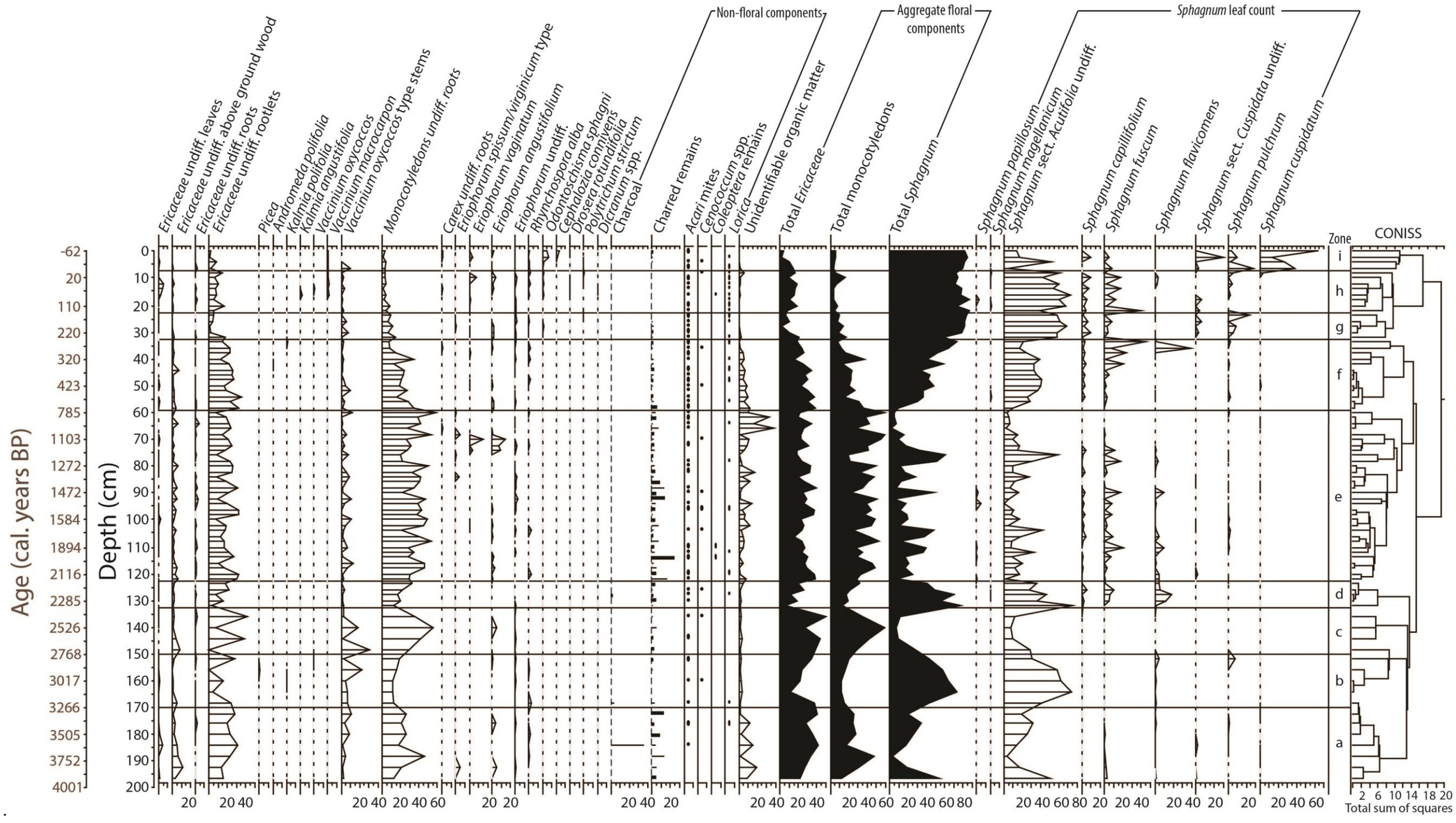

Figure 6.26 FBB12 macrofossil assemblage diagram plotted against depth with secondary age axis.

Peat components displayed with depth bars are derived from averaged quadrat counts (n=15) under low-power magnification (x10). Peat components displayed in solid black denote aggregates of different components. Individual *Sphagnum* leaf counts are also displayed with depth bars and represent proportion of aggregate *Sphagnum* based on random selection of 100 leaves identified at high magnification (x400). All data are presented as percentages with the exception of presence/absence data, which are displayed as black dots. Zones were assigned after CONISS cluster analysis.

Table 6.5 FBB12 plant macrofossil assemblage description

Zone	Depth (cm)	Vegetation assemblage description	Age (cal yr BP)
FBB12-i	0 - 7	***Sphagnum* rich peat changes to *S.* sect. *Cuspidata* dominated**. *S. capillifolium* and *S. fuscum* are present but main input is initially from *S. pulchrum* (*ca.* 25%) and *S. cuspidatum* (*ca.* 35%). *S. pulchrum* then decreases and *S. cuspidatum* increases to *ca.* 65 % at the surface. *Cephalozia connivens* and *O. sphagni* are increasing towards the surface. *R. alba, E. vaginatum, E. angustifolia* and *V. macrocarpon* present.	-62 - -5
FBB12-h	7 - 23	***Sphagnum* dominated peat** which experiences a subtle decrease in concentration as total Ericaceae and total monocots increase (average *ca.* 15% and *ca.* 10%). Initially, S. *papillosum* and S. *magellanicum* are present before S. *pulchrum* returns in in low concentrations accompanied by S. *magellanicum*. *O. sphagni*, *Drosera rotundifolia*, *R. alba* and *Eriophorum* spp. are present. Remains of *Dicranum* spp. and P. *strictum* are identifiable, along with *V. macrocarpon* and small pulses *K. angustifolia* and *V. oxycoccos*.	-5 - 146
FBB12-g	23 - 33	**Sustained increase in total *Sphagnum***, which remains *S.* sect. *Acutifolia* dominated (mix of *S. capillifolium* and *S. fuscum*) but concentrations of *S. pulchrum* to *ca.* 20% at 24 cm. Total monocots and total Ericaceae continue to decrease and UOM is sustained at low levels throughout the remainder of core. Monocot. components remain similar to preceding zone. *Odontoschisma sphagni* remains are present and there is an abrupt occurrence of *Polytrichum strictum* at 24 cm.	146 - 246
FBB12 -f	33 - 59	**Increasing total *Sphagnum* abundance** accompanied by a reduction in total monocots, total Ericaceae and total UOM. *Sphagnum* is mainly sect. *Acutifolia* undiff. although S. *capillifolium* is present throughout along with *S. fuscum* which increase from 42 cm towards the end of the zone. S. *pulchrum* is present in low concentrations and pulses of S. *flavicomens* and S. *cuspidatum* occur at 36 cm and 50 cm respectively. Initially *V. oxycoccos* type is present but reduces in the latter half of the zone *A. polifolia* and then *K. polifolia* remains are identifiable. Identifiable monocot. remains initially composed of *Eriophorum* spp. but these are then accompanied by *R. alba* and *Carex* are present at 34 cm. Reduction of charred remains	246 - 739
FBB12 -e	69 - 123	**Change to abruptly fluctuating monocot. dominated peat.** *Sphagnum* concentrations are low, dominated by sect. *Acutifolia*. Low pulses *of S. papillosum* present in the first half of the zone and small inputs from *S. pulchrum* throughout. UOM increases, reaching peak core concentrations of *ca.* 35% 66 – 62 cm. Varied monocot. remains identifiable: *Eriophorum* spp. are present throughout whilst *R. alba* is initially sporadically present then returns towards the end of the zone accompanied by *Carex* spp. Increased concentrations of *E. angustifolium* and *E. vaginatum* occur between 74 – 68 cm (both *ca.* 10%). Pulses of *Vaccinium* spp. contribute to total Ericaceae. Increased sporadic input of charred remains.	793 - 2164
FBB12 -d	123 - 133	**Abrupt increase in *Sphagnum*** to *ca.* 75% decreasing to *ca.* 45% towards the end of the zone. Majority of *Sphagnum* is sect. *Acutifolia* undiff. but, of the identifiable leaves, *S. flavicomens* initially increases (coinciding with a pulse of *S. magellanicum*) before being replaced by increasing abundances of *S. fuscum* and, to a lesser extent, *S. capillifolium*. Throughout the zone, total Ericaceae and total monocots double from 10% and 15% respectively. Reduction to background abundances of *V. oxycoccos* type and UOM input continues to be low.	2164 2358
FBB12 -c	133 - 150	**Decrease in total *Sphagnum*, replaced by total monocots and total Ericaceae**. *S.* sect *Acutifolia* dominated peat decreases to sustained concentrations of *ca*. 10%. Whilst total monocots increase to 140 cm (*ca*. 55%; *Eriophorum* remains identified) whilst total Ericaceae increase 144 cm then again at 148 cm (*ca*. 50%). UOM is consistently low.	2358 - 2768
FBB12 -b	150 - 170	**Initial increase in *Sphagnum* sect. *Acutifolia*; *ca.* 70% then decrease.** *S. flavicomens* present in background concentrations and a small pulse of *S. pulchrum* occurs at the end of the zone. Total Ericaceae and, to a lesser extent, total monocots increase towards the end of the zone. Sequential remains of *K. polifolia, Picea* then *V. oxycoccos* are present along with *R. alba* and *Eriophorum* spp.	2768 - 3266
FBB12-a	170 - 198	**Mix of major components and fluctuating conditions.** Total Ericaceae subtly increases (*ca.* 30%) and total monocots and UOM generally decrease throughout the zone *(ca.* 30% and *ca.* 10% respectively). Total *Sphagnum*, dominated by *S.* sect. *Acutifolia*, fluctuates around *ca.* 50% to *ca.* 5%. *Vaccinium oxycoccos* type gradually increases and low pulses of *Eriophorum* spp. and *Rhynchospora alba* occur. Large abrupt inputs of charcoal at 184 cm.	3266 - 3975

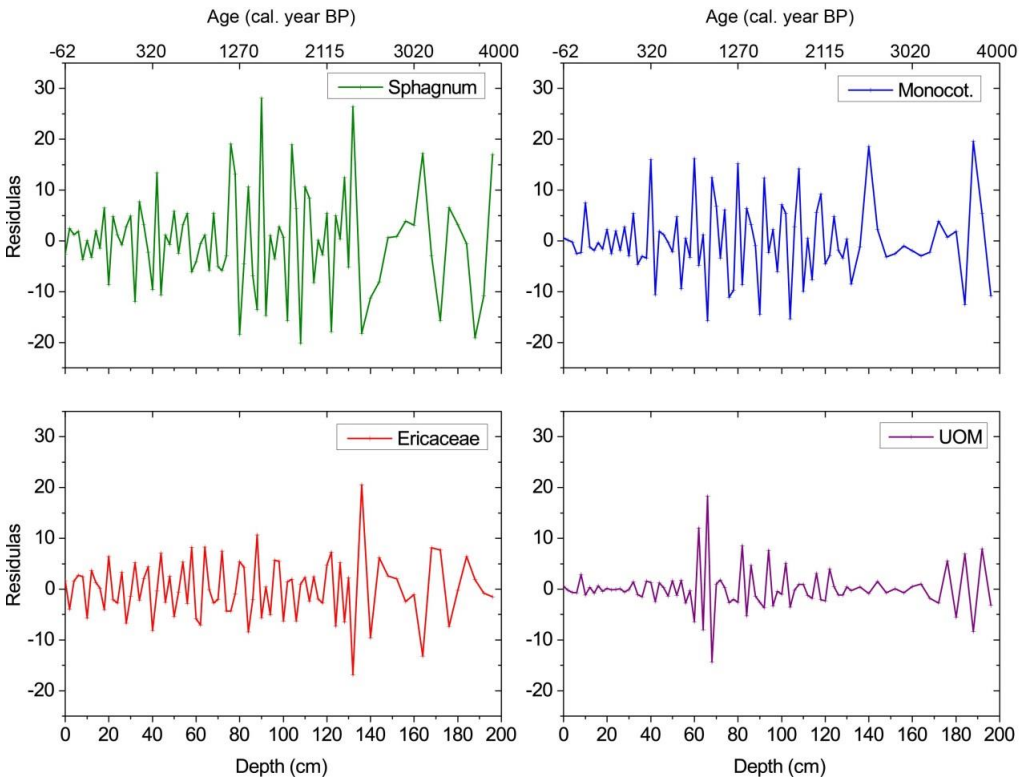

Figure 6.27 Variability of the FBB12 major peat forming components plotted against depth, with a secondary age axis.
The variability is reported using the residuals from LOESS smoothing: sampling proportion = 0.09 (equivalent to n=6) and 1 polynomial degree applied. The y-axes (residuals) scales are consistent between components for comparative purposes.

6.4.1.1 Statistical treatment of FBB12 macrofossil data: DCA

The DCA eigenvalue for axis one is 0.5 and the gradient length is 2.98, indicating that a dominant driver of vegetation change has been detected and a unimodal response model is appropriate for the ordination of the plant macrofossils within this core. Therefore, if the species distribution along axis one supports hydrological change as the dominant vegetation driver, the DCA axis one scores can be used as a semi-quantitative water table reconstruction.

Visual interpretations of the species distribution across axis one are broadly indicative of a hydrological gradient: UOM is located towards the positive end of axis one with some monocot. and ericaceous species, whilst *R. alba* and components of *S.* sect *Cuspidata* are located at the negative end of the gradient (Figure 6.28). The ordination locations of these taxa indicate that the

positive end of axis one represents drier conditions and the negative end represents wetter conditions.

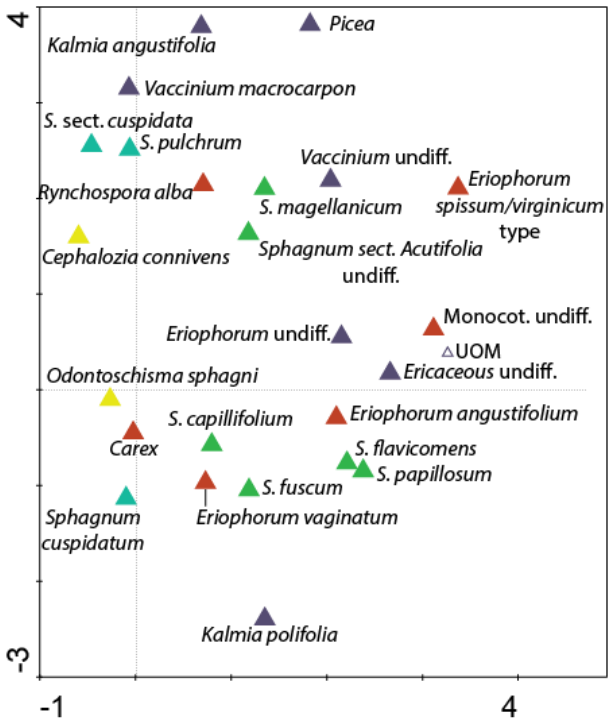

Figure 6.28 FBB12 plant macrofossil species DCA axis one (x-axis) and two (y-axis) scores.
Key: purple = shrubs; orange = grasses and sedges; yellow = liverworts; green = *S.* sect. *Acutifolia* and *S.* sect. *Sphagnum*; turquoise = *S.* sect. *Cuspidata*; empty triangle = UOM.

The relative positions of ericaceous undiff., monocot. undiff. and the *Sphagnum* sections also support the presence of a water table gradient along axis one. It may be expected that ericaceous remains should be located on a drier axis one position than monocots; however, the difference between the two groups is small. Total monocots is composed of many species with very different water table tolerances. Therefore, this positive axis one location could indicate that the monocot. undiff. components mainly originate from drier species in FBB12.

The DCA sample scores from axis one and two can be used to further explore the relationship between hydrological change and vegetation assemblage (Figure 6.29). The wettest zone in the assemblage diagram is inferred to be FBB12-i, at the surface of the peat core. These samples have been ordinated towards the negative extreme of axis one, supporting water table as the

environmental driver. Samples in zone FBB12-e are located at the most positive end of axis one, indicating that this is the driest period of the record. Generally, there is a clear clustering of zones with the exception of FBB12-a; however, this may be expected from this zone since it contains fluctuating changes in the main vegetation components.

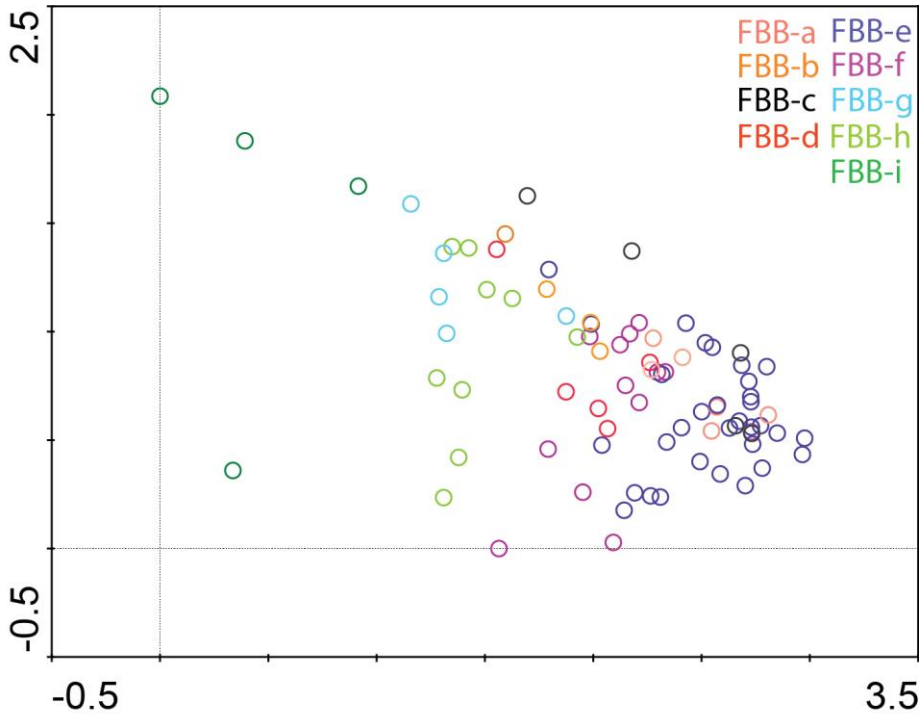

Figure 6.29 FBB12 plant macrofossil DCA sample scores coloured by zones allocated in stratigraphic diagram (Figure 7.1-1)

The DCA species ordination trends support the use of the DCA axis one as a semi-quantitative reconstruction of water table depth (Figure 6.30A). The record begins with alternations between dry and wet conditions until 124 cm. These appear more gradual than the higher frequency fluctuations in the remainder of the record; however, this may be a feature of the reduced sampling resolution in the early section of the core. The peatland is sustained in drier, fluctuating conditions from 122cm to 80 cm, before an increase to drier conditions at 64 cm. The most striking feature of the record is the decrease to wetter conditions from 64 cm to the surface. These inferred water table trends are in general agreement with the conclusions inferred from the assemblage diagram. Changes in the variability of the DCA axis one scores (Figure 6.30B) support the earlier conclusions obtained from the aggregate

vegetation components surrounding the stability of the record (see Figure 6.27): the record is variable until 68 cm when it decreases to 46 cm then increases again to 20 cm.

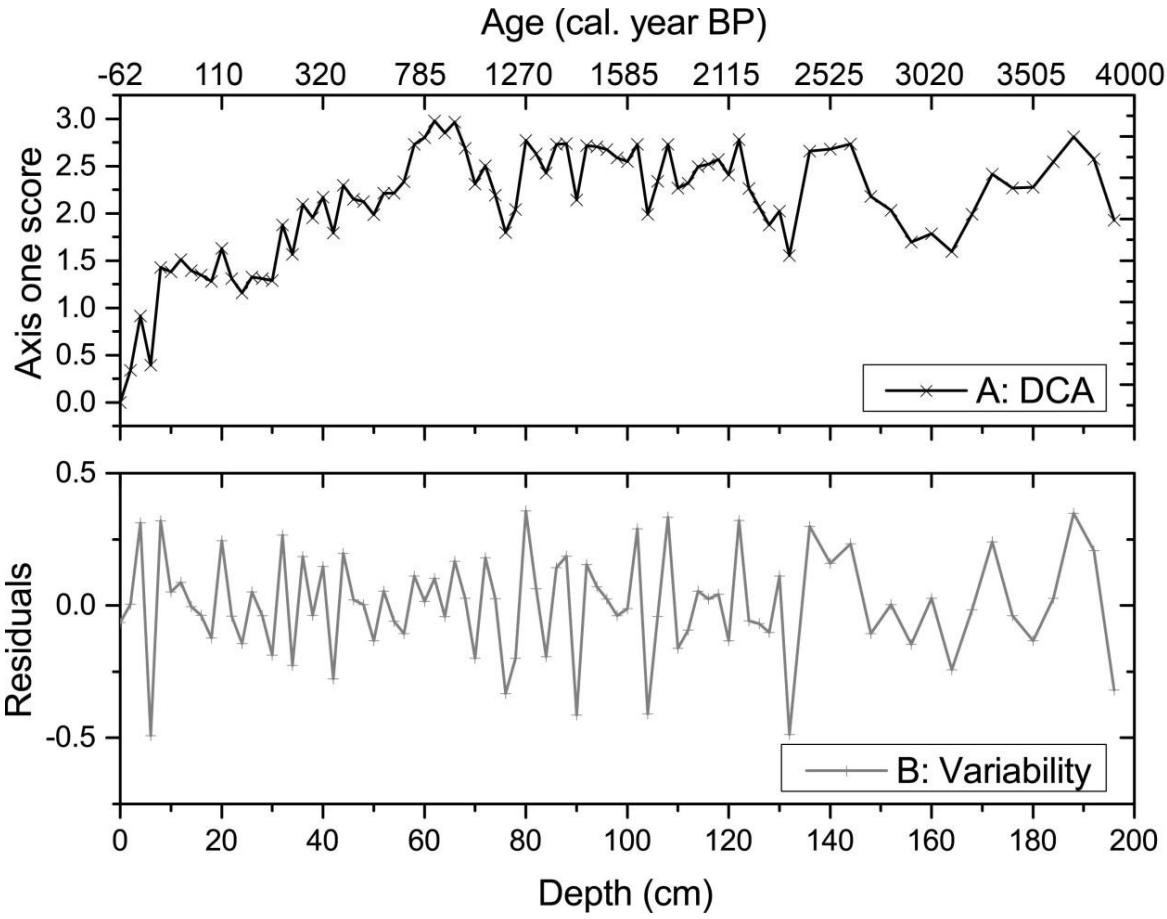

Figure 6.30 A: FBB12 plant macrofossil DCA axis one scores and B. Variability of the DCA axis one scores obtained using the residuals from LOESS smoothing: sampling proportion = 0.09 (equivalent to n=6) and 1 polynomial degree applied.

6.4.1.2 Statistical treatment of FBB12 macrofossil data: nMDS

The nMDS model for the FBB12 macrofossil assemblage had a stress of 0.13, which is sufficiently low for the interpretation of the model results (Figure 6.31). The nMDS species distributions are similar to the results from the DCA: UOM, monocots and Ericaceae are located to the positive end of axis one whilst *S.* sect. *Cuspidata* and V. *macrocarpon* are located towards the negative end (Figure 6.31B). The similarity that exists between DCA and nMDS species scores is reflected in the similar sample scores: the DCA and nMDS

down core reconstructions are positively correlated (r = 0.94, p <0.001). The nMDS and DCA axis one scores are similar throughout the record with only small divergences in the magnitude response; therefore, the same major climatic interpretations would be extracted from the ordination and multidimensional scaling methods (Figure 6.31D).

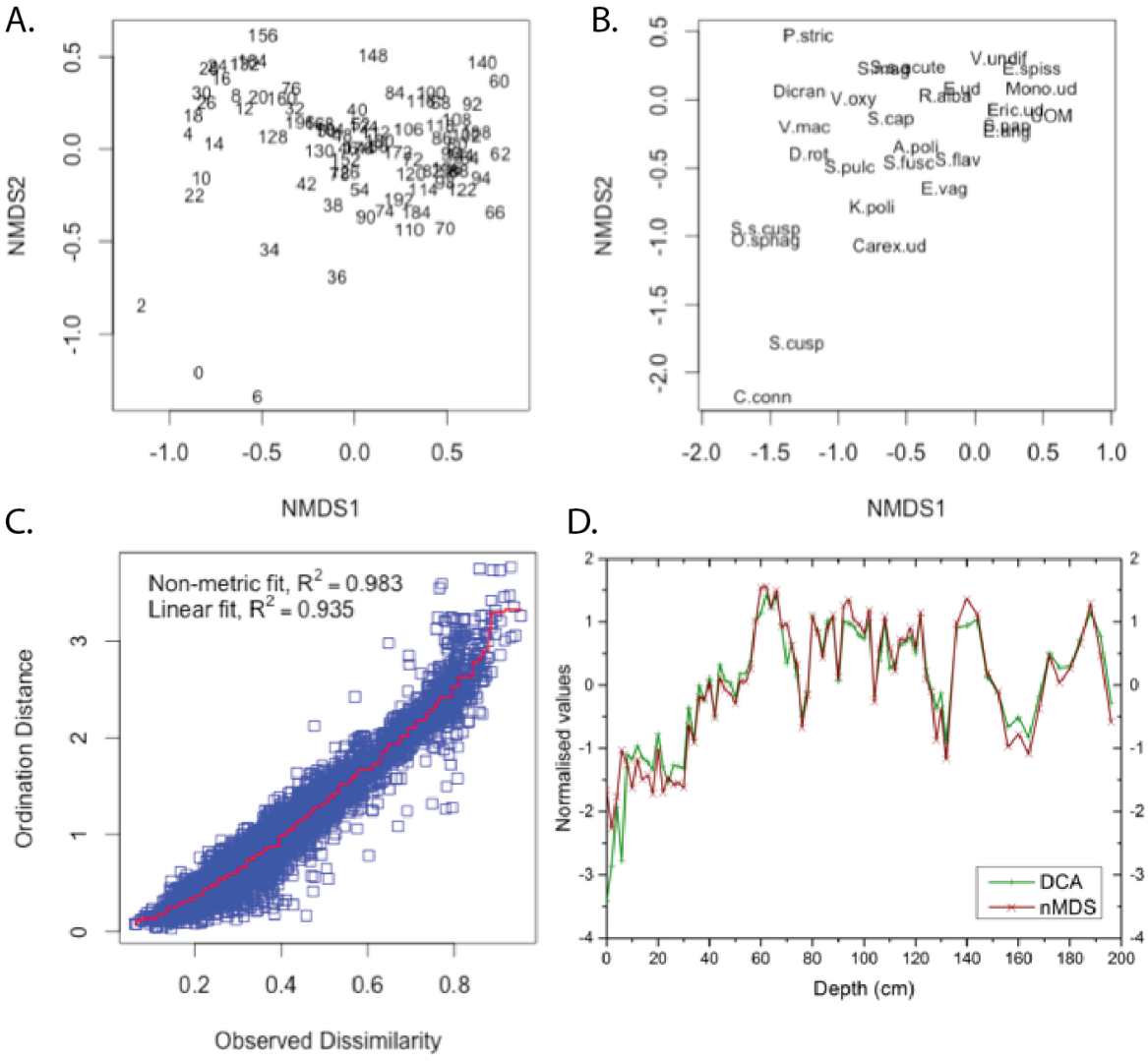

Figure 6.31 FBB12 plant macrofossil assemblage nMDS results. A: sample scores, indicated by depth (in cm); B: species scores. C: nMDS model, measure of dissimarlity between observed and rpecited results; D: normalised comaprison of DCA and nMDS Axis one reconstructions

6.4.1.3 Statistical treatment of FBB12 macrofossil data: DHI

The DCA and nMDS indicate that changes in the WTD are responsible for the majority of the fluctuations in the macrofossil assemblage; therefore, the DHI, which attributes all changes to fluctuations in water table depth, can be applied to the data set as an alternative method of inferring hydrological conditions (Figure 6.32).

A comparison of the three updated models reveals that there is no statistically significant difference between the medians of the full updated index and the index excluding UOM ($U = 2971$, $T = 7404$, $p = 0.127$); however, both indices are statistically different from the index excluding roots ($p < 0.001$). The index excluding roots predominately reconstructs higher DHI values than the full index (Figure 6.32). Whilst the reconstruction obtained when roots are excluded has statistically different values from the other indices, they are positively correlated ($p < 0.05$). Therefore, since it is the direction of change that is of importance when making hydrological inferences, the trends obtained from all updated indices would be similar.

The index excluding UOM and the full updated index reconstruct similar DHI values, with the exception of 68 – 62 cm when the direction of change remains similar but the index excluding UOM infers wetter conditions than the full updated index. The reconstructed difference indicates that the species present are more indicative of wetter conditions, perhaps driven by the low concentrations of *S. pulchrum* and *S. cuspidatum*, than the presence of UOM would suggest. The differences between the indices indicate that, rather than being a product of increased decomposition, UOM either originated from algal pool mud or a non-climatic driver at these depths. Whilst the presence of algal pool mud was not noted in the field; the presence of *S. cuspidatum* and *S. pulchrum* (albeit in low concentrations) indicate that algal mud is a possibility. There is no overwhelming evidence of a disturbance event: charred remains are common around this period but are reduced in concentrations compared with other points in the core.

The medians of the updated index and the Daley and Barber derived index are statistically different ($U = 415$, $T = 9960$, $p = <0.001$); however, the trends are weakly correlated between the two indices ($r = 0.532$, $p < 0.001$). Trends between Daley and Barber index and the full index deviate during two main

periods: 200 - 154 cm and 60 - 30 cm. As evident in the assemblage diagram, total *Sphagnum* increases from 188 cm to 160 cm, indicating a wetting trend. This trend is evident in the Daley and Barber derived index but less so in the updated index. Total *Sphagnum* also generally increases between 60 and 30 cm, again indicative of a wetting trend as evident in the Daley and Barber derived index. These assertions indicate that the updated index is, at points, insensitive to wetting trends.

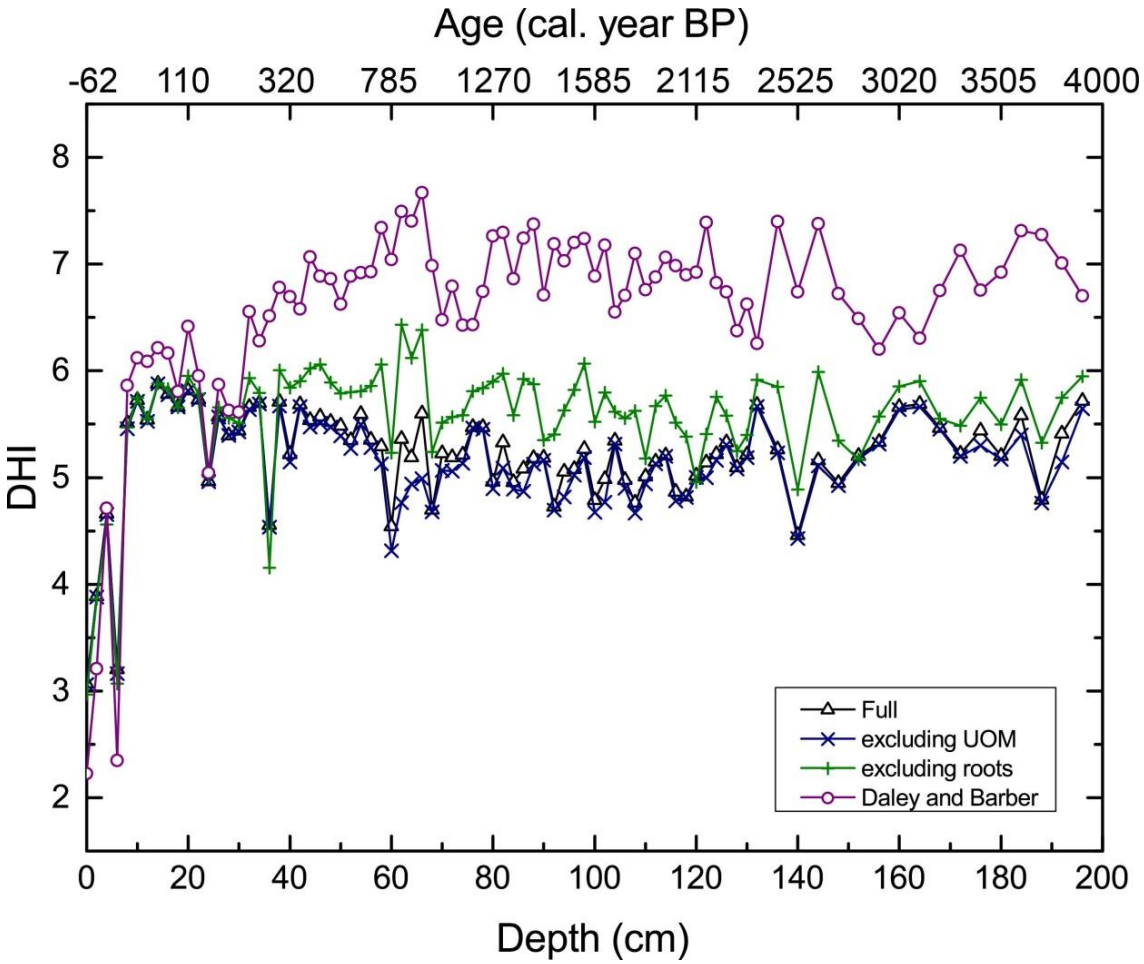

Figure 6.32 FBB12 plant macrofossil DHI reconstructions

6.4.1.4 FBB12 macrofossil hydrological reconstructions

Normalised comparisons of the DCA and nMDS axis one scores and the DHI reconstructions reveal similar trends across the FBB12 record (DCA and DHI: $r = 0.907$, $p < 0.001$; Figure 6.33). The main sequence of vegetation-inferred hydrological changes can be interpreted as an initial wetting trend to 156 cm, before drying to 140 cm. A shorter-lived wet period occurs to 128 cm before

fluctuating to drier conditions until 80cm. A wetter period then occurs until 70 cm, when it possibly dries to 60 cm (uncertainty owing to the divergence in UOM of the DHI index reconstructions), before an overwhelming wet trend to the surface.

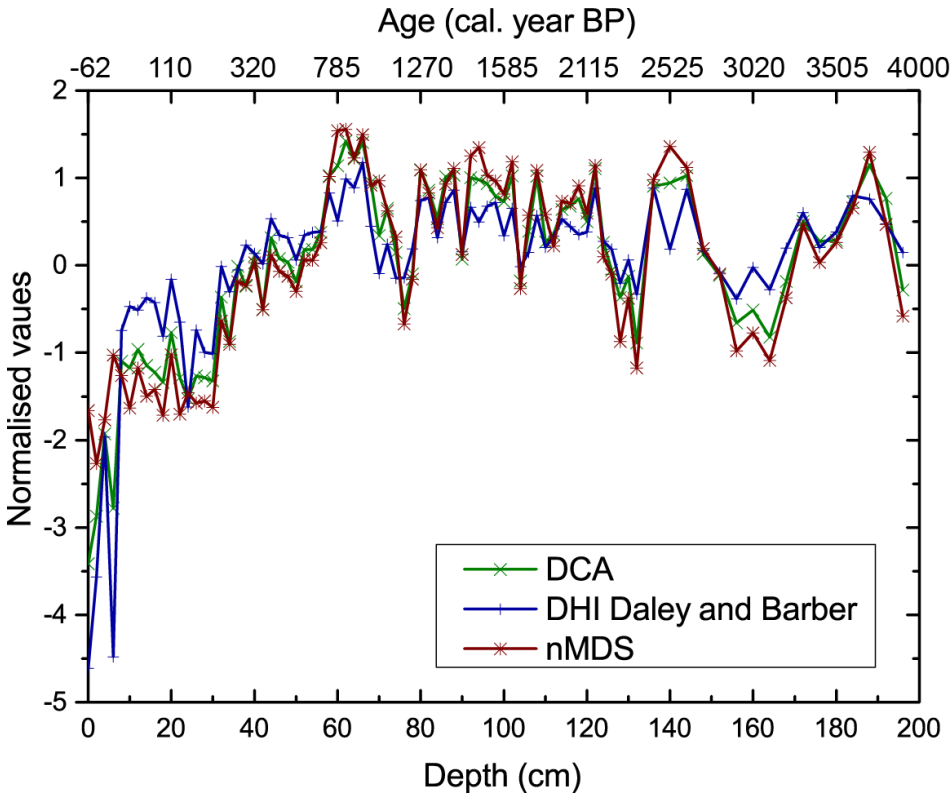

Figure 6.33 FBB12 plant macrofossil DCA, nMDS and DHI normalised comparisons of reconstructed environmental change.

6.4.2 Testate amoebae

The testate amoebae assemblage data have been allocated into seven zones of similar species composition (Figure 6.34; Table 6). The most dominant taxon throughout the record is *A. flavum* with average concentrations of 39%, although it commonly accounts for *ca.* 60% of the total assemblage *A. muscorum* is present throughout the whole record, frequently reaching 30% of the total assemblage in central sections of the core. *H. subflava* is not consistently present in the FBB12 record: it occurs around background levels in zones FBB12-b and FBB12-e to –g, but elsewhere contributes important inputs (*ca.* 30-40%). Other smaller taxa contributions include *H. sphagni* and *T. arcula* (both consistently *ca.* 10% in zones FBB12-c to -e) and *A wrightianum* (more sporadically *ca.* 10% throughout most of the record).

The full assemblage change by zone is summarised in Table 6.6. The testate amoebae assemblage can be broadly separated into three main sections:

1. zones FBB12-a and –b: dominated by *A. flavum* with low species richness, analysed in low resolution;
2. zones FBB12-c and –d: elevated *A. muscorum, H subflava* and *T. arcula* with continued prominent input from A*. flavum*
3. zones FBB12-e to –g: still dominated by fluctuating *A. flavum* but reduced *A. muscorum, H. sphagni, H. subflava* and later *T. arcula* whilst increased *H. elegans, H. papilio and P. spinosa*.

A. flavum dominates throughout and is a key indicator of wet (e.g. Amesbury *et al*., 2013; Turner *et al*., 2013), stable conditions (Sullivan and Booth, 2011) suggesting that near surface water tables were characteristic of the FBB12 record. *H. subflava* is a drier indicator, becoming more abundant in zone FBB12-c. This coincides with an increase in *A. muscorum*, a dry taxon, which is sustained until FBB12-d. The other aforementioned taxa that increase in section two also have dry preferences indicating that the water table lowered in this section. The reduction of these taxa in section three and the increase in *P. spinosa* and the more adaptable H. *papilio* suggests that the peatland became wetter or at least more variable. A greater number of taxa are present from zone FBB12-e to –g.

Non-testate fauna were only identified during the higher resolution analyses; therefore, their absence in the early zones is not significant. Chironomids are sporadically present in FBB12-c, –d and –f and Cladocera are present throughout, both indicating the presence of standing water. Since these organisms are present during the proposed drier middle section, it is likely that conditions were not consistently dry during this time, rather, the water table likely fluctuated.

Changes in the variability of the most abundant taxa (*A. flavum, A. muscorum, H. sphagni* and *H. subflava*) were assessed by plotting the residuals generated from LOESS smoothing (Figure 6.35). Focusing on the period of higher resolution sampling (132 – 0 cm), *A. flavum* abundances are variable, with high frequency and amplitude fluctuations until *ca.* 60 cm. The

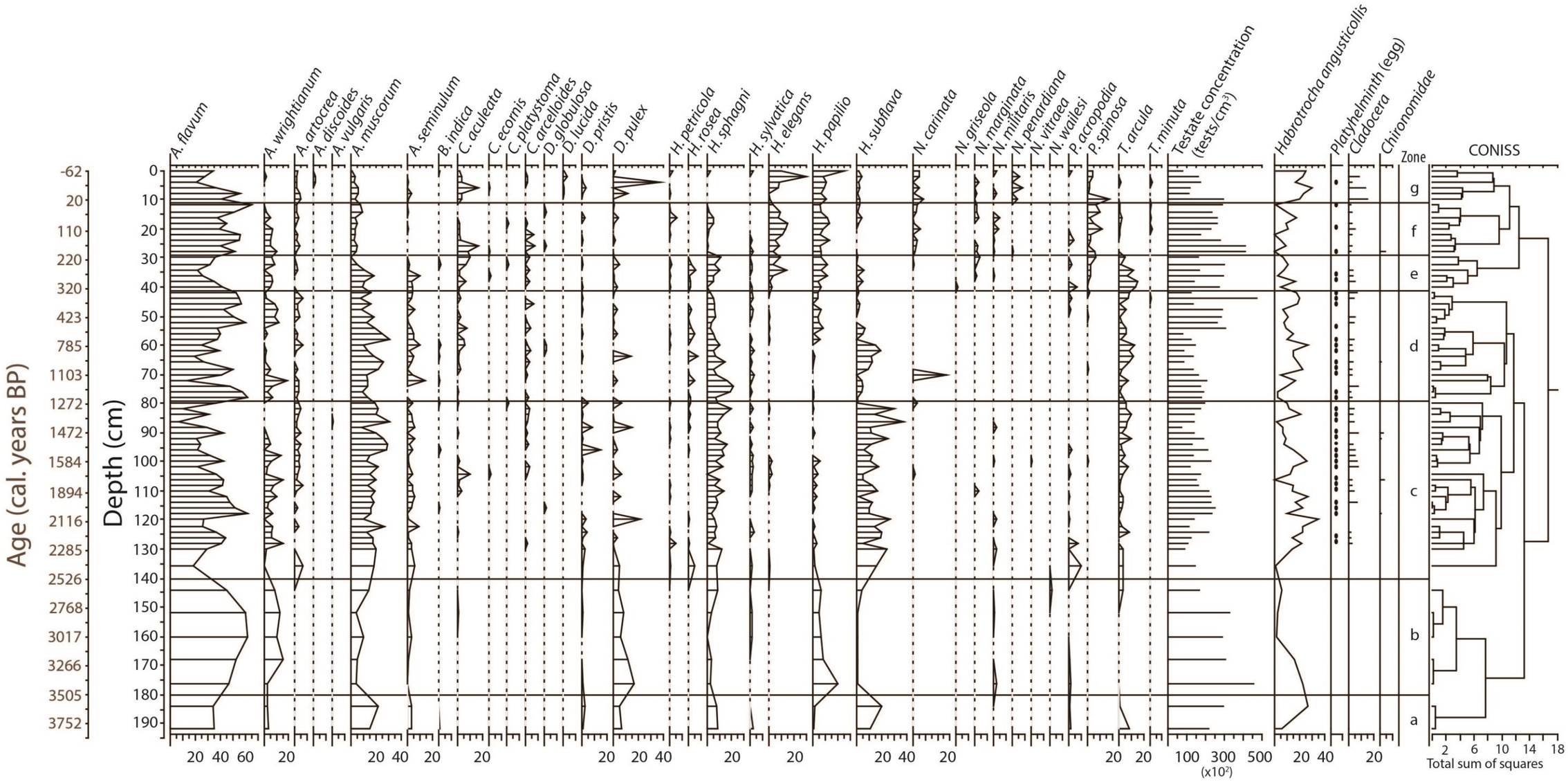

Figure 6.34 FBB12 testate amoebae assemblage diagram plotted against depth with a secondary age axis.

All data are percentages of the 100 tests identified at each level. Concentration data is displayed as depth bars, concentrations of tests per sample are represented by the bar graph and the presence of non-testate fauna is indicated by the black dots or as frequencies indicated by bar graphs. Zones have been allocated based on the results of the CONISS cluster analysis.

Table 6.6 FBB12 testate amoebae assemblage descriptions

Zone	Depth (cm)	Faunal assemblage description	Age (cal yr BP)
FBB12-g	0 -11	Many species are now present. *A. flavum* is the most prominent species present despite a reduction in concentration compared with the preceding zone. *H. papilio* and *H. elegans* increase towards the surface along with *D. pulex* which peaks earlier at 4 cm. *C. aculeata* increases to 6 cm then decreases to the surface. The concentration of *N. carinata* fluctuates and small abundances of *T. arcula* and *T. minuta* are present at 4 cm.	-63 - 29
FBB12-f	11-29	Elevated abundances of *A. flavum, H. elegans, H. papilio* and *P. spinosa*. Initially higher concentrations of *C. aculeata* that decreases towards the end of the zone. *A. artocrea, A. muscorum, Nebela carinata and N. militaris* are present in low concentrations. *T. arcula* is initially absent, then is present in low concentrations accompanied by *T. minuta*. A subtle reduction in *A. wrightianum* occurs.	29 - 210
FBB12-e	29-41	The zone is characterised by reduced *A. flavum* abundances although they do increase from 34cm to the end of the zone. The opposite trend is evident in *A. muscorum*, which increases to 36 cm before decreasing. *A. seminulum* and *H. papilio* are present in low concentrations and further decrease to the end of the zone, accompanied by a decrease in *P. spinosa* and *T. arcula. H. Sphagni*, *H. elegans* and *H. papilio* increase and there is fluctuation in the small input of *C. arcelloides.*	210 - 330
FBB12-d	41-79	Increased concentrations of *A. flavum* to *ca.* 40% with a decreasing trend towards 64 cm and then an increase towards the end of the zone. A similar trend is evident in *A. wrightianum* and *H. papilio* increases to the end of the zone when *H. elegans* is present. Conversely, *A. muscorum* increases to 58 cm, reaching *ca.* 30%, before decreasing. H. *subflava* also initially increases but then decreases ahead of *A. muscorum* at 62 cm. *H. sphagni* decreases throughout the zone, whilst *T. arcula* is present but fluctuating. *A. artocrea, B. indica, C. arcelloides* and *D. pulex* are sporadically present.	330 - 1256
FBB12-c	79-140	Average concentrations of *A. flavum* decrease to *ca*. 25%, although they do temporarily increase at 118 cm. *A. wrightianum* decreases (becoming absent at 88 cm), *H papilio* decreases to background concentrations, becoming more sporadic and *D. pulex* exhibits low abrupt fluctuations. The mean concentrations of *A. muscorum,* (*ca*. 20%), *H. sphagni* (*ca.* 10%) and *H. subflava* (*ca*. 205%) are increased relative to the preceding zone, with the latter species increasing throughout the zone. *T. arcula* is generally present at around 10% throughout and *A. discoides* are now present in low concentrations. Towards the middle and latter section of the zone, sporadic low concentrations of *Cyclopyxis arcelloides* and *Centropyxis aculeata* are present.	1256 - 2525
FBB12-b	140-180	*A. flavum* increases towards the centre of the zone (reaching *ca*. 60%) then gradually decreases back to 40% towards the end of the zone. *A. wrightianum* increases to stable concentrations of *ca*. 10-15% whilst *A. muscorum* gradually increases throughout. Concentrations of *D. pulex* and *H. papilio* gradually decrease. Consistently low concentrations of *H. subflava and A. seminulum*. *T. arcula* is present towards the end of the zone, accompanied by *Nebela wailesi* and *H. elegans*.	2525 - 3458
FBB12-a	180-196	Most dominant species is *A. flavum*, accompanied by *A. muscorum* and *H. subflava*. Low stable concentrations of *A. wrightianum, A. seminulum*, *D. pulex and H. sphagni*. *T. arcula* is initially present then declines.	3458 - 3900

smoothed residuals of the other major taxa are lower than *A. flavum*, influenced by their relative concentrations. However, they also experience higher variability from 132 to 60 cm than near the peat surface: *H. subflava* is most variable between 132 – *ca*. 80 cm, whilst *H. Sphagni* continues to experience pronounced variability until *ca*. 60 cm. Between 132 cm and *ca*. 36 cm, *A. muscorum* contains high frequency variability that is characterised by three abrupt prominent peaks. *H. subflava, A. muscorum* and *H. sphagni* become increasingly stable towards the surface as concentrations decrease. *A. Flavum* is generally more stable near the peat surface than the middle of the record and this stability is enhanced around 40 cm.

An average of twelve species of testate amoebae were identified per sample and the species richness increased as depth decreased ($r = -0.479$, $p < 0.001$; Figure 6.36A). A decreasing trend in species richness began at 136 cm, culminating at 118 cm (n=6) before increasing to temporary elevated levels around 104 cm (n=17). Peak species richness occurs at 32 cm (n = 21) after a longer term increasing trend from *ca*. 76 cm; however, it quickly decreases and fluctuates to the peat surface. A comparison with the macrofossil water table inferences reveals that the number of testate species is higher when the peatland is wetter (DHI: $r = -0.384$, $p < 0.001$; DCA: $r = -0.459$, $p < 0.001$). This relationship may be explained by the larger water table tolerances of the drier species compared with the wetter species, which would contribute to the increased overall of species tolerances under wetter conditions. The increase in species richness under wet conditions may also be assisted by preservation, since decay rates will be reduced, perhaps facilitating the preservation of more vulnerable species. However, there is no significant relationship between concentration and species richness ($r = 0.0891$, $p = 0.450$), indicating that preservation alone cannot account for the observed trends.

The concentrations of testate amoebae are variable throughout the core, decreasing from 176 cm to 130 cm and remaining low until *ca*. 56 cm (Figure 6.36B). The macrofossil assemblage record indicates a reduction in *Sphagnum* from *ca*. 120 – 56 cm; therefore, the testate amoebae concentration may be influenced by the change in host: the pH will be altered along with the water film required for survival (Tolonen, 1986; Charman *et al*.,

2000; Wilmshurst *et al.*, 2003; discussed further in Section 8.1). Concentrations increase from *ca.* 56 to 26 cm (during which the macrofossils indicate a wetting trend) before exhibiting a stepwise decrease in concentration to the surface in the active peat (Figure 6.36B). The SDI increases from 136 – 120 cm before increasing to 102 cm, assisted by the increase in number of species present (Figure 6.36C). The index then fluctuates before increasing from 46 cm to 38 cm reaching the peak SDI of the record and indicating a stable testate amoebae community at this point, coinciding with increased species richness and species evenness (Figure 6.36A and D).

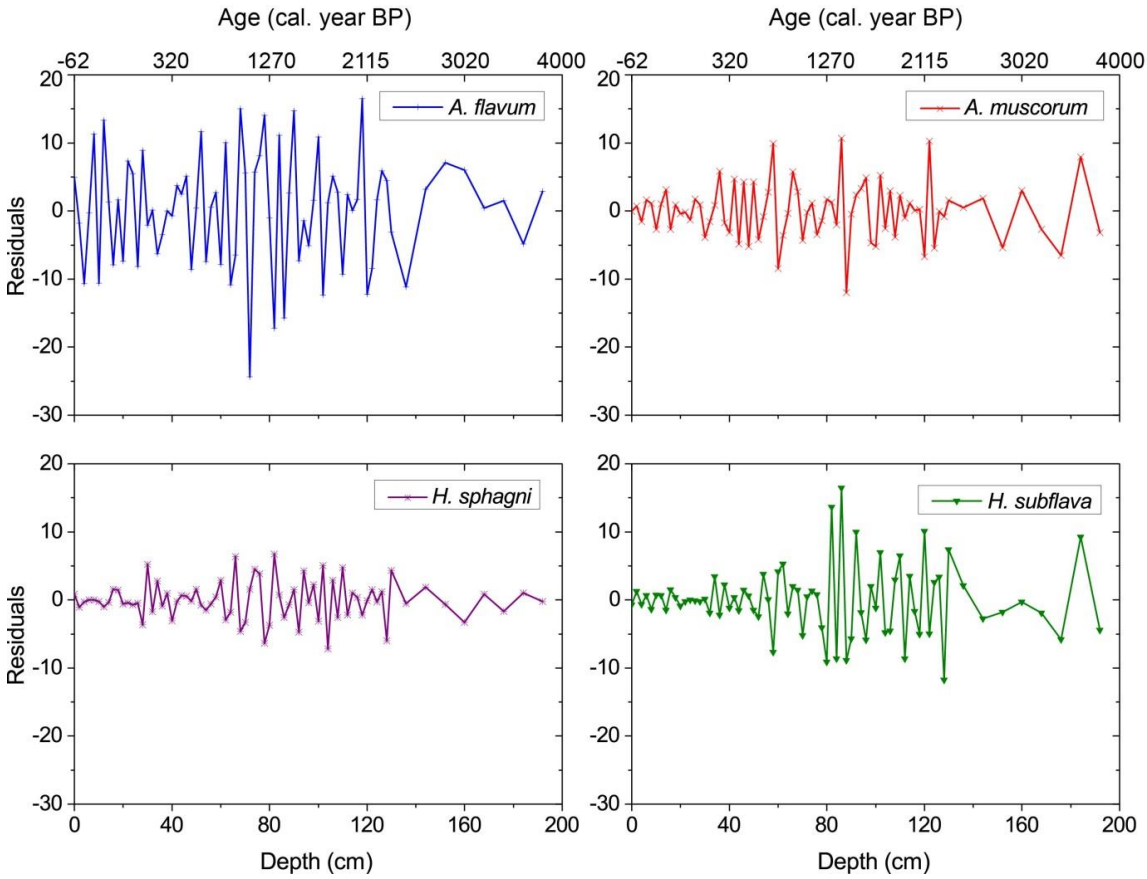

Figure 6.35 Variability of the four most abundant testate amoebae taxa A: *A. flavum*; B: *A. muscorum*; C *H. sphagni*; D: *H. subflava*) using the residuals from LOESS smoothing. A sampling proportion of 0.09 (equivalent to n=6 in the higher resolution sampling period) and 1 polynomial degree were applied.

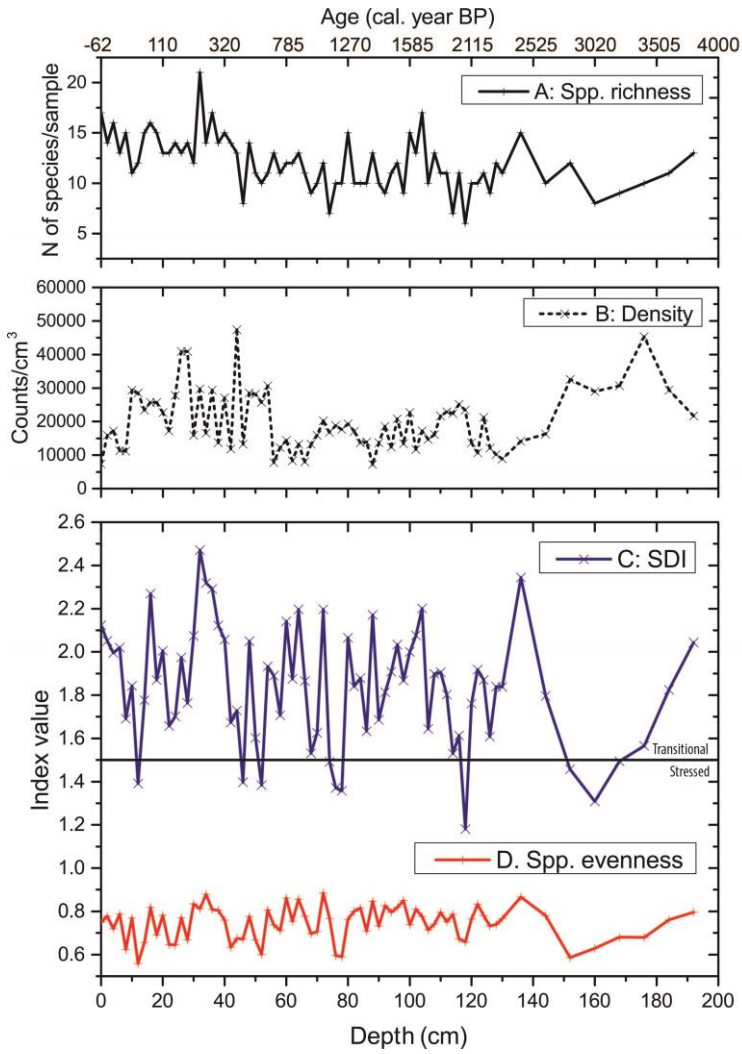

Figure 6.36 FBB12 testate amoebae ecological measures.
A: Species richness (number of species per sample); B: Concentrations of individuals (counts per cm^3 of peat; determined used Lycopodium counts); C: Shannon Diversity index; D: Species evenness (indicates the relative abundance of species, calculated using the SDI and the natural log of species with zero = no evenness and 1 = evenness).

6.4.2.1 Statistical treatment of FBB12 testate amoebae data: DCA

The gradient length of first DCA axis is 2.49, indicating that a unimodal response model is appropriate for the ordination of the testate amoebae within this core and the eigenvalue is 0.285. Generally, the distribution of the dominant species score across the DCA axis one is suggestive of a hydrological gradient: drier species such as *H. subflava* and *A. muscorum* are located towards the positive end of the axis and wetter species such as *A. flavum* are located towards negative end (Figure 6.37).

Some of the rare wetter species within the assemblage do not align with the hydrological trend: *A. vulgaris* and *N. wailesi* are both are located towards the positive (dry) end of axis one. It is likely that the DCA has been unable to appropriately capture the preferences of these sparse species. There are also discrepancies in the species distribution towards the negative (wet) end of the axis one: *N. marginata, T. minuta and N. militaris* are generally indicative of dry conditions and would therefore be expected to be located closer to the positive end of the gradient. However, the DCA may be representing a segment of their expected water table tolerances since they are generally present in low concentrations and are unlikely to have a prominent effect on any environmental interpretations made from the DCA axis one scores.

The influence of rare species on the ordination was investigated by eliminating the problematic rare species rather than just downweighting their influence (Figure 6.38). Omitting the problematic rare taxa from the ordination had the effect of decreasing the gradient length to 2.448 and the eigenvalue to 0.283, and had little effect on the ordination location of the dominant species. Therefore, the original DCA axis one score will be used as a reconstruction of past hydrological conditions. The DCA axis one and two sample scores identify periods of similarity within the assemblage: samples towards the negative (wet) end of the axis are from zones FBB12-i and –h and the samples from zones FBB-e, -d, c and –a are towards the positive (dry) end (Figure 6.39). FBB12-c samples are well constrained along axis one whilst within-zone variability is evident towards the peat surface.

The DCA axis one scores indicate that the peat became wetter to 176 cm and was stable before drying to 130 cm. A further drying occurred between 102 to 86 cm at which the peatland became the driest of any other point in the core (Figure 6.40A). The variability is pronounced in the period of higher resolution sampling until 70 cm where it peaks (Figure 6.40B). The DCA indicates a move to wetter condtions from 86 cm to the surface peat, which is the wettest point in the record. The record is stable from 66 – 24 cm then variability increases slightly to the surface.

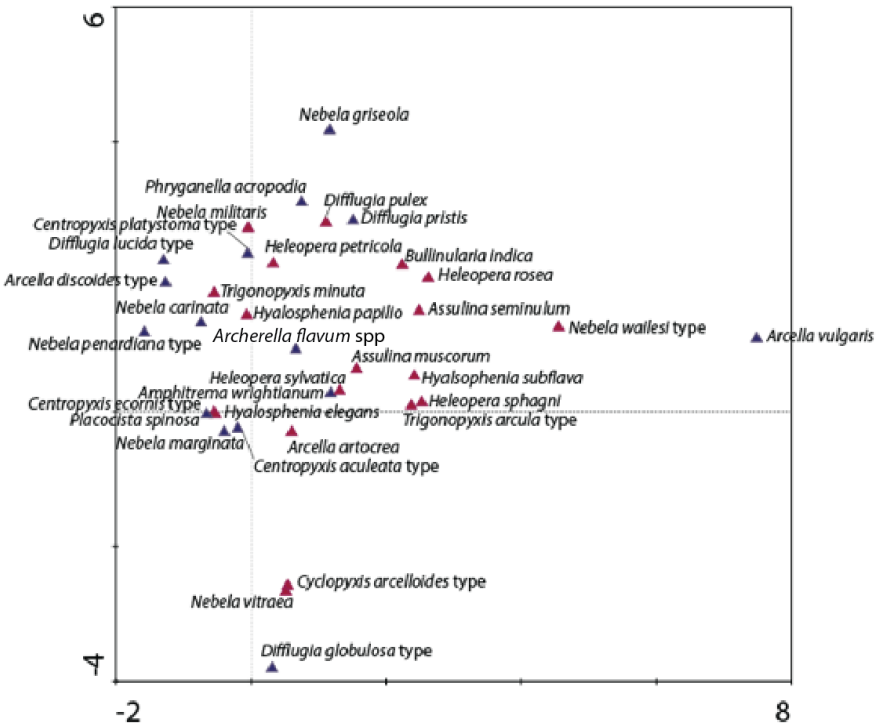

Figure 6.37 FBB12 testate amoebae DCA axis one (x-axis) and two (y-axis) species scores Red symbols represent species with drier WTD preferences and blue symbols represent species with wetter water table depth preferences. Colours (and thus dry or wet preferences) have been assigned based on the training sets of Amesbury *et al.*, (2013) and Lamarre *et al.*, (2013).

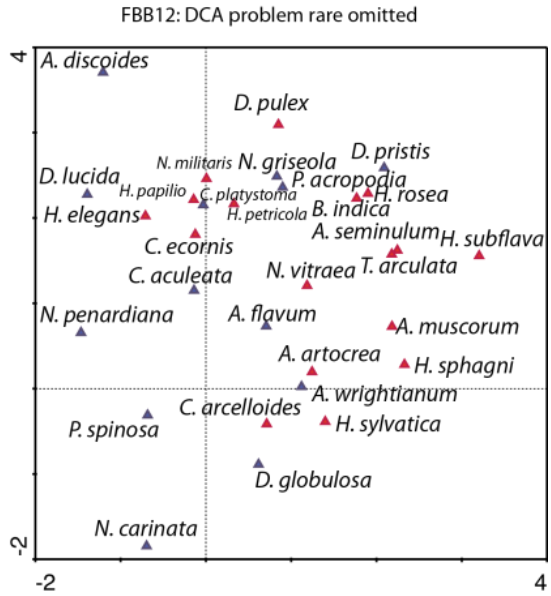

Figure 6.38 Alternative FBB12 testate amoebae DCA with rare species omitted. Red symbols represent species with drier WTD preferences and blue symbols represent species with wetter water table depth preferences. Colours (and thus dry or wet preferences) have been assigned based on the training sets of Amesbury *et al.*, (2013) and Lamarre *et al.*, (2013).

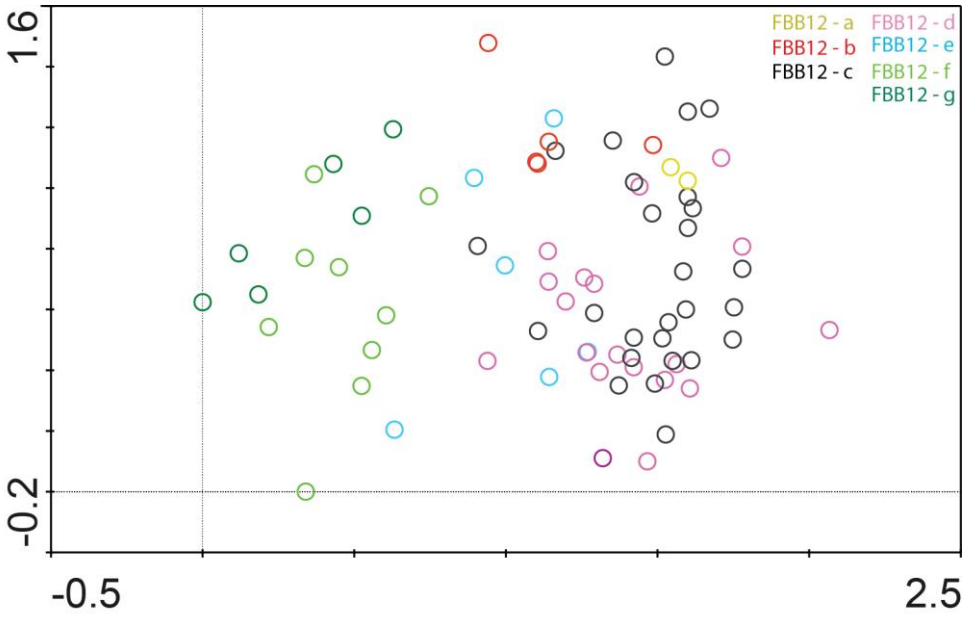

Figure 6.39 FBB12 testate amoebae DCA axis one (x-axis) and two (y-axis) sample scores coloured by zones allocated by CONISS (see Figure 6.34)

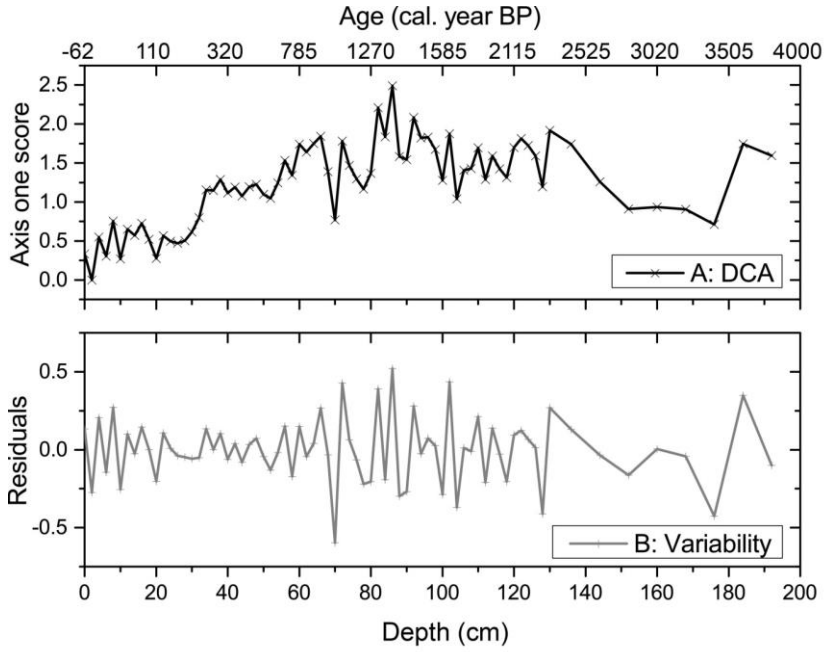

Figure 6.40 A: DCA Axis one scores for each sample representing changes in hydrological conditions down core. Lower values indicate wetter conditions. B: variability of the DCA axis one scores using the residuals from LOESS smoothing. A sampling proportion of 0.09 (equivalent to n=6 in the higher resolution sampling period) and 1 polynomial degree were applied.

6.4.2.2 Statistical treatment of FBB12 testate amoebae data: nMDS

The nMDS model obtained from the FBB12 testate amoebae assemblage data has a stress of 0.15, which allows for interpretation of the nMDS axes one and two (Figure 6.41). The species distribution across the primary nMDS axis is similar to the results obtained from the DCA axis one: *A. discoides N. penardiana* and *D. lucida* are located are towards the negative end of the axis whilst *H. subflava* and T. *arcula* are located towards the positive end of the axis (Figure 6.37 - Figure 6.41). The main difference in the species distribution along axis one of the nMDS and the DCA is that *A. vulgaris*, the most positively ordinated species in the DCA, is absent in the nMDS owing to the low abundance. The broad similarity between the first axes of the DCA and the nMDS suggests that the same underlying environmental variable and associated response from the testate amoebae have been detected. The scaling of the species along axis two does differ between the nMDS and the DCA; however, the source of the secondary environmental driver is unclear from the species distributions. The downcore reconstructions using the nMDS and DCA axis one scores are similar ($r = 0.96$, $p < 0.001$); therefore, analyses of the trends would lead to similar climatic interpretations (Figure 6.41D).

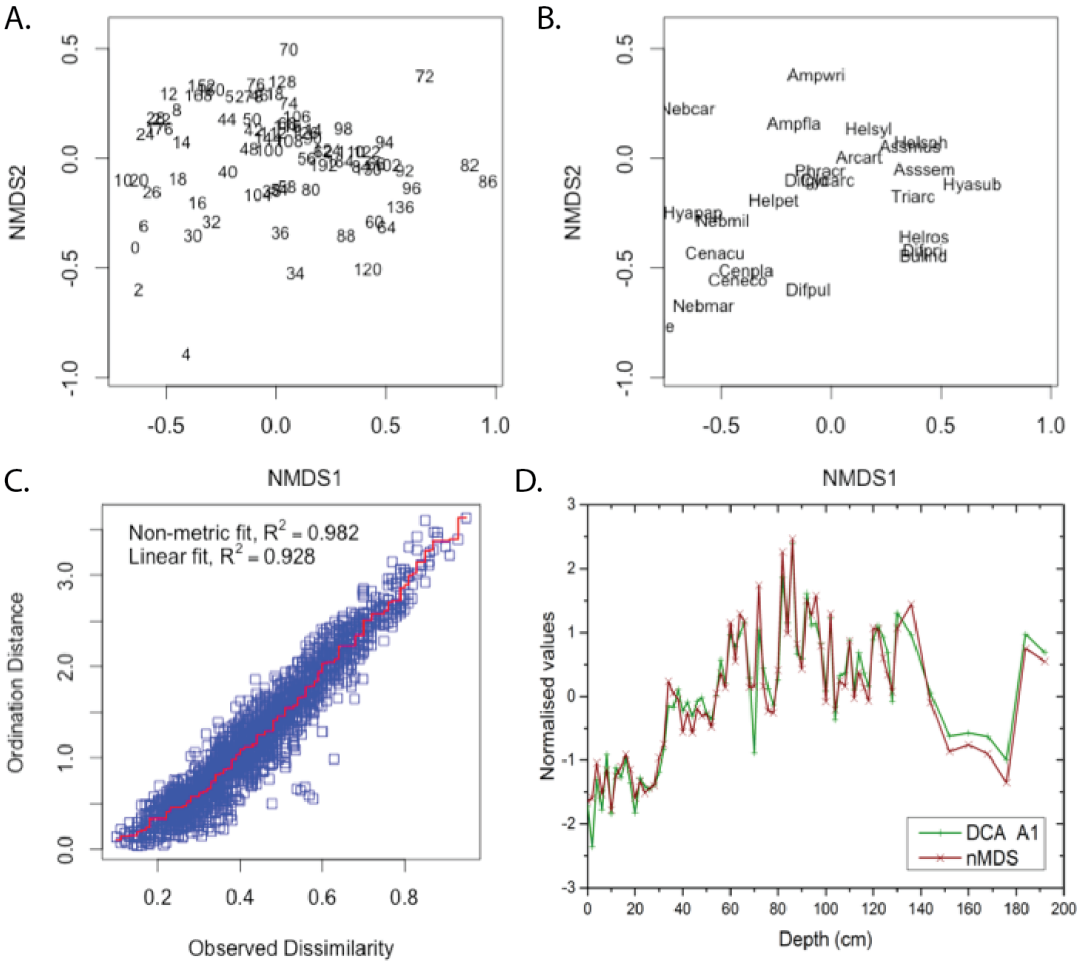

Figure 6.41 FBB12 testate amoebae nMDS results.
A: sample scores, indicated by depth (in cm); B: species scores. C: nMDS model, measure of dissimarlity between observed and predicted results; D: normalised comaprison of DCA and nMDS axis one reconstructions, lower values indicate wetter conditions.

6.4.2.3 Statistical treatment of FBB12 testate amoebae data: transfer functions

The results from the FBB12 testate amoebae DCA and nMDS indicate that water table depth is likely the dominant influence on assemblage change; therefore, the transfer functions can be applied to the testate amoebae assemblage data. The medians of the reconstructions obtained using the ATLANTIC.NA WA.inv.tol and WA.inv models are statistically different (U = 1744, T = 4519, p = <0.001); however, they are positively correlated (r = 0.934, p = <0.001; Figure 6.42). The WA.inv reconstruction has a 4.83% greater error than WA.inv.tol and generally reconstructs wetter conditions, although both model results overlap within error ranges throughout. The

direction of change is generally consistent between models with the exception of 74 – 72 cm, 58 – 56 cm and 26 cm (highlighted in red; Figure 6.42). Between 74 – 72 cm the WA.inv model reconstruction reveals a pronounced drying whilst the WA.inv.tol model decreases slightly. This coincides with a decrease in *A. flavum* and increase in *A. wrightianum* and *A. seminulum*. *A. wrightianum* has a wet water table preference whilst *A. seminulum* prefers dry conditions; therefore, the WA.inv.tol model would have been driven by the *A. wrightianum* increase, unlike the WA.inv model. It is unclear from the assemblage diagram what is driving the divergences at 58 – 56 cm and 26 cm; however, they are unlikely to affect the interpretation of larger scale environmental change.

The median values of the reconstructions obtained using the QUEBEC WA.cla.tol and WA.cla models are also statistically different ($U = 1643$, $T = 4418$, $p =<0.001$; Figure 6.43) as are the relationships between the two models ($r = 0.795$, $p <0.001$). There are more occurrences of diverging trends within the QUEBEC model reconstructions than the ATLANTIC.NA models (highlighted in red; Figure 6.43). Comparisons between the two transfer functions reveal that the ATLTANTIC.NA and QUEBEC models are statistically different at the 0.05 level using ANVOA on ranks ($DF = 5$, $H = 274.186$ $p < 0.01$). Despite the statistical differences between the reconstructions, visual comparisons of the different testate transfer functions reveal similar hydrological trends with ATLANTIC.NA WA.inv and QUEBEC WA.cla reconstructions being the most similar ($r = 0.961$, $p <0.01$; Table 6.7)

The main hydrological trends contained with both reconstructions indicate that the peatland initially became wetter until *ca.* 170 cm, dried to 90 cm before a wetting trend to the surface peat (Figure 6.42). Changes in the variability of the ATLANTIC.NA and QUEBEC reconstructions are assessed by plotting the residuals generated from LOESS smoothing (Figure 6.44). Both transfer functions contain more variation between *ca.* 130 and 70 cm, representing oscillating water tables and reflects the increased variation in the major taxa (Figure 6.35).

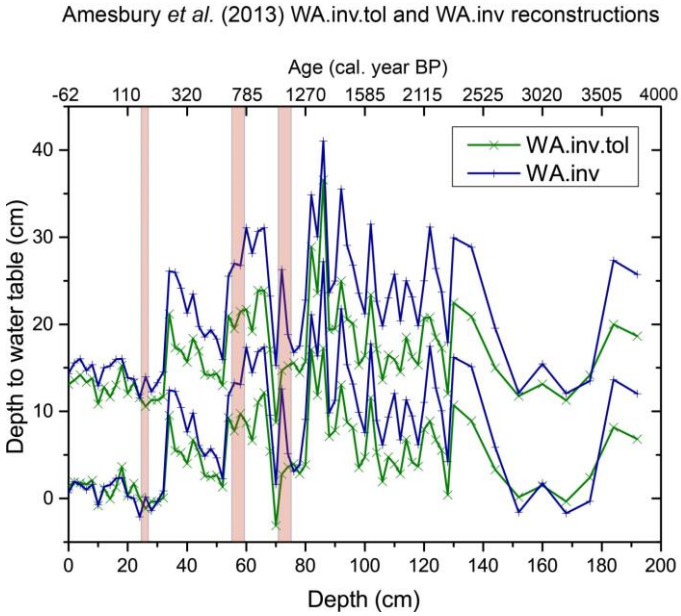

Figure 6.42 Upper and lower estimates of FBB12 testate amoebae reconstructions using ATLANTIC.NA WA.inv.tol and WA.inv models. Red bands indicate periods of diverging trends. Lower y-axis values indicate wetter conditions.

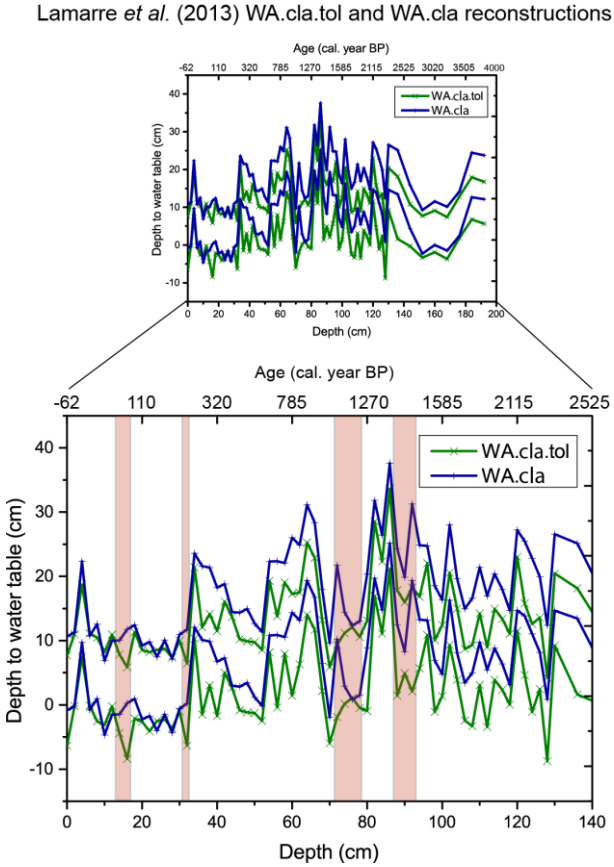

Figure 6.43 Upper and Lower estimates of FBB12 transfer function reconstructions from QUEBEC WA.inv.tol and WA.inv, red bands indicate periods of diverging trends. Lower y-axis values indicate wetter conditions.

Table 6.7 Table of Pearson correlation coefficients between transfer function models. All significant at the P < 0.001 level

	ATLANTIC.NA WA.inv	QUEBEC WA.cla.tol	QUEBEC WA.cla
ATLANTIC.NA WA.inv.tol	**0.93**	**0.90**	**0.93**
ATLANTIC.NA WA.inv		**0.80**	**0.96**
QUEBEC WA.cla.tol			**0.86**

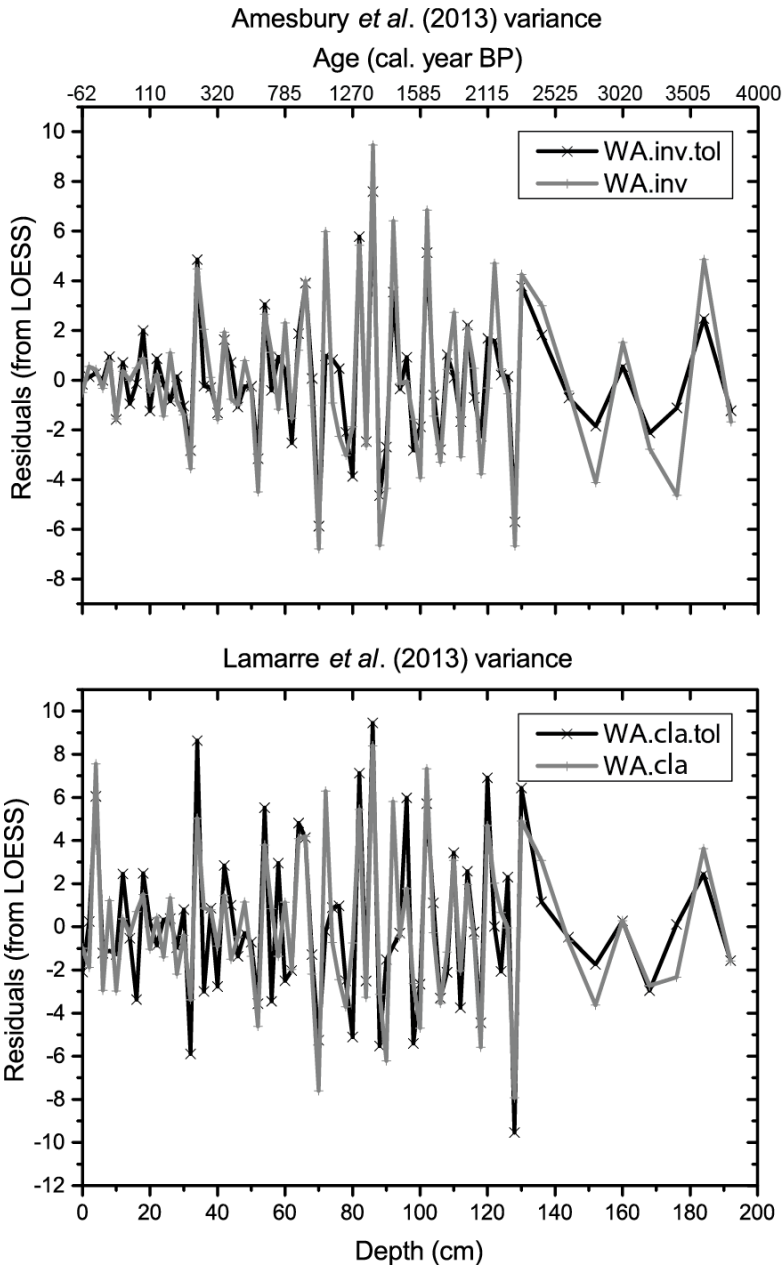

Figure 6.44 FBB12 testate amoebae transfer function reconstructions variability based on the residuals from LOESS smoothing. A sampling proportion of 0.09 (equivalent to n=6 in the higher resolution sampling period) and 1 polynomial degree were applied.

A normalised comparison of the ATLANTIC.NA and QUEBEC transfer function reconstructions and the DCA and nMDS axis one scores may highlight periods of divergence between the reconstructions and, therefore, indicate when non-hydrological drivers were controlling the testate assemblage (Figure 6.45). Generally, the major trends are similar in the weighted average, ordination and scaling methods of transformation, with the exception of the *ca.* 70 cm and the surface samples (24 – 0 cm). Pearson product moment coefficients indicate that the DCA reconstruction is more similar to the QUEBEC WA.cla reconstruction (r = 0.87) when compared with ATLANTIC.NA reconstruction (r = 0.81) and the QUEBEC WA.cla.tol reconstruction (r = 0.67)

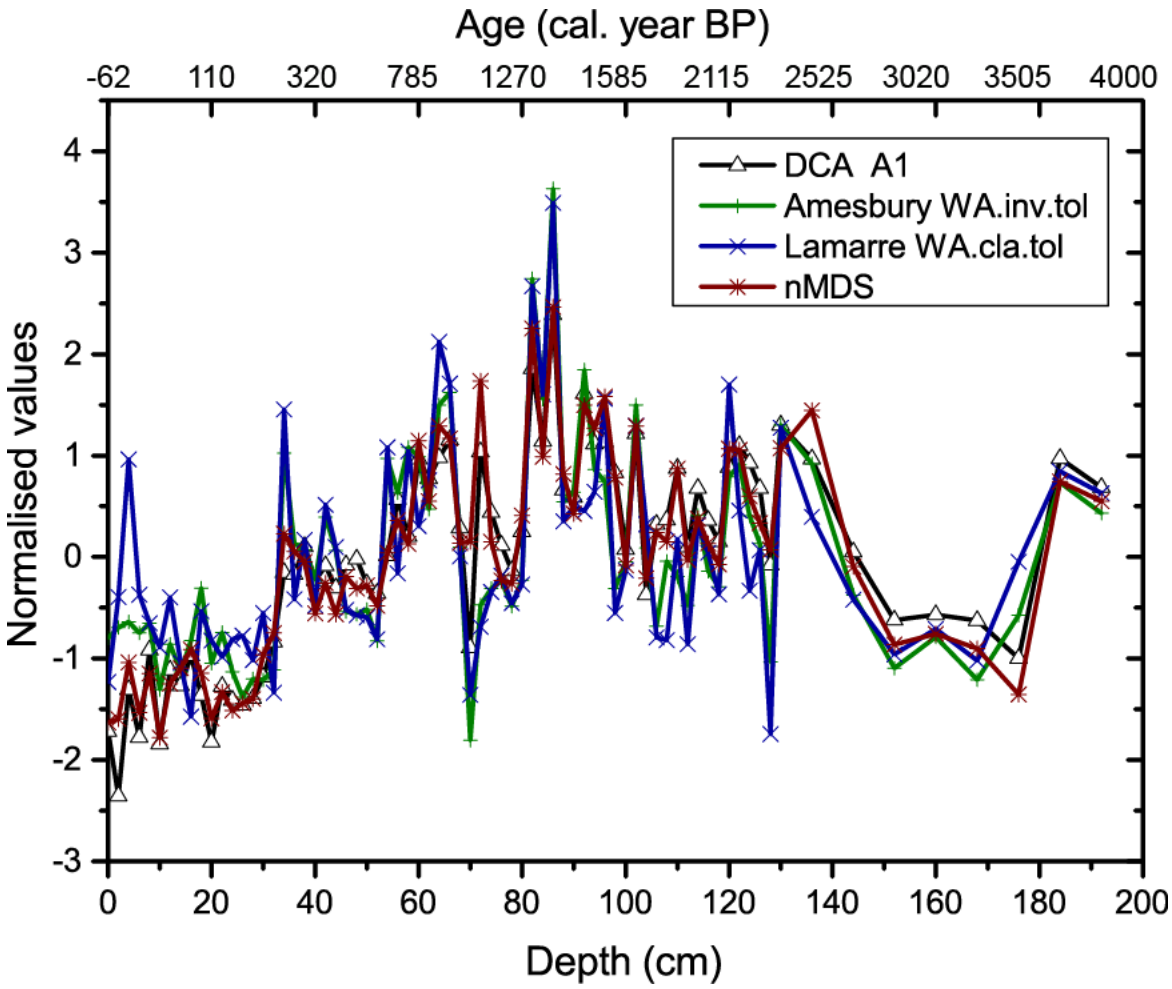

Figure 6.45 FBB12 testate amoebae normalised data transformation comparison. Lower y-axis values indicate wetter conditions.

6.4.3 Full FBB12 palaeoecological comparison

A comparison of the plant macrofossil and testate amoebae inferred hydrological changes over the last 2000 year is presented using the normalised values of the Daley and Barber derived DHI index for the plant macrofossils and the normalised records from ATLANTIC.NA WA.inv.tol and QUEBEC WA.cla.tol for the testate amoebae (Figure 6.46). The main difference between the trends of the testate amoebae and plant macrofossil reconstructions occurs within the surface peat: the macrofossil DHI indicates a wetting phase, as supported by the presence S. sect. *Cuspidata*, which thrives in pools, whilst the testate amoebae reconstruction indicates a slight drying trend within the last *ca.* 250 cal yr BP. It is possible that the hydrological signal reconstructed by the testate amoebae at these depths is complicated by the vertical habitats of the testate amoebae on the *Sphagnum* stems since the testate amoebae will be living rather than fossil. It is, therefore, important that the environmental conditions reconstructed over the last few centuries are considered alongside surface peat processes (discussed further in Section 8.1). Throughout the FBB12 reconstruction, there is a less pronounced response registered in the macrofossils compared with the testate amoebae. Reasons for this, and associated implications, are discussed in Section 8.1. The main reconstructed peat hydrological changes over the time period of interest can be summarised as a drying trend from *ca.* 2000 – 1300 cal yr BP, followed by a pronounced wet shift to 1100 cal yr BP and then an overall wetting trend to the present day within fluctuating conditions.

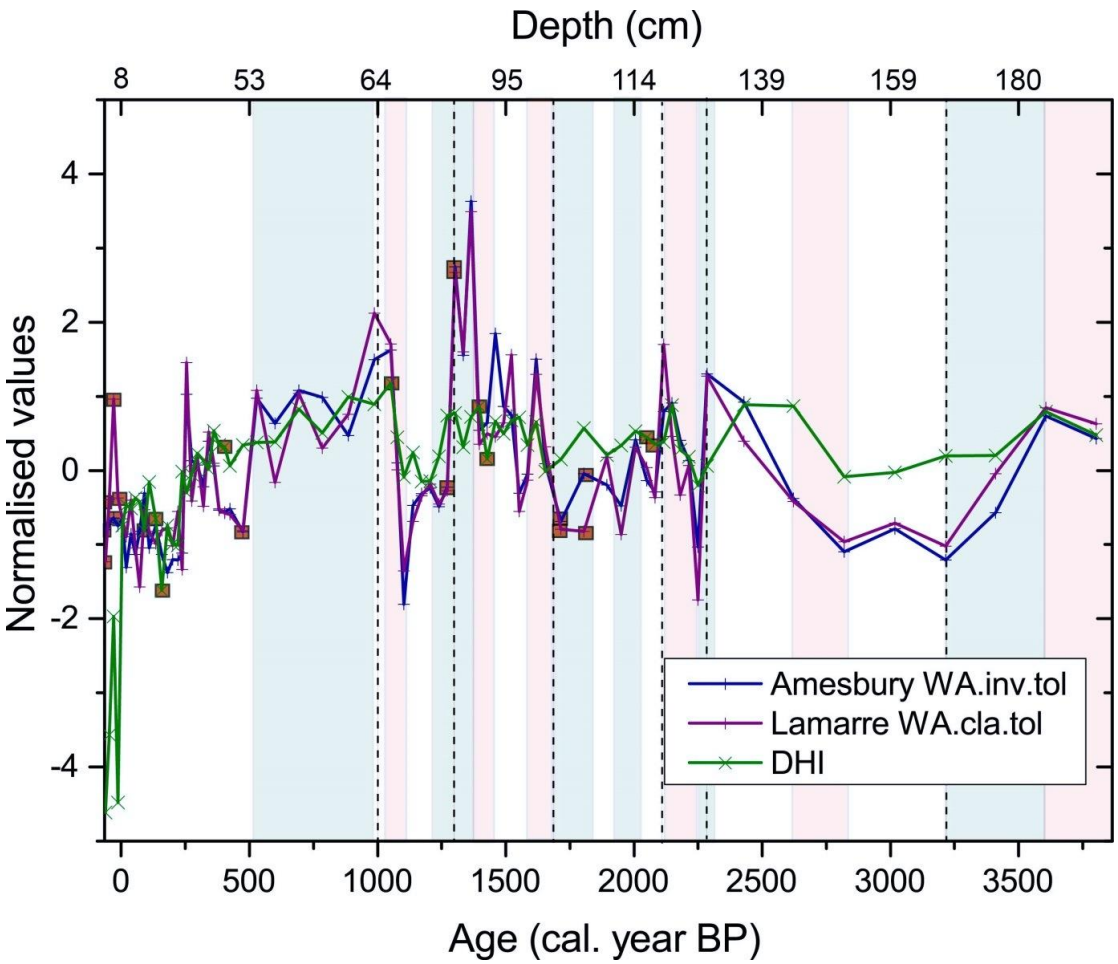

Figure 6.46 FBB12 normalised ecohydrological reconstructions. Consistent trends within proxies to wetter conditions are shaded blue and drier trends shaded red. Any white areas indicate periods where trends in the proxies disagree or are unclear and dashed lines separate similar periods of hydrological conditions. Samples that are likely to be driven by major factors other than hydrological change (as identified by differences in ordination and weighted averaging-based techniques) are highlighted by red boxes around individual points along with any divergences in the transfer function trends. Lower y-axis values indicate wetter values

6.5 Villagedale Bog

6.5.1 VDB12 plant macrofossils

The plant macrofossil data from VDB12 have been separated into six zones of similar vegetation assemblages (Figure 6.47). The boundary between zones VDB12-e and –f was lowered by one sample as a visual inspection of the assemblage data indicated that the prominent change in the majority of taxa occurred ahead of the CONISS zone placement. The zonal separation highlighting the full complexity of change within the record is outlined in Table 6.8. The main assemblage changes can be summarised within three distinct sections:

1. zones VDB12-a and –b: *Sphagnum* dominated peat
2. zone VDB12-c: abrupt decrease in *Sphagnum* reveals monocot. dominated peat, in conjunction with an increase in ericaceous remains
3. zones VDB12-d to –f: return to *Sphagnum* dominated peat with fluctuating conditions.

The prominent peat-forming component is *S.* sect. *Acutifolia*, which commonly accounts for *ca.* 80% of the record in section one and *ca.* 60% in section three. Four primary pulses of *S.* sect *Cuspidata* commence at the end of zone VDB12-c: prominent increases in *S. cuspidatum* occur at 68 cm and 48 cm, before it is replaced by stronger pulses of *S. pulchrum ca.* 38 cm and 8cm. The abrupt *S.* sect. *Cuspidata* pulses generally co-vary with more sustained pulses of stepwise increases in *S. papillosum* and *S. magellanicum* that are centred around 100cm (VDB12-b), 64 cm (VDB12-d) and 30 cm (VDB12-e).

Periods of *S.* sect. *Acutifolia* dominance may generate climatically complacent records (e.g. Hughes *et al.*, 2006). This complacency is often exacerbated by low availability of *S.* sect. *Acutifolia* stem leaves, which are required for identification to species level. Such conditions are characteristic of section one; therefore, it is likely that this period will register relatively less change than the remainder of the record. Other proxy records are required to reveal whether this is reflective of a period of climatic stability or of plant macrofossil insensitivity.

The dominance of the *Sphagnum* contribution to the vegetation record suggests that VDB12 is a fairly wet habitat. This is confirmed by low UOM concentrations (consistently <10%), usually indicative of dry periods of high decomposition, and the presence of *R. alba*, *V. macrocarpon and S. cuspidatum* within the assemblage, which are characteristic of wet conditions. The main differences between the responses of total Ericaceae and monocots occur in zones VDB12-c and VDB12-e: instances of ericaceous remains peak ahead of the main peak in monocots in VDB12-c, whereas ericaceous materials decrease ahead of monocots in VDB12-e.

The increase in UOM, Ericaceae and monocots indicate a subtle long-term drying trend. However, the increased pulses of *S. cuspidatum* and *S. pulchrum* in zones VDB12-c to -f are suggestive of fluctuations to wetter conditions towards the peat surface. The assemblage is initially more stable within the *S.* sect *Acutifolia* dominance; however, this is disturbed by the abrupt shift in zone VD12-c. A comparison of the major aggregate vegetation components reveals that total *Sphagnum*, monocots and Ericaceae contain low variability until 84 cm when the latter two components become more variable (Figure 6.48). Elevated variability occurs from 72 - 40 cm in total Ericaceae and 72 - 32 cm in total *Sphagnum* and total monocots at which points they become more stable towards the peat surface. The trends in variability indicate that the vegetation assemblage continues to fluctuate into zone VDB12-e after the abrupt shift in zone VDB12-d. These vegetation changes could be either driven by less stable climatic conditions or they could also be related to the destabilising effect of the major vegetation change evident in zone VDB12-d.

Whilst sporadic, low abundances of charred remains were detected in the record, there is no evidence to suggest that a fire triggered the abrupt change in zone VDB12-d. Charred remains are particularly concentrated at the boundary of VDB12-a and -b, indicating that a fire event may have been centred around 1191 cal yr BP; however, there is no macrofossil or chronological evidence to indicate that it disturbed the peat surface at the coring location.

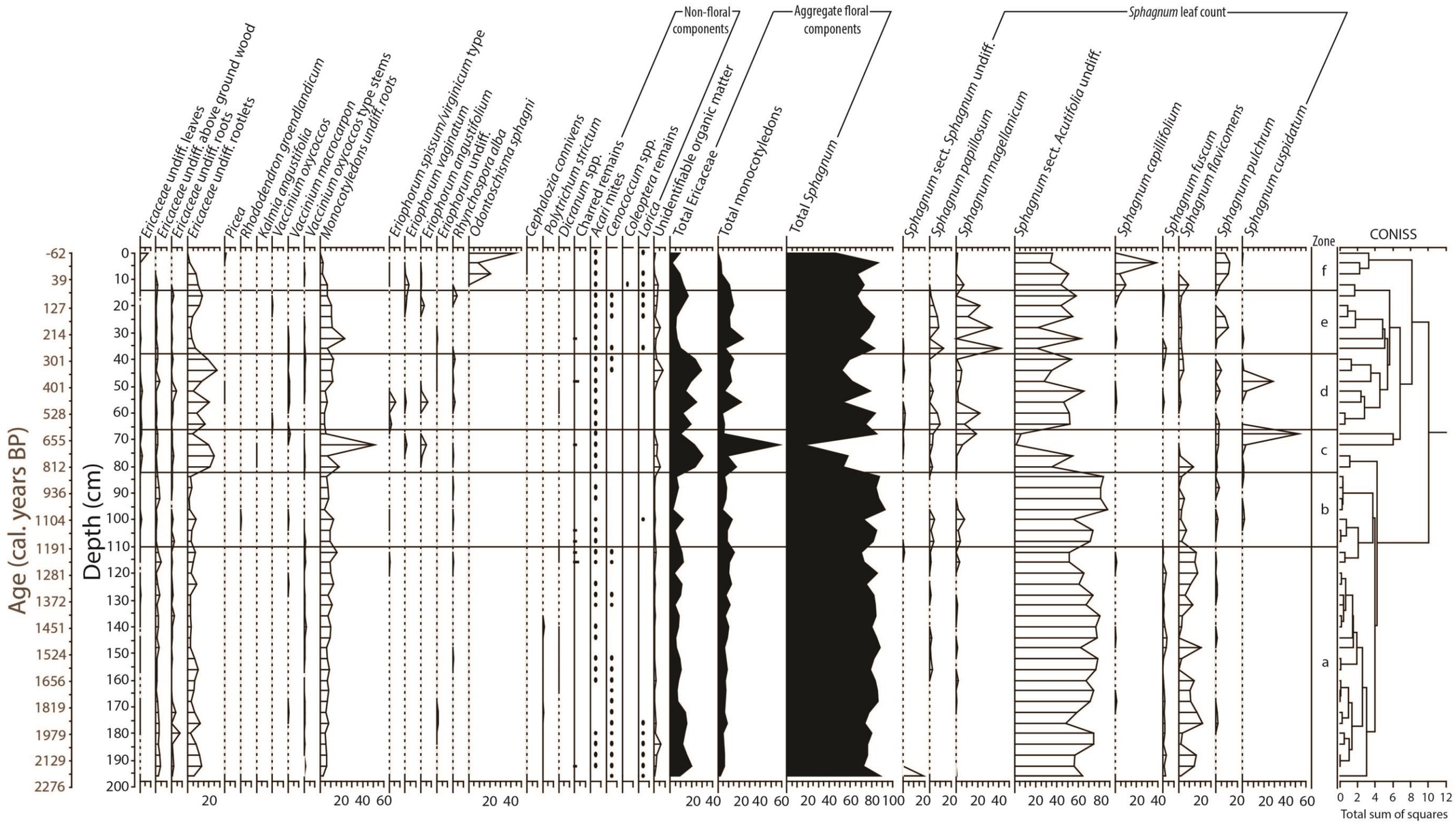

Figure 6.47 VDB12 macrofossil assemblage diagram plotted against depth with secondary age axis.

Peat components displayed with depth bars are derived from averaged quadrat counts (n=15) under low-power magnification (x10). Peat components displayed in solid black denote aggregates of different components. Individual *Sphagnum* leaf counts are also displayed with depth bars as proportion of aggregate *Sphagnum* based on random selection of 100 leaves identified at high magnification (x400). All data are presented as percentages with the exception of presence/absence data that are displayed as black dots and charred remains are presented within the bar graph. Zones were assigned after CONISS cluster analysis.

Table 6.8 Description of VDB12 plant macrofossil assemblage.

Zone	Depth (cm)	Vegetation assemblage description	Age (cal yr BP)
VDB12 -f	0 - 14	**Decrease in total monocots. and Ericaceae**. *S* sect. *Acutifolia* undiff. generally decrease although identifiable remains of *S. capillifolium* increase. *S. pulchrum* increases to *ca*. 20%. *Odontoschisma sphagni* remains increase (44% at surface), and *Eriophorum* spp. are present.	-62 - 74
VDB12 -e	14 - 38	**Reduced fluctuations of total *Sphagnum* centred around 80%**. Ericaceous remains reduce to *ca*. 5% alongside more subtle decreases in monocots. Increase in *S. magellanicum* (42%) and *S papillosum* (13%) but concentrations decrease to smaller values throughout the zone. A pulse of *S. pulchrum* is centred on 28 cm, reaching 12% and there are minimal amounts of *S. cuspidatum* at the start of the zone before disappearing entirely.	74 - 284
VDB12 -d	38 - 66	**Return to increased *Sphagnum* (*ca.* 80%) with reduced levels of monocots (*ca.* 5%) and ericaceous remains (15-20%),** although latter two groups do increase throughout the zone. *Sphagnum* decreases to *ca.* 50% near the end of the zone. Conditions appear more variable than other *Sphagnum* dominated zones (VDB-a –b). Increase *in S. cuspidatum* at 48 cm *ca.* 25%, accompanied by small amount of *S. pulchrum*. Increase in *S. magellanicum* and *S. papillosum* when *S. cuspidatum* decreases. *S.* sect. *Acutifolia* dominates. Evidence of *Eriophorum* species, *R. alba* and *V. macrocarpon*.	284 - 607
VDB12 -c	66 - 82	**Reduction in total *Sphagnum* to 15%, culminating at 72 cm**. This is a two-stage decrease owing to the staggered pattern of monocot. and ericaceous increase (increased ericaceous material peaking at 31% at 76 cm with monocots peaking at 60% at 72 cm). Some charred remains are present in one sample towards the end of the zone. Increased UOM to 6%. *V. macrocarpo*n and *K. angustifolia* present. Low levels of *S. papillosum* and *S. magellanicum* increase towards the end of the zone. *S. sect Acutifolia* decreases and *S. flavicomens* is absent from second half of the zone. *S. Cuspidatum* peaks to *ca*. 50% at end of the zone	607-840
VDB12 -b	82 - 110	**Total *Sphagnum* generally increases to *ca.* 90% with a reduction in ericaceous and monocot. remains.** *S.* sect. *Acutifolia* generally increases, dominating total *Sphagnum* whilst *S. flavicomens* reduces throughout accounting for *ca.* 5-10%. *S. papillosum* and *S. magellanicum* are initially present in higher concentrations (*ca*. 5 and 10% respectively) but then are absent from 96 cm when *S.* sect. *Cuspidata* are present in background concentrations, coinciding with *R. alba*. Charred remains are only present around the initial zone boundary. *R. groenlandicum* and *V. macrocarpon* remains evident at 100 cm.	840 - 1191
VDB12-a	110 - 196	***Sphagnum* dominated zone**, **generally fluctuating between 70 – 80%.** *S.* sect. *Acutifolia* dominates and *S. flavicomens* input is variable, peaking around 15% in at periods with *S. cuspidatum* present in low concentrations. Small amounts of *S. papillosum* and *S. magellanicum* are present from 160 cm and 172 cm respectively. Total Ericaceae initially accounts for 20% of the assemblage before fluctuating around 10% and total monocots initially account for 5%, gradually increasing throughout the zone to *ca*. 10% of the assemblage. Small amounts of UOM are present throughout with a temporary peak at 184 cm (7%). Small sporadic amounts of *Eriophorum* species and *V. macrocarpon* present, with some identifiable *R. alba* in both the middle and towards the end of the zone. *P. strictum* present in low concentrations until 136 cm, accompanied by *Dicranum* spp. from 164 cm.	1191 - 2217 -

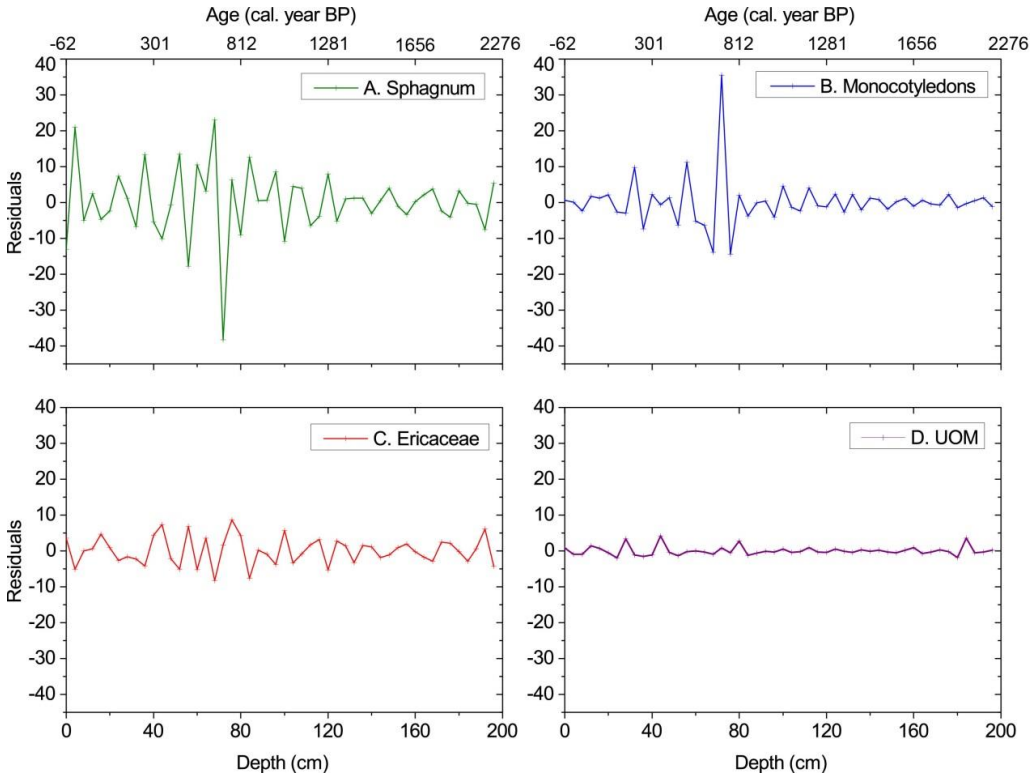

Figure 6.48 VDB12 variability of the major peat forming components plotted against depth, with a secondary age axis.
The variability is reported using the residuals from LOESS smoothing: sampling proportion = 0.12 (equivalent to n=6) and 1 polynomial degree applied. The y-axes (residuals) scales are consistent between components for comparative purposes.

6.5.1.1 Statistical treatment of VDB12 macrofossil data: DCA

The eigenvalue for DCA axis one is 0.419 and the gradient length is 2.85, indicating that a unimodal response model is appropriate for the ordination of the plant macrofossils within this core. A visual investigation of the species ordination locations across axis one identifies the presence of a broad hydrological gradient (Figure 6.49). Dry species such as *Picea* and *P. strictum* are located towards the positive end of the axis and wet species such as *S. cuspidatum* and *V. macrocarpon* are located towards the negative end of the axis.

Although the key indicator species are indicative of a hydrological gradient, some individual species have not been ordinated in locations to support this. For example, *O. sphagni* is located towards the dry end of the axis, which contradicts field and literature observations that suggest that it should be

located alongside *Sphagnum* in a wetter location (Figure 6.1 and 6.3). This distribution is likely a result of poor liverwort preservation down core, preventing the DCA from extracting a representative hydrological position for the species. Despite the unsatisfactory axis one position, *O. sphagni* is not present beyond the living peat in zone VDB12-f; therefore, it will not influence any hydrological reconstructions beyond this point.

Assuming a hydrological driver, the ordination location of the pseudo-taxon UOM is more central than may be expected: UOM is representative of decomposition, a process that is enhanced in dry conditions; therefore, UOM would be expected to be ordinated towards the dry end of axis one. Algal pool mud can be mistaken for UOM; however, in this record UOM does not coincide with *S. cuspidatum* which would be indicative of pool conditions. UOM occurs in low abundance throughout VDB12; therefore, since the DCA cannot optimally address rare species, its rarity is likely the driving factor behind the UOM ordination location. The misplacement of UOM would not affect overall reconstructions based on species scores owing to its low abundance throughout.

The relative location of Ericaceae and *Sphagnum* components along the first axis of the DCA is indicative of responses to hydrological change: ericaceous remains are all located towards the negative end of axis one, alongside the wet indicators, whereas *Sphagnum* spp. are generally more positive. Whilst this may be appropriate for *Vaccinium* species with wet preferences, ericaceous undiff. would be expected to be located in a drier ordination location than S. sect. *Acutifolia*. Since the majority of preserved ericaceous remains are roots or rootlets, the ordination location may have arisen from overlying conditions being drier than the sampling period. An example of this occurs in zone VDB12-c, which exhibits a two stage decrease in total *Sphagnum* and a two stage increase in total monocots whilst Ericaceae peak a sample ahead of monocots in a single increasing trend.

DCA was repeated three times to explore the effect of the surface samples, rare species and roots on the ordination (Figure 6.49, Table 6.9). The most effective DCA alteration was the exclusion of the roots and the surface species: the eigenvalue increased to 0.497 and the gradient length was 2.365. The ordination locations of some individual species in this DCA are improved:

S. pulchrum is more negative (wetter), and Ericaceae undiff. are more positive (drier) than the original ordination from the full DCA. *Picea* has been ordinated further towards the negative (wetter) end of axis one; however, this may be influenced by enhanced leaf preservation in wetter conditions. Owing to the improved species ordination locations, the axis one scores from the DCA excluding roots and surface species will be used to represent past changes in the peatland WTD.

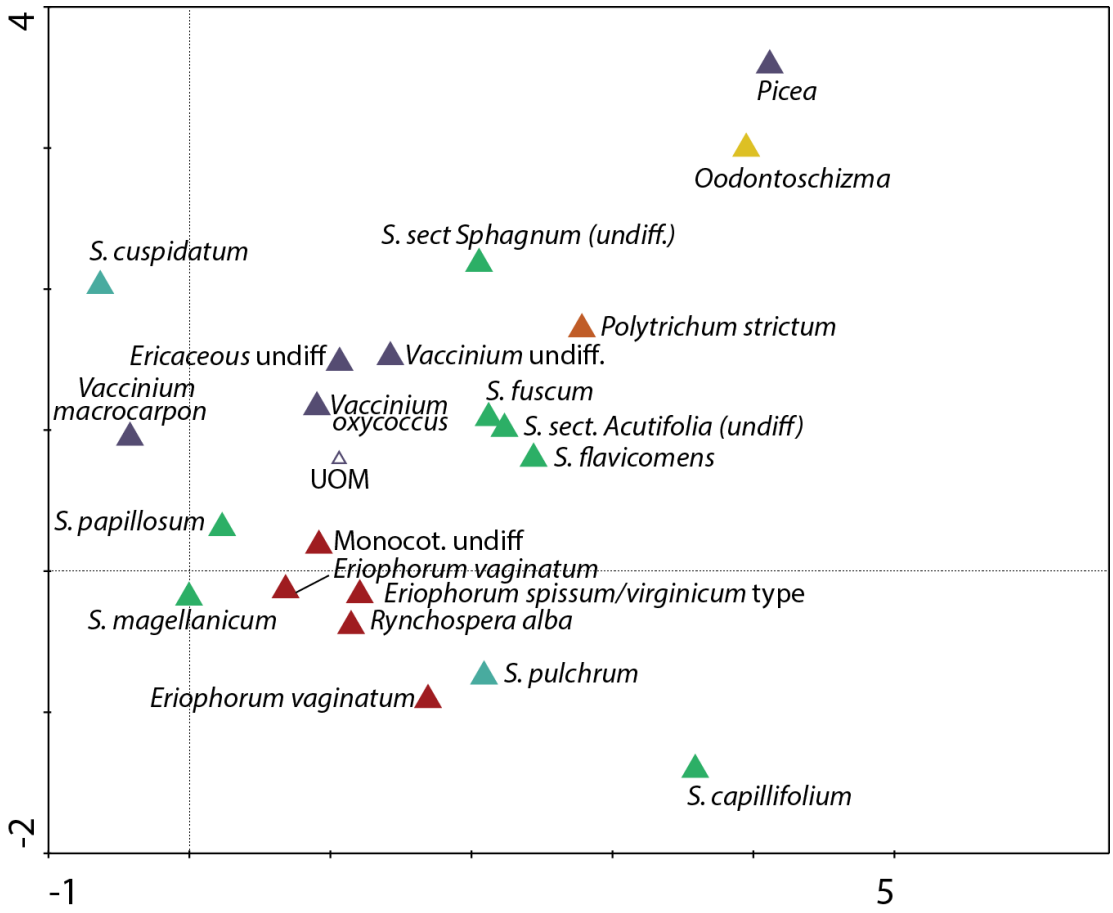

Figure 6.49 VDB12 plant macrofossil species DCA axis one (x-axis) and two (y-axis) distributions.
Similar vegetation types are grouped by colour: purple = woody shrubs; red = monocots. and sedges; yellow = liverwort; orange = brown moss; green = *S.* sect. *Sphagnum* and *S.* sect. *Acutifolia*; blue = *S.* sect. *Cuspidata*; no fill = UOM.

Table 6.9 VDB12 plant macrofossil DCA statistics

DCA	Eigen value	Gradient length
1. Full	0.419	**2.85**
A. Excluding surface samples	0.429	2.27
B. Rare species excluded	0.296	1.953
C. Roots and surface species excluded	**0.497**	2.365

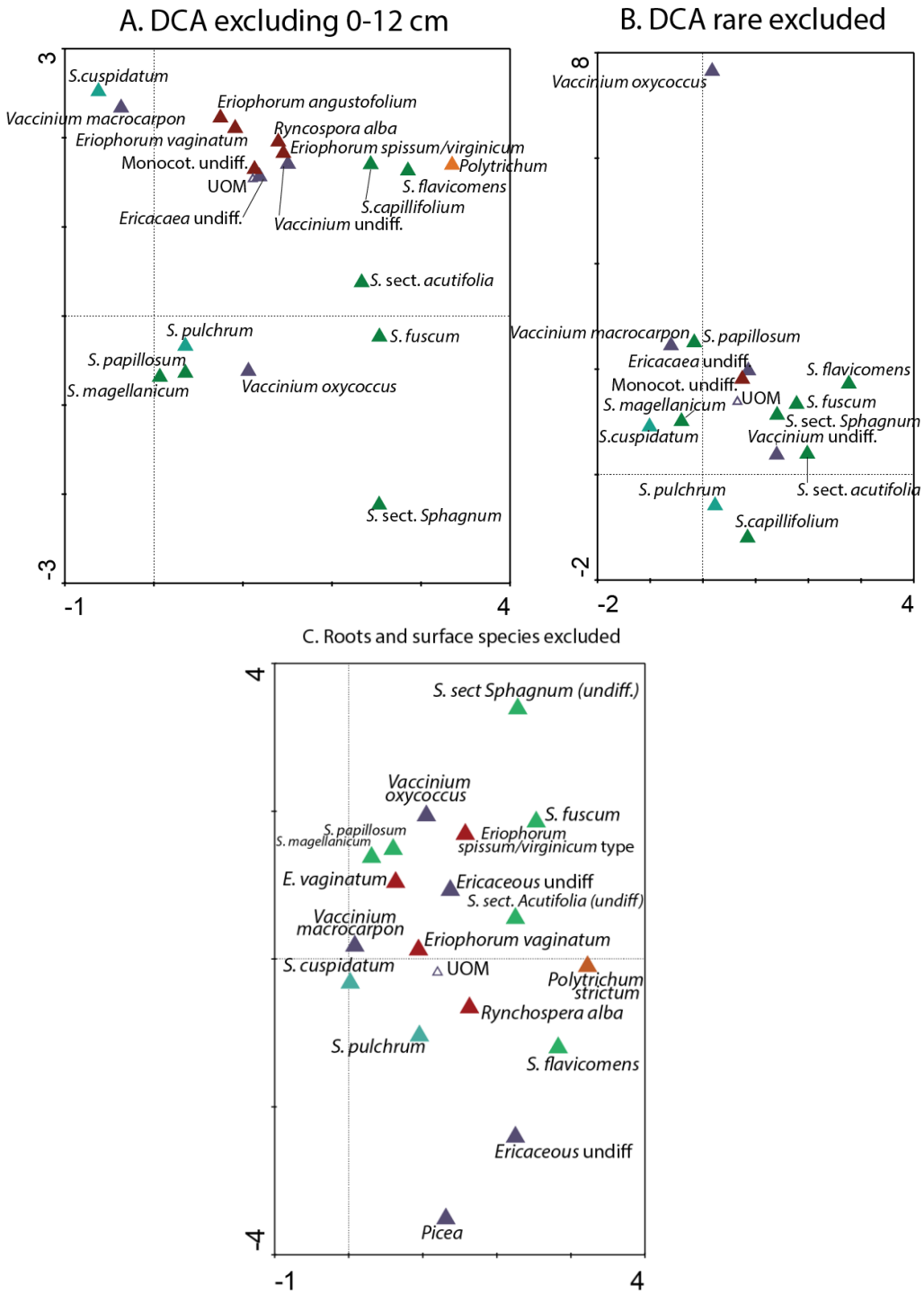

Figure 6.50 Alternative VDB12 plant macrofossil species DCA axis one (x-axis) and two (y-axis) distributions.

A: excludes the surface samples that contain enhanced preservation relative to the remainder of the core; B: rare species (<10%) are excluded form the DCA rather than simply down weighted; C: excludes the roots and surface samples. Similar vegetation types are grouped by colour: purple = Ericaceae; red = monocots. and sedges; yellow = liverwort; orange = brown moss; green = *S.* sect. *Sphagnum* and *S.* sect. *Acutifolia*; blue = *S.* sect. *Cuspidata*; no fill = UOM.

The sample scores of the first and second DCA axis have been plotted to identify periods of similar vegetation assemblage within the core (Figure 6.51). Samples from zone VDB12-f are located at the positive end of axis one. Whilst VDB12-c to –e are located at the negative end of the axis that was previously identified as the drier end, these sample distributions could also be related to preservation. The ordination locations of the samples compliment the findings of the variability within the major species: zone VDB12-c is highly variable, zones VDB12-e and -f contain some variability and the VDB12-a and –b s are more tightly constrained.

The DCA axis one scores reveal stable conditions until 120 cm that are drier than elsewhere in the record. A gradual wetting trend occurs until 100 cm when there is a return to drier conditions until 76 cm. An abrupt, pronounced wet shift then occurs, ending at 68 cm. Drier conditions return at 64 cm although the water table depth then abruptly fluctuates to the surface of the core. The variability in the DCA axis one scores echo the earlier conclusions obtained from the variability of the major vegetation components (Figure 6.52) but the decrease in stability after the pronounced wetting continued until *ca.* 16 cm.

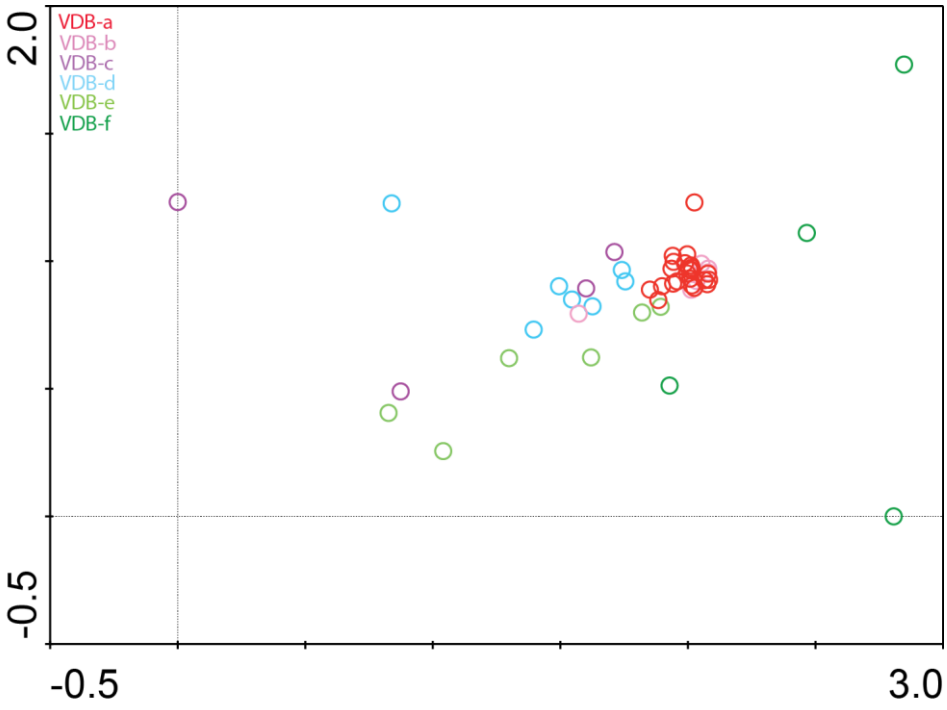

Figure 6.51 VDB12 plant macrofossil sample DCA axis one (x) and two (y) scores. Zone colourations correspond with the CONISS-based zonation of the assemblage diagram (Figure 6.47).

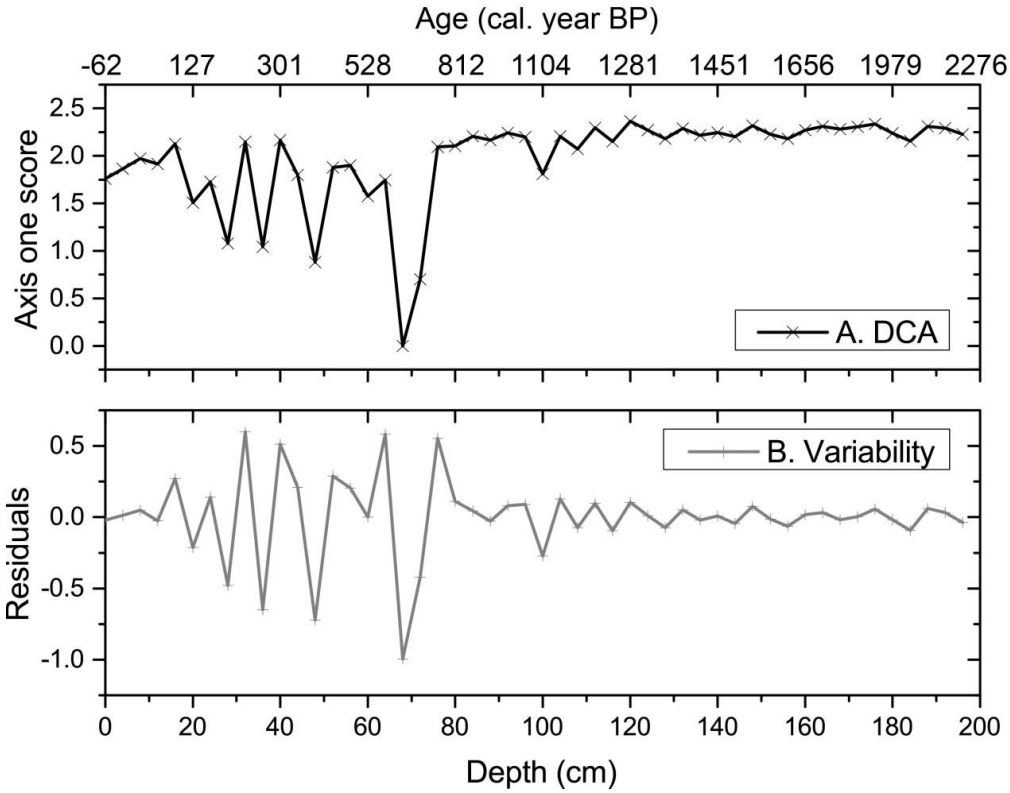

Figure 6.52 A: VDB12 DCA axis one scores (lower y-axis values indicate wetter conditions) and B: variability reported using the residuals from LOESS smoothing: sampling proportion = 0.12 (equivalent to n=6) and 1 polynomial degree applied

6.5.1.2 Statistical treatment of VDB12 macrofossil data: nMDS

The nMDS model for the VDB12 macrofossil assemblage had a stress of 0.11, indicating that the model results can be interpreted as a response to the major environmental control (Figure 6.53). The species distributions along axis one differ from the first axis of the DCA (Figure 6.52) since the wetter species are now located towards the positive end of the axis whilst drier species are located towards the negative end (Figure 6.53B). Despite the opposing gradient direction, the relative species distributions are similar to the original DCA ordination: *S. cuspidatum* is located towards one end of the axis, followed by *V. macrocarpon* and *S. magellanicum*, whilst *P. strictum* and the *Sphagnum* sections undiff. are located towards the opposing end. The comparable species distributions obtained in both the DCA and the nMDS are reflected in the similar axis one sample scores ($r = 0.92$, $p < 0.001$; Figure 6.53). The main differences between the two reconstructions occur between 200 – 170 cm (the nMDS is more variable than the DCA); around 80 cm (the

nMDS responds ahead of the DCA) and between 4 – 0 cm; however, the overall trends are similar throughout the main period of interest and environmental interpretations obtained from these results would be comparable.

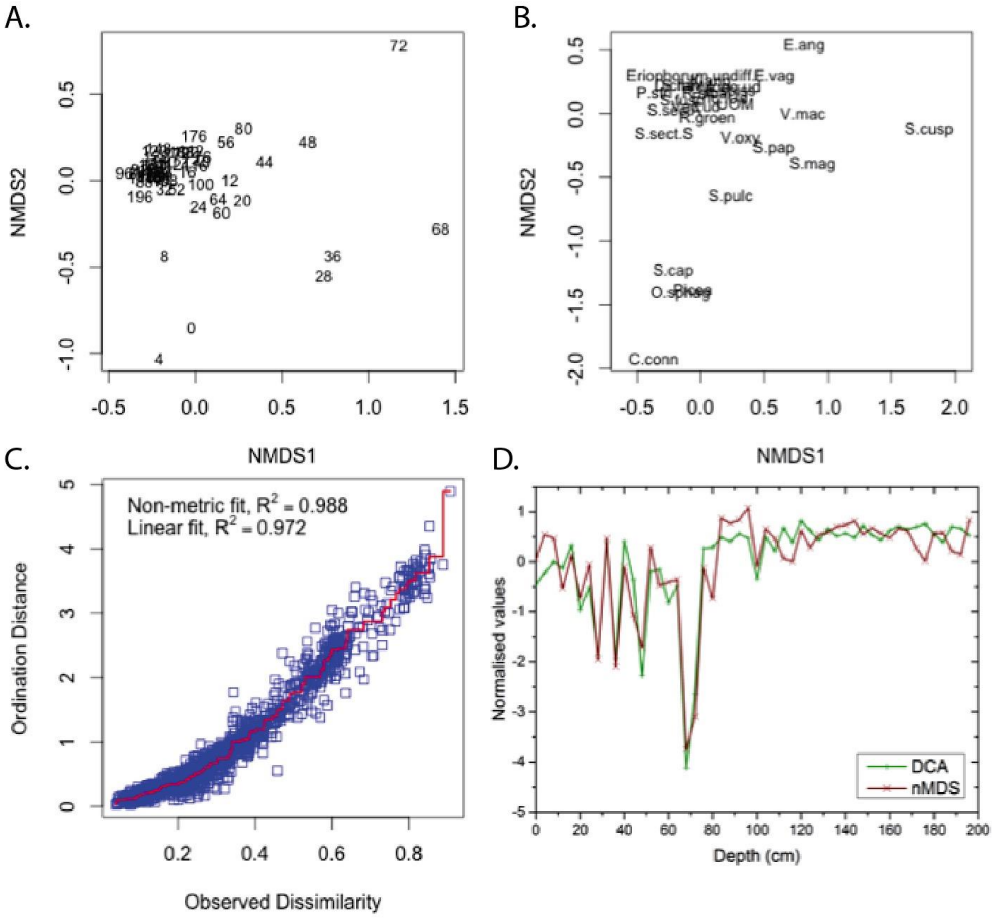

Figure 6.53 VDB12 plant macrofossil nMDS results.
A: nMDS axis one and two sample scores; B: nMDS axis one and two species scores C: formation ofnMDS model and associated stress; D: normalised comparison of the DCA and NMDS axis one scores (lower y-axis values indicate wetter conditions).

6.5.1.3 Statistical treatment of VDB12 macrofossil data: DHI

The approach of applying the DHI is supported by the results of the DCA and nMDS, which suggested WTD was the most likely dominant control on vegetation assemblage. There is no statistical difference between the medians of the three updated indexes as determined by one-way ANOVA on ranks (H = 3.418, 2 DF p=0.0181; Figure 6.54). The full updated DHI has a more similar relationship with the index that excludes UOM than the index that excludes

roots ($r = 0.999$, $p < 0.001$ and $r = 0.986$, $p < 0.001$ respectively). The index that excludes roots generally reconstructs higher magnitudes of change than the other indices. Excluding UOM had no effect on the reconstructed trends indicating that the presence of UOM was associated with decomposition and was likely not contributed by other factors such as pool layers or disturbance events. The statistical similarity of the three updated indices indicates that the final interpretations of environmental change would not be altered by excluding roots and/or UOM.

Owing to the statistical similarity of the three updated indices, comparisons with the Daley and Barber derived index can be made using the full index. The medians of the indices are statistically different ($U = 368$, $T = 3407$, $p < 0.001$) although the there is a weak but significant relationship between them ($r = 0.726$, $p = <0.001$). In the first zones (VDB12-a), the Daley and Barber index shows less variation that the updated index, although the opposite is true from *ca*. 80 to the surface. The full updated DHI index appears to be more sensitive to fluctuations within dry conditions than the Daley and Baber DHI, whereas the opposite is true in wet conditions.

The Daley and Barber index contains a trend to wetter conditions from 112 cm to 100 cm, which is in agreement with the total *Sphagnum* content in macrofossil diagram (Figure 6.47). A drying trend occurs from 100 cm, culminating at 80 cm before an abrupt shift to wetter conditions, whereas the updated index becomes wetter to 80 cm, then dries to 76 before becoming wetter again. Comparisons with the macrofossil assemblage diagram fail to conclusively indicate which DHI reconstruction is most representative of the plant macrofossil response to WTD at this point.

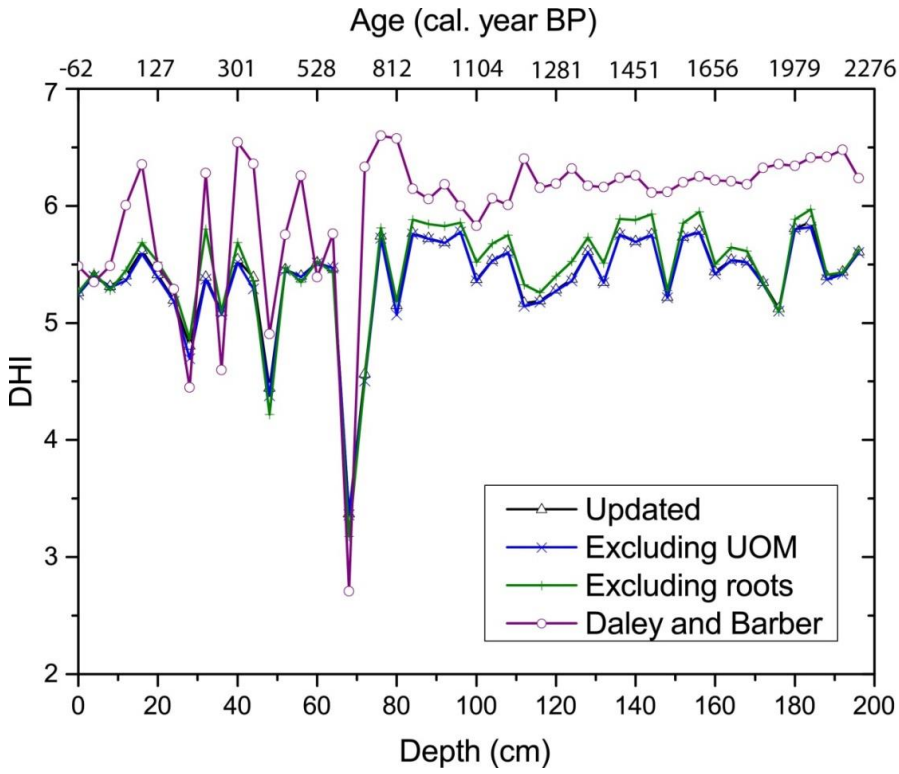

Figure 6.54 VDB12 plant macrofossil DHI reconstructions using the Daley and Barber (2012) index and three obtained from the updated index: full, excluding UOM and excluding roots. Lower y-axis values indicate wetter conditions.

6.5.1.4 VDB12 macrofossil hydrological reconstructions

A normalised comparison of data transformation methods indicates that the Daley and Barber derived DHI is more similar to DCA than the updated DHI ($r = 0.826$, $p < 0.001$ and $r = 0.806$, $p < 0.001$ respectively; Figure 6.55). The DCA deviates from the trends of the DHI indices between 84 - 76 cm when the DCA shows a steady decline to wetter conditions whilst the DHI indices both indicate drying conditions. At this point, the nMDS and updated DHI are more similar; however, this enhanced similarity is not consistent throughout the record. The updated DHI increases to drier conditions at 60 cm which differs from the decrease evident in the DCA, nMDS and the Daley and Barber derived DHI. During this period of deviation, *S. magellanicum* increases whilst *S.* sect. *Cuspidata* and total Ericaceae decrease. This change in assemblage may indicate a move to drier conditions; however, since wet indicators such as *V. macrocarpon* are also present at this time, the hydrological signal is unclear and may be representative of fluctuating conditions. The DHI comparisons

reveal that that there is potential for improvement within the Daley and Barber (2012) DHI; however the current updated index requires further refinement by the inclusion of more sites and more surface sample measurements before it can be confidently interpreted as a record of environmental change.

The hydrological trends obtained from the plant macrofossils indicate that the WTD was low and stable between 2000 - 1100 cal yr BP, containing small fluctuations. The peatland became drier *ca.* 1100 – 800 cal yr BP before a pronounced, abrupt wet shift *ca.* 600 cal yr BP. The WTD was then more variable towards the present day, containing pronounced fluctuations until *ca.* 200 cal yr BP when the water table increasingly lowered until *ca.* 100 cal yr BP.

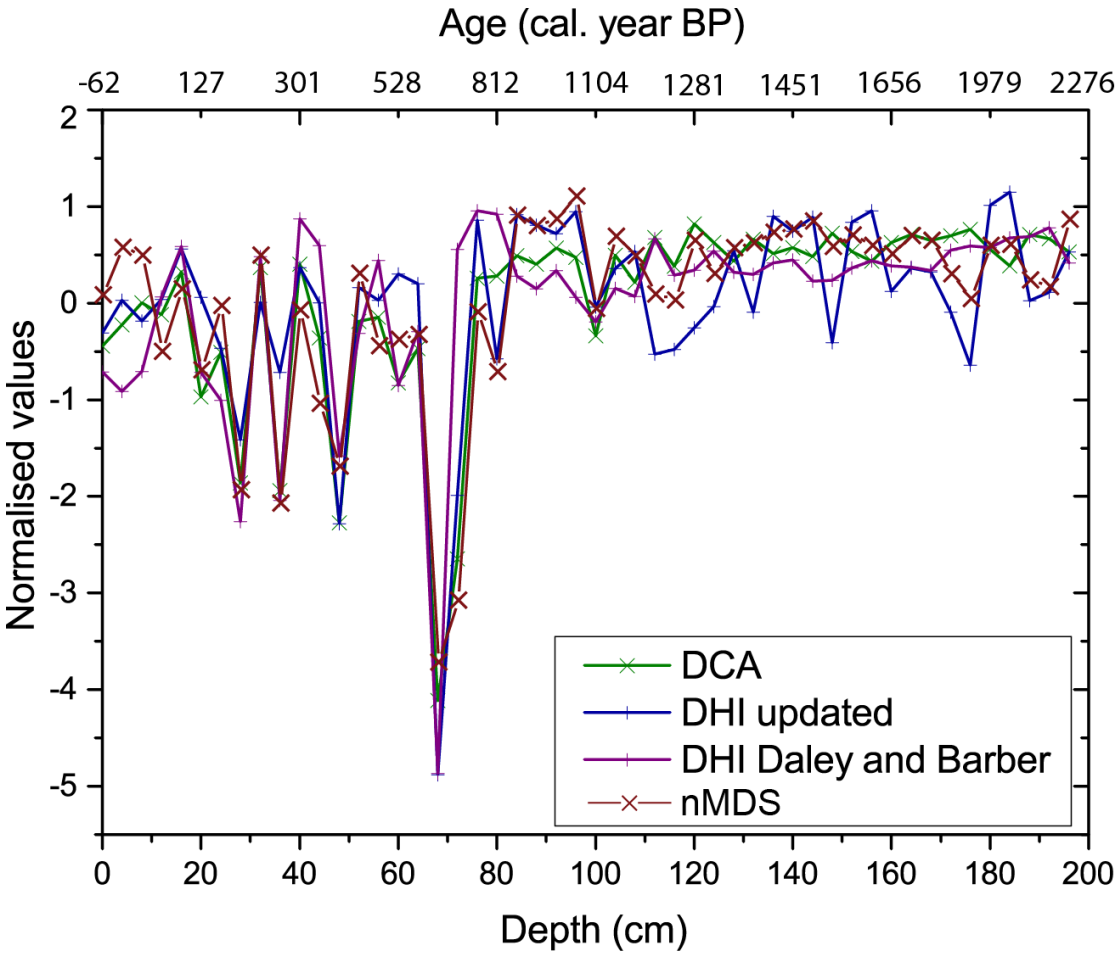

Figure 6.55 VDB plant macrofossil normalised data transformations. Lower y-axis values indicate wetter conditions.

6.5.2 VDB12 testate amoebae

The testate amoebae assemblage data have been visually separated into seven zones of similar species distribution using results from CONISS analysis (Figure 6.56; Table 6.10). The zone boundary between VDB12-e and –f was altered by one sample to account for a larger, more consistent change in species abundance evident in the assemblage diagram. The faunal assemblage at VDB12 is diverse with many different species varying in dominance throughout the record. *A. flavum* is the most prominent with an average abundance of 30%, accounting for *ca.* 60% in the central zones VDB12-d and –e. *H. subflava* is a dominant taxa towards the beginning and end of the record (although supressed in VDB12-e) with an average abundance of 14%.

The opposing water table preferences of the most dominant taxa indicate the variable nature of VDB12 hydrological change: *A. flavum* is regarded as a key indicator of wetter conditions (e.g. Amesbury *et al.,* 2013, Turner *et al*., 2013), often dependant on stable hydrological conditions (Sullivan and Booth, 2011), whereas *H. subflava* is generally indicative of drier conditions. During the early stages of the record, *H. subflava* is more abundant, with reduced concentrations of *A. flavum;* later stages exhibit a reverse in these conditions.

A discoides is more abundant in the initial stages of the record and is associated with wet conditions (e.g. Turner *et al*., 2013) found in pools and wet hollows (e.g. Tolonen, 1986). Regional transfer training sets reveal that *A. discoides* is located on a wetter water table gradient than *A. flavum* (Amesbury *et al*., 2013, Lamarre *et al*., 2013). Therefore, it is likely that zone VDB-a contained fluctuating wet/dry conditions, owing to interplay of *A. discoides, H. subflava D. pulex* and the dry indicator *T. arcula.* The peatland likely became drier in VDB12-b as indicated by the reduction in *A. discoides* and increase in dry *A. muscorum.* More stable wet conditions occurred around zones VDB12-d and especially -e (owing to the increase in *A. wrightianum*) which then dried towards the surface (VDB12-f-g).

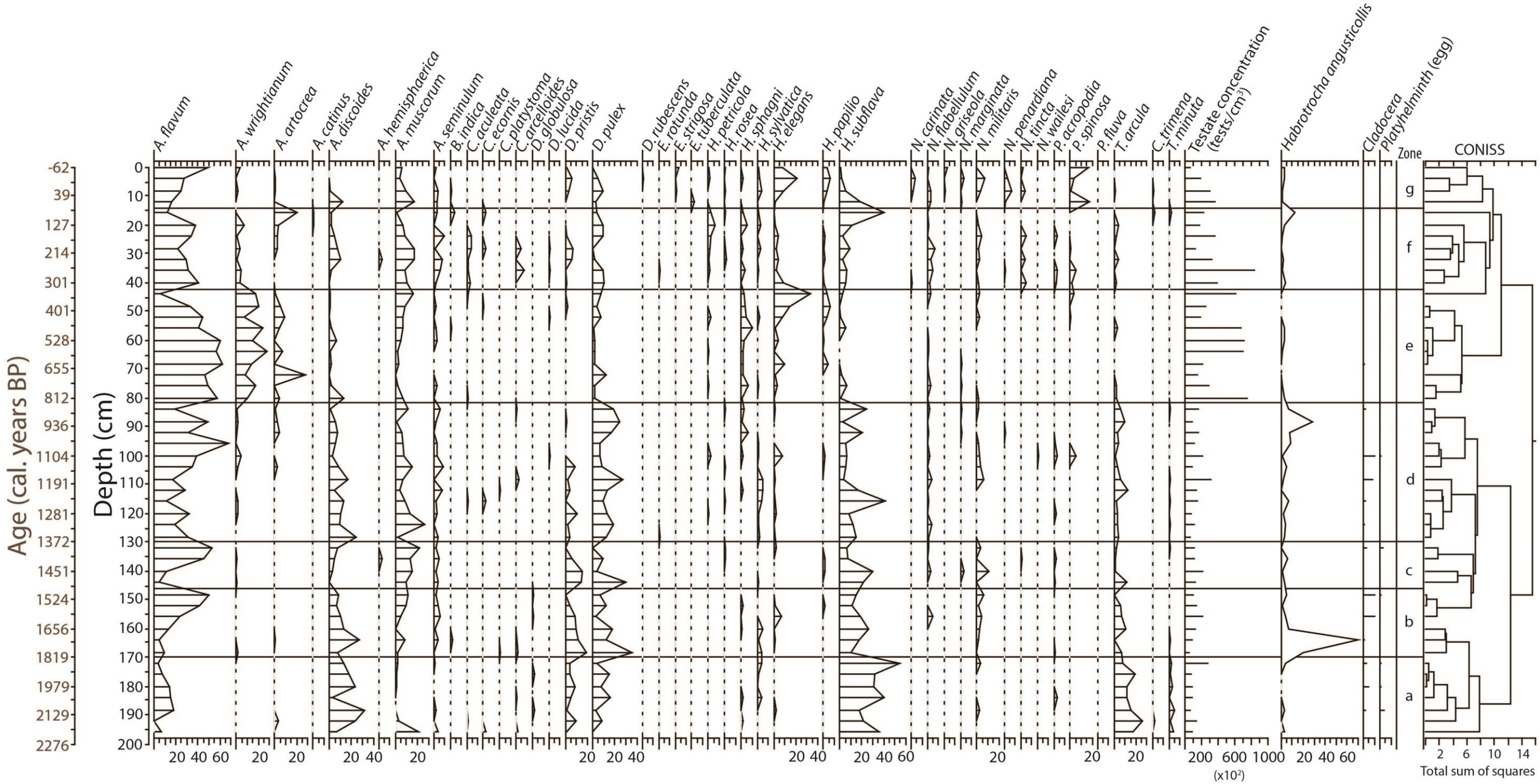

Figure 6.56 VDB12 testate amoebae assemblage diagram plotted against depth with a secondary age axis.

All data are percentages of the 100 tests identified at each level. Concentration data is displayed as depth bars, concentrations of tests per sample are represented by the bar graph and the frequencies of non-testate fauna are indicated bar graphs or, in the case of rotifers, a line graph. Zones have been allocated based on the results of the CONISS cluster analysis.

Table 6.10 Description of VDB testate amoebae assemblage

Zone	Depth (cm)	Faunal description	Age (cal yr BP)
VDB12-g	0 - 14	***A. flavum* increases to the surface from 12% to 49%.** *H. Elegans* increases to 21% at 4 cm; whereas *H. subflava* decreases from 40% to 1%. *A. muscorum* and *A. discoides* also decrease to surface. *D. pulex* and *D. pristis* increase to 8 cm and 4 cm respectively although are absent from the surface sample. Other taxa present in near surface samples in low concentrations include *N. militaris and P. spinosa*. *T. arcula* is generally absent from this zone.	-62 - 74
VDB12-f	14 - 42	***A. flavum* concentrations are sustained around 30 – 40%.** *A. artocrea* is present in lower concentrations than the previous zone and *A. muscorum* is elevated to 18% at 32 cm before decreasing. *A. flavum* generally decreases when *A. discoides* and *A. muscorum* increase. *D. pulex* accounts for *ca*. 10% of the assemblage and decreases at a similar point to *A. flavum*. *H. subflava* fluctuates *ca.* 5% but increases to 40% at the end of the zone.	74-320
VDB12-e	42 - 82	**Dominated by *A. flavum* which accounts for 58 – 62% of this zone then a decreasing trend begins at 60 cm.** *A. artocrea* has an abrupt peak of 28% at 72 cm – the taxon's highest concentration in the record. *D. Pulex* fluctuates but is not dominant. *A wrightianum* increases to 64 cm then fluctuates. *H. subflava* is present in low concentrations with the exception of the middle of the zone. *A discoides* and *T. arcula* decrease to background levels and the latter becomes absent at certain points. *A muscorum* increases from 72 cm to the end of the zone. *H. elegans* increase towards the end of the zone, reaching 33% at 44 cm.	320 – 840
VDB12-d	82 - 130	***A. flavum* is suppressed (*ca*. 15%) until 108 cm then increases to 96 cm (68%) before a more subtle decrease towards the end of the zone**. *A. discoides* and *A. muscorum* decrease throughout. *D. pulex* and *H subflava* exhibit similar trends although *H subflava* increase ahead of *D. pulex* which peaks at a similar time to *A. arcula*. These taxa are generally elevated when *A. flavum* is reduced. *A. artocrea* and *N. militaris* are present in the latter half of the zone.	840-1372
VDB12-c	130 - 146	***A. flavum* abruptly decrease to low concentrations (5-11%) but return to *ca.* 50% at the end of the zone**. *A. muscorum* and *A. discoides* increase throughout whilst *D. pristis* and *D. pulex* decrease. *H. subflava* increases to 140 cm then decrease towards the end of the zone. *N. flabellum* is present in low concentrations throughout with *P. spinosa a*nd *T. arcula*. *H. elegans* is present at the end of the zone.	1372 - 1495
VDB12-b	146 - 170	**Increasing concentrations of *A. flavum*, reaching 50% at 148 cm and *A. muscorum*.** *H. subflava* increases ahead of *A. flavum* reaching smaller peaks of *ca.* 30% before decreasing. *A. discoides, D. pulex* and *D. pristis* generally decrease. *T. arcula* fluctuate around *ca.* 10% and other species present in low concentrations include *N. flabellum* and *A. seminulum*. Cladocera increase throughout and the beginning of the zones sees a large abrupt increase in rotifers.	1495 - 1819
VDB12-a	170 - 196	**Initial high abundances of *H. subflava* (35%), *A. muscorum* (21%) and *T. arcula* (17%).** *H. subflava* increases in a series of three increments to 55% at 172 cm. *T. arcula* generally decreases throughout the zone and *A. muscorum* abruptly decreases to background levels from 192 cm. *A. discoides* fluctuates around 20% throughout and *D. pulex* fluctuates around 15%. *A. flavum* concentrations are low at the beginning of the zone but abruptly increase to 18% at 188 cm before decreasing throughout the remainder of the zone. Small concentrations of *T. minuta* are present throughout (<5%).	1819 - 2217

Based on the trends of the dominant taxa, the record can be summarised into three main sections:

1. zones VDB12-a to –c: high concentrations of *H. subflava* , decreasing with *A. discoides* and *T. arcula* as *A. flavum* and *D. pulex* increases. Indicative of initially dry conditions becoming wetter;
2. zones VDB12-d to –e: *A. flavum* dominance with an increase in *A. wrightianum* and *A. artocrea* in latter half of the section indicating wet conditions that increasingly become wetter;
3. zones VDB12-f and –g: *A. flavum* abundance decreases but still dominates as many more species are present in fluctuating abundances. *A. muscorum*, *D. pulex*, *H. elegans* and *H. subflava* also contribute to the assemblage indicating drier and/or more unstable conditions.

The variability of the four most abundant taxa changes throughout the record: initially *A. flavum* and *D. pulex* are more stable than *H. subflava* and *A. discoides*; however *D. pulex* becomes more variable at 172 cm and *A. flavum* exhibits large fluctuations from 152 cm (Figure 6.57). All four of the major taxa exhibit increases in variability between 76 cm and 48 cm. The onset of this increased variability coincides with an increase in the number of species present. The increased stability from *ca*. 48 cm is proximal to the reversal in the major species trends: e.g. *A. flavum* starts to decrease to the surface peat, whereas *H subflava* and *A. muscorum* beginning to increase.

Testate amoebae concentrations are stable but gently fluctuating from 200 - 84 cm, at which point it abruptly becomes more variable (Figure 6.58). There are three pronounced increases in concentration centred on 80 cm, 60 cm and 40 cm when the density of testate amoebae increase four fold. The testate concentration then decreases from 36 cm to the surface, returning to similar levels as the early stage of the record. A steady decrease in the number of testate amoebae present occurs from 12 cm to the surface in the living peat.

The average number of species present in each sample was thirteen (SD: 3.48; Figure 6.58). The species richness has a weak but significant relationship with depth, increasingly towards the peat surface ($r = -0.597$, $p < 0.001$). A divergence in this trend occurs between 84 -72 cm when the number of

species decreased to the lowest core level (n=8), before a stepwise increase to maximum species richness within the catotelm at 28 cm (n=21). Preservation may assist with this increase towards the surface; however, the fluctuation in trend indicates that other factors must also be influencing the species richness. The peak species richness coincides with an increase in the stability of the major species (Figure 6.57). The number of species present then decreases in the active peat, aside from the sample at 8 cm.

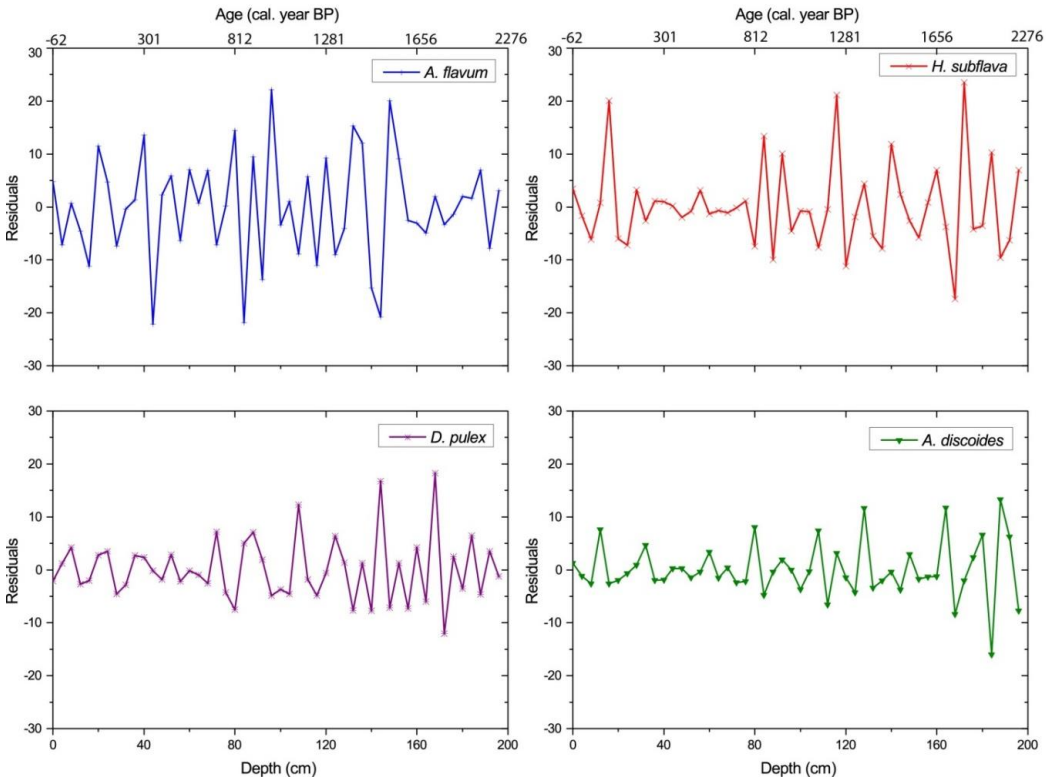

Figure 6.57 VDB12 variability of the four main testate amoebae taxa determined using the residuals from LOESS smoothing: sampling proportion = 0.12 (equivalent to n=6) and 1 polynomial degree applied

The SDI of VDB12 testate amoebae assemblage is above the 1.5 boundary indicative of stressed populations for the majority of the record, with an average index value of 1.93 (SD: 0.32; Figure 6.58). The main period of SDI reduction below 1.5 occurs between 72 – 64 cm, coinciding with the reduction in species richness driven by *A. flavum* dominance and assisted by large inputs from *A. wrightianum* (as reflected in the reduction in species evenness). The move to sustained wetter conditions may have passed a threshold that resulted in an increase in the holding capacity of the wetter species (indicated by increased concentration) that could out compete the dry

species. The SDI was sustained by high test concentrations between 128 -100 cm before the most pronounced decrease in SDI occurs to 68 cm.

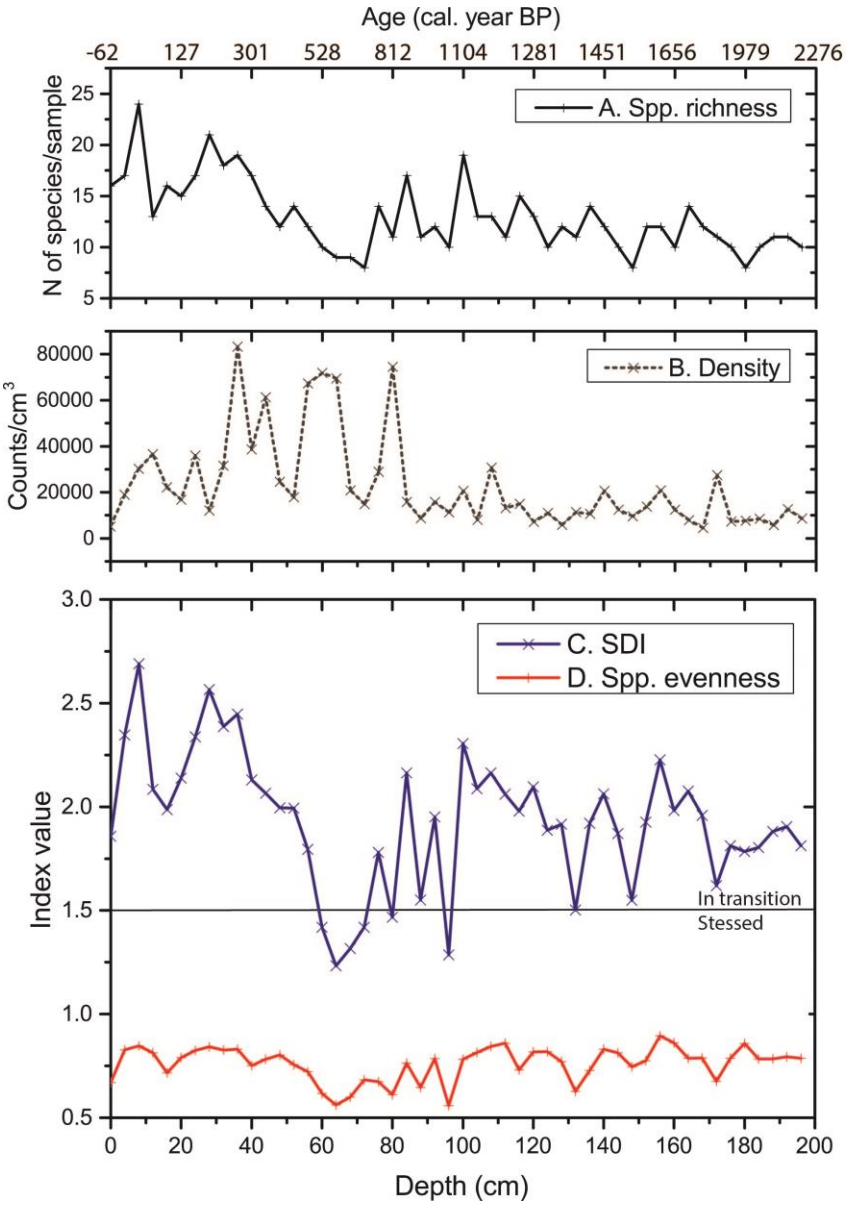

Figure 6.58 VDB12 testate amoebae ecological measures. A: Species richness (number of species per sample); B: Concentrations of individuals (counts per cm^3 of peat; determined used L*ycopodiu*m counts); C: Shannon Diversity index (calculated using the number of species per sample and the total number of species in the core; insert equation); D: Species evenness (indicates the relative abundance of species, calculated using the SDI and the natural log of species with zero = no evenness and 1 = evenness).

6.5.2.1 Statistical treatment of VDB12 testate amoebae data: DCA

The gradient length of the VDB12 testate amoebae DCA axis one is 2.338, indicating that a unimodal response model is appropriate for the ordination of the testate amoebae within this core, and the eigenvalue is 0.374. The ordination locations of the dominant species *A. flavum* and *H. subflava* infer that the wetter species are located towards the negative end of axis one and the dry indicator species are towards the positive end of the gradient (Figure 6.59). However, two of the other dominant species have unexpected ordinations: *A. discoides* indicates wetter condition but is placed amongst drier species in the ordination and *A. muscorum* would be expected to be located further towards the dry end of the axis. *A. discoides* may respond to seasonal WTD fluctuations (Barber and Langdon, 2007); therefore, the current characterisation of the water table preference of this species may be poorly constrained.

There are also are discrepancies across axis one within the rarer taxa: e.g. the key wet indictor *D. globulosa* is the most positive species, located near the key dry indicator *T. minuta*. Additionally, *B. indica* is ordinated centrally but would be expected to be located near the positive end of the axis. One of the main limitations of DCA is its sensitivity to rare taxa; however, the low abundances of these species will limit their influence on the DCA axis one scores. The DCA was repeated with the rare species removed to investigate their influence on the ordination the other species. The performance statistics of the DCA with rare species removed slightly weakened compared with the full DCA (eigenvalue = 0.371, gradient length = 2.328) and it did not noticeably alter the relative ordination locations of the dominant species or the DCA axis one scores (Figure 6.6). Therefore, it is appropriate to use the original DCA for environmental reconstructions, preserving the better performance statistics and the full dataset.

To identify periods within the record that have similar assemblages, sample scores were plotted against the first and second DCA axes (Figure 6.61). The zone located towards the most negative end of axis one is VDB12-g, whereas VDB12-a is located towards the most positive end of axis one. Generally, the zones are sequentially located more negatively, indicating the persistence of a wetting trend throughout the record. VDB12-e and –f are interspersed in

terms of axis one, indicating that they represent similar hydrological conditions; however VDB12-e is located more positively on axis two.

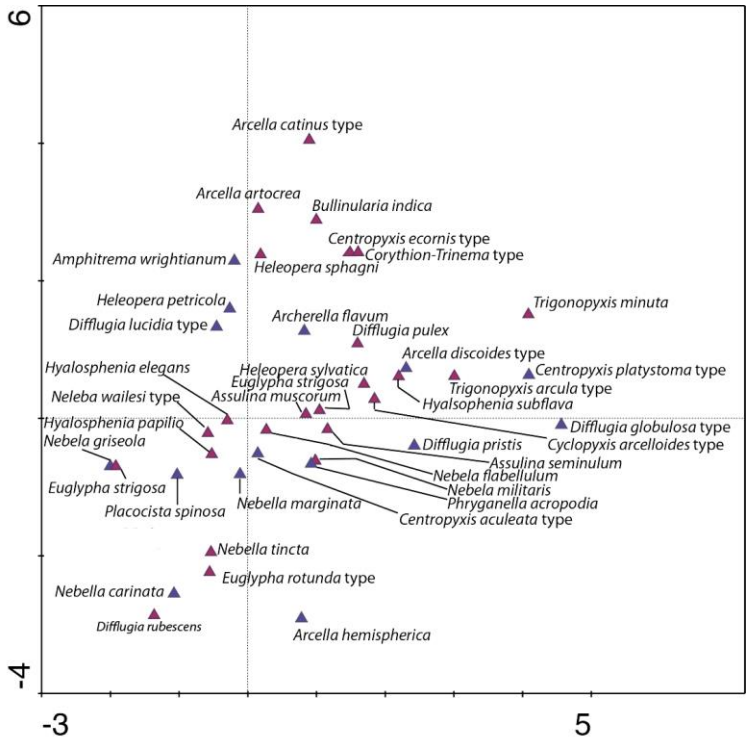

Figure 6.59 VDB12 testate amoebae DCA species axis one (x-axis) and two (y-axis) scores.
Taxa coloured blue to indicate wetter WTD preferences and red to indicate drier WTD preferences. Colour coding is based on the training sets of Amesbury *et al*. (2013) and Lamarre *et al*. (2013).

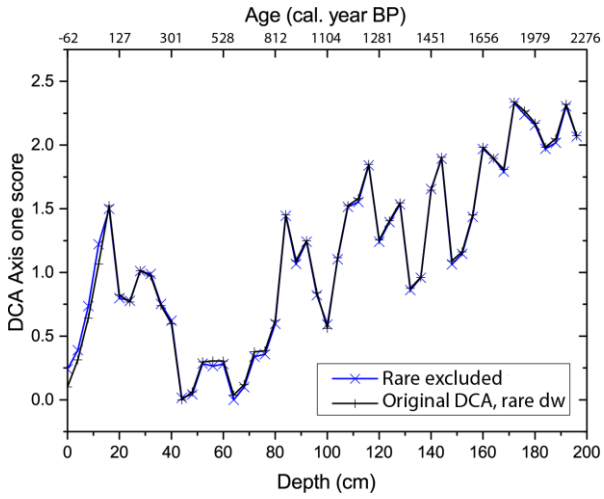

Figure 6.60 VDB12 testate amoebae DCA axis one scores from the original DCA with rare species downweighted and the DCA conducted with the rare (<10%) species removed. Environmental interpretations would be the same in both reconstructions. Lower y-axis values indicate wetter conditions.

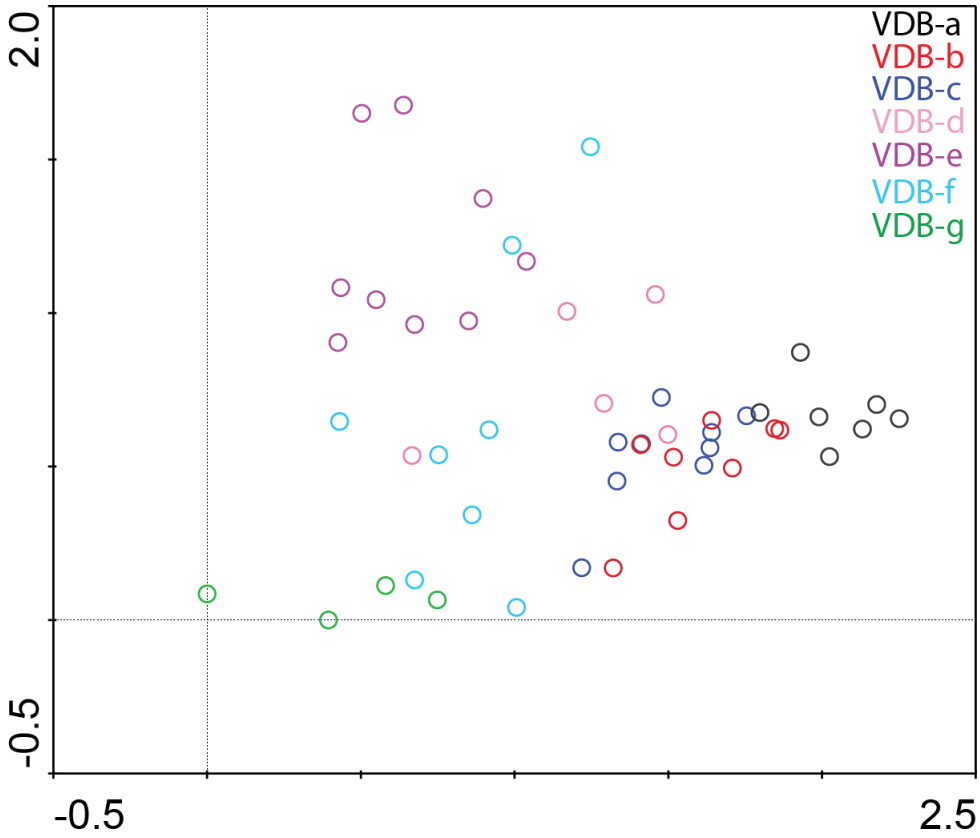

Figure 6.61 VDB12 testate amoebae DCA axis one (x-axis) and two (y-axis) sample scores coloured by zones allocated by CONISS analysis.

6.5.2.2 Statistical treatment of VDB12 testate amoebae data: nMDS

The nMDS model obtained from the VDB12 testate amoebae assemblage data had a stress of 0.14, which allows for careful interpretation of the nMDS axes one and two scores (Figure 6.62). The species distribution across the primary nMDS axis is similar to the results obtained from the first DCA axis: *T. minuta, D. globulosa and T. arcula* are located towards the positive end of the axis whilst *A. wrightianum*, *E. strigosa* and *N. griseola* are located towards the negative end of the axis (Figure 6.62B). The broad similarity between the first axes of the DCA and the nMDS suggests that the same underlying environmental variable and associated response from the testate amoebae have been detected. The scaling of the species along axis two differs between the nMDS and the DCA; however, the source of the secondary environmental driver is unclear from the species distributions. The downcore reconstructions using the nMDS and DCA axis 1 scores are similar ($r = 0.97$, $p = <0.001$);

therefore, the similar trends would generate similar climatic interpretations (Figure 6.62).

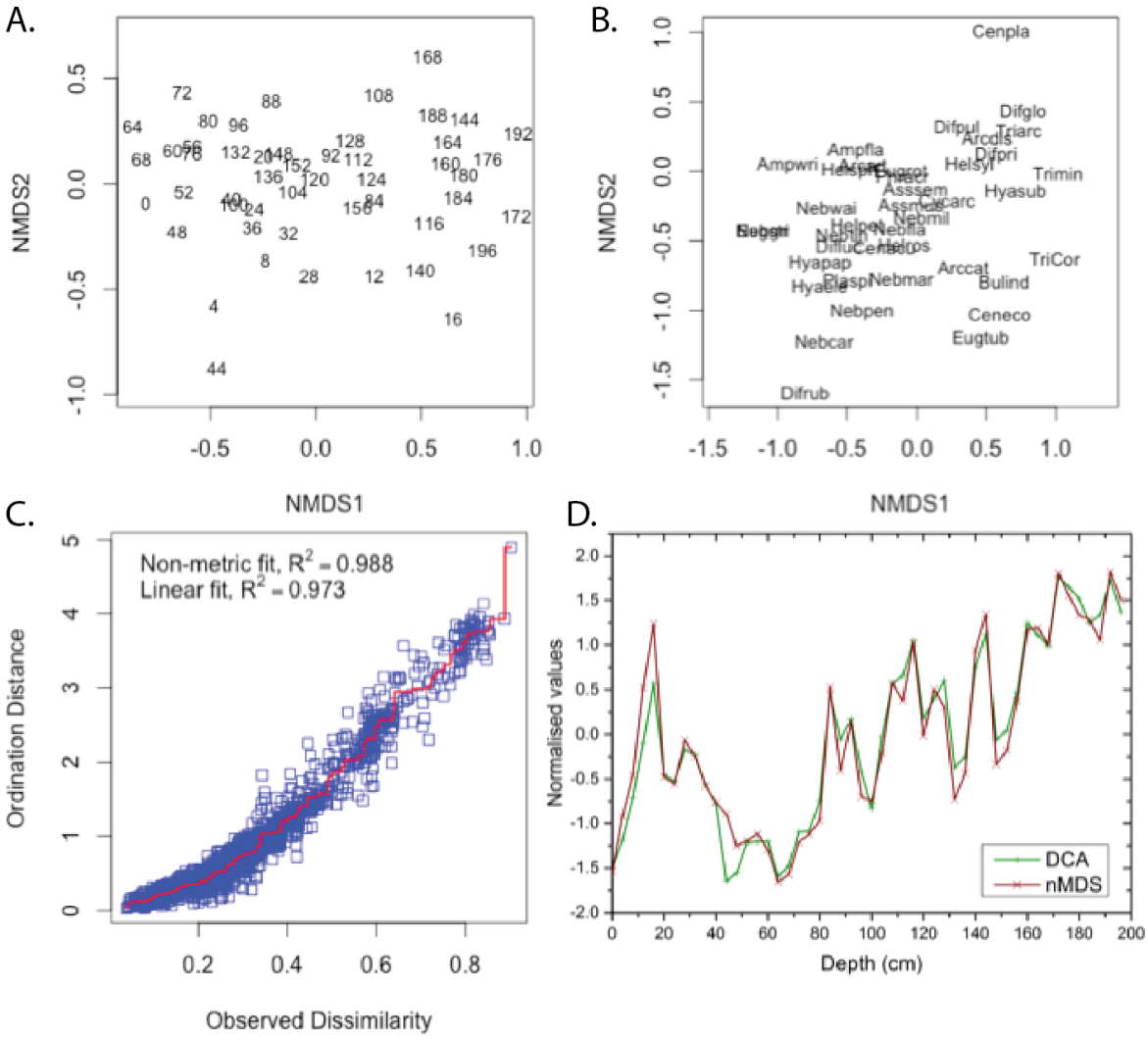

Figure 6.62 VDB12 testate amoebae nMDS results.
A: nMDS axis one and two sample scores; B: nMDS axis one and two species scores; C: formation of nMDS model and assocaited stress; C: normalised comparison of the DCA and NMDS axis one scores (lower y-axis values indicate wetter conditions).

6.5.2.3 Statistical treatment of VDB12 testate amoebae data: transfer functions

Owing to the presence of a hydrological gradient within the VDB12 testate amoebae DCA and nMDS, the ATLANTIC.NA (Amesbury *et al.*, 2012) and QUEBEC (Lamarre *et al.*, 2013) transfer functions models were applied to the data, attributing all assemblage changes to WTD. A comparison of the

ATLANTIC.NA models indicates that the WA.inv reconstruction has a 14% greater error than WA.inv.tol reconstruction. There is a statistically significant difference between the median of the WA.inv.tol and WA.inv (U = 728, T = 2003, p <0.001;Figure 6.63); however, the trends are statistically positively related (r = 0.935, p <0.001). Therefore, whilst the absolute values are different and the WA.inv experiences a greater amplitude of change, the directions of change are similar. Two points show different directions of change; however, they are unlikely to have a prominent effect on the environmental interpretation (highlighted in red; Figure 6.63).

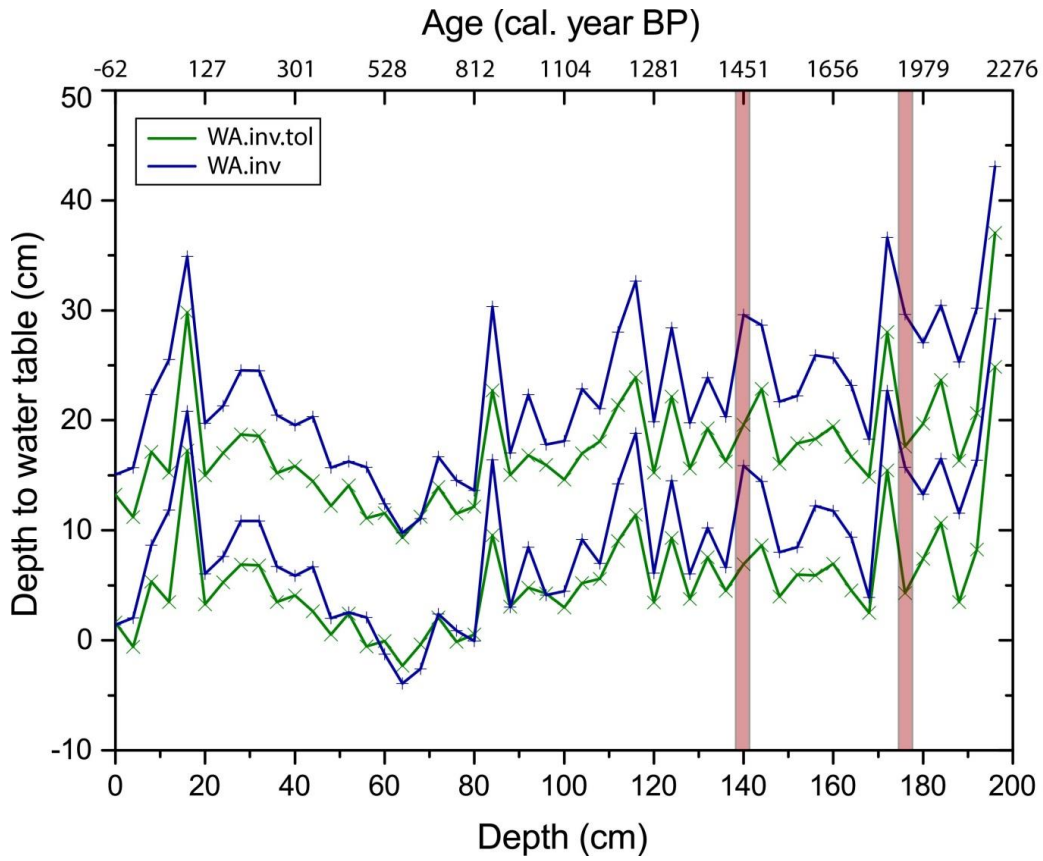

Figure 6.63 Upper and lower estimates of VDB12 water table depth obtained from the ATLANTIC.NA WA.inv.tol and WA.inv models from Amesbury *et al.* (2012). Red bands indicate divergences in the direction of change between the two models.

The median values of the WTD reconstructions obtained using the QUEBEC WA.cla.tol and WA.cla models are significantly different (U = 767, T = 2-42, p <0.001). Despite the differences in absolute values, there is a significantly positive relationship between the trends of the two reconstructions (r = 0.914, p <0.001). Pearson's correlation indicates that the two QUEBEC model

reconstructions are less similar than the two ATLANTIC.NA model reconstructions. The WA.cla model generally reconstructs drier conditions than the WA.cla.tol model; however the absolute reconstructed values are remarkably similar between 72 and 60 cm. There were more prominent divergences in trends of the QUEBEC model reconstructions than the ATLANTIC.NA reconstructions (highlighted in red; Figure 6.64). The divergences are unlikely to alter large-scale environmental interpretations aside from altering the timing of peak change. However, the interpretations must be made cautiously especially between 56 – 48 cm since several consecutive samples have diverging trends.

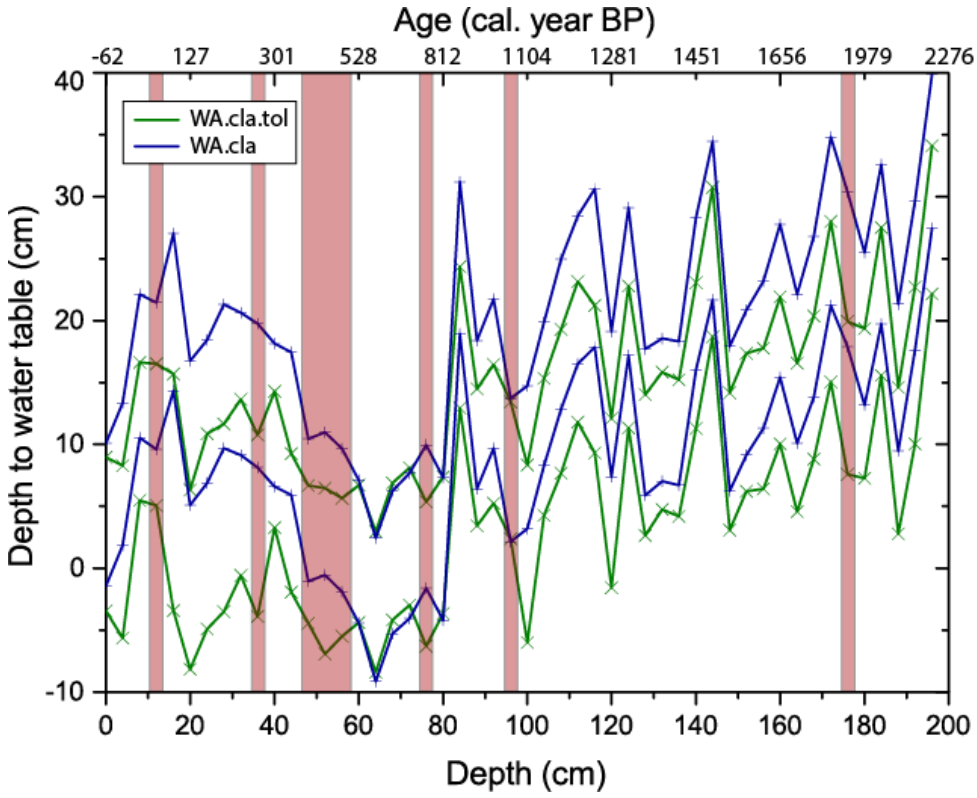

Figure 6.64 Upper and lower estimates of VDB12 water table depth obtained from the QUEBEC WA.cla.tol and WA.cla models from Lamarre *et al*. (2013). Red bands indicate divergences in the direction of change between the two models.

A comparison of the variability of each model from both transfer functions reveals that the ATLANTIC.NA WA.inv reconstruction generally contains more pronounced variation than the ATLANTIC.NA WA.inv.tol. The variation between QUEBEC model reconstructions is more similar than the ATLANTIC models, although more pronounced differences are evident towards the surface (Figure 6.65). In the first half of the record (from 200 – *ca.* 80 cm) the

QUEBEC models contain more variation than the ATLANTIC.NA reconstructions. Both experience a pronounced change in variability at 84 cm then conditions in both transfer functions are more stable until *ca.* 20 cm. The ATLANTIC.NA model reconstruction then exhibit more pronounced variability than the QUEBEC reconstruction.

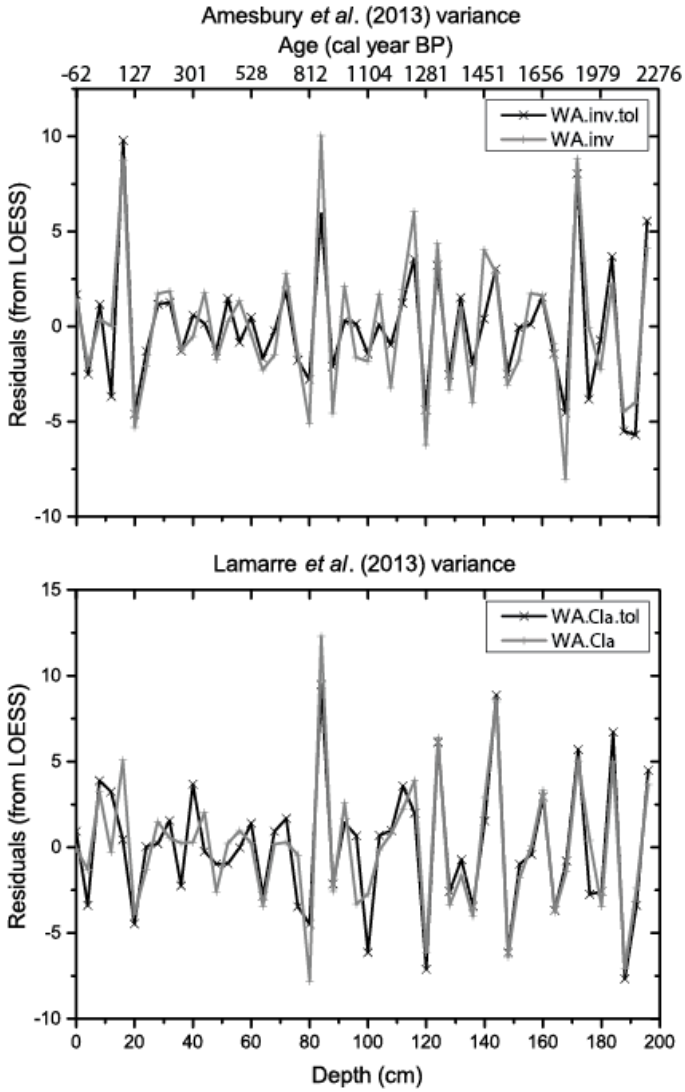

Figure 6.65 Variability of models using residuals from LOESS with a sampling proportion of 0.12 (equivalent to n=6) and 1 polynomial degree.

6.5.2.4 VDB12 testate amoebae hydrological reconstructions

There is no statistically significant difference in the medians of the ATLANTIC.NA WA.inv.tol and the QUEBEC WA.cla.tol models (U = 987, T = 2788, p = 0.07) and the trends of both reconstructions are statistically related (r = 0.78, p = <0.001). Both transfer functions reveal a wetting trend to 80

cm, although this is more pronounced in the QUEBEC model than the ATLANTIC.NA model (Figure 6.66). Both models reveal a temporary increase to drier conditions around 80 cm before an abrupt wetting event, after which values fluctuate at a new base level. The ATLANTIC.NA model indicates a drying trend from 64 cm to 24 cm whilst QUEBEC is more variable.

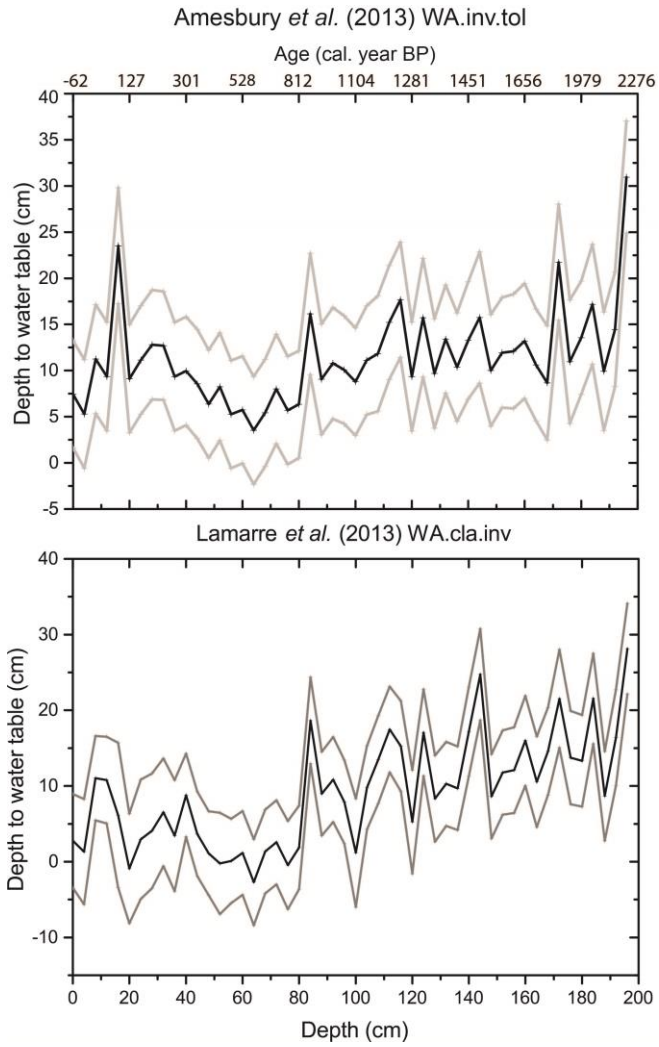

Figure 6.66 VDB12 testate amoebae transfer function reconstructions (black lines) with sample errors (grey lines)

A normalised comparison of the two transfer function reconstructions and the DCA and nMDS axis ones scores reveal similar trends in water table reconstructions (Figure 6.67). The main periods of dissimilarity between the transfer functions and ordination reconstructions occur between 196-160 cm and 48-44 cm (dry excursions are generally not identified by the DCA and the nMDS) and around 132 cm (the DCA and nMDS become drier ahead of the

transfer function shift at 128 cm). The normalised comparison also highlights periods of conflicting trends within the transfer functions at 168 cm when the ATLANTIC.NA reconstruction becomes drier ahead of the QUEBEC reconstruction and, more generally, from 56 cm to the living peat surface. The testate amoebae WTD reconstructions indicate a general trend toward wetter conditions until *ca*. 530 cal yr BP before the peatland becomes drier towards the living peat (*ca*. 100 cal yr BP).

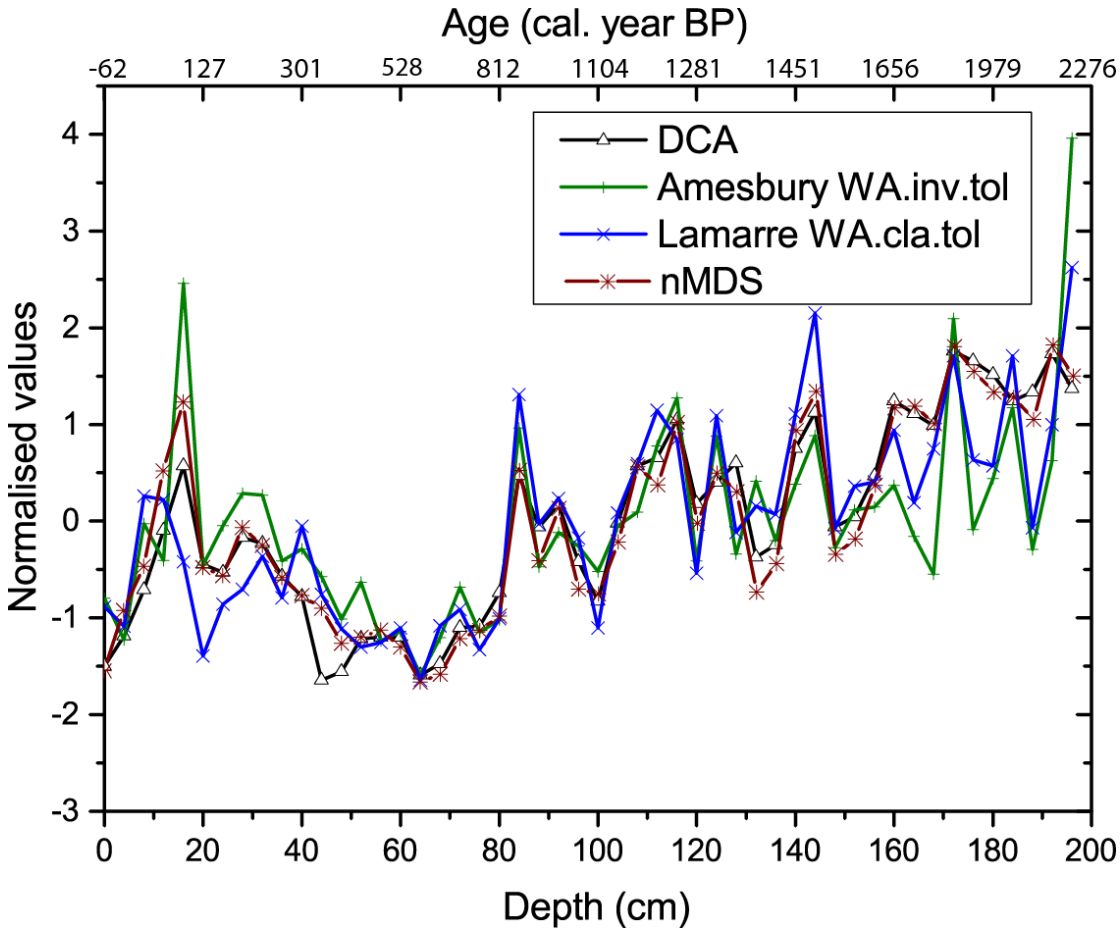

Figure 6.67 VDB12 testate amoebae normalised reconstructions. Lower y-axis values indicate wetter conditions.

6.5.3 Full VDB12 palaeoecological comparison

The plant macrofossil WTD reconstructions obtained using the Daley and Barber (2012) DHI and the testate amoebae reconstructions obtained using Amesbury *et al*. (2012) and Lamarre *et al*., (2013) transfer functions indicate a fluctuating series of wet and dry trends within a larger scale, gradual wetting trend to *ca.* 600 cal yr BP (Figure 6.68). The testate amoebae transfer function reconstructions contain an abrupt decrease to wetter conditions *ca*. 875 cal yr BP, whilst this occurs *ca.* 150 years later in the plant macrofossils. The peatland then generally dries to *ca*. 100 cal yr BP in the surface living peat.

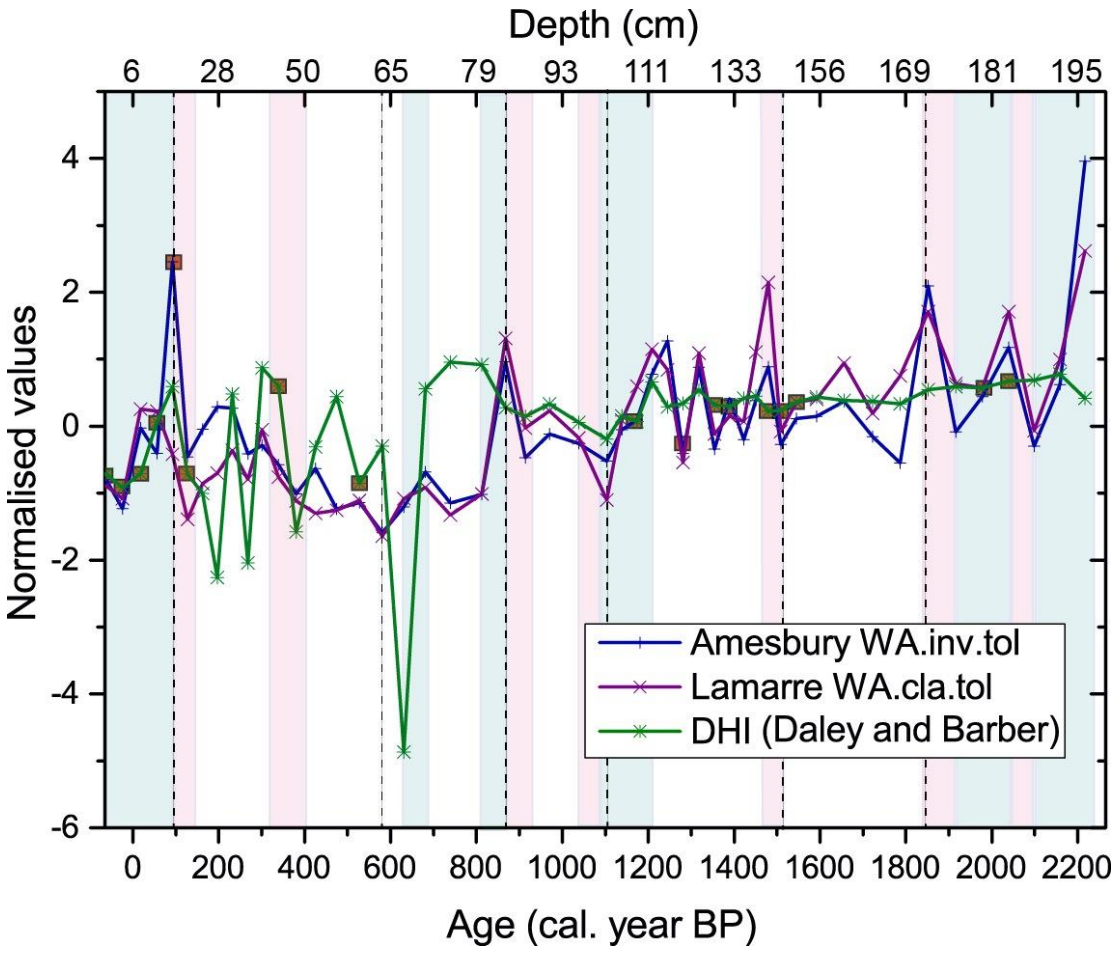

Figure 6.68 VDB12 ecohydrological reconstruction
Consistent trends between proxies to wetter conditions are shaded blue and drier trends shaded red. Any white areas indicate periods where trends in the proxies disagree or are unclear, dashed lines separate similar periods of hydrological conditions. Samples that are likely driven by factors other than hydrological conditions (as identified by differences in ordination and weighted averaging-based techniques) are highlighted by red boxes around individual points along with any divergences in the transfer function trends. Lower y-axis values indicate wetter conditions.

6.6 Saco Heath

6.6.1 Plant macrofossils

The SCH10 plant macrofossil data have been separated into nine zones of similar vegetation assemblages (Figure 6.69; Table 6.11). The vegetation record is dominated by *Sphagnum*, which commonly accounts for *ca.* 80% of the overall record. *S.* sect. *Acutifolia* is the main peat-forming species (*ca.* 70%), accompanied by *S. pulchrum* in low concentrations (*ca.* 5 – 10%) throughout. Of the identifiable *S.* sect. *Acutifolia*, *S. fuscum* is present in all samples except from 172 cm, which coincides with a decrease in total *Sphagnum* to 30%. *S. fuscum* dominates in the deepest sample (200 cm), representing *ca*. 60% of the total vegetation assemblage but more commonly accounts for *ca.* 10% throughout the remainder of the record. *S. flavicomens* generally accounts for *ca*. 10% of the total assemblage until 84 cm where it becomes more abundant, accounting for *ca*. 20% of the vegetation.

There are three main excursions to low levels of total *Sphagnum*:

1. SCH10-b: total *Sphagnum* falls to 30%, replaced by ericaceous remains (increased from *ca*. 15% to *ca*. 60%) and UOM (increased from 0% to 10%). Charred remains are present in one sample of this zone in low concentrations.
2. SCH10-d: *Sphagnum* accounts for *ca.* 40% of the assemblage, whilst total ericaceous components increase to *ca*. 50% and total monocots show their first main increase to 10%. UOM has a renewed increase around 104 cm to *ca.* 40%, which marks the peak UOM core abundance. This zone contains high amounts of charcoal and charred remains, suggesting a fire may have affected the site
3. SCH10-h: total *Sphagnum* reaches a point of minimum abundance (*ca*. 10%). Ericaceous remains increase to 75% along with a 10% increase in monocots and UOM. *Vaccinium* species peak at *ca*. 15% at 16 cm

There is a large increase in the variability of all major vegetation components around 100 cm (Figure 6.70), indicating instability in the vegetation assemblage. Zones SCH10-f and -g, located between the second and third *Sphagnum* decrease, experience more abruptly fluctuating conditions in the major vegetation components than the other

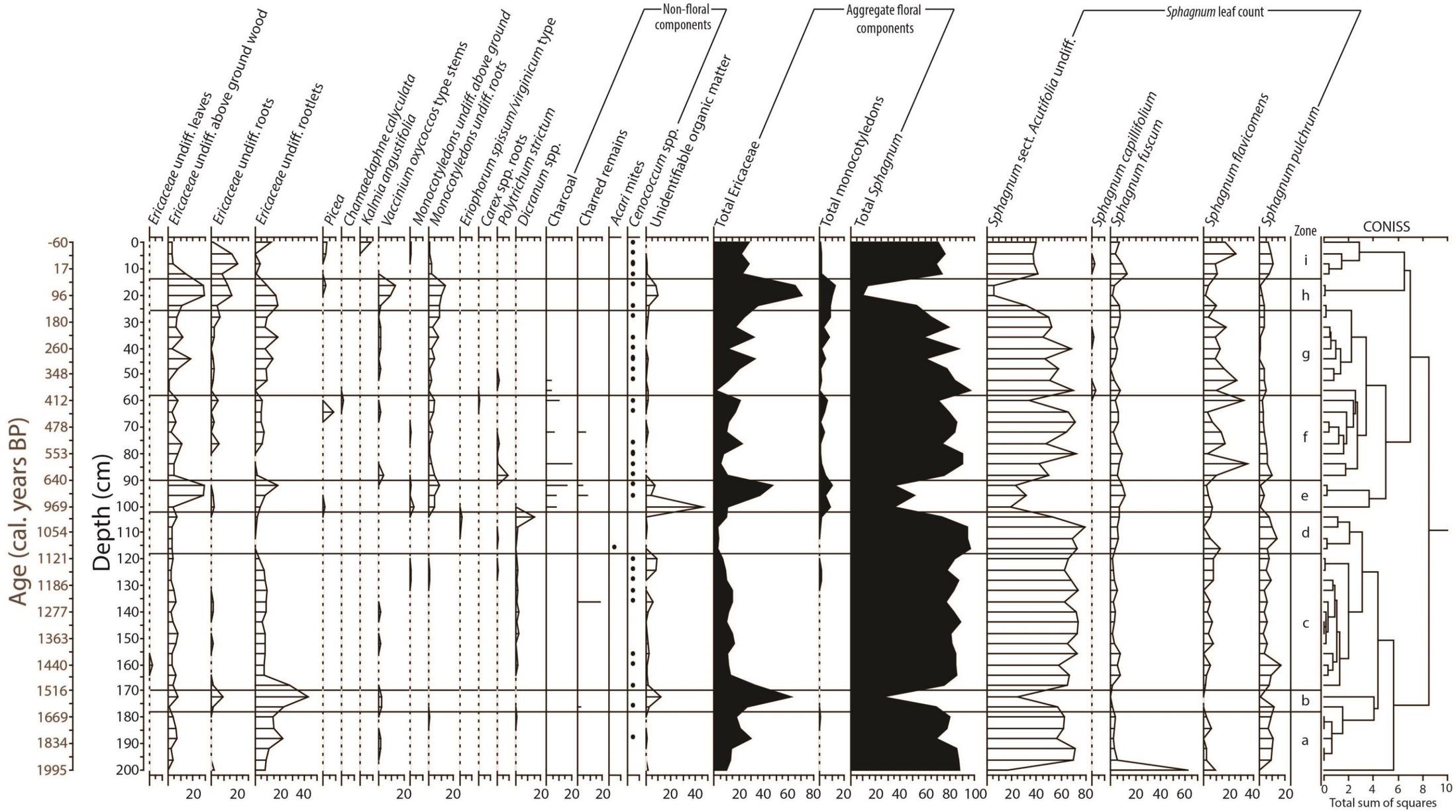

Figure 6.69 SCH10 macrofossil assemblage diagram plotted against depth with secondary age axis.

Peat components displayed with depth bars are derived from averaged quadrat counts (n=15) under low-power magnification (x10). Peat components displayed in solid black denote aggregates of different components. Individual *Sphagnum* leaf counts are also displayed with depth bars as proportion of aggregate *Sphagnum* based on random selection of 100 leaves identified at high magnification (x400). All data are presented as percentages with the exception of presence/absence data that are displayed as black dots. Zones were assigned after CONISS cluster analysis

Table 6.11 Description of SCH10 plant macrofossil assemblage

Zone	Depth (cm)	Vegetation assemblage description	Age (cal yr BP)
SCH10-i	0 - 14	***Sphagnum* increases to *ca.* 70%, mainly *S.* sect. *Acutifolia*** (with *S. flavicomens* increasing to the surface) and 10% S. *pulchrum*. Reduction in monocots and UOM. Ericaceae decrease to *ca*. 25%. *Picea* and *Kalmia angustifolia* present.	-60 - 50
SCH10-h	14 - 26	**Abrupt reduction in *Sphagnum* to *ca.* 10% at 20-16 cm.** Increase in Ericaceae to 70%, monocots *ca*. 10% and UOM to *ca*. 10%. Peak in *Vaccinium* species and *Picea* remains.	50 - 148
SCH10-g	26 - 58	**Step-wise decreasing trend in total *Sphagnum* from *ca.* 80% at the beginning of the zone to *ca.* 50% at the end**. More frequent fluctuations that other high *Sphagnum* zones. Step-wise increase in monocots to *ca.* 15% at the end of the zone and *ca.* 40% Ericaceae. Low pulses of UOM. *Polytrichum* present at the start of the zone then is absent for the remainder of the record.	148 - 399
SCH10-f	58 - 90	**Increase in *Sphagnum* concentrations (fluctuating around 80%).** Monocots reduce but are still present and Ericaceae increase in a stepwise trend. Background levels of UOM. Still some charcoal present. *Polytrichum strictum ca.* 10% at beginning of zone but decreases and is absent for the latter half of the zone. *Vaccinium* stems sporadically present and *Picea* remains identified at 64 cm.	399 - 640
SCH10-e	90 - 102	**Decreased period of total *Sphagnum to ca.* 40%.** UOM initially abruptly increases to 45% before decreasing to *ca*. 10% at 96 cm. Monocots fluctuate around 10%. Delay in Ericaceae response but does increase to 40% then 50% from 96 cm. *Picea* present at the beginning of the zone. Charcoal and charred remains present.	640 - 990
SCH10-d	102 - 118	**Increase in total *Sphagnum* to 90%** until 108 cm then decrease. Some *S. pulchrum* but mainly S. *sect. Acutifolia*. Low Ericaceae (5%), increasing toward the end of the zone (*ca*. 15%). *Dicranum* spp. have a short lived increase to *ca*. 15% at 100 cm, replacing background concentrations of *Polytrichum strictum. Eriophorum spissum/virginicum* type are present at a similar depth.	990 - 1108
SCH10-c	118 - 170	**Return to higher abundance of total *Sphagnum***, fluctuating around 80 – 90%. Ericaceae decrease to *ca.* 15% and generally gently decrease throughout. Minimal input from monocots although increase slightly at 124cm. Fluctuating UOM and *Dicranum* spp. present (<5%) and a small inputs of *Polytrichum strictum* occur towards the end of the zone.	1108 - 1516
SCH10-b	170 - 178	**Low *Sphagnum*, moderate-high Ericaceae and increase in UOM.** Short period of decreased *Sphagnum* (to *ca*. 25%) with an increase in Ericaceae (to 60%) and UOM (*ca*. 10%) Charred remains and *Vaccinium* species present.	1516 - 1638
SCH10-a	178 - 200	**High *Sphagnum*, moderate Ericaceae and low UOM**. *Sphagnum* accounts for 90% of the assemblage at 200 cm, and decreases to the end of the zone reaching 80%. Mainly *S. sect. Acutifolia* with *ca*. 10% *S. pulchrum*. Monocots are either present in low concentrations or absent. Ericaceae increase from 10% at the start of the zone to *ca*. 20% at the end. *Vaccinium* species are generally present (<5%) and *Dicranum* species appear (<5% at the end of the zone).	1638 - 1995

sections of elevated *Sphagnum* abundance. The variability remains elevated towards the peat surface in all major vegetation components, with the exception of UOM.

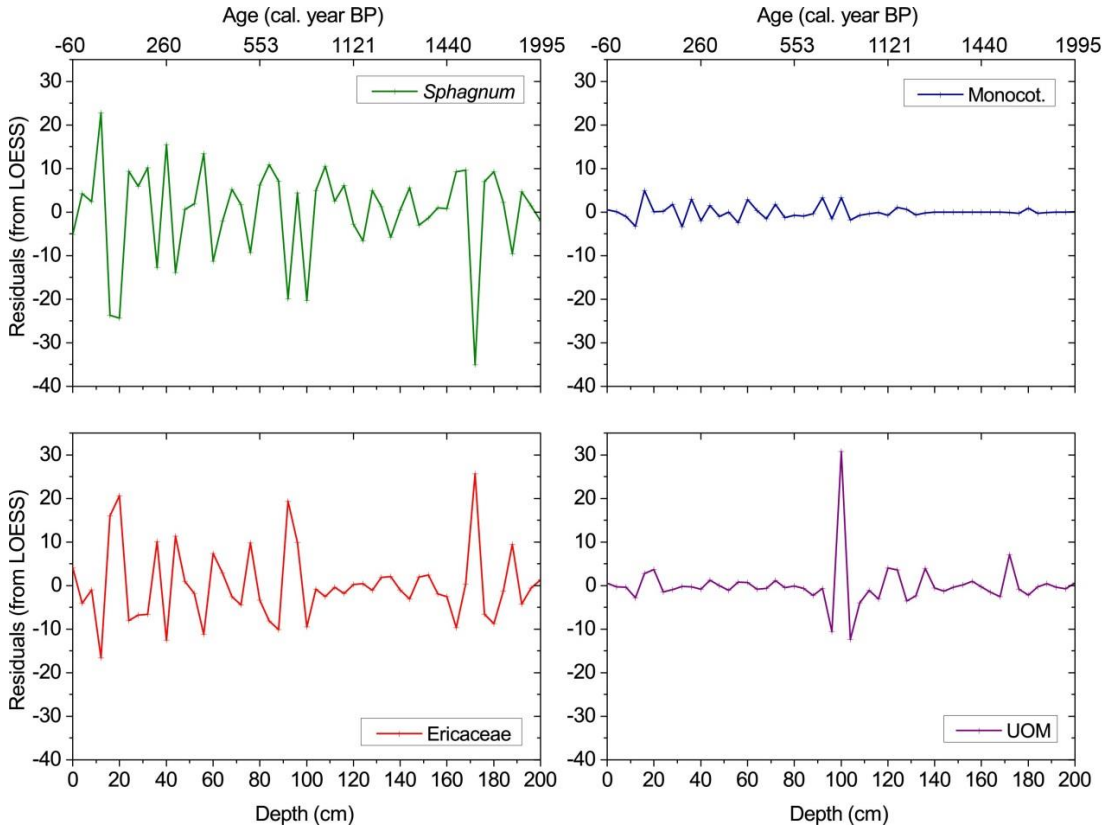

Figure 6.70 SCH10 variability of the major peat forming components plotted against depth, with a secondary age axis.
The variability is reported using the residuals from LOESS smoothing: sampling proportion = 0.12 (equivalent to n=6) and 1 polynomial degree applied.

Acari mites were only detected at 108 cm, the level with maximum *Sphagnum* abundance (>90%) in zone SCH10-d. Mites were more frequently present in the records from other sites in this study; however, the reason for their rarity in SCH10 is unclear. *Cenococcum* species were generally present throughout the core although they were absent at 108 cm during the *Sphagnum* increase and occur less frequently in older peat.

SCH10 is a fairly dry site as supported by the absence of key pool indicators such as *S. cuspidatum*, *R. alba* and *V. macrocarpon*. Aside from the prominent short-lived *Sphagnum* reductions in zones SCH10-b, -e and –h, there is little evidence of long term hydrological change. However, the

increase in *S. flavicomens* in the latter half of the record may indicate wetter conditions from zone SCH10-f towards the surface living peat.

6.6.1.1 Statistical treatment of SCH10 plant macrofossil data: DCA

The DCA axis one has an eigenvalue of 0.248 and a gradient length of 1.81, indicating that full unimodal species turnover may not have been captured within the record. The species ordination locations across the first DCA axis are not strongly indicative of a hydrological gradient (Figure 6.71). The dry indicating UOM is placed at the negative end of axis one with monocots undiff. and *Vaccinium* species whilst *Dicranum* species and *Eriophorum* species are located towards the positive end. Whilst the ordination interpretation is limited by the absence of preserved leaf fragments to facilitate the identification of *Dicranum* or *Eriophorum* to species level, these species are not especially characteristic of either wet or dry conditions. Therefore, it is unlikely that these species would inhabit opposing ends of the gradient if available moisture was the ordination driver.

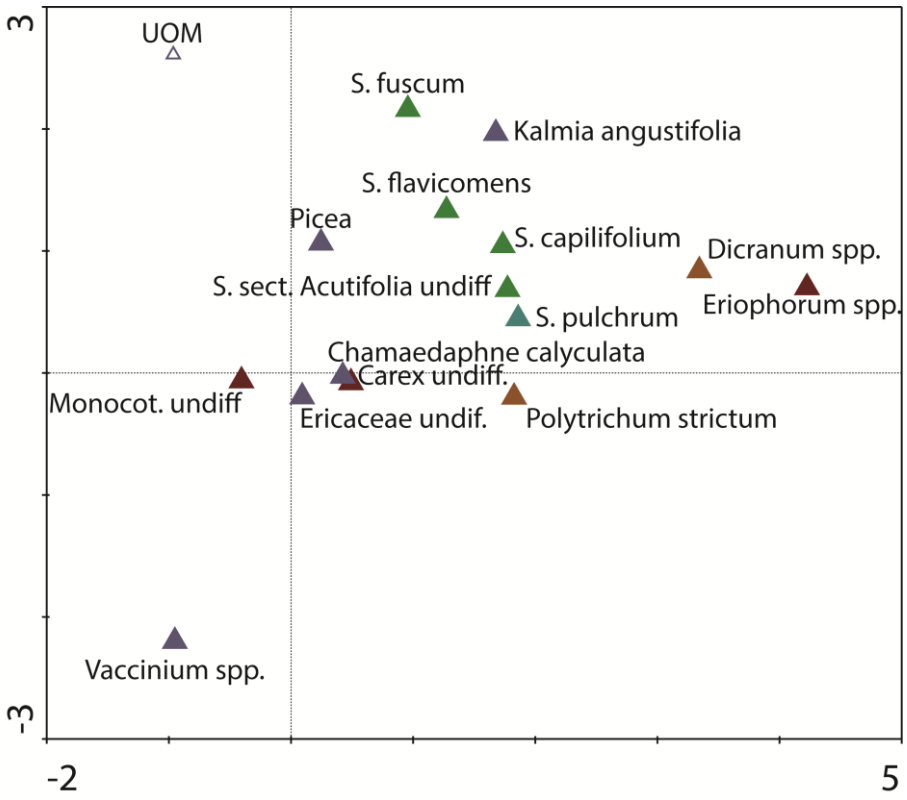

Figure 6.71 SCH10 DCA axis one (x) and two (y) species distribution. Similar vegetation types are grouped by colour: purple = woody shrubs; red = monocots. and sedges; orange = brown moss; green = *S.* sect. *Acutifolia*; blue = *S.* sect. *Cuspidata*; no fill = UOM.

Three possible explanations may contribute to this trend in species ordination:

1. Hydrological change is driving the assemblage change and the *Dicranum* and *Eriophorum* species present inhabit wet conditions;
2. Hydrological change is driving the assemblage change but the short water table gradient within SCH10 is restricting the ordination;
3. Hydrological change is not the main driver of the vegetation assemblage.

The wet indicator *S. pulchrum* would be expected to be more positively ordinated than its current location in order to support hypothesis one; therefore, it is unlikely to be the sole reason behind the ordination trends. Furthermore, if hydrological change was not the dominant driver of assemblage change then it may be expressed across the second DCA axis; however, no clear hydrological trend exists to suggest that water table is a secondary driver.

A short water table gradient may explain the ordination trends since SCH10 is a dry site throughout the entire record with no key indicators of very wet conditions such as *S. cuspidatum* or *R. alba*. In the absence of these species, shifts to increased total *Sphagnum* may be indicative of wetter conditions, especially those containing increases in *S. flavicomens* and/or *S. pulchrum*. *Sphagnum* components would therefore be expected to be located at an end of the ordination axis if the water table was driving the record; however, they are located centrally on axis one. The central ordination may indicate that the DCA has struggled to characterise the hydrological preference of the *Sphagnum* components. *S.* sect. *Acutifolia* and particularly *S. fuscum* have large water table tolerances which may have limited the vegetation responses to changing hydrological conditions, thus generating an insensitive record of change (e.g. Hughes *et al.*, 2006). The second hypothesis is therefore feasible: the DCA may have been restricted by the short gradient length.

The plants located towards the positive end of axis one (*Dicranum, Eriophorum* and *P. strictum*) surround zone SCH12-e (Figure 6.71). During zone SCH12-e and SCH12-f, charcoal is present in high concentrations, indicating that a fire has occurred on the peatland surface. This disturbance is registered in the age-depth model (Chapter 5:), which reveals a reduction in

accumulation rates, bracketed by radiocarbon measurements at 100 and 88 cm. The age difference between these depths is 348 years, whereas the preceding 12 cm of peat accumulated in 99 years and, similarly, the succeeding 12 cm accumulated in 101 years. Therefore, the accumulation rate during SCH10-e is not typical for the time period, and is around three times slower than the average accumulation rate over the last 2000 years (mean for 12 cm is 123 years). This scale of accumulation rate change indicates that the fire was unlikely to have been superficial and thus has the potential to override the effect of water table on the vegetation assemblage patterns.

Peatland fires are controlled by vegetation structure (Sillasoo *et al.*, 2011) and, whilst no direct link has been detected between hydrological state and burning, the depth of the penetration of a peatland fire may be enhanced by sustained lower WTD (Benscoter and Vitt, 2008). Prior to the fire, ericaceous and *Dicranum* species increased alongside *Eriophorum spissum/virginicum* type in zone SCH10-d indicating that the water table was lower which may have encouraged burning. *Picea* is present at the start of zone SCH10-e and would have provided fuel for the fire and facilitated fire expansion. UOM then substantially increase by (*ca.* >40%) during the fire. After the fire, monocot. species enter the assemblage and ericaceous species thrived, perhaps aided by the dry, nutrient rich conditions. Finally, *P. strictum* and *Vaccinium* species enter the assemblage and *Sphagnum* begins to return to higher concentrations. Previous investigations into sequential vegetation change associated with peatland fires have found varying results (Tuittila *et al.*, 2007; Sillasoo *et al.*, 2011). For example, *E. vaginatum* has been shown to become highly competitive in disturbed ecosystems (Silvan *et al.*, 2004); however, this response was not evident in SCH10. *Calluna vulgaris* has also been shown to dominate after a peatland fire (Sillasoo *et al* 2011), whilst this species is not present on eastern North American peatlands, a response in similar shrub species (e.g. *Chamaedaphne calyculata* and *Kalmia angustifolia*) is not detected.

It is difficult to clearly deduce the point at which the peatland recovers from the fire in zone SCH10-e using the vegetation assemblage data. Peatland vegetation assemblages post-fire vary, depending on the nature of the fire and the vegetation assemblage prior to the fire (Johnson 1992). Fires have

been shown to boost *Sphagnum* abundances (Clymo and Dyckett 1986) owing to the removal of competition from shrub vegetation. The depth at which the *Sphagnum* returns to the previous, higher concentrations (at the beginning of zone SCH10-f) could, therefore, represent the point of peatland recovery. However, zone SCH10-f and -g display more unstable, highly fluctuating conditions than the previous *Sphagnum* rich zone (SCH10-c; Figure 6.70). The increased variability could be a result of more unstable climatic conditions or could indicate peatland reestablishment after the fire event. Primary post-fire vegetation succession maintains the original pre-fire vegetation structure and composition, whilst secondary succession may occur after deep fires leaving bare peat which is colonised by species such as *Polytrichum* (Masing, 1960). *Polytrichum* does occur at the beginning of zones SCH10-f, after the fire, therefore, secondary succession may have occurred at this site.

Whilst there is strong evidence to support the presence of a fire in SCH10-e, there is little evidence from the macrofossils of burning in the other two zones of reduced *Sphagnum*. Small amounts of charred remains were present in zone SCH10-b; however, this is not conclusive enough to support a burning event that could be solely responsible for such a pronounced effect on the vegetation. The vegetation shift in zone SCH10-h occurred in recent peat (*ca.* 148 – 50 cal yr BP). However, there is no documentary evidence of a fire at this time (Kludge, 1991).

An alternative hypothesis for the increased ericaceous remains in SCH10-h, supported by the absence of charcoal, may be that this is an artefact of the current surface shrubby vegetation. Roots account for around half of the ericaceous increase in SCH10-h and the roots of the surface vegetation may culminate around this depth of 12 – 24 cm. The increase in UOM could represent a prolonged phase of deeper water table levels and increased acrotelm depth. Decomposition is likely to proceed faster at this location than at the more northern sites owing to the temperature gradient (Section 4.4).

The influence of fire on the SCH10 coring location has been discussed above using the macrofossil evidence in combination with the age depth model obtained within this thesis. These conclusions can be compared with published charcoal analysis from a separate core from Saco Heath (Clifford and Booth, 2013), which was obtained from the peatland edge rather than a

more central location similar to SCH10. Clifford and Booth (2013) identified fire events at 460 – 600 cal yr BP and a fire-induced hiatus from 600 – 1500 cal yr BP. This corresponds with the fire in zone SCH10-e (990 – 640 cal yr BP); however, the longer hiatus duration in the edge core compared with SCH10 indicates the central SCH10 coring location was less affected by the fire. Other smaller fire events were registered in the edge core at 2350, 2050, 1530 and 180 – 50 cal yr BP. The fires at 1530 and 180 – 50 cal yr BP do correspond with the low *Sphagnum* zones in SCH10; however, the lack of charred remains in SCH10 and the consistency of the age-depth model at these points suggests that the SCH10 coring location was not directly burned at these times. Rather, these WTD fluctuations at SCH10 may be responding to disturbances towards the edge of the peatland.

To assess the effects of the low *Sphagnum* zones on the DCA axis one species scores, three additional DCA were completed using different combinations of samples from the possible fire disturbed areas (Figure 6.72). The first alternative DCA (A) omitted all samples from zone SCH10-e to the surface, assuming that, post-fire, the importance of readjustment and associated vegetation succession would increase, reducing hydrological influences. The second alternative DCA (B) omitted all low *Sphagnum* zones to investigate whether they are associated with fire and whether a hydrological signal can be obtained from the remainder of the record. Finally, alternative DCA (C) omitted samples from zone SCH10-e owing to the direct fire evidence in this zone, thus assuming that the other low-*Sphagnum* events could be driven by other factors, including hydrological change. The eigenvalue is the highest in DCA A that only included zones a-f; however, this improvement is small (Table 6.12).

The species distributions from the DCA-C (all zones except SCH10-e) are similar to the original full DCA, indicating that there are other points in the core that are also driven by disturbance, or that the effect of the fire in SCH10-e on the vegetation change is similar to a different driver, which could be WTD. The species ordination reveals a stronger trend towards hydrological change in the locations of the *Sphagnum* species when all low-*Sphagnum* zones are removed (DCA-B). However, a hydrological trend in the full assemblage data remains unclear. This may indicate that water table depth is influencing the vegetation distribution, but that the response of the plants is

supressed owing to the dominance of *S.* sect. *Acutifolia*. DCA-A, which only includes the first half of the record, fails to reveal a clear hydrological driver, although it has located *S. pulchrum* and *V. macrocarpon* towards the negative end of the axis and *S. fuscum* towards the positive end. This supports the hypothesis that the SCH10 macrofossil ordination is restricted by the complacency of the vegetation record and the insufficient species turnover as represented by the low gradient lengths (Table 6.12).

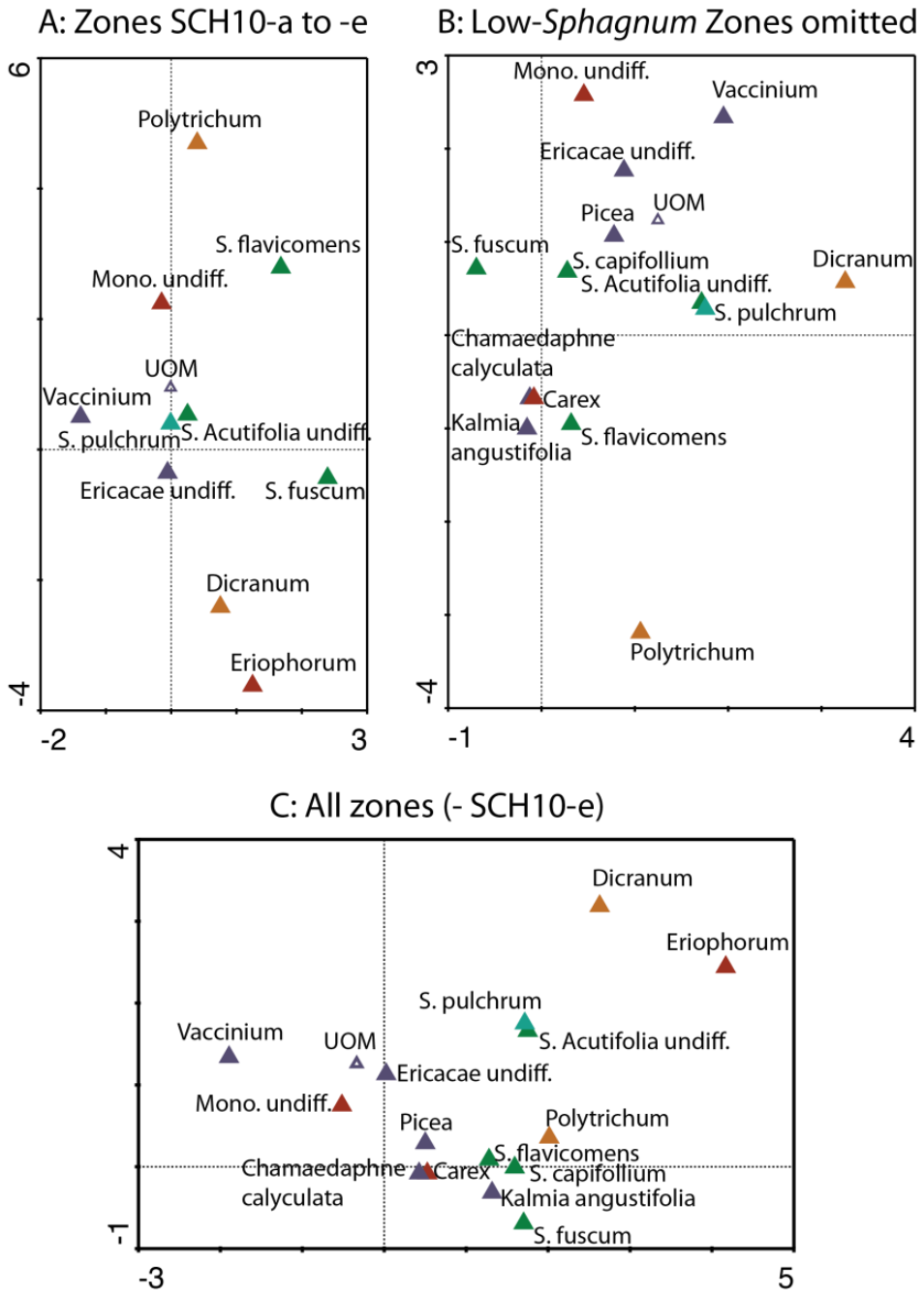

Figure 6.72 Alternative SCH10 plant macrofossil DCA, colours follow key in Figure 6.71.

Table 6.12 Axis one eigenvalues and gradient lengths for different DCA conditions

DCA	Eigen value	Gradient length
1. Full	0.248	**1.81**
A. Only zones SCH10-a to -f	**0.297**	1.716
B. All low *Sphagnum* zones omitted	0.153	1.552
C. All depths excluding SCH10-e	0.211	1.694

The DCA axis one and two sample scores reveal that samples located to the negative end of axis one are all located within the three main zones of decreased *Sphagnum* (SCH10-b, -e and -h). The samples from SCH10-d are located at the positive end of axis one and are from a zone of generally increased *Sphagnum*. These trends indicate that drier samples are located towards the negative end of the axis, whilst wetter samples are located towards the positive end of the axis. Samples from zones - a and -i are located within a similar ordination space, so there is some association between the top and bottom of the profile.

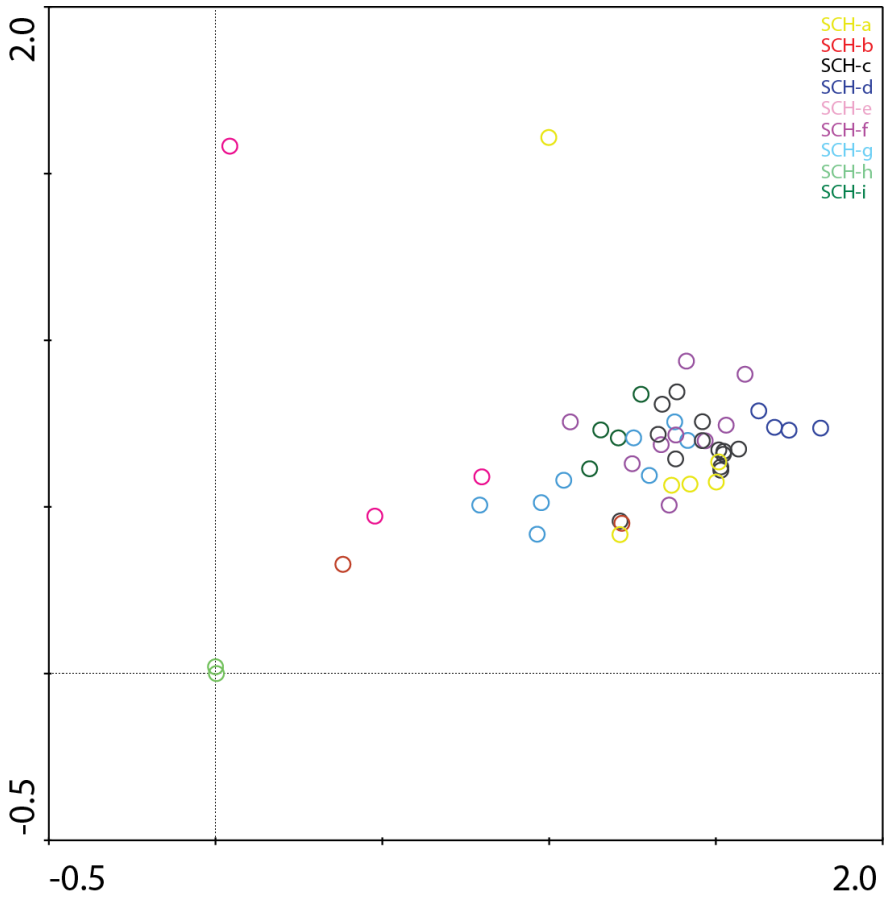

Figure 6.73 SCH10 DCA axis one (x) and two (y) sample distributions, samples coloured by zones allocated during CONISS analysis (see Figure 6.69)

6.6.1.2 Statistical treatment of SCH10 macrofossil data: nMDS

The nMDS model for the SCH10 macrofossil assemblage had a stress of 0.11, which allows for the careful interpretation of model results (Figure 6.74). The species distributions along the first nMDS axis are similar to the results of the DCA axis one ordination (Figure 6.74B): *Vaccinium*, ericaceous and monocot. species are located towards the negative end of axis one, whilst *Eriophorum* and *Dicranum* species are located towards the positive end. The similar species distributions are reflected in the comparison of the nMDS and DCA reconstructions using the first axes sample scores ($r = 0.97$, $p < 0.001$; Figure 6.74D). The absolute values of the sample scores differ between reconstructions but the direction of change is the same throughout, and interpretations of environmental conditions would therefore be the same.

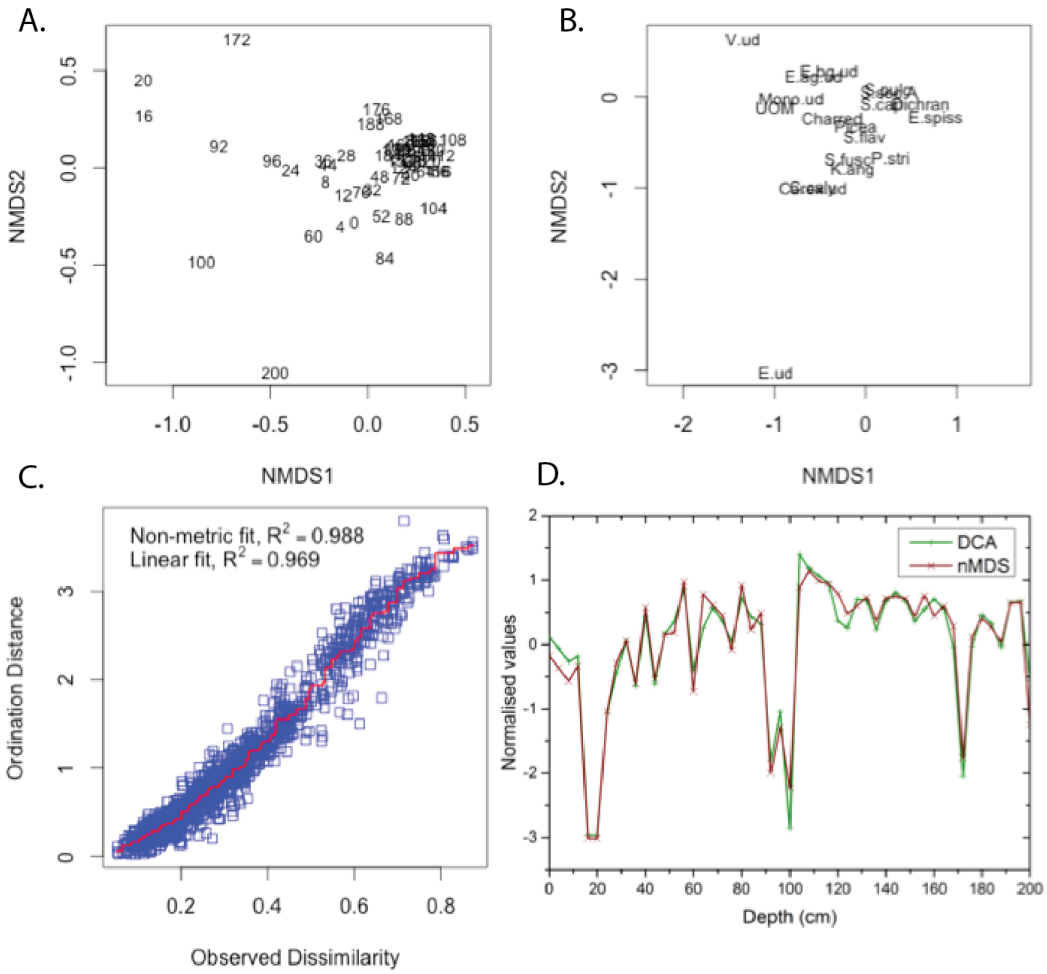

Figure 6.74 SCH10 plant macrofossil nMDS results.
A: nMDS axis one and two sample scores; B: nMDS axis one and two species scores. C: formation of nMDS model and assocaited stress; D: normalised comparison of the DCA and NMDS axis one scores (more negative scores indicate drier conditions).

6.6.1.3 Statistical treatment of SCH10 macrofossil data: DHI

The distribution of the species along the first axis of the DCA and nMDS models indicate that transformation methods based on weighted averaging techniques used to reconstruct hydrological changes must be interpreted with caution, owing to the insensitivity of the SCH10 macrofossil record to water table depth and the disturbance event. The DHI only considers hydrological changes; therefore, whilst it may provide further insight into differences in water table height over time, it cannot account for any non-hydrological changes, such as the fire in SCH10-e. During, and potentially after this period, the macrofossil hydrological reconstructions may be unreliable and proxy reconstructions will be required to determine environmental change.

There is no statistical difference between the three updated indexes (full, -UOM and –roots) as determined by one-way ANOVA on ranks ($F(2, 150)$ $H = 0.594$, $p=0.743$; Figure 6.75). The updated DHI is more similar to DHI excluding roots (0.976, $p < 0.001$) than DHI excluding UOM (0.948, $p < 0.001$). The trends in the updated indices are coherent with the exception of the sample at 100 cm: the index excluding UOM decreases whilst the full index and the index excluding roots increases. The UOM in this sample is unlikely to be related to climatic driven changes in the vegetation assemblage, rather it was likely driven by the fire.

The index excluding UOM does not deviate from the updated index in zone SCH10-b, suggesting that this period of reduced *Sphagnum* was a true drying event that has not been driven by fire disturbance. There is a difference in the magnitude of the full updated and the index without UOM reconstructions in the low-*Sphagnum* zone SCH10-h. This could be indicative of a disturbance; however, the trends remain similar, as indicated by the Pearson product-moment correlation coefficient of the samples in the SCH10-h zone (full index and –UOM index; 0.99). Therefore, since both indices remain strongly correlated, disturbance at this point of the record is unlikely.

The statistical similarities in the three updated DHI indices facilitate comparisons of the full updated index with the existing index derived by Daley and Barber (2012). The medians of Daley and Barber derived index and the updated index are statistically different ($U = 141$, $T = 1467$, $P < 0.001$) and there is no significant relationship between the two reconstructions ($r =$

0.272, p = 0.053). A comparison of DHI reconstructions and the pattern of changes in vegetation assemblage reveals that the three zones of reduced *Sphagnum* are more clearly represented in the Daley and Barber derived index than the full updated index. Whilst the full updated index appears to be more complacent to dry periods than the Daley and Barber derived index, the former index does appear to be more sensitive to changes towards wetter conditions. The complacency of the full updated index to dry shifts may be a result of the surface sampling strategy: the surface samples were collected across a microtopographical gradient in two currently wet peatlands, with large pool complexes. Therefore, the drier end of the species tolerances may not be fully reflected in the current state of the updated index.

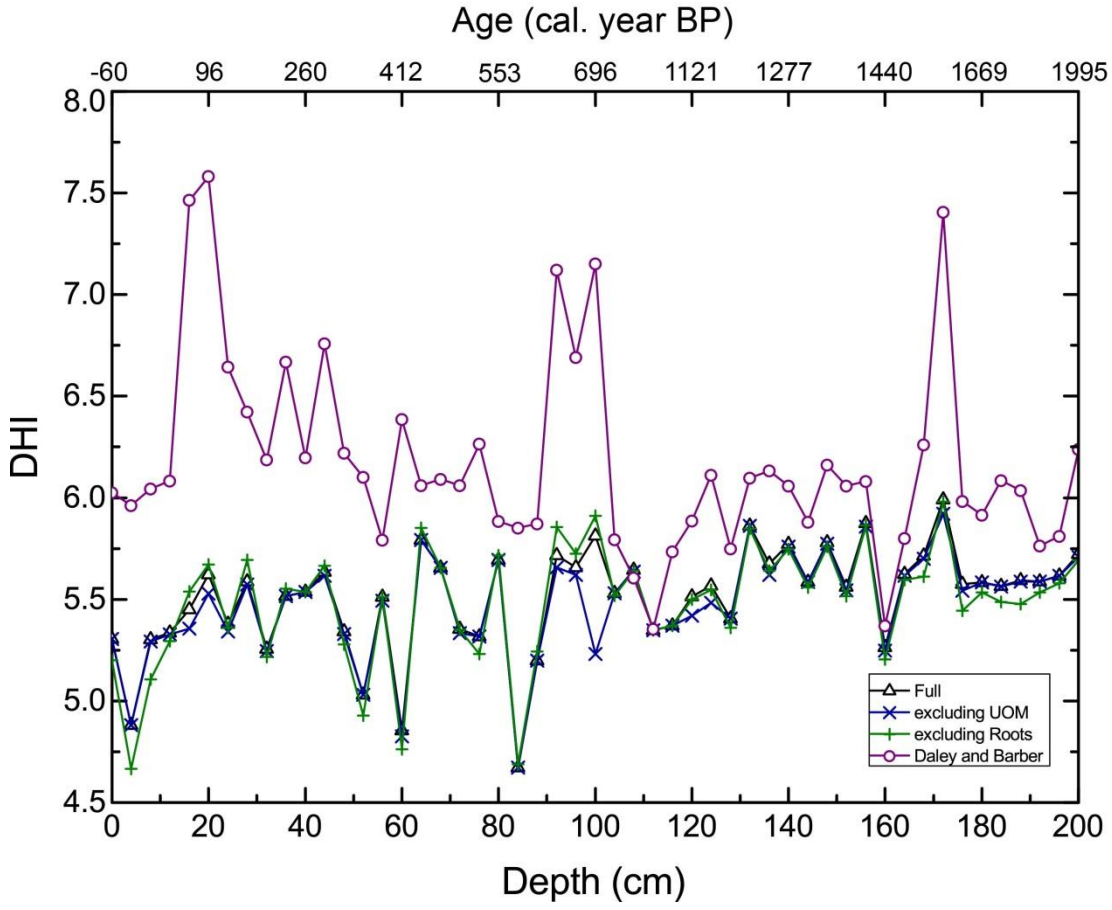

Figure 6.75 SCH10 plant macrofossil data transformed using DHI. Lower y-axis values indicate wetter conditions.

Whilst it has been established that the DCA axis one has a dampened response owing to the short hummock-hollow gradient, a comparison of normalised data from DCA axis one, the Daley and Baber derived index and the full updated index (Figure 6.75) reveals that the Daley and Barber index is more similar to the trends identified in the DCA axis one scores ($r = 0.935$, $P < 0.001$) than the updated DHI ($r = 0.146$, $p = 0.307$). Since a clear vegetation response to hydrological changes was not detected within the first axis of the DCA or the nMDS, the degree of similarity within the DHI, DCA and nMDS is surprising.

The updated DHI was created as initial priming work to assess the effectiveness of a more regionally specific index; therefore, it is still in developmental stages. Comparisons between the updated index and the Daley and Barber (2012) index within all study sites reveal that the North American regionally specific updated index does show potential to enhance hydrological characterisations. However, the current form of the index is limited by the small field measurement sample size and associated weak characterisation of some North American specific peatland species (such as *S. flavicomens*). Within this study, comparisons between the updated index and the index omitting UOM have revealed useful information about the peatland record by identifying possible disturbance events and periods of non-hydrologically driven occurrences of this quasi-species. It is therefore recommended that all future studies transforming plant macrofossil data by DHI should also adopt this approach within the data screening process. The reconstructions obtained from the updated index and the index omitting roots are remarkably similar at all sites within this study; therefore, the inclusions of these below-ground components are not a primary cause for concern when interpreting DHI results.

Hydrological interpretations of the proxy reconstructions must not be made between 104 and 88 cm owing to fire disturbance. The three environmental reconstructions (Figure 6.75) indicate that The WTD may have been high between 2000-1500 cal yr BP then experienced a subtle increase towards *ca*. 1000 cal yr BP years whilst containing conditions dry enough to encourage burning. A fluctuating drying trend to lower WTD may have occurred after the fire *ca*. 550 to 150 cal yr BP, culminating in the lowest WTD of the last 2000 years around 100 cal yr BP.

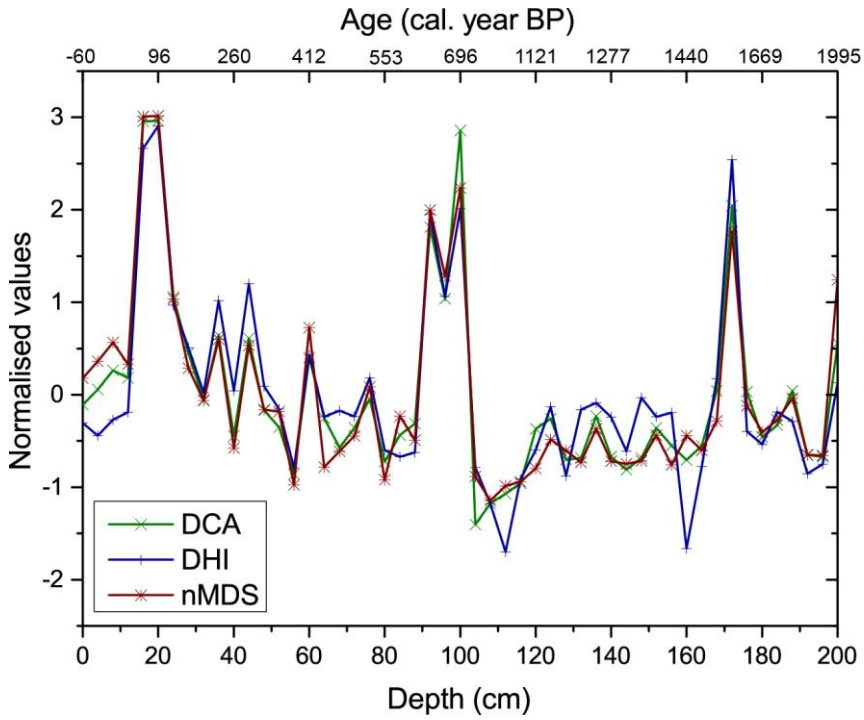

Figure 6.76 SCH10 plant macrofossil DCA axis one scores and DHI normalised. Lower y-axis values indicate wetter conditions. Species with wetter preferences were more positively located along the first axes of theca and nMDS than those with drier preferences. This direction of species distributions along the first axes is opposite to all other sites within this study. The DCA and nMDS y-axes scores have been reversed from the original plots (with lower values indicating now indicating wetter rather than drier conditions) to match those of the other study sites complement the direction of change within the DHI y-axis.

6.6.1 Testate amoebae

Testate amoebae data have been visually separated into eight zones of similar assemblages (Figure 6.77; Table 6.13). Three species dominate the SCH10 testate amoebae assemblage: *H. subflava, D. pulex and A. discoides.* Whilst the largest single species abundance peak is attributed to *D. pulex* (*ca.* 80%), *H. subflava* is the most abundant across the entire record: the average abundance of *H. subflava* is 34% compared with 20% for *D. pulex*. Additionally, the abundance of *D. pulex* varies more than *H. subflava* with respective standard deviations of 20.3 and 17.9.

Despite the uncertainties surrounding the distribution of *H. subflava* and *D. pulex* (Section 3.5.4.1), their presence indicates dry conditions. *A. discoides* is commonly found in wetter conditions (Tolonen, 1986; Turner *et al.*, 2013); however, it can also be found alongside relatively dry taxa (Charman *et al.,*

2007; Booth, 2008) and requires relatively lower moisture content than would be expected based on water table depth preferences (Charman *et al.,* 2007). This co-existence of wetter and drier species may be indicative of fluctuating conditions, either seasonally or interannually. Alternatively, dry species have less specific WTD tolerances than wet species (Charman *et al.,* 2007); therefore, the peatland could be towards the wet range of the dry species. Since the dominant SCH10 taxa typically have a preference for dry conditions this indicates that the peatland is likely to have been dry throughout, with fluctuating conditions.

Four other species also consistently contribute to the testate amoebae assemblage throughout the record: *A. muscorum*, *N. flabellum, N. militaris* and *Trigonopyxis arcula* type. These species are all generally associated with dry conditions: *T. arcula* is a reliable indicator of drier conditions (Charman *et al*., 2000; Charman *et al*., 2007; Lamarre *et al*., 2013); *N. militaris* is associated with dry conditions (Booth, 2008); *A. muscorum* have a wide water table depth tolerance; and *N. flabellum* is commonly dry, but to a lesser extent than the aforementioned species. The lack of reliable wet indicators, such as *Amphitrema wrightianum* or *Nebela marginata*, support the earlier conclusions from the dominant testate amoebae species and the plant macrofossils that SCH10 is a generally dry site. The assemblage diagram suggests a subtle overall drying trend across the 2 m peat record, owing to the elevated concentrations of *D. pulex* and decreasing *A. discoides* towards the surface. The distribution of Cladocera supports the suggestion of an overall drying trend, Cladocera require habitats of standing surface water and are present in the in the early peat zones whilst are absent from *ca.* 148 cm to the surface, with the exception of one sample (44 cm).

On initial inspection, the testate amoebae assemblage data show little resemblance to the trends evident in the macrofossil data. Therefore, the testate amoebae may be responding to a different environmental driver or contain a stronger response to hydrological change than the plant macrofossils. During the fire event (*ca.* 102-90 cm), there is a peak in *D. pulex* which then decreases as *A. flavum* increases and *H. papilio* returns. Therefore, shifts in testate amoebae taxa (primarily indicated by *D. pulex*) could represent a short-lived response to disturbance, either in combination with, or in isolation of, climate. The variability in the four most dominant

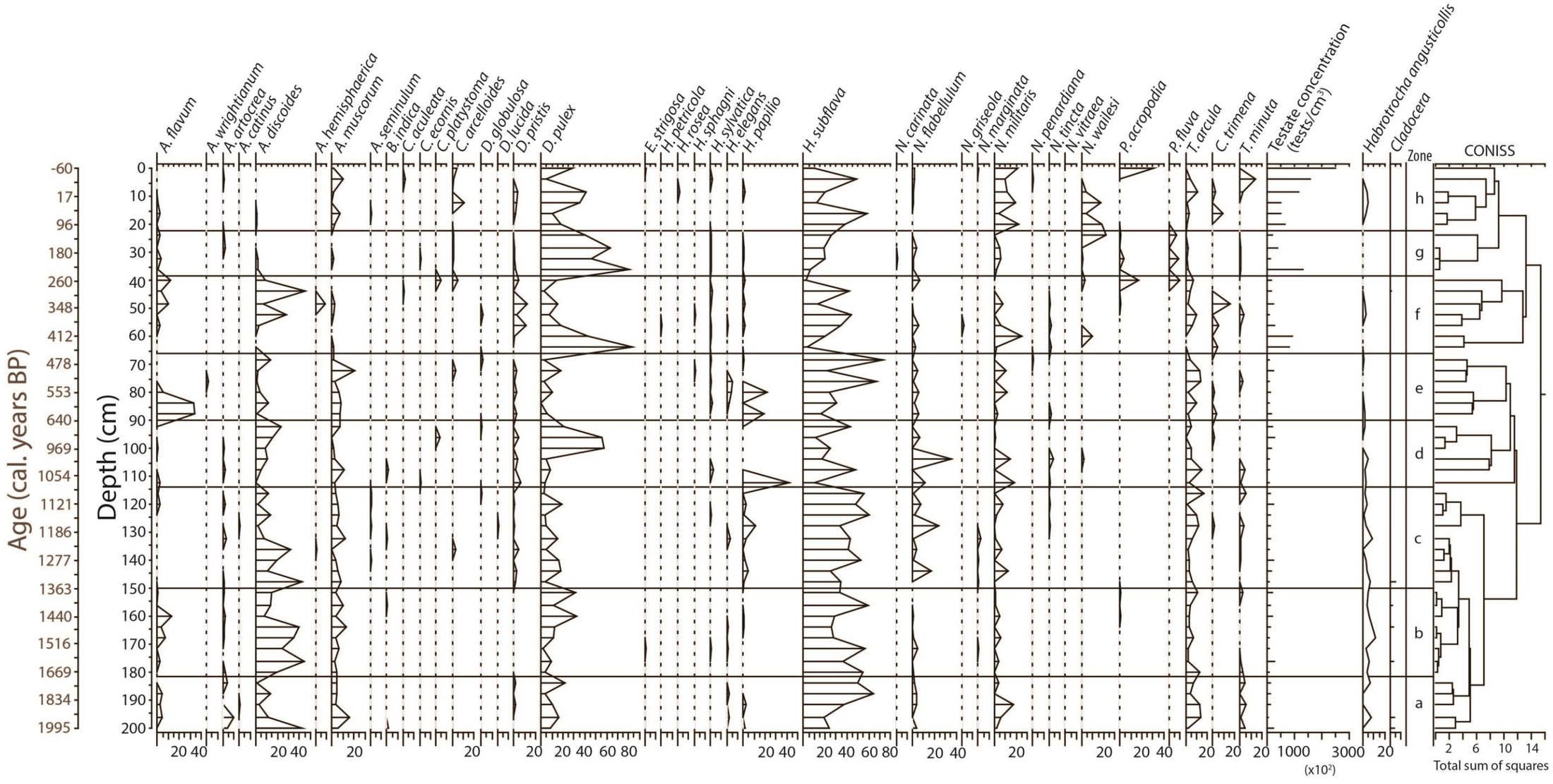

Figure 6.77 SCH10 testate amoebae assemblage diagram plotted against depth with a secondary age axis.

All data are percentages of the 100 tests identified at each level. Concentration data is displayed as depth bars, concentrations of tests per sample are represented by the bar graph and the frequencies of non-testate fauna are indicated bar graphs or, in the case of rotifers, a line graph. Zones have been allocated based on the results of the CONISS cluster analysis.

Table 6.13 SCH10 description of testate amoebae assemblage data

Zone	Depth (cm)	Faunal assemblage description	Age (cal yr BP)
SCH10-h	0 - 22	**More species contribute to the assemblage during this zone.** *N militaris* is present *ca.* 20% throughout and *N. wailesi* is also present *ca.* 20% but is absent by 4cm. There is a double peak feature in *A. muscorum* and *H. subflava* at 16 and 4 cm with a *D. pulex* increase in between.	-60 - 113
SCH10-g	22 - 38	***H. subflava* gradually increase throughout the zone from <5% to *ca.* 30%.** *D. pulex* begins the zone *ca.* 15% but abruptly increases to *ca.* 80% at 36 cm before decreasing to *ca.* 30% at the end of the zone. *A. discoides, A. flavum and T. arcula* decrease to background concentrations by 36 cm.	113 - 245
SCH10-f	38 - 66	***D. pulex* gradually decreases from *ca.* 80% at 64 cm to *ca.* 20% at the end of the zone.** *N. militaris* also increases throughout the zone from 20%. The lower concentrations of *D. pulex* towards the end of the zone are replaced by *ca.* 20-40% of *A. discoides* and increasing *H. subflava ca.* 40%. *T. arcula* are present in the latter half of the zone <10%. Noticeable increase in *A. discoides* at 52cm and 44cm. New species present include *N. wailesi type, P. arcopodia and P. fulva*.	245 - 454
SCH10-e	66 - 90	**The zone beings with an increase of *A. flavum* from 0 – *ca.* 35% (maximum core abundance**). *D. pulex* decreases to 10-15% at the beginning of the zone. *H. elegans* is present at its maximum core abundance around 76 cm but is still <10%. *H. papilio* is present *ca.* 20% at the beginning of the zone but decreases to *ca.* 0% for the reminder of the zone. Only occurrence of *A. wrightianum* (less at <5%) at 75cm.	454 - 640
SCH10-d	90 - 114	***H. papilio* abruptly increases to *ca.* 40% at 112 cm followed by an abrupt increase *in N. flabellum* at 104 cm to *ca.* 35% then both are absent for the remainder of the zone.** *A. discoides* steadily increases from 0% to *ca.* 20% at 92 cm. Whilst present in low concentrations at the start of the zones, *D. Pulex* abruptly increase to *ca.* 60%, at 100 cm before decreasing at the end of the zone. *H. subflava* fluctuates around 30%. *N. militaris* and *T. arcula* decrease in latter half of zone. The only core occurrence of *C. platystoma* is at 98 cm; however, it is <5%.	640-1082
SCH10-c	114 - 150	***H. subflava* dominates with step-wise increases in abundance at 136 cm and 124 cm.** Similarly, *H. papilio* and *N. flabellum* increase at *ca.* 144cm, and 126 cm. *T. arcula* is more prominent in the latter half of zone *ca.* 20%. *D. pulex* and *A discoides* experience stepwise reductions to 5% and 10% respectively at the end of the zone.	1082 - 1363
SCH10-b	150 - 182	***A. discoides* returns to *ca.* 40% between 176 cm – 164 cm and concentrations of *H. subflava* decrease to *ca.* 30% at 164 cm, although increase throughout the remainder of the zone to 40%.** *A discoides* decreases to 160 cm whilst *A. flabellum* (15%) and *A. muscorum* (*ca.* 10%) increase. *H. subflava* is generally in antiphase with *A. discoides. D. pulex* increases throughout the zone reaching *ca.* 30% by 152 cm.	1363 - 1802
SCH10-a	182 - 200	***A. discoides* initially dominates (*ca.* 45%), accompanied by *A. muscorum, D. pulex* and *H. subflava. A. discoides* instantly decreases (to *ca.* 10%) until 184** cm, replaced by higher concentrations of *H. subflava* (*ca.* 55%) and smaller portions *of D. pulex, N. militaris. T. arcula* is present, generally following the trends of *D. pulex*.	1702 - 1995

species decreases around 120 cm, before *D. pulex* and *H. subflava* increase at 112 cm (Figure 6.78). *H. subflava* contains increased variation to *ca*. 64 cm, whilst *D. pulex* is less consistent indicating pronounced variation around 92 cm and again 68 - 64 cm. Variability increases in *T. arcula* after 120 cm and *A. discoides* decreases after 50 cm, coinciding with a decrease in total abundance (Figure 6.79).

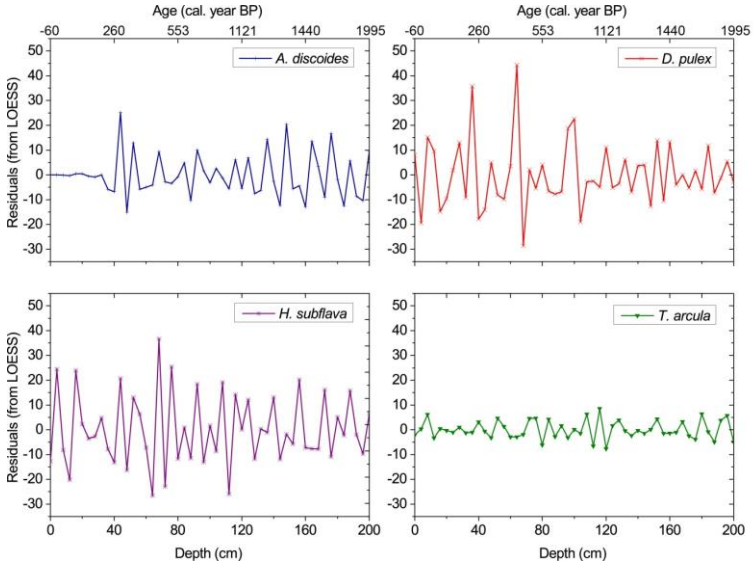

Figure 6.78 SCH10 variability of the four most dominant testate amoebae species plotted against depth, with a secondary age axis. The variability is reported using the residuals from LOESS smoothing: sampling proportion = 0.12 (equivalent to n=6) and 1 polynomial degree applied. The y-axes (residuals) scales are consistent between components for comparative purposes.

On average, ten species were present in each sample (SD: 2.44; Figure 6.79A). From *ca.* 180 cm the number of species present generally increased to 128 cm before decreasing to 92 cm when six species were present. This is the point of lowest species richness in the record and, after temporarily increasing to 76 cm, this decrease is repeated at 60 cm. The number of species present in each sample becomes more variable towards the peat surface.

The average concentrations of testate amoebae are 30165 tests cm^{-3} (SD: 45466; Figure 6.79). Concentrations are stable from 200 cm to 64 cm, at which point they more than double (Figure 6.79B). Whilst the increase is not sustained; it does commence a significant increasing trend towards the peat

surface (r = -0.550, p <0.0001), which may be related to increased preservation in the more freshly accumulating peat. An abrupt increase in concentration occurs at 36 cm and coincides with a dominance of *D pulex*. This species was also present at the aforementioned 64 – 60 cm increase in concentration and both these peaks coincide with a reduction in species richness.

The SDI average for SCH10 was 1.61 (SD: 0.24), with the highest value of 2.41 at 40 cm and the lowest value of 0.72 at 64 cm (Figure 6.79). The macrofossils revealed the disturbance of a fire in zone SCH10-d, which contains a zonal SDI average of 1.56. Whilst this is less than the SDI average for the entire record, similarly low SDIs also occur in SCH10-b and SCH10-g, indicating that the balance of the testate amoebae population has not been markedly altered by the fire.

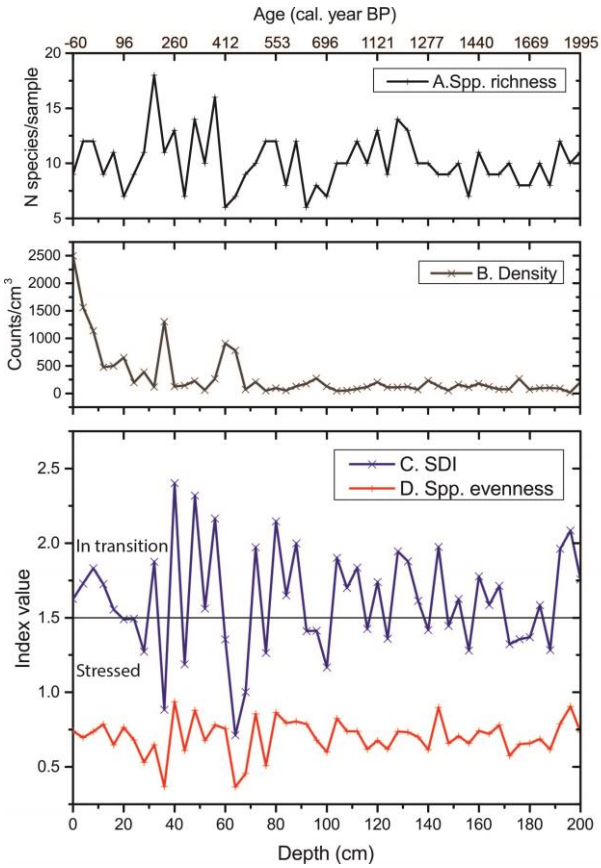

Figure 6.79 SCH10 testate amoebae ecological measures.
A: Species richness (number of species per sample); B: Concentrations of individuals (counts per cm^3 of peat; determined used L*ycopodiu*m counts); C: Shannon Diversity index (calculated using the number of species per sample and the total number of species in the core; insert equation); D: Species evenness (indicates the relative abundance of species, calculated using the SDI and the natural log of species with zero = no evenness and 1 = evenness).

6.6.1.1 Statistical treatment of SCH10 testate amoebae data: DCA

The DCA axis one gradient length was 2.33, indicating that a unimodal response model is appropriate for the ordination of the testate amoebae within this core, and an eigenvalue of 0.381. The relative position of the dominant species along axis one suggests that, if WTD is controlling the testate amoebae assemblage, the positive end of the axis is wetter and the negative end is drier: *A. discoides* is more positive than *D. pulex* and *H. subflava*. This wet-dry distribution is supported by the position of *N. militaris*, which is present throughout the record, and is ordinated more negatively, towards the dry end (Figure 6.80). However, taxa with both wet and dry tolerances are interspersed along axis one which may suggest that WTD is not the sole dominant driver of assemblage change. For example, the key wet indicators *D. globulosa* and *A. wrightianum* are located at the positive end, accompanied by the dry indicating *B. indica*, *T. arcula, A. muscorum* and *A. seminulum*. With the exception of *T. arcula* and *A. muscorum*, these species are rarely present in the assemblage; therefore, the DCA may have struggled to characterise their environmental preferences. Since the ordinations of the dominant taxa are indicative of a water table gradient, it is therefore appropriate to use the DCA sample score to suggest likely large scale changes in WTD.

To identify periods of the record with similar assemblages, sample scores were plotted against the first and second DCA axes (Figure 6.81). Zones SCH10-h and g, located close to the surface of the core, are generally located to the left of axis one and zones SCH10-a and –b, located in the deepest sections of the record, are located towards the right of the axis one. The remainder of the zones are poorly clustered. There is no clear grouping in the testate data amoebae that can be attributed to the fire event, unlike the plant macrofossils.

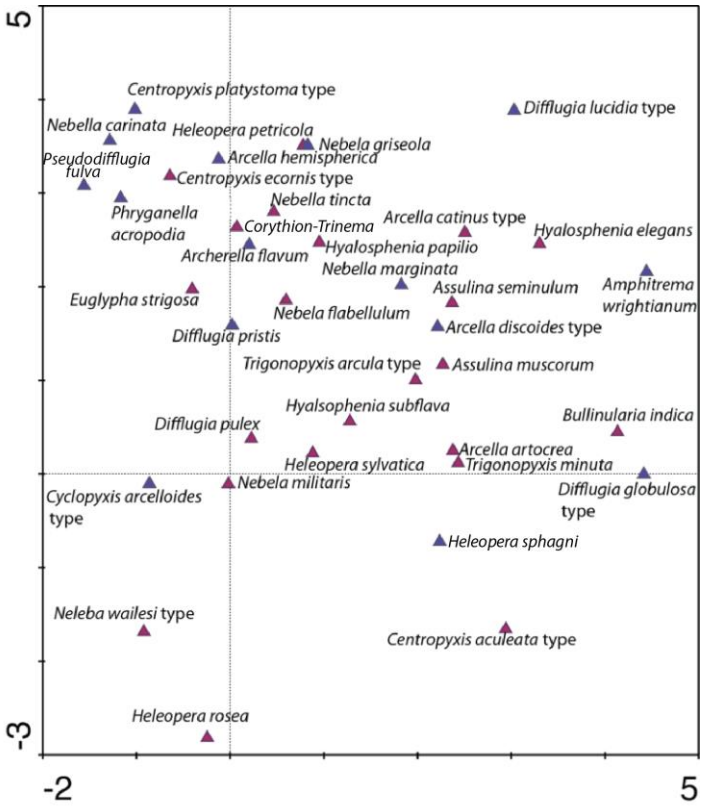

Figure 6.80 SCH10 testate amoebae DCA axis one (x-axis) and two (y-axis) scores.
Red and blue colours indicate dry and wet preferences respectively based on the training sets of Amesbury *et al.* (2013) and Lamarre *et al.* (2013).

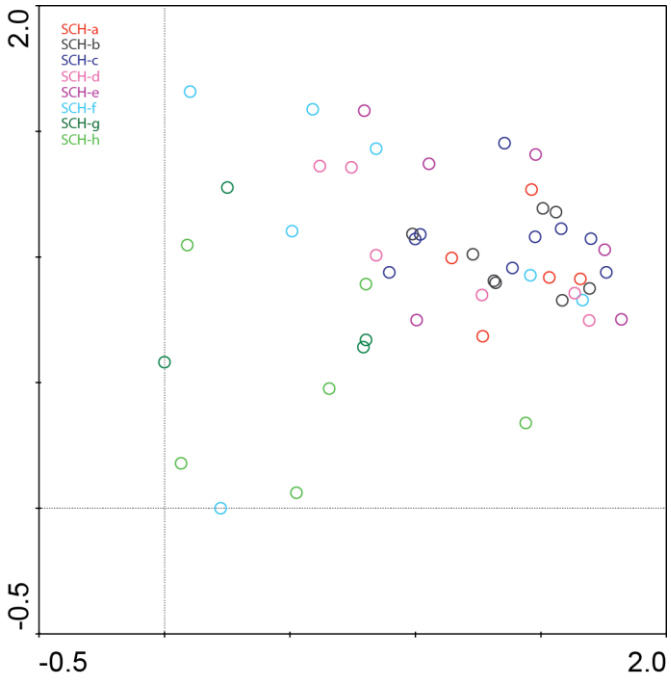

Figure 6.81 SCH10 testate amoebae DCA axis one (x-axis) and axis two (y-axis) sample scores. Samples are coloured by zones corresponding allocated from the CONISS cluster analysis (see Figure 6.77).

6.6.1.2 Statistical treatment of SCH10 testate amoebae data: nMDS

The nMDS model obtained from the VDB12 testate amoebae assemblage data had a stress of 0.16, indicating that interpretation of the first and second nMDS axes is possible (Figure 6.82). The species distribution across the primary nMDS axis is similar to the results obtained from the first DCA axis one: *D. lucidia, D. globulosa* and *A. wrightianum* are located towards the positive end of the axis whilst *P. acropodia, N. wailesi and C. platystoma* are located towards the negative end of the axis (Figure 6.82). Therefore, whilst wetter and drier preferring species are interspersed along axis one, it appears that the positive end of axis one represents wetter conditions than the negative end of the axis. The broad similarity between the first axes of the DCA and the nMDS suggests that the same underlying environmental variable and associated response from the testate amoebae have been detected. The down-core reconstructions using the nMDS and DCA axis one scores are similar ($r = 0.96$, $p < 0.001$) and, although the direction of change deviated ast some points (e.g. 180 – 162 cm and 128 cm), the main environmental interpretations of both results would be the same (Figure 6.82).

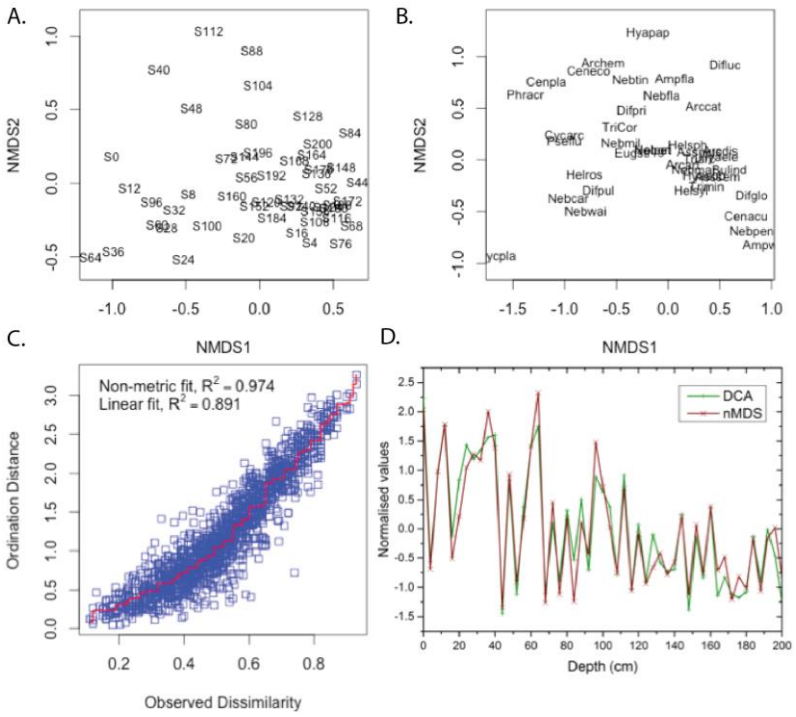

Figure 6.82 SCH10 testate amoebae nMDS results.
A: nMDS axis one and two sample scores; B: nMDS axis one and two species scores; C: formation of nMDS model and assocaited stress; D: normalised comparison of the DCA and NMDS axis one scores (lower y-axis values indicate wetter conditions).

6.6.1.3 Statistical treatment of VDB12 testate amoebae data: transfer functions

Results from the DCA and nMDS indicate that the testate amoebae are responding to WTD, supporting the use of transfer functions to transpose the data. There is significant difference between the medians of the two SCH10 reconstructions obtained using the ATLANTIC.NA WA.inv.tol and WA.inv models (U = 826, T = 2152, p = 0.002); however, they do contain a significant positive relationship (r = 0.823, p <0.001), representing the similar trends (Figure 6.83). The average sample prediction error associated with the WA.inv model reconstruction is 4.8% greater than the WA.inv model.

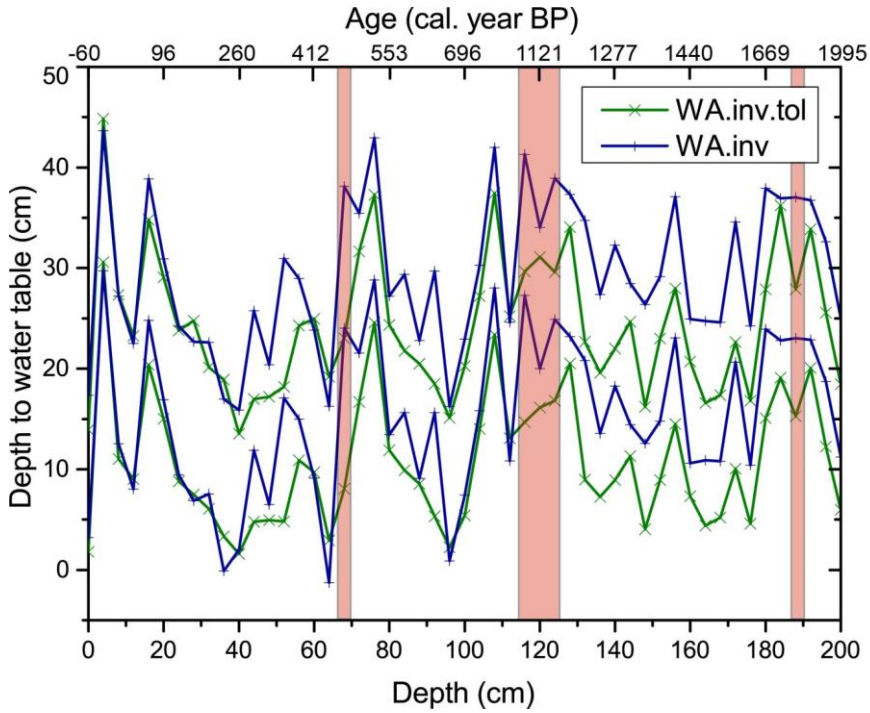

Figure 6.83 Upper and lower estimates of SCH10 water table depth obtained from the ATLANTIC.NA WA.inv.tol and WA.inv models from Amesbury *et al.* (2012). Red bands indicate divergences in the direction of change between the two models.

The model ATLANTIC.NA WA.inv.tol and WA.inv reconstructions are remarkably similar both in terms of the direction of change and the absolute values between 40 cm and the surface. The reconstruction range of both models overlap in all samples, although at several points, such as 52 cm, this overlap is small. Generally, the WA.inv.tol model reconstructs wetter conditions than the WA.inv model, as perhaps expected owing the narrower

tolerances of the wetter species. However, the WA.inv model reconstructs wetter conditions than the WA.inv.tol model at several depths towards the latter half of the record. Examples of such depths are 64 cm and 36 cm, both of which are dominated by *D. pulex*.

Whilst the direction of change is generally similar in both model reconstructions, they do diverge at three main points in the record (highlighted in red). The abundance of *H. subflava* increases between 192 – 188 cm and 72 - 68 cm; therefore, the differences in trends between the WA.inv.tol and WA.inv models may be attributed to the dominance of the dry species with a large WTD tolerance. The reconstruction difference at 68 cm is further exacerbated by the presence of *D. globulosa*, the wettest species with a very small tolerance, at 72 cm. At both divergences the differences are only present in one sample and are not sufficient enough adversely alter any environmental interpretations. However, a group of samples between 124 - 116 cm contain divergent trends: the WA.inv.tol model reveals a wetting trend whilst the WA.inv model indicates generally sustained drier conditions. This period is again dominated with *H. subflava*. In the context of the entire record, this difference would not have a pronounced effect on the interpretation; however, it may be useful to be aware of these differences.

The median values of QUEBEC WA.cla.tol and WA.cla reconstructions are significantly different ($U = 874$, $T = 2200$, $p=0.004$) whilst they contain a significant positive relationship ($r=0892$, $p <0.001$). The errors associated with the QUEBEC WA.cla model are 4.19% larger than those associated with to the QUEBEC WA.cla.tol model. The QUEBEC reconstructions are similar to the ATLANTIC.NA reconstructions in that the absolute values of both models are in the most agreement from *ca*. 40 cm to the surface peat, compared with the remainder of the record. There are two prominent deviations in the directions of the QUEBEC model; however, they would not result in differences within the main trends or environmental inferences (Figure 6.84). There are no clear trends within the variability of the ALTANTIC.NA and QUEBEC reconstructions, rather variability abruptly fluctuates between samples (Figure 6.85). A decrease in variability is centred *ca.* 90 cm, following and preceding temporary increases.

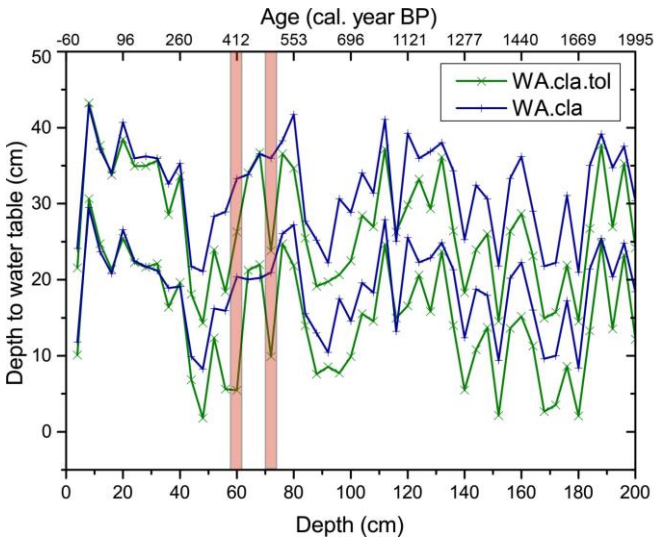

Figure 6.84 Upper and lower estimates of SCH10 water table depth obtained from the QUEBEC WA.cla.tol and WA.cla models from Lamarre *et al.* (2012). Red bands indicate divergences in the direction of change between the two models

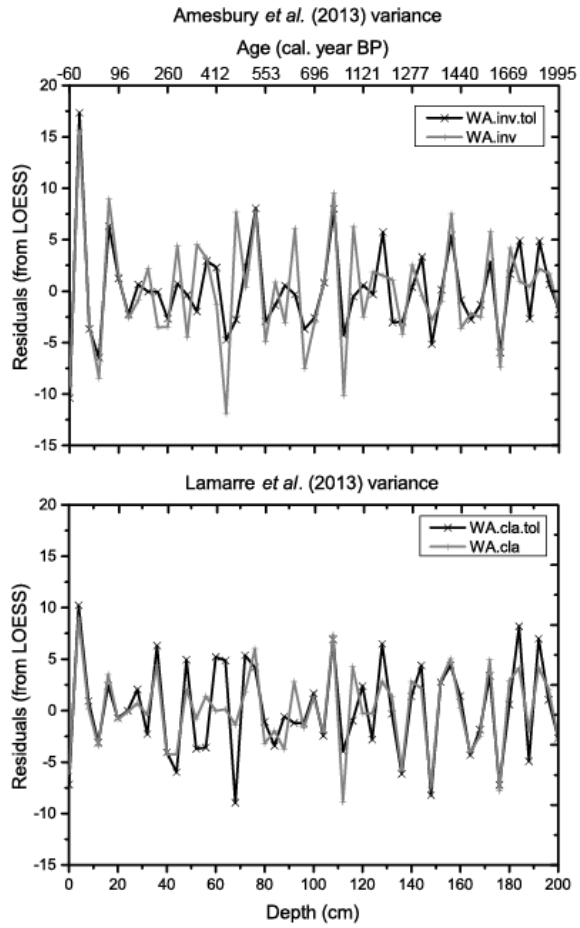

Figure 6.85 Variability of models using residuals from LOESS with a sampling proportion of 0.12 (equivalent to n=6) and 1 polynomial degree, before normalisation

6.6.1.4 SCH10 testate amoebae hydrological reconstructions

The population medians of the four transfer function reconstructions were shown to be statistically different using one way ANOVA on ranks (H=28.470, 3 DF, p = <0.01); however, there is no statistical difference between ATLANTIC.NA WA.inv model and the QUEBEC WA.cla and WA.cla.tol models. Of all model reconstruction, the most similar relationship exists between the QUEBEC WA.cla and WA.cla.tol (r=0.892, p <0.001). Generally, trends between transfer function reconstructions are consistent for the first half of the record until *ca.* 108 cm where they diverge more frequently and to a greater extent.

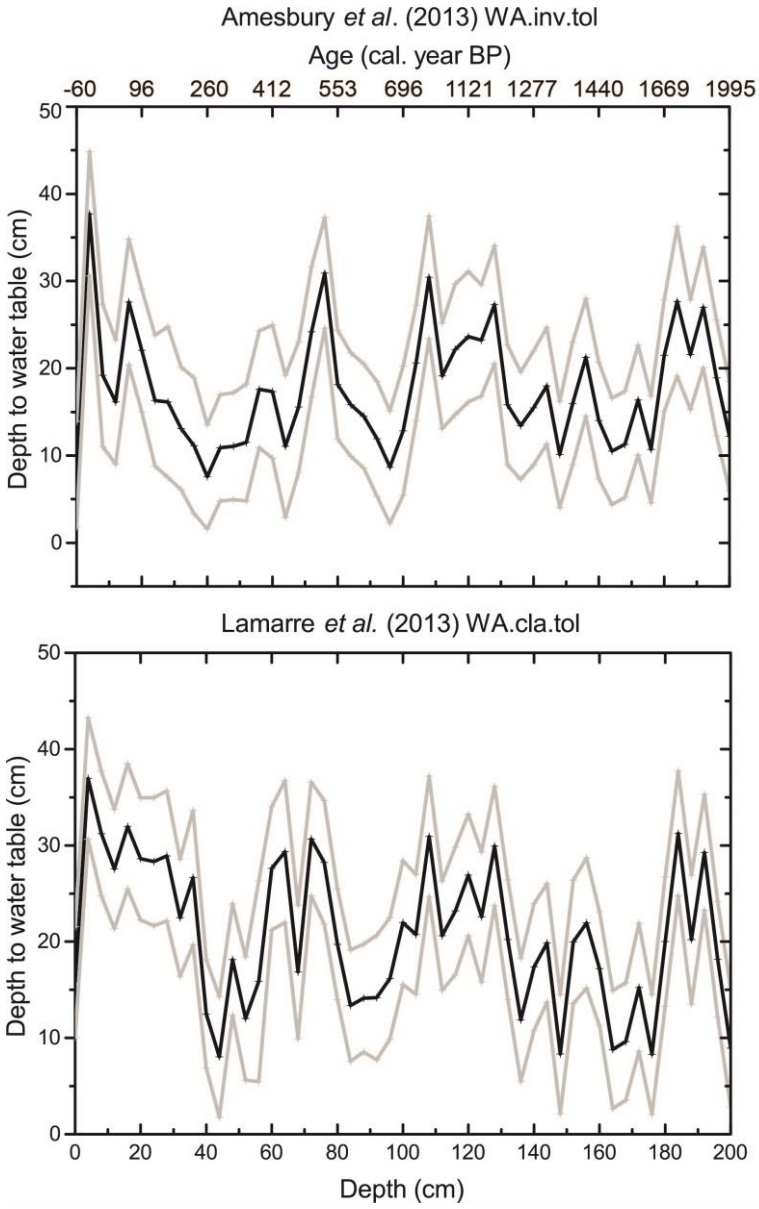

Figure 6.86 SCH10 testate amoebae transfer function reconstructions (black lines) with sample errors (grey lines)

The broad scale trends in the DCA and nMDS axis one scores and the transfer function reconstructions move in similar directions, with the noticeable exception of the period from 116 cm to 68 cm (Figure 6.67). The similarities support the conclusion made from the macrofossil record that, in the central section of the record, the ecological assemblages are driven mainly by the fire disturbance and are then influenced by the assemblage recovery from this event. Furthermore, the similarities between the weighted averaging techniques and the ordination and scaling methods in the early and later stages of the record indicate that the species response to the fire may be similar to a drought event. Environmental reconstructions can therefore be made before the fire. The DCA and nMDS axis one have more similarities with the transfer functions from 68 cm to the live peat. However, it is important to note that the fire will have altered the physical and chemical properties of the peat so it is unclear whether the peatland would respond to environmental factors in the same way as it would have done before the fire event.

The testate amoebae reconstructions indicate a drier period *ca*. 2000 – 1670 cal yr BP, which abruptly became wetter from *ca*. 1670 – 1500 cal yr BP before returning to a brief drier period around 1400 cal. yr BP. The wet conditions at 1300 cal yr BP gradually dry in a series of fluctuations to 1200 cal yr BP and the dry conditions persist until the fire event occurs. The water table post-fire could have increased in height *ca.* 400 – 260 cal yr BP before drying to the peat surface.

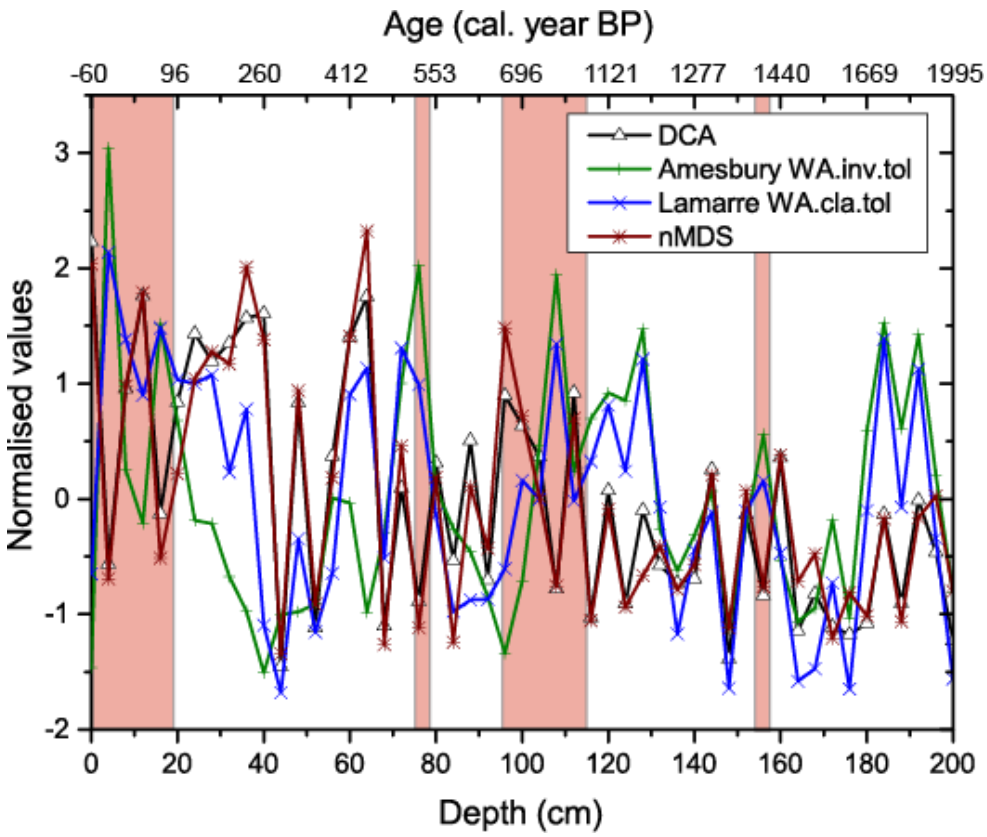

Figure 6.87 SCH10 testate amoebae normalised water table reconstructions obtained from DCA and transfer functions. Lower y-axis values indicate wetter conditions.

Full SCH10 paleoecology comparison

A comparison of the plant macrofossil and testate amoebae inferred hydrological changes are provided by the normalised values of the DHI index (macrofossils) and the normalised records from Amesbury *et al.* (2013) WA.inv.tol and Lamarre *et al.* (2013) WA.cla.tol (testate amoebae; Figure 6.88). The main period of the SCH10 record that is likely influenced by drivers other than hydrological change is *ca.* 1000 – 650 cal yr BP. This was identified as the fire event in the macrofossil record; therefore, no hydrological inferences can be made from the assemblage changes during this time aside from the conclusion that the peatland would have been dry to facilitate burning.

The plant macrofossils and testate amoebae reconstructions contain different trends until *ca.* 1650 cal yr BP. The differences between the records may be a result of a slower response time in the macrofossils compared with the testate amoebae. Therefore, whilst a WTD consensus between proxies is lacking in the early stages of the record, it is likely that the peatland was becoming

wetter. Both proxies indicate a drying trend from *ca.* 1400 – 1150 cal yr BP, which is registered earlier in the testate amoebae than the plant macrofossil record and in shorter lived in the latter reconstruction. The proxy reconstructions indicate a possible drying after the fire; however the colonisation and succession of the vegetation and associated effects on testate amoebae may be driven by factors such as increased nutrients and peat structure rather than revealing a true hydrological feature. A wetting trend may have occurred from *ca.* 500 – 300 cal yr BP before the water table lowered towards the present day peat surface.

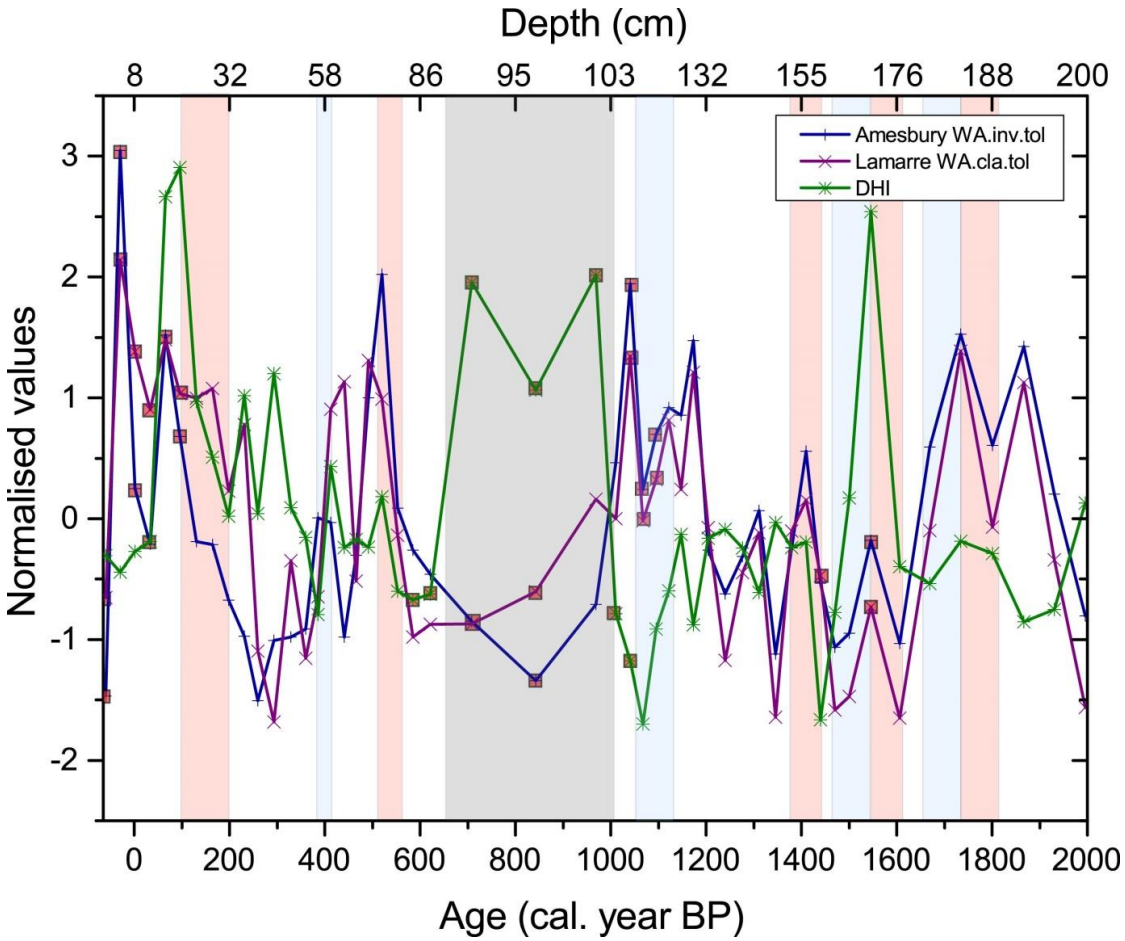

Figure 6.88 SCH10 normalised palaeo-ecohydrological reconstructions with fire indicated in grey box.
Coherent trends both proxies towards wetter conditions are indicated by blue bars and trends towards drier conditions are indicated by red bars. Red boxes around individual points indicate divergences between ordination and weighted averaging techniques. Lower y-axis values indicate wetter conditions.

Chapter 7: Carbon accumulation

This chapter presents the carbon (C) accumulation histories of each study site. These have been developed using the radiocarbon and cryptotephra age-depth models outlined in Chapter 5 in combination with bulk density and inferred carbon (C) content measurements presented in Section 7.2.1. The inferred C content was obtained at contiguous 1 cm resolution, assuming 50% of the organic matter is C based on results from Turunen *et al*. (2002) *sensu* Charman *et al*. (2013) and Loisel and Yu (2013; Section 3.4.3). The appropriateness of the 50% assumption within this regional and temporal setting has been confirmed through a comparative test using average values of measured C from proximal peatlands (Section 7.1). Carbon accumulation rates (CAR) are presented at the individual sample resolution and have also been averaged into 100-, 200- and 500- year intervals (bins) to identify longer-term CAR trends. Whilst only four 500-year segments can be calculated within these 2000-year records, this time period is often the focus of longer-term studies. Therefore, the results reported here will be useful to compare amoung other sites and regions.

The primary aim of the thesis is to characterise the relationship between environmental change and peatland C accumulation. To address this aim, the drivers behind the C accumulation histories presented here will be investigated in Chapter 8 using results from the vegetation assemblages and the reconstructed hydrological changes outlined in Chapter 6.

7.1 Testing the sensitivity of C histories to inferred C content

C content of peat has been calculated based on the assumption that 50% of the organic matter content is C (Section 3.4.3). However, the C content of organic matter does vary based on differences in vegetation composition and decomposition processes (Chambers *et al*., 2011). A recent proximal study reported measured average C content from three early - late Holocene peatland records in northern Newfoundland (BVB; 45.97%, SD = 9.17), central Nova Scotia (PTB; 48.76 %, SD = 1.92) and Maine (SDY; 48.96 %, SD = 8.3; Charman *et al.,* submitted). The reported C contents are all lower than the

assumed 50% in this study; however, the values are supressed by the lower early Holocene C content remaining after being exposed to decompositional processes for a greater length of time than subsequent peat deposits. Average C content of each site during the last 2000 years is closer to 50% ranging from 47.49% to 49.29% (Table 7.1).

To test the sensitivity of CAR to the values of assumed C content, the measured average late Holocene C content of the most proximal site reported in Charman *et al.* (submitted) have been applied to the study sites of this thesis (Table 7.1). Dependent t-tests reveal that there are no significant differences (at the 99.9% confidence interval) between the site-specific mean CAR when calculated using different C contents. Therefore, the overall trends and interpretations of CAR would not change. Whilst recalculating C histories with the Charman *et al.* (submitted) values does not account for vegetation-driven changes in C content of the peat over the last 2000 years, it demonstrates that the C history calculations are not highly sensitive to the C content used. Therefore, this provides the confidence that the major trends in the data can be identified assuming 50% of the organic matter content is C.

Table 7.1 Comparison of C accumulation rates and cumulative C when %C is altered. Updated values have been obtained using the published % C values from proximal sites (Charman *et al.*, submitted).

Ph.D. Site	Proximal site (% C 2000 years)	50% cumulative C (kg m^{-2})	Updated cumulative C (kg m^{-2})	50% μ CAR (g C m^{-2} yr^{-1})	Updated μ CAR (g C m^{-2} yr^{-1})
SCH10	SDY (49.28)	83.31	82.19	48.75	47.73
VDB12	SDY (49.28)	69.09	68.09	36.89	36.36
FBB12	PTB (48.76)	52.62	49.98	34.9	33.15
JRB12	BVB (45.97)	81	77.34	43.04	41.07

The sensitivity of the bulk density and inferred C content method was assessed using triplicate analyses from three discrete sample levels. Uncertainty associated with bulk density and inferred C content measurement may reflect the natural differences within the individual peat layers (e.g. slightly different proportions of decayed vegetation type) and may be generated whilst using the volumetric sampler and the balance. The standard deviation of the three measurements from the three sample layers ranged between 6 – 13 % of the bulk density and inferred C content mean which

generates an uncertainty in the order of magnitude of 0.001 g cm^{-3}. Error on this scale would not alter main interpretations of the data that are of interest to this study.

7.2 C accumulation histories

7.2.1 Bulk density and inferred C content

The bulk density and inferred C content varies between the four sites over the last 2000 years (Figure 7.1). FBB12 has the highest average bulk density (0.095 g cm^{-3}, SD 0.018) and the highest average inferred C content (0.047 g cm^{-3}, SD 0.009). JRB12 has the lowest average bulk density (0.077 g cm^{-3}, SD 0.03) and the lowest average inferred C content (0.037 g cm^{-3}, SD 0.009). VDB12 and SCH10 have intermediate average bulk densities of 0.08 g cm^{-3} (SD = 0.03) and 0.086 g cm^{-3} (SD 0.03) respectively with average inferred C contents of 0.038 g cm^{-3} (SD 0.009) and 0.043 g cm^{-3} (SD 0.013). An independent t-test reveals that the mean bulk densities of each site are significantly different at the 95% confidence interval. The mean inferred C content of SCH10 and FBB12 are also statistically different from all sites, whilst VDB12 and JRB12 are not statistically different at the 95% confidence interval.

Within the fluctuations of the bulk density measurements and inferred C content, general trends can be detected in the northern sites: JRB12 increases to *ca.* 1000 cal yr BP then decreases to the present day and FBB12 also initially increases, reaching sustained high values at *ca.* 1200 cal yr BP before decreasing from *ca.* 800 cal yr BP. The southern sites are more variable and initially differ from the northern sites: VDB12 decreases to *ca.* 1500 cal yr BP, increases to *ca.* 400 cal yr BP and then decreases to the present day. Trends within SCH10 are more complex with an increase to *ca.* 1600 cal yr BP, a decrease to lower values until *ca.* 1200 cal yr BP then an increase to 900 cal yr BP. SCH10 values generally decrease to *ca.* 250 cal yr BP and exhibit an abrupt dramatic increase before decreasing to the present day.

Similar trends in bulk density and inferred C content occur in JRB12, FBB12 and SCH10 *ca.* 1800 cal yr BP when values are reduced before a subsequent increase; however, this is not clearly demonstrated in the VDB12 record.

SCH10, VDB12 and FB12 contain elevated values centred *ca.* 900 cal yr BP. JRB12 values are elevated *ca*. 1050 cal yr BP; however, these are interrupted by a temporary decrease centred on *ca*. 900 cal yr BP.

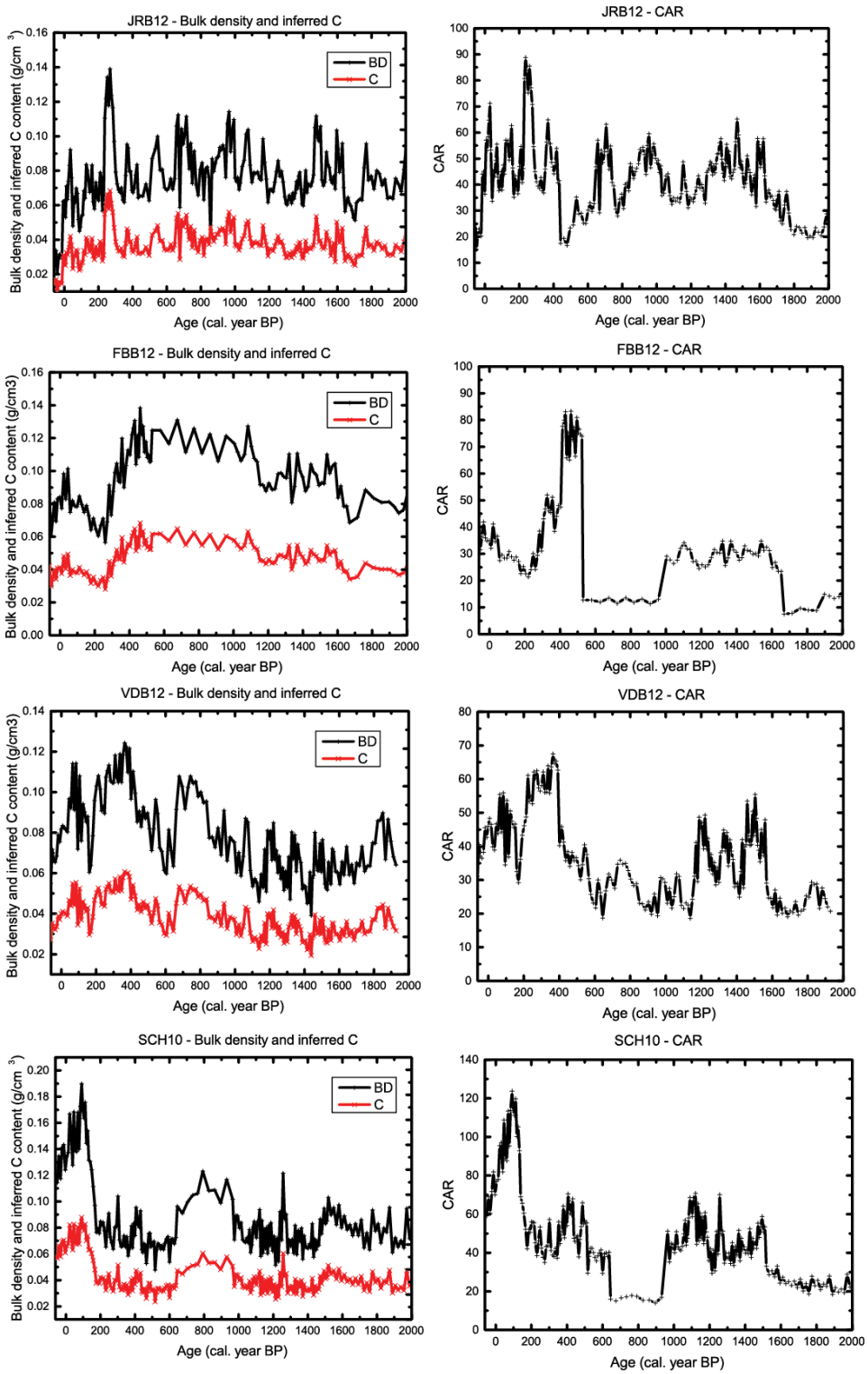

Figure 7.1 Bulk density, inferred C and CAR by site over the last 2000 years. Sites arranged from north (JRB12; top) to south (SCH10, bottom). Scales of the y-axes are optimised on a site-by-site basis; therefore, the y-axis scales differ between sites.

7.2.2 CAR

Over the last 2000 years, the average CAR is highest at SCH10 (48.75 ± 3.06 g C m^{-2} yr^{-1}; 95% confidence interval), followed by JRB12 (43.04 ± 1.71 g C m^{-2} yr^{-1}; 95% confidence interval) and VDB12 (36.89 ± 1.77 g C m^{-2} yr^{-1}; 95% confidence interval (Figure 7.2). FBB12 has the lowest average CAR (34.90 ± 3.47 g C m^{-2} yr^{-1}; 95% confidence interval). An independent t-test reveals that there is no significant difference between the mean CAR of VDB12 and FBB12 at the 95% confidence interval; however, the mean CAR of SCH10 and JRB12 are statistically different from all sites.

CAR varied over the last 2000 years (Figure 7.2). All sites reveal a period of elevated CAR *ca*. 1600 cal yr BP. This begins earlier, is less pronounced and less sustained at JRB12 than the other sites, which register higher CARs until *ca.* 1250 years BP in VDB12 and *ca.* 1050 cal yr BP in SCH10 and VDB12. During this period SCH10 and VDB12 reveal two further periods of CAR increase: the first is evident at VDB12 (centred *ca*. 1400 cal yr BP) then at SCH10 (centred *ca*. 1350 cal yr BP) and the second respectively occurs between *ca.* 1300 and 1250 cal yr BP.

The elevated CAR ends *ca*. 1400 cal yr BP at JRB12, *ca.* 1200 cal yr BP at VDB12, *ca.* 1100 cal yr BP at FBB12 and *ca.* 1050 cal yr BP at SCH10. Around 1150 cal yr BP, CAR are roughly halved at FBB12 (until *ca.* 650 cal yr BP) and at SCH10 (until *ca.* 750 cal yr BP). During this period VDB12 and JRB12 CAR exhibit generally opposing trends: VDB12 initially decreases with fluctuations at reduced rates until *ca.* 750 cal yr BP but temporarily increases to *ca.* 850 cal yr BP. Conversely, JRB12 contains a temporary increase before decreasing to *ca.* 1000 cal yr BP, then abruptly, temporarily increases *ca.* 850 cal yr BP.

The lowest CAR of SCH10, VDB12 and FBB12 occurs in the middle section of the 2000-year record *ca.* 1000 cal yr BP. However, minimum JRB12 CAR occurs *ca.* 550 cal yr BP. SCH10 fluctuates at slightly elevated levels from *ca.* 600 cal yr BP until *ca.* 200 cal yr BP, when it roughly doubles before decreasing to the surface. VDB12 increases to *ca.* 450 cal yr BP then decreases to the surface and FBB12 CAR is elevated until *ca.* 450 cal yr BP, decreases to *ca.* 250 cal yr BP then increases and fluctuates to the surface. JRB12 has a two-phase increase centred on *ca*. 450 cal yr BP and *ca.* 300 cal yr BP before decreasing to the surface.

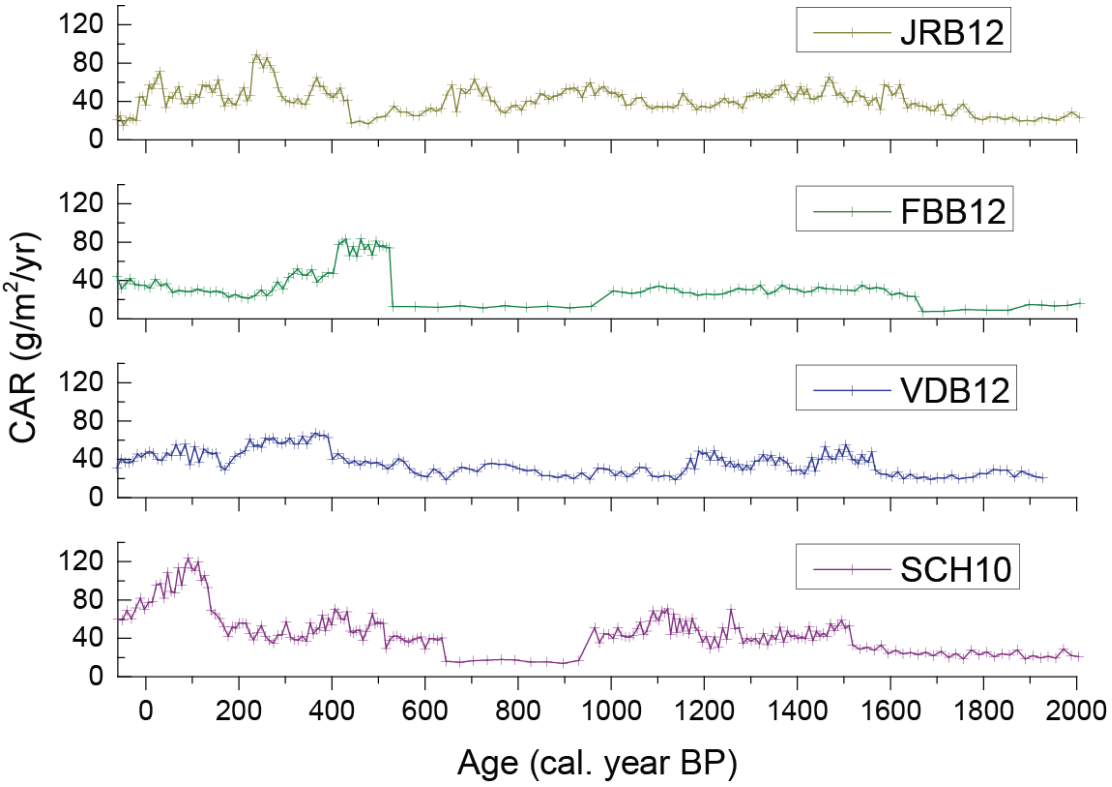

Figure 7.2 Carbon accumulation rates by site (arranged from north (JRB12; top) to south (SCH10; bottom) over last 2000 years.

7.2.3 Cumulative C

Cumulative C is the sum of the total C that has accumulated over a specific time period of interest. Cumulative C has been calculated for each site within this study over the last 2000 years based on inferred C content obtained at contiguous 1 cm intervals. The error has been estimated using the maximum sample specific error identified from three triplicate sample test (12.7% of inferred C). Cumulative C was greatest at SCH10 (83.31 ± 10.6 kg m^{-2}) and similar at JRB12 (81.10 ± 10.3 kg m^{-2}), whilst lower at VDB12 (69.09 ± 8.81 kg m^{-2}) and FBB12 (52.62 ± 6.73 kg m^{-2}; Figure 7.3). The C addition is consistent throughout the last 2000 years at VDB12 and JRB12, with a subtle slowdown in JRB12 *ca.* 650-550 cal yr BP. The FBB12 record begins with a reduced rate of cumulative C between 2000 and 1750 cal yr BP and both SCH10 and FBB12 experience a decrease in C addition between *ca.* 1100 and *ca.* 700/600 cal yr BP respectively. After this reduction of C accumulation in FBB12, the addition of C temporarily occurs at a greater rate than elsewhere in the FBB12 the record.

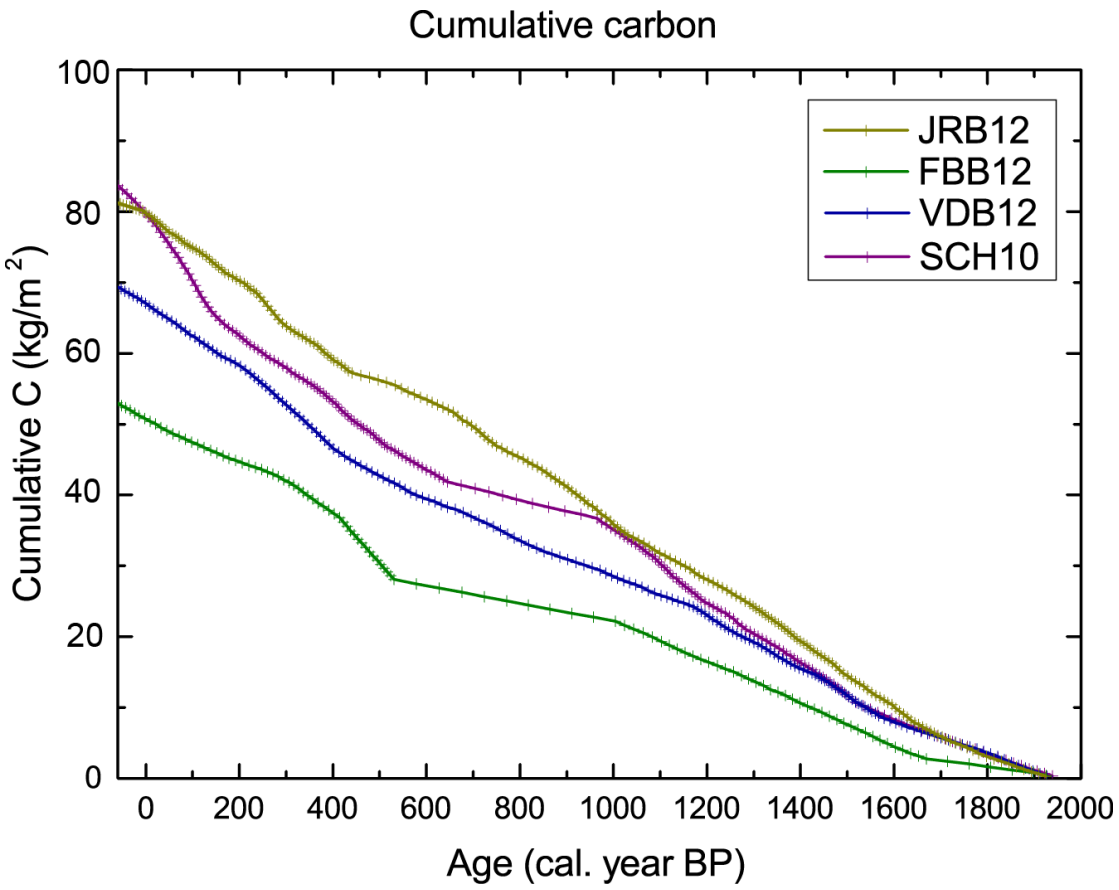

Figure 7.3 Cumulative C by site over the last 2000 years. Key arranged from north (JRB12) to south (SCH10).

7.2.4 CAR over different temporal resolutions

The CAR for the four sites have been calculated over 100-, 200- and 500-year time segments. Over 100-year periods, all sites initially exhibit similar trends, increasing to 1500 cal yr BP (Figure 7.4). SCH10 CAR continues to increase to 1100 cal yr BP whilst the others decrease. The most noticeable decrease in CAR occurs between 1000-900 cal yr BP in SCH10. CAR is supressed between 1000-600 cal yr BP in FBB12 whilst SCH10 experiences a stepwise increase in CAR from 1000 – 400 cal yr BP and VDB12 and JRB12 fluctuate between 1000 – 600 cal yr BP. JRB12, FBB12 and VDB12 generally decrease from *ca.* 500 cal yr BP to the surface peat with the timing of the onset of decrease differing by 100 years, whilst SCH10 increases to 100 cal yr BP.

There is no clear north – south trend across the transect over 100-year intervals: FBB12, an intermediate site, commonly has the lowest CAR.

However, FBB12 CAR is the highest at 500 cal yr BP, at which point the other sites decrease with increasing latitude. VDB12 CAR values are always intermediate of the other sites, with JRB12 experiencing the highest rates until 1400 cal yr BP and SCH10 containing the highest between 1400 and 1100 cal yr BP. The SCH10 CAR increase to the present day could appear anomalous; however, the elevated values are on trend. A possible explanation for the elevated SCH10 CAR during this period could be the current woody surface vegetation and associated roots (Chapter 6).

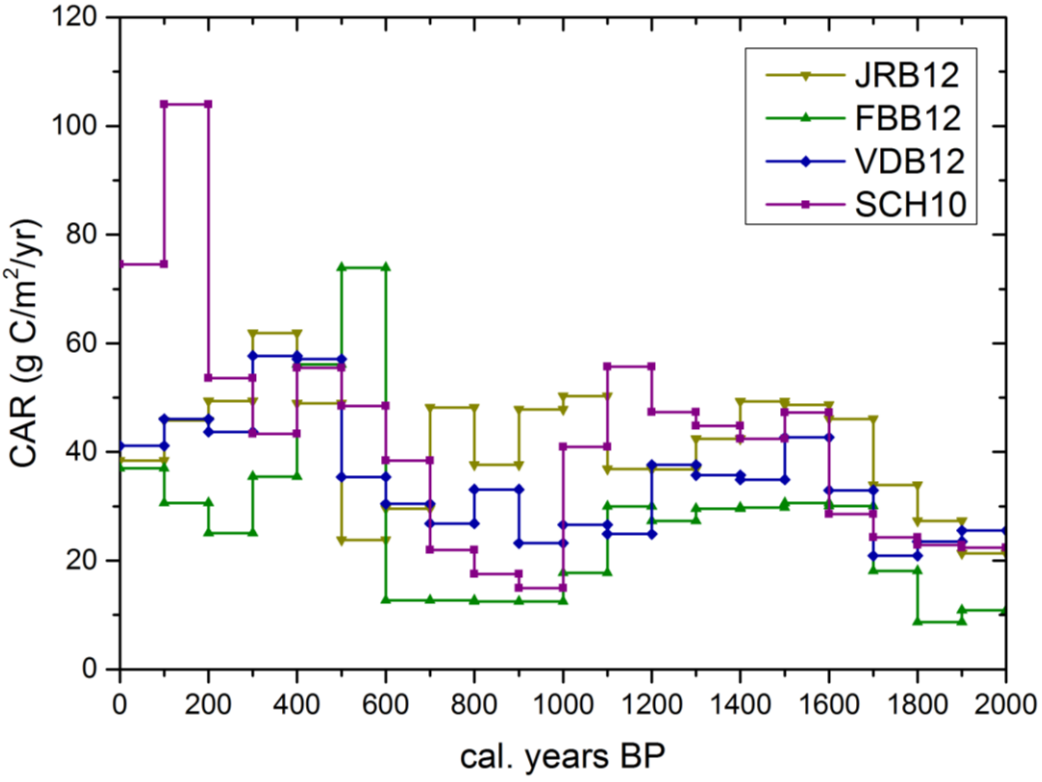

Figure 7.4 Mean C accumulation rates: 100-year intervals with key arranged from north (JRB12) to south (SCH10)

The average variability (measured using standard deviations from the mean) in CAR calculated over 100 year segments is reduced from 2000 – 1700 cal yr BP and 900 – 800 cal yr BP at all sites (Figure 7.5). Variability increases *ca.* 1500 cal yr BP and *ca.* 400 – 300 cal yr BP. FBB12 has the most consitent variation between the 100 year intervals throughout the whole records whilst SCH10 commonly had the highest variation with the exception of 0 – 100 and 300 – 400 cal yr BP, when JRB12 contains the peak variability of the entire record.

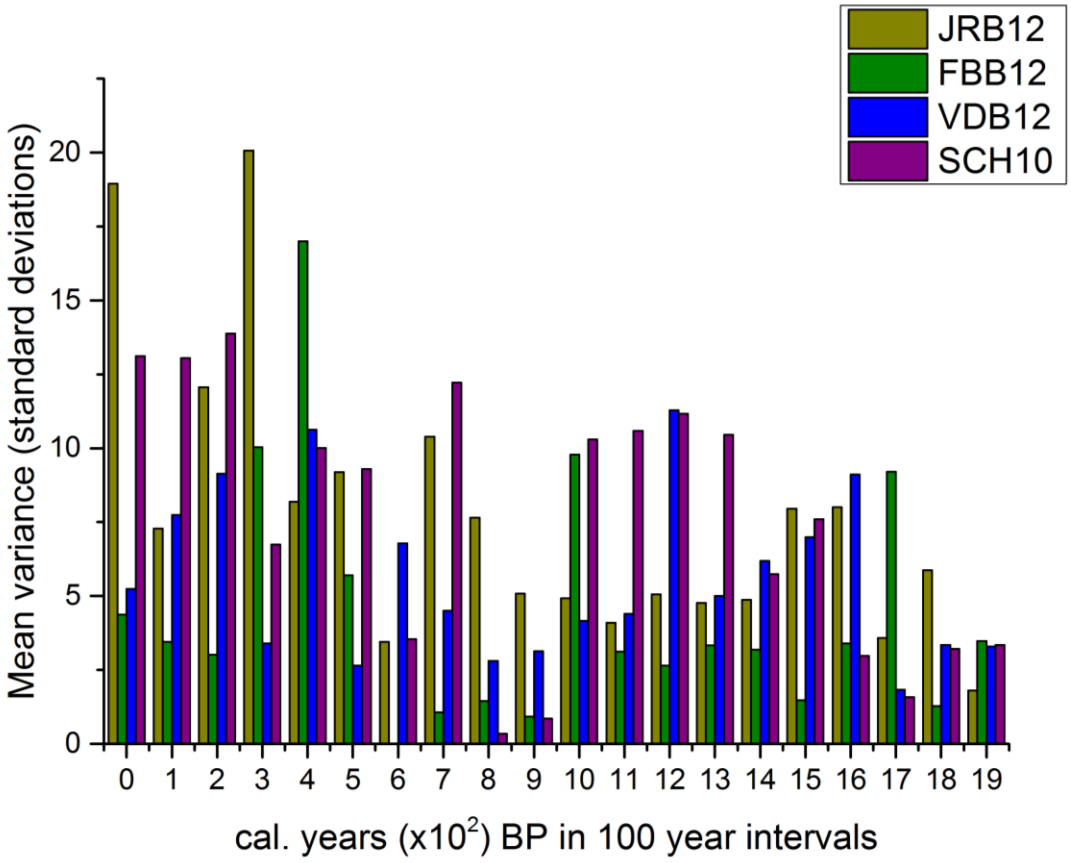

Figure 7.5 Mean variability of C accumulation rates in 100-year intervals. Key arranged from north (JRB12) to south (SCH10)

The 200-year CAR intervals contain similar trends to the 100-years CAR intervals although the timings of changes have altered with the extended resolution (Figure 7.6). Over 200-year periods, all sites initially exhibit similar trends, increasing to 1400 cal yr BP. SCH10 CAR continues to increase to 1000 years BP whilst the others decrease. The most noticeable decrease in CAR occurs between 1000-800 cal yr BP in SCH10 and between 1000-600 cal yr BP in FBB12. This corresponds with a slowdown in cumulative C at both sites (Figure 7.3). VDB12 and JRB12 CAR are stable during this period although JRB12 contains a subtle decrease. All sites increase at 600 to 400 cal yr BP, although this is less pronounced in JRB12 and corresponds with the slowdown in JRB12 cumulative C (Figure 7.3). JRB12 reveals a greater CAR increase at 400 to 200 years BP when VDB12 continues to increase whilst SCH10 and FBB12 decrease. JRB12 and VDB12 show similar decreases to the present day, whereas FBB12 subtly increases and SCH10 dramatically increases.

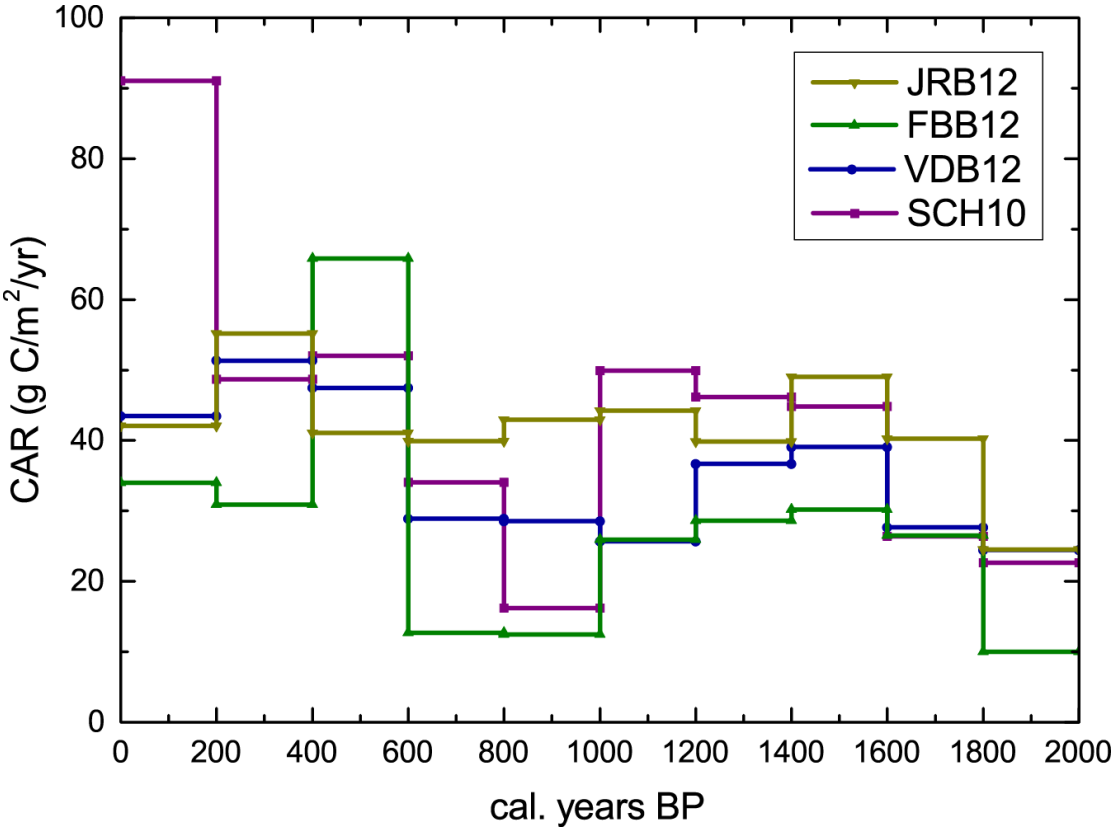

Figure 7.6 Mean C accumulation rates: 200-year intervals with key arranged from north (JRB12) to south (SCH10)

Average variability in CAR calculated over 200 year segments differs between sites (Figure 7.7). JRB12 variability generally increases towards the present day with the most stable conditions between 1400 and 1200 cal yr BP. SCH10 variability increases to 1000 cal yr BP, aburptly decreases to more stable conditions at 800 years BP before an increase in variability to the present day. VDB12 and FBB12 exhibit less clear trends in variability: they both increase to 1600 cal yr BP and decrease to 1400 cal yr BP. Trends diverge from 1200 cal yr BP and FBB12 becomes more stable between 800 and 600 cal yr BP. Both increase to maximum variability at 400 cal yr BP and become more stable to the present day. Similar CAR variability trends occur from 2000 – 1600 cal yr BP when all sites increase, although SCH10 experiences a more subtle increase than the other sites. The variability trends are also similar at SCH10 and FBB12 from 1400 – 800 cal yr BP when both records increase before a subsequent decrease.

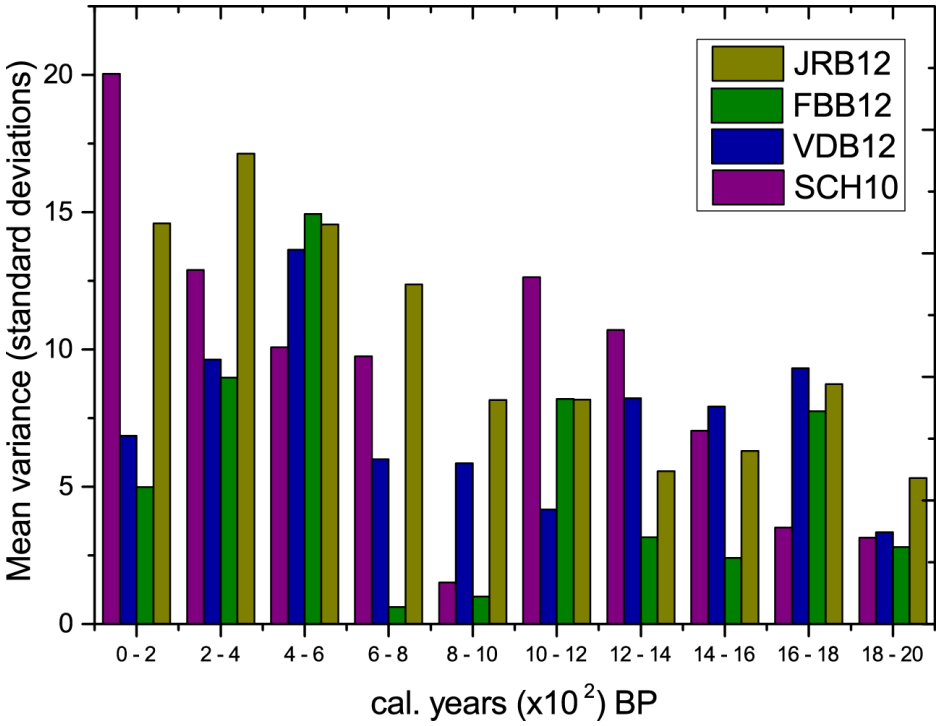

Figure 7.7 Mean variability of C accumulation rates in 200-year segments. Key arranged from north (JRB12) to south (SCH10)

At the 500-year timescale, CAR increase at all sites increase to 1500 years BP (Figure 7.8). SCH10, VDB12 and JRB12 CAR decrease at 1000 years BP whilst FBB12 continues to increase. The divergent trend at 1000 years BP is driven by an abrupt FBB12 CAR increase between 600 and 500 years BP, which is more influential than the previous sustained period of CAR suppression. All sites increase at 500 year BP to the present day with the exception of FBB12.

Average variability calculated in 500-year intervals decreases in all sites from 2000 - 1000 years BP (Figure 7.9). JRB12, FBB12 and SCH10 increase to 500 - 1000 years BP, whilst VDB12 decreases. FBB12 decreases to the present day whilst the other sites increase. FBB12 ends at a similar level of variation as JRB12, owing to the preceding dramatic increase in FBB12. With the exception of the large increase in FBB12, SCH10 contains the most variability over 500-year intervals. FBB12 CAR are the most stable between 2000 and 1000 years BP and VDB12 CAR are the most stable from 1000 years BP to present.

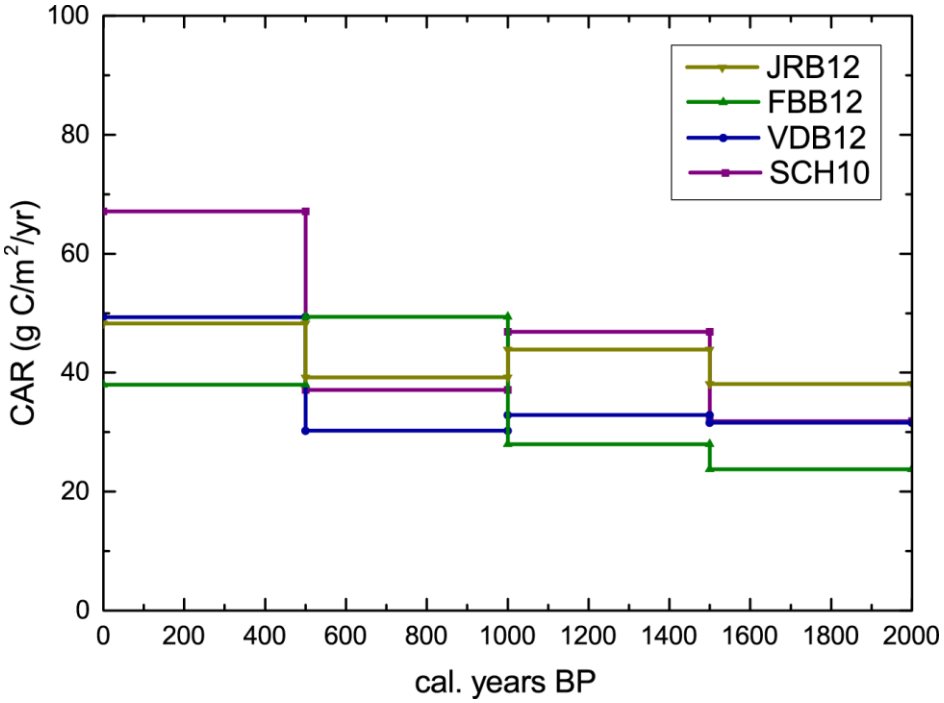

Figure 7.8 Mean C accumulation rates: 500-year intervals with key arranged from north (JRB12) to south (SCH10)

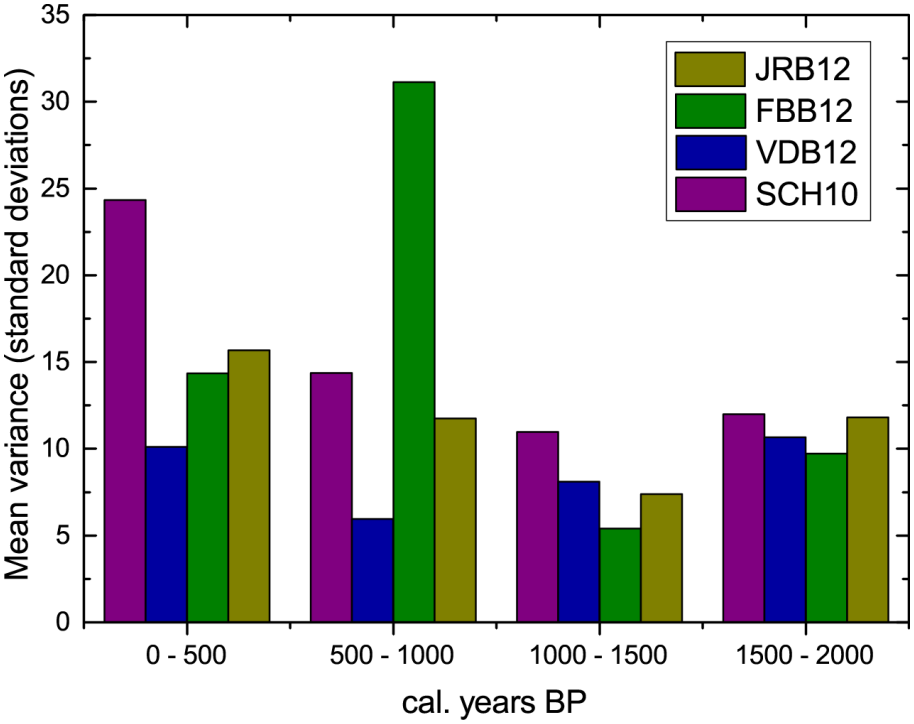

Figure 7.9 Mean C accumulation rates: 500-year intervals with key arranged from north (JRB12) to south (SCH10)

Chapter 8: Discussion

The aim of this thesis is to characterise the relationship between late Holocene ombrotrophic peatland hydrological conditions and carbon accumulation rates (CAR) across a climate gradient in eastern North America. Four research objectives were outlined in Section 1.2:

1. Robust core chronologies will be developed to enhance spatial and temporal comparisons of reconstructed climatic change.
2. Peatland water table reconstructions will be obtained from four sites across Maine, Nova Scotia and Newfoundland to improve the characterisation of late Holocene climate change in eastern North America.
3. Late Holocene carbon accumulation rates will be reconstructed using inferred carbon content and age-depth models to investigate temporal and spatial variations in carbon (C) sequestrations.
4. The extent to which late Holocene peatland carbon accumulation rates fluctuate with vegetation patterns, climatic conditions and disturbance events will be assessed.

This chapter is structured in two main sections based on these objectives. The first section characterises late Holocene environmental change in eastern North America, using the results from objective one to address objective two. The extent to which the peatland water table reconstructions obtained within this thesis are driven by climate is assessed (Section 8.1) before the spatial and temporal differences between the palaeoenvironmental reconstructions presented in Chapter 6 are compared with other regional climatic records (Section 8.2). The timing of environmental change around the North Atlantic region before the onset of the Medieval Climate Anomaly (MCA) will be tested using the White River Ash (WRA) as a tephra pinning point between palaeo-archives (Section 8.3). The second section of this discussion characterises changes in C accumulation across the eastern North American climate gradient, using the peatland palaeoenvironmental reconstructions (Section 8.1 - 8.3) and C accumulation histories to characterise changes in CAR and identify the dominant CAR drivers over the last 2000 years (Section 8.4).

8.1 Reconstructed peatland environmental change: considerations

Converting proxy reconstructions of peatland water table fluctuations into inferences of past environmental change requires an assessment of the responsiveness of peatland autogenic systems and the sensitivity of the proxies; however, disentangling the influence of these controls on the reconstructions presents challenges. Internal homeostatic mechanisms (Ingram, 1982; Belyea and Baird, 2006) limit water table fluctuations; therefore, reconstructed water tables may not represent the full magnitude of the responsible climatic change. The non-linear peatland response, compounded by the inability of biological proxies to isolate the relative influence of precipitation and temperature from the reconstructions, prevents the conversion of reconstructed peatland water table depths (WTD) to direct climate parameters. Incorporating organic geochemical techniques into peatland palaeoecological studies may move towards directly reconstructing temperature (e.g. using Glycerol Dialkyl Glycerol Tetraethers (GDGTs; Weijers *et al*., 2007)) and precipitation (e.g. using oxygen and hydrogen stable isotopes on cellulose and *n*-alkanes; Daley *et al*., 2009; Nichols and Huang, 2012). However, these techniques require further understanding and development before they can be used as reliable quantitative indicators of climatic change. This thesis does not seek to directly quantify past climate change from the water table reconstructions, rather emphasis is placed on characterising the relative peatland expressions of climate change across the study region.

Comparisons between multiple regional ombrotrophic peatland water table reconstructions, independent palaeoclimate reconstructions and/or climatic instrumental records that reveal consistent changes may be used to extract overriding regional climatic signals from background site-specific noise, long-term autogenic development and proxy-related uncertainty reflected in the records (e.g. Hughes *et al*., 2000; Barber and Charman, 2003; Langdon *et al*., 2003; Charman *et al*., 2006). The relatively low magnitude of late Holocene climate change requires sensitive proxies to reveal a clear signal within the accompanying noise; therefore, environmental interpretations within this thesis will be restricted to periods of prominent change.

8.1.1 Proxy sensitivity to environmental change

Plant communities have threshold responses to changes in WTD (Barber *et al*., 2003), which often result in complacent responses to small and/or short-lived WTD changes (e.g. Hughes *et al*., 2006). Macrofossil reconstructions may therefore lag behind other proxy records (e.g. Blundell and Barber, 2005). Such complacency was detected at each site within this thesis (Chapter 6) as the macrofossil records generally exhibited more muted changes compared with the testate amoebae reconstructions. The macrofossil assemblages of JRB12, VDB12 and SCH10 were dominated by *S.* sect. *Acutifolia*, often primarily composed of the eurytopic species *S. fuscum* (Daniels and Eddy, 1990). The frequently high abundance of this species most likely drove the relative complacency in the macrofossil records compared with the testate amoebae assemblages. A striking example of the *S. fuscum*-induced complacency is evident in the VDB12 record between 2000 and *ca.* 1200 cal yr BP when the macrofossil reconstructions reveal stable hydrological conditions whilst the testate amoebae reconstructions infer more oscillating conditions (Figure 8.1). *S. fuscum*-driven complacency was also detected in the one existing published water table reconstruction from eastern Newfoundland (Nordan's Pond Bog; Hughes *et al*., 2006). The dominance of *S. fuscum* in the ombrotrophic peatlands of eastern North America emphasises the need for multiple proxy reconstructions to characterise peatland environmental change in this region.

S. sect. *Acutifolia* dominance cannot explain all apparent occurrences of macrofossil complacency: for example, the FBB12 macrofossil record is not consistently dominated by *S.* sect. *Acutifolia* between 1600 – 1300 cal yr BP; however, the vegetation response is less variable compared with the testate amoebae reconstruction (Figure 8.1). Such macrofossil stability may be influenced by the differences in the life cycles of the plants, which are perennial, and the testate amoebae, which have rapid reproduction rates of between 10 and 27 generations per year (Charman, 2001). The plants may be more resistant to change than the testate amoebae and may require more sustained or extreme environmental forcing to exhibit a similar magnitude of response. This period of muted vegetation response in FBB12 does contain fluctuating hydrological conditions as inferred from the testate amoebae; therefore, perhaps the environmental conditions did not exceed the threshold required to

generate full-scale plant community changes that are evident in the testate amoebae.

The different length of vegetation and testate amoebae lifecycles may result in the macrofossil response lagging behind the testate amoebae: for example, in JRB12 *ca*. 1100 cal yr BP and in SCH10 *ca.* 1450 cal yr BP, the testate amoebae indicate drier conditions ahead of the plant macrofossils. This difference in response time to hydrological change has also been demonstrated in other studies (e.g. Väliranta *et al*., 2012). A lag in response between testate amoebae and plant macrofossils may be indicative of the speed of onset of the environmental change and its duration. Extracting such information from the proxy reconstructions is, however, complicated since a lag between the records may also be influenced by responsiveness of the ecological community at the time of change and antecedent environmental conditions.

Plant macrofossils are not always the more complacent proxy, the vegetation exhibits more pronounced variation than the testate amoebae in VDB12 between *ca*. 650 – 200 cal yr BP. As previously noted, the initial section of the VDB12 vegetation record was a stable *S. fuscum* hummock until *ca*. 700 cal yr BP when a pronounced abrupt shift to temporary wetter conditions occurred. After this point the macrofossils indicate a wetter community with increased variability. Environmental drivers may have forced the vegetation to cross an ecological threshold *ca*. 700 cal yr BP, defined as a point at which "a community or ecosystem switches from one stable state to another, usually within a relatively short time-interval" (Willis *et al*., 2010). Before this pronounced change in the macrofossils, the testate amoebae indicate a temporary wet phase followed by an abrupt shift to sustained wetter conditions. This sustained step-wise hydrological change may have been required to trigger a change in the resistant *S. fuscum* hummock to wetter conditions.

Generally, the vegetation and testate amoebae species with wet preferences have narrower ecological tolerances than more generalist species with dry preferences (Figure 8.2; Väliranta *et al*., 2012). Wet-indicating species may not only have quicker responses to environmental change than drier species, but also the response of the floral and faunal assemblages to drying conditions may be muted by the less discriminant species associated with drier conditions.

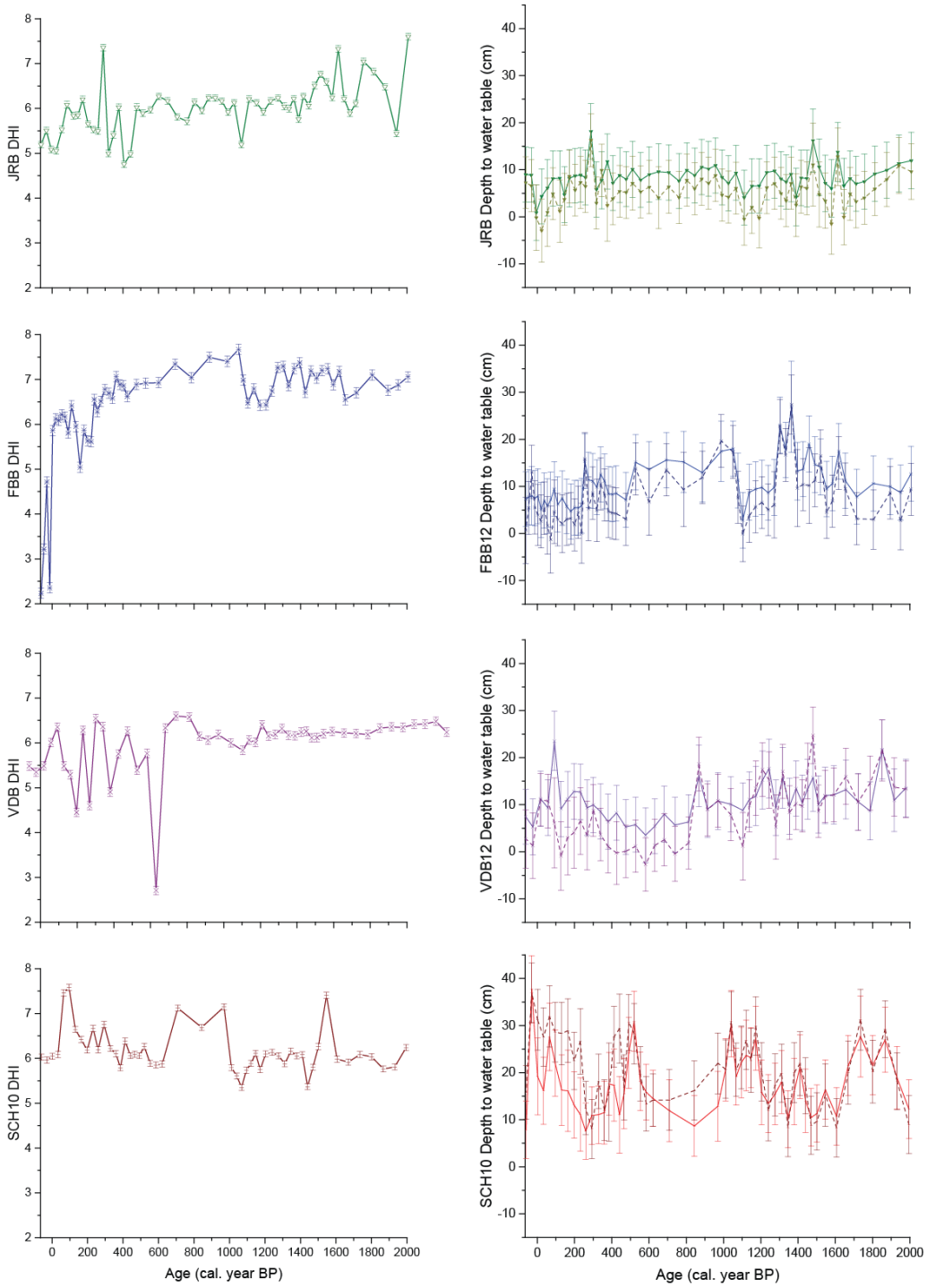

Figure 8.1 Plant macrofossil DHI reconstructions (left column) with standard error presented and testate amoebae transfer function reconstructions (Amesbury *et al.*, 2013 in solid line; Lamarre *et al.*, 2013 in dashed line; right column) with transfer function error of prediction presented. Sites arranged from northeast (JRB12, top) to southwest (SCH10; bottom). Lower y-axis values indicate wetter conditions.

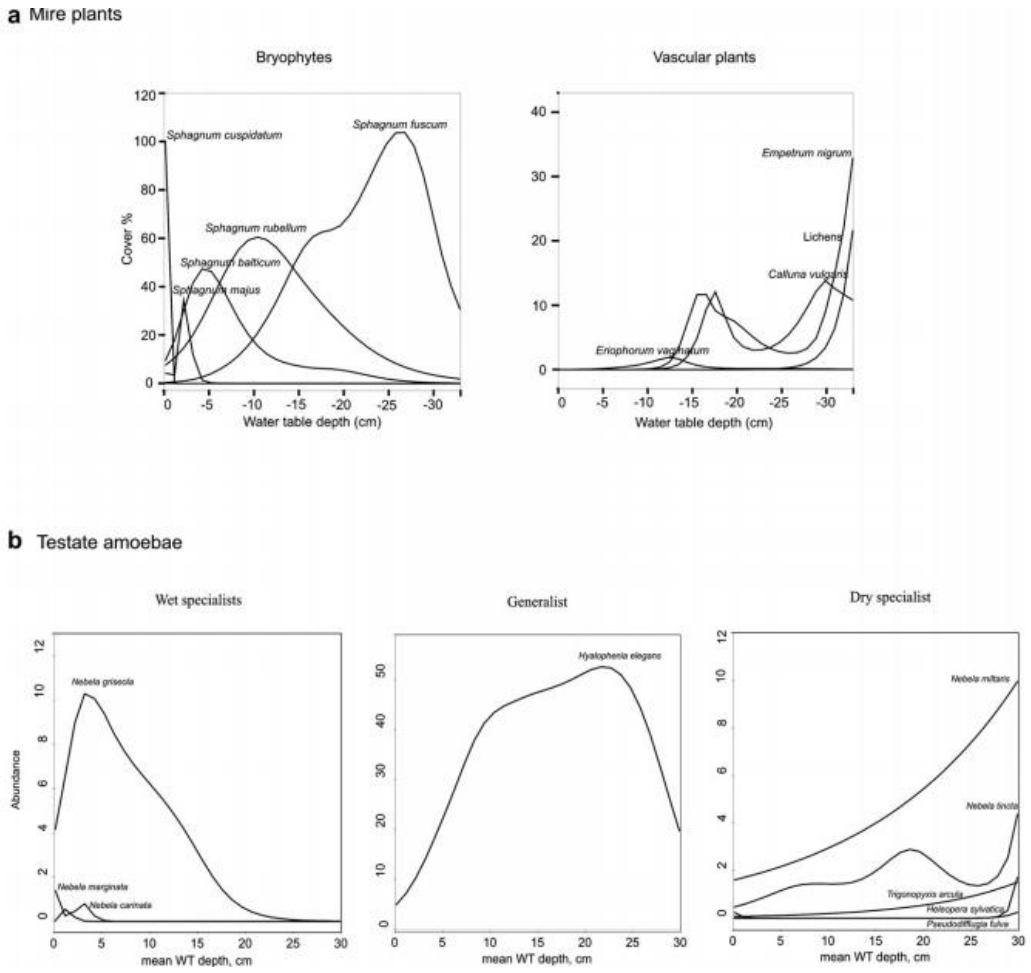

Figure 8.2 Modelled relationship between modern mire plants (a) and testate amoebae (b) species and the current mean water table depth at each measurement plot in Kontolanrahka Bog based on Generalised Additive Models from Väliranta *et al.* (2012). Wet species generally show narrower tolerances than drier species.

Based on the differences in the ecological response to hydrological conditions, peatland environmental studies have traditionally focused on the identification of wet shifts and phases. More recently, studies have indicated that dry phases can be detected in peatland ecohydrological reconstructions, representing prolonged periods of high frequency or magnitude drought, and should be investigated alongside wet phases (e.g. Booth *et al.*, 2006; Swindles *et al.*, 2012). However, when investigating drying peatland responses it is important to consider ecological lags or subsequent threshold responses that may occur, masking the true extent and characteristics of the drier environmental conditions.

8.1.2 Constraining ecological environmental preferences and preservation issues

Whilst the testate amoebae may be more sensitive to water table fluctuations than the plant macrofossils, the ecological preferences of several testate amoebae taxa remain uncertain and thus hinder quantitative environmental reconstructions. The water table tolerances of three taxa, all of which dominate at points in the records obtained within this thesis, are particularly uncertain: *Difflugia pulex, Hyalosphenia subflava* and *Arcella discoides*. Both *D. pulex* and *H. subflava* are commonly assigned as indicators of low water table depths (WTD); however, both species have weak modern analogues (e.g. Charman *et al.*, 2007; Booth, 2008; Mitchell *et al.*, 2008; Turner *et al.*, 2013; Section 3.5.4). The water table preference of *D. pulex* is one of the main differences between the two transfer functions applied in this study (Amesbury *et al.,* 2013 and Lamarre *et al.,* 2013; Section 3.5.4). Despite the different water table tolerances of *D. pulex* in the training sets, the difference between the two transfer function reconstructions are within the model errors (Figure 8.1), demonstrating that the real utility of transfer functions lies in the reconstructed direction of hydrological change rather than the magnitude of change, which should be viewed with some caution (*sensu* Swindles *et al.*, 2013; Turner *et al.*, 2013).

The ability of *D. pulex, A. discoides* and *H. subflava* to thrive under variable conditions (Sullivan and Booth, 2011) suggests that they could be indicators of disturbance: for example, during the hiatus in SCH10, attributed to the fire, *D. pulex* increases in abundance. This response of *D. pulex* to a prominent fire disturbance has not been noted elsewhere in the literature; however, few studies have investigated testate amoebae response to substantial burning events. *T. arcula* has previously been suggested as a burning indicator (Warner, 1990) and *H. subflava* concentrations have been shown to increase in response to a severe moorland wild-fire (Turner *et al.*, 2013). Neither taxon contained pronounced responses to the fire event in SCH10. Further research into characterising the testate amoebae response to burning events is therefore required to test whether a consistent change in taxa, such as *D. pulex*, may be indicative of a severe fire in ombrotrophic peatlands.

Testate amoebae assemblages may be influenced by changes in vegetation since, in a peatland ecosystem, the plants are the producers and the testate

amoebae are the consumers. Changes between *Sphagnum*-dominated and sedge/shrub-dominated vegetation shape the testate amoebae habitats by altering the pH and water film potential of the host plants for survival (Tolonen, 1986; Charman *et al*., 2000; Wilmshurst *et al*., 2003). For example, *Sphagnum* plants have greater surface areas with more consistent water films and have the potential to generate more acidic surroundings compared with sedges and shrubs. Testate amoebae assemblages also vary within *Sphagnum* species: higher species richness has been associated with *S. angustifolium, S. flexuosum* and *S. palustre* compared with *S. magellanicum* (Mieczan, 2009). Since water table changes trigger changes in peatland vegetation composition, it is difficult to isolate the effect of water table and vegetation driven changes in testate amoebae assemblages. The influence of the plants on the testate amoebae cannot, therefore, be assessed from the records obtained within this study without additional proxies providing independent assessments of external environmental change.

8.2 Late Holocene environmental change in eastern North America

There is a paucity of terrestrial late Holocene climate records from the Maine, Nova Scotia and Newfoundland. The existing palaeo-reconstructions have been predominantly obtained from sparsely dated lake sediments with longer temporal foci, often extending into the Late Glacial (Figure 8.3). The different temporal focus often results in late Holocene environmental change being characterised by a few data points with relatively poor chronological control. Therefore, this thesis contributes to the spatial and temporal characterisation of eastern North America MCA-Little Ice Age (LIA) climate change.

A summary of the available environmental reconstructions indicates that late Holocene climatic conditions across the eastern coast of North America were spatially and temporally complex: terrestrial and marine records from the same region often show opposing trends, potentially indicating differences in the strength of oceanic and atmospheric drivers, whilst temperature and precipitation regimes often differ between the northern and southern regions (Figure 8.4). During the MCA, reconstructions of more southern regions of eastern North America revealed drier conditions than the north, whilst the northern regions were wetter but more variable. MCA temperature

reconstructions were predominantly warmer than previous conditions in the north, whilst southern temperatures appear to have been initially cooler. Conditions in southern regions were cool and wet during the LIA, whilst precipitation in more northern regions initially decreased before increasing. Comparisons between results obtained within this thesis and existing records are used to highlight climatic differences across the transect and to assess the extent to which MCA-LIA climatic differences are replicable across the study region.

The trigger of the MCA-LIA transition has been attributed to an increased frequency of solar minima (e.g. Shindell *et al*., 2001; Mann *et al*., 2009) and increased volcanic activity (Gao *et al*., 2008); however, the heterogeneous global expression of reconstructed MCA-LIA climatic conditions requires a combination of oceanic and atmospheric drivers to account for the sustained climatic change (Section 2.8.3). The LIA is thought to have persisted owing to the reversal of the MCA La Niña-like conditions, a strengthened Atlantic Meridional Overturning Circulation (AMOC; e.g. Seager *et al*., 2007; Wanamaker *et al*., 2012) and a more negative North Atlantic Oscillation (NAO; e.g. Trouet *et al*., 2009). The relative contribution of each driver is, however, unclear (Section 2.8.3).

The Labrador Sea area was warmer during the LIA than during the MCA, a change driven by weaker Westerly winds that reduced heat loss. Sea ice in the Labrador Sea region increased during the LIA, strengthening the freshwater flow and weakening the AMOC (Massé *et al*., 2008). Cold fresh water from Labrador may force *ca*. 100 km northward excursions in the latitude of the Gulf Stream (Rossby and Benway, 2000) and such extensions have been associated with the positive phase of the NAO (Joyce *et al*., 2000) and a strengthened AMOC (Frankignoul *et al*., 2001). The combination of the weaker AMOC and the negative NAO reduced northward ocean heat transport during the LIA with a 10% estimated decrease in the strength of the Gulf Stream (Lund *et al*., 2006). Owing to the proximity of the study sites to the Gulf Stream and Labrador Current, it is hypothesised that the reconstructed MCA-LIA peatland environmental change will predominantly reflect changes in the NAO and the AMOC and that comparisons of the WTD reconstructions across the transect may therefore reveal changes in the northward extent of the Gulf Stream.

The climatic expression of the persistent negative LIA-like NAO conditions reveals colder temperatures in northern Europe, Maine and the rest of the USA when compared with Newfoundland, Labrador, Quebec and western Greenland (NOAA, 2012). A negative NAO also generates wetter summers in eastern North America than during a positive NAO (Trouet *et al.*, 2009). It is therefore hypothesised that the influence of the NAO will generate a more pronounced peatland response in the southern sites as MCA (LIA) precipitation decreases (increases) and evaporation increases (decreases), than the northern sites with less (more) evaporation.

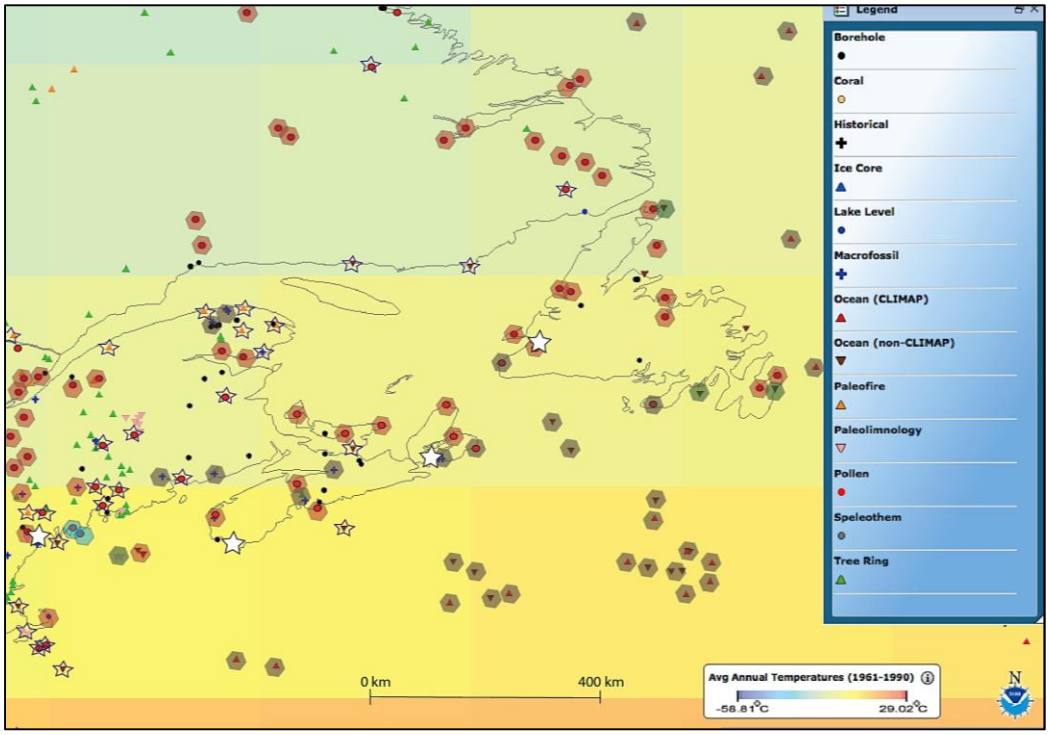

Figure 8.3 Example of scarcity of late Holocene palaeoenvironmental reconstructions in eastern North America with adequate chronological control using NOAA's palaeoclimate database interactive map (last accessed 01/05/2015).
White stars indicate location of study sites within this thesis. Purple outlined stars indicate records with multiple data points and chronological measurements during the last 2000-years; red hexagons indicate weak chronological control (single chronological measurements within the last 2000 years); brown hexagons indicate that the temporal focus of the records do not include the last 2000 years; green hexagon indicates modern reconstructions that do not extend across the last 2000 years (bore hole temperature estimates are also limited to the last 500 years); blue hexagons indicate unpublished data.

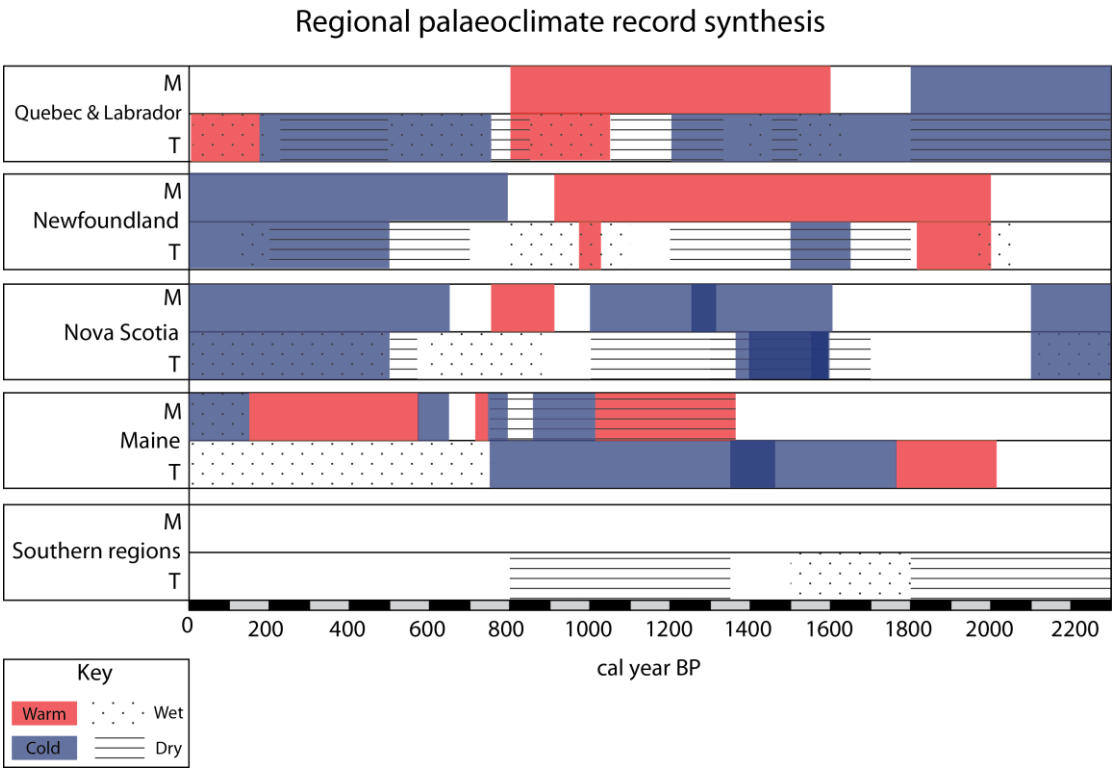

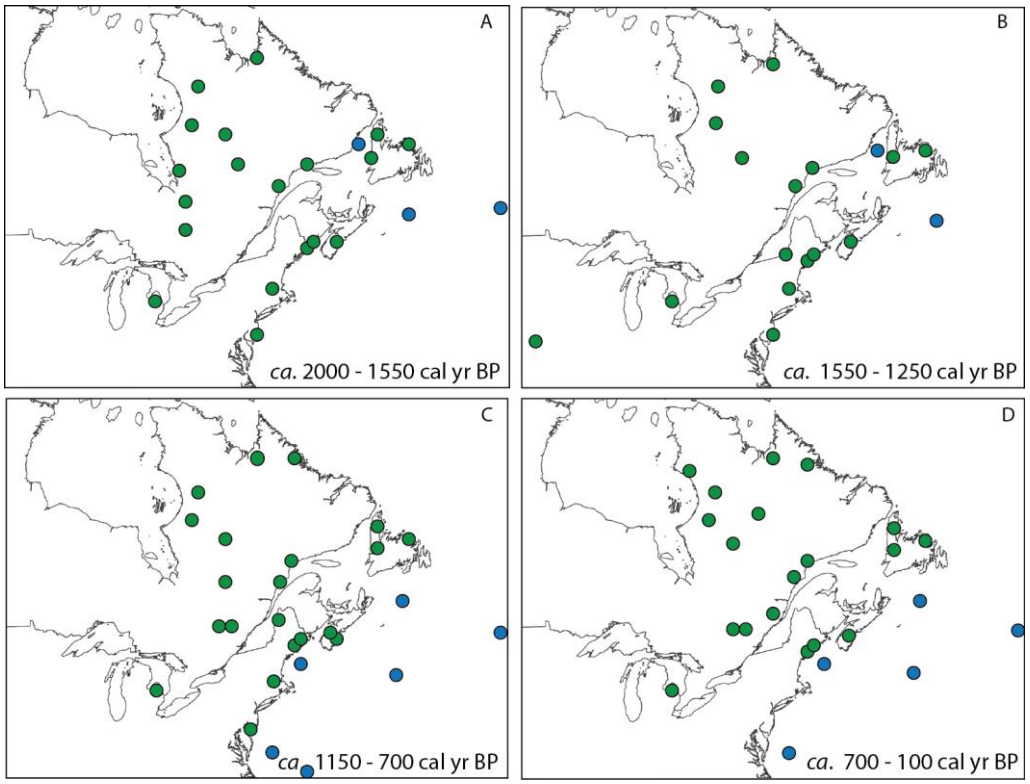

Figure 8.4 Summary of reconstructed temperature and precipitation trends over the 2300 cal yr BP in eastern North America by region (obtained from synthesis of regional records, Section 2.9). M = records obtained from marine sediments, t = records obtained from terrestrial records. The approximate locations of the records in synthesis identified in the bottom four panels separated by major time interval, green circles indicate terrestrial records, blue indicated marine records.

8.2.1 Characterisation of late Holocene environmental change across the eastern coast of North America

The reconstructed environmental changes of the peatlands obtain within this study (Figure 8.5, Table 8.1) are compared with other regionally proximal climatic reconstructions (Figure 8.6) to characterise climate change over the last 2000 years. The majority of the dominant changes reconstructed from the study sites in this thesis are in agreement with the other regional records; therefore, they are likely representing responses to climatic change rather than being dominated by internal peatland dynamics.

8.2.1.1 Pre-MCA

The peatland WTD reconstructions obtained within this thesis generally indicate drier conditions *ca*. 2000 cal yr BP. Similar dry conditions are also reconstructed in records from the St Lawrence North Shore region (Magnan and Garneau, 2014), Michigan and Minnesota (Booth *et al*., 2006;Figure 8.6) and southern Nova Scotia (Spooner *et al*., 2014). Records from the northwest regions of the transect indicate that the temperatures decreased during this drier period: permafrost aggradation increased in subarctic Quebec (Cayer and Bhiry, 2014), temperatures reconstructions were cooler in the Laurentian Fan (Marchitto and deMenocal, 2003; Balestra *et al*., 2013) and the duration of sea ice in the Gulf of St. Lawrence increased (Dhahri, 2010). Conversely, temperature reconstructions obtained from Newfoundland, in the northeast of the transect, are indicative of a warming trend in both marine (Levac, 2003) and terrestrial (Rosenberg *et al*., 2004) records.

Around 1450 – 1300 cal yr BP, JRB12 becomes wetter; however a similar increase in the summer moisture balance does not occur until *ca*. 1300 cal yr BP in FBB12. This is the main difference between the reconstructed WTD of the two most northern sites within this thesis over the 2000-year reconstruction. The earlier trend towards wetter conditions further north is supported by a peatland WTD reconstruction in northeastern Newfoundland (Nordan's Pond Bog; Hughes *et al*., 2006) in which conditions change even earlier than in JRB12 (*ca*. 1750 cal yr BP). This earlier in response may be an artefact of the lower sampling resolution and weaker chronological control in the Nordan's Pond Bog or it may represent a true lag in the peatland response to climate change across the study transect (discussed further in Section 8.3).

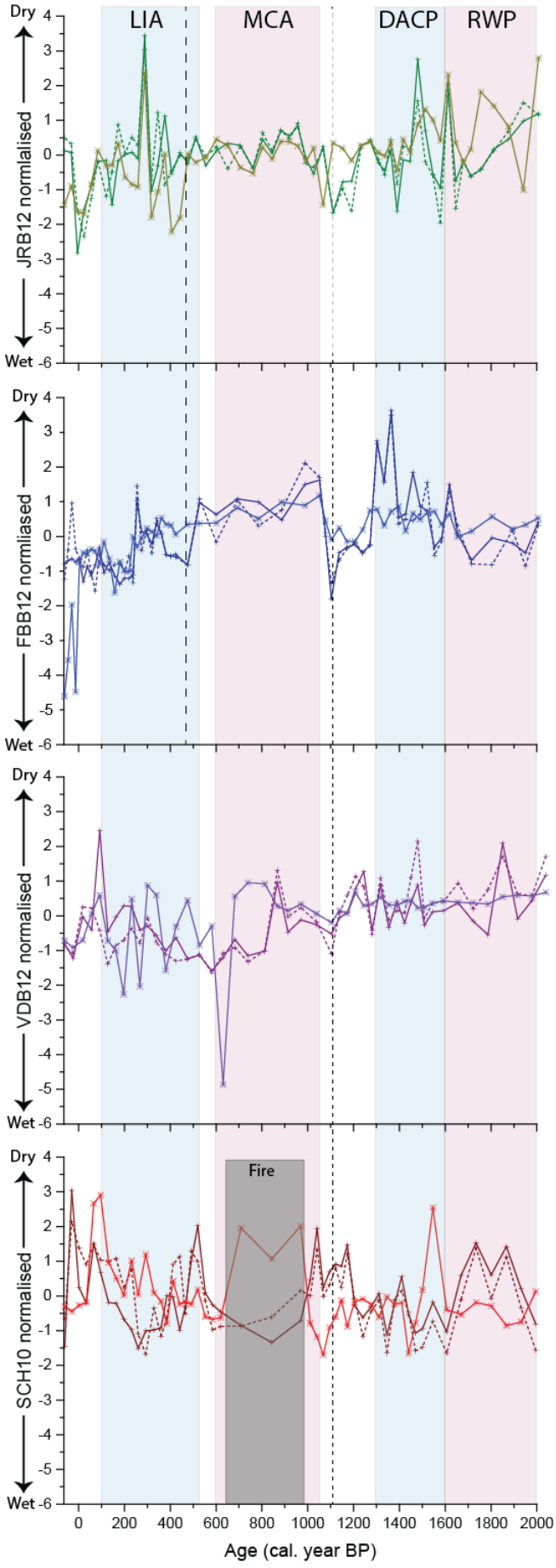

Figure 8.5 The four peatland environmental reconstructions obtained using plant macrofossils (lighter solid line) and testate amoebae reconstructed environmental change using Amesbury *et al.*, (2013) training set (darker solid line) and Lamarre *et al.*, (2013) training set (darker dashed line).

Lower y-axis values indicate wetter conditions. Broad timings of the four main climatic periods of last 2000 years are indicated: Roman Warm Period (RWP; *ca.* 2000 – 1600 cal yr BP), Dark Ages Cold Period (DACP; *ca.* 1600 – 1300 cal yr BP), Medieval Climate Anomaly (MCA; c*a.* 1050 – 600 cal BP) and the Little Ice Age (LIA; *ca.* 550 – 100 cal yr BP). Blue shading represents cooler conditions and red shading representing warmer conditions. The presence and timings of these periods are not well constrained in this region eastern North America; therefore, they serve only a guide for discussion.

the

the

yr

of

as

Table 8.1 Summary of main reconstructed water table changes distinguished by dominant changes which broadly correspond with named climatic periods over the last 2000 years. Each period is described from north (JRB12; top) to south (SCH10; bottom).

Roman Warm Period

Time (cal yr BP)	Site	Reconstructed water table conditions
2000-1700	JRB12	Fluctuating (potentially wetting)
2000-1700	FBB12	Wet (fluctuating)
2000-1700	VDB12	Potentially wetting
2000-1700	SCH10	Dry (fluctuating)

Dark Ages Cool Period

Time (cal yr BP)	Site	Reconstructed water table conditions
1700-1300	JRB12	Drier (fluctuating) to *ca.* 1500 cal yr BP then wetter
1700-1300	FBB12	Drying
1700-1300	VDB12	Fluctuations around consistent water table levels
1700-1250	SCH10	Shift to wet at 1700 cal yr BP then wet containing drying trend

Pre-Medieval Climate Anomaly

Time (cal yr BP)	Site	Reconstructed water table conditions
1300-1100	JRB12	Contains a pronounced wetter phase
1300-1100	FBB12	Pronounced wet phase becoming wetter
1250-1100	VDB12	Wetting
1175-1050	SCH10	Shift to drier conditions (containing wetting trend)

Medieval Climate Anomaly

Time (cal yr BP)	Site	Reconstructed water table conditions
1100-500	JRB12	Pronounced return to drier stable conditions
1100-500	FBB12	Pronounced dry shift then wetting trend
1100-900; 900-600	VDB12	Wet conditions before drying; then pronounced wet shift
1050-600	SCH10	Fire

Little Ice Age

Time (cal yr BP)	Site	Reconstructed water table conditions
500-300	JRB12	Variable, ending in dry pronounced conditions
500-300	FBB12	Overall wet trend but variable
600-100	VDB12	Drying trend
600-300	SCH10	Wet then temporary drying to 400 cal yr BP before wetting again to 300 cal yr BP

Latter stages of LIA - present

Time (cal yr BP)	Site	Reconstructed water table conditions
300-0	JRB12	Wetting trend
300-0	FBB12	Wetting trend
300-100, 100-0	VDB12	Variable, drying; then wetting trend
300-100, 100-0	SCH10	Drying then variable

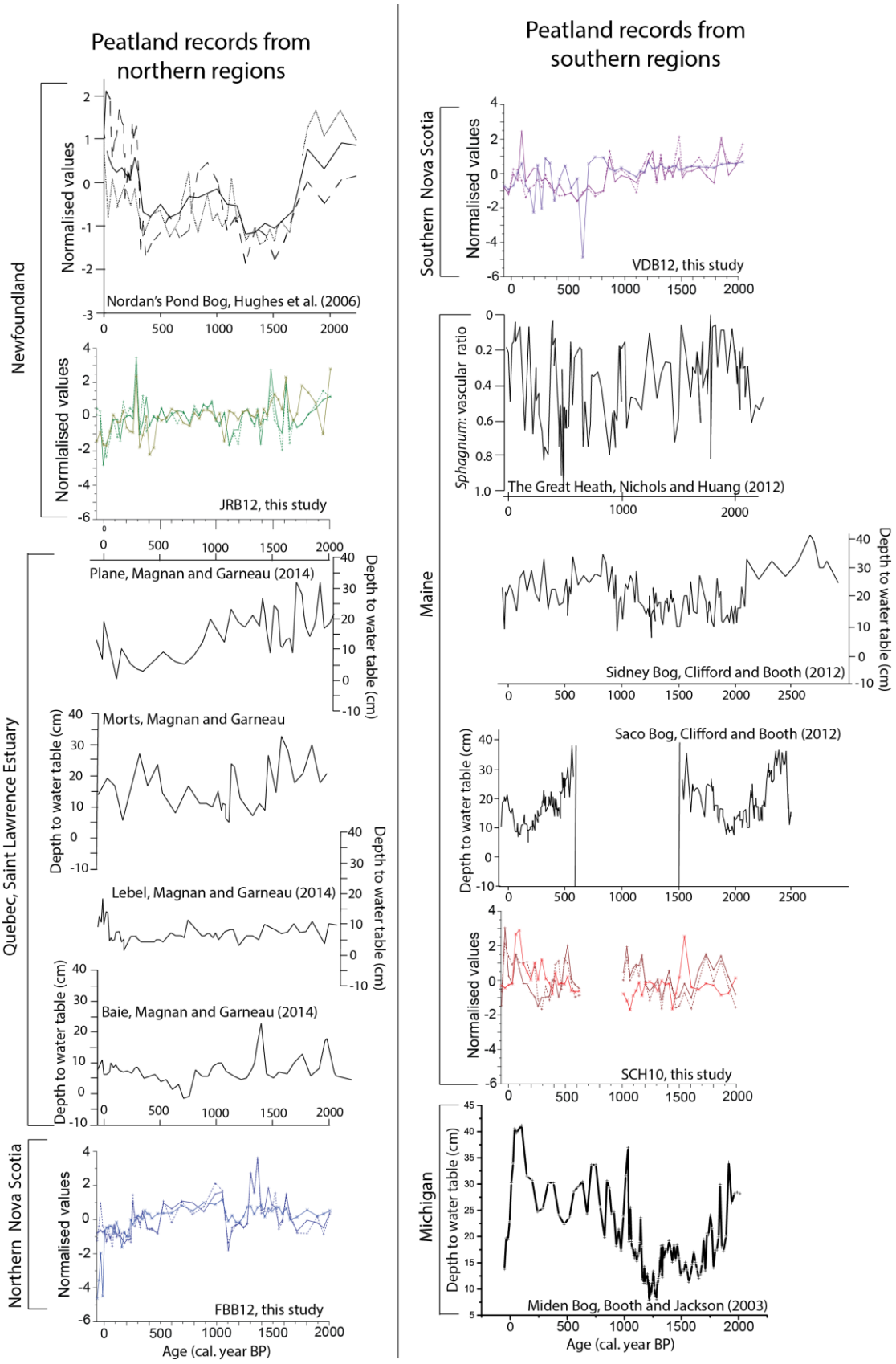

Figure 8.6 Proximal reconstructed peatland water table depths from other published studies (black) and this study (coloured) separated by geographical region. Lower y-axis values indicate wetter conditions whilst higher y-axis values indicate drier conditions.

To assess whether a lag in JRB12 and FBB12 response *ca.* 1450 cal yr BP is a feature generated by chronological uncertainty, the testate amoebae WTD reconstructions generated by the Amesbury *et al.* (2013) transfer function were plotted with full chronological errors in the R software package 'Bacon' (Blaauw and Christen, 2011). All three proxy reconstructions obtained from each site could be treated this way; however, the output would be noisy and thus difficult to compare. Therefore, since the plant macrofossils were potentially complacent around this time (Section 8.1.1) and the transfer functions are in agreement (Figure 8.1), the Amesbury *et al.* (2013) reconstruction was deemed an appropriate record to test the lag in response across the transect of sites. The sustained drying in FBB12 and the JRB12 wet trend around 1500 cal yr BP do occur outside of the chronological uncertainty indicating a true lag in response time (Figure 8.7). The lag between the response of two northern sites and the lack of similar trends in the southern sites at this point potentially indicates that the strength of a more northern climatic driver, such as the Labrador Current or the polar front, increased in strength prior to the MCA.

Peatland hydrological reconstructions from the Gulf of St Lawrence, Quebec, indicate wetter conditions after *ca.* 1600 cal yr BP (Magnan and Garneau, 2014;Figure 8.6), which may represent an earlier response to an increased summer moisture balance evident in the study sites from this thesis. However, when assessing the degree of concurrent changes between the more continental Quebec records and oceanic climates typical of the study region, differences in accumulation rates must be considered: the Quebec records generally accumulate at around half the speed of typical accumulation rates in oceanic raised peatlands. Whilst the Quebec records are often analysed at a higher resolution temporally equitable to the records in this study, the implication of the slower accumulation rate is that each 1 cm sample will encompass a longer time period resulting in longer averaged values of ecological change, and this restricts the testing of concurrent change.

The trend towards wetter conditions that began in the northern peatlands *ca.* 1450 cal yr BP, follows a short-lived shift to drier conditions *ca.* 1500 cal yr BP that extended across the study region into Maine (Great Heath; Nichols and Huang, 2012;Figure 8.6). This increase in summer moisture balance is less clear in more southern sites, which indicate a subtle drying trend from *ca.*

1500 – 1100 cal yr BP in SCH10, VDB12 and Sidney Bog, Maine (Clifford and Booth, 2013;Figure 8.6). This period coincided with cooler conditions in the northwest of the transect represented by increased palsa formation (Payette and Rochefort, 2001; Asselin and Payette, 2006).

Dry conditions were reconstructed from a Massachusetts lake record *ca.* 1200 – 800 cal yr BP (Oswald and Foster, 2011) and *ca.* 1350 – 750 cal yr BP from marine sediments obtained from Chesapeake Bay (Cronin *et al.*, 2010). Conversely, this period corresponds to a wet phase in both JRB12 and FBB12 (more pronounced in the latter more southern site) and in two peatlands from the Gulf of St Lawrence (Baie and Lebel; Magnan and Garneau, 2014;Figure 8.6). The differences in the magnitude of change between the northern sites of this thesis may be influenced by the antecedent conditions (since the JRB12 had a wetter baseline at prior to this shift); therefore further wetting may have a lower threshold response. The 1300 – 1100 cal yr BP wet phase is one of the most pronounced features of the northern sites over the last 2000 and is discussed further in Section 8.3.1.

8.2.1.2 MCA

The two most northerly sites within this study exhibit a more abrupt end to the wet conditions *ca.* 1100 cal yr BP at the onset of the MCA, than VDB12 which has more sustained wet conditions (until *ca.* 900 cal yr BP) and SCH10 which experiences a wet trend within a dry phase (discussed further in Section 8.3.1). The northern sites from this study are therefore drier during the MCA, whilst containing a very subtle wetting trend. A WTD reconstruction from northeastern Newfoundland indicated that water tables rose between 1100 – 800 cal yr BP (Hughes *et al.*, 2006); however, Quebec peatland water tables exhibited a similar response to JRB12 and FBB12 *ca.* 1000 cal yr BP (Magnan and Garneau, 2014; Figure 8.6). The lowered water tables correspond with warmer temperatures across the northern region of the transect in north-western Quebec (Arseneault and Payette, 1997), southwestern Quebec (Paquette and Gajewski, 2013) and northwestern Newfoundland (Rosenberg *et al.*, 2004). Drier conditions at VDB12 are less sustained than JRB12 and FBB12, indicative of shorter-lived MCA climatic conditions; however, the testate amoebae and plant macrofossil reconstructions disagree at this point, generating an uncertain climatic reconstruction. Significant regional drying

was reconstructed using wetland pollen *ca*. 1000 cal yr BP in southern Nova Scotia (Spooner *et al*., 2014); however the degree of persistence of this dry period also remains unresolved.

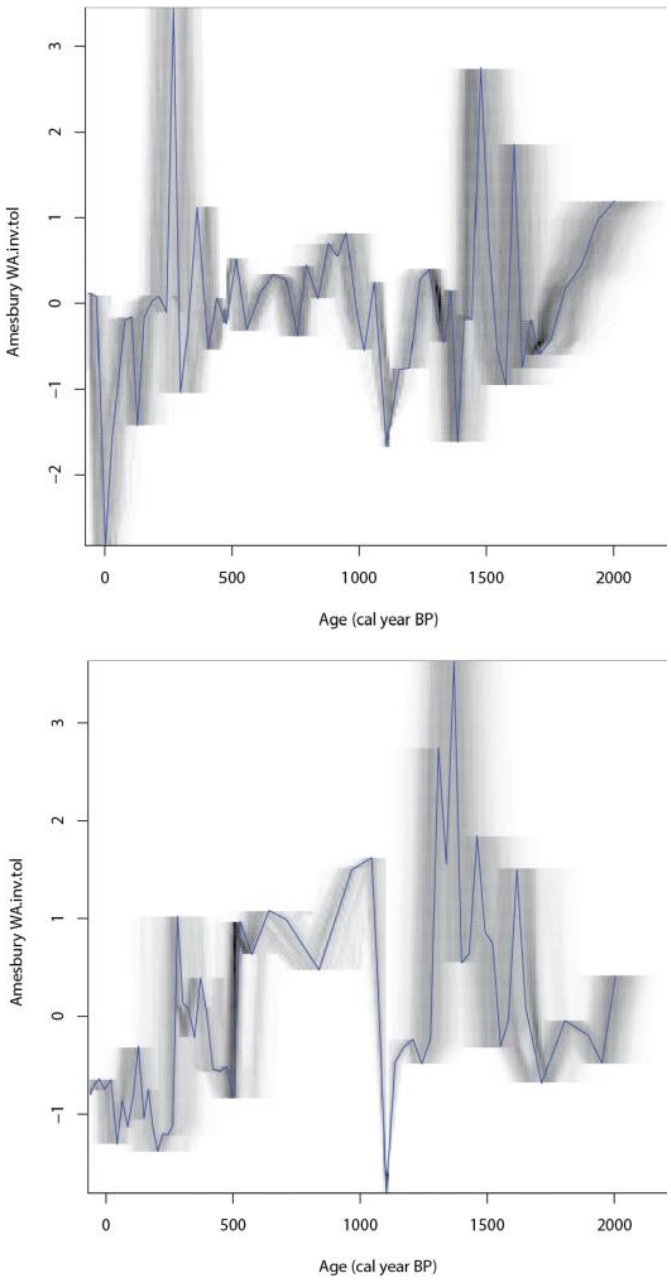

Figure 8.7 Testate amoebae water table reconstructions (using Amesbury *et al*., 2013 training set) for JRB12 (top) and FBB12 (bottom) presented with chronological uncertainty derived from Bacon age-depth Bayesian modelling. Darker narrower periods indicate increased chronological control. Lower y-axis values indicate wetter conditions.

Whilst terrestrial reconstructions indicate an increase in temperatures from *ca.* 1000 cal yr BP, temperature reconstructions from the marine records disagree: cooler occurred conditions in the Laurentian Fan (Balestra *et al*. 2013), the Laurentian Slope (Marchitto and deMonocal, 2003), the Gulf of Maine (Wanamaker *et al*., 2011) and the Bay of Islands (Levac, 2003). Furthermore, there was no evidence of MCA warming in Nova Scotian coastal waters (Keigwin *et al*., 2003). A proposed marine temperature supressing mechanism has been attributed to the persistence of a fresher, colder Labrador Current (Keigwin *et al* 2003), which would be generated under positive NAO. This mechanism may explain the warmer marine reconstructions *ca.* 1350 - 1000 cal yr BP further south in Chesapeake Bay (Cronin *et al*., 2010), since the lower latitude regions will be less influenced by the cold Labrador Current.

The water table reconstructions obtained from the Great Lake regions and western US revealed droughts *ca.* 800 and 700 cal yr BP (Booth *et al*., 2006;Figure 8.6); however, concurrent drought events across the eastern coast of North America are less obvious: drier conditions are evident *ca.* 800 cal yr BP in FBB12 and JRB12, persisting from earlier-MCA conditions but they do not exhibit an obvious dry event. Similarly, the peatland reconstructions in northeastern Newfoundland (Hughes *et al*., 2006), Quebec (Magnan and Garneau *et al*., 2014) and Maine (Clifford and Booth, 2013) demonstrate a temporary lowering of the WTD but not a pronounced dry event (Figure 8.6). These records suggest that the later MCA droughts in western US were more pronounced than the eastern coast of North America and thus likely driven by Pacific originating drivers such as the Pacific Decadal Oscillation (PDO), as postulated by Booth *et al*., (2006). Alternatively, the lack of response in the more eastern records may be highlighting the difficulty of locating dry events within dry baseline periods (see Section 8.1.1).

A pronounced wet shift occurs at VDB12 *ca*. 850 cal yr BP and this increase in available moisture is also reflected in records from Quebec (van Bellen *et al*., 2013; Magnan and Garneau, 2014;Figure 8.6), southwestern Nova Scotia (Neil *et al*., 2014) and Maine (Nichols and Huang, 2012). The MCA is therefore characterised by an initial water table lowering in the northern sites of the transect *ca.* 1000-600 cal yr BP; however, this was short-lived in the southern regions and the Gulf of St Lawrence (Figure 8.6). The wetter conditions in the

southern peatlands coincides with chironomid-inferred 1 °C summer temperature increase between 790 -590 cal yr BP in Nunavut, Canada (Rolland *et al.*, 2009) and a varved lake reconstruction from the west of Baffin Island reveals a rapid 0.5 °C rise in summer temperatures at 755 - 730 cal yr BP until 590 cal yr BP (Moore *et al.*, 2001).

8.2.1.3 LIA

Wet conditions occur *ca.* 600-500 cal yr BP in Maine (SCH10), Nova Scotia (VDB12; FBB12; Lennox *et al.*, 2010), Quebec (Magnan and Garneau, 2014;Figure 8.6) and Newfoundland (JRB12). This period is associated with cooler temperatures across the eastern coast of North America (Rosenberg *et al.*, 2004; Dionne and Richard, 2006; Payette, 2007; Lamarre *et al.*, 2012; Nichols and Huang, 2012; Lafontaine-Boyer and Gajewski, 2014; Spooner *et al.*, 2014). Hydrological changes in Saco Heath during the last 500 years are similar in both the record obtained from the centre of the bog (SCH10; this study) and the edge core (Clifford and Booth, 2013). However, the hydrological responses were less similar pre-MCA, before the fire event (Figure 8.6).

Whilst all regional peatland reconstructions contain wetter conditions during the LIA compared with the MCA, a more subtle difference in the response of the northern and southern peatlands occurs *ca.* 500 cal yr BP: JRB12 and FBB12 exhibit a pronounced wet phase (*ca.* 500-400 cal yr BP) whilst VDB12 contains peak wet conditions (following the later MCA gradual wetting trend) but begins to dry and SCH10 has become drier. Wetter peat conditions in the northern region of the transect are confirmed by the elevated peatland WTD in Quebec *ca.* 400 – 140 cal yr BP (Lamarre *et al.*, 2012), which coincide with cooler reconstructed temperatures across Quebec (Arlen-Pouliot and Bhiry, 2005; Paquette and Gajewski, 2013).

The WTD of JRB12 lowered to *ca.* 300 cal yr BP, accompanied by a drying in Quebec (Magnan and Garneau, 2014) and a similar, but reduced, drying response is evident in FBB12 until *ca.* 250 cal yr BP (with overlapping chronological uncertainty; Figure 8.7). This corresponds with the coolest reconstructed temperatures over the last 1400 years in southern Quebec (*ca.* 350 – 250 cal yr BP; Lafontaine-Boyer and Gajewski, 2014). FBB12 and JRB12 then exhibit a wet trend, whilst drier conditions persist in Quebec (Magnan

and Garneau, 2014), north eastern Newfoundland (Hughes *et al.*, 2006), Maine (this study; Nichols and Huang, 2012) and Michigan (Booth *et al*, 2006). Between 200-100 cal yr BP, the SCH10 and VDB12 dry whilst FBB12 and JRB12 exhibit a wetting trend.

8.2.1.4 Summary of peatland expression of climate change over the last 2000 years

A comparison of the four water table reconstructions indicates that the trends in the two northern sites (JRB12 and FBB12) are the most similar over the last 2000 years (Figure 8.8, Table 8.2). The greater similarities between the northern sites may suggest that they are most acutely influenced by the dynamics of the Labrador Sea, whilst the characterisation of more southern climate change suggests that the water balance at SCH10 is mainly dictated by the associated strength of the Gulf Stream. Therefore, VDB12 is likely responding to a combination of a more delayed northern polar waters signal and the strength of the Gulf Stream (Table 8.2). These trends support the hypothesis that dominant MCA-LIA expression of climate change across eastern North America was determined by the NAO and the AMOC, accepting the first of the four hypotheses obtained from the literature review and outlined in Section 2.10.

The peatland responses are regionally inconsistent from *ca.* 300 cal yr BP to present. This may represent a complex pattern of climatic change during this period or reflect the complication of extracting a climate signal within more recently deposited peat, which is subject to active surface processes and weakened ^{14}C chronological control. Additional peat records are therefore required from this time period, with better dating control (such as the inclusion of ^{210}Pb dating of the surface peat) to confidently characterise the peatland response to environmental change over the last *ca*. 300 cal yr BP. There is also a lack of reliability between regional peatland responses between *ca*. 2000 - 1600 cal yr BP, representing variable or unstable climatic conditions.

It is clear from the comparisons of reconstructed environmental change that a consistent climatic signal does not occur throughout the traditionally defined MCA and LIA timings. Rather these periods contain several phases of environmental change, which may be influenced by different aspects of the

local and global climate systems. Within-core peatland responses to the MCA appear to be less variable than the LIA and this is particularly evident in environmental records from Northern Nova Scotia and Newfoundland. However, this contradicts assertions that the MCA was characterised by unusually high hydroclimatic variability relative to the surrounding periods (Hughes and Diaz, 1994; Graham *et al.*, 2010). The variability was decadal to centennial scale in North America (Cook *et al.*, 2004; Booth *et al.*, 2006; Seager *et al.*, 2007; Cook *et al.*, 2010) therefore, perhaps the shorter end of this temporal scale of variability was not detected in the sampling resolution of this study. Alternatively, the stability in northern peatland water tables may indicate that climatic conditions in northern regions of eastern North American were more stable than elsewhere or that the peatlands are less responsive in drier conditions (Section 8.1.1). Obtaining high-resolution direct reconstructions of precipitation and temperature from this region is required to test the reason for perceived increased MCA peatland stability.

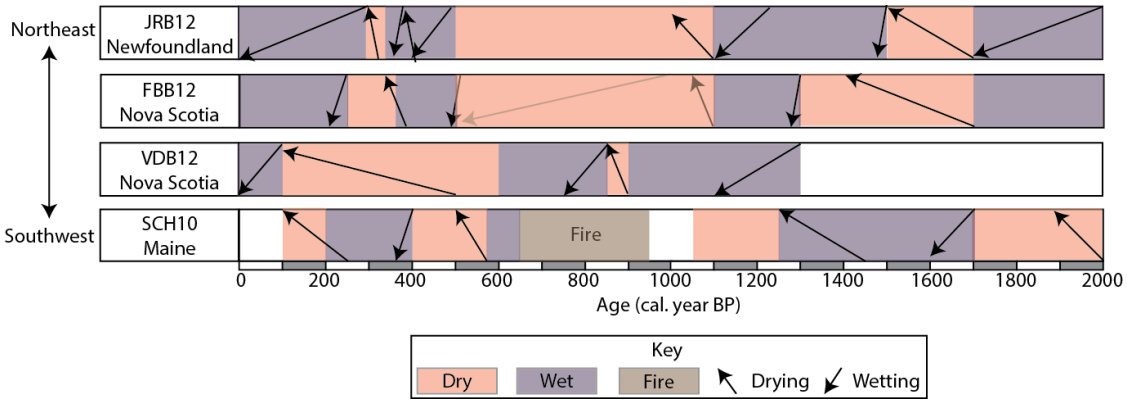

Figure 8.8 Summary of the main reconstructed water table conditions (pink represents dry and purple represents wet) with directional shifts in wetness indicated by arrows. Sites arranged from northeast (JRB12; top) to southwest (SCH10; bottom).

Table 8.2 Summary of peatland responses reconstructed within this study that are associated with the MCA and LIA

Age (cal yr BP)	**Period**	**Reconstructed peatland response**
ca. 1500 - 1100	Pre-MCA	Stronger northern peatland wetting response
ca 800 – 600	MCA	Northern sites dry and southern sites more variable
ca. 600 – 400	LIA	Sites become wetter (timing of changes not contemporaneous)
*ca*300 -200	LIA	Northern sites drier whilst southern sites wetter
ca. 200 – 100	LIA	Northern sites of are wetter whilst southern sites are drying

8.2.2 Comparing proxy records with climate drivers

A comparison of the terrestrial palaeoclimate records from eastern North America, the marine records from the North Atlantic, the ice core data from Greenland and terrestrial records from western Europe (Figure 8.9) reveals warmer, drier conditions occurred *ca.* 1000 cal yr BP, at the start of the MCA, and cooler wetter conditions occurred *ca.* 500 cal yr BP, during the LIA. This transatlantic expression of environmental change highlights the important role that the North Atlantic plays in modulating climate. However, it is clear from the compilation of palaeoenvironmental records that the regional expression of climate change is variable throughout the last 2000 years.

Isolating the effect of dominant climatic drivers from environmental archives is difficult owing to system noise masking the prominent signal and internal feedback mechanisms or non-climatic drivers that may modulate reconstructions from environmental archives. Reconstructed strengths of individual climatic drivers are compared below with the peatland WTD reconstructions obtained within this study to identify likely dominant influences (Figure 8.10). It is hypothesised that the WTD reconstructions obtained within this thesis are predominantly driven by changes in the NAO and AMO based on the conclusions obtained from Section 8.2. No significant correlations existed between any of the peatland WTD reconstructions and any of the climatic drivers throughout the entirety of the records. However, the influence of different drivers on peatland environmental conditions may vary over time and visual comparisons of the trends in environmental reconstructions and strength of climatic drivers may reveal dominant forces at different points within the record.

8.2.2.1 External forcing

Solar forcing has been postulated as a driver of peatland water table change across this study region, in Maine, (Nichols and Huang, 2012) and Newfoundland, (Hughes *et al*., 2006). Solar forcing is reduced *ca*. 500 and 1300 cal yr BP, which coincides with observations of higher peatland water tables. The similarities between solar activity and WTD are especially pronounced at FBB12 (Figure 8.10). The solar influence is elevated at *ca*. 1650, 650, 350, 200 cal yr BP, occasionally coinciding with drier periods, and sustained elevated solar levels occur between *ca*. 1000 and 700 cal yr BP,

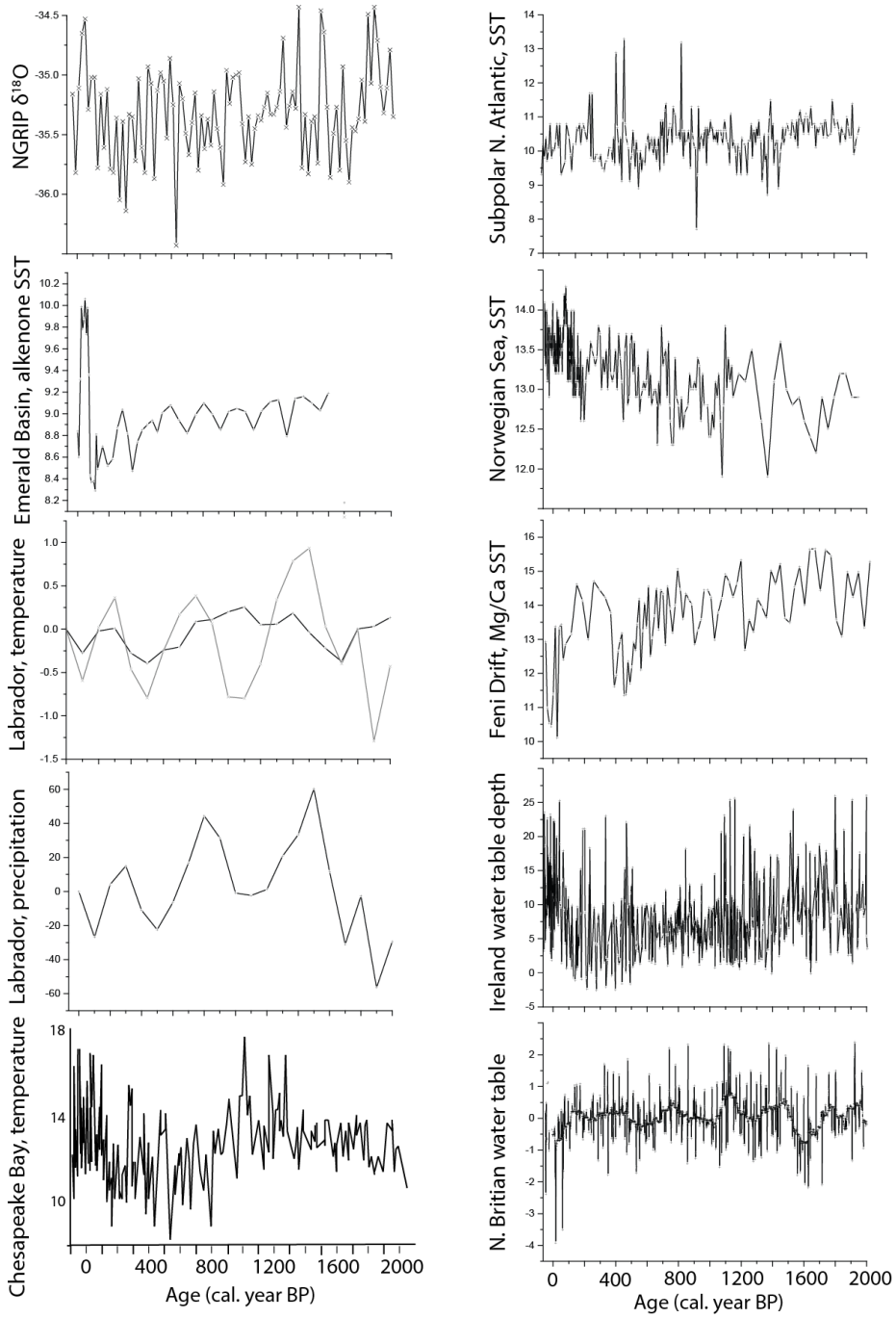

Figure 8.9 Palaeoenvironmental records obtained from around the North Atlantic region: more western North Atlantic regions in left panel, more eastern regions in right panel.

Lower y-axis values indicate cooler and/or wetter conditions depending on the proxy, whilst higher y-axis values indicate warmer and/or drier conditions. Left panel: NGRIP δ18O from ice core (NGRIP members, 2004); Emerald Basin alkenone sea surface temperature reconstruction (Keigwin *et al.*, 2003); Labrador pollen temperature and precipitation reconstructions (Viau *et al.*, 2009) grey line: January temperature anomalies; black line: July temperature anomalies; Chesapeake Bay Mg/Ca temperature reconstruction (Cronin *et al.*, 2003). Right panel: Subpolar North Atlantic alkenones temperatures (Sicre *et al.*, 2011); Norwegian radiolarians sea surface temperatures (Dolven *et al.*, 2002); Feni Drift sea surface temperature (Mg/Ca of planktonic foraminifera (Richter *et al.*, 2009); compilation of Irish (Swindles *et al.*, 2013) and British (Charman *et al.*, 2006) peatland water table depth reconstructions).

which coincide with drier conditions (Steinhilber *et al.*, 2009; Figure 8.10). Therefore, solar forcing does appear to be influential in shaping the peat hydrological responses over the last 2000 years in the study sites. Increased volcanic activity has been postulated to assist decreased solar activity with the triggering of the LIA (Section 2.8.3). However, volcanic activity does not correspond with changes in the records obtained within this thesis (Zielinski *et al.*, 1994; Figure 8.10).

8.2.2.2 Atlantic climate drivers

The indices of the Atlantic multidecadal oscillation (AMO) represent temperature differences in the North Atlantic, reflecting changes in the Atlantic Meridional Overturning Circulation (AMOC). The observed index does not extend beyond 400 years; however, during this time there are similarities between the temperature of the North Atlantic and the peatland responses from this study (Figure 8.10): when the AMO becomes more positive, the peatlands become drier, although the similarities are less obvious in SCH10. This supports the hypothesis of Booth *et al.* (2006) that the AMO, and associated North Atlantic warmth, is contributing to the expression of climate change in North America as dictated by the strength of the Gulf Stream and the Labrador Current.

The NAO is positive during the MCA until *ca.* 900 - 600 cal yr BP before decreasing towards the LIA, when it fluctuates but remains in a decreasing trend until *ca.* 200 cal yr BP (Cook *et al.*, 1998; Figure 8.10). Therefore, it appears likely that the NAO was influential in driving the peatland responses to MCA-LIA change in the study region, supporting conclusions from Section 8.2. The NAO was suggested to be the driver of mid-late Holocene peatland water table changes based on the comparison of a WTD reconstruction from Maine (Nichols and Huang, 2012) with a regional record for storminess (Noren *et al.*, 2002) and thus NAO activity.

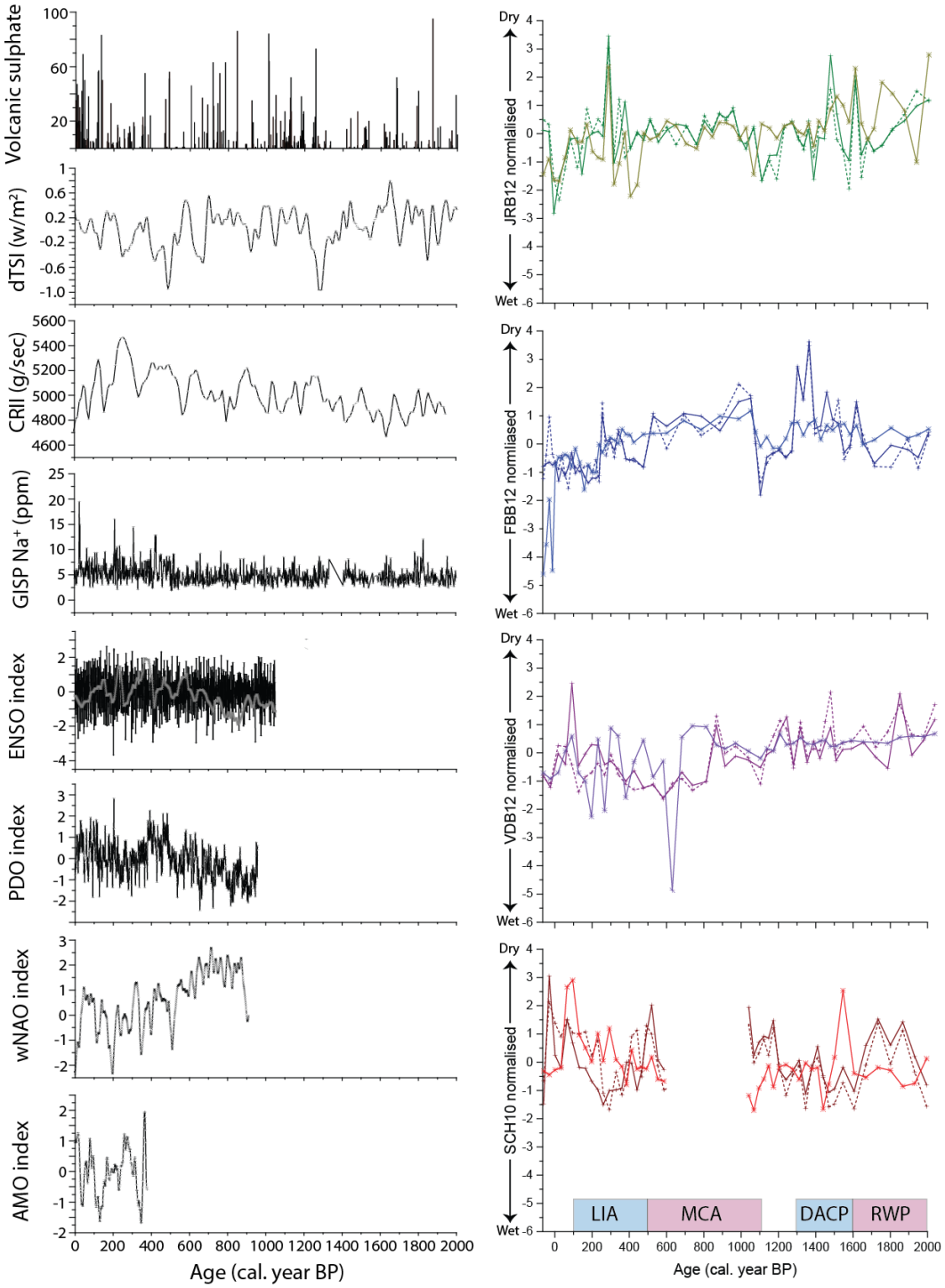

Figure 8.10 Reconstructed characteristics of climatic drivers (left panel) and reconstructed peatland WTD obtained within this study (right panel).

Approximate timings of RWP, DACP, MCA and LIA indicated for comparative purposes. Volcanic sulphate data obtained from GISP2 ice core (Zielinski and Mershon, 1997); dTSI represents total solar irradiance (Steinhilber *et al.*, 2009); CRII represents cosmic ray induced ionization rate (Usoskin and Kovaltsov, 2008); Na+ content of the GISP2 ice core as a proxy of sea salt aerosol loading of the atmosphere over Greenland (O'Brien *et al.*, 1995); ENSO index reconstruction (Li *et al.*, 2011); PDO (MacDonald and Case, 2005); wNAO (Cook *et al* 1998), AMO (Gray, 2004).

8.2.2.3 Pacific climate drivers

The link between PDO and the reconstructed peatland environmental change is less consistently clear compared with the records of Atlantic drivers (Figure 8.10). However, the trough in PDO around 300 cal yr BP does coincide with wet conditions at SCH10 and drier conditions in FBB12 and JRB12 (Figure 8.10). There does not appear to be an obvious consistent peatland response to changes in ENSO, (Figure 8.10), although the trough around 850 cal yr BP does coincide with a move to wetter conditions in VDB12 and smaller, wetter responses are evident in the more northern sites.

8.2.2.4 MCA-LIA drivers responsible for climatic change in eastern North America

The NAO is attributed as a driving influence of the MCA-LIA climate (e.g. Trouet *et al*., 2009; Moffa-Sánchez *et al*., 2014) and has been postulated as the driver of peatland WTD change as reconstructed from other regions of eastern North America (Nichol and Huang, 2012) and Europe (e.g. Charman *et al*., 2012). The similarities between the NAO index and the WTD reconstructions obtained within this study indicate that the NAO is instrumental in driving WTD change at the study sites, as supported by the patterns of reconstructed MCA-LIA climate change (Section 8.2). The persistently positive NAO generated wet winters and dry summers during the MCA, whilst the predominantly negative NAO during the LIA generated comparatively drier winters and wetter summers (Trouet *et al*., 2009; Nichols and Huang, 2012; Charman *et al*., 2012). The NAO therefore contributes to a major shift in precipitation seasonality during the MCA-LIA transition, reflected in the generally drier peatland response during the MCA in the study sites compared with the wetter peatland response in the LIA.

Peat records from the Great Lake region (Minnesota and Michigan) indicate that a late Holocene extreme drought event was centred on 1000 cal yr BP (Booth *et al*., 2006; Figure 8.6). Similar drought periods have also been detected further north in Ontario (Booth and Jackson, 2003) and in many palaeoclimatic records extending across the western US (Cook *et al*., 2004). Since this drying extended across the North American content into Chesapeake Bay (Cronin *et al*., 2003; Willard *et al*., 2003), Maine (Nichols and Huang, 2012, this study), Nova Scotia (this study; although to a lesser extent

in VDB12), Quebec (Magnan and Garneau, 2014) and Newfoundland (Hughes *et al.*, 2006, this study), the hypothesis that Pacific and Atlantic originating drivers contributed the MCA climatic expression (Booth *et al.*, 2006) is supported. The persistence of the MCA drought in the northern regions, compared with the more southern and continental sites suggests that the cooler Labrador Sea conditions (driven by increased Westerly winds during the positive NAO) were likely responsible for the persistence of MCA climatic conditions.

The wetter conditions at the start of the LIA on the eastern coast of North America (*ca.* 600 – 400 cal yr BP) are replicated on the western seaboard of the North Atlantic. Suggests mechanisms contributing to this change are solar variations and the North Atlantic Deep Water (NADW) formation, driving the cold conditions (e.g. Charman, 2010; Swindles *et al.*, 2013; Figure 8.9). The peatland expression of the LIA climate change was more prominent than the MCA in the western regions of the North Atlantic (Figure 8.9). Peatland records from Ireland indicate a second strong wetter or colder LIA pulse *ca.* 250 cal yr BP. Whilst this wet phase is present at some of the eastern north American peatlands in this study (e.g. SCH10), the timing differs in the sites further north. Cooler conditions associated with this second LIA pulse register in the Greenland Ice Core (NGRIP) and the Gulf of Maine; however, they are not prominent in the oceanic records from the eastern Atlantic (Figure 8.9). This may suggest that some of the forcing behind the second LIA phase originates in the western North Atlantic, potentially in the Labrador Sea associated with increased ice rafting. This hypothesis is supported by decreasing terrestrial temperature reconstructions obtained from Labrador during this time period (Viau *et al.*, 2006; Figure 8.9).

Whilst the NAO and AMOC do appear to be associated with climatic reconstructions obtained within this thesis, the relative changes between the northern and southern sites do not fully support the previous hypothesis that MCA-LIA associated environmental change would be more prominent in the southern sites than the northern sites (Section 8.2). Average LIA reconstructed water tables are higher in the northern site compared with the southern sites of this study; however, the LIA WTD are variable and the extent of the peatland WTD change in the north likely exceeds that simply driven by enhanced evaporation. Therefore, precipitation is a potential limiting factor

dictating peatland WTD changes during the MCA-LIA and it is likely that regional MCA-LIA precipitation patterns across the eastern seaboard are more complex than currently appreciated. This hypothesis may be tested in future studies combining geochemical and palaeoecological proxies, which may be able to isolate the relative roles of precipitation and temperature.

8.3 Tephra isochrons: testing the synchroneity of environmental change

The presence of well-defined tephra horizons provides the dating resolution required to assess the synchroneity of environmental responses to climatic change across sites in different regions (e.g. Langdon and Barber, 2004; Lane *et al.*, 2012). Synchroneity of environmental change may be assessed based on the timing, duration, shape and magnitude of the recorded environmental response (Blaauw *et al.*, 2007; Rohling and Pälike, 2005).

8.3.1 Utilising the White River Ash (WRA): transatlantic comparisons of environmental change

The WRA tephra was detected in all four sites within this study and one existing Newfoundland peat record (Pyne-O'Donnell *et al.*, 2012). Recently, the WRA has been correlated with the 'AD 860B' tephra found in Greenland and western Europe (Jensen *et al.*, 2014); therefore, this tephra isochron from Mount Bona-Churchill, Alaska provides the ideal opportunity to test the synchroneity of environmental change across the Atlantic region. The WRA was deposited in AD *ca.* 846-847 (Coulter *et al.*, 2012), thus it can be used to identify of any lead and lags in the environmental response associated with the onset of the MCA.

Environmental reconstructions are obtained from the testate amoebae and plant macrofossil records obtained within this study (Chapter 6) and age models have been constructed in 'Bacon' using a combination of tephra and radiocarbon measurements (Chapter 5). Nordan's Pond Bog, eastern Newfoundland is currently the only published record from the eastern coast of North America with the tephrostratigraphies and environmental reconstructions obtained from the same core (**Error! Reference source not found.**). Hydrological conditions have been reconstructed using testate

amoebae inferred water table depths (Hughes *et al*., 2006) and $\delta^{18}O$ from *Sphagnum* cellulose (Daley *et al*., 2009). The age-depth model has been remodelled in 'Bacon' to combine the full tephrochronology (Pyne O'Donnell *et al*., 2012) with the radiocarbon measurements (Daley *et al*., 2009).

The comprehensive Holocene Tephra Database for Northern Europe (Swindles *et al*., 2011) reveals that the WRAe has been identified in one Scandinavian, three German, one Scottish and fourteen Irish published records. However, of these nineteen sites, only three records have completed environmental reconstructions and tephra analysis on the same core: Langlands Moss, Scotland (Langdon and Barber, 2002) and Glen West and Dead Island, Northern Ireland (Swindles *et al*., 2013). All three sites are peatlands and hydrological reconstructions have been obtained using testate amoebae water table transfer functions. Chronologies have been remodelled in Bacon using the improved age for the 'AD 860B'/WRAe tephra (AD 846-847; Coulter *et al*., 2012) for this discussion. The WRAe was also identified in NGRIP (Coulter *et al*., 2012); therefore the oxygen isotope record based on the Greenland Ice Core Chronology 2005 (GICC05; Vinther *et al*., 2006) can be used in the transatlantic comparison (**Error! Reference source not found.**).

WRAe tephrochronologies have been obtained in other European sites; however, the water table depth reconstructions for the same sites have been completed using different cores. Since this discussion focuses on comparing the synchroneity of environmental change, the data cannot be transferred across cores with adequate accuracy. An example of such a site is Dosenmoor, Germany, which contains the WRAe tephra (van den Bogaard *et al*., 2002) and has published peatland hydrological reconstructions (Barber *et al*., 2004). Tephra analysis could be completed retrospectively on the Barber *et al*. (2004) cores to widen the Atlantic comparison. The WRAe is also detected on the western coast of North America as a proximal ash deposit, presenting an opportunity to extend environmental comparisons across North America and the North Atlantic. However, signals of environmental change containing the proximal WRAe are limited by the magnitude of ashfall and associated disturbance to the environmental proxies and archives. Disentangling the effect of proximal tephra deposition and environmental change is complex and is beyond the scope of this discussion.

The environmental reconstructions obtained within this thesis reveal that the WRAe coincides with the end of a two-step trend towards wetter conditions in JRB12, FBB12 and VDB12 (**Error! Reference source not found.**). A dry shift occurs after the WRAe in all three sites. The most southerly site in this thesis, SCH10, has a more complex environmental response during the study period, with divergences in the proxy records (Chapter 6). However, the testate amoebae reconstructions indicate that the WRAe was also deposited during a wetting trend but, unlike the other study sites, the wetting trend continues slightly beyond the tephra deposition. SCH10 prominently dries ahead of the wet trend; therefore, the WRAe is not deposited in a wet phase (as was the case for the other sites) but rather a wetting trend within a dry phase. The SCH10 wetting trend at the WRAe deposition does contain the two-step trend event in the other sites; therefore, it is likely a delayed but more sustained wetting period in the south. The lower magnitude and sustained wet response at SCH10 may be indicative of a weaker climate driving force or it may have been influenced by the drier antecedent conditions.

The Nordan's Pond record from northeast of Newfoundland indicates a different environmental response from the sites studied within this thesis: the testate amoebae record indicates that the peatland is in a wet phase at the WRAe deposition, although this is less pronounced than the sites located further southwest. The wet conditions persist (to *ca*. 1003 cal yr BP, before drying to *ca*. 923 cal yr BP) beyond conditions reconstructed further south. The *Sphagnum* oxygen isotope values from Nordan's Pond indicate that the WRAe is deposited at the end of a trend to colder surface air temperatures, which are then sustained beyond the tephra deposition. It is possible that the lag in response between Nova Scotia, southwestern Newfoundland and Nordan's Pond is a feature of the lower sampling resolution in the latter record. However, the lag may represent a more sustained driver generating the cool, wet peatland conditions further north in eastern Newfoundland. Possible driving mechanisms behind the wet conditions prior to the tephra deposition may include changes strength of the Labrador Current, the extent of sea ice, the extension of the polar front and the Atlantic storm track, or a combination of these factors which may be influenced by the NAO and the AMOC (Section 2.7.2.3). Future studies could increase the resolution of the

water table reconstructions from Nordan's Pond Bog or other proximal sites to test the hypothesis.

The oxygen isotope ($\delta^{18}O$) record from Nordan's Pond indicated a shift to cooler conditions *ca.* 200 years before the cooling associated with the abrupt '8.2 ka event' was recorded in the Greenland ice core (Daley *et al.*, 2009); however, a similar lag does not exist during the smaller magnitude cool phase associated with the WRAe deposition. The resolution of the NGRIP $\delta^{18}O$ record (20 years) reflects local surface air temperature with the removal of noise (North Greenland Ice Core Project Members, 2004). The WRAe is deposited towards the end of a cooling trend to more negative values in the NGRIP $\delta^{18}O$ record which begin in 1310 cal yr BP (North Greenland Ice Core Project Members, 2004). The cold conditions do fluctuate beyond the WRAe deposition before the abrupt transition to warmer conditions (from 1070-1030 cal yr BP) that are sustained until 950 cal yr BP. The NGRIP record therefore appears to warm ahead of Nordan's Pond, which may reflect the reduced influence of the cold conditions of the Labrador Sea in Greenland compared with Newfoundland. Alternatively, the suppressed temperature in eastern Newfoundland may be influenced by regional microclimates, since fog banks dominate in this region during spring and early summer (McManus *et al.*, 1991).

The trends in the three European testate amoebae reconstructions containing WRAe are similar to those from eastern North America, indicating that the WRAe was deposited at the end of a wet-shift that precedes and follows drier conditions. The drier conditions before the WRAe are more sustained than the subsequent temporary dry trend in the Dead Island record (Swindles *et al.*, 2013). It is unclear whether this brief subsequent drying followed by a long term wetting trend is characteristic of the European records since the other records do not extend beyond this period in adequate resolution. The dry conditions following the WRAe deposition are sustained, although less pronounced in northern Nova Scotia and Newfoundland and shorter lived in southern Nova Scotia.

In each of the European records, the WRAe was deposited after the peak wet conditions associated with the wet phase; however, the subsequent move to drier conditions was quicker in Glen West (Swindles *et al.*, 2013) than the

other two European and eastern North American peatlands. This may indicate that the Glen West peatland was more sensitive to drying than the other sites and presents the possibility that environmental conditions changed earlier in the western Atlantic. However, this earlier change is not supported by the other European peatlands. Furthermore, the WRAe is deposited near to the surface of this site, therefore, conditions recorded after the tephra deposition may be influenced by processes within the active peat layer or the signal may be reworked by more recent environmental change.

The peatland conditions at the point of WRAe deposition in Ireland were the second of two abrupt shifts to wetter conditions separated by an abrupt pronounced shift to drier conditions (Swindles *et al*., 2013). The Langland Moss water table reconstruction (Langdon and Barber, 2005) is at a lower sampling resolution than the Irish sites, thus higher resolution sampling would be required to confirm this feature in the Scottish record. The two-step feature is also present in the records from eastern North America; however, the interrupting dry shift is less pronounced in the west Atlantic records compared with the Irish records. This may indicate that the Irish records are more sensitive to dry conditions, or that this first part of the two-phase wet shift was less prominent on the eastern Atlantic compared with the western Atlantic.

The transatlantic peatland response to environmental change at the time of the WRA deposition appears to be a concurrent end to a centennial scale wet phase, with the exception of the Nordan's Pond Bog record in which the wet conditions are more sustained. Northern Ireland may have been the first of the studied regions to end of the wet phase as indicated through the record generated at Glen West peatland; however, this is not confirmed from the other sites located east of the Atlantic Ocean. The peatlands from this thesis exhibit a drying trend that leads the end of the colder period and subsequent abrupt warming evident in Greenland, although Greenland appears to be warming before the northeastern Newfoundland Nordan's Pond record. Since the response is more sustained in northeastern Newfoundland, followed by Greenland then the rest of the sites further south, these potential response lags may suggest that the driver of the cool conditions is originating in the Labrador Sea and could be attributed to the Labrador Current or presence of sea ice in this area. Alternatively, the leading responses may indicate greater

site sensitivity to environmental change. Increasing the number of future study sites in this region is, therefore, a priority to test the potential drivers of climate change around AD 846-847.

The northern origin of the climate driver could explain the peatland response in Maine: areas further south would be less influenced by changes in the Labrador Current than the more northern sites, generating a more supressed, delayed peatland response. There is also potential for a more sustained wetting trend in Maine than in sites further north since the site would be less affected by the driver's weaker influence and autogenic processes could continue the wetting trend. Alternatively, the peatlands further north may have been closer to a threshold response during the wetter phase than was evident in SCH10. The more northern sites may have required a smaller magnitude of warming to generate a larger response. Conversely, the different response in Maine may indicate that the interactions of a combination of drivers are influencing climatic conditions at this point, or it could also be indicative of the larger wet-shift required to alter communities under the more severe water table deficit. More records containing both the WRAe and environmental reconstructions on the same cores from Maine are required to test these hypotheses.

Whilst tephra facilitates the investigation of environmental synchroneity and teleconnections, the accuracy of the comparisons of the environmental response is dependent on the temporal sampling resolution. Therefore both chronological and stratigraphic precision is required for the comparison of environmental synchroneity. This echoes conclusions from a study on the mid-Holocene Hemlock decline in North America. The selected sampling density was shown to have a critical impact on the age of the decline since aliasing is generated by lower resolutions that incorporate earlier reconstructed troughs within the record's fluctuations (Liu *et al.*, 2012). The importance of adequate sampling resolution may have been overshadowed by the recent emphasis placed on the need to improve chronological accuracy and precision. Sampling at the Nyguist rate, a sampling resolution of twice the frequency in the original signal of interest, may avoid aliasing (Shannon and Weaver, 1949). However the rate of accumulation must also be considered since the interval between observations in water table reconstructions is not

constant and the sample thickness may encompass different time periods as the accumulation rate varies (Lui *et al*., 2012)

The comparison of environmental responses at the time of the WRAe deposition indicates that a wet-shift occurred in the peatlands across the Atlantic before the onset of the MCA. The results from this comparison indicate that the changes Labrador Sea region contributed to this wet event prior to the MCA. Therefore, it is hypothesised that similar drivers to those active in generating the LIA are driving climatic change before the MCA. The NAO was negative before the MCA (Cook *et al*., 2002), which decreased Westerly winds, allowing sea-ice formation and a weakened convection, thus reducing the strength of the Gulf Stream and AMOC. Once the NAO became more positive and the AMOC strengthened at the onset of the MCA, the drier and warmer conditions may then have been sustained by other features of the climate system, such as the PDO (as indicated by similar hydroclimatic responses across North America; Booth *et al*., 2006). The hypothesis that the NAO and AMOC drove climatic changes originating in the Labrador Sea could be tested within future studies by increasing the sampling resolutions to match the highest resolution available (i.e. NGRIP, 20 years) in each record if possible. Furthermore, environmental reconstructions from more records containing the WRAe could be included to further the investigation, particularly in the Maine region, northeastern Newfoundland and Europe.

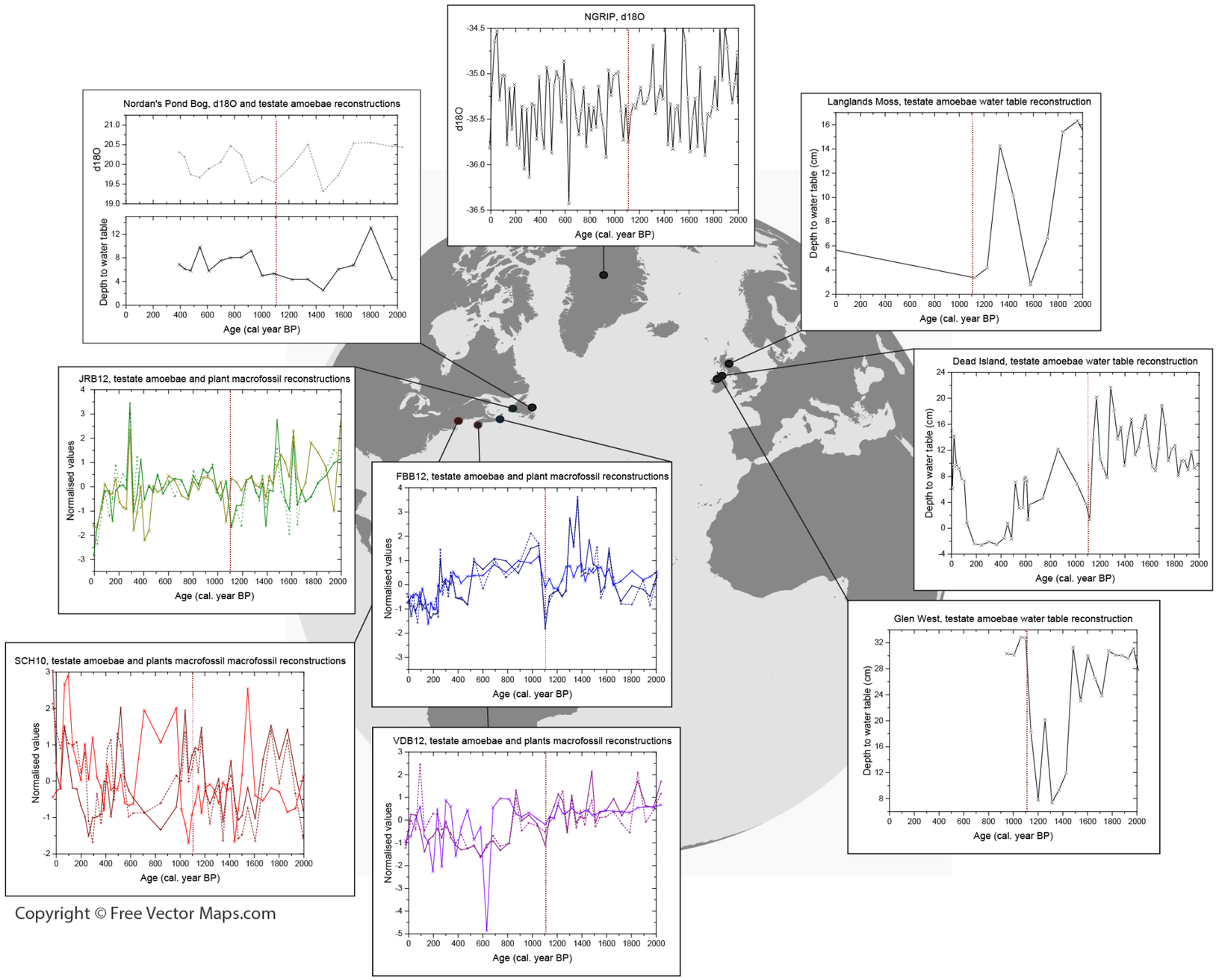

Figure 8.11 Transatlantic comparison of environmental reconstructions at the time of the WRA.
Coloured reconstructions represented record generated within this thesis whilst other published reconstructions are in black (age models have been re-modelled in Bacon). Nordan's Pong Bog: Daley *et al*. (2009; top) and Hughes *et al*. (2006; bottom); NGRIP: Vinther *et al*. (2006); Langlands Moss: Langdon and Barber (2002); Dead Island and Glen West: Swindles *et al*. (2013).

8.3.2 Mount St Helens isochron

The Mount St Helens We cryptotephra (AD 1482) is more regionally confined than the WRAe, being detected only in the northern two records of this study and Nordan's Pond Bog (Pyne-O'Donnell *et al.*, 2012). This spatial distribution may be indicative of a patchy tephra fall-out distribution pattern (e.g. Davies *et al.*, 2010) or it may show that the southernmost limit of detectable cryptotephra deposition for this eruption lies close to Newfoundland. If the cryptotephra did not extend further south, it reveals that the atmospheric circulation differs between the northern and southern study sites in this thesis. The negative NAO corresponding with MSH deposition has weaker Westerly winds, allowing southern winds to extend northwards. The northerly MSH tephra distribution may have therefore been limited by weakened Westerlies and restricted northerly influence. Analyses from more sites at the southern end of the study transect are required to distinguish between the southern limit and patchy distribution hypotheses.

The MSH We tephra was deposited in 468 cal yr BP, at the beginning of the LIA. At the point of tephra deposition, Nordan's Pond Bog, JRB12 and FBB12 were in a wet phase as $\delta^{18}O$ values indicate temperatures began to warm (Figure 8.12). The wet shift is more pronounced in FBB12 than the other two more northern sites and the wetter conditions persist until *ca.* 375 cal yr BP. Whilst the MSH tephra was not found at the southern sites, the testate amoebae reconstructed can be presented with full chronological uncertainties to compare environmental characteristics (Figure 8.12). The most southerly site, SCH10, also became wetter at this point, whilst VDB12 contained a long term fluctuating drying trend although experienced the wetter phase earlier than the other sites.

Currently, too few sites have identified the MSH cryptotephra to identify potential drivers of environmental change around this time; therefore, efforts should focus on obtaining more records to understand the temporal and spatial pattern of LIA climate change in eastern North America. The MSH isochron, located at the start of the LIA, highlights the climatic variability during this period: the northern sites appear to become wetter near the start of the LIA, become drier and then become wetter again. This lack of a

consistent climate trend containing a cold wet period that was temporarily interrupted by warming, drying trends, may complicate the characterisation of LIA across sites with weak chronological control.

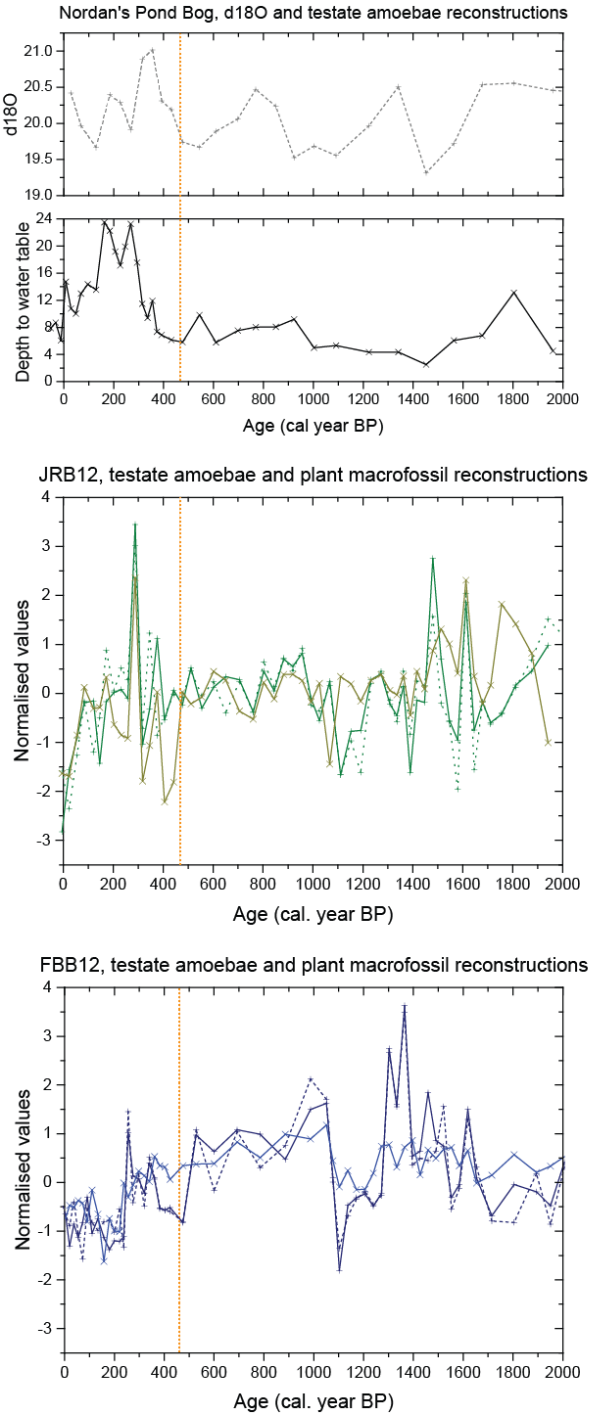

Figure 8.12 Peatland environmental change at the deposition time of the MSH We tephra. Top: records from Nordan's Pond Bog (Newfoundland; Hughes *et al*. 2006; Daley *et al*. 2010); middle: JRB12 (southwestern Newfoundland; this study); lower: FBB12 (Nova Scotia; this study). Lower y-axis values indicate wetter/colder conditions.

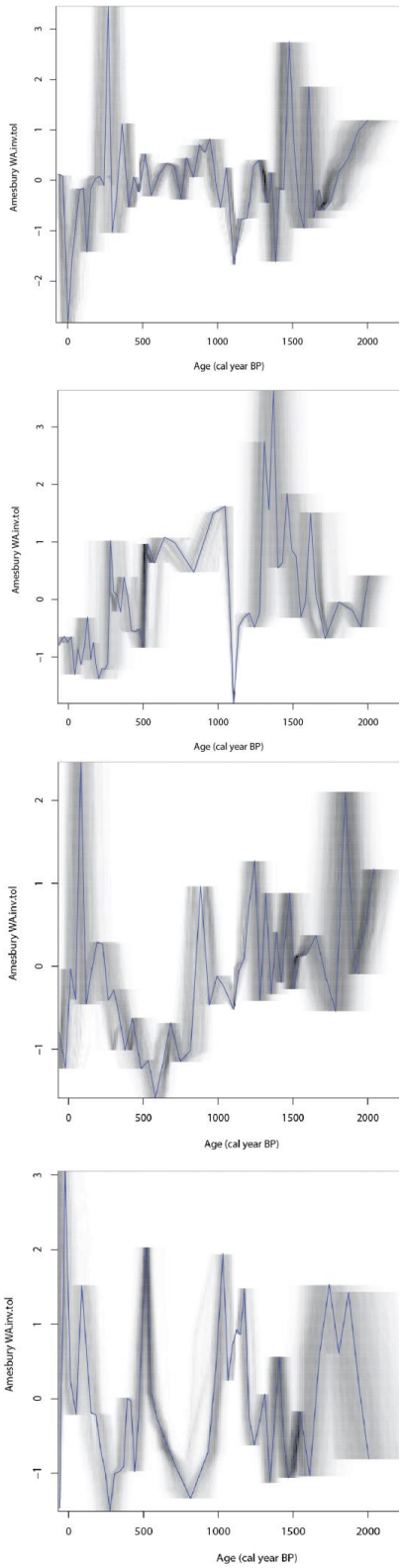

Figure 8.13 Testate amoebae water table reconstructions (using Amesbury *et al.*, 2013 training set) for JRB12 (top), FBB12 (second top), VDB12 (second from bottom) and SCH10 (bottom) presented with chronological uncertainties derived from Bacon age-depth modelling. Darker narrower periods indicate increased chronological control

8.4 Late Holocene peat carbon accumulation in eastern North America

Peat accumulation occurs when rates of net primary productivity (NPP) exceed rates of decomposition. Both variables increase with temperature; however, it is unclear whether NPP or decomposition will be more enhanced under projected future climate warming. Modelling studies focusing on climate driven changes in carbon (C) respiration indicate that decay will increase, depleting C stocks (e.g. Ise *et al.*, 2008; Dorrepaal *et al.*, 2009), whilst results from empirical studies indicate that NPP C gains will outweigh decay C losses (e.g. Yu *et al.*, 2012; Charman *et al.*, 2013). The likely responses of peatlands to projected future climate change must be better understood in order to estimate the C sink capacity and peat C flux to the atmosphere (Frolking *et al.*, 2011; Yu, 2012).

The spatial and temporal patterns of peatland C accumulation over the last 2000 years across a climatic gradient in eastern North America are investigated in this section by addressing the following objectives:

1. Characterise spatial and temporal patters of carbon accumulation rates (CAR);
2. Evaluate whether the changes in CAR during the last 2000 years are associated with reconstructed climate change in eastern North America. Emphasis is placed on characterising variations in CAR during the most pronounced periods of late Holocene climate change, termed the Medieval Climate Anomaly (MCA; AD 900 - 1350) and the Little Ice Age (LIA; AD 1400 - 1850);
3. Investigate the relationship between peat substrate composition, water table depth (WTD), temperature, fire and CAR;
4. Assess the vulnerability of the peatland carbon store to climate warming in eastern North America.

Characterising the drivers of CAR within complex dynamic peatland systems is complicated by the interactions of non-linear relationships, externally driven change and physical peat characteristics. The importance of secondary gradients and their associated feedbacks in controlling CAR may increase in importance under certain circumstances. Therefore, whilst the individual roles

of potential CAR controls are initially characterised within this chapter (Section 8.4.3.1 – 8.4.3.4), multivariate modelling of CAR has been conducted in Section 8.4.3.5 to account for the interactions between the explanatory variables.

8.4.1 Spatial patterns of peat C accumulation

8.4.1.1 Spatial trends in peat accumulation over the last 100 years

A north-south temperature gradient exists across the study sites: average annual temperatures and summer temperatures decrease with increasing latitude (Section 4.4.1). The difference in summer temperatures is most pronounced between SCH10 and JRB12, the sites at either end of the transect, with a difference of 5˚C, whilst VDB12 and FBB12 have similar summer temperatures that are only 1ºC warmer than JRB12. Growing degree days above 0˚C (GGD0) also decrease with increasing latitude (JRB12 contains 56% of SCH10 GGD0) and the two most southerly study sites receive more summer solar radiation and total sun hours than the northern two study sites (Table 4.1).

Many peatland studies have identified mean temperatures over the summer months (June, July, August) as one of the main controls of NPP and thus CAR on millennial timescales (e.g. Yu *et al.*, 2009; Garneau *et al.*, 2014; Loisel *et al.*, 2014) and on shorter timescales, such as during the MCA-LIA transition (e.g. Loisel and Garneau, 2010; Charman *et al.*, 2013). NPP is also influenced by other temperature related variables such as growing season length (Lund *et al.*, 2010) and photosynthetically active radiation (PAR; Loisel *et al.*, 2012; Charman *et al.*, 2013). Therefore, it is hypothesised that the southern most study site will be accumulating more carbon than the northern most site, all other variables being constant, owing to its warmer summer temperatures, greater number of GGD0 and higher solar radiation (hypothesis 2; Section 2.10).

Modern correlations between peat C accumulation and climatic conditions were determined using the averaged modelled climate variables for AD 1901 – 2010 (Table 8.3; Section 4.4.1) from each site and the amount of C accumulated over the same time period from each corresponding core. AD 1901 was located within each core based on the Bayesian age-depth models

(Chapter 5). The accuracy of the chronological placement of this period is limited since modern samples are associated with large ^{14}C errors: the core depths corresponding to a weighted average age of AD 1901 have 2σ age ranges of ± 83 years for SCH10 and JRB12, ± 92 years for FBB12 and ± 99 years for VDB12. Despite the large chronological uncertainty, the significant correlations identified between the climatic variables and accumulated C at the weighted average age estimate also remain significant across the 2σ range of chronological uncertainty for AD 1901, with the exception of one variable (mean summer available moisture (Table 8.3). Therefore, whilst the chronological uncertainty attributed to the last century of peat growth is substantial, the inferred relationship between climate and modern carbon accumulation in eastern North America can provide valuable context for the investigation of late Holocene carbon and climate interactions. Future studies should further investigate links between modern climate and carbon accumulation rates in eastern North America to test whether the presented correlations persist under improved chronological accuracy. Such improved chronologies could be achieved using other dating techniques such as ^{210}Pb, Spheroidal Carbonaceous Particles (SCPs) and by the locating the carbon bomb spike generated through atmospheric nuclear weapons testing *ca*. AD 1963.

Northern hemisphere summer temperatures (averaged over June, July and August; JJA) were significantly correlated with cumulative C ($r = 0.99$, $p = <0.05$), as were maximum temperatures and GGD0 (both $r = 0.96$, $p = <0.05$). All three climate variables were also significantly correlated with cumulative C across the 2σ age range for AD 1901. Therefore, C accumulation trends across the study sites over the last 100 years had a positive relationship with temperature, supporting the hypothesis that the southern sites will be accumulating more C than the northern sites. Contemporary summer solar radiation and sun hours were not correlated with cumulated C; therefore, these variables may be at best secondary drivers of C accumulation across the last 100 years at the study sites.

There is a significant correlation between cumulative C and JJA available moisture ($r = -0.96$, $p <0.05$); however, whilst this relationship persisted when the maximum 2σ AD 1901 age was considered, it did not remain significant. Available moisture is a measure of the balance between precipitation and

evapotranspiration; therefore, since there were no significant correlations between cumulative C and any of the precipitation variables, it is likely that temperature is more influential than precipitation in driving the relationship over the last 100 years. This echoes conclusions from other studies that suggest that precipitation changes will be of secondary importance to temperature and PAR (e.g. Charman *et al.*, 2013) in driving carbon accumulation. The summer moisture availability determines the peatland water table depth (Charman, 2010); therefore, the reconstructed water table depth can be used to test whether a relationship between peat accumulation and summer moisture deficit exists throughout the last 2000 year (Section 8.4.2).

8.4.1.2 Spatial trends in peat accumulation over the last 2000 years

Regional temperature reconstructions indicate that, across the study region, the current latitudinal summer temperature gradient persisted over the last 2000 years: Northern Quebec remained *ca.* 5ºC cooler than southeastern United States despite climate fluctuations (Viau *et al.*, 2006; Figure 8.14). The reconstructed temperature records therefore support the hypothesis that C accumulation will be greater in the southern sites than the northern sites over the last 2000 years. The total cumulative carbon is highest in SCH10, the most southern site in this study, over the last 2000 years, indicating that warmer temperatures in the south encouraged C accumulation (Figure 8.15). However, there is no clear north-south trend in cumulative C across the study region: cumulative C in SCH10, VDB12 and FBB12 increases with decreasing latitude, whilst the most northern core JRB12 contains similar total C to SCH10. Aside from the surface peat, JRB12 consistently contains higher cumulative C than the other sites; therefore, additional influences aside from temperature must be influencing the elevated cumulative C in JRB12 over the last 2000 years.

All modern modelled climate variables for JRB12 are in agreement with the north-south trends of the other sites. Therefore, there are no obvious climatic influences that can account for the elevated levels of C accumulation in JRB12 (Table 8.3). Microclimate and site specific effects that have not been accounted for may be influencing CAR: for example, exposure generated by distance from, and density of, tree margins (Magnan *et al.*, 2014) and surrounding topographical features may influence wind characteristics and

pathways of peat development (Loisel and Yu, 2013). However, of the variables that are accounted for within this study, the main difference between JRB12 and the other sites is the age of peat formation: JRB12 started accumulating at *ca*. 3250 cal yr BP and is younger than SCH10 (*ca*. 5000 cal yr BP), VDB12 (*ca*. 6000 cal yr BP) and FBB12 (*ca*. 10250 cal yr BP; Chapter 5). The basal peat age is correlated with cumulated C over the last 2000 years at the 90% level (r = -0.941); therefore, the younger stage of the peatland may be accounting for the increased C in JRB12.

The correlation between peat accumulation rates and peat basal age in other studies has been attributed to lower decomposition in younger sites (e.g. Garneau *et al*., 2014; Loisel and Yu, 2013b). The temporal focus of this study has been limited to 2000 years across all sites; therefore, whilst local climatic influences may vary rates of decomposition, differences in temporal foci cannot account for the elevated cumulative C in JRB12. Higher CAR in earlier stages of peat growth have been attributed to successional vegetation change from sedge dominated fens to *Sphagnum* dominated bogs (e.g. Loisel *et al*., 2014); however, this cannot explain the elevated CAR in JRB12 since it is a consistently *Sphagnum*-dominated bog over the time period of interest. A decline in peat accumulation with increasing peatland age was hypothesised by Clymo, (1984; 1992), suggesting that, over time, the peat mass approaches a steady state when the rate of peat loss by decay (owing to the size of the catotelm) approaches the constant rate of peat addition. However, all sites contain a similar depth of peat (ranging from 380 – 450 cm; Chapter 5), despite the differing age of peat formation. Therefore, whilst the ages of the peatlands may be contributing to the accumulated C trends, the degree of influence that the peatland ages, and thus the proximity of each peatland to the point of maturity, has on the cumulated C content cannot be assessed further in the absence of more detailed field investigations into basin morphometries

Table 8.3 Pearson correlation coefficients: relationship between climatic variables and total amount of cumulative C from AD 1901 to 2001.The sensitivity of the correlations is tested within the age-depth model uncertainty using the 2σ age range. Bold indicate significant relationships.

Climate variable	**Weighted mean age r^2**	**Max age r^2**	**Min age r^2**
Spring temperature	0.85	0.77	0.83
Summer temperature	**0.99**	**0.99**	**0.999**
Autumn temperature	0.50	0.50	0.53
Winter temperature	-0.19	-0.24	-0.20
Minimum temperature	-0.06	-0.13	-0.08
Maximum temperature	**0.96**	**0.999**	**0.99**
Average annual temperature	0.77	0.72	0.76
Spring precipitation	0.09	0.21	0.17
Summer precipitation	-0.77	-0.70	-0.75
Autumn precipitation	-0.93	-0.81	-0.88
Winter precipitation	-0.88	-0.82	-0.85
Average annual precipitation	-0.87	-0.75	-0.81
Precipitation during driest month	-0.40	-0.22	-0.30
Precipitation during wettest month	-0.82	-0.70	-0.76
Mean summer available moisture	**-0.96**	-0.94	**-0.97**
Growing degree days above 0˚C	**0.96**	**0.95**	**0.97**
Average daily sun hours	0.49	0.56	0.55
Summer solar radiation	0.79	0.75	0.79
Snow depth (Oct – April)	-0.63	-0.62	-0.64
Length of growing season	0.27	0.18	0.25
Physical variable			
Latitude	-0.62	-0.61	-0.64
Longitude	0.91	0.85	0.90
Height above sea level	-0.12	0.13	0.00
Basal age	-0.25	-0.01	-0.12
Peat thickness	-0.62	-0.52	-0.55

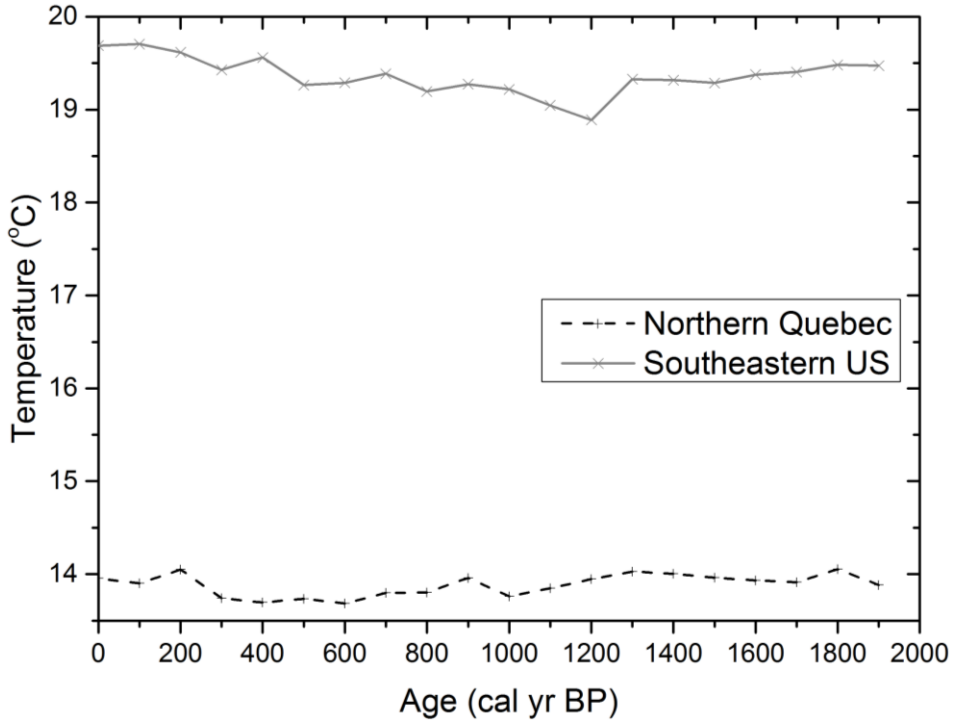

Figure 8.14 Pollen-inferred summer temperatures for Northern Quebec and Southeastern US (adapted from Viau *et al.*, 2006).

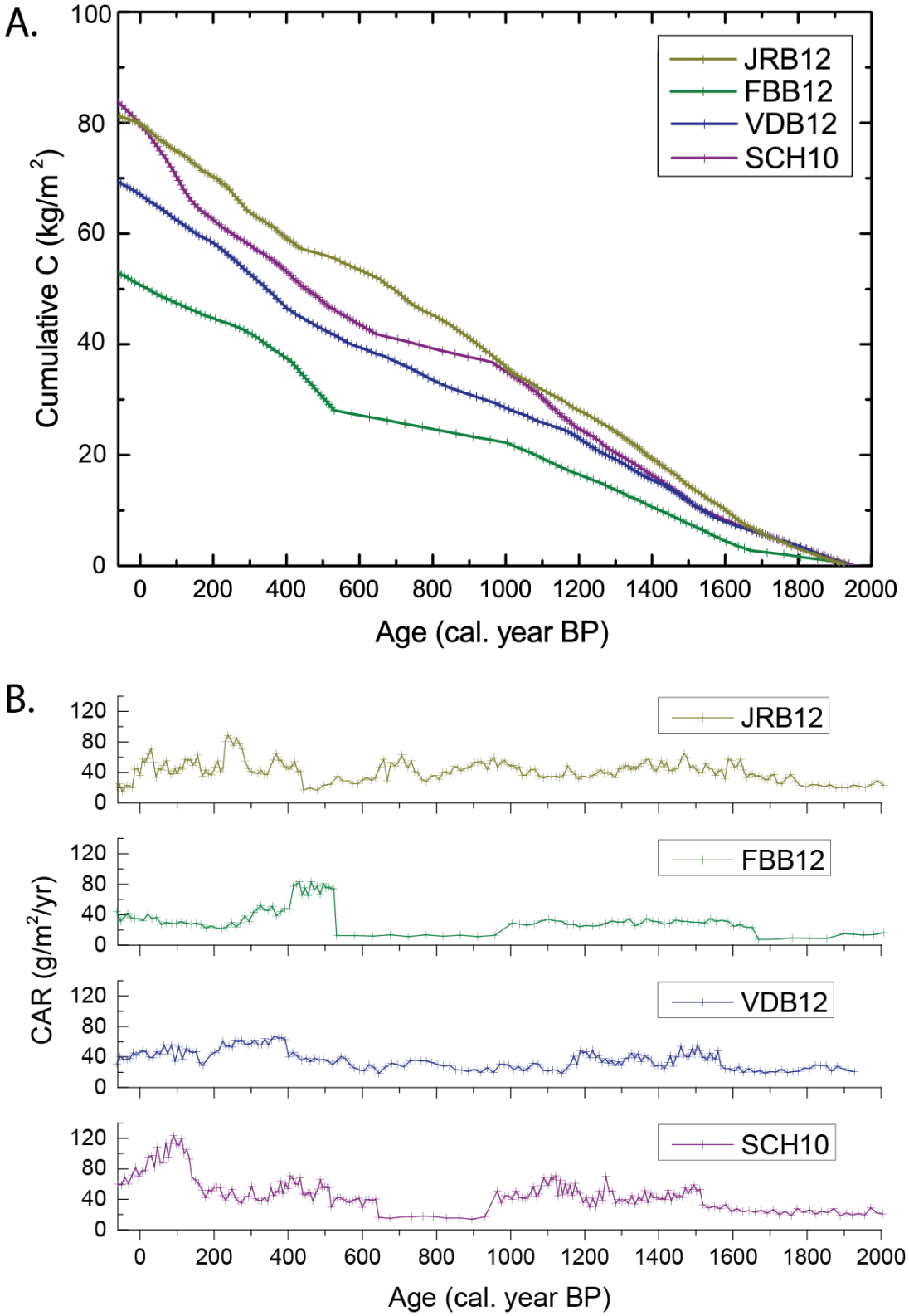

Figure 8.15 CAR and cumulative carbon content over the last 2000 year by site. Sites have been presented north (JRB12) – south (SCH10).

8.4.2 Temporal patterns of peat accumulation over the last 2000 years

It is hypothesised that CAR increased during the warmer MCA owing to higher NPP, relative to cooler LIA with reduced NPP and increased cloudiness. This hypothesis is based on the demonstrated relationships between C accumulation and PAR during the growing season using modelled climate data (*sensu* Charman *et al.*, 2013). The hypothesis is not supported by the measured changes in CAR across all study sites (Figure 8.16). Whilst the regional timings of the MCA in eastern North America are poorly constrained, CAR during the traditional MCA (*ca*. 1050 – 600 cal yr BP) were lower in the three southern sites, nearing some of the lowest values over the 2000-year period. High CAR values were evident in JRB12, the most northern site, at the start of the MCA until *ca*. 900 cal yr BP when CAR fluctuated in a decreasing trend. CAR increased later in the two most southerly sites at *ca*. 650 cal yr BP. This CAR increase was *ca.* 100 years before the assumed onset of the Northern Hemisphere LIA (Jones and Mann, 2004); however, there is currently no overwhelming consensus as to the onset or timings of the LIA in eastern North America owing to the spatial heterogeneity of climate reconstructions obtained from this region and the paucity of records (Section 8.2). The associated CAR increase occurs later, and more abruptly, in FBB12 (*ca*. 500 cal yr BP), whilst JRB12 does not experience an LIA CAR increase until *ca*. 450 cal yr BP. Comparisons of CAR with full chronological errors reveal that the occurrence of the CAR increase in the two southern sites before the two northern sites is outside of chronological uncertainty (Figure 8.17). During the second phase of the LIA (*ca*. 400 – 200 cal yr BP), the CAR response differs across the peatlands without an obvious north-south trend. The acrotelm-catotelm boundary corresponds with *ca*. 300 cal yr BP in all sites; therefore, any CAR trends from this point may be influenced by active peat processes and will be elevated relative to the remainder of record since the progress of decomposition will be reduced (Clymo, 1984).

The MCA (*ca*. 1050 – 600 cal yr BP) is generally associated with drier conditions along the eastern coast of North America (Section 8.2.1), as supported by the increase in the depth to water table at all four study sites at the onset of the MCA (Figure 8.16). A fire occurred shortly after the MCA onset at SCH10, decreasing CAR. Subsequent MCA CAR trends may therefore only partially relate to peatland water table depth (WTD) or climatic conditions

at this site. Warmer MCA conditions have also been reconstructed from palaeoclimatic records across the region (Section 8.2.1). Whilst secondary gradients may be modelled, it is difficult to isolate the influence of precipitation and temperature from empirical data. The prominent MCA increase in depth to water table in FBB12 was associated with a decline to sustained low CAR. Similarly, the drier conditions persisting until *ca*. 800 cal yr BP in VDB12 were associated with reduced CAR. Therefore, the broad relationship between CAR and WTD in VDB12 and FBB12 during the MCA conflicts with conclusions from empirical studies demonstrating that carbon accumulation during the MCA was driven by warmer temperatures (e.g. Charman *et al*., 2013; Loisel *et al*., 2012) and correlations between the modern climate data and cumulated C obtained within this study (Section 8.4.1.1). However, the drier MCA conditions at JRB12 do coincide with increased CAR (either suggesting that temperatures also increased or that the moisture balance was more favourable to peat growth) and this relationship persists until *ca*. 700 cal yr BP when CAR decreases despite sustained WTD. These initial conclusions indicate that precipitation may be a more dominant control on peat accumulation than temperature in regions proximal to the moisture threshold for peat growth.

The differences in CAR trends across the study sites indicate that the warming and associated drying of the MCA likely forced the southern sites across a threshold at which the hydrological balance was no longer conducive to peat growth. This hypothesis is supported by the differences in magnitude of MCA reconstructed WTD at the study sites: during the initial MCA CAR depression (*ca.* 1000 cal yr BP), FBB12 and SCH10 WTD are respectively *ca*. 20 cm and 30 cm below the peat surface, whilst JRB12 does not does not exceed *ca.* 10 cm (Table.8.4). Whilst a fire occurred at SCH10, FBB12 CAR do not respond to subsequent MCA WTD fluctuations, which also suggests that a WTD – CAR threshold has been surpassed. C accumulation at the most northerly site, JRB12, may have benefited from the less pronounced MCA warming and drying compared with the southern sites by encouraging, rather than inhibiting, NPP.

The VDB12 testate amoebae reconstructed WTD change at the onset of the MCA is greater, whilst more gradual, than JRB12. VDB12 CAR is suppressed at the onset of the MCA owing to a prior decrease in depth to water table. The

gradual and temporary nature of the MCA drying at this site does not trigger a response in CAR until *ca.* 850 – 700 cal yr BP. The suppressed CAR at VDB12 at the onset of the MCA, therefore, cannot be attributed to a threshold response similar to the other southerly sites. Rather, a combination of the antecedent water table conditions, the gradual rate of drying and short-duration of the dry conditions is responsible for lower CAR at VDB12.

Table.8.4 WTD change associated with the MCA

Testate amoebae reconstructed WTD	**JRB12**	**FBB12**	**VDB12**	**SCH10**
Prior to MCA	5 cm	0 cm	5 cm	20 cm
MCA onset	10 cm	20 cm	18 cm	30 cm
Difference	**5 cm**	**20 cm**	**13 cm**	**10 cm**
Plant macrofossil reconstructed WTD				
Prior to MCA	5	6.25	5.5	5
MCA onset	6	7.5	6.5	7
Difference	**1**	**1.25**	**1**	**2**

The persistent drier conditions appear to have moved JRB12 towards the moisture threshold at which C was no longer effectively accumulating *ca.* 500 cal yr BP. Alternatively, the reduction in CAR compared with WTD trends *ca.* 500 cal yr BP in JRB12, as well as *ca.* 1100-1300 cal yr BP in FBB12 and during the RWP in JRB12, VDB12 and SCH10, may be attributed to secondary decay occurring during the succeeding dry periods. A recent modelling study indicated the potential for pronounced persistent drying to elevate decomposition and C losses below the peat surface (Frolking *et al.*, 2014). Under such conditions, CAR values would contain low biases owing to secondary decay at a later date. The effect of secondary decay on CAR has yet to be tested in empirical studies. Episodes of secondary decay may be identified within palaeo C accumulation records when periods of unexpectedly low CAR are succeeded by prolonged and/or pronounced reconstructed dry conditions, such as *ca.* 500 cal yr BP in JRB12. This study investigates peatlands at the latitudinal moisture limit of peat growth; therefore, it is difficult to confidently distinguish between periods of CAR reduced by

secondary C decomposition and periods of CAR that are limited by a lack of sufficient available moisture. There is therefore a need for future studies to obtain direct reconstructions of temperature and precipitation either using biomarkers within the peat (e.g. using glycerol dialkyl glycerol tetraethers (GDGTs) and deuterium or oxygen isotopes) or from proximal lake records (e.g. using chironomid-inferred temperatures or isotopic analyses) to further explore the influence of secondary C decomposition on CAR.

The modern data comparison revealed a tentative correlation between cumulative C and summer moisture availability (Section 8.4.1.1), which is supported by the broad-scale consistent changes between the reconstructed water table depth and CAR over the last 2000 years (Figure 8.16). Whilst the WTD and CAR relationship is particularly clear during the last *ca*. 500 years, CAR trends differ from trends in reconstructed water table depth during the MCA in SCH10, VDB12, FBB12, and during the Roman Warm Period (RWP) in SCH10, VDB12 and JRB12 (discussed above). Fluctuations in summer moisture availability are, therefore, likely driving CAR at all sites during the LIA but not surpassing a threshold within responses associated with the warmer periods of the MCA and RWP. The breakdown of the relationship between WTD and CAR under dry conditions at the sites close to the limit of peat growth or due to antecedent conditions highlights the difficulties of establishing the influence of WTD on CAR over long time scales. Changes in relationships between WTD and CAR over time can also limit the amount of CAR variability that can be explained using multivariate modelling (Section 8.4.3.5). Therefore, findings from this thesis suggest that future studies should prioritise identifying intermittent relationships over different timescales using bandwidth modelling.

The peatland-C debate largely focuses on determining whether future warmer temperatures will relatively enhance decomposition or increase NPP. This study reveals that, for peatlands located near the southern limit of peat growth, maintaining an optimum balance of precipitation and evapotranspiration for peat accumulation is a primary control of CAR. Results indicate that WTD appears to influence CAR on multi-centennial rather than millennial timescales. Furthermore, relationships between CAR and WTD may not persist over the entire last 2000 years of interest in this study. Carbon accumulation rates in peatlands across Maine and Nova Scotia were shown to

be at their lowest during the dry conditions of the MCA, a partial analogue for future warming, and the RWP. Under sustained future warming it is likely that peatlands in these locations will become weaker C sinks or even sources of net C release to the atmosphere as the bioclimatic zones for peat formation change (Gallego-Sala *et al.*, 2010; Gallego-Sala and Prentice, 2013).

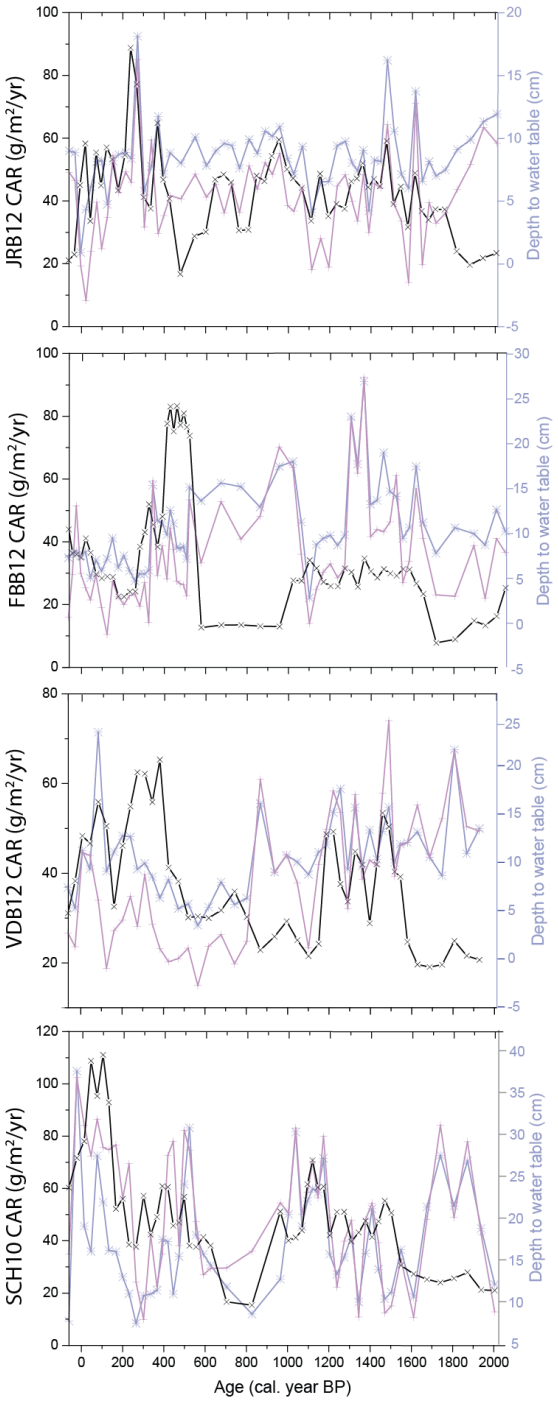

Figure 8.16 CAR (in black) and testate amoebae reconstructed water table depths using the (Amesbury *et al.* (2013) transfer function (in blue) and the (Lamarre *et al.* (2013) transfer function (in purple).

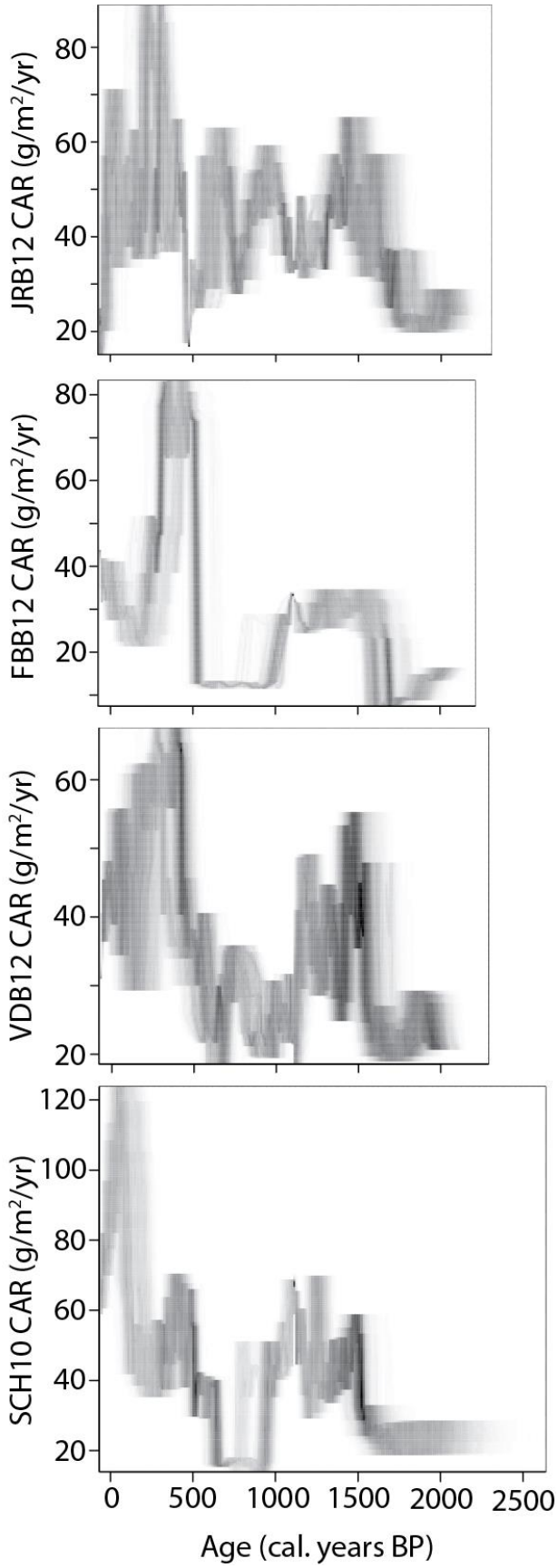

Figure 8.17 CAR by site over the last 2000 years with modelled chronological uncertainties (using Bacon (Blaauw and Christen, 2011) package in R (R Core Development Team, 2014).

8.4.3 Constraining the contribution of peat C accumulation drivers over the last 2000 years

8.4.3.1 Temperature

The best available reconstructed temperature records for eastern North America over the last 2000 years are pollen inferred July temperatures estimated in 100 year intervals for North America, Northern Quebec and south eastern US (Viau *et al*., 2006; Figure 8.14). The spatial and temporal resolution of the temperature estimates is coarse relative to the scale of the sampling strategy in this thesis: all study sites would fall under the category of Northern Quebec despite being located in a very different bioclimatic region. Therefore, whilst the temperature reconstructions of Viau *et al*. (2006) can serve as a guide to broad trends of centennial temperature changes, the relationship between local temperature changes and carbon accumulation cannot be optimally tested with the currently available data.

There are no significant relationships between the CAR of each study site and any of the three regionally appropriate Viau *et al*. (2006) temperature reconstructions (Table 8.5). The lack of relationship between temperature and CAR on 100 year time periods over the last 2000 years in this study is, perhaps, surprising owing to the modern correlation between carbon accumulation and summer temperatures (Section 8.4.1.1) and the importance of temperature on peat CAR detected in other palaeo-peatland studies (e.g. Charman *et al*., 2013). A significant correlation does exist between CAR and North American temperature anomalies when the CAR from all sites are aggregated into 500-year time intervals ($r = 0.655$, $p < 0.01$). Therefore, temperature may be a more influential CAR control in the study sites on longer time scales.

Table 8.5 Pearson correlation coefficients between CAR and Viau *et al*. (2006) temperature reconstructions over 100-year intervals. No significant relationships have been detected (p= >0.05)

	SCH10	VDB12	FBB12	JRB12	Average
North America	-0.00474	-0.14958	-0.32904	0.376119	-0.06958
Northern Quebec	0.008573	-0.19967	-0.28644	0.004456	-0.14714
Southeast United States	0.38035	0.367974	0.092174	0.137269	0.33722 4

The absence of detected significant correlations between CAR and temperature on the time scale of this study may be influenced by the broad spatial scale of the Viau *et al*. (2006) temperature reconstructions. To minimise the effect of the different spatial scales of the records from this study and the Viau *et al*. (2006) reconstructions, the average CAR across all four sites was also tested. This did not reveal a significant correlation. Therefore, more local temperature reconstructions for each site are required to test the relationship between peat accumulation and temperature over the climatic gradient at the spatial scale of this study. Palaeotemperature reconstructions can be obtained from peat using branched chained lipids (GDGTs; Peterse *et al*., 2010; Weijers *et al*., 2007). GDGT-based temperature reconstructions have the advantage of being obtained from the same sample depths as the CAR measurements, minimising chronological uncertainty and problems with different sampling resolutions. However, the current standard error of calibration for the GDGT-based temperature reconstructions is larger than late Holocene temperature change (5 ºC; Weijers *et al*., 2011) with a potential warm bias owing to the insulating effect of vegetation and the heat capacity of the soil water (Weijers *et al.,* 2011). Despite calibration problems, the direction of reconstructed temperature change, rather than absolute values, agree with trends of temperature related reconstructions from other proxies and palaeoarchives (Nichols *et al*., 2014). Large reconstruction errors and uncertainty surrounding absolute reconstructed values is also a feature of testate amoebae water table reconstructions; therefore, improvements in the reconstruction calibration of both proxies are required.

Regional temperature patterns over the last 2000 years could also be investigated using chironomid inferred summer air temperature (C-IT) records in combination with temperature reconstructions obtained using isotopic analysis on the chitin from the midge head capsules. Very few late Holocene C-IT records have been obtained from the study region and those that do exist have coarse sampling resolution: e.g. the record from Newfoundland contains 8 samples from the last *ca.* 2000 years (Rosenberg *et al*., 2005). C-IT would not, however, escape the problem associated with GDGTs of the large reconstruction error encompassing the magnitude of late Holocene climate change: the root mean square error of prediction of the C-IT North American transfer function is at least 2.6°C (Walker *et al*., 1997). The trends of

temperature change still provide useful climatic comparisons across records. The C-IT from Newfoundland differs from the Viau *et al*. (2006) summer temperature reconstructions, indicating that temperatures 2000 cal yr BP were the coolest of the last *ca*. 9000 years and then fluctuated but increased towards *ca*. 1000 cal yr BP before decreasing to the present day. Therefore, there is a requirement for future studies to focus on characterising relative late Holocene temperature changes reconstructed from both peat and lake sediments in eastern North America.

8.4.3.2 Water table depth

The significant correlation between summer moisture deficit and accumulated C over the last 100 years suggests that reconstructed WTD over the last 2000 years would also correlate with CAR (Section 8.4.1.1). Visual comparisons of CAR and WTD support this hypothesis, indicating that trends are similar at certain periods of the last 2000 years (Section 8.4.2). The correlation strength of CAR and WTD at each study site is tested along with the aggregated full sites on a sample-by-sample basis as well as 100- and 500- year intervals. Comparisons of the two transfer functions used to reconstruct WTD in this thesis fail to reveal which transfer function performs better (Chapter 6). Therefore, both transfer functions are used as representations of WTD change for the comparison with CAR.

Significant correlations between CAR and WTD exist in SCH10 and JRB12 but not VDB12 or FBB12 (Table 8.6). However, the significant correlations between CAR and WTD only occur for one transfer function in each site and the correlated transfer function does not remain consistent: SCH10 CAR is related to the Lamarre et al. (2013) WTD reconstruction and JRB12 CAR is related to the Amesbury et al. (2013) reconstruction. Both transfer functions at all sites contain similar broad trends in reconstructed WTD, within reconstruction errors (Figure 8.1); therefore, the difference in correlation with CAR is perhaps surprising. The lack of correlation consistency between transfer function reconstructions and CAR, both within and between sites, may reflect the weak strength of correlations however, it also emphasises that the identification of relationships using palaeo-reconstructions depends upon the optimum performance of the statistical techniques applied.

Table 8.6 Pearson correlation coefficients between carbon accumulation and reconstructed WTD by site on multidecadal timescales.

Significant correlations in bold with * denoting p = <0.01 and ^ denoting p = <0.05.

	SCH10	VDB12	FBB12	JRB12	All sites
Amesbury *et al.* (2013) WTD	0.20	0.07	-0.14	**0.31^**	**0.17^**
Lamarre *et al.* (2013) WTD	**0.43***	-0.12	-0.27	0.26	**0.23***

Despite the inconsistent responses of CAR to WTD at the individual site level, both transfer function reconstructions are significantly correlated with CAR when all sites are considered together (Table 8.6). The correlation between the Lamarre *et al*. (2013) reconstructions and CAR are stronger and more significant than the Amesbury *et al*. (2013) reconstructions. The relationship between WTD and CAR at all sites is positive, indicating that when the depth to water table increases, under drier conditions, CAR increases. This relationship agrees with the negative correlation detected between summer moisture availability and amount of accumulated C (wetter, less C; Section 8.4.2). Field studies and laboratory experiments characterising the effect of lower water tables on CAR have reported conflicting results, which vary over different timescales, depending on the balance of production and decomposition (e.g. Alm, *et al*., 1999; Laiho *et al*., 2004; Minkkinen *et al*., 1999; reviewed by Laiho, 2006). The reason for the discrepancy, which continues within palaeo-peatland studies, is that the effect of water table drawdown on CAR is complex, depending on the length and severity of the drying event which may trigger changes in other interlinked variables such as: aeration, vegetation type, soil temperature, acidity and characteristics of organic matter. Whilst it may be assumed that drying would enhance rates of decomposition, thus lowering CAR, the potential for enhanced decomposition is limited by the extent of previous decomposition, the type of litter and the threshold at which the decomposer organisms become water limited (Laiho, 2006). Therefore, if the peat has already been extensively decomposed, the litter is recalcitrant and the associated warming temperatures enhance NPP, it is likely that peat addition would exceed decomposition, thus enhancing long-term C accumulation.

The relationship between CAR and WTD within this study varies with time: only the Lamarre *et al*. (2013) WTD reconstruction and CAR relationship at SCH10 remains at the 100-year level ($r = 0.449$, <0.05). The weakening of the relationship between CAR and WTD over longer time periods differs from the relationship between CAR and temperature, which appears to strengthen. Therefore, in terms of estimating the peat-carbon response to future climate change, short-term changes in summer moisture availability may be important for estimating short-term changes in carbon accumulation in sites near to the limit of peat growth, whilst temperature changes may be important for the longer-term future of peatland C stores. A similar relationship between carbon accumulation and water table depth has been detected in other regional palaeo-peatland studies (e.g. Klein *et al*. (2013) in southern central Alaska), attributed to increased decomposition. However, regional studies, such as this thesis and Klein *et al*. (2013), contradict the larger spatial scale studies which fail to detect prominent relationship between CAR and reconstructed WTD (e.g. Charman *et al*., 2013).

The reduced influence of WTD on CAR in studies with large spatial scales is perhaps unexpected since WTD influences other CAR variables such as vegetation assemblage and the occurrence of fire events. Whilst the lack of correlation between WTD and CAR may be real, the inconsistencies between correlations of different transfer functions and CAR detected in this study warns that some of the current conclusions on the relationship between WTD and CAR may be influenced by uncertainties associated with the testate amoebae WTD reconstructions. Refinements of the characterisation of species' responses to WTD changes and improvements in transfer function training sets are therefore urgently required to reduce reconstruction errors and enhance the confidence with which the relationship between WTD and CAR can be established. Obtaining multiple proxy records of hydrological change, e.g. using testate amoebae and stable isotopes, is also essential to reduce WTD reconstruction uncertainties when comparing with CAR.

The findings from this study highlight the complexity of isolating the influence of NPP and decomposition from CAR. Depending on ecosystem thresholds, drier conditions can supress or increase plant productivity whilst increasing peat decay (Fenner and Freeman, 2011; Frolking *et al*., 2014). CAR may also increase under drier conditions if the ecosystem shifts to woodier

vegetation, which is associated with higher density and/or recalcitrant peat (Breeuwer *et al.,* 2008; Loisel and Garneau, 2010; tested in Section 8.4.3.2). Understanding moisture thresholds of change are important for understanding CAR controls: NPP increases under higher temperature require precipitation to exceed evapotranspiration and facilitate peat growth (Cai and Yu, 2011; Jones and Yu, 2010).

8.4.3.3 Peat vegetation composition

Peatland vegetation assemblages, determined by the height of the water table and internal self-regulating processes (Loisel and Yu, 2013c) as well as external disturbances such as increased nitrogen (N) deposition or tephra loading (e.g. Hughes *et al*., 2013), form the basis of the preserved peat substrate the peat susceptibility to decomposition. Whilst changes in major vegetation types can significantly influence CAR (e.g. van Bellen *et al*., 2011; Loisel and Yu, 2012), few studies have fully characterised the role of plant type on CAR. *Sphagnum* has a lower bulk density, contains less C and has a higher C:N ratio than vascular plants; therefore, if hydrological conditions allow for rapid peat burial, there is the potential for vascular plants to have higher accumulation rates (Loisel *et al*., 2014). However, the recalcitrant polymers of *Sphagnum* are more resistant to decay; thus *Sphagnum* dominated assemblages have a greater capacity for enhanced C accumulation over longer time scales than assemblages dominated by vascular plants (e.g. Malmer *et al*., 2003).

The vegetative components of the four study sites are categorised into Ericaceae, monocotyledons, bryophytes and UOM using the data from Chapter 6. The bryophytes are predominantly composed of *Sphagnum,* which is also separated into sections and correlations between *Sphagnum* sections and CAR are tested separately. UOM is decomposed vegetative material, included to act as an indicator of rates of decay. There is no consistent response of CAR to vegetation type across the four sites (Table 8.7). Monocots are significantly correlated with CAR at all sites except from VDB12 on a multidecadal timescale. However, the nature of the relationship between monocot. abundance and CAR varied between sites: FBB12 contained a negative relationship between CAR and monocots indicating higher CAR when the abundance of monocots is decreased, whilst SCH10 and JRB12 contained a

positive CAR and monocot relationship. The positive correlation between CAR and monocot abundance in SCH10 and JRB12 compared with the negative CAR and monocot correlation in FBB12 may be influenced by the differences in decay potential: SCH10 and JRB12 accumulated almost twice as fast as FBB12 over the last 2000 years. The quicker burial of the monocot. remains may have decreased the aerobic decay potential, preserving the enhanced labile C store at SCH10 and JRB12 to a greater extent than FBB12 (Beilman *et al.*, 2009; Loisel and Garneau, 2010). The slower accumulating FBB12 would have facilitated enhanced decay of the labile material, depleting the C store when monocots dominate (e.g. Nichols *et al.*, 2014; van Bellen *et al.*, 2011). The role of vegetation in controlling peat C is clearly intertwined with hydrological conditions and the rate of peat burial, thus decay potential (Loisel *et al.*, 2014). This hypothesis may also explain the negative relationship between bryophytes, primarily *S.* sect. *Acutifolia*, and CAR at SCH10 and JRB12.

When the vegetation assemblage and CAR data across all sites are aggregated, monocot. abundance is negatively correlated with CAR and this relationship continues at the 100-year timescale ($r=-0.37$, $p=0.01$). The overall negative relationship between CAR and monocots supports the increasing number of studies that have reported a reduced capacity for C accumulation as monocots increase (Murray *et al.*, 1989; Hughes *et al.*, 2013; Kuiper *et al.*, 2014; Loisel and Yu, 2013). The relationship between CAR and bryophytes ($r=0.309$, $p<0.01$), specifically *S.* sect. *Acutifolia* (0.237, $p < 0.05$), became positive when extended across all sites at 100 year time periods. Monocots, rich in cellulose, decompose quicker than *Sphagnum*, which contains more complex lipids (Verhoeven and Toth, 1995) and acidifies its surrounding inhibiting decomposition by organisms (van Breemen, 1995), thus encouraging C accumulation.

UOM is significantly related to CAR at VDB12 and JRB12, indicating that CAR increases when decomposition increases. Whilst this relationship may seem counterintuitive, the drier, warmer conditions encouraging decomposition also encourage NPP. Therefore, the UOM – CAR relationship at these sites suggests that NPP rather than decomposition is the primary control of CAR over the last 2000 years. The positive relationship between UOM and CAR is in agreement with earlier conclusions: when conditions are drier and water table depths are lower, CAR increases.

The results from this study indicate complex relationships been vegetation components and CAR that are dependent on local accumulation regimes and on the timescales of interest. When all sites are aggregated, only the significant negative relationship between CAR and monocots remains. In warmer future conditions, monocot.-dominated vegetation communities may thrive in the southern regions of this study at the expense of the cooler, wetter preferring *Sphagnum* communities, which are vulnerable to prolonged episodic drying (Williams and Flanagan, 1996). Under such circumstances, carbon accumulation in peatlands close to the current climatic limit of peat growth may decrease, potentially creating positive feedbacks to climate warming.

Table 8.7 Pearson correlation coefficients between groups of vegetation and CAR by site at a multidecadal timescale. Significant correlations in bold (p = <0.05) with * denoting p = < 0.01.

	SCH10	VDB12	FBB12	JRB12	All sites
Ericaceae	0.27	0.22	0.05	-0.12	0.11
Monocotyledons	**0.36**	0.14	**-0.29**	**0.340**	**-0.24***
Bryophytes	**-0.30**	-0.239	0.20	**-0.329**	0.09
S. sect. Acutifolia	**-0.30**	**-0.32**	0.21	**-0.299**	0.06
UOM	0.12	**0.36**	-0.07	**0.310**	0.06

8.4.3.4 Fire

No significant correlations were detected between CAR and charcoal over the last 2000 years at the individual site level. However, when all sites were considered together, a negative significant relationship emerged (r = -0.168, p = <0.05). The relationship between charred material and CAR strengthens over the 100-year time scale (-0.339, p = <0.01). If severe fires penetrate the vegetated surface, they not only disturb the system and trigger new, unique trajectories of ecological change (Klinger, 1996) whilst directly liberating C through burning, but also encourage decomposition (Turestsky *et al*., 2011). Increased frequency or severity of fire events under warmer drier climates could, therefore, diminish peat C accumulation (Kuhry, 1994; Weider *et al*

2009). Whilst this study indicates a correlation between fire and CAR on centennial timescales, this relationship was not present over millennial timescales in a peatlands study in Quebec (van Bellen *et al.*, 2012). Millennial-scale studies of CAR, fire regimes and peatland hydrological change in eastern North America are therefore required to test whether the relationship exists between CAR and fire exists in more oceanic peatlands compared with those of Quebec.

Peatland fires have been shown to release around 2.5 – 3.25 kg C m^{-2} to the atmosphere in a single event (Pitkanen *et al.*, 1999; Turetsky *et al.*, 2008). In the 100 years preceding the SCH10 fire (*ca.* 1000-700 cal yr BP; Chapter 7) average CAR was 45.21 g C m^{-2} yr^{-1} that decreased to 16.2 g C m^{-2} yr^{-1} during the fire. The peatland stopped accumulating C and may have lost some stored C during the fire; however, CAR values cannot be negative and pin-pointing the date of onset and end of the fire event is difficult. Even with the over estimation of accumulated C during this fire event, the broadly estimated equivalent C loss (based on the accumulation rates before the fire) is 0.05 g/m^2 C or 11% of the total C accumulated over the last 2000 years. This approximate calculation does not consider any changes in accumulation rates after the fire; however, it does demonstrate the impact that fire can have on the peatland carbon store.

8.4.3.5 Multivariate modelling

Summer temperature, water table depth, vegetation type and fire are varying secondary gradients that are not consistently strongly correlated with CAR across the study sites over the last 2000 years. When all sites are aggregated, temperature is related with CAR on longer time scales of 500 year periods, whilst WTD, vegetation components and fire events correlated with CAR over shorter multidecadal to centennial timescales. These findings indicate that there is no single dominant driver of CAR over the last 2000 years in the four eastern North American study sites; rather, combinations of the variables must be interacting to generate the estimated CAR.

To identify the combination of known environmental variables that can account for the highest variability in CAR, multivariate modelling was conducted at the multidecadal, centennial and multi-centennial timescale for each individual site and across an aggregate of all four sites. The multivariate

models cannot be expected to account for all CAR variations since all potential variables have not been characterised. Two main variables that have been omitted from this study are PAR and nitrogen (N) deposition: PAR has been shown to be influential to CAR (Loisel *et al.*, 2012; Charman *et al.*, 2013); however, accurate reconstructions of PAR are difficult to obtain at the spatial scale of this study. N_2 deposition and N_2 fixation by bacteria may be also be an important control of CAR (e.g. Loisel *et al.*, 2014); however, rates of N_2 have not changed drastically over the time period of interest and are likely below the critical threshold for plant community change in the study area making it a secondary control on CAR. The relative combinations of the influential variables may change over time and, if these changes do not oscillate on the time periods investigated, they will not be captured in the multiple-regression modelling. Despite the limitations of omitted variables and non-stationary relationships over time, the multivariate modelling can reveal the relative importance of the measured variables over last 2000 years.

At the multidecadal level, the variation in CAR at all sites over the last 2000 years is best accounted for by a combination of change in WTD, charred material, Ericaceae abundance and monocot. abundance. However, the adjusted r^2 value was only 0.123 ($p < 0.001$) indicating that the model is not characterising the majority of the CAR variations. At the individual site level, the variation of CAR was best explained when monocots were included in the regression model at all sites apart from VDB12. Charred remains also contributed to all models with the exception of JRB12.

At the centennial scale, the variation in the combination of all sites was best accounted for by a similar combination of variables as the multidecadal scale, although ericaceous remains no longer contributed to the regression models and the inclusion of the SE US temperature reconstruction enhanced the model performance (Table 8.9). Monocots are an explanatory variable at all sites over 100-year time periods (although were not significant at VDB12) and temperature became important in the northern three sites. The CAR variation is also investigated over 500 year periods and, whilst this equates to only four time slices within the last 2000 years precluding any firm conclusion of drivers of CAR, the inclusion of a temperature reconstruction enhanced the model performance at SCH10, FBB12 and JRB12, whilst there are no clear explanatory variables in VDB12.

The multivariate modelling fails to explain the majority of the variations in the study sites CAR over the last 2000 years; however, of the measured variables, the importance of vegetation composition, fire and temperature in determining CAR is evident. The role of temperature in explaining CAR variation is more important than the earlier correlations based on centennial scales suggested (Section 0). Further work should develop higher resolution temperature reconstructions to determine whether this parameter is as influential on shorter time scales, or whether its importance increases as time progresses. WTD does assist with the explanation of CAR when all sites are combined; however, only the reconstructions using the Lamarre *et al*. (2013) transfer function assist the multiple regression models. This echoes earlier conclusions that multiple proxy reconstructions for the same environmental variable are required to thoroughly test relationships with CAR, since they can be influenced by the efficiency of the statistical techniques to convert proxy data to environmental reconstructions.

The performance of the multiple regression models may be improved by the inclusion of more appropriate temperature reconstructions for the temporal and spatial scale of the study (Section 8.4.3.1) and the characterisation of other influential variables (such as PAR and N). However, it is clear that explaining or predicting rates of carbon accumulation from environmental factors is highly complex owing to the interrelationship of the variables, influences of peatland self-regulation that cannot be easily accounted for and the non-stationary relationships that exist between CAR and the explanatory variables.

Table 8.8 Multivariate modelling to account for carbon accumulation rates on multidecadal timescales. Bold indicate significant relationships.

	Adj. R2	p	F	t
All sites	**0.123**	**<0.001**	**8.511**	
WTD (Lamarre *et al*., 2013)		**0.025**		2.251
Charred material		**0.011**		-2.552
Ericaceae		**0.01**		2.613
Monocots		**0.01**		-2.610
JRB12	**0.089**	**0.031**	**3.726**	
Monocots.		**0.014**		2.551
Ericaceae		0.149		-1.463
FBB12	**0.141**	**0.009**	**4.270**	
Monocots.		**0.013**		-2.579
Ericaceae		**0.021**		2.369
Charred material		0.092		-1.714
VDB12	**0.146**	**0.013**	**4.840**	
UOM		**0.016**		2.496
Charred remains		0.093		1.720
SCH10	**0.236**	**0.001**	**6.142**	
WTD (Lamarre *et al*., 2013)		**0.041**		2.1
Monocots.		**0.02**		2.402
Charred remains		0.101		-1.674

Table 8.9 Multivariate modelling to account for carbon accumulation rates on centennial timescales. Bold indicates significant relationships.

	Adj. R2	P	F	t
All sites	**0.163**	**0.002**	**4.834**	
Monocots		0.098		-1.674
WTD (Lamarre *et al*., 2013)		0.165		1.404
Charred material		0.111		-1.614
Temperature (SE US)		0.0191		1.319
JRB12	**0.26**	**0.05**	**3.222**	
Monocot		**0.026**		2.457
Sphagnum		0.228		1.253
Temperature (N. America)		**0.032**		2.352
FBB12	**0.21**	**0.05**	**3.527**	
Monocots.		**0.018**		-2.617
Temperature (SE US)		0.182		-1.390
VDB12	**0.363**	**0.027**	**3.712**	
WTD (Lamarre *et al*., 2013)		0.054		-2.087
Monocots		0.163		-1.467
Charred remains		**0.016**		2.707
Temperature (SE US)		**0.046**		2.178
SCH10	**0.366**	**0.008**	**6.476**	
Charred material		**0.004**		-3.355
Monocots		**0.008**		2.979

8.4.4 Assessment of the C store vulnerability in peatlands at the southern limit of peat growth

The peatland C response to projected future climate change likely varies depending on the proximity of the peatlands to current climatic limits of peat growth (Yu *et al.*, 2014); however, few studies have focused on characterising the sensitivity of such peatlands. Carbon accumulation in peatlands located at the current southern limit of peat growth in eastern North America appears to be particularly sensitive to previous dry periods such as the MCA and the RWP, associated with pronounced suppression of CAR (Section 8.4.2). Whilst the investigation of individual and combined climate variables failed to identify the dominant combination of variables explaining CAR change over the last 2000 years (Section 0), the most prominent changes in CAR coincide with sustained or pronounced dry periods. Therefore, maintaining a level at which available moisture encourages peat accumulation is essential to determining CAR in this location.

The detrimental effects of warmer, drier periods on the peatlands of Maine and Nova Scotia contrast with results from carbon accumulation patterns at other Northern Hemisphere peatlands, which appear to benefit from the same conditions (e.g. Charman *et al.*, 2013). From the current study site locations, the limit for CAR suppression under drier conditions appears to be northern Nova Scotia. However, confirmation of this location should be tested by the inclusion of more palaeo-records from additional sites in future studies. Modelling results indicate that future climate change will likely result in a dramatic decrease in the Newfoundland bioclimatic zone of blanket peat growth (Gallego-Sala and Prentice, 2013) as conditions become too warm and dry for peat accumulation. The bioclimatic limit for all peat formation may therefore extend northwards in eastern North America if future warming is more persistent or severe than previous MCA conditions. Whilst carbon accumulation may increase in majority of northern peatlands under warmer conditions (Yu *et al.*, 2012; Charman *et al* 2013), the reduction of the carbon sinks in southern regions, owing to low moisture levels, must be assessed when estimating the overall peatland CAR balance of northern peatlands under future warming conditions.

Chapter 9: Conclusions

The primary aim of this thesis was to characterise the relationship between late Holocene peatland hydrological conditions and carbon (C) accumulation rates (CAR) across a climate gradient in eastern North America. Towards this aim, four objectives were outlined in Section 1.2 and have been addressed throughout this thesis:

1. Robust core chronologies will be developed to enhance spatial and temporal comparisons of reconstructed climatic change (Chapter 5)
2. Peatland water table reconstructions will be obtained from four sites across Maine, Nova Scotia and Newfoundland to improve the characterisation of Late Holocene climate change in eastern North America (Chapter 6)
3. Late Holocene carbon accumulation rates will be reconstructed using inferred carbon contents and age-depth models to investigate temporal and spatial variations in C sequestrations (Chapter 7).
4. The extent to which late Holocene peatland carbon accumulation rates fluctuate with vegetation patterns, climatic conditions and disturbance events will be assessed (Chapter 8).

This chapter firstly summarises the main findings obtained from this investigation into late Holocene peatland environmental change in eastern North America, structured according to the research objectives. Secondly, this chapter builds on the main research conclusions, assessing both limitations and the research contributions of this work, by identifying areas of further research priorities.

9.1 Main findings

9.1.1 Development of robust stratigraphic chronologies in eastern North America

- The wealth of late Holocene cryptotephras deposited in eastern North America is only now being fully realised: an additional tephra from the Pacific Northwest region of the United States has been identified and

this study reports the first findings of tephra from the even more distal source regions of Kamchatka, Mexico and Japan.

- The deposition of the White River Ash is prevalent across Newfoundland, Nova Scotia and Maine. This transatlantic isochron facilitates comparisons of climatic change prior to the Medieval Climate Anomaly (MCA): the end of a centennial-scale wet phase occurred at a similar time in more southern regions of eastern North America and northwest Europe whilst cooler, wetter conditions were more sustained in northeastern Newfoundland and Greenland. The lag in response time within the records proximal to the Labrador Sea region suggests that the North Atlantic Oscillation (NAO) was the dominant driver of Medieval climate change in eastern North America through its interaction with the Atlantic Meridional Overturning Circulation (AMOC).

9.1.2 Late Holocene climate change in eastern North America

- The onset of the MCA was associated with lower peatland water table depths, reflecting warmer and drier conditions, which were more persistent in northern Nova Scotia and Newfoundland than in regions further south. Peatland water tables were higher and more variable during the Little Ice Age (LIA) than during the MCA, reflecting cooler and wetter conditions.
- The peatland water table reconstructions obtained from Newfoundland and northern Nova Scotia are more similar over the last 2000 years than those obtained from southern Nova Scotia and Maine. These trends support the hypothesis that the dominant MCA and LIA expressions of climate change in eastern North America were influenced by the strength of the NAO and the AMOC.

9.1.3 Late Holocene carbon accumulation rates in eastern North America

- Carbon accumulation rates (CAR) in peatlands located at the current southern limit of peat growth in eastern North America appear to be particularly sensitive to previous dry periods such as the MCA and the Roman Warm Period, associated with pronounced suppression of CAR.

Peak CAR over the last 2000 years occurred during the wetter LIA, further indicating CAR sensitivity to the regional moisture balance.

- The total amount of accumulated C over the last 2000 years generally increases with decreasing latitude indicating that warmer temperatures enhanced net primary productivity (NPP) where the peatlands were not moisture limited. However, the most northerly peatland contradicts the trends of the other study sites, accumulating similar amounts of C as the most southerly site. CAR at the most northerly site do not appear to have been moisture limited over the last 2000 years, contributing to the elevated total carbon stock. However, other microclimatic and allogenic drivers of peat accumulation that have not been not accounted for within this study may also be contributing to the north-south deviation in CAR trends.

9.1.4 Controls on late Holocene carbon accumulation rates in eastern North America

- Short-term (multi-decadal - centennial) fluctuations in peatland CAR are influenced by changes in summer moisture availability, whilst temperature changes become increasingly important over longer (multi-centennial) timescales. The influence of CAR controls over different timescales must be considered when determining future peatland-carbon responses to climate change.
- The combined influence of vegetation type, water table depth, temperature and fire failed to account for the majority of variations in CAR over the last 2000 years. This suggests that the relationship between these explanatory variables and CAR did not remain constant over time, and there may be other influential variables contributing to CAR change that have not been accounted for within this study. However, sustained or pronounced dry periods coincided with the most prominent decreases in CAR over the last 2000 years, indicating that peatland water table depth was a limiting CAR control at certain points within the records. Maintaining the balance at which available moisture encourages peat accumulation is therefore an essential determinant of CAR in eastern North America.

9.2 Recommendations for future research

- This study has highlighted the importance of maintaining the optimal available moisture balance for primary productivity and C sequestration. Future studies may focus on identifying the threshold at which available moisture becomes an overriding limiting factor, switching peatlands from carbon sources to sinks or vice versa.

- Whilst climate is a dominant driver of CAR, a better understanding of the autogenic controls on CAR, water table dynamics and peatland lateral expansion is required to fully characterise patterns of peatland C sequestration and storage. Site-specific studies comparing CAR and water table reconstructions obtained from multiple cores have provided valuable insights into the importance of such internal dynamics. Further studies of this nature from more varied regions of peat development are required to obtain a comprehensive understanding of the autogenetic processes. These results could then be incorporated within models to test the sensitivity of peatlands to both internal and external processes.

- The geographical limits of peatlands that may be susceptible to CAR suppression under future drier conditions should be identified within subsequent research projects. This could be achieved by increasing the number of palaeo-peatland records obtained from areas proximal to the current moisture limits of peat growth (in eastern North America and other regions of the world, such as southwest Europe) to identify the boundaries of accumulation rate suppression responses to the MCA. More accurate limits could then be obtained using bioclimatic modelling that considers both the reconstructed palaeo-responses and projected future climatic conditions. Such information is vital for obtaining robust estimates of the overall peatland C balance under projected warming conditions. The likely limit of CAR suppression under projected warming could also guide conservation priorities to protect sensitive peatlands from anthropogenic disturbances that may exacerbate immediate C emissions. Furthermore, the vulnerability of the peatland C stores must be assessed within countries using

peatlands as C credits (within the second commitment period (2013-2020) of the Kyoto Protocol, United Nations Framework Convention on Climate Change, Durban, 2011), since these carbon stocks have the potential to exacerbate rather than mitigate C emissions.

- The majority of palaeo-peatland studies focus on the fixation of atmospheric carbon dioxide (CO_2) and its respiration during decay; however, the release of methane (CH_4) is also an important component of the peatland C cycle: omitting CH_4 from the C balance could overestimate net C storage by 19% (Friborg, 2003). Efforts towards understanding past CH_4 cycling are underway. A recent study analysed C and hydrogen isotopic ratios of leaf wax biomarkers (*n*-alkanes) to reconstruct CH_4 recycling in a *Sphagnum* peatland, owing to the symbiotic relationship that exists between *Sphagnum* and methanotrophic bacteria (Nichols *et al*., 2014). Further investigations are required to link the reconstructed proportion of recycled methane contributing to the *Sphagnum* C pool obtained within this approach with estimates of atmospheric CH_4 concentrations. Comparisons of C isotopic values of *n*-alkanes characteristic of *Sphagnum* and vascular plants may also reveal changes in levels of CH_4 production. The CH_4 signal will deplete the C isotopic values of the *Sphagnum n*-alkanes (owing to the *Sphagnum*-methanotroph symbiosis) relative to the vascular plant's *n*-alkanes. The effectiveness of this approach is currently being assessed within two of the eastern North American study sites from this thesis (Mackay, Bendle and Moossen *et al*., in prep). Combining organic geochemical approaches within more traditional palaeo-peatland studies may further enhance environmental understandings of these systems by providing reconstructions of hydrological, temperature and vegetation changes that can be obtained from the same peat sample. Whilst understanding of these techniques requires further refinement, their development should be a priority as they present an opportunity to extract direct climatic parameters from the peatland records that can be combined with the palaeoecological reconstructions of water table depth to obtain more informative climatic reconstructions.

- The detailed deposition distribution of ultra-distal tephras in eastern North America should be characterised through generating tephrostratigraphies from more sites. This work is currently in progress within northeastern regions of the United States (Jensen and Booth *et al*., in prep); however, there is an abundance of Canadian peatlands and lakes in Nova Scotia, Newfoundland, Quebec and Labrador with potential for such exploration. The characterisation of these isochrons in more sites would not only facilitate further investigations into the degree of synchroneity of past climate changes across the tropics and the mid-to high latitudes, but they could also be used within atmospheric transport models to reconstruct past atmospheric circulation patterns. Both aspects would assist with refining the role of oceanic and atmospheric climate drivers within periods of past climatic change.

- Environmental reconstructions from more records containing the White River Ash could be developed to expand the investigation into transatlantic climatic synchroneity at the onset of the MCA and further test hypotheses that the dominant late Holocene climatic drivers in this region were the NAO and the AMOC. The assessment of degree of climatic synchroneity at the point of the tephra deposition is currently limited by the existing sampling resolutions. Future studies may consider increasing sampling resolutions to match the highest resolution available (i.e. NGRIP, 20 years) in each record, if accumulation rates allow.

- The identification of three new ultra-distal tephra source regions within this study highlights the need to look beyond expected source regions when correlating cryptotephras. There is potential for future studies in eastern North America to identify cryptotephras originating from other additional sources regions: for example, tephra from the 2010 eruption of Eyjafjallajökull, Iceland approached Newfoundland (Davies *et al*., 2010); therefore, there is the possibility that Icelandic ash has reached this region in the past, despite conflicting with dominant atmospheric circulation patterns.

- One of the main current limitations within cryptotephra studies is the availability of comparable reference material to obtain firm correlations; therefore, there is the urgent need to investigate more proximal ashes and enhance the availability of comparative databases, such as Tephrabase (Newton *et al.*, 1997; *sensu* Kuehn *et al.*, 2013). Improvements in the availability of tephra reference material would facilitate the inclusion of trace element analysis alongside the major and minor chemistry of the shards towards refining source region correlations to precise eruption correlations.

Throughout this thesis, the degree of insight into the mechanisms and characteristics of environmental change that can currently be extracted from palaeo-peatland records is demonstrated. The future research priorities identified within this section highlight that we are still to discover the true extent of the information that these archives contain and the way in which they can enhance our understanding of the climate system.

Appendices

Appendix A

Major oxide concentrations (wt %) of all individual glass shards from cryptotephras at Saco Heath, Villagedale Bog, Framboise Bog, Jeffrey's Bog analysed at the Tephra Analytical Unit (TAU), School of Geosciences, University of Edinburgh. *n* = number of analyses, totals <95% are shown in red italics. Microprobe operating conditions: Cameca SX100 electron probe microanalyser with accelerating voltage of 15 keV. Rhyolitic (Lipari, ID 3506) and basaltic (BCR2g) secondary standards were used to test analytical consistency. A focused 3 µm beam diameter was used and is described in Hayward (2012).

n	SiO_2	TiO_2	Al_2O_3	FeO	MnO	MgO	CaO	Na_2O	K_2O	Total
SCH10-42: Villagedale Tephra (21/04/13)										
1	68.30	0.48	16.82	2.77	0.06	0.85	3.26	5.31	1.82	99.68
2	68.55	0.52	16.78	3.08	0.07	0.99	3.52	5.16	1.67	100.33
3	*68.70*	*0.45*	*13.09*	*2.79*	*0.06*	*0.71*	*3.01*	*4.32*	*1.82*	*94.95*
4	68.97	0.45	16.15	3.08	0.07	0.95	3.05	4.81	1.75	99.28
5	70.16	0.48	15.39	3.00	0.06	0.82	3.07	5.37	1.93	100.27
6	71.84	0.13	13.06	1.00	0.04	0.21	1.49	4.35	3.47	95.61
7	72.69	0.37	14.92	2.51	0.07	0.56	2.35	5.26	2.09	100.82
8	74.10	0.13	14.70	1.14	0.04	0.23	1.62	3.78	3.35	99.09
9	74.61	0.18	11.47	3.30	0.07	0.52	2.80	3.52	2.18	98.65
10	74.80	0.53	10.64	2.04	0.03	0.09	0.44	4.07	3.57	96.20
11	76.30	0.31	12.13	1.75	0.07	0.38	2.06	3.67	2.38	99.03
SCH10-57: Uncorrelated (06/02/13)										
1	68.20	0.39	14.53	2.83	0.09	0.63	2.78	4.69	2.79	96.92
2	70.05	0.40	14.45	2.72	0.12	0.66	2.66	4.49	2.86	98.40
3	70.22	0.38	14.82	2.57	0.13	0.62	2.86	4.57	2.75	98.92
4	71.07	0.38	15.24	2.68	0.10	0.66	2.57	5.24	2.97	100.91
5	74.62	0.36	14.59	1.62	0.02	0.27	2.66	4.44	2.15	100.74
6	76.41	0.33	11.86	1.72	0.07	0.21	1.94	3.68	2.34	98.56
7	76.81	0.31	11.90	2.14	0.06	0.33	2.05	3.93	2.55	100.07
SCH10-118: White River Ash (eastern lobe) (21/04/13)										
1	*68.12*	*0.19*	*14.36*	*1.35*	*0.04*	*0.40*	*1.72*	*4.19*	*2.84*	*93.23*
2	*69.11*	*0.18*	*12.78*	*1.42*	*0.03*	*0.40*	*1.67*	*4.17*	*3.22*	*92.98*
3	*69.38*	*0.17*	*13.24*	*1.66*	*0.05*	*0.40*	*1.84*	*3.74*	*3.03*	*93.51*
4	*69.75*	*0.19*	*13.07*	*1.39*	*0.04*	*0.47*	*1.98*	*4.17*	*3.10*	*94.17*
5	*69.84*	*0.16*	*13.70*	*1.47*	*0.03*	*0.33*	*1.84*	*4.20*	*3.05*	*94.63*
6	70.02	0.20	13.57	1.54	0.05	0.41	1.94	4.10	3.18	95.01
7	*70.20*	*0.17*	*12.49*	*1.38*	*0.04*	*0.41*	*1.86*	*4.17*	*3.07*	*93.77*
8	70.59	0.19	13.94	1.47	0.03	0.32	1.70	4.19	3.09	95.51

n	SiO_2	TiO_2	Al_2O_3	FeO	MnO	MgO	CaO	Na_2O	K_2O	Total
9	70.68	0.20	13.47	1.59	0.07	0.38	1.88	4.07	3.01	95.35
10	70.77	0.18	14.13	1.51	0.05	0.40	1.88	3.75	3.12	95.78
11	70.89	0.20	13.18	1.62	0.05	0.41	1.94	4.26	3.08	95.63
12	70.90	0.19	14.10	1.47	0.05	0.41	1.85	4.34	3.20	96.50
13	70.98	0.21	13.80	1.56	0.05	0.45	2.09	4.21	3.12	96.47
14	71.19	0.19	14.46	1.44	0.05	0.39	1.77	4.32	2.98	96.80
15	*71.31*	*0.17*	*12.11*	*1.38*	*0.04*	*0.40*	*1.79*	*3.62*	*3.00*	*93.82*
16	71.46	0.20	14.11	1.46	0.05	0.35	1.88	4.56	3.24	97.29
17	71.65	0.18	16.25	1.43	0.04	0.30	2.60	4.81	2.66	99.93
18	71.66	0.14	13.43	1.61	0.03	0.39	1.67	4.24	3.22	96.39
19	71.71	0.20	13.61	1.51	0.04	0.38	1.91	4.10	3.19	96.66
20	72.30	0.17	14.22	1.42	0.05	0.36	1.85	4.31	3.26	97.94
21	72.31	0.20	12.93	1.39	0.04	0.38	1.93	4.07	3.13	96.39
22	72.65	0.21	12.98	1.69	0.04	0.39	1.87	4.46	3.25	97.54
23	72.70	0.15	13.65	1.02	0.05	0.31	1.70	4.05	3.46	97.09
24	72.73	0.18	13.90	1.53	0.05	0.34	1.95	4.04	3.23	97.95
25	72.87	0.19	14.48	1.48	0.01	0.35	1.84	4.21	3.20	98.63
26	73.05	0.20	13.91	1.60	0.05	0.40	1.96	4.27	3.23	98.66
27	73.49	0.17	13.80	1.31	0.05	0.35	1.77	4.44	3.21	98.60
28	73.55	0.18	14.28	1.83	0.04	0.42	1.97	4.66	3.25	100.18
29	74.25	0.15	13.81	1.26	0.04	0.35	1.84	4.10	3.29	99.11

SCH10-131: White River Ash (eastern lobe) (06/02/13)

1	69.30	0.45	14.01	3.05	0.07	0.80	2.89	4.44	1.95	96.96
2	*70.29*	*0.21*	*13.07*	*1.50*	*0.06*	*0.39*	*1.92*	*4.01*	*2.95*	*94.41*
3	*70.31*	*0.19*	*13.15*	*1.49*	*0.05*	*0.35*	*1.86*	*4.09*	*3.08*	*94.55*
4	70.50	0.15	14.01	1.39	0.04	0.34	1.70	4.01	2.95	95.09
5	70.68	0.19	14.20	1.30	0.05	0.38	1.93	4.43	3.13	96.29
6	71.01	0.19	14.94	1.52	0.05	0.40	1.93	4.54	3.07	97.64
7	71.11	0.19	14.23	1.71	0.05	0.47	1.95	4.41	3.02	97.14
8	*71.27*	*0.12*	*12.79*	*1.11*	*0.04*	*0.23*	*1.48*	*3.77*	*3.29*	*94.10*
9	71.54	0.22	9.75	3.61	0.06	0.04	0.24	5.31	4.27	95.04
10	71.58	0.19	14.92	1.68	0.05	0.40	1.92	4.25	3.05	98.03
11	71.94	0.18	13.93	1.49	0.03	0.42	1.98	4.63	3.17	97.75
12	72.60	0.27	12.41	2.04	0.05	0.43	2.33	3.94	2.23	96.31
13	72.95	0.19	14.49	1.56	0.05	0.37	1.96	4.03	3.11	98.71
14	72.98	0.20	14.34	1.57	0.06	0.36	1.94	4.35	3.21	99.02
15	73.22	0.12	13.53	1.20	0.05	0.23	1.50	4.09	3.31	97.24
16	73.30	0.18	13.60	1.21	0.05	0.39	1.75	4.37	3.23	98.08
17	73.56	0.16	13.96	1.23	0.06	0.34	1.68	4.14	3.33	98.46
18	74.26	0.16	15.37	1.16	0.05	0.35	1.72	4.22	3.13	100.41
19	77.12	0.37	12.22	2.11	0.06	0.34	1.80	3.59	2.39	99.99

SCH10-150: White River Ash (eastern lobe) (22/04/13)

n	SiO_2	TiO_2	Al_2O_3	FeO	MnO	MgO	CaO	Na_2O	K_2O	Total
1	*69.18*	*0.20*	*13.15*	*1.45*	*0.05*	*0.35*	*1.88*	*4.30*	*3.01*	*93.57*
2	*69.34*	*0.20*	*13.87*	*1.49*	*0.06*	*0.37*	*1.75*	*3.91*	*2.83*	*93.81*
3	70.84	0.19	14.18	1.41	0.05	0.42	1.81	4.14	3.06	96.11
4	*70.95*	*0.25*	*10.38*	*3.45*	*0.04*	*0.30*	*2.62*	*3.10*	*2.15*	*93.24*
5	*71.08*	*0.15*	*12.61*	*1.34*	*0.03*	*0.28*	*1.61*	*3.41*	*3.15*	*93.65*
6	71.67	0.19	14.58	1.41	0.05	0.39	1.91	4.01	3.11	97.34
7	71.89	0.19	14.76	1.35	0.03	0.38	1.79	3.73	3.05	97.18
8	72.05	0.21	13.89	1.63	0.06	0.41	1.91	4.16	2.97	97.29
9	72.09	0.18	14.06	1.53	0.04	0.34	1.72	4.29	3.10	97.36
10	72.26	0.21	15.11	1.38	0.05	0.37	1.86	4.32	3.10	98.66
11	*72.71*	*0.07*	*12.42*	*0.77*	*0.06*	*0.07*	*0.82*	*3.44*	*4.41*	*94.78*
12	72.73	0.19	14.96	1.30	0.05	0.38	1.88	4.28	3.09	98.86
13	72.87	0.17	14.71	1.59	0.04	0.36	1.72	4.23	3.22	98.91
14	73.08	0.20	14.12	1.70	0.05	0.40	1.89	4.50	3.18	99.12
15	73.24	0.21	14.29	1.56	0.05	0.38	1.87	4.33	3.09	99.01
16	73.51	0.21	14.49	1.68	0.04	0.38	1.98	4.12	3.08	99.49
17	*73.90*	*0.07*	*12.00*	*0.56*	*0.08*	*0.04*	*0.58*	*3.75*	*3.95*	*94.94*
VDB12-42: Villagedale Tephra (21/04/13)										
1	65.93	0.57	15.57	3.57	0.09	1.14	3.94	4.84	1.61	97.26
2	66.93	0.44	15.66	2.31	0.08	0.66	3.55	4.99	1.65	96.27
3	67.30	0.48	14.95	3.03	0.06	0.81	3.11	4.63	1.72	96.08
4	67.61	0.36	17.04	2.74	0.04	0.64	4.03	5.73	1.58	99.76
5	67.78	0.42	14.38	2.69	0.04	0.85	2.98	4.63	1.86	95.64
6	68.05	0.50	15.06	3.31	0.08	1.05	3.15	4.57	1.85	97.63
7	68.50	0.51	14.71	3.45	0.07	0.96	3.17	4.72	1.77	97.85
8	68.53	0.49	14.58	2.24	0.07	0.30	2.78	4.81	2.04	95.82
9	69.03	0.48	15.19	3.09	0.08	0.83	2.98	4.97	1.72	98.37
10	69.13	0.46	14.67	2.89	0.06	0.74	3.23	4.63	1.67	97.46
11	69.22	0.48	15.51	2.79	0.06	0.83	2.98	5.24	1.78	98.90
12	69.24	0.48	14.93	2.77	0.06	0.73	3.40	5.46	1.50	98.57
13	69.59	0.39	15.12	2.96	0.06	0.80	3.02	5.39	1.85	99.17
14	70.47	0.46	14.85	2.61	0.06	0.76	2.85	5.04	1.94	99.04
VDB12-53: Possible Japanese tephra (21/04/13)										
1	74.48	0.36	12.36	2.29	0.06	0.35	3.08	3.99	2.04	99.02
2	76.10	0.39	12.96	2.21	0.06	0.31	2.09	3.67	2.18	99.97
VDB12-90: Mexican source (Volcán Ceboruco) (05/02/13)										
1	*63.27*	*0.55*	*14.27*	*2.99*	*0.11*	*0.84*	*2.47*	*4.90*	*2.80*	*92.21*
2	*64.69*	*0.37*	*15.59*	*2.45*	*0.06*	*0.39*	*1.83*	*5.16*	*2.91*	*93.46*
3	65.48	0.58	16.52	2.21	0.07	0.44	2.63	5.38	2.46	95.78
4	65.53	0.43	15.00	4.86	0.15	0.17	1.23	5.82	5.73	98.93
5	66.29	0.36	15.04	2.67	0.09	0.60	1.91	5.18	3.31	95.44
6	*66.61*	*0.26*	*14.13*	*1.68*	*0.10*	*0.34*	*1.04*	*5.28*	*3.53*	*92.98*

Appendix A

n	SiO_2	TiO_2	Al_2O_3	FeO	MnO	MgO	CaO	Na_2O	K_2O	Total
7	*67.13*	*0.23*	*14.75*	*1.84*	*0.09*	*0.39*	*1.34*	*4.74*	*3.34*	*93.85*
8	67.47	0.62	14.66	3.25	0.12	0.79	2.18	5.17	3.04	97.30
9	67.83	0.53	15.96	2.34	0.11	0.57	1.86	5.16	3.17	97.53
10	*68.16*	*0.22*	*14.65*	*1.99*	*0.08*	*0.35*	*1.16*	*4.83*	*3.34*	*94.77*
11	68.49	0.23	16.89	1.82	0.08	0.24	1.35	5.84	3.09	98.02
12	69.07	0.28	15.19	2.08	0.10	0.42	1.65	5.21	3.25	97.26
13	69.48	0.26	15.37	1.75	0.10	0.36	1.24	5.10	3.62	97.29
14	69.58	0.26	15.52	1.84	0.11	0.42	1.29	5.26	3.35	97.63
15	69.62	0.25	15.29	1.89	0.11	0.38	1.32	5.29	3.47	97.60
16	69.70	0.24	15.31	1.70	0.10	0.32	1.43	5.73	3.47	98.00
17	69.71	0.25	14.54	1.81	0.11	0.38	1.32	5.41	3.37	96.89
18	69.93	0.26	15.60	2.01	0.11	0.38	1.38	5.43	3.25	98.36
19	70.13	0.24	14.72	1.93	0.11	0.36	1.38	5.36	3.24	97.47
20	70.16	0.26	15.65	1.97	0.10	0.37	1.40	5.26	3.52	98.70
21	70.22	0.24	15.31	1.83	0.10	0.34	1.39	5.34	3.44	98.23
22	70.23	0.25	14.14	2.05	0.10	0.28	1.11	5.01	3.57	96.74
23	70.29	0.23	15.43	1.94	0.09	0.33	1.32	5.04	3.33	98.00
24	70.39	0.25	15.22	1.69	0.10	0.38	1.26	5.55	3.42	98.26
25	70.51	0.27	14.53	2.02	0.10	0.35	1.43	5.19	3.38	97.78
26	70.54	0.25	15.11	1.94	0.10	0.39	1.34	5.31	3.29	98.24
27	70.73	0.25	14.73	1.75	0.11	0.29	1.17	5.01	3.48	97.53
28	70.73	0.22	14.87	1.90	0.10	0.33	1.37	5.04	3.45	98.01
29	70.86	0.27	15.05	1.93	0.13	0.35	1.36	5.10	3.46	98.51
30	71.06	0.32	15.84	2.05	0.10	0.43	1.39	5.43	3.43	100.04
31	71.11	0.26	14.94	1.92	0.08	0.30	1.18	5.36	3.42	98.56
32	71.13	0.26	15.95	1.83	0.14	0.39	1.34	5.84	3.56	100.43
VDB12-100: White River Ash (eastern lobe) (21/04/13)										
1	*68.20*	*0.18*	*13.08*	*1.47*	*0.04*	*0.34*	*1.88*	*4.01*	*2.99*	*92.18*
2	*68.42*	*0.17*	*13.97*	*1.47*	*0.04*	*0.37*	*1.83*	*4.15*	*2.97*	*93.42*
3	*68.96*	*0.21*	*12.43*	*1.58*	*0.07*	*0.38*	*1.87*	*3.88*	*3.00*	*92.38*
4	*69.26*	*0.17*	*12.91*	*1.22*	*0.04*	*0.34*	*1.66*	*4.00*	*3.15*	*92.74*
5	70.01	0.16	14.18	1.39	0.04	0.34	1.77	4.44	3.04	95.37
6	*70.39*	*0.17*	*13.23*	*1.47*	*0.05*	*0.36*	*1.83*	*4.07*	*3.05*	*94.63*
7	71.01	0.24	15.30	2.05	0.10	0.38	1.15	5.30	3.44	98.98
8	71.22	0.21	13.55	1.57	0.05	0.39	1.95	4.30	3.21	96.45
9	71.35	0.18	14.11	1.59	0.05	0.39	1.77	4.19	3.05	96.67
10	71.55	0.18	12.92	1.49	0.04	0.30	1.84	4.04	3.14	95.49
11	71.70	0.17	13.99	1.41	0.04	0.39	1.82	3.72	3.23	96.47
12	72.51	0.19	13.89	1.21	0.04	0.41	1.80	4.35	3.11	97.50
13	72.86	0.20	14.11	1.56	0.04	0.37	1.89	4.28	3.17	98.49
14	73.09	0.20	15.47	1.37	0.04	0.44	1.93	4.69	3.24	100.48
15	73.10	0.14	12.55	1.14	0.04	0.23	1.57	3.99	3.26	96.04
16	73.45	0.12	13.82	1.11	0.04	0.25	1.46	3.83	3.39	97.46
17	73.82	0.12	13.18	1.17	0.04	0.21	1.45	4.17	3.45	97.60

n	SiO_2	TiO_2	Al_2O_3	FeO	MnO	MgO	CaO	Na_2O	K_2O	Total
18	74.01	0.21	14.70	1.60	0.04	0.40	1.90	3.91	3.12	99.89
19	74.09	0.12	13.70	1.10	0.04	0.21	1.47	3.99	3.53	98.25
VDB12-176: Ksudach 1 (05/02/13)										
1	*68.15*	*0.25*	*12.87*	*2.75*	*0.08*	*0.53*	*2.22*	*4.72*	*1.30*	*92.88*
2	*69.28*	*0.32*	*12.21*	*2.92*	*0.10*	*0.50*	*2.30*	*4.56*	*1.25*	*93.43*
3	*69.56*	*0.14*	*12.44*	*1.40*	*0.04*	*0.27*	*1.53*	*3.79*	*3.11*	*92.27*
4	*70.33*	*0.28*	*10.94*	*2.46*	*0.12*	*0.39*	*1.90*	*4.31*	*1.30*	*92.02*
5	70.95	0.40	13.36	2.59	0.13	0.57	2.19	4.75	1.35	96.29
6	71.53	0.17	13.99	1.40	0.07	0.39	1.88	4.50	3.18	97.11
7	71.85	0.34	12.70	2.60	0.11	0.46	2.14	4.91	1.42	96.52
8	72.25	0.19	14.56	1.58	0.04	0.37	1.91	4.33	3.17	98.39
9	72.27	0.35	14.00	2.71	0.13	0.51	2.28	5.08	1.33	98.67
10	*72.49*	*0.18*	*12.99*	*1.34*	*0.04*	*0.35*	*1.93*	*1.71*	*2.88*	*93.90*
11	72.62	0.40	13.63	3.03	0.13	0.58	2.35	5.23	1.35	99.32
12	72.81	0.37	13.87	2.30	0.12	0.41	2.02	5.14	1.37	98.42
13	72.99	0.32	14.66	2.34	0.12	0.43	2.03	4.51	1.51	98.91
14	73.03	0.30	13.51	2.06	0.10	0.39	2.27	4.62	2.12	98.41
15	73.32	0.32	13.65	2.01	0.11	0.33	1.97	5.09	1.39	98.18
16	73.39	0.38	14.97	2.73	0.15	0.53	2.37	5.01	1.33	100.85
17	*73.40*	*0.18*	*14.39*	*1.35*	*0.04*	*0.39*	*2.00*	*0.20*	*1.24*	*93.19*
18	74.34	0.30	16.10	1.93	0.10	0.22	2.02	5.40	1.37	101.78
19	*74.38*	*0.24*	*11.63*	*1.29*	*0.05*	*0.13*	*0.53*	*3.10*	*3.62*	*94.98*
20	76.07	0.12	12.44	0.99	0.03	0.13	0.86	2.97	4.91	98.53
21	78.23	0.13	12.72	0.83	0.01	0.15	0.98	1.07	3.75	97.87
FBB12-31: Possible Layer-T (Mount St Helens) (04/02/13)										
1	64.54	0.54	15.06	3.86	0.08	1.21	3.69	4.53	1.78	95.30
2	*66.57*	*0.48*	*13.70*	*2.66*	*0.06*	*0.74*	*2.84*	*4.91*	*1.91*	*93.86*
3	67.61	0.45	19.71	2.69	0.07	0.87	4.46	5.63	1.59	103.06
4	67.89	0.42	14.07	2.58	0.04	0.80	2.75	4.68	1.91	95.14
5	*68.17*	*0.34*	*13.40*	*2.24*	*0.07*	*0.57*	*2.52*	*4.71*	*2.07*	*94.08*
6	69.64	0.39	15.25	2.62	0.07	0.77	2.81	4.77	1.89	98.20
7	71.32	0.24	14.80	1.96	0.04	0.52	2.19	4.34	2.10	97.52
8	71.33	0.37	15.15	2.58	0.06	0.67	2.75	4.67	2.17	99.75
9	71.42	0.32	12.87	1.84	0.03	0.43	1.77	4.48	2.31	95.45
10	*71.53*	*0.28*	*12.68*	*1.61*	*0.04*	*0.36*	*1.69*	*4.38*	*2.39*	*94.97*
11	71.61	0.47	16.15	2.87	0.06	0.76	3.04	5.33	1.87	102.15
12	71.85	0.37	14.66	2.25	0.04	0.53	2.35	4.70	2.15	98.90
13	72.30	0.36	14.41	2.28	0.04	0.47	2.27	4.52	2.23	98.88
14	72.85	0.34	13.73	2.16	0.06	0.46	1.93	4.66	2.32	98.51
FBB12-47: Possible Mount St Helens Set W (Wn/We) (23/04/13)										
1	*71.48*	*0.20*	*11.53*	*1.21*	*0.03*	*0.16*	*1.68*	*3.89*	*2.30*	*92.47*
2	72.75	0.28	12.39	2.44	0.07	0.52	2.49	4.08	1.72	96.75

n	SiO_2	TiO_2	Al_2O_3	FeO	MnO	MgO	CaO	Na_2O	K_2O	Total
3	74.76	0.21	12.62	1.54	0.03	0.26	1.52	4.49	2.39	97.83
4	74.77	0.20	12.67	1.44	0.04	0.24	1.32	4.17	2.58	97.42
FBB12-70: White River Ash (eastern lobe) (20/04/13)										
1	*68.45*	*0.17*	*12.75*	*1.21*	*0.05*	*0.43*	*1.75*	*4.41*	*3.13*	*92.34*
2	*68.65*	*0.11*	*12.86*	*1.02*	*0.03*	*0.26*	*1.58*	*4.22*	*3.17*	*91.88*
3	*68.68*	*0.16*	*13.95*	*1.42*	*0.05*	*0.32*	*1.85*	*4.44*	*3.10*	*93.97*
4	*69.00*	*0.20*	*14.24*	*1.34*	*0.03*	*0.35*	*1.78*	*3.88*	*2.94*	*93.77*
5	*70.02*	*0.02*	*13.42*	*1.30*	*0.00*	*0.35*	*1.73*	*3.92*	*3.26*	*94.02*
6	*70.55*	*0.23*	*12.23*	*2.21*	*0.03*	*0.53*	*2.33*	*4.22*	*2.04*	*94.37*
7	*70.72*	*0.13*	*12.78*	*1.08*	*0.05*	*0.22*	*1.50*	*4.01*	*3.22*	*93.71*
8	*70.87*	*0.26*	*11.63*	*1.74*	*0.04*	*0.38*	*1.69*	*3.80*	*2.20*	*92.62*
9	70.91	0.19	13.97	1.49	0.05	0.37	1.72	4.21	3.13	96.03
10	70.96	0.16	13.86	1.47	0.05	0.37	1.68	4.24	2.95	95.75
11	*71.09*	*0.19*	*10.97*	*1.77*	*0.04*	*0.38*	*1.84*	*3.03*	*3.20*	*92.53*
12	*71.27*	*0.20*	*12.90*	*1.46*	*0.05*	*0.41*	*1.77*	*3.66*	*3.13*	*94.84*
13	71.58	0.20	12.88	1.48	0.05	0.35	1.77	3.95	3.13	95.39
14	71.70	0.18	13.57	1.44	0.05	0.33	1.72	4.74	3.28	97.02
15	71.70	0.20	11.99	1.56	0.03	0.37	1.94	4.33	3.20	95.31
16	72.02	0.21	13.97	1.70	0.05	0.42	1.90	4.31	3.15	97.73
17	72.08	0.12	13.05	1.28	0.02	0.24	1.59	3.77	3.42	95.57
18	72.09	0.18	13.97	1.72	0.04	0.38	1.87	3.56	3.15	96.97
19	72.24	0.11	13.29	1.11	0.05	0.24	1.50	4.14	3.22	95.88
20	72.41	0.10	12.99	0.93	0.02	0.21	2.22	3.73	2.86	95.46
21	72.58	0.33	12.52	2.18	0.05	0.48	2.37	4.19	2.14	96.85
22	72.90	0.20	13.62	1.48	0.04	0.40	1.86	4.19	3.13	97.80
23	72.99	0.12	12.75	1.13	0.04	0.16	1.42	3.59	3.46	95.66
24	73.00	0.15	11.87	1.08	0.04	0.21	1.58	4.00	3.54	95.47
25	73.58	0.21	13.66	1.48	0.05	0.38	1.91	3.86	3.21	98.34
26	74.02	0.11	12.35	1.04	0.04	0.16	1.24	3.65	3.58	96.20
27	74.49	0.11	13.61	1.03	0.05	0.30	1.41	4.49	3.27	98.76
FBB12-105: White River Ash (eastern lobe) (24/04/13)										
1	64.18	1.17	15.20	4.89	0.16	1.26	2.74	5.21	2.94	97.76
2	64.53	1.04	15.87	4.71	0.19	1.18	2.88	5.66	2.86	98.93
3	66.93	0.57	15.83	3.95	0.08	1.16	3.84	4.95	1.64	98.94
4	*68.43*	*0.16*	*14.16*	*1.37*	*0.04*	*0.34*	*1.77*	*2.93*	*2.90*	*92.10*
5	*68.90*	*0.69*	*13.98*	*1.60*	*0.03*	*0.14*	*2.94*	*4.93*	*1.74*	*94.95*
6	*70.58*	*0.17*	*13.70*	*1.32*	*0.05*	*0.32*	*1.71*	*3.94*	*3.15*	*94.95*
7	71.58	0.20	13.80	1.58	0.05	0.42	2.00	4.25	3.04	96.92
8	72.45	0.18	13.11	1.58	0.03	0.39	1.94	3.82	3.16	96.65
9	72.45	0.19	14.40	1.51	0.05	0.40	1.81	4.58	3.02	98.40
10	72.70	0.16	14.09	1.46	0.04	0.39	1.96	4.14	3.04	97.98
11	72.75	0.18	12.97	1.49	0.05	0.35	1.78	3.89	3.17	96.63
12	73.00	0.13	12.74	1.01	0.04	0.26	1.45	4.12	3.23	95.99

n	SiO_2	TiO_2	Al_2O_3	FeO	MnO	MgO	CaO	Na_2O	K_2O	Total
13	73.44	0.15	14.10	1.45	0.04	0.36	1.89	3.95	3.36	98.74
14	73.74	0.20	13.61	1.58	0.04	0.40	2.00	4.36	3.15	99.09
15	73.77	0.14	13.94	1.02	0.04	0.27	1.82	4.01	3.27	98.27
16	74.57	0.22	13.76	1.56	0.03	0.29	1.34	4.27	2.70	98.74
17	75.32	0.22	13.57	1.51	0.03	0.27	1.39	4.17	2.56	99.05
18	76.87	0.23	14.11	1.27	0.04	0.27	1.50	4.78	2.47	101.54
FBB12-162: Possible Japanese tephra (05/02/13)										
1	*70.55*	*0.01*	*12.18*	*0.72*	*0.06*	*0.01*	*0.51*	*3.82*	*4.71*	*92.58*
2	*72.41*	*0.34*	*11.05*	*2.12*	*0.06*	*0.43*	*2.42*	*3.56*	*2.21*	*94.61*
3	72.45	0.60	12.65	3.12	0.13	0.76	3.52	3.97	0.78	97.98
4	72.85	0.35	11.08	2.23	0.07	0.41	2.54	3.67	2.23	95.42
5	73.86	0.02	14.52	0.59	0.06	0.06	0.62	4.69	4.38	98.79
6	74.04	0.60	12.90	3.42	0.13	0.74	3.20	4.50	0.81	100.34
7	74.31	0.28	14.62	1.59	0.02	0.23	2.82	3.99	2.05	99.92
8	75.29	0.28	12.01	2.17	0.06	0.47	2.32	3.51	2.23	98.33
9	75.35	0.34	11.41	2.07	0.04	0.40	2.19	3.30	2.35	97.45
10	75.54	0.03	11.68	0.76	0.06	0.00	0.39	3.29	4.52	96.27
11	75.84	0.31	11.91	2.14	0.04	0.43	2.13	3.58	2.30	98.69
JRB12-71: Mount St Helens (West set) (21/04/13)										
1	73.18	0.20	12.84	1.52	0.03	0.23	1.42	4.61	2.38	96.41
2	73.36	0.18	13.20	1.47	0.03	0.24	1.37	4.29	2.54	96.68
3	73.78	0.16	12.00	1.51	0.03	0.19	1.47	4.04	2.35	95.54
4	74.07	0.23	12.42	1.34	0.03	0.14	0.87	4.22	2.65	95.98
5	74.25	0.19	14.27	1.51	0.04	0.28	1.73	4.52	2.31	99.11
6	74.42	0.21	13.07	1.47	0.03	0.23	1.49	4.41	2.53	97.85
7	74.54	0.22	13.81	1.50	0.04	0.23	1.38	4.56	2.48	98.76
8	74.63	0.23	13.63	1.39	0.03	0.23	1.39	4.44	2.39	98.36
9	75.01	0.23	12.01	1.19	0.02	0.28	1.53	4.51	2.45	97.24
10	75.02	0.23	13.44	1.43	0.04	0.22	1.44	3.73	2.51	98.06
11	75.05	0.23	11.78	1.35	0.02	0.16	0.95	4.22	2.80	96.56
12	75.20	0.84	13.15	2.83	0.05	0.41	1.25	4.23	3.38	101.35
13	75.47	0.21	13.07	1.52	0.03	0.24	1.40	4.83	2.45	99.23
14	75.54	0.23	12.57	1.32	0.04	0.23	1.35	4.66	2.49	98.42
15	75.84	0.23	13.51	1.44	0.03	0.26	1.55	4.58	2.62	100.07
16	76.01	0.22	13.03	1.52	0.03	0.29	1.41	5.08	2.63	100.23
17	76.16	0.23	14.66	1.41	0.03	0.26	1.48	4.70	2.34	101.28
18	76.69	0.23	12.54	1.21	0.04	0.19	0.86	4.59	2.75	99.08
19	76.80	0.23	13.40	1.49	0.04	0.26	1.45	4.57	2.52	100.75
JRB12-131: White River Ash (eastern lobe) (04/02/13)										
1	*67.70*	*0.16*	*14.39*	*1.40*	*0.04*	*0.31*	*1.64*	*4.17*	*3.12*	*92.94*
2	*68.84*	*0.16*	*13.36*	*1.58*	*0.03*	*0.34*	*1.67*	*4.07*	*3.08*	*93.12*
3	*68.87*	*0.19*	*12.85*	*1.44*	*0.04*	*0.36*	*1.84*	*4.24*	*3.12*	*92.95*

Appendix A

n	SiO_2	TiO_2	Al_2O_3	FeO	MnO	MgO	CaO	Na_2O	K_2O	Total
4	*69.38*	*0.15*	*13.48*	*1.58*	*0.04*	*0.33*	*1.88*	*4.06*	*2.95*	*93.86*
5	*69.91*	*0.19*	*12.79*	*1.53*	*0.02*	*0.39*	*1.90*	*4.03*	*3.09*	*93.84*
6	69.99	0.17	14.12	1.58	0.05	0.40	1.74	4.07	3.17	95.30
7	70.41	0.11	11.95	1.13	0.05	0.21	1.41	3.72	3.18	92.17
8	70.43	0.13	12.29	1.31	0.04	0.24	1.55	3.82	3.41	93.22
9	70.53	0.14	12.19	1.19	0.05	0.27	1.56	4.02	3.36	93.30
10	70.70	0.16	13.08	1.31	0.03	0.31	1.87	3.97	3.11	94.55
11	70.86	0.19	13.25	1.45	0.03	0.39	1.86	4.11	3.14	95.28
12	70.86	0.21	13.83	1.59	0.04	0.37	1.88	4.17	3.25	96.20
13	70.92	0.20	14.30	1.61	0.06	0.36	1.89	4.26	3.00	96.60
14	71.17	0.16	14.40	1.43	0.05	0.38	1.98	3.94	3.04	96.53
15	*71.34*	*0.17*	*12.52*	*1.33*	*0.04*	*0.34*	*1.68*	*3.77*	*3.21*	*94.41*
16	71.73	0.20	13.50	1.62	0.05	0.37	1.88	3.99	3.10	96.45
17	71.82	0.19	13.89	1.37	0.03	0.35	1.80	4.24	3.18	96.88
18	71.86	0.22	12.54	1.61	0.05	0.40	1.49	3.60	3.43	95.20
19	72.01	0.19	15.80	1.50	0.05	0.38	1.79	3.98	3.17	98.87
20	72.25	0.21	13.64	1.56	0.04	0.39	1.83	4.03	3.17	97.12
21	72.27	0.21	13.43	1.37	0.04	0.40	1.92	4.18	3.13	96.96
22	72.39	0.13	14.05	1.22	0.04	0.27	1.60	4.27	3.32	97.28
23	72.41	0.20	14.17	1.47	0.04	0.44	1.97	4.26	3.30	98.27
24	72.69	0.12	13.58	1.42	0.05	0.24	1.59	4.00	3.11	96.81
25	72.92	0.18	14.01	1.39	0.05	0.34	1.81	3.98	3.33	98.00
26	72.97	0.13	13.79	1.06	0.05	0.26	1.52	3.93	3.61	97.32
27	73.06	0.17	14.26	1.38	0.06	0.33	1.77	3.77	3.25	98.04
28	73.18	0.21	14.47	1.49	0.05	0.37	1.97	4.07	3.18	99.00
29	73.23	0.19	14.22	1.45	0.05	0.35	1.93	4.28	3.30	99.00
30	73.44	0.20	13.68	1.54	0.05	0.41	1.94	4.40	3.10	98.76
31	73.67	0.17	14.14	1.46	0.05	0.33	1.68	4.17	3.37	99.04
32	73.78	0.18	14.33	1.28	0.05	0.35	1.80	3.90	3.13	98.80
33	73.82	0.17	14.27	1.43	0.05	0.36	1.65	4.43	3.05	99.22
34	74.58	0.15	13.63	1.08	0.06	0.30	1.62	4.21	3.18	98.81
35	74.62	0.25	14.30	1.26	0.05	0.27	1.61	4.18	3.42	99.97
36	74.79	0.16	14.40	1.32	0.05	0.27	1.68	4.13	3.33	100.12

Standards
Reference values
Basaltic standard (BCR2g) accepted range

SiO_2	TiO_2	Al_2O_3	FeO	MnO	MgO	CaO	Na_2O	K_2O	P_2O_5
53.3-54.9	2.21-2.31	13.3-13.7	12.21-12.61	-	3.54-3.64	7.01-7.23	3.05- 3.27	1.74-1.84	0.33-0.37

Lipari standard (ID 3506) accepted range

73.43-74.63	0.07-0.09	12.52-12.92	1.70- 1.80	0.07-0.09	-	0.70-0.74	3.96- 4.16	5.08-5.25	-

Lipari consensus values (Kuehn *et al.*, 2011): recommended values and (uncertainty at 95% confidence)

74.1 (1.4)	0.074 (0.020)	13.1 (0.5)	1.55 (0.05)	0.065 (0.031)	0.041 (0.022)	0.73 (0.06)	4.07 (0.22)	5.11 (0.27)	0.010 (0.02)

04/02/13 am
Basaltic standard (BCR2g)

	SiO_2	TiO_2	Al_2O_3	FeO	MnO	MgO	CaO	Na_2O	K_2O	P_2O_5	Total
1	55.18	2.27	13.80	12.42	0.18	3.58	7.43	2.98	1.85	0.35	100.01
2	54.80	2.26	13.57	12.39	0.20	3.63	7.10	3.31	1.92	0.33	99.51
3	54.73	2.25	13.38	12.53	0.17	3.80	7.09	3.32	1.69	0.34	99.30
μ	54.90	2.26	13.58	12.45	0.18	3.67	7.21	3.20	1.81	0.34	99.61
Lipari standard (ID 3506)											
1	74.05	0.08	12.97	1.28	0.08	0.03	0.76	3.94	5.14	0.01	98.33
2	74.79	0.08	12.93	1.42	0.04	0.06	0.70	4.01	5.16	0.01	99.21
3	74.60	0.08	12.81	1.45	0.06	0.02	0.78	4.05	5.11	0.01	98.99
4	73.97	0.07	13.30	1.56	0.04	0.04	0.79	4.11	5.12	0.01	99.03
μ	74.35	0.08	13.00	1.43	0.06	0.04	0.76	4.03	5.13	0.01	98.89

04/02/13 pm
Basaltic standard (BCR2g)

1	55.03	2.28	14.07	12.08	0.19	3.62	7.17	3.18	1.86	0.32	99.81
2	55.05	2.28	13.30	12.19	0.19	3.65	7.26	3.11	1.87	0.33	99.24
3	55.29	2.27	13.18	11.90	0.20	3.55	7.26	3.31	1.84	0.32	99.12
4	54.57	2.27	13.31	12.61	0.18	3.59	7.19	3.53	1.82	0.30	99.38
5	54.96	2.27	13.66	12.75	0.18	3.64	7.22	3.38	1.81	0.31	100.18
6	54.41	2.27	13.06	12.36	0.21	3.57	7.26	3.24	1.83	0.32	98.54
7	54.18	2.28	13.28	12.26	0.19	3.35	7.34	3.20	1.87	0.31	98.27
8	53.43	2.29	13.16	12.62	0.20	3.61	6.88	3.01	1.75	0.31	97.27
9	54.47	2.28	13.27	11.75	0.20	3.41	7.25	3.28	1.75	0.32	98.00
10	53.91	2.29	13.25	11.81	0.22	3.60	7.15	3.41	1.82	0.31	97.77
11	54.71	2.29	13.33	12.24	0.19	3.57	6.93	3.44	1.85	0.32	98.86
12	54.91	2.28	13.53	12.01	0.20	3.76	7.21	1.52	1.70	0.33	97.45
μ	54.58	2.28	13.37	12.22	0.20	3.58	7.18	2.88	1.81	0.32	98.66
Lipari standard (ID 3506)											
1	73.46	0.07	12.82	1.36	0.07	0.02	0.75	3.92	5.26	0.01	97.76
2	71.91	0.08	12.47	1.55	0.07	0.00	0.69	3.86	5.32	0.01	95.96
3	73.16	0.08	11.87	1.45	0.07	0.07	0.77	3.97	5.25	0.01	96.69
4	73.72	0.08	12.55	1.64	0.07	0.05	0.82	4.25	5.18	0.00	98.36

5	73.25	0.08	12.84	1.62	0.09	0.03	0.77	4.20	5.04	0.00	97.92
6	74.06	0.08	12.77	1.37	0.07	0.02	0.75	4.21	5.16	0.01	98.50
7	72.94	0.08	12.13	1.75	0.07	0.00	0.74	3.81	5.09	0.01	96.60
8	72.36	0.08	12.33	1.63	0.06	0.04	0.84	3.95	5.25	0.00	96.54
9	72.36	0.08	12.03	1.56	0.07	0.07	0.70	4.13	5.25	0.01	96.25
10	72.56	0.07	12.46	1.62	0.07	0.07	0.79	4.10	5.20	0.01	96.93
11	70.51	0.07	12.63	1.83	0.07	0.04	0.79	4.10	5.07	0.00	95.13
12	77.17	0.08	13.01	1.29	0.07	0.06	0.79	0.25	3.35	0.01	96.10
μ	73.12	0.08	12.49	1.56	0.07	0.04	0.76	3.73	5.04	0.01	96.90
05/02/13 am											
Lipari standard (ID 3506)											
1	72.71	0.09	12.98	1.32	0.07	0.09	0.79	4.00	5.04	0.00	97.09
2	73.42	0.07	12.89	1.56	0.06	0.07	0.76	4.15	5.12	0.01	98.11
3	75.28	0.07	13.09	1.31	0.06	0.05	0.66	4.01	5.38	0.00	99.92
4	75.10	0.08	13.23	1.43	0.06	0.04	0.73	4.16	5.25	0.01	100.08
5	74.61	0.08	13.50	1.71	0.08	0.03	0.76	4.65	5.11	-0.01	100.52
6	74.09	0.08	13.21	1.36	0.08	0.03	0.77	3.90	5.24	0.00	98.77
7	74.60	0.09	13.76	1.59	0.06	0.01	0.85	4.27	5.33	0.00	100.56
8	74.73	0.07	13.25	1.61	0.06	0.05	0.69	4.01	5.13	0.01	99.60
9	75.23	0.08	12.67	1.77	0.06	0.06	0.70	4.20	5.15	0.00	99.91
10	75.80	0.07	13.20	1.43	0.05	0.08	0.74	4.15	5.49	0.01	101.03
11	75.89	0.08	12.76	1.60	0.08	0.03	0.77	4.18	5.38	0.01	100.78
12	73.67	0.08	12.65	1.70	0.07	0.05	0.93	4.26	5.23	0.00	98.64
13	72.62	0.08	12.13	1.43	0.07	0.05	0.71	3.88	5.19	0.01	96.18
14	73.98	0.08	13.10	1.70	0.06	0.05	0.74	4.26	5.10	0.00	99.07
15	72.30	0.07	12.98	2.93	0.06	0.01	0.69	4.02	4.97	0.00	98.04
16	75.51	0.07	13.15	1.43	0.06	0.06	0.81	3.94	5.53	0.01	100.57
μ	74.35	0.08	13.03	1.62	0.07	0.05	0.76	4.12	5.23	0.00	99.30
06/02/13 am Basaltic standard (BCR2g)											
1	54.78	2.27	13.91	12.53	0.19	3.47	7.14	3.28	1.82	0.34	99.73
2	55.50	2.26	14.10	12.50	0.20	3.52	7.02	3.50	1.81	0.34	100.75
3	54.14	2.27	12.87	12.03	0.20	3.70	7.06	3.56	1.83	0.34	98.00
4	54.97	2.26	14.49	12.41	0.20	3.59	7.18	3.59	1.84	0.35	100.87
5	55.33	2.26	13.24	12.50	0.20	3.66	7.16	3.33	1.92	0.33	99.94
6	54.70	2.27	13.85	11.95	0.19	3.60	7.10	3.16	1.84	0.37	99.04
7	55.22	2.28	13.86	12.88	0.19	3.67	7.15	3.22	2.02	0.35	100.84
8	55.60	2.25	13.34	13.15	0.19	3.64	7.36	3.43	1.92	0.34	101.22
9	55.52	2.26	13.71	12.22	0.18	3.64	7.19	3.18	1.93	0.32	100.16
10	55.47	2.27	13.97	13.24	0.20	3.68	7.09	3.12	1.91	0.34	101.30
11	55.84	2.28	13.45	12.81	0.20	3.57	7.50	3.44	1.83	0.34	101.26
12	57.24	2.26	13.44	12.69	0.21	3.66	7.30	3.34	1.88	0.33	102.37
μ	55.36	2.27	13.69	12.58	0.20	3.62	7.19	3.35	1.88	0.34	100.46
Lipari standard (ID 3506)											
1	74.13	0.08	12.76	1.45	0.05	0.04	0.81	4.05	5.20	-0.01	98.57

2	74.79	0.08	12.98	1.49	0.06	0.07	0.75	4.20	5.14	0.02	99.59
3	74.53	0.08	12.87	1.60	0.06	0.04	0.76	4.05	5.01	0.00	98.99
4	75.19	0.08	14.18	1.55	0.07	0.07	0.81	4.00	5.15	0.01	101.10
5	74.27	0.07	13.11	1.53	0.07	0.06	0.77	3.99	5.21	0.01	99.09
6	73.79	0.08	13.28	1.74	0.06	0.02	0.72	4.00	5.27	0.00	98.95
7	75.12	0.07	12.65	1.50	0.06	0.01	0.81	4.28	5.23	0.00	99.72
8	75.37	0.08	13.20	1.44	0.08	0.06	0.74	4.09	5.23	0.01	100.32
9	75.27	0.08	12.56	1.27	0.05	0.05	0.74	4.17	5.31	0.01	99.50
10	75.38	0.07	12.99	1.70	0.06	0.05	0.80	3.94	5.36	0.00	100.36
11	75.43	0.07	13.06	1.56	0.06	0.06	0.78	4.22	4.98	0.00	100.22
12	75.72	0.08	13.19	1.53	0.08	0.02	0.90	4.15	5.15	0.01	100.84
μ	74.92	0.08	13.07	1.61	0.06	0.05	0.78	4.10	5.19	0.01	99.77
20/04/2013											
Lipari standard (ID 3506)											
1	73.90	0.09	12.87	1.61	0.06	0.05	0.77	3.99	5.30	0.02	99.01
2	73.96	0.07	12.52	1.51	0.07	0.03	0.77	4.32	5.23	0.00	98.85
3	74.23	0.09	12.33	1.59	0.08	0.04	0.80	4.03	5.23	0.00	98.77
μ	74.03	0.08	12.57	1.57	0.07	0.04	0.78	4.11	5.25	0.01	98.88
21/04/2013											
Basaltic standard (BCR2g)											
1	54.87	2.25	14.43	12.13	0.21	3.61	7.12	3.26	1.72	0.32	99.92
2	55.30	2.27	14.20	12.20	0.21	3.62	7.33	3.37	1.78	0.33	100.60
3	54.48	2.27	13.49	12.28	0.21	3.60	7.13	3.08	1.81	0.33	98.68
4	54.53	2.26	13.99	12.83	0.21	3.60	7.14	3.38	1.75	0.31	100.02
5	54.30	2.26	13.17	12.60	0.20	3.44	7.20	3.19	1.89	0.29	98.55
μ	54.70	2.26	13.86	12.41	0.21	3.57	7.18	3.26	1.79	0.32	99.55
Lipari standard (ID 3506)											
1	74.82	0.07	13.27	1.42	0.06	0.02	0.79	3.84	5.21	0.02	99.89
2	73.91	0.08	12.37	1.62	0.07	0.02	0.78	4.04	5.10	0.02	98.36
3	74.04	0.08	12.55	1.48	0.07	0.03	0.72	3.90	5.21	0.00	98.44
μ	74.26	0.08	12.73	1.51	0.07	0.02	0.76	3.93	5.17	0.01	98.90
22/04/2013											
Basaltic standard (BCR2g)											
1	54.85	2.26	13.82	12.66	0.21	3.59	7.08	3.40	1.78	0.30	99.96
2	54.60	2.27	14.18	12.01	0.20	3.55	7.06	3.66	1.75	0.30	99.58
3	55.64	2.28	14.70	12.59	0.20	3.61	7.24	1.42	1.80	0.29	99.77
4	54.81	2.28	13.08	12.47	0.20	3.58	7.26	2.84	1.83	0.30	98.66
5	54.14	2.27	13.19	12.72	0.19	3.50	7.21	3.50	1.87	0.28	98.89
6	54.67	2.25	13.46	12.66	0.21	3.76	7.10	3.32	1.82	0.30	99.56
7	54.19	2.26	13.30	12.37	0.20	3.58	7.15	3.35	1.86	0.31	98.57
8	54.23	2.28	12.74	12.29	0.21	3.62	7.27	2.99	1.78	0.31	97.72
9	54.48	2.28	13.60	12.30	0.20	3.62	7.09	3.05	1.85	0.29	98.77
10	53.91	2.27	13.76	12.92	0.20	3.55	7.18	3.58	1.89	0.29	99.56

μ	54.55	2.27	13.58	12.50	0.20	3.60	7.16	3.11	1.82	0.30	99.10
Lipari standard (ID 3506)											
1	74.00	0.07	13.45	1.63	0.06	0.05	0.80	3.91	5.39	0.01	99.77
2	73.95	0.09	12.86	1.71	0.07	0.03	0.76	4.35	5.35	0.01	99.55
3	74.13	0.08	13.50	1.70	0.05	0.05	0.79	4.38	5.27	0.01	100.31
4	73.87	0.07	12.74	1.49	0.08	0.06	0.72	4.04	5.24	0.00	98.68
5	73.91	0.08	13.73	1.70	0.08	0.06	0.79	4.25	5.22	0.01	100.19
6	74.06	0.08	13.65	1.52	0.06	0.03	0.76	4.19	5.13	0.00	99.86
7	73.77	0.08	12.56	1.40	0.07	0.01	0.71	3.65	5.45	0.00	98.07
8	74.25	0.07	14.09	1.35	0.09	0.03	0.70	4.14	5.11	0.01	100.21
9	73.56	0.08	12.83	1.67	0.06	0.03	0.79	4.19	5.28	0.00	98.86
10	74.01	0.07	14.14	1.57	0.07	0.04	0.68	4.14	5.21	0.00	100.29
μ	73.95	0.08	13.36	1.57	0.07	0.04	0.75	4.12	5.27	0.01	99.58
23/04/2013											
Basaltic standard (BCR2g)											
1	53.76	2.27	14.18	12.85	0.20	3.62	7.13	3.35	1.76	0.30	99.42
2	53.94	2.29	13.30	11.97	0.21	3.55	7.18	3.26	1.77	0.32	97.80
3	53.08	2.27	13.02	12.63	0.20	3.66	7.00	3.56	1.78	0.32	97.51
4	54.28	2.29	13.50	12.58	0.19	3.57	7.18	3.24	1.79	0.33	98.96
5	53.17	2.26	13.55	12.88	0.21	3.66	7.10	3.08	1.82	0.33	98.06
6	54.27	2.27	13.21	12.46	0.19	3.66	7.20	3.07	1.83	0.33	98.50
7	53.40	2.26	13.00	12.47	0.20	3.58	7.02	3.22	1.81	0.33	97.29
8	53.83	2.29	13.72	12.63	0.20	3.57	7.13	3.39	1.83	0.32	98.93
9	53.68	2.27	14.13	12.39	0.20	3.61	7.02	3.11	1.80	0.33	98.55
10	54.06	2.25	12.90	12.75	0.19	3.52	7.24	3.49	1.76	0.31	98.50
μ	53.75	2.27	13.45	12.56	0.20	3.60	7.12	3.28	1.80	0.32	98.35
Lipari standard (ID 3506)											
1	73.47	0.07	12.66	1.49	0.08	0.02	0.78	4.01	5.15	-0.01	98.08
2	73.69	0.08	12.79	1.52	0.06	0.03	0.72	4.31	5.23	0.02	98.79
3	72.80	0.08	13.08	1.33	0.09	0.03	0.79	4.18	5.26	0.00	98.00
4	73.37	0.08	12.83	1.63	0.07	0.04	0.71	4.11	5.10	0.00	98.32
5	73.05	0.07	12.35	1.53	0.07	0.02	0.76	3.83	5.16	0.00	97.22
6	73.89	0.08	13.65	1.56	0.07	0.06	0.74	4.05	5.12	0.02	99.58
7	73.51	0.07	12.61	1.66	0.07	0.04	0.69	4.07	5.22	0.00	98.29
8	73.18	0.08	12.96	1.53	0.08	0.03	0.82	4.05	5.19	0.00	98.27
9	73.39	0.07	13.40	1.57	0.07	0.04	0.79	4.40	5.07	0.01	99.16
10	74.39	0.08	12.45	1.54	0.07	0.03	0.74	3.89	5.13	0.00	98.71
μ	73.47	0.08	12.88	1.54	0.07	0.03	0.75	3.49	5.16	0.00	98.44
23/04/13 pm											
Basaltic standard (BCR2g)											
1	54.60	2.26	14.51	11.92	0.19	3.66	7.24	3.21	1.82	0.35	99.77
2	54.48	2.26	13.53	12.18	0.19	3.39	6.98	3.33	1.74	0.31	98.40
3	55.51	2.26	13.19	12.80	0.20	3.47	7.12	3.74	1.77	0.33	100.39
μ	54.86	2.26	13.74	12.30	0.19	3.51	7.11	3.43	1.78	0.33	99.52

Lipari standard (ID 3506)											
1	74.84	0.07	13.25	1.52	0.08	0.04	0.69	4.27	5.22	0.00	100.36
2	74.40	0.08	12.38	1.54	0.07	0.05	0.72	4.01	5.13	0.00	98.76
3	74.28	0.08	12.97	1.58	0.07	0.02	0.75	4.12	5.16	0.02	99.39
μ	74.51	0.08	12.87	1.55	0.07	0.04	0.72	4.13	5.17	0.01	99.50
24/04/13 am											
Basaltic standard (BCR2g)											
1	54.75	2.28	14.00	12.53	0.19	3.64	6.89	3.38	1.82	0.35	99.81
2	54.48	2.26	12.57	12.03	0.21	3.53	7.05	2.89	1.87	0.35	97.24
3	53.79	2.28	13.45	12.47	0.21	3.57	7.09	3.29	1.92	0.33	98.43
4	55.18	2.26	14.02	12.96	0.20	3.47	7.19	3.39	1.86	0.35	100.88
5	54.51	2.28	14.27	12.35	0.21	3.51	7.19	3.53	1.85	0.33	100.05
6	54.68	2.27	13.87	12.35	0.20	3.68	7.20	3.37	1.80	0.34	99.77
7	54.42	2.28	13.94	12.19	0.20	3.62	7.16	3.45	1.84	0.33	99.44
8	54.69	2.27	14.36	12.94	0.20	3.58	6.86	3.49	1.76	0.33	100.49
9	54.10	2.26	13.82	12.60	0.21	3.55	7.12	3.52	1.76	0.34	99.30
10	54.86	2.29	13.84	12.01	0.20	3.55	7.28	3.14	1.78	0.35	99.31
μ	54.55	2.27	13.81	12.44	0.20	3.57	7.10	3.35	1.83	0.34	99.47
Lipari standard (ID 3506)											
1	73.90	0.08	12.99	1.45	0.07	0.04	0.74	4.31	5.30	0.01	99.26
2	74.31	0.07	13.15	1.39	0.08	0.05	0.73	4.13	5.26	0.01	99.54
3	73.77	0.08	13.33	1.75	0.07	0.03	0.71	4.23	5.24	0.01	99.57
4	73.59	0.09	13.11	1.51	0.08	0.05	0.70	4.15	5.23	0.01	98.89
5	73.98	0.08	13.00	1.79	0.07	0.05	0.78	4.05	5.16	0.01	99.34
6	73.44	0.08	13.70	1.70	0.08	0.02	0.75	4.22	5.15	0.00	99.49
7	73.77	0.08	13.35	1.58	0.06	0.05	0.76	4.29	5.31	0.02	99.62
8	73.53	0.08	13.30	1.66	0.06	0.04	0.73	4.16	5.22	0.01	99.14
9	74.61	0.08	13.43	1.34	0.07	0.04	0.71	4.13	5.33	0.01	100.11
10	74.06	0.08	13.11	1.60	0.07	0.03	0.76	4.08	5.33	0.01	99.50
11	73.97	0.08	13.08	2.68	0.07	0.06	0.72	4.23	5.12	0.01	100.38
μ	73.90	0.08	13.23	1.68	0.07	0.04	0.74	4.21	5.24	0.01	99.26
24/04/13 pm											
Lipari standard (ID 3506)											
1	74.47	0.08	13.21	1.47	0.05	0.02	0.68	4.04	5.13	0.02	99.16
2	74.39	0.08	12.45	1.46	0.07	0.05	0.70	4.11	5.12	0.01	98.44
3	74.12	0.08	12.84	1.66	0.08	0.05	0.73	4.19	5.14	0.00	98.88
4	74.09	0.07	12.88	1.69	0.08	0.05	0.76	4.00	5.30	0.02	98.93
5	73.43	0.08	12.36	1.70	0.07	0.04	0.72	4.05	5.13	0.01	97.59
μ	74.12	0.08	12.75	1.60	0.07	0.04	0.72	4.08	5.16	0.01	98.60
25/04/2013											
Basaltic standard (BCR2g)											
1	55.36	2.24	13.55	12.86	0.21	3.60	7.08	2.43	1.82	0.36	99.52
2	54.60	2.28	13.84	12.86	0.20	3.57	7.12	2.07	1.79	0.37	98.72

3	54.86	2.27	13.39	12.27	0.20	3.55	6.98	3.76	1.76	0.35	99.40
4	54.54	2.25	12.53	12.12	0.19	3.40	7.20	2.92	1.79	0.36	97.31
μ	54.84	2.26	13.33	12.53	0.20	3.53	7.10	2.80	1.79	0.36	98.74
Lipari standard (ID 3506)											
1	74.47	0.08	13.21	1.47	0.05	0.02	0.68	4.04	5.13	0.02	99.52
2	74.39	0.08	12.45	1.46	0.07	0.05	0.70	4.11	5.12	0.01	98.80
3	74.12	0.08	12.84	1.66	0.08	0.05	0.73	4.19	5.14	0.00	99.25
4	74.09	0.07	12.88	1.69	0.08	0.05	0.76	4.00	5.30	0.02	99.29
5	73.43	0.08	12.36	1.70	0.07	0.04	0.72	4.05	5.13	0.01	97.96
μ	74.10	0.08	12.75	1.60	0.07	0.04	0.72	4.08	5.16	0.01	98.96

Appendix B

Major oxide concentrations (wt %) of individual glass shards obtained from reference material. Ksudach 1 (KS1) shards from Olivebacked Lake were analysed at the Tephra Analytical Unit (TAU), School of Geosciences, University of Edinburgh and those from Lifebuoy Lake were analysed at Queen's University Belfast. Analyses of Lifebuoy Lake samples were completed over two days; therefore * indicates second day runs and associated secondary standard data (tholeiitic obsidian (ATho); accepted values (ref μ) from Óskarsson *et al*., 1982 show that SiO_2 was slightly high and Na_2O slightly low on this day). Edinburgh microprobe operating conditions: Cameca SX100 electron probe microanalyser with accelerating voltage of 15 keV. Belfast microprobe operating conditions: JEOL FEGSEM 6500F with accelerating voltage of 15 keV, beam current 5 nA and beam rastered to about 5x5 μm. *n* = number of analyses, totals <95% are shown in red italics. The Jala Pumice from Volcán Ceboruco (P1) and MSH Layer T shards were analysed at the University of Alberta on a JEOL 8900 using a 10 μm beam, 6 nA current, and 15KeV voltage. Bracketing standard data (OC = Old Crow tephra) for each reference material is included and accepted standard values for analyses completed at the University of Alberta have been taken from Kuehn *et al*. (2011).

Ksudach 1 (KS1)												
n	**SiO_2**	**TiO_2**	**Al_2O_3**	**FeO**	**MnO**	**MgO**	**CaO**	**Na_2O**	**K_2O**	**P_2O_5**	**Cl**	**Total**
KS1 OLIVEBACKED LAKE (20/03/2009)												
1	75.35	0.36	12.21	3.02	0.16	0.74	1.67	4.60	1.53	0.20	0.17	95.73
2	74.86	0.38	13.39	2.33	0.14	0.44	2.11	4.63	1.46	0.07	0.17	98.90
3	74.66	0.41	13.83	2.42	0.14	0.40	2.05	4.52	1.41	0.00	0.15	98.69
4	74.64	0.40	12.94	2.37	0.12	0.40	2.08	5.43	1.44	-0.01	0.17	96.16
5	74.25	0.42	13.73	2.55	0.14	0.46	2.30	4.53	1.37	0.05	0.19	97.24
6	74.19	0.40	13.67	2.45	0.14	0.40	2.21	4.92	1.44	0.00	0.17	99.57
7	74.06	0.39	13.63	2.53	0.14	0.42	2.05	5.09	1.42	0.10	0.17	97.80
8	73.48	0.40	13.95	2.74	0.14	0.55	2.29	4.96	1.26	0.07	0.16	100.35
9	73.31	0.43	13.58	2.81	0.15	0.54	2.49	5.14	1.34	0.06	0.15	99.00
10	71.42	0.30	16.42	1.13	0.09	0.15	3.01	6.21	1.09	0.03	0.14	98.55
11	71.06	0.69	13.85	4.03	0.22	0.79	3.01	4.93	1.19	0.08	0.15	96.83

12	68.79	0.19	17.96	1.39	0.25	0.41	3.85	6.33	0.74	0.03	0.05	100.41
KS1 LIFEBUOY LAKE (18/02/2014)												
1*	74.28	0.33	14.14	2.37	0.24	0.29	1.92	4.74	1.42	0.11	0.17	97.42
2*	74.18	0.33	13.94	2.52	0.17	0.25	1.95	4.94	1.41	0.14	0.18	97.85
3*	73.68	0.35	14.14	2.65	0.14	0.41	2.11	4.88	1.35	0.11	0.16	97.27
4	73.50	0.40	13.92	2.60	0.08	0.44	2.14	5.22	1.36	0.13	0.20	97.24
5	73.22	0.40	13.92	2.91	0.11	0.45	2.09	5.33	1.31	0.08	0.18	97.12
6	73.03	0.32	13.94	2.58	0.10	0.47	2.07	5.87	1.38	0.04	0.17	95.60
7*	73.02	0.43	14.23	2.68	0.26	0.43	2.07	5.27	1.37	0.10	0.16	96.44
8	72.93	0.35	13.79	2.88	0.24	0.41	2.11	5.63	1.40	0.09	0.17	96.95
9	72.89	0.43	13.97	2.76	0.24	0.45	2.09	5.59	1.37	0.08	0.12	97.47
10	72.85	0.44	14.29	2.88	0.05	0.58	2.24	5.03	1.33	0.13	0.18	96.81
11	72.79	0.44	14.19	2.84	0.12	0.35	2.09	5.68	1.29	0.04	0.19	95.59
12	72.43	0.46	13.79	3.07	0.30	0.51	2.05	5.83	1.34	0.06	0.17	95.76
13	72.16	0.62	13.77	3.51	0.16	0.65	2.46	5.11	1.32	0.10	0.14	97.66
14	71.94	0.37	14.32	3.26	0.19	0.49	2.36	5.48	1.31	0.06	0.20	96.60
15	71.17	0.26	15.74	1.75	0.08	0.20	2.78	6.68	1.08	0.09	0.18	96.12
16	*66.26*	*0.46*	*17.73*	*2.25*	*0.17*	*0.34*	*4.32*	*7.30*	*0.90*	*0.16*	*0.11*	*93.34*
μ	72.87	0.40	14.25	2.62	0.16	0.44	2.36	5.35	1.31	0.08	0.16	97.30
σ	1.90	0.10	1.25	0.57	0.06	0.14	0.58	0.67	0.17	0.05	0.03	1.55

	SiO_2	**TiO_2**	**Al_2O_3**	**FeO**	**MnO**	**MgO**	**CaO**	**Na_2O**	**K_2O**	**P_2O_5**	**Cl**	**Total**
KS1: Lifebuoy Lake bracketing standard data												
Lipari1	72.39	0.03	12.81	1.53	0.00	0.03	0.63	4.02	4.90	0.04	0.32	96.70
Lipari2	73.34	0.04	12.93	1.59	0.01	0.05	0.64	3.91	5.03	0.03	0.34	97.92
Lipari3	73.83	0.07	12.99	1.65	0.17	0.04	0.71	4.13	5.04	0.01	0.32	98.96
μ	73.19	0.05	12.91	1.59	0.06	0.04	0.66	4.02	4.99	0.03	0.33	97.86
σ	0.73	0.02	0.09	0.06	0.10	0.01	0.04	0.11	0.08	0.02	0.01	1.13
Atho1	74.35	0.27	11.79	3.28	0.18	0.10	1.69	4.42	2.75	0.10	0.01	98.96
Atho2	74.51	0.27	12.01	3.38	0.13	0.09	1.67	4.54	2.75	0.02	0.01	99.39
Atho3	74.93	0.23	12.08	3.36	0.06	0.09	1.66	4.10	2.72	0.02	0.05	99.31
μ	74.60	0.26	11.96	3.34	0.12	0.09	1.67	4.35	2.74	0.05	0.02	99.22
σ	0.30	0.02	0.15	0.05	0.06	0.01	0.02	0.23	0.02	0.05	0.02	0.23
*Atho4	75.46	0.29	12.13	3.37	0.10	0.08	1.69	4.02	2.85	0.01	0.08	100.07
*Atho5	75.53	0.22	12.14	3.42	0.12	0.08	1.74	3.97	2.87	0.05	0.08	100.22
*Atho6	75.97	0.21	12.26	3.38	0.14	0.08	1.69	4.18	2.73	0.01	0.07	100.74
μ	75.65	0.24	12.18	3.39	0.12	0.08	1.71	4.06	2.82	0.02	0.08	100.34

σ	0.28	0.04	0.07	0.03	0.02	0.00	0.03	0.11	0.08	0.02	0.01	0.35
KS1: Olivebacked Lake bracketing standard data												
Lipari1	73.71	0.07	12.74	1.58	0.07	0.05	0.70	4.15	5.19	-0.02	0.38	98.62
Lipari2	73.29	0.08	12.69	1.50	0.07	0.06	0.81	3.95	5.12	0.02	0.38	97.97
Lipari3	73.90	0.08	12.89	1.56	0.06	0.03	0.75	3.93	5.08	0.03	0.37	98.68
Lipari4	74.61	0.08	13.00	1.67	0.05	0.03	0.70	3.91	5.04	0.01	0.37	99.48
Lipari5	73.71	0.08	12.95	1.55	0.07	0.01	0.72	3.77	5.09	0.00	0.38	98.32
Lipari6	74.58	0.08	12.83	1.51	0.06	0.03	0.74	3.97	4.97	0.04	0.37	99.18
Lipari7	73.70	0.09	12.96	1.64	0.08	0.05	0.65	4.04	5.11	-0.01	0.38	98.68
Lipari8	73.16	0.08	12.55	1.53	0.07	0.05	0.84	4.02	5.07	-0.01	0.38	97.74
Lipari9	73.44	0.08	13.23	1.65	0.07	0.02	0.81	3.95	5.12	0.00	0.38	98.75
Lipari10	75.13	0.09	12.88	1.58	0.07	0.02	0.69	3.91	4.99	-0.03	0.39	99.72
μ	73.92	0.08	12.87	1.58	0.07	0.04	0.74	3.96	5.08	0.00	0.38	98.71
σ	0.64	0.00	0.19	0.06	0.01	0.02	0.06	0.10	0.06	0.02	0.01	0.62
Ref μ	74.48	0.27	12.07	3.43	0.10	0.10	1.75	4.31	2.72			99.23

Jala Pumice (P1)

n	**SiO_2**	**TiO_2**	**Al_2O_3**	**FeO**	**MnO**	**MgO**	**CaO**	**Na_2O**	**K_2O**	**Cl**	**Total**
1	70.34	0.22	15.57	2.02	0.10	0.31	1.27	4.97	3.38	0.07	98.26
2	68.22	0.25	15.29	1.80	0.05	0.34	1.28	4.69	3.38	0.15	95.43
3	69.60	0.31	15.45	1.92	0.07	0.28	1.31	4.98	3.05	0.08	97.05
4	70.36	0.30	15.86	1.95	0.11	0.32	1.31	4.92	3.26	0.08	98.47
5	70.31	0.26	15.63	2.03	0.10	0.34	1.37	4.94	3.33	0.09	98.40
6	71.34	0.33	15.87	1.89	0.15	0.35	1.34	5.01	3.36	0.13	99.76
7	70.07	0.23	15.18	1.83	0.08	0.32	1.31	4.96	3.25	0.15	97.37
8	70.89	0.24	15.63	2.00	0.09	0.31	1.31	5.03	3.24	0.11	98.84
9	70.61	0.24	15.67	1.85	0.13	0.33	1.28	5.43	3.31	0.13	98.98
10	70.45	0.30	16.14	2.00	0.05	0.31	1.30	4.97	3.35	0.15	99.01
11	70.42	0.32	15.94	1.96	0.10	0.33	1.28	5.05	3.33	0.07	98.79
12	70.61	0.29	15.70	2.03	0.09	0.33	1.31	5.26	3.30	0.08	99.00
13	68.94	0.27	15.53	1.90	0.05	0.37	1.34	5.09	3.33	0.07	96.88
14	70.13	0.40	15.78	1.88	0.13	0.30	1.35	4.94	3.44	0.11	98.45
15	70.87	0.24	15.64	1.87	0.07	0.34	1.28	4.89	3.42	0.08	98.70
16	70.45	0.32	15.70	1.90	0.06	0.36	1.32	4.97	3.31	0.09	98.47
17	69.90	0.22	15.49	1.92	0.06	0.38	1.39	5.25	3.28	0.15	98.03
18	68.27	0.32	15.27	1.92	0.06	0.36	1.32	4.97	3.18	0.10	95.76
19	69.65	0.28	15.47	1.96	0.11	0.34	1.30	5.09	3.50	0.05	97.75

20	70.28	0.24	15.64	1.92	0.14	0.35	1.29	5.25	3.39	0.09	98.60
21	69.15	0.19	15.38	1.90	0.09	0.33	1.23	4.98	3.29	0.10	96.64
22	70.51	0.29	15.72	1.85	0.13	0.32	1.33	4.85	3.43	0.11	98.53
23	69.88	0.27	15.62	1.83	0.09	0.33	1.29	5.24	3.31	0.09	97.94
24	70.39	0.25	15.88	2.07	0.06	0.40	1.39	4.85	3.30	0.12	98.70
25	70.44	0.29	15.85	1.92	0.14	0.35	1.28	5.19	3.34	0.08	98.87
μ	70.08	0.27	15.64	1.92	0.09	0.34	1.31	5.03	3.32	0.10	98.11
σ	0.76	0.04	0.22	0.07	0.03	0.03	0.04	0.16	0.09	0.03	1.05

P1 bracketing standard data											
ID	**SiO_2**	**TiO_2**	**Al_2O_3**	**FeO**	**MnO**	**MgO**	**CaO**	**Na_2O**	**K_2O**	**Cl**	**Total**
3506-10	74.69	0.04	13.49	1.65	0.10	0.03	0.72	4.09	5.07	0.35	100.16
3506-11	74.46	0.14	13.23	1.58	0.06	0.05	0.71	3.96	5.01	0.37	99.47
3506-12	74.09	0.11	13.17	1.53	0.08	0.04	0.72	3.78	5.12	0.33	98.89
3506-13	74.61	0.05	13.22	1.65	0.04	0.03	0.72	4.00	5.10	0.35	99.70
3506-14	74.80	0.03	13.11	1.64	0.08	0.01	0.75	3.79	5.10	0.36	99.60
μ	74.53	0.08	13.24	1.61	0.07	0.03	0.73	3.92	5.08	0.35	99.56
σ	0.28	0.05	0.15	0.05	0.02	0.02	0.02	0.13	0.05	0.01	0.46
3506-15	74.00	0.04	12.96	1.60	0.05	0.05	0.73	4.12	5.00	0.35	98.82
3506-16	74.36	0.07	13.13	1.61	0.02	0.02	0.72	3.68	5.10	0.32	98.95
3506-17	74.55	0.11	13.24	1.61	0.07	0.01	0.75	3.82	5.20	0.39	99.65
3506-18	73.91	0.00	13.33	1.58	0.06	0.02	0.77	3.99	5.07	0.31	98.97
3506-19	74.65	0.08	13.14	1.49	0.04	0.04	0.70	3.84	5.17	0.37	99.43
μ	74.30	0.06	13.16	1.58	0.05	0.03	0.73	3.89	5.11	0.35	99.16
σ	0.33	0.04	0.14	0.05	0.02	0.02	0.03	0.17	0.08	0.03	0.36
μ ref. value	**74.10**	**0.07**	**13.10**	**1.55**	**0.07**	**0.04**	**0.74**	**4.06**	**5.13**	**0.34**	**99.09**
σ	0.96	0.03	0.34	0.06	0.03	0.02	0.05	0.28	0.26	0.03	
OC-7	72.49	0.24	12.76	1.68	0.07	0.30	1.45	3.61	3.46	0.28	96.26
OC-8	73.00	0.34	12.95	1.64	0.09	0.25	1.39	3.60	3.62	0.20	97.04
OC-9	72.65	0.32	12.86	1.54	0.05	0.23	1.44	3.60	3.60	0.31	96.54
OC-10	72.20	0.31	12.75	1.70	0.04	0.25	1.43	3.47	3.63	0.23	95.95
OC-11	72.34	0.24	12.76	1.53	0.11	0.25	1.33	3.56	3.56	0.30	95.91
μ	72.54	0.29	12.82	1.62	0.07	0.26	1.41	3.57	3.57	0.26	96.34
σ	0.31	0.05	0.09	0.08	0.03	0.02	0.05	0.06	0.07	0.05	0.47
OC-12	73.82	0.31	12.56	1.73	0.06	0.27	1.43	3.74	3.33	0.29	97.47
OC-13	72.59	0.31	12.83	1.59	0.03	0.26	1.39	3.56	3.60	0.35	96.44

OC-14	*71.05*	*0.27*	*12.43*	*1.69*	*0.05*	*0.26*	*1.42*	*3.17*	*3.70*	*0.28*	*94.23*
OC-15	*71.57*	*0.29*	*12.57*	*1.58*	*0.05*	*0.28*	*1.31*	*3.23*	*3.60*	*0.24*	*94.68*
OC-16	*71.46*	*0.31*	*12.44*	*1.59*	*0.04*	*0.26*	*1.32*	*3.04*	*3.65*	*0.24*	*94.28*
μ	72.10	0.30	12.57	1.64	0.05	0.27	1.37	3.35	3.58	0.28	95.42
σ	1.12	0.02	0.16	0.07	0.01	0.01	0.06	0.29	0.14	0.04	1.46
μ ref. value	**71.90**	**0.30**	**12.57**	**1.63**	**0.05**	**0.28**	**1.42**	**3.67**	**3.56**	**0.27**	**95.68**
σ	1.00	0.05	0.34	0.14	0.03	0.03	0.05	0.26	0.26	0.05	
Laki-1	50.11	3.28	13.06	14.15	0.26	5.36	9.91	3.02	0.45	0.01	99.61
Laki-2	49.84	3.12	13.49	14.13	0.25	5.29	9.59	2.92	0.45	0.00	99.09
Laki-3	49.81	3.20	13.05	14.26	0.22	5.20	9.86	2.87	0.47	0.02	98.96
Laki-4	49.81	3.12	13.22	14.17	0.29	5.15	9.75	3.04	0.46	0.01	99.01
μ	49.89	3.18	13.21	14.18	0.25	5.25	9.78	2.96	0.46	0.01	99.17
σ	0.15	0.08	0.21	0.06	0.03	0.09	0.14	0.08	0.01	0.01	0.30
Laki-5	50.39	3.08	13.07	14.32	0.22	5.26	9.75	2.89	0.55	0.00	99.51
Laki-6	50.47	3.04	12.99	14.29	0.16	5.37	9.51	2.93	0.47	0.02	99.24
Laki-7	50.25	3.13	13.04	14.42	0.21	5.18	9.60	2.87	0.46	0.05	99.20
Laki-8	50.29	3.20	12.87	14.20	0.24	5.25	9.53	3.07	0.51	0.02	99.17
μ	50.35	3.11	12.99	14.31	0.20	5.26	9.60	2.94	0.50	0.03	99.28
σ	0.10	0.07	0.09	0.09	0.03	0.08	0.11	0.09	0.04	0.02	0.16
μ ref. value	49.70	3.08	13.00	14.10	0.23	5.39	9.70	2.85	0.46	0.02	99.09
σ	1.40	0.22	0.50	0.60	0.10	0.25	0.38	0.25	0.04	0.01	

MSH-Layer T: visible distal sample from NE Washington State

n	SiO_2	TiO_2	Al_2O_3	FeO	MnO	MgO	CaO	Na_2O	K_2O	Cl	Total
1	67.77	0.53	15.70	3.41	0.11	0.93	3.25	4.42	1.80	0.07	97.99
2	67.03	0.56	14.92	3.00	0.08	0.81	2.49	5.13	1.97	0.17	96.16
3	68.64	0.44	15.59	3.21	0.02	0.74	3.34	4.65	1.71	0.13	98.46
4	68.57	0.39	15.60	2.89	0.01	0.69	3.25	4.49	1.77	0.08	97.74
5	69.06	0.47	15.37	2.93	0.02	0.71	2.96	4.86	1.86	0.08	98.32
6	68.83	0.46	15.10	3.11	0.04	0.67	2.94	4.59	1.85	0.09	97.69
7	69.86	0.57	14.90	3.50	0.07	0.80	2.66	4.44	2.08	0.11	98.99
8	70.19	0.43	15.10	2.95	0.01	0.69	2.77	4.50	2.00	0.10	98.74
9	68.40	0.37	14.33	2.58	0.10	0.63	2.43	4.64	2.08	0.15	95.70
10	69.79	0.38	14.25	2.62	0.08	0.56	2.31	4.54	2.01	0.10	96.64

11	71.61	0.38	14.57	2.77	0.07	0.43	2.36	4.64	2.10	0.17	99.11
12	*68.57*	*0.40*	*13.74*	*2.68*	*0.07*	*0.52*	*2.16*	*4.53*	*2.09*	*0.12*	*94.89*
13	70.69	0.38	14.37	2.42	0.06	0.48	2.39	4.62	2.08	0.16	97.66
14	72.18	0.42	14.91	2.02	0.08	0.44	2.07	4.63	2.56	0.19	99.50
15	71.56	0.39	14.31	2.69	0.08	0.44	2.19	4.51	2.20	0.08	98.45
16	71.04	0.37	14.08	2.37	0.04	0.45	2.27	4.56	2.10	0.13	97.41
17	71.11	0.28	14.29	2.49	0.08	0.48	2.29	4.44	1.94	0.10	97.49
18	*68.92*	*0.46*	*13.39*	*2.10*	*0.00*	*0.45*	*1.62*	*4.55*	*2.63*	*0.14*	*94.24*
19	70.88	0.42	13.94	2.05	0.04	0.45	1.66	4.35	2.75	0.18	96.73
20	74.03	0.50	13.98	2.37	0.03	0.48	2.14	4.18	2.39	0.13	100.24
21	72.50	0.32	13.48	2.14	0.01	0.42	1.96	4.22	2.35	0.14	97.56
22	73.15	0.45	13.52	2.16	0.08	0.45	1.83	4.16	2.48	0.11	98.38
23	73.50	0.32	13.48	2.32	0.06	0.38	1.85	4.23	2.41	0.17	98.72
24	74.57	0.33	13.61	2.03	0.00	0.45	1.80	3.98	2.46	0.16	99.38
25	72.86	0.29	13.28	2.23	0.01	0.40	1.88	3.71	2.33	0.10	97.09
26	73.79	0.35	13.12	1.83	0.04	0.38	1.72	4.09	2.54	0.11	97.97
μ	70.73	0.41	14.34	2.57	0.05	0.55	2.33	4.45	2.18	0.13	97.74
σ	2.13	0.08	0.78	0.46	0.03	0.15	0.51	0.28	0.29	0.04	1.40

MSH Layer T: upper 20cm of proximal coarse lapilli fall, Independence Pass

n	SiO_2	TiO_2	Al_2O_3	FeO	MnO	MgO	CaO	Na_2O	K_2O	Cl	Total
1	70.19	0.44	15.83	3.07	0.02	0.82	3.02	4.88	1.84	0.12	97.91
2	71.34	0.34	15.42	2.74	0.11	0.62	2.52	4.98	1.98	0.15	96.96
3	71.46	0.36	15.30	2.65	0.07	0.61	2.57	5.09	1.99	0.08	98.20
4	71.82	0.36	15.17	2.58	0.05	0.63	2.46	5.07	1.96	0.10	98.54
5	71.84	0.44	15.32	2.50	0.09	0.56	2.52	4.72	2.06	0.14	98.32
6	72.02	0.32	15.15	2.53	0.06	0.56	2.33	4.92	2.15	0.15	95.76
7	72.13	0.36	15.20	2.55	0.06	0.55	2.50	4.63	2.06	0.16	98.76
8	72.27	0.39	15.22	2.52	0.07	0.54	2.36	4.59	2.12	0.10	99.79
9	72.78	0.35	15.01	2.60	0.03	0.49	2.45	4.25	2.09	0.15	98.41
10	*72.81*	*0.38*	*15.00*	*2.17*	*0.06*	*0.51*	*2.17*	*4.66*	*2.24*	*0.17*	*94.96*
11	72.82	0.34	14.85	2.28	0.06	0.51	2.16	4.76	2.26	0.15	96.22
12	72.97	0.29	14.89	2.16	0.05	0.44	2.18	4.97	2.11	0.10	98.36
13	73.17	0.36	14.99	2.23	0.01	0.48	2.18	4.50	2.12	0.12	98.34
14	73.36	0.36	14.63	1.91	0.09	0.54	2.01	4.85	2.29	0.12	97.42
15	*73.61*	*0.26*	*14.65*	*2.07*	*0.06*	*0.46*	*2.05*	*4.54*	*2.28*	*0.20*	*90.60*
16	*73.74*	*0.26*	*14.64*	*2.11*	*0.04*	*0.44*	*1.97*	*4.49*	*2.31*	*0.20*	*94.05*
17	73.95	0.32	14.47	2.00	0.08	0.39	1.97	4.46	2.38	0.13	99.08

18	74.21	0.32	14.46	1.98	0.03	0.38	1.92	4.44	2.28	0.14	98.76
μ	72.58	0.35	15.01	2.37	0.06	0.53	2.30	4.71	2.14	0.14	97.25
σ	1.01	0.05	0.35	0.30	0.02	0.10	0.27	0.24	0.14	0.03	2.18
MSH Layer T: Lower portion of proximal coarse lapilli fall, Independence Pass											
1	68.86	0.52	16.47	3.31	0.05	0.91	3.33	4.90	1.80	0.08	99.73
2	69.55	0.53	15.79	3.04	0.10	0.79	3.12	5.30	1.82	0.19	98.22
3	69.66	0.54	16.10	3.13	0.03	0.79	3.20	4.77	1.87	0.14	98.06
4	69.67	0.49	16.57	3.13	0.05	0.76	2.90	4.67	1.82	0.18	96.30
5	69.73	0.54	15.90	3.22	0.03	0.90	3.10	4.81	1.86	0.14	98.94
6	69.74	0.47	15.95	3.26	0.06	0.89	3.11	4.79	1.89	0.08	99.42
7	69.85	0.48	16.01	3.16	0.06	0.82	3.19	4.79	1.75	0.12	98.87
8	69.90	0.43	15.94	3.07	0.06	0.82	3.11	5.03	1.74	0.11	99.23
9	69.92	0.45	16.06	3.06	0.10	0.86	3.07	4.81	1.79	0.09	98.44
10	69.96	0.54	15.87	3.16	0.09	0.81	3.06	4.84	1.81	0.07	99.00
11	70.03	0.51	15.95	3.30	0.08	0.80	3.03	4.36	1.98	0.21	95.38
12	70.05	0.47	16.06	3.17	0.08	0.83	3.07	4.57	1.81	0.12	98.50
13	70.12	0.49	16.03	2.99	0.12	0.73	3.06	4.84	1.73	0.10	98.32
14	70.28	0.44	15.94	2.83	0.10	0.76	2.92	5.12	1.73	0.09	95.98
15	70.28	0.49	16.08	2.94	0.01	0.84	3.03	4.68	1.80	0.06	100.34
16	70.36	0.48	15.86	3.08	0.07	0.82	3.01	4.60	1.85	0.09	98.96
17	70.65	0.49	15.44	3.12	0.06	0.78	2.78	4.72	2.06	0.12	98.79
18	71.50	0.45	15.38	2.74	0.07	0.78	2.72	4.52	1.85	0.21	99.69
19	71.79	0.37	14.90	2.68	0.03	0.70	2.74	4.96	1.92	0.10	99.26
μ	70.10	0.48	15.91	3.07	0.07	0.81	3.03	4.79	1.84	0.12	98.49
σ	0.66	0.04	0.37	0.17	0.03	0.05	0.16	0.22	0.08	0.05	1.30

MSH-Layer T bracketing standard data											
ID	**SiO_2**	**TiO_2**	**Al_2O_3**	**FeO**	**MnO**	**MgO**	**CaO**	**Na_2O**	**K_2O**	**Cl**	**Total**
3506-1	73.76	0.05	13.24	1.37	0.07	0.02	0.77	4.23	5.12	0.32	98.89
3506-2	74.02	0.09	13.16	1.30	0.03	0.06	0.81	4.05	5.14	0.28	98.89
3506-3	73.94	0.09	13.22	1.44	0.04	0.05	0.72	4.06	5.12	0.27	98.88
3506-4	73.83	0.03	13.26	1.51	0.09	0.04	0.77	4.14	5.14	0.31	99.05
3506-5	73.11	0.08	13.12	1.47	0.06	0.07	0.70	4.29	5.16	0.33	98.31
3506-6	72.67	0.07	13.12	1.41	0.05	0.04	0.73	4.08	5.35	0.30	97.76
μ	73.56	0.07	13.19	1.42	0.06	0.05	0.75	4.14	5.17	0.30	98.63
σ	0.54	0.02	0.06	0.07	0.02	0.02	0.04	0.10	0.09	0.02	0.50
3506-7	74.35	0.04	13.16	1.42	0.06	0.04	0.78	4.24	5.13	0.34	99.48
3506-8	74.04	0.09	13.29	1.43	0.09	0.04	0.69	4.16	5.13	0.27	99.16

3506-9	74.30	0.09	13.05	1.46	0.04	0.02	0.78	4.08	5.14	0.29	99.19
3506-10	74.58	0.08	13.22	1.42	0.08	0.03	0.75	4.11	5.12	0.26	99.57
3506-11	74.36	0.07	13.19	1.41	0.06	0.02	0.73	3.91	5.08	0.34	99.09
3506-12	74.72	0.10	13.06	1.45	0.11	0.04	0.76	4.17	5.09	0.32	99.74
μ	74.39	0.07	13.16	1.43	0.07	0.03	0.75	4.11	5.11	0.30	99.37
σ	0.23	0.02	0.09	0.02	0.02	0.01	0.03	0.11	0.02	0.04	0.26
μ ref. value	**74.10**	**0.07**	**13.10**	**1.55**	**0.07**	**0.04**	**0.74**	**4.06**	**5.13**	**0.34**	**99.09**
σ	0.96	0.03	0.34	0.06	0.03	0.02	0.05	0.28	0.26	0.03	
OC-1	71.82	0.30	12.49	1.58	0.06	0.27	1.47	3.75	3.55	0.24	95.48
OC-2	*70.43*	*0.37*	*12.36*	*1.48*	*0.08*	*0.28*	*1.40*	*3.76*	*3.42*	*0.27*	*93.80*
OC-3	*70.70*	*0.31*	*12.43*	*1.53*	*0.08*	*0.28*	*1.38*	*3.73*	*3.73*	*0.24*	*94.35*
OC-4	*70.62*	*0.27*	*12.35*	*1.51*	*0.04*	*0.27*	*1.44*	*3.68*	*3.63*	*0.19*	*93.97*
OC-5	*70.76*	*0.24*	*12.25*	*1.45*	*0.06*	*0.27*	*1.47*	*3.57*	*3.69*	*0.23*	*93.93*
OC-6	*70.62*	*0.32*	*12.40*	*1.48*	*0.04*	*0.29*	*1.42*	*3.50*	*3.60*	*0.22*	*93.84*
μ	*70.83*	*0.30*	*12.38*	*1.50*	*0.06*	*0.28*	*1.43*	*3.66*	*3.60*	*0.23*	*94.23*
σ	0.50	0.05	0.08	0.04	0.02	0.01	0.03	0.11	0.11	0.02	0.64
OC-7	73.55	0.30	12.94	1.67	0.04	0.29	1.48	3.90	3.61	0.23	97.94
OC-8	74.31	0.30	12.98	1.54	0.01	0.33	1.52	3.63	3.76	0.25	98.58
OC-9	72.54	0.33	12.62	1.55	0.06	0.26	1.39	3.94	3.59	0.23	96.45
OC-10	72.25	0.33	12.59	1.50	0.07	0.25	1.43	3.48	3.85	0.30	95.98
OC-11	72.12	0.23	12.55	1.63	0.07	0.24	1.39	3.65	3.51	0.24	95.58
OC-12	71.83	0.26	12.48	1.47	0.09	0.26	1.40	3.64	3.62	0.27	95.25
μ	72.77	0.29	12.69	1.56	0.06	0.27	1.44	3.71	3.66	0.25	96.63
σ	0.96	0.04	0.21	0.07	0.03	0.03	0.05	0.18	0.12	0.03	1.34
μ ref. value	**71.90**	**0.30**	**12.57**	**1.63**	**0.05**	**0.28**	**1.42**	**3.67**	**3.56**	**0.27**	**95.68**
σ	1.00	0.05	0.34	0.14	0.03	0.03	0.05	0.26	0.26	0.05	

Appendix C

C.1 Similarity coefficient tables

Correlations by similarity coefficient (SC; Borchardt *et al*., 1972) for cryptotephras at Saco Heath, Villagedale Bog, Framboise Bog and Jeffrey's Bog. Original geochemical data are available in Supplementary Information Appendix A.

C.2 Correlations by similarity coefficient (SC)

	SCH-42	**SCH-57**	**SCH-118**	**SCH-131**	**SCH-150**	**VDB-42**	**VDB-53**	**VDB-90**	**VDB-100**	**VDB-176**	**FBB-31**	**FBB-47**	**FBB-70**	**FBB-105**	**FBB-162**	**JRB-71**	**JRB-131**
SCH-42	1.00																
SCH-57	0.86	1.00															
SCH-118	0.65	0.76	1.00														
SCH-131	0.64	0.74	**0.97**	1.00													
SCH-150	0.66	0.76	**0.98**	**0.96**	1.00												
VDB-42	**0.98**	0.87	0.67	0.66	0.67	1.00											
VDB-53	0.76	0.82	0.77	0.77	0.78	0.77	1.00										
VDB-90	0.68	0.76	0.85	0.85	0.86	0.69	0.76	1.00									
VDB-100	0.65	0.75	**0.98**	**0.99**	**0.97**	0.66	0.77	0.85	1.00								
VDB-176	0.80	0.84	0.77	0.75	0.76	0.82	0.83	0.77	0.76	1.00							
FBB-31	0.84	**0.92**	0.76	0.75	0.77	0.86	0.88	0.77	0.76	0.88	1.00						
FBB-47	0.63	0.70	0.86	0.86	0.87	0.64	0.78	0.82	0.86	0.71	0.73	1.00					
FBB-70	0.62	0.71	**0.93**	**0.95**	**0.92**	0.63	0.77	0.83	**0.94**	0.72	0.72	0.86	1.00				
FBB-105	0.63	0.73	**0.95**	**0.97**	**0.95**	0.65	0.78	0.84	**0.96**	0.74	0.74	0.88	0.96	1.00			
FBB-162	0.73	0.81	0.79	0.77	0.79	0.75	**0.91**	0.76	0.78	0.85	0.87	0.77	0.75	0.77	1.00		
JRB-71	0.63	0.70	0.84	0.85	0.85	0.64	0.76	0.82	0.85	0.71	0.72	**0.97**	0.86	0.87	0.75	1.00	
JRB-131	0.64	0.74	**0.97**	**0.98**	**0.96**	0.65	0.78	0.85	**0.99**	0.75	0.75	0.87	**0.95**	**0.97**	0.78	0.85	1.00

Appendix C

Correlations by similarity coefficient (SC) for cryptotephras at study sites with the existing Nordan's Pond Bog record and known North American proximal reference material (Pyne-O'Donnell *et al.*, 2012; this study).

	SCH-42	SCH-57	SCH-118	SCH-131	SCH-150	VDB-42	VDB-53	VDB-90	VDB-100	VDB-176	FBB-31	FBB-47	FBB-70	FBB-105	FBB-162	JRB-71	JRB-131
NDN-95	0.65	0.72	0.86	0.86	0.87	0.66	0.79	0.84	0.86	0.74	0.76	**0.96**	0.87	0.88	0.78	**0.95**	0.87
NDN-160	0.66	0.77	**0.96**	**0.95**	**0.98**	0.60	0.78	0.86	0.96	0.77	0.77	0.88	**0.91**	**0.94**	0.80	0.86	**0.96**
NDN-185	0.61	0.68	0.77	0.76	0.78	0.62	0.68	0.83	0.77	0.68	0.69	0.80	0.76	0.76	0.67	0.81	0.77
NDN-230	0.77	0.82	0.82	0.80	0.82	0.79	0.86	0.81	0.81	0.89	0.89	0.79	0.78	0.80	0.89	0.78	0.80
NDN-300	0.79	0.86	0.80	0.79	0.81	0.81	0.79	0.83	0.79	0.84	0.86	0.74	0.77	0.79	0.80	0.74	0.79
NDN-365	0.68	0.78	0.84	0.84	0.84	0.70	0.80	0.93	0.84	0.78	0.79	0.84	0.84	0.84	0.78	0.85	0.84
NDN-430	0.81	0.82	0.68	0.67	0.69	0.81	0.69	0.70	0.68	0.72	0.77	0.62	0.65	0.67	0.70	0.62	0.67
NDN-455	0.76	0.85	0.83	0.82	0.83	0.77	0.84	0.86	0.82	0.85	0.86	0.80	0.80	0.82	0.83	0.79	0.82
NDN-490	0.60	0.68	0.82	0.81	0.82	0.61	0.70	0.83	0.81	0.68	0.69	0.86	0.81	0.81	0.69	0.87	0.82
NDN-545	0.76	0.84	0.83	0.82	0.83	0.77	0.80	0.86	0.82	0.84	0.84	0.81	0.79	0.81	0.82	0.80	0.81
Layer T	0.84	**0.91**	0.77	0.75	0.77	0.86	0.86	0.75	0.76	0.88	**0.95**	0.73	0.72	0.74	0.87	0.72	0.75
MSH We	0.65	0.72	0.86	0.85	0.86	0.66	0.79	0.85	0.86	0.74	0.76	**0.96**	0.86	0.87	0.77	**0.95**	**0.86**
MSH Wn	0.68	0.74	0.89	0.89	**0.90**	0.70	0.82	0.85	0.89	0.78	0.79	**0.91**	0.89	**0.91**	0.80	0.89	0.89
WRAe	0.65	0.76	**0.97**	**0.97**	**0.98**	0.67	0.79	0.87	**0.97**	0.76	0.77	0.88	**0.92**	**0.95**	0.79	0.86	**0.97**
N'berry Pum.	0.61	0.68	0.76	0.75	0.76	0.62	0.69	0.84	0.76	0.69	0.69	0.79	0.75	0.75	0.68	0.80	0.76
Aug. Unit G	0.80	0.84	0.77	0.75	0.77	0.81	0.85	0.75	0.76	0.86	0.88	0.75	0.73	0.75	0.86	0.73	0.75
Aniakchak	0.81	0.88	0.79	0.79	0.81	0.83	0.78	0.82	0.79	0.85	0.86	0.73	0.76	0.79	0.80	0.73	0.78
E. Lake Teph.	0.60	0.68	0.81	0.80	0.81	0.61	0.70	0.83	0.81	0.69	0.69	0.85	0.81	0.81	0.68	0.86	0.81
Mazama Ash	0.77	0.85	0.82	0.81	0.83	0.78	0.81	0.85	0.82	0.85	0.86	0.79	0.79	0.81	0.83	0.79	0.81

Correlations by similarity coefficient (SC) for cryptotephras at Saco Heath, Villagedale Bog, Framboise Bog and Jeffrey's Bog with a selection of Icelandic rhyolitic (*), Mexican (+) and Japanese (^) Holocene tephras from published studies (see Supplementary References) and the Kamchatkan KS1 eruption (this study).

	SCH-42	SCH-57	SCH-118	SCH-131	SCH-150	VDB-42	VDB-53	VDB-90	VDB-100	VDB-176	FBB-31	FBB-47	FBB-70	FBB-105	FBB-162	JRB-71	JRB-131
***"AD860B"**	0.68	0.80	**0.93**	**0.92**	**0.94**	0.70	0.79	0.87	0.93	0.80	0.80	0.83	0.88	0.90	0.83	0.82	**0.92**
***Helka 1104**	0.67	0.74	0.82	0.81	0.81	0.68	0.72	0.73	0.82	0.72	0.73	0.79	0.79	0.82	0.72	0.78	0.82
*** Tjørnuvík A**	0.71	0.78	0.78	0.78	0.79	0.72	0.82	0.77	0.78	0.78	0.79	0.83	0.77	0.79	0.81	0.82	0.79
***Landnam**	0.63	0.72	0.76	0.76	0.77	0.64	0.72	0.83	0.76	0.71	0.73	0.80	0.76	0.76	0.70	0.82	0.76
***Loch Portain B**	0.62	0.70	0.73	0.72	0.73	0.63	0.69	0.77	0.73	0.67	0.67	0.76	0.73	0.73	0.69	0.76	0.74
***Hekla H-S**	0.78	0.84	0.77	0.77	0.78	0.79	0.87	0.76	0.77	0.82	0.85	0.74	0.74	0.76	0.84	0.73	0.77
***Kebister**	0.73	0.78	0.80	0.79	0.81	0.74	0.82	0.77	0.80	0.79	0.80	0.83	0.78	0.80	0.81	0.83	0.80
+Huitzilzingo	0.58	0.66	0.76	0.77	0.77	0.59	0.75	0.77	0.77	0.67	0.67	0.79	0.80	0.79	0.74	0.79	0.78
+Lower Almolya	0.63	0.73	0.86	0.88	0.88	0.64	0.74	0.82	0.87	0.72	0.73	0.90	0.88	0.89	0.73	**0.92**	0.87
+Volcun Ceboruco	0.69	0.78	0.86	0.85	0.86	0.70	0.76	**0.95**	0.86	0.78	0.78	0.81	0.82	0.84	0.78	0.80	0.85
+Tephra II	0.69	0.80	**0.92**	**0.91**	**0.93**	0.70	0.80	**0.90**	**0.92**	0.80	0.81	0.85	0.88	**0.91**	0.83	0.84	**0.91**
^Ko-c1	0.77	0.83	0.78	0.76	0.78	0.78	**0.93**	0.74	0.77	0.87	0.89	0.75	0.74	0.76	**0.95**	0.74	0.76
^Ko-c2	0.79	0.84	0.76	0.74	0.76	0.81	**0.92**	0.73	0.73	0.87	0.91	0.74	0.73	0.75	**0.93**	0.72	0.75
^Ta-a	0.69	0.79	0.84	0.83	0.85	0.70	0.89	0.83	0.84	0.81	0.82	0.82	0.81	0.83	**0.92**	0.80	0.84
^Ta-b	0.72	0.83	0.82	0.80	0.82	0.74	**0.92**	0.79	0.81	0.86	0.86	0.79	0.78	0.80	**0.96**	0.78	0.81
^Ta-c2	0.74	0.82	0.80	0.79	0.81	0.75	**0.90**	0.78	0.79	0.87	0.87	0.79	0.77	0.79	**0.97**	0.77	0.79
KS1	0.84	0.75	0.75	0.73	0.73	0.82	0.83	0.76	0.73	**0.95**	0.87	0.69	0.70	0.72	0.84	0.68	0.73

List of References

Aaby, B. 1976. Cyclic climatic variations in climate over the past 5500 years reflected in raised bogs. *Nature* 263, 281–284.

Aaby, B. and Tauber, H. 1975. Rates of peat formation in relation to degree of humification and local environment, as shown by studies of a raised bog in Denmark. *Boreas* 4, 1–17.

Ahn, J., Brook, E.J., Mitchell, L., Rosen, J., McConnell, J.R., Taylor, K., Etheridge, D. and Rubino, M. 2012. Atmospheric CO_2 over the last 1000 years: A high-resolution record from the West Antarctic Ice Sheet (WAIS) Divide ice core. *Global Biogeochemical Cycles* 26, GB2027.

Alloway, B.V., Lowe, D.J., Larsen, G., Shane, P.A.R. and Westgate, J.A. 2013. Tephrochronology, in Elias, S.A. (ed.). The Encyclopaedia of Quaternary Sciences, 2nd ed., vol. 4. Elsevier, Amsterdam, pp. 277-304.

Alm, J., Schulman, L., Walden, J., Nykanen, H., Martikainen, P.J. and Silvola, J. 1999. Carbon balance of a boreal bog during a year with an exceptionally dry summer. *Ecology* 80, 161-174.

Amesbury, M.J., Charman, D.J., Fyfe, R.M., Langdon, P.G. and West, S. 2008. Bronze Age upland settlement decline in southwest England: testing the climate change hypothesis. *Journal of Archaeological Science* 35, 87-98.

Amesbury, M.J., Barber, K.E. and Hughes, P.D.M. 2011. The methodological basis for fine-resolution, multi-proxy reconstructions of ombrotrophic peat bog surface wetness. *Boreas* 40, 161–174.

Amesbury, M.J., Barber, K.E. and Hughes, P.D.M. 2012. Can rapidly accumulating Holocene peat profiles provide sub-decadal resolution proxy climate data? *Journal of Quaternary Science* 27(8), 757-770.

Amesbury, M.J., Mallon, G., Charman, D.J., Hughes, P.D.M., Booth, R.K., Daley, T.J. and Garneau, M. 2013. Statistical testing of a new testate amoeba-based transfer function for water-table depth reconstruction on ombrotrophic peatlands in north-eastern Canada and Maine, United States. *Journal of Quaternary Science* 28, 27–39.

Ammann, C.M., Joos, F., Schimel, D.S., Otto-Bliesner, B.L. and Tomas, R.A. 2007. Solar influence on climate during the past millennium: results from transient simulations with the NCAR Climate System Model. *Proceedings of the National Academy of Sciences of the United States of America* 104, 3713–8.

Andersen, K.K., Azuma, N., Barnola, J.M., Bigler, M., Biscaye, P., Caillon, N., Chappellaz, J., Clausen, H.B., Dahl-Jensen, D. and Fischer, H. 2004. High-resolution record of Northern Hemisphere climate extending into the last interglacial period. *Nature* 431, 147–151.

Andrews, B.J., Gardner, J.E., Tait, S., Ponomareva, V., and Melekestsev, I.V. 2007. Dynamics of the 1800 ^{14}C yr BP caldera-forming eruption of Ksudach volcano, Kamchatka, Russia, in Eichelberger, J., Gordeev, E., Kasahara, M., Izbekov, P., and Lees, J., eds., *Volcanism and subduction: The Kamchatka region*. Geophysical Monograph Series: Washington DC, American Geophysical Union, 172, 325–342.

Andrus, R.E., Wagner, D.J. and Titus, J.E. 1983. Vertical zonation of *Sphagnum* mosses along hummock-hollow gradients. *Canadian Journal of Botany* 61(12), 3128-3139.

Aoki, K. and Machida, H. 2006. Major element composition of volcanic glass shards of the late Quaternary widespread tephra in Japan — distinction of tephras using K_2O–TiO_2 diagrams. *Bulletin of the Geological Survey of Japan* 57, 239–258 (in Japanese with English captions).

Arlen-Pouliot, Y. and Bhiry, N. 2005. Palaeoecology of a palsa and a filled thermokarst pond in a permafrost peatland, subarctic Québec, Canada. *The Holocene* 15, 408–419.

Armentano, T. and Menges, E. 1986. Patterns of Change in the Carbon Balance of Organic Soil-Welands of the Temperate Zone. *Journal of Ecolology* 74, 755–774.

Arseneault, D. and Payette, S. 1997. Reconstruction of millennial forest dynamics from tree remains in a subarctic tree line peatland. *Ecology* 78, 1873–1883.

Ashok, K., Behera, S.K., Rao, S.A., Weng, H. and Yamagata, T. 2007. El Niño Modoki and its possible teleconnection. *Journal of Geophysical Research Oceans* 112, C11007.

Asselin, H. and Payette, S. 2006. Origin and long-term dynamics of a subarctic tree line. *Ecoscience* 13, 135–142.

Aurela, M., Riutta, T., Laurila, T., Tuovinen, J.P., Vesala, T., Tuittila, E.S., Rinne, J., Haapanala, S. and Laine, J. 2007. CO_2 exchange of a sedge fen in southern Finland - the impact of a drought period. *Tellus B* 59, 826–837.

Backéus, I. 1985. *Aboveground production and growth dynamics of vascular bog plants in central Sweden*. PhD Thesis, Uppsala University.

Baillie, M.G.L. 1995. *A Slice through Time: dendrochronology and precision dating*. Routledge, London.

Baird, A.J., Belyea, L.R. and Morris, P.J. 2009. Upscaling of Peatland-Atmosphere Fluxes of Methane: Small-Scale Heterogeneity in Process Rates and the Pitfalls of " Bucket-and-Slab " Models, in *Carbon Cycling in Northern Peatlands* (eds A.J. Baird, L.R. Belyea, X. Comas, A.S. Reeve and L.D. Slater), American Geophysical Union, Washington, D.C..

Baker, A., Caseldine, C.J., Gilmour, M.A., Charman, D., Proctor, C.J., Hawkesworth, C.J. and Phillips, N. 1999. Stalagmite luminescence and peat humification records of palaeomoisture for the last 2500 years. *Earth and Planetary Science Letters* 165, 157–162.

Bakus, G. J. 2007. *Community Analysis: Ordination and Other Multivariate Techniques*, in Quantitative Analysis of Marine Biological Communities: Field Biology and Environment, John Wiley & Sons, Inc., Hoboken, NJ, USA.

Balestra, B., Bertini, A., de Vernal, A., Monechi, S. and Reale, V. 2013. Late Quaternary sea surface conditions in the Laurentian Fan: Evidence from coccolith and dinocyst assemblages. *Palaeogeography Palaeoclimatology. Palaeoecology.* 387, 200–210.

Barber, K.E. 1981. Peat Stratigraphy and Climatic Change: A Palaeoecological Test of the Theory of Cyclic Peat Bog Regeneration. Rotterdam: A. A. Balkema.

Barber, K.E. 1993. *Peatlands as scientific archives of past biodiversity*. Biodiversity Conservation 2, 474–489.

Barber, K. 1994. Deriving Holocene palaeoclimates from peat stratigraphy: some misconceptions regarding the sensitivity and continuity of the record. Quaternary Newsletter 72, 1–9.

Barber, K.E., Chambers, F.M., Maddy, D., Stoneman, R. and Brew, J.S. 1994. A sensitive high-resolution record of late Holocene climatic change from a raised bog in northern England. *The Holocene* 4, 198–205.

Barber, K., Dumayne-Peaty, L., Hughes, P., Mauquoy, D. and Scaife, R. 1998. Replicability and variability of the recent macrofossil and proxy-climate record from raised bogs: field stratigraphy and macrofossil data from Bolton Fell Moss and Walton Moss, Cumbria, England. Journal of Quaternary Science 13, 515–528.

Barber, K., Maddy, D., Rose, N., Stevenson, A., Stoneman, R. and Thompson, R. 2000. Replicated proxy-climate signals over the last 2000 yr from two distant UK peat bogs: new evidence for regional palaeoclimate teleconnections. *Quaternary Science Reviews* 19, 481–487.

Barber, K.E. and Langdon, P.G. 2001. *Peat stratigraphy and climate change*, in Brothwell, D.R, Pollard, A.M. (eds), Handbook of Archaeological Sciences. John Wiley and Sons Ltd., Chichester, pp. 210–226.

Barber, K.E. and Charman, D., 2003. *Holocene palaeoclimate records from peatlands,* in Mackay, A.W., Battarbee, R.W., Birks, H.J.B. & Oldfield, F. (eds), Global Change in the Holocene. Edward Arnold, London, pp. 210 – 226.

Barber, K.E., Chambers, F.M. and Maddy, D. 2003. Holocene palaeoclimates from peat stratigraphy: macrofossil proxy climate records from three oceanic raised bogs in England and Ireland. *Quaternary Science Reviews* 22, 521–539.

Barber, K.E., Chambers, F.M. and Maddy, D. 2004. Late Holocene climatic history of northern Germany and Denmark: peat macrofossil investigations at Dosenmoor, Schleswig-Holstein, and Svanemose, Jutland. *Boreas* 33, 132–144.

Barber, K.E. and Langdon, P.G. 2007. What drives the peat-based palaeoclimate record ? A critical test using multi-proxy climate records from northern Britain. *Quaternary Science Reviews* 26, 3318–3327.

Barsugli, J.J. and Battisti, D.S. 1998. The basic effects of atmosphere- ocean thermal coupling on midlatitude variability. *Journal of the Atmospheric Sciences* 55, 477–493.

Bastien, D.F. and Garneau, M. 1997. Macroscopic Identification Key of 36 Sphagnum Species in Eastern Canada. *Geological Survey of Canada, Miscellaneous Report 61*. Natural Resources Canada.

Baumgartner, S., Beer, J., Masarik, J., Wagner, G., Meynasdier, L. and Synal, H.A. 1998. Geomagnetic modulation of the ^{36}Cl flux in the GRIP ice core, Greenland. *Science* 279, 1330–1332.

Bayliss, A., McCormac, G. and van der Plicht, H. 2004. An illustrated guide to measuring radiocarbon from archaeological samples. *Physics Education* 39, 137–144.

Beget, J.E., Mason, O. and Anderson, P. 1992. Age, extent and climatic significance of the c. 3400 BP Aniakchak tephra, western Alaska, USA. *The Holocene* 2, 51–56.

Beilman, D.W., Vitt, D.H., Bhatti, J.S. and Forest, S. 2008. Peat carbon stocks in the southern Mackenzie River Basin: uncertainties revealed in a high-resolution case study. *Global Change Biology* 14, 1221–1232.

Beilman, D.W., MacDonald, G.M., Smith, L.C. and Reimer, P.J. 2009. Carbon accumulation in peatlands of West Siberia over the last 2000 years. *Global Biogeochemical Cycles* 23, GB1012.

Belyea, L.R. 2007. Climatic and topographic limits to the abundance of bog pools. *Hydrological processes* 687, 675–687.

Belyea, L.R. 2009. Nonlinear Dynamics of Peatlands and Potential Feedbacks on the Climate System, in A.J. Baird, L.R. Belyea, X. Comas, A.S. Reeve and L.D. Slater (eds), *Carbon Cycling in Northern Peatlands*, American Geophyscial Union, Washington, D.C..

Belyea, L.R. and Clymo, R.S. 2001. Feedback control of the rate of peat formation. *Proceedings of the Royal Society of London: Biological Sciences* 268, 1315–21.

Belyea, L. and Baird, A. 2006. Beyond "The Limits to Peat Bog Growth": Cross-scale Feedback in Peatland Development. *Ecological Monographs*. 76, 299–322.

Bendle, J. A. P. and Rosell-Melé, A. 2007. High-resolution alkenone sea surface temperature variability on the North Icelandic Shelf: implications for Nordic Seas palaeoclimatic development during the Holocene. *The Holocene* 17, 9–24.

Bennett. K.D. 1994. Confidence intervals for age estimates and deposition times in late-Quaternary sediment. *The Holocene* 4, 337–348.

Bennett, K.D. 1996. Determination of the number of zones in a biostratigraphical sequence. *New Phytologist* 132, 155-170.

Benscoter, B.W. and Vitt, D.H. 2008. Spatial patterns and temporal trajectories of the bog ground layer along a post-fire chronosequence. *Ecosystems* 11, 1054–1064.

Berger, A., Loutre, M.F., Lema, D.G.G., Cyclotron, C. and Louvam-la-neuve, B.I. 1991. Insolation values for the climate of the last 10 million years. *Quaternary Science Reviews* 10, 297–317.

Bergeron, Y., Cyr, D., Girardin, M.P., Carcaillet, C., 2010. Will climate change drive 21st century burn rates in Canadian boreal forest outside of its natural variability: collating global climate model experiments with sedimentary charcoal data. *International Journal of Wildland Fire* 19, 1127-1139.

Biester, H., Knorr, K.H., Schellekens, J., Basler, A. and Hermanns, Y.M. 2013. Comparison of different methods to determine the degree of peat decomposition in peat bogs. *Biogeosciences* 11, 2691-2707.

Birks, H.H. 2007. Plant macrofossil introduction, in Elias, S.A (ed.) *Encyclopedia of Quaternary Science, Volume 3*..Elsevier, Amsterdam, 2266-2288.

Bjerknes, J. 1964. Atlantic air-sea interaction. *Advances in Geophysics* 10, 82.

Bjerknes, J. 1969. Atmospheric teleconnections from the equatorial Pacific. *Monthly Weather Reviews* 97, 163–172.

Blaauw, M. 2010. Methods and code for "classical" age-modelling of radiocarbon sequences. *Quaternary Geochronology* 5, 512–518.

Blaauw, M. and Christen, J.A., 2005. Radiocarbon peat chronologies and environmental change. *Journal of the Royal Statistical Society. Series C (Applied Statistics)* 54, 805–816.

Blaauw, M. and Christen, J.A. 2011. Flexible Paleoclimate Age-Depth Models Using an Autoregressive Gamma Process. *Bayesian Analysis* 6, 457–474.

Blaauw, M., Heuvelink, G.B.M., Mauquoy, D., van der Plicht, J. and van Geel, B. 2003. A numerical approach to ^{14}C wiggle-match dating of organic deposits: best fits and confidence intervals. *Quaternary Science Reviews* 22, 1485–1500.

Blaauw, M., van der Plicht, J. and van Geel, B. 2004. Radiocarbon dating of bulk peat samples from raised bogs: non-existence of a previously reported "reservoir effect"? *Quaternary Science Reviews* 23, 1537–1542.

Blaauw, M., Christen, J.A., Mauquoy, D., van der Plicht, J. and Bennett, K.D. 2007. Testing the timing of radiocarbon-dated events between proxy archives. *The Holocene* 17, 283–288.

Blackford, J. 2000. Palaeoclimatic records from peat bogs. *Trends in Ecology and Evolution* 15, 193–198.

Blackford, J.J. and Chambers, F.M. 1993. Determining the degree of peat decomposition for peat- based palaeoclimaticstudies. *International Peat Journal 5*, 7-24.

Blackford, J.J. and Chambers, F.M., 1995. Proxy climate record for the last 1000 years from Irish blanket peat and a possible link to solar variability. *Earth and Planetary Science Letters* 133, 145–150.

Blockley, S.P.E., Pyne-O'Donnell, S.D.F., Lowe, J.J., Matthews, I.P., Stone, A., Pollard, A.M., Turney, C.S.M. and Molyneux, E.G., 2005. A new and less destructive laboratory procedure for the physical separation of distal glass tephra shards from sediments. *Quaternary Science Reviews* 24, 1952-1960.

Blundell, A. and Barber, K. 2005. A 2800-year palaeoclimatic record from Tore Hill Moss, Strathspey, Scotland: the need for a multi-proxy approach to peat-based climate reconstructions. Quaternary Science Reviews 24, 1261–1277.

Blundell, A., Charman, D.J. and Barber, K. 2008. Multiproxy late Holocene peat records from Ireland: towards a regional palaeoclimate curve. Journal of Quaternary Science 23, 59–71.

Blytt, A.G. 1876. Essay on the Immigration of the Norwegian Flora during Alternating Rainy and Dry Periods. Cammermayer, Kristiana.

Bobrov, A.A., Charman, D.J. and Warner, B.G., 1999. Ecology of testate amoebae (Protozoa: Rhizopoda) on peatlands in western Russia with special attention to niche separation in closely related taxa. *Protist* 150, 125–136.

Booth, R.K. 2001. Ecology of testate amoebae (protozoa) in two Lake Superior coastal wetlands: Implications for paleoecology and environmental monitoring. *Wetlands* 21, 564–576.

Booth, R.K. 2002. Testate amoebae as paleoindicators of surface-moisture changes on Michigan peatlands: modern ecology and hydrological calibration. *Journal of Paleolimnology* 28, 329–348.

Booth, R.K. 2008. Testate amoebae as proxies for mean annual water-table depth in Sphagnum-dominated peatlands of North America. *Journal of Quaternary Science* 23, 43–57.

Booth, R.K. 2010. Testing the climate sensitivity of peat-based paleoclimate reconstructions in mid-continental North America. Quaternary Science Reviews 29, 720–731.

Booth, R.K. and Jackson, S.T. 2003. A high-resolution record of late-Holocene moisture variability from a Michigan raised bog, USA. *The Holocene* 13, 863–876.

Booth, R.K., Jackson, S.T. and Gray, C.E. 2004. Paleoecology and high-resolution paleohydrology of a kettle peatland in upper Michigan. *Quaternary Research* 61, 1–13.

Booth, R.K., Notaro, M., Jackson, S.T. and Kutzbach, J.E. 2006. Widespread drought episodes in the western Great Lakes region during the past 2000

years: geographic extent and potential mechanisms. *Earth and Planetary Science Letters* 242, 415–427.

Booth, R.K., Lamentowicz, M. and Charman, D.J. 2010. Preparation and analysis of testate amoebae in peatland palaeoenvironmental studies. *Mires and Peat* 7, 1–7.

Borchardt, G.A., Aruscavage, P.J.and Millard, H. 1972. Correlation of the Bishop Ash, a Pleistocene marker bed using instrumental neutron activation analysis. *Journal of Sedimentary Petrology* 42, 301–306.

Boygle, J.E., 1994. Tephra in lake sediments: An unambiguous geochronological marker? PhD. Thesis, University of Edinburgh, Edinburgh.

Bradley, R.S. 2000. Enhanced: 1000 years of climate change. *Science* 288, 1353–1355.

Bradley, R.S. 2003. Climate forcing during the Holocene, in: Mackay, A.W., Battarbee, R.W., Birks, H.J.B., Oldfield, F. (Eds.), *Global Change in the Holocene: Approaches to Reconstructing Fine-Resolution Climate Change*. Arnold, London.

Bradley, R.S. and Jones, P.D. 1995. *Climate since AD 1500*. Routledge, London.

Bragazza, L. 1997. Sphagnum niche diversification in two oligotrophic mires in the southern Alps of Italy. *Bryologist* 507–515.

Bragazza, L., Tahvanainen, T., Kutnar, L., Rydin, H., Limpens, J., Hájek, M., Grosvernier, P., Hájek, T.S., Hajkova, P., Hansen, I., Lacumin, P. and Gerdol, R. 2004. Nutritional constraints in ombrotrophic Sphagnum plants under increasing atmospheric nitrogen deposition in Europe. *New Phytologist* 163 609-616

Braitseva, O.A., Melekestsev, I.V., Ponomareva, V.V. and Kirianov, V.Yu. 1996. The caldera- forming eruption of Ksudach volcano about cal. AD 240, the greatest explosive event of our era in Kamchatka. *Journal of Volcanology and Geothermal Research* 70, 49–66.

Braitseva, O.A., Ponomareva, V.V., Sulerzhitsky, L.D., Melekestsev, I.V. and Bailey, J. 1997. Holocene key-marker tephra layers in Kamchatka, Russia. *Quaternary Research* 47, 125–139.

Bray, J.R. 1971. Solar-climate relationships in the Post-Pleistocene. *Science* 171, 1242.

Breeuwer, A., Heijmans, M., Robroek, B.J.M., Limpens, J. and Berendse, F. 2008. The effect of increased temperature and nitrogen deposition on decomposition in bogs, *Oikos,* 117, 1258-1268.

Brien, S.R.O., Mayewski, P.A., Meeker, L.D., Meese, D.A., Twickler, M.S. and Whitlow, S. 1995. Complexity of Holocene Climate as Reconstructed from a Greenland Ice Core. *Science* 270, 1962–1964.

Briffa, K.R., Jones, P.D. and Schweingruber, F.H. 1992. Tree-ring density reconstructions of summer temperature patterns across western North America since 1600. *Journal of Climate* 5, 735–754.

Brown, A.D. 2006. *Late-Holocene palaeoclimates: cross-validation of multiple proxies from lake and bog archives in northern England*. PhD thesis. University of Southampton.

Bruce, J.P. 2011 *Climate change information for adaption*. Institute for Catastrophic Loss Reduction Report.

Bryden, H.L. and Imawaki, S. 2001. Ocean Heat Transport, in Siedler, G. *et al*. (eds), *Ocean Circulation and Climate: Observing and Modelling the Global Ocean*. Academic Press, San Diego, San Francisco, New York, Boston, London, Sydney, Tokyo, p. 715.

Bryden, H.L., Longworth, H.R. and Cunningham, S. A. 2005. Slowing of the Atlantic meridional overturning circulation at 25 degrees N. *Nature* 438, 655–7.

Bubier, J.L., Moore, T.R. and Bledzki, L. A. 2007. Effects of nutrient addition on vegetation and carbon cycling in an ombrotrophic bog. *Global Change Biology* 13, 1168–1186.

Cai, S. and Yu, Z. 2011. Response of a warm temperate peatland to Holocene climate change in northeastern Pennsylvania. *Quaternary Research* 75, 531–540.

Caseldine, C., Baker, A and Barnes, W.L. 1999. A rapid, non-destructive scanning method for detecting distal tephra layers in peats. *The Holocene* 9, 635–638.

Caseldine, C.J., Baker, A., Charman, D.J. and Hendon, D. 2000. A comparative study of optical properties of NaOH peat extracts: implications for humification studies. *The Holocene* 10, 649–658.

Cayer, D. and Bhiry, N. 2014. Holocene Climate and Environmental Changes in Western Subarctic Québec as Inferred from the Sedimentology and the Geomorphology of a Lake Watershed. *Arctic, Antarctic and Alpine Research* 46, 55–65.

Chambers, F.M. and Blackford, J.J. 2001. Mid- and late-Holocene climatic changes: a test of periodicity and solar forcing in proxy-climate data from blanket peat bogs. *J. Quat. Sci.* 16, 329–338.

Chambers, F.M. and Charman, D.J., 2004. Holocene environmental change: contributions from the peatland archive. *The Holocene* 14, 1–6.

Chambers, Frank M., Barber, K.E, Maddy, D. and Brew, J. 1997. A 5500-year proxy-climate and vegetation record from blanket mire at Talla Moss, Borders, Scotland. *The Holocene* 7, 391–399.

Chambers, F.M., Mauquoy, D., Brain, S. A., Blaauw, M. and Daniell, J.R.G. 2007. Globally synchronous climate change 2800 years ago: Proxy data from peat in South America. *Earth Planet. Sci. Lett.* 253, 439–444.

Chambers, F.M., Beilman, D.W. and Yu, Z. 2011. Methods for determining peat humification and for quantifying peat bulk density, organic matter and carbon content for palaeostudies of climate and peatland carbon dynamics. *Mires and Peat* 7, 1–10.

Chambers, F.M., Booth, R.K., De Vleeschouwer, F., Lamentowicz, M., Le Roux, G., Mauquoy, D., Nichols, J.E. and van Geel, B. 2012. Development and refinement of proxy-climate indicators from peats. *Quat. Int.* 268, 21–33.

Charman, D. 2007. Summer water deficit variability controls on peatland water-table changes: implications for Holocene palaeoclimate reconstructions. *The Holocene* 17, 217–227.

Charman, D.J. 1999. Testate amoebae and the fossil record: issues in biodiversity. *Journal of Biogeography* 26, 89–96.

Charman, D.J. 2001. Biostratigraphic and palaeoenvironmental applications of testate amoebae. *Quat. Sci. Rev.* 20, 1753–1764.

Charman, D.J. 2002. *Peatlands and Environmental Change*. Wiley, Chichester, UK.

Charman, D.J. 2010. Centennial climate variability in the British Isles during the mid–late Holocene. *Quat. Sci. Rev.* 29, 1539–1554.

Charman, D.J. and Warner, B.G., 1992. Relationship between testate amoebae (Protozoa: Rhizopoda) and microenvironmental parameters on a forested peatland in northeastern Ontario. *Can. J. Zool.* 70, 2474–2482.

Charman, D.J. and Warner, B.G. 1997. The ecology of testate amoebae (Protozoa: Rhizopoda) in oceanic peatlands in Newfoundland, Canada: modelling hydrological relationships for palaeoenvironmental reconstruction. *Ecoscience* 555–562.

Charman, D.J. and Garnett, M.H. 2005. Chronologies for recent peat deposits using wiggle-matched radiocarbon dates: problems with old carbon contamination. *Radiocarbon* 47, 135-145.

Charman, D.J., Hendon, D. and Packman, S. 1999. Multiproxy surface wetness records from replicate cores on an ombrotrophic mire: implications for Holocene palaeoclimate records. *J. Quat. Sci.* 14, 451–463.

Charman, D.J., Hendon, D. and Woodland, W. 2000. The identification of peatland testate amoebae. *Quaternary Research Association Technical Guide* no. 9. London.

Charman, D.J., Brown, A.D., Hendon, D. and Karofeld, E. 2004. Testing the relationship between Holocene peatland palaeoclimate reconstructions and instrumental data at two European sites. *Quaternary Science Reviews* 23, 137–143.

Charman, D.J., Blundell, A., Chiverrell, R.C., Hendon, D. and Langdon, P.G. 2006. Compilation of non-annually resolved Holocene proxy climate records : stacked Holocene peatland palaeo-water table reconstructions from northern Britain. *Quaternary Science Reviews* 25, 336–350.

Charman, D.J., Blundell, A. and ACCROTELM Members. 2007. A new European testate amoebae transfer function for palaeohydrological reconstruction on ombrotrophic peatlands. *J. Quat. Sci.* 22, 209–221.

Charman, D.J., Barber, K.E., Blaauw, M., Langdon, P.G., Mauquoy, D., Daley, T.J., Hughes, P.D.M. and Karofeld, E. 2009. Climate drivers for peatland palaeoclimate records. *Quat. Sci. Rev.* 28, 1811–1819.

Charman, D.J., Beilman, D.W., Blaauw, M., Booth, R.K., Brewer, S., Chambers, F.M., Christen, J. a., Gallego-Sala, a., Harrison, S.P., Hughes, P.D.M., Jackson, S.T., Korhola, a., Mauquoy, D., Mitchell, F.J.G., Prentice, I.C., van der Linden, M., De Vleeschouwer, F., Yu, Z.C., Alm, J., Bauer, I.E., Corish, Y.M.C., Garneau, M., Hohl, V., Huang, Y., Karofeld, E., Le Roux, G., Loisel, J., Moschen, R., Nichols, J.E., Nieminen, T.M., MacDonald, G.M., Phadtare, N.R., Rausch, N., Sillasoo, Ü., Swindles, G.T., Tuittila, E.-S., Ukonmaanaho, L., Väliranta, M., van Bellen, S., van Geel, B., Vitt, D.H. and Zhao, Y. 2013. Climate-related changes in peatland carbon accumulation during the last millennium. *Biogeosciences* 10, 929–944.

Chertkoff, D. G. and Gardner, J. E. 2004. Nature and timing of magma interactions before, during, and after the caldera-forming eruption of Volcán Ceboruco. Mexico. Contribu. *Mineral Petrol* 146, 715-735.

Chiverrell, R.C. 2001. A proxy record of late Holocene climate change from May Moss, northeast England. *J. Quat. Sci.* 16, 9–29.

Christen, J.A. and Fox, C. 2010. A general purpose sampling algorithm for continuous distributions (the t-walk). *Bayesian Anal.* 5, 263–281.

Chylek, P., Folland, C., Frankcombe, L., Dijkstra, H., Lesins, G. and Dubey, M., 2012. Greenland ice core evidence for spatial and temporal variability of the Atlantic Multidecadal Oscillation. Geophys. Res. Lett. 39, L09705.

Ciais, P., C. Sabine, G. Bala, L. Bopp, V. Brovkin, J. Canadell, A. Chhabra, R. DeFries, J. Galloway, M. Heimann, C. Jones, C. Le Quéré, R.B. Myneni, S.P. and

P.T., 2013. Carbon and Other Biogeochemical Cycles, in: Stocker, T.F., D. Qin, G.-K. Plattner, M. Tignor, S.K. Allen, J. Boschung, A. Nauels, Y. Xia, V.B. and P.M.M. (Ed.), Cli- Mate Change 2013: *The Physical Science Basis. Contribution of Working Group I to the Fifth Assessment Report of the Intergovernmental Panel on Climate Change.* Cambridge University Press, Cambridge, United Kingdom and New York, NY, USA.

Clifford, M.J. and Booth, R.K., 2013. Increased probability of fire during late Holocene droughts in northern New England. *Clim. Change* 119, 693–704.

Clymo, R., 1984. The limits to peat bog growth. Philos. Trans. R. Soc. London, *Biol. Sci.* 303, 605–654.

Clymo, R.S., 1991. Peat growth, in: Shane, L. C.K., Cushing, E.J. (Ed.), *Quaternary Landscapes.* University of Minnesota Press, Minneapolis, pp. 76–112.

Clymo, R.S and Duckett, J.G. 1986. Regeneration of Sphagnum. *New Phytologist* 102 589-614.

Clymo, R., Turunen, J. and Tolonen, K. 1998. Carbon accumulation in peatland. *Oikos* 81, 368–388.Cobb, K.M., Charles, C.D., Cheng, H. and Edwards, R.L. 2003. El Nino/Southern Oscillation and tropical Pacific climate during the last millennium. *Nature* 424, 271–276.

Cole-Dai, J., Mosley-Thompson, E., Wight, S.P. and Thompson, L.G. 2000. A 4100-year record of explosive volcanism from an East Antarctica ice core. *Journal of Geophysical Research* 105, 24431-24441.

Cole-Dai J, Ferris D, Lanciki A, Savarino J, Baroni M and Thiemens M.H. 2009. Cold decade (AD 1810–1819) caused by Tambora (1815) and another (1809) stratospheric volcanic eruption. *Geophysical Research Letters* 36, L22703.Conroy, J.L., Restrepo, A., Overpeck, J.T., Steinitz-Kannan, M., Cole, J.E., Bush, M.B. and Colinvaux, P.A. 2009. Unprecedented recent warming of surface temperatures in the eastern tropical Pacific Ocean. *Nat. Geosci.* 2, 46–50.

Cook, E.R., D'Arrigo, R.D. and Briffa, K.R. 1998. A reconstruction of the North Atlantic Oscillation using tree-ring chronologies from North America and Europe. *The Holocene* 8, 9–17.

Cook, E.R., Palmer, J.G. and D'Arrigo, R.D. 2002. Evidence for a 'Medieval Warm Period' in a 1,100 year tree-ring reconstruction of past austral aummer temperatures in New Zealand. *Geophysical Research Letters* 29, 1667.

Cook, E.R., Woodhouse, C.A., Eakin, C.M., Meko, D.M. and Stahle, D.W. 2004. Long-term aridity changes in the western United States. *Science* 306, 1015–1018.

Cook, E.R., Seager, R., Jr, R.R.H., Vose, R.S., Herweijer, C. and Woodhouse, C. 2010. Megadroughts in North America : placing IPCC projections of hydroclimatic change in a long-term palaeoclimate context. *Journal of Quaternary Science* 25, 48–61. Coulter, S.E., Pilcher, J.R., Hall, V. A., Plunkett, G. and Davies, S.M. 2010. Testing the reliability of the JEOL FEGSEM 6500F electron microprobe for quantitative major element analysis of glass shards from rhyolitic tephra. *Boreas* 39, 163–169.

Coulter, S.E., Pilcher, J.R., Plunkett, G., Baillie, M., Hall, V. a., Steffensen, J.P., Vinther, B.M., Clausen, H.B. and Johnsen S.J. 2012. Holocene tephras highlight complexity of volcanic signals in Greenland ice cores. *J. Geophys. Res. Atmos.* 117.

Cronin, T., Dwyer, G., Kamiya, T., Schwede, S. and Willard, D. 2003. Medieval Warm Period, Little Ice Age and 20th century temperature variability from Chesapeake Bay. *Glob. Planet. Change* 36, 17–29.

Cronin, T.M., Hayo, K., Thunell, R.C., Dwyer, G.S., Saenger, C. and Willard, D. A. 2010. The Medieval Climate Anomaly and Little Ice Age in Chesapeake Bay and the North Atlantic Ocean. *Palaeogeogr. Palaeoclimatol. Palaeoecol.* 297, 299–310.

Crowley, T.J. 2000. Causes of climate change over the past 1000 years. *Science* 289, 270–277.

Crowley, T.J., Baum, S.K., Kim, K., Hegerl, G.C. and Hyde, W.T. 2003. Modeling ocean heat content changes during the last millennium. *Geophys. Res. Lett.* 30.

D'Arrigo, R., Wilson, R. and Jacoby, G. 2006. On the long- term context for late twentieth century warming. *J. Geophys. Res. Atmos.* 111.

Dahl-Jensen, D., Mosegaard, K., Gundestrup, N., Clow, G.D., Johnsen, S.J., Hansen, A.W., Balling, N. 1998. Past Temperatures Directly from the Greenland Ice Sheet. *Science* 282, 268–271.

Daley, T.J. 2007. *Tracking Holocene climate change using peat bog stable isotopes*, PhD Thesis, University of Southampton.

Daley, T.J. and Barber, K.E. 2012. Multi-proxy Holocene palaeoclimate records from Walton Moss, northern England and Dosenmoor, northern Germany, assessed using three statistical approaches. *Quat. Int.* 268, 111–127.

Daley, T.J., Street-Perrott, F. A., Loader, N.J., Barber, K.E., Hughes, P.D.M., Fisher, E.H. and Marshall, J.D. 2009. Terrestrial climate signal of the "8200 yr B.P. cold event" in the Labrador Sea region. *Geology* 37, 831–834.

Daniels, R.E. and Eddy, A. 1990. *A handbook of European Sphagna*. Natural Environment Research Council, Swindon, UK.

Davies, S.M., Hoek, W.Z., Bohncke, S.J.P., Lowe, J.J., Pyne O'Donnell, S. and Turney, C.S.M. 2005. Detection of Lateglacial distal tephra layers in the Netherlands. *Boreas* 34, 123–135.

Davies, S.M., Elmquist, M., Bergman, J., Wohlfarth, B. and Hammarlund, D. 2007. Cryptotephra sedimentation processes within two lacustrine sequences from west central Sweden. *The Holocene* 3, 1–13.

Davies, S.M., Wastegård, S., Rasmussen, T.L., Svensson, A., Johnsen, S.J., Steffensen, J.P. and Andersen, K.K. 2008. Identification of the Fugloyarbanki tephra in the NGRIP ice core: a key tie- point for marine and ice- core sequences during the last glacial period. *J. Quat. Sci.* 23, 409–414.

Davies, S.M., Larsen, G., Wastegård, S., Turney, C.S.M., Hall, V. A., Coyle, L. and Thordarson, T. 2010. Widespread dispersal of Icelandic tephra: how does the Eyjafjöll eruption of 2010 compare to past Icelandic events? *J. Quat. Sci.* 25, 605–611.

Davies, S.M., Wastegård, S., Abbott, P.M., Barbante, C., Bigler, M., Johnsen, S.J., Rasmussen, T.L., Steffensen, J.P. and Svensson, A. 2010b. Tracing volcanic events in the NGRIP ice-core and synchronising North Atlantic marine records during the last glacial period. *Earth Planet. Sci. Lett.* 294, 69–79.

Davis, A.M., McAndrews, J. H. and Wallace, B. L. 1988. Paleoenvironment and the archaeological record at the L'Anse aux Meadows Site, Newfoundland. *Geoarchaeology: An International Journal* 3, 53-64.

Davis, B. A. S. and Brewer, S. 2011. A unified approach to orbital, solar, and lunar forcing based on the Earth's latitudinal insolation/temperature gradient. *Quat. Sci. Rev.* 30, 1861–1874.

De Vleeschouwer, F., Van Vliët Lanoé, B. and Fagel, N. 2008. Long term mobilisation of chemical elements in tephra-rich peat (NE Iceland). *Appl. Geochemistry* 23, 3819–3839.

De Vries, H. 1958. Variation in concentration of radiocarbon with time and location on Earth. K. Nederlandse Akad. *Wet. Proceedings, Ser. B* 61, 94–102.

Delworth, T., Manabe, S. and Stouffer, R.J. 1993. Interdecadal variations of the thermohaline circulation in a coupled ocean-atmosphere model. *J. Clim.* 6, 1993–2011.

Delworth, T.L. and Greatbatch, R.J. 2000. Multidecadal thermohaline circulation variability driven by atmospheric surface flux forcing. *J. Clim*. 13, 1481–1495.

Denton, G.H. and Broecker, W.S. 2008. Wobbly ocean conveyor during the Holocene? *Quaternary Science Review* 27: 1939-1950.

Delworth, T.L. and Mann, M.E. 2000. Observed and simulated multidecadal variability in the Northern Hemisphere. *Clim. Dyn*. 16, 661–676.

Dhahri, N. 2010. *Natural variability of pelagic and benthic conditions in the Gulf of St. Lawrence during the late Holocene.* PhD thesis. Universite du Quebec a Montreal, Canada.

Diaz, H.F., Trigo, R., Hughes, M.K., Mann, M.E., Xoplaki, E. and Barriopedro, D. 2011. Spatial and Temporal Characteristics of Climate in Medieval Times Revisited. Bull. *Am. Meteorol. Soc.* 92, 1487–1500.

Dickson, R., J., L., Meincke, J., Rhines, P. and Swift, J. 1996. Long-term coordinated changes in the convective activity of the North Atlantic. *Prog. Oceanogr.* 38, 214–295.

Dionne, J.-C. and Richard, P.J.H. 2006. Origine, âge et taux d'accrétion verticale de la tourbière à palses de Blanc-Sablon, basse Côte-Nord, Golfe du Saint-Laurent, Québec. *Géographie Phys. Quat.* 60, 199–205.

Dorrepaal, E., Toet, S., van Logtestijn, R.S.P., Swart, E., van de Weg, M.J., Callaghan, T. V. and Aerts, R. 2009. Carbon respiration from subsurface peat accelerated by climate warming in the subarctic. *Nature* 460, 616–619.

Dugmore, A.J. 1989. Tephrochronological studies of Holocene glacier fluctuations in South Iceland, in: Oerlemans, J. (Ed.), *Glacier Fluctuations and Climate Change*. Kluwer Academic: Dordrecht, pp. 37–55.

Dugmore, A.J. and Newton, A.J. 1992. Thin Tephra Layers in Peat Revealed by X-Radiography. *Journal of Archaeological Science* 19, 163–170.

Dugmore, A.J. and Newton, A.J. 1997. Holocene Tephra Layers in the Faroe Islands. *Frodskaparrit (The Faroese Journal of Natural and Medical sciences)* 4, 141-154.

Dugmore, A.J., Newton, A.J., Sugden, D.E., and Larsen, G. 1992. Geochemical stability of fine- grained silicic Holocene tephra in Iceland and Scotland. *J. Quat. Sci.* 7, 173–183.

Dugmore, A.J., Larsen, G. and Newton, A.J., 1995. Seven tephra isochrones in Scotland. *The Holocene* 5, 257–266.

Dugmore, A. I., Newton, A. I., Edwards, K. I., Larsen, G., Blackford, J. J. and Cook, G. T. 1996. Long-distance marker horizons from small-scale eruptions: British tephra deposits from the AD 1510 eruption of Hekla, Iceland. *Journal of Quaternary Science* 11, 51 1-516.

Dolven, J.K., Cortese, G. and Bjorklund, K.R. 2002. A high-resolution radiolarian-derived paleotemperature record for the Late Pleistocene-Holocene in the Norwegian Sea. *Paleoceanography* 17, 1072.

Dugmore, A.J., Larsen, G. and Newton, A.J., 2004. Tephrochronology and its application to late Quaternary environmental reconstruction, with special reference to the North Atlantic islands. In: Buck C.E., Millard A.R. (Eds.), *Tools for Constructing Chronologies: Crossing Disciplinary Boundaries*. Lecture Notes in Statistics, vol. 177. Springer, London, pp. 173-188.

Dupont, L.M. 1986. Temperature and rainfall variation in the Holocene based on comparative palaeoecology and isotope geology of a hummock and a hollow (Bourtangerveen, The Netherlands). *Rev. Palaeobot. Palynol.* 48, 71–88 95–116 133–159.

Eddy, J.A. 1976. The maunder minimum. *Science* 192, 1189-1202

Enfield, D.B., Mestas-Nunez, A.M. and Trimble, P.J. 2001. The Atlantic multidecadal oscillation and its relation to rainfall and river flows in the continental U.S. *Geophysical Research Letters* 28, 2077–2080.

Eppinga, M.B., de Ruiter, P.C., Wassen, M.J. and Rietkerk, M. 2009. Nutrients and hydrology indicate the driving mechanisms of peatland surface patterning. *The American Naturalist* 173, 803–18.

Feng, S., Oglesby, R.J., Rowe, C.M., Loope, D.B. and Hu, Q. 2008. Atlantic and Pacific SST influences on Medieval drought in North America simulated by the Community Atmospheric Model. *Journal of Geophysical Research* 113, D11101.

Fenner, N. and Freeman, C. 2011. Drought-induced carbon loss in peatlands, *Nature Geoscience,* 4, 895-900.

Ferdinandsen, C. and Winge, Ö. 1925. *Cenococcum Fr. A monographic study*. K. Veterinaer-og Landbohoiskoles Aarsskrift 332–382.

Fiacco Jr., R.J., Palais, J.M., Germani, M.S., Zielinski, G.A. and Mayewski, P.A. 1993. Characteristics and Possible source of a 1479 A.D. Volcanic ash layer in a Greenland Ice Core. *Quaternary Research* 39, 267-273.

Fiacco Jr., R.J., Thordarson, T., Germani, M.S., Self, S., Palais, J.M., Whitlow, S. and Grootes, P.M. 1994. Atmospheric aerosol loading and transport due to the 1783-1784 Laki eruption in Iceland, interpreted from ash particles and acidity in the GISP2 ice core. *Quaternary Research* 42, 231-240.

Filion, L. 1984. A relationship between dunes, fire and climate recorded in the Holocene deposits of Quebec. *Nature* 309, 543–546.

Finkel, R.C. 1997. Beryllium 10 concentrations in the Greenland Ice Sheet Project 2 ice core from 3-40 ka. *Journal of Geophysical Research* 102, 699–706.

Flannigan, M.D., Logan, K. A., Amiro, B.D., Skinner, W.R. and Stocks, B.J. 2005. Future Area Burned in Canada. *Climate Change* 72, 1–16.

Folland, C.K., Colman, A.W., Rowell, D.P. and Davey, M. 2001. Predictability of northeast Brazil rainfall and real-time forecast skill, 1987-98. *Journal of Climate* 14, 1937–1958.

Folland, C.K., Knight, J., Linderholm, H.W., Fereday, D., Ineson, S. and Hurrell, J.W. 2009. The Summer North Atlantic Oscillation: Past, Present, and Future. *Journal of Climate* 22, 1082–1103.

Frankcombe, L.M., von der Heydt, A. and Dijkstra, H. A. 2010. North Atlantic Multidecadal Climate Variability: An Investigation of Dominant Time Scales and Processes. *Journal of Climate* 23, 3626–3638.

Frankignoul, C., de Coëtlogon, G., Joyce, T.M. and Dong, S. 2001. Gulf Stream Variability and Ocean-Atmosphere Interactions. *Journal of Physical Oceanography* 31, 3516–3529.

Freeman, C., Ostle, N. and Kang, H. 2001. An enzymic "latch" on a global carbon store. *Nature* 409, 149.

Friborg, T. Soegaard, H., Christensen, T.R., Lloyd, C.R., Panikov, N.S. 2003. Siberian wetlands: where a sink is a source. *Geophys. Res. Lett*. 30, 2129.

Froese, D.G., Jensen, B.J., 2005. Stop 2: White River Ash-eastern lobe, in Froese, D.G., Westgate, J.A., Alloway, B.V. (Eds.), *Field Trip Guide for the International Field Conference and Workshop on Tephrochronology and Volcanism, Dawson City, Yukon Territory, Canada*. Institute of Geological and Nuclear Sciences, New Zealand, pp. 53-56. Science Report 2005/26.

Froggatt, P.C. 1983. Toward a comprehensive Upper Quaternary tephra and ignimbrite stratigraphy in New Zealand using electron microprobe analysis of glass shards. *Quaternary Research* 19, 188–200.

Froggatt, P.C. 1992. Standardization of the chemical analysis of tephra deposits, report of the ICCT working group. *Quaternary International* 13, 93–96.

Frolking, S., Roulet, N.T., Tuittila, E., Bubier, J.L., Quillet, A., Talbot, J. and Richard, P.J.H. 2010. A new model of Holocene peatland net primary

production, decomposition, water balance, and peat accumulation. *Earth System Dynamics* 1, 1–21.

Frolking, S., Talbot, J., Jones, M.C., Treat, C.C., Kauffman, J.B., Tuittila, E.S. and Roulet, N. 2011. Peatlands in the Earth's 21st century coupled climate-carbon system. *Environmental Review* 19, 371-396.

Frolking, S., Talbot, J. and Subin, Z.M. 2014. Exploring the relationship between peatland net carbon balance and apparent carbon accumulation rate at century to millennial time scales. *The Holocene* 24, 1167–1173.

Furukawa, R., Yoshimoto, M. and Yamagata, K. 1997. Did Hokkaido Komagatake volcano erupt in 1694? Reappraisal of the eruptive ages of 17th - 18th centuries in Hokkaido. *Kazan* 42, 269-279.

Gajewski, K. 1988. Late Holocene climate changes in eastern North America estimated from pollen data. *Quat. Res.* 29, 255–262.

Gallego-Sala, A. V. and Prentice, I.C., 2013. Blanket peat biome endangered by climate change. *Nat. Clim. Chang.* 3, 152–155.

Gallego-Sala, A., Clark, J., House, J., Orr, H., Prentice, I.C., Smith, P., Farewell, T. and Chapman, S. 2010. Bioclimatic envelope model of climate change impacts on blanket peatland distribution in Great Britain. *Clim. Res.* 45, 151–162.

Gao, C., Robock, A. and Ammann, C. 2008. Volcanic forcing of climate over the past 1500 years: An improved ice core-based index for climate models. *J. Geophys. Res.* 113, D23111.

Gardner, J.E. and Tait, S., 2000. The caldera-forming eruption of Volcán Ceboruco, Mexico. *Bull. Volcanol.* 62, 20–33.

Garneau, M., van Bellen, S., Magnan, G., Beaulieu-Audy, V., Lamarre, A. and Asnong, H., 2014. Holocene carbon dynamics of boreal and subarctic peatlands from Quebec, Canada. *The Holocene* 24, 1043–1053.

Gauch, H.G., Whittaker, R.H. and Singer, S.B. 1981. A comparative study of nonmetric ordinations, *Journal of Ecology* 69, 135-152.

Gehrels, M.J., Newnham, R.M., Lowe, D.J., Wynne, S., Hazell, J. and Caseldine, C. 2008. Towards rapid assay of cryptotephra in peat cores : Review and evaluation of various methods. *Quaternary International* 178, 68–84.

Godwin, H. 1956. The history of the British flora. Cambridge University Press, UK.

Gomaa, F., Todorov, M., Heger, T.J., Mitchell, E. A. D. and Lara, E. 2012. SSU rRNA phylogeny of Arcellinida (Amoebozoa) reveals that the largest Arcellinid genus, Difflugia Leclerc 1815, is not monophyletic. *Protist* 163, 389–99.

Goodrich, G.B. and Walker, J.M. 2011. The influence of the PDO on winter precipitation during high-and low-index ENSO conditions in the eastern United States. *Phys. Geogr.* 32, 295–312.

Gordon, A.D. and Birks, H.J.B. 1972, Numerical methods in Quaternary palaeoecology I. Zonation of pollen diagrams. *New Phytologist*, 71, 961-979.

Gore, A.J., 1983. *Mires : swamp, bog, fen and moor*. Elsevier Scientific Pub. Co., New York, N.Y.

Gorham, E. 1991. Northern Peatlands: Role in the Carbon Cycle and Probable Responses to Climatic Warming. *Ecol. Appl.* 1, 182–195.

Graham, N.E., Ammann, C.M., Fleitmann, D., Cobb, K.M. and Luterbacher, J. 2010. Support for global climate reorganization during the “Medieval Climate Anomaly.” *Clim. Dyn.* 37, 1217–1245.

Graham, N.E., Hughes, M.K., Ammann, C.M., Cobb, K.M., Hoerling, M.P., Kennett, D.J., Kennett, J.P., Rein, B., Stott, L. and Wigand, P.E. 2007. Tropical Pacific–mid-latitude teleconnections in medieval times. *Clim. Change* 83, 241–285.

Gray, S.T. 2004. A tree-ring based reconstruction of the Atlantic Multidecadal Oscillation since 1567 A.D. *Geophys. Res. Lett.* 31, L12205.

Grosse-Brauckmann, G. 1972. Uber pflanzliche makrofossilien mitte-leuropaïscher torfe. I. Gewebereste krautiger pflanzen und ihremerkmale. *Telma* 2, 19–55.

Grove, J. 2004. *Little Ice Ages Ancient and Modern*. London, Routledge.

Grove, J.M. and Switsur, R. 1994. Glacial geological evidence for the Medieval Warm Period. *Clim. Change* 26, 143–169.

Gunnarson, B.E., Borgmark, A. and Wastergard, S. 2003. Holocene humidity fluctuations in Sweden inferred from dendrochronology and peat stratigraphy. *Boreas* 32, 347–360.

Haigh, J.D., Winning, A.R., Toumi, R. and Harder, J.W. 2010. An influence of solar spectral variations on radiative forcing of climate. *Nature* 467, 696–9.

Hall, V.A. and Pilcher, J.R. 2002. Late-Quaternary Icelandic tephras in Ireland and Great Britain: detection, characterization and usefulness. *The Holocene* 12, 223–230.

Hall, M. and Hayward, C. 2014. Preparation of micro-and crypto-tephras for quantitative microbeam analysis. *Geol. Soc. London, Spec. Publ.* 398, 21–28.

Hall, V. A., Pilcher, J. R. and McVicker, S. J. 1993. Tephra-linked studies and environmental archaeology, with special reference to Ireland. Circaea The *Journal of the Association for Environmental Archaeology* 11, 17-22.

Hammond R.F., van der Krogt, G. and Osinga, T. 1990. Vegetation and water tables on two raised bog remnants in County Kildare. In Doyle, G.J., editor, *Ecology and conservation of Irish peatlands*, Dublin: Royal Irish Academy, 121–34.

Hannon, G.E., Hermanns-Audardottir, M. and Wastegard, S., 1998. Human impact at Tjornuvik in the Faroe Islands. Frodskaparrit 46, 215-228.

Haslam, C.J. 1987. *Late Holocene peat stratigraphy and climatic change: a macrofossil investigation from the raised mires of North Western Europe*. PhD thesis, Univeristy of Southampton.

Haslett, J. and Parnell, A. 2008. A simple monotone process with application to radiocarbon- dated depth chronologies. *J. R. Stat. Soc. Ser. C (Applied Stat.)* 57, 399–418.

Hayward, C. 2011. High spatial resolution electron probe microanalysis of tephras and melt inclusions without beam-induced chemical modification. *The Holocene* 22, 119–125.

Heiri, O., Tinner, W. andLotter, A.F. 2004. Evidence for cooler European summers during periods of changing meltwater flux to the North Atlantic. *Proc. Natl. Acad. Sci. U.S.A.* 101, 15285–8.

Hendon, D. and Charman, D.J. 1997. The preparation of testate amoebae (Protozoa: Rhizopoda) samples from peat. *The Holocene* 7, 199–205.

Hendon, D., Charman, D.J. and Kent, M. 2001. Palaeohydrological records derived from testate amoebae analysis from peatlands in northern England: within-site variability, between-site comparability and palaeoclimatic implications. *The Holocene* 11, 127–148.

Higuera, P., Brubaker, L., Anderson, P., Hu, F. and Brown, T. 2009. Vegetation mediated the impacts of postglacial climate change on fire regimes in the south-central Brooks Range, Alaska. *Ecol. Monogr.* 79, 201–219.

Hill, M.O. and Gauch, H.G. 1980. Detrended correspondence analysis, an improved ordination technique. *Vegetatio* 42: 47–58.

Hogg, E.H. 1997. Temporal scaling of moisture and the forest-grassland boundary in western Canada. *Agric. For. Meteorol.* 84, 115–122.

Houlder, D. J. 2000. *ANUCLIM user guide, version 5.1.* Centre for Resource and Environmental Studies, Australian National University, Canberra.

Hu, Q. and Feng, S. 2001. Variations of teleconnection of ENSO and interannual variation in summer rainfall in the central United States. *J. Clim.* 14, 2469–2480.

Hu, F.S., Kaufman, D., Yoneji, S., Nelson, D., Shemesh, A., Huang, Y., Tian, J., Bond, G., Clegg, B. and Brown, T. 2003. Cyclic Variation and Solar Forcing of Holocene Climate in the Alaskan Subarctic. *Science* 301, 1890–1893.

Hughes, M.K. and Diaz, H.F. 1994. Was there a “Medieval Warm Period”, and if so, where and when? *Clim. Change* 26, 109–142.

Hughes, P.D.M. and Barber, K.E. 2004, Contrasting pathways to ombrotrophy in three raised bogs from Ireland and Cumbria, England, *The Holocene,* 14, 1, 65-77.

Hughes, P.D.M., Barber, K.E., Langdon, P.G. and Mauquoy, D. 2000. Mire-development pathways and palaeoclimatic records from a full Holocene peat archive at Walton Moss, Cumbria, England. *The Holocene* 10, 465–479.

Hughes, P.D.M., Blundell, A., Charman, D.J., Bartlett, S., Daniell, J.R.G., Wojatschke, A. and Chambers, F.M. 2006. An 8500cal. year multi-proxy climate record from a bog in eastern Newfoundland: contributions of meltwater discharge and solar forcing. *Quat. Sci. Rev.* 25, 1208–1227.

Hughes, P.D.M., Lomas-Clarke, S.H., Schulz, J. and Jones, P. 2007. The declining quality of late-Holocene ombrotrophic communities and the loss of *Sphagnum* austinii (Sull. ex Aust.) on raised bogs in Wales. *The Holocene* 17, 613–625.

Hughes, P.D.M., Mallon, G., Essex, H.J., Amesbury, M.J., Charman, D.J., Blundell, a., Chambers, F.M., Daley, T.J. and Mauquoy, D. 2012. The use of k-values to examine plant "species signals" in a peat humification record from Newfoundland. *Quat. Int.* 268, 156–165.

Hughes, P.D.M., Mallon, G., Brown, A., Essex, H.J., Stanford, J.D. and Hotes, S. 2013. The impact of high tephra loading on late-Holocene carbon accumulation and vegetation succession in peatland communities. *Quaternary Science Reviews* 67, 160-175.

Hunt, J.B. and Hill, P.G. 1993. Tephra geochemistry: a discussion of some persistent analytical problems. *The Holocene* 3, 271–278.

Hunt, J.B. and Hill, P.G. 1996. An inter-laboratory comparison of the electron probe microanalysis of glass geochemistry. *Quat. Int.* 34, 229–241.

Hunt, J.B. and Hill, P.G. 2001. Tephrological implications of beam size—sample- size effects in electron microprobe analysis of glass shards. *J. Quat. Sci.* 16, 105–117.

Hurrell, J.W. 1995. Decadal trends in the North Atlantic Oscillation: Regional temperatures and precipitation. *Science* 269, 676–679.

Hurrell, J.W., Visbeck, M., Busalacchi, A., Clarke, R.A., Delworth, T.L., Dickson, R.R., Johns, W.E., Koltermann, K.P., Kushnir, Y. and Marshall, D. 2006. Atlantic

climate variability and predictability: A CLIVAR perspective. *J. Clim.* 19, 5100–5121.

Hutchinson, M.F. 2004. *Anusplin Version 4.3.* Centre for Resource and Environmental Studies. Aust. Natl. Univ. Canberra, ACT.

Hutchinson, M.F., McKenney, D.W., Lawrence, K., Pedlar, J.H., Hopkinson, R.F., Milewska, E. and Papadopol, P. 2009. Development and testing of Canada-wide interpolated spatial models of daily minimum-maximum temperature and precipitation for 1961-2003. *J. Appl. Meteorol. Climatol.* 48, 725–741.

Ingram, H.A.P. 1982. Size and shape in raised mire ecosystems: a geophysical model. *Nature* 297, 300–303.

IPCC, 2007: Climate Change 2013: The Physical Science Basis. Contribution of Working Group I to the Fith Assessment Report of the Intergovernmental Panel on Climate Change [Solomon, S., D. Qin, M. Manning, Z. Chen, M. Marquis, K.B. Averyt, M.Tignor and H.L. Miller (eds.)]. Cambridge University Press, Cambridge, United Kingdom and New York, NY, USA.

Ise, T., Dunn, A.L., Wofsy, S.C. and Moorcroft, P.R. 2008. High sensitivity of peat decomposition to climate change through water-table feedback. *Nature Geoscience* 1, 763–766.

Ivanov, K.E. 1953. *Hydrology of mires*. Gidrometeoizdat, Leningrad.

Ivanov, K.E. 1981. *Water movement in mirelands*. Academic Press, London.

Jackson, S.T. and Charman, D.J. 2010. Editorial: Peatlands-paleoenvironments and carbon dynamics. *PAGES news* 18, 3–4.

Jensen, B.J.L. 2007. Tephrochronology of middle to late Pleistocene loess in east-central Alaska. MSc Thesis, University of Alberta, p. 120.

Jensen B. J. L., Pyne-O'Donnell, S., Plunkett, G., Froese, D.G., Hughes, P.D.M., Sigl, M., McConnell, J.R., Amesbury, M.J., Blackwell, P.G., van den Bogaard, C., Buck, C.E., Charman, D.J., Clague, J.J, Hall, V.A., Koch, J., Mackay, H., Mallon, G., McColl, L. and Pilcher, J.R. 2014a. Transatlantic distribution of the Alaskan White River Ash. *Geology* 42, 875-878.

Jensen, B.J.L, Kuehn, S.K. and Froese, D.G. 2014b. *Geochemical characterization of the Mount St. Helens "Spirit Lake" Stage.* Tephra 2014 - Maximizing the potential of tephra for multidisciplinary science, August 2014, Portland, OR.

Johnson, E.A. 1992 *Fire and vegetation dynamics – studies from the North American boreal forest*. Cambridge Univeristy Press.

Johnsen, S. J., Dahl- Jensen, D., Gundestrup, N., Steffensen, J. P., Clausen, H. B., Miller, H., Masson-Delmotte, V., Sveinbjornsdottir, A.E. and White, J. 2001. Oxygen isotope and palaeotemperature records from six Greenland ice- core stations: Camp Century, Dye- 3, GRIP, GISP2, Renland and NorthGRIP. *Journal of Quaternary Science*, *16*(4), 299-307.

Jones, P.D. and Bradley, R.S. 1992. Climatic variations over the last 500 years, in: Bradley, R.S., Jones, P.D. (Eds.), *Climate Since AD 1500*. Routledge, London, pp. 649–665.

Jones, P.D. and Mann, M.E. 2004. Climate over past millennia. *Rev. Geophys.* 42, RG2002.

Jones, M.C. and Yu, Z. 2010. Rapid deglacial and early Holocene expansion of peatlands in Alaska. *Proc. Natl. Acad. Sci. U. S. A.* 107, 7347–52.

Jones, A. R., Thomson, D. J., Hort, M. and Devenish, B. 2007. The U.K. Met Office's next-generation atmospheric dispersion model, NAME III', in Borrego C. and Norman A.-L. (Eds) *Air Pollution Modeling and its Application XVII* (Proceedings of the 27th NATO/CCMS International Technical Meeting on Air Pollution Modelling and its Application), Springer, pp. 580-589.

Joosten, H. and Clarke, D. 2002. W*ise Use of Mires and Peatlands: Background and Principles including a Framework for Decision-Making*. Totnes UK Int. Mire Conserv. Gr. Int. Peat Soc.

Joyce, T.M., Deser, C. and Spall, M.A. 2000. The relation between decadal variability of subtropical mode water and the North Atlantic Oscillation. *J. Clim*. 13, 2550–2569.

Juggins, S. 2013. Quantitative reconstructions in palaeolimnology: new paradigm or sick science? *Quat. Sci. Rev.* 64, 20–32.

Jungclaus, J.H., Haak, H., Latif, M. and Mikolajewicz, U. 2005. Arctic–North Atlantic interactions and multidecadal variabil- ity of the meridional overturning circulation. *J. Clim.* 18, 4013–4031.

Katsui, Y., Yokohama, L., Fujita, T. and Ehara, S. 1975. Komagatake. Report of the Volcanoes in Hokkaido, Part 4, Committee for prevention of the Natural Disasters of Hokkaido, Sapporo, 194 (in Japanese).

Keenan, D.J. 2003. Volcanic ash retrieved from the GRIP ice core is not from Thera. *Geochem. Geophys. Geosyst.* 4, 1097.

Keigwin, L.D., Sachs, J.P. and Rosenthal, Y. 2003. A 1600-year history of the Labrador Current off Nova Scotia. *Clim. Dyn.* 21, 53–62

Kelly, P. and Wigley, T. 1990. The influence of solar forcing trends on global mean temperature since 1861. *Nature* 347, 460-462.

Kelly, P. and Wigley, T. 1992. Solar cycle length, greenhouse forcing and global climate. *Nature* 360, 328-330.

Kent, M. and Coker, P. 1992. *Vegetation description and analysis: a practical approach*. Wiley, Chichester, UK.

Kerr, R.A. 2000. A North Atlantic Climate Pacemaker for the Centuries. *Science* 288, 1984–1985.

Kessler, W.S. 2002. Is ENSO a cycle or a series of events? *Geophys. Res. Lett.* 29, 40–41.

Khider, D., Stott, L.D., Geay, J.E., Thunell, R. and Hammond, D.E. 2011. Assessing El Niño Southern Oscillation variability during the past millennium. *Paleooceanography* 26, PA3222.

Kilian, M., Plicht, J. and Van der, van Geel, B. 1995. Dating raised bogs: new aspects of ams 14c wiggle matching, a reservoir effect and climatic change. *Quat. Sci. Rev*. 14, 959–966.

Klein, E.S., Booth, R.K., Yu, Z., Mark, B.G. and Stansell, N.D. 2013. Hydrology-mediated differential response of carbon accumulation to late Holocene climate change at two peatlands in Southcentral Alaska. *Quat. Sci. Rev.* 64, 61–75.

Klinger, L.F. 1996. The myth of the classic hydrosere model of bog succession, *Arctic and Alpine Research,* 28, 1, 1-9.

Knight, J.R. 2005. A signature of persistent natural thermohaline circulation cycles in observed climate. *Geophys. Res. Lett.* 32, L20708.

Knight, J.R., Folland, C.K. and Scaife, A. A. 2006. Climate impacts of the Atlantic Multidecadal Oscillation. *Geophys. Res. Lett.* 33, L17706.

Kobayashi, T., Nairn, I., Smith, V. and Shane, P. 2005. Proximal stratigraphy and event sequence of the c. 5600 cal. yr BP Whakatane rhyolite eruption episode from Haroharo volcano, Okataina Volcanic Centre, New Zealand. New Zeal. *J. Geol. Geophys.* 48, 471–490.

Kovach, W.L. 1995. *Multivariate Data Analysis*. Quaternary Research Association, London.

Kuehn S.C. and Foit, F.F. 2006. Correlation of widespread Holocene and Pleistocene tephra layers from Newberry Volcano, Oregon, using glass compositions and numerical methods. *Quaternary International* 148, 113-137.

Kuehn, S.C., Froese, D.G. and Shane, P.A.R. 2011. The INTAV intercomparison of electron-beam microanalysis of glass by tephrochronology laboratories, results and recommendations. *Quaternary International* 246, 19-47.

Kuehn, S.C., Bursik, M.I., Pouget, S. 2013. *Improved integration and discoverability of tephra data for multidisciplinary applications.* Abstract V13A-2591 presented at 2013 Fall Meeting, AGU, San Francisco (9-13 Dec 2013).

Kuhry, P. 1994. The role of fire in the development of *Sphagnum*-dominated peatlands in western boreal Canada. *Journal of Ecology* 82, 899-910.Kuhry, P. and Turunen, J. 2006. Postglacial development of boreal and subarctic peatlands, in: Wieder, R.K., Vitt, D.H., (Eds.), Boreal Peatland Ecosystems. Springer-Verlag, pp. 25–46.

Kuiper, J.J., Mooij, W.M., Bragazza, L. and Robroek, B.J. 2014, Plant functional types define magnitude of drought response in peatland CO_2 exchange, *Ecology,* 95, 1, 123-131.

Kyle, P.R., Ponomareva, V.V., Rourke Schluep, R. 2011. Geochemical characterization of marker tephra layers from major Holocene eruptions, Kamchatka Peninsula, Russia. *Geology Review* 53, 1059-1097.

Lafontaine-Boyer, K. and Gajewski, K. 2014. Vegetation dynamics in relation to late Holocene climate variability and disturbance, Outaouais, Quebec, Canada. *The Holocene* 24, 1515–1526.

Laiho, R. 2006. Decomposition in peatlands: Reconciling seemingly contrasting results on the impacts of lowered water levels. *Soil Biol. Biochem.* 38, 2011–2024.

Laiho, R. and Prescott, C.E. 2004. Decay and nutrient dynamics of coarse woody debris in northern coniferous forests: a synthesis. *Can. J. For. Res.* 34, 763–777.

Laine, A., Byrne, K., Kiely, G. and Tuittila, E. 2009. The short-term effect of altered water level on carbon dioxide and methane fluxes in a blanket bog. *Suoseura* 60, 65–83.

Lamarre, A., Garneau, M. and Asnong, H. 2012. Holocene paleohydrological reconstruction and carbon accumulation of a permafrost peatland using testate amoeba and macrofossil analyses, Kuujjuarapik, subarctic Québec, Canada. *Rev. Palaeobot. Palynol.* 186, 131–141.

Lamarre, A., Magnan, G., Garneau, M. and Boucher, É. 2013. A testate amoeba-based transfer function for paleohydrological reconstruction from boreal and subarctic peatlands in northeastern Canada. *Quat. Int.* 306, 88–96.

Lamb, H.H. 1965. The Early Medieval Warm Epoch and its Sequel. *Palaeogeogr., Palaeoclim. Palaeoecol* 1, 13–37.

Lamb, H.H. 1977. *Climate: Present, Past and Future*. Methuen, London.

Lamentowicz, M. and Mitchell, E. A D. 2005. The ecology of testate amoebae (Protists) in sphagnum in North-western Poland in relation to peatland ecology. *Microb. Ecol*. 50, 48–63.

Lamentowicz, M., Cedro, A., Gałka, M., Goslar, T., Miotk-szpiganowicz, G., Mitchell, E. A. D. and Pawlyta, J. 2008. Last millennium palaeoenvironmental

changes from a Baltic bog (Poland) inferred from stable isotopes, pollen, plant macrofossils and testate amoebae. *Palaeogeogr. Palaeoclimatol. Palaeoecol.* 265, 93–106.

Lamentowicz, M., Lamentowicz, L., van der Knaap, W.O., Gabka, M. and Mitchell, E. A. D. 2010. Contrasting species-environment relationships in communities of testate amoebae, bryophytes and vascular plants along the fen-bog gradient. *Microb. Ecol.* 59, 499–510.

Lane, C.S., Blockley, S.P.E., Lotter, A.F., Finsinger, W., Filippi, M.L. and Matthews, I.P. 2012. A regional tephrostratigraphic framework for central and southern European climate archives during the Last Glacial to Interglacial transition : comparisons north and south of the Alps. *Quaternary Science Reviews* 36, 50–58. Lane C. S., Chorn B. T. and Johnson T. C. 2013a. Ash from the Toba super eruption in Lake Malawi shows no volcanic winter in East Africa at 75 ka. *PNAS* 110:8025-8029.

Lane C. S., Brauer A., Blockley S. P. E., Dulski P., 2013b. Volcanic ash reveals time-transgressive abrupt climate change during the Younger Dryas. Geology 41(12),1251-1254.

Langdon, P.G. and Barber, K.E. 2002. The 'AD 860' tephra in Scotland: new data from Langlands Moss, East Kilbride. *Quaternary Newsletter* 97, 11-18.

Langdon, P.G. and Barber, K.E. 2004. Snapshots in time: precise correlations of peat-based proxy climate records in Scotland using mid-Holocene tephras. *The Holocene* 14, 21–33.

Langdon, P.G. and Barber, K.E., 2005. The climate of Scotland over the last 5000 years inferred from multiproxy peatland records : inter-site correlations and regional variability. *Journal of Quaternary Science* 20, 549–566.

Langdon, P.G., Barber, K.E. and Hughes, P.D.M. 2003. A 7500-year peat-based palaeoclimatic reconstruction and evidence for an 1100-year cyclicity in bog surface wetness from Temple Hill Moss, Pentland Hills, southeast Scotland. *Quat. Sci. Rev.* 22, 259–274.

Langdon, P.G., Caseldine, C.J., Croudace, I.W., Jarvis, S., Wastegård, S., and Crowford, T.C. 2011. A chironomid-based reconstruction of summer temperatures in NW Iceland since AD 1650. *Quat. Res.* 75, 451–460.

Larsen, G., Dugmore, A., J. and Newton, A.J. 1999. Geochemistry of historic silicic tephra in Iceland. The Holocene 9, 463-471.

Lappalainen, E. 1996. *Global Peat Resources: Jyska*: Int. Peat Soc. Geol. Surv. Finl.

Lean, J. and Rind, D. 1998. Climate forcing by changing solar radiation. *J. Clim*. 11, 3069–3094.

Legendre, P. and Legendre, L. 1998. *Numerical Ecology*, 2nd English edition. Elsevier Science BV, Amersterdam.

Lemieux, C.J., Beechey, T.J. and Gray, P.A. 2011. Prospects for Canada's protected areas in an era of rapid climate change. *Land use policy* 28, 928–941.

Lennox, B., Spooner, I., Jull, T. and Patterson, W.P. 2010. Post-glacial climate change and its effect on a shallow dimictic lake in Nova Scotia, Canada. *J. Paleolimnol*. 43, 15–27.

Lerbekmo, J.F., Westgate, J.A., Smith, D.G.W. and Denton, G. 1975. New data on the character and history of the White River volcanic eruption, Alaska, in Suggate, R.P., Cresswell, M.M. (Eds.), *Quaternary Studies*. Royal Society of New Zealand, Wellington, pp. 203–209.

Levac, E. 2003. Palnological records from Bay of Islands. Newfoundland: Direct correlation of Holocene Palaeoceanographic and climatic changes. *Palnology* 27, 135–154.

Lévesque, P.E.M., Dinel, H. and Larouche, A. 1988. *Guide to the idenfication of plant macrofossis in Canadian peatlands.* Land Resource Research Centre, Ottawa, Ontario.

Li, W., Li, L., Fu, R., Deng, Y. and Wang, H. 2011. Changes to the North Atlantic sub-tropical high and its role in the intensification of summer rainfall variability in the southeastern United States, *Journal of Climate,* 24, 1499-1506.

Libby, W. F., Anderson, E.C. and Arnold, J.R. 1949. Age Determination by Radiocarbon Content: World-Wide Assay of Natural Radiocarbon. *Science* 109, 227–228.

Liu, Y., Brewer, S., Booth, R.K., Minckley, T.A. and Jackson, S.T. 2012. Temporal density of pollen sampling affects age determination of the mid-Holocene hemlock (Tsuga) decline. *Quat. Sci. Rev.* 45, 54–59.

Lockwood, M. 2001. Long-term variations in the magnetic fields of the Sun and the heliosphere: their origin, effects and implications. *J. Geophys. Res.* 106, 16021–16038.

Loisel, J. and Garneau, M., 2010. Late Holocene paleoecohydrology and carbon accumulation estimates from two boreal peat bogs in eastern Canada: Potential and limits of multi-proxy archives. *Palaeogeogr. Palaeoclimatol. Palaeoecol.* 291, 493–533.

Loisel, J. and Gallego-Sala, A. V., Yu, Z. 2012. Global-scale pattern of peatland Sphagnum growth driven by photosynthetically active radiation and growing season length. *Biogeosciences* 9, 2737–2746.

Loisel, J. and Yu, Z. 2012. Recent acceleration of carbon accumulation in a boreal peatland, south-central Alaska. *J. Geophys. Res.* 118, 1–13.

Loisel, J. and Yu, Z. 2013a. Recent acceleration of carbon accumulation in a boreal peatland, south central Alaska. *J. Geophys. Res. Biogeosciences* 118, 41–53.

Loisel, J. and Yu, Z. 2013b. Holocene peatland carbon dynamics in Patagonia. *Quat. Sci. Rev.* 69, 125–141.

Loisel, J. and Yu, Z. 2013c. Surface vegetation patterning controls carbon accumulation in peatlands. *Geophys. Res. Lett.* 40, 5508–5513.

Loisel, J., Yu, Z., Beilman, D.W., Camill, P., Alm, J., Amesbury, M.J., Anderson, D., Andersson, S., Bochicchio, C., Barber, K., Belyea, L.R., Bunbury, J., Chambers, F.M., Charman, D.J., De Vleeschouwer, F., Fia kiewicz-Kozie , B., Finkelstein, S. a., Ga ka, M., Garneau, M., Hammarlund, D., Hinchcliffe, W., Holmquist, J., Hughes, P., Jones, M.C., Klein, E.S., Kokfelt, U., Korhola, a., Kuhry, P., Lamarre, a., Lamentowicz, M., Large, D., Lavoie, M., MacDonald, G., Magnan, G., Makila, M., Mallon, G., Mathijssen, P., Mauquoy, D., McCarroll, J., Moore, T.R., Nichols, J., O'Reilly, B., Oksanen, P., Packalen, M., Peteet, D., Richard, P.J., Robinson, S., Ronkainen, T., Rundgren, M., Sannel, a. B.K., Tarnocai, C., Thom, T., Tuittila, E.-S., Turetsky, M., Valiranta, M., van der

Linden, M., van Geel, B., van Bellen, S., Vitt, D., Zhao, Y., Zhou, W., 2014. A database and synthesis of northern peatland soil properties and Holocene carbon and nitrogen accumulation. *The Holocene* 24, 1028–1042.

Longworth, H., Marotzke, J. and Stocker, T.F. 2005. Ocean gyres and abrupt change in the thermohaline circula- tion: A conceptual analysis. *J. Clim.* 18, 2403–2416.

Lowe, D.J. 2011. Tephrochronology and its application: A review. *Quat. Geochronol.* 6, 107–153.

Lowe, D. and Hunt, J. 2001. A summary of terminology used in tephra-related studies. *Les Sossier l'Archeo-Logis* 17–22.

Lowe, J., and 41 others. 2012. Volcanic ash layers illuminate the resilience of Neanderthals and early modern humans to natural hazards. *Proceedings of the National Academy of Sciences* 109, 13532–13537.

Lund, D.C., Lynch-Stieglitz, J. and Curry, W.B. 2006. Gulf Stream density structure and transport during the past millennium. *Nature* 444, 601–604.

Lund, M., Lafleur, P.M., Roulet, N.T., Lindroth, A., Christensen, T.R., Aurela, M., Chojnicki, B.H., Flanagan, L.B., Humphreys, E.R., Laurila, T., Oechel, W.C., Olejnik, J., Rinne, J., Schubert, P. and Nilsson, M.B. 2010. Variability in exchange of CO_2 across 12 northern peatland and tundra sites. *Glob. Chang. Biol.* 2436–2448.

Lund, M., Christensen, T.R., Lindroth, A. and Schubert, P. 2012. Effects of drought conditions on the carbon dioxide dynamics in a temperate peatland. *Environ. Res. Lett.* 7, 045704.

MacDonald, G.M. and Case, R.A. 2005. Variations in the Pacific Decadal Oscillation over the past millennium, *Geophysical Research Letters* 32, 8.

Mackay, H., Hughes, P.D.M. and Langdon, P.G. 2013. Constraining peatland environmental change: exploiting the emerging eastern North American crypto-tephrostratigraphic record. Abstract PP13C-1897 presented at 2013 Fall Meeting, AGU, San Francisco (9-13 Dec 2013). http://adsabs.harvard.edu/abs/ 2013AGUFMPP13C1897M [last accessed 28 Sept 2014].

Mackey, B.G., McKenney, D.W., Yang, Y., McMahon, J.P. and Hutchinson, M.F. 1996. Site regions revisited: a climatic analysis of Hills' site regions for the province of Ontario using a parametric method. *Can. J. For. Res.* 26, 333–354.

Madden, B. and Doyle, G.J. 1990. Primary production on Mongan Bog. In: Doyle, G.J. (Ed.), *Ecology and Conservation of Irish Peatlands*. Royal IrishAcademy, Dublin, pp. 147–161.

Magnan, G. and Garneau, M. 2014. Evaluating long-term regional climate variability in the maritime region of the St. Lawrence North Shore (eastern Canada) using a multi-site comparison of peat-based paleohydrological records. *J. Quat. Sci.* 29, 209–220.

Magnan, G., Garneau, M. and Payette, S. 2014. Holocene development of maritime ombrotrophic peatlands of the St. Lawrence North Shore in eastern Canada. *Quat. Res*. 82, 96–106.

Magny, M. 1993. Climatic contribution can provide an answer for prehistoric lake dwellings. *Compte-Rendus Académie des Sci. Paris* 316, 1619–1625.

Magny, M. 2004. Holocene climate variability as reflected by mid-European lake-level fluctuations and its probable impact on prehistoric human settlements. *Quat. Int.* 113, 65–79.

Mallon, G. 2012. *Patterns of mid-Holocene climate change: evidence from the peat archive.* PhD thesis. Univeristy of Southampton.

Malmer, N. 1988. Patterns in the growth and the accumulation of inorganic constituents in the Sphagnum cover on ombrotrophic bogs in Scandinavia. *Oikos* 53, 105–120.

Malmer, N., Albinsson, C., Svensson, B.M. and Walle, B. 2003. Interferences between Sphagnum and vascular plants : effects on plant community structure and peat formation. *Oikos* 3, 469–482.

Manley, G. 1974. Central England Temperatures: Monthly means 1659 to 1973, *Quaterly Journal of the Royal Meteorological Society,* 100, 389-405.

Mann, M.E., Zhang, Z., Hughes, M.K., Bradley, R.S., Miller, S.K., Rutherford, S. and Ni, F. 2008. Proxy-based reconstructions of hemispheric and global

surface temperature variations over the past two millennia. *Proc. Natl. Acad. Sci.* U. S. A. 105, 13252–7.

Mann, M.E., Zhang, Z., Rutherford, S., Bradley, R.S., Hughes, M.K., Shindell, D., Ammann, C., Faluvegi, G. and Ni, F. 2009. Global signatures and dynamical origins of the Little Ice Age and Medieval Climate Anomaly. *Science* 326, 1256–60.

Mann, M.E., Schmidt, G. A., Miller, S.K. and LeGrande, A.N. 2009b. Potential biases in inferring Holocene temperature trends from long-term borehole information. *Geophys. Res. Lett.* 36, L05708.

Mantua, N.J. and Hare, S.R. 2002. The Pacific decadal oscillation. *J. Oceanogr.* 58, 35–44.

Manzini, E., Cagnazzo, C., Fogli, P.G., Bellucci, A. and Müller, W.A. 2012. Stratosphere- troposphere coupling at inter- decadal time scales: Implications for the North Atlantic Ocean. *Geophys. Res. Lett.* 39.

Marchitto, T.M. and Demenocal, P.B. 2003. Late Holocene variability of upper North Atlantic Deep Water temperature and salinity. *Geochemistry, Geophys. Geosystems* 4.

Margalef, R. 1972. *Homage to Evelyn Hutchinson, or why there is an upper limit to diversity.* Connecticut Academy of Arts and Sciences.

Markel, E.R. and Booth, R.K. 2010. Testate amoebae and 13C of Sphagnum as surface-moisture proxies in Alaskan peatlands. *The Holocene* 20, 463–475.

Marshall, J., Kushnir, Y., Battisti, D., Chang, P., Czaja, A., Dickson, R., Hurrell, J., McCartney, M., Saravanan, R. and Visbeck, M. 2001. North Atlantic climate variability: phenomena, impacts and mechanisms. *Int. J. Climatol.* 21, 1863–1898.

Masarik, J., Beer, J. and Duebendorf, C. 1999. Simulation of Particle fluxes and cosmogenic nuclide production in the Earth's atmosphere. *Journal of Geophysical Research* 104, 1–15.

Masing, V. 1960. Hochmoorbrände und die Entwicklung der Vegetation auf den Moor-Brandflächen. Tartu Riikliku Ülikooli Toim. *Botaanika* 93, 96–122.

Maslin, M. and Thomas, E. 2003. Balancing the deglacial global carbon budget: the hydrate factor. *Quat. Sci. Rev.* 22, 1729–1736.

Massé, G., Rowland, S.J., Sicre, M.-A., Jacob, J., Jansen, E. and Belt, S.T. 2008. Abrupt climate changes for Iceland during the last millennium: evidence from high resolution sea ice reconstructions. *Earth Planet. Sci. Lett.* 269, 565–569.

Matthes, F.E. 1939. Report of committee on glaciers, April 1939. *Eos, Trans.* Am. Geophys. Union 20, 518–523.

Matthews, J. A. and Briffa, K.R. 2005. The "Little Ice Age": Re-Evaluation of an Evolving Concept. Geogr. Ann. Ser. *A Phys. Geogr.* 87, 17–36.

Mauquoy, D. 1997. *Testing the Sensitivity of the Palaeoclimatic Signal from Ombrotrophic Peat Stratigraphy,* Unpublished PhD thesis, University of Southampton.

Mauquoy, D. and Barber, K. 1999. A replicated 3000 yr proxy-climate record from Coom Rigg Moss and Felecia Moss, the Border Mires, northern England. *Journal of Quaternary Sceince* 14, 263–275.

Mauquoy, D. and van Geel, B. 2007. Mire and peat macros, in: Elias, S.A. (ed.) *Encycl. Quat. Sci., Vol 3.* Elsevier, Amsterdam. 2315–2336.

Mauquoy, D., Geel, B. Van, Blaauw, M., Plicht, J. Van Der, van Geel, B. and van der Plicht, J. 2002. Evidence from northwest European bogs shows "Little Ice Age" climatic changes driven by variations in solar activity. *The Holocene* 12, 1–6.

Mauquoy, D., Yeloff, D., Van Geel, B., Charman, D.J. and Blundell, A. 2008. Two decadally resolved records from north-west European peat bogs show rapid climate changes associated with solar variability during the mid-late Holocene. *J. Quat. Sci.* 23, 745–763.

Mauquoy, D., Hughes, P.D.M. and van Geel, B. 2010. A protocol for plant macrofossil analysis of peat deposits. *Mires and Peat* 7, 1–5.

Mayewski, P. a., Rohling, E.E., Curt Stager, J., Karlén, W., Maasch, K. a., David Meeker, L., Meyerson, E. a., Gasse, F., van Kreveld, S., Holmgren, K., Lee-Thorp, J., Rosqvist, G., Rack, F., Staubwasser, M., Schneider, R.R., Steig, E.J., 2004. Holocene climate variability. *Quat. Res.* 62, 243–255.

McClymont, E.L., Mauquoy, D., Yeloff, D., Broekens, P., van Geel, B., Charman, D.J., Pancost, R.D., Chambers, F.M. and Evershed, R.P. 2008. The disappearance of Sphagnum imbricatum from Butterburn Flow, UK. *The Holocene* 18, 991–1002.

McCune, B. and Grace, J.B. 2002. *Analysis of ecological communities*. MjM Software Design. USA, Glenden Beach, OR.

McKenney, D.W., Pedlar, J.H., Papadopol, P. and Hutchinson, M.F. 2006. The development of 1901–2000 historical monthly climate models for Canada and the United States. *Agric. For. Meteorol.* 138, 69–81.

McKenney, D.W., Hutchinson, M.F., Papadopol, P., Lawrence, K., Pedlar, J., Campbell, K., Milewska, E., Hopkinson, R.F., Price, D. and Owen, T. 2011. Customized spatial climate models for North America. *Bull. Am. Meteorol. Soc.* 92, 1611–1622.

McManus, G.E., Conway, C.M., Mercer, D.J. and Wood, C. 1991. *Atlas of Newfoundland and Labrador,* St John's, Nfld: Breakwater

McMullen, J.A., 2000 *Palaeoecology and the conservation management of lowland raised bogs*, PhD thesis, University of Southampton.

McMullen, J., Barber, K. and Johnson, B. 2004. A palaeoecological perspective of vegetation succession on raised bog microforms. *Ecol. Monogr.* 74, 45–77.

McPhaden, M.J., Zebiak, S.E. and Glantz, M.H. 2006. ENSO as an integrating concept in earth science. *Science* 314, 1740–1745.

Meade, R. 1992. Some early changes following the rewetting of a vegetated cutover peatland surface at Danes Moss, Cheshire, UK, and their relevance to conservation management. *Biological Conservation,* 61, 1, 31-40.

Melekestsev, I.V., Braitseva, O.A., Ponomareva, V.V., and Sulerzhitsky, L.D. 1996. Holocene catastrophic caldera-forming eruptions of Ksudach volcano. Kamchatka. *Volcanology and Seismology* 17, 395–421.

Mieczan, T. 2009. Ecology of testate amoebae (Protists) in Sphagnum peatlands of eastern Poland: Vertical micro-distribution and species assemblages in relation to environmental parameters. *Ann. Limnol. - Int. J. Limnol.* 45, 41–49.

Milankovitch, M. 1941. Canon of Insolation and the Ice-Age Problem (in German), in: *Special Publications of the Royal Serbian Academy*, Vol 132. Israel Program for Scientific Translations, p. 484.

Miller, R.L. 2012. Adjustment to Radiative Forcing in a Simple Coupled Ocean–Atmosphere Model. *J. Clim*. 25, 7802–7821

Minchin, P.R. 1987. An evaluation of the relative robustness of techniques for ecological ordination, in: *Theory and Models in Vegetation Science*. Springer, pp. 89–107.

Minkkinen, K., Vasander, H., Jauhiainen, S., Karsisto, M. and Laine, J. 1999. Post-drainage changes in vegetation composition and carbon balance in Lakkasuo mire, Central Finland. *Plant and Soil* 207, 107–120.

Mitchell, E.A.D. and Gilbert, D., 2004. Vertical micro-distribution and response to nitrogen deposition of testate amoebae in Sphagnum. *J. Eukaryot. Microbiol.* 51, 480–490.

Mitchell, E.A.D., Butler, A.J., Warner, B.G. and Gobat, J.M. 1999. Ecology of testate amoebae (Protozoa: Rhizopoda) in *Sphagnum* peatlands in the Jura Mountains, Switzerland and France. *Ecoscience* 565–576.

Mitchell, E.A.D., Buttler, A., Grosvernier, P., Rydin, Hå., Albinsson, C., Greenup, A.L., Heijmans, M.M.P.D., Hoosbeek, M.R. andSaarinen, T. 2000. Relationships among testate amoebae (Protozoa), vegetation and water chemistry in five Sphagnum- dominated peatlands in Europe. *New Phytol.* 145, 95–106.

Mitchell, E. A. D., Charman, D.J. and Warner, B.G. 2008. Testate amoebae analysis in ecological and paleoecological studies of wetlands: past, present and future. *Biodivers. Conserv.* 17, 2115–2137.

Mitchell, E. A. D., Payne, R.J., van der Knaap, W.O., Lamentowicz, Ł., Gąbka, M. and Lamentowicz, M. 2013. The performance of single- and multi-proxy transfer functions (testate amoebae, bryophytes, vascular plants) for reconstructing mire surface wetness and pH. *Quat. Res.* 79, 6–13.

Moffa-Sánchez, P., Born, A., Hall, I.R., Thornalley, D.J.R. and Barker, S. 2014. Solar forcing of North Atlantic surface temperature and salinity over the past millennium. *Nat. Geosci.* 7, 275–278.

Moore, J.J., Hughen, K.A., Miller, G.H. and Overpeck, J.T. 2001. Little Ice Age recorded in summer temperature reconstruction from varved sediments of Donard Lake, Baffin Island, Canada. *Journal of Paleolimnology* 503–517.

Moore T.R., Bubier J.L., Frolking S.E., Lafleur, P.M. and Roulet, N.T., 2002. Plant biomass and production and CO_2 exchange in an ombrotrophic bog. *J. Ecol.* 90, 25 – 36.

Moore, T.R., Lafleur, P.M., Poon, D.M.I., Heumann, B.W., Seaquist, J.W. and Roulet, N.T. 2006. Spring photosynthesis in a cool temperate bog. *Glob. Chang. Biol.* 12, 2323–2335.

Morgan, T.J., Herod, A.A., Brain, S. A, Chambers, F.M., Kandiyoti, R. 2005. Examination of soil contaminated by coal-liquids by size exclusion chromatography in 1-methyl-2-pyrrolidinone solution to evaluate interference from humic and fulvic acids and extracts from peat. *J. Chromatogr. A* 1095, 81–8.

Morris, P.J., Waddington, J.M., Benscoter, B.W. and Turetsky, M.R. 2011a. Ecohydrology Bearings — Invited Commentary Conceptual frameworks in peatland ecohydrology : looking beyond the two-layered (acrotelm – catotelm) model 11, 1–11.

Morris, P.J., Belyea, L.R. and Baird, A.J. 2011b. Ecohydrological feedbacks in peatland development: a theoretical modelling study. *J. Ecol.* 99, 1190–1201.
Mullineaux, D.R. 1996. Pre-1980 Tephra-Fall Deposits Erupted from Mount St. Helens. *U.S. Geological Survey, Washington, Professional Paper* 1563, 99.

Murray, K.J., Harley, P.C., Tenhunen, J.T. and Walz, H. 1989, Water content effects on photosynthetic response of *Sphagnum* mosses from the foothills of the Philip Smith Mountains, Alaska, *Oecologia, 79,* 2, 244-250.

Nanayama, F., Satake, K., Furukawa, R., Shimokawa, K., Atwater, B. F., Shigeno, K. and Yamaki, S. 2003. Unusually large earthquakes inferred from tsunami deposits along the Kuril trench. *Nature* 424, 660-663.

National Aeronautics and Space Administration (NASA), 2011, http://earthobservatory.nasa.gov/Features/NAO/NAO_2.php, last accessed 05/07/2013.

National Oceanic and Atmospheric Administration (NOAA), 2011, http://www.climate.gov/news-features/climate-current-events/winter-temperatures-influenced-north-atlantic-oscillation-la, last accessed 23/05/2014.

Neil, K., Gajewski, K. and Betts, M. 2014. Human-ecosystem interactions in relation to Holocene environmental change in Port Joli Harbour, southwestern Nova Scotia, Canada. *Quat. Res.* 81, 203–212.

Nesje, A. and Dahl, S.O. 2003. The "Little Ice Age" – only temperature? *The Holocene* 13, 139–145.

Newman, M., Compo, G.P. and Alexander, M.A. 2003. ENSO-forced variability of the Pacific decadal oscillation. *J. Clim.* 16, 3853–3857.

Newton, A.J. and Metcalfe, S.E. 1999. Tephrochronology of the Toluca Basin, central Mexico. *Quaternary Science Reviews* 18, 1039-1059.

Newton A. J., Gittings B. and Stuart N. 1997. *Designing a scientific database Query Server using the World Wide Web: The example of Tephrabase.* Innovations in GIS 4, Taylor and Francis, London, 251-266.

Newton, A.J., Dugmore, A.J. and Gittings, B.M., 2007. Tephrabase : tephrochronology and the development of a centralised European database. *Journal of Quaternary Science* 22, 737–743.

Nichols, J.E. and Huang, Y. 2012. Hydroclimate of the northeastern United States is highly sensitive to solar forcing. *Geophys. Res. Lett.* 39.

Nichols, J.E., Booth, R.K., Jackson, S.T., Pendall, E.G. and Huang, Y. 2006. Paleohydrologic reconstruction based on *n*-alkane distributions in ombrotrophic peat. *Organic Geochemistry* 37, 1505–1513.

Nichols, J.E., Peteet, D.M., Moy, C.M., Castaneda, I.S., McGeachy, A. and Perez, M. 2014. Impacts of climate and vegetation change on carbon accumulation in a south-central Alaskan peatland assessed with novel organic geochemical techniques. *The Holocene* 24, 1146–1155.

Noren, A.J., Bierman, P.R., Steig, E.J., Lini, A. and Southon, J. 2002. Millennial-scale storminess variability in the northeastern United States during the Holocene epoch. *Nature* 419, 821–824.

North Greenland Ice Core Project members. 2004. High-resolution record of Northern Hemisphere climate extending into the last interglacial period. *Nature* 431, 147-151.

O'Brien, S.R., Mayewski, P.A., Meeker, L.D., Meese, D.A., Twickler, M.S. and Whitlow, S.I. 1995. Complexity of Holocene Climate as Reconstructed from a Greeland Ice Core. *Science* 270, 1962-1964.

Ogden, C.G. and Hedley, R. 1980. *An atlas of freshwater testate amoebae*. Oxford University Press, New York.

Ogilvie, A.E.J. and Jónsson, T. 2001. "Little Ice Age" Research: A Perspective from Iceland. *Clim. Change 48*, 9–52.

Oglesby, R., Feng, S., Hu, Q. and Rowe, C. 2012. The role of the Atlantic Multidecadal Oscillation on medieval drought in North America: Synthesizing results from proxy data and climate models. *Glob. Planet. Change* 84-85, 56–65.

Ortega-Guerrero, B. and Newton, A.J. 1998. Geochemical characterization of late Pleistocene-Holocene tephra layers from the Basin of Mexico, central Mexico. *Quaternary Research* 50 90-106.

Okland, R.H. 1990, *Vegetation ecology: theory, method and applications with reference to Fennoscandia*, Botanical Garden and Museum, University of Oslo, Norway.

Óskarsson N., Sigvaldason G.E., Steinthórsson S., 1982. A dynamic model of rift zone petrogenesis and the regional petrology of Iceland. *Journal of Petrology* 23:28-74.

Osvald, H. 1923. *Die Vegetation des Hochmoores Komosse*. Vensk. Va ̈xtsociolo- giska Sa ̈llskapets Handl. 1, 436.

Oswald, W.W. and Foster, D.R. 2011. A record of late-Holocene environmental change from southern New England, USA. *Quat. Res.* 76, 314–318.

Overbeck, F. 1947. Studien zur Hochmoor- entwicklung in Niedersachsen und die Bestimmung der Humifizierung bei stratigraphisch-pollenanalytischen Moorunter- suchungen (Studies of raised bog development in Lower Saxony and the determination of humification in stratigraphical. *Planta* 35, 1–56.

Overbeck, F. 1975. *Botanisch-geologische Moorkunde*. K. Wachholz, Neumunster.

PAGES 2k Consortium, 2013. Continental-scale temperature variability during the past two millennia. *Nat. Geosci.* 6, 339–346.

Palais, J.M., Germani, M.S. and Zielinski, G.A. 1992. Inter-hemispheric transport of volcanic ash from a 1259 AD volcanic eruption to the Greenland and Antarctic Icesheets. *Geophysical Research Letters* 19, 801-804.

Paquette, N. and Gajewski, K. 2013. Climatic change causes abrupt changes in forest composition, inferred from a high-resolution pollen record, southwestern Quebec, Canada. *Quat. Sci. Rev.* 75, 169–180.

Parris, A.S., Bierman, P.R., Noren, A.J., Prins, M.A. and Lini, A. 2010. Holocene paleostorms identified by particle size signatures in lake sediments from the northeastern United States. *J. Paleolimnol.* 43, 29–49.

Patterson, R.T. and Kumar, A. 2000. Use of Arcellacea (Thecamoebians) to gauge levels of contamination and remediation in industrially polluted lakes, in: *Environmental Micropaleontology*. Springer, pp. 257–278.

Payette, S. 2007. Contrasted dynamics of northern Labrador tree lines caused by climate change and migrational lag. *Ecology* 88, 770–780.

Payette, S. and Delwaide, A. 2004. Dynamics of subarctic wetland forests over the past 1500 years. *Ecol. Monogr.* 74, 373–391.

Payette, S. and Rochefort, L. 2001. *Écologie des tourbières du Québec-Labrador.* Presses Université Laval.

Payne, R.J., 2012. Volcanic impacts on peatland microbial communities: A tephropalaeoecological hypothesis-test. *Quat. Int.* 268, 98–110.

Payne, R. and Blackford, J. 2008. Distal volcanic impacts on peatlands: palaeoecological evidence from Alaska. *Quat. Sci. Rev.* 27, 2012–2030.

Payne, R.J. and Mitchell, E.A.D. 2009. How many is enough? Determining optimal count totals for ecological and palaeoecological studies of testate amoebae. *J. Paleolimnol.* 42, 483–495.

Payne, R., Gehrels, M., 2010. The formation of tephra layers in peatlands: An experimental approach. *Catena* 81, 12–23.

Payne, R. J., Kilfeather, A. A., van der Meer, J. J. M. and Blackford, J. J., 2005. Experiments on the taphonomy of tephra in peat. *Suoseura* 64, 147-156.

Payne, R.J., Kishaba, K., Blackford, J.J. and Mitchell, E.A.D. 2006. Ecology of testate amoebae (Protista) in south-central Alaska peatlands: building transfer-function models for palaeoenvironmental studies. *The Holocene* 16, 403–414.

Payne, R., Blackford, J. and van der Plicht, J. 2008. Using cryptotephras to extend regional tephrochronologies: An example from southeast Alaska and implications for hazard assessment. *Quaternary Research* 69, 42–55.

Payne, R.J., Edwards, K. J. and Blackford, J. J., 2013. Volcanic impacts on the Holocene vegetation history of Britain and Ireland? A review and meta-analysis of the pollen evidence. *Vegetation History and Archaeobotany* 22, 153-164.

Peet, R.K. 1974. The measurement of species diversity. *Annu. Rev. Ecol. Syst.* 285–307.

Pelletier, L., Garneau, M. and Moore, T.R. 2011. Variation in CO 2 exchange over three summers at microform scale in a boreal bog, Eastmain region, Québec, Canada. J*. Geophys. Res.* 116, G03019.

Persson, C. 1971. Tephrochronological investigation of peat deposits in Scandinavia and on the Faroe Islands. *Sveriges Geol. Unders.* 65, 3–34.

Peterse, F., Nicol, G.W., Schouten, S. andDamsté, J.S.S. 2010. Influence of soil pH on the abundance and distribution of core and intact polar lipid-derived branched GDGTs in soil. *Org. Geochem.* 41, 1171–1175.

Philander, S.G. 1990. *El Niño, La Niña, and the Southern Oscillation*. Academic Press, London.

Philips, M.E., 1954, *Eriophorum angustifolium* Roth, *The Journal of Ecology,* 612-622.

Pielou, E.C., 1975. *Ecology diversity*. New York.

Pierce, D.W., Barnett, T.P., Schneider, N., Saravanan, R., Dommenget, D. and Latif, M. 2001. The role of ocean dynamics in producing decadal climate variability in the North Pacific. *Clim. Dyn.* 18, 51–70.

Pilcher, J.R. and Hall, V.A. 1992. Towards a tephrochronology for the Holocene of the north of Ireland. *The Holocene* 2, 255–259.

Pilcher, J.R., Hall, V.A., and McCormac, F.G. 1995. Dates of Holocene Icelandic volcanic eruptions from tephra layers in Irish peats. *The Holocene* 5, 103-110.

Pitkanen, K. Turunen, J. and Tolonen, K. 1999. The role of fire in the carbon dynamics of a mire, eastern Finland. *The Holocene* 9, 453–462.

Plunkett, G. and Swindles, G.T. 2008. Determining the Sun's influence on Late Glacial and Holocene climates: a focus on climate response to centennial-scale solar forcing at 2800 cal. BP. *Quaternary Science Reviews* 2, 175-184.

Pollard, A.M., Blockley, S.P.E. and Ward, K.R. 2003. Chemical alteration of tephra in the depositional environment: theoretical stability modelling. *J. Quat. Sci.* 18, 385–394.

Pollard, A. M., Blockley, S.P.E., Lane, C.S., 2006. Some numerical considerations in the geochemical analysis of distal microtephra. *Appl. Geochemistry* 21, 1692–1714.

Pollard, A.M., Blockley, S.P.E. and Lane, C.S. 2008. Reply to the comment on "Some numerical considerations in the geochemical analysis of distal microtephra", by N.J.G. Pearce, C.A. Bendall and J.A. Westgate. *Appl. Geochemistry* 23, 1365–1366.

Preece, S.J., McGimsey, R.G., Westgate, J.A., Pearce, N.J.G., Hart, W.K. and Perkins, W.T. 2014. Chemical complexity and source of the White River Ash, Alaska and Yukon. Geosphere 10, 1020-1042.

Proctor, C.J., Baker, A., Barnes, W.L. and Gilmour, M.A. 2000. A thousand year speleothem proxy record of North Atlantic climate from Scotland. *Clim. Dyn.* 16, 815–820.

Pyne-O'Donnell, S.D.F, 2011. The taphonomy of Last Glacial-Interglacial Transition (LGIT) distal volcanic ash in small Scottish lakes. *Boreas* 40, 131–145.

Pyne-O'Donnell, S. D. F., Hughes, P.D.M., Froese, D.G., Jensen, B, J.L., Kuehn, S.C., Mallon, G., Amesbury, M.J., Charman, D.J., Daley, T.J., Loader, N.J., Mauquoy, D., Street-Perrott. F.A. and Woodman-Ralph, J. 2012. High-precision ultra-distal Holocene tephrochronology in North America. *Quaternary Science Reviews* 52, 6-11.

Qian, S.S. King, R.S. and Richardson, C.J. 2003, Two statistical methods for the detection of environmental thresholds, *Ecological Modelling,* 166, 87-97.

Qin, Y., Mitchell, E. A. D., Lamentowicz, M., Payne, R.J., Lara, E., Gu, Y., Huang, X. and Wang, H., 2013. Ecology of testate amoebae in peatlands of central China and development of a transfer function for paleohydrological reconstruction. *J. Paleolimnol.* 50, 319–330.

R Development Core Team. 2014. R: A language and environment for statistical computing. Vienna, Austria: R Foundation for Statistical Computing. Retrieved from http://www.R-project.org.

Ramsey, C.B. 2008. Deposition models for chronological records. *Quat. Sci. Rev.* 27, 42–60.

Rasmusson, E.M. and Carpenter, T. 1982. Variations in tropical sea surface temperature and surface wind fields associated with the Southern Oscillation/El Nino. *Mon. Weather Rev* 110, 354–384.

Rasmussen, S.O., Vinther, B.M., Clausen, H.B. and Andersen, K.K. 2007. Early Holocene climate oscillations recorded in three Greenland ice cores. *Quat. Sci. Rev*. 26, 1907–1914.

Ratcliffe, D.A. and Walker, D. 1958. The Silver Flowe, Galloway, Scotland. *Journal of Ecology*, 46, 407-445.

Reichler, T., Kim, J., Manzini, E. and Kröger, J. 2012. A stratospheric connection to Atlantic climate variability. *Nat. Geosci.* 5, 783–787.

Reimer, P.J., Baillie, M.G.L., Bard, E., Bayliss, A., Beck, J.W., Blackweel, P.., Bronl Ramsey, C., Buk, C.E., Burr, G.S., L., E.R., Friedrich, M., Grootes, P.M., Guilderson, T.P., Hajdas, I., Heaton, T.J., Hoog, A.., Hughen, K.., Kaiser, K.., Kromer, B., McCormac, F.G., Manning, S.., Reimer, R.., Richards, D.., Southon, J.., Talamo, S., Turney, C.S.., va der Plicht, J., Weyhenmeyer, C.E. 2009. IntCal09 and Marine09 Radiocarbon Age Calibration Curves 0-50,000 Years cal BP. Radiocabon 51, 1111–1150.

Reimer, P. J., Bard, E., Bayliss, A., Beck, J. W., Blackwell, P. G., Bronk Ramsey, C., Grootes, P. M., Guilderson, T. P., Haflidason, H., Hajdas, I., HattŽ, C., Heaton, T. J., Hoffmann, D. L., Hogg, A. G., Hughen, K. A., Kaiser, K. F., Kromer, B., Manning, S. W., Niu, M., Reimer, R. W., Richards, D. A., Scott, E. M., Southon, J. R., Staff, R. A., Turney, C. S. M., and van der Plicht, J., 2013. IntCal13 and Marine13 Radiocarbon Age Calibration Curves 0-50,000 Years cal BP. *Radiocarbon* 55, 4.

Renouf, M.A.P. and Bell, T. 2009. Contraction and expansion in Newfoundland prehistory, AD 900–1500, in Maschner, H., Mason, O. and McGhee, R. *The Northern World* AD 900 1400, 263–278. The University if Utah Press, Salt Lake City, UT.

Rhodes, T.E. and Davis, R.B. 1995. Effects of late Holocene forest disturbance and vegetation change on acidic Mud Pond, Maine, USA. *Ecology* 734–746.

Richter, T.O., Peeters, F.J.C. and van Weering, T.C.E. 2009. Late Holocene (0–2.4kaBP) surface water temperature and salinity variability, Feni Drift, NE Atlantic Ocean. *Quat. Sci. Rev.* 28, 1941–1955.

Riehle, J.R. 1985. A reconnaissance of the major Holocene tephra deposits in the upper Cook Inlet, Alaska. *J. Volcanol. Geotherm. Res*. 26, 37–54.

Rietkerk, M., Dekker, S.C., Wassen, M.J., Verkroost, A W.M. and Bierkens, M.F.P. 2004. A putative mechanism for bog patterning. *Am. Nat.* 163, 699–708.

Rind, D. and Overpeck, J. 1993. Hypothesized causes of decade-to-century-scale climate variability: Climate model results. *Quat. Sci. Rev.* 12, 357–374.

Robock, A. 2002. Volcanic eruptions, in Munn, T. (Ed.), *The Earth System: Physical and Chemical Dimensions of Global Environmental Change.* Encyclopaedia of Global Environmental Change, Volume 1. Wiley, Chichester, pp. 738-744.

Roedel, W. 1994. *Physik unserer Umwelt: Die Atmosphäre*, 2nd, revis. ed. Springer-Verlag, Berlin.

Rogers, J.C. 1984. The association between the North Atlantic Oscillation and the Southern Oscillation in the Northern Hemisphere. *Mon Wea Rev* 112, 1999–2015.

Rohling, E.J. and Pälike, H. 2005. Centennial-scale climate cooling with a sudden cold event around 8,200 years ago. *Nature* 434, 975–979.

Roland, T.P., Caseldine, C.J., Charman, D.J., Turney, C.S.M. and Amesbury, M.J. 2014, Was there a '4.2 ka event' in Great Britain and Ireland? Evidence from the peatland record, *Quaternary Science Reviews,* 83, 11-27.

Roland, T. P., Mackay, H. and Hughes, P.D. M. 2015. Tephra analysis in ombrotrophic peatlands: A geochemical comparison of acid digestion and density separation techniques. *Journal of Quaternary Science* 30, 3-8.

Rolland, N., Larocque, I., Francus, P., Pienitz, R. and Laperrière, L. 2009. Evidence for a warmer period during the 12th and 13th centuries AD from chironomid assemblages in Southampton Island, Nunavut, Canada. *Quat. Res.* 72, 27–37.

Rosenberg, S.M., Walker, I.R., Mathewes, R.W. and Hallett, D.J. 2004. Midge-inferred Holocene climate history of two subalpine lakes in southern British Columbia, Canada. *The Holocene* 14, 258–271.

Rossby, T. and Benway, R.L. 2000. Slow variations in mean path of the Gulf Stream east of Cape Hatteras. *Geophys. Res. Lett.* 27, 117–120.

Roy, M., Dell'Oste, F., Veillette, J.J., de Vernal, A., Hélie, J.-F. and Parent, M. 2011. Insights on the events surrounding the final drainage of Lake Ojibway based on James Bay stratigraphic sequences. *Quat. Sci. Rev.* 30, 682–692.

Ruddiman, W.F. 2007. The early anthropogenic hypothesis: challenges and responses. *Rev. Geophys.* 45.

Ruokolainen, L., and Kauko S. Differences in performance of four ordination methods on a complex vegetation dataset. *Annales Botanici Fennici*. Finnish Zoological and Botanical Publishing Board, 2006.

Rydin, H. 1985. Effect of water level on desiccation of *Sphagnum* in relation to surrounding *Sphagna*. *Oikos* 45, 374–379.

Rydin, H. and McDonald, A.J.S., 1985. Tolerance of *Sphagnum* to water level. *J. Bryol*. 13, 571–578.

Rydin, H. and Jeglum, J.K. 2006. *The Biology of Peatlands*. OUP Oxford.

Sageman, B.B. and Bina, C.R. 1997. Diversity and species abundance patterns in Late Cenomanian black shale biofacies, Western Interior, US. *Palaios* 12, 449–466.

Sato, H. 1971. 14C age of Tarumae volcanic ash d member – 14C age of the Quaternary deposits in Japan (65). *Earth Science* 25, 185-186 (in Japanese).

Sawada, M., A. E. Viau, G. Vettoretti, W. Peltier, R. and Gajewski, K. 2004. Comparison of North American pollen based temperature and global lake-status with CCCma AGCM2 output at 6 ka. *Quaternary Science Reviews* 23, 225-244.

Schlesinger, M.E. and Ramankutty, N. 1994. An oscillation in the global climate system of period 65-70 years. *Nature* 367, 723–726.

Schönborn, W. 1992. Adaptive polymorphism in soil-inhabiting testate amoebae (Rhizopoda): its importance for delimitation and evolution of asexual species. *Arch Protistenkd* 142, 139–155.

Schoning, K., Charman, D.J. and Wastegoard, S. 2005. Reconstructed water tables from two ombrotrophic mires in eastern central Sweden compared with instrumental meteorological data. *The Holocene* 1, 111–118.

Schurer, A.P., Tett, S.F.B. and Hegerl, G.C. 2014. Small influence of solar variability on climate over the past millennium. *Nat. Geosci.* 7, 104–108.

Seager, R., Graham, N., Herweijer, C., Gordon, A.L., Kushnir, Y. and Cook, E. 2007. Blueprints for Medieval hydroclimate. *Quat. Sci. Rev.* 26, 2322–2336.

Seager, R., Tzanova, A. andNakamura, J. 2009. Drought in the Southeastern United States: Causes, Variability over the Last Millennium, and the Potential for Future Hydroclimate Change. *J. Clim.* 22, 5021–5045.

Sernander, R. 1908. On the evidences of postglacial changes of climate furnished by the peat- mosses of Northern Europe. *Geol. Föreningens Förhandlingar* 30, 465–473.

Shabber, A., Bonsal, B. and Khandekar, M. 1997. Canadian precipitation patterns associated with the southern oscillation. *J. Clim.* 10, 3016–3027.

Shane, P. 2000. Tephrochronology: a New Zealand case study. *Earth-Science Reviews* 49, 223-259.

Shane, P., Nairn, I. a., Martin, S.B. and Smith, V.C. 2008. Compositional heterogeneity in tephra deposits resulting from the eruption of multiple magma bodies: Implications for tephrochronology. *Quat. Int.* 178, 44–53.

Shannon, C.E. 1948. *A mathematical theory of communication.* Bell Syst. tech. J. 623–656.

Shannon, C.E. and Weaver, W. 1949. The mathematical theory of information. *The Bell System Technical Journal* 27, 379-423, 623-656.

Sheinbaum, J. 2003. Current theories on El Niño-Southern Oscillation: A review. *Geofisica Internacional* 42, 291–305.

Shindell, D.T., Schmidt, G. A, Mann, M.E., Rind, D., Waple, A. 2001. Solar forcing of regional climate change during the Maunder Minimum. *Science* 294, 2149–52.

Sicre, M.A., Hall, I.R., Mignot, J., Khodri, M., Ezat, U., Truong, M.X., Eiríksson, J., Knudsen, K.L. 2011. Sea surface temperature variability in the subpolar Atlantic over the last two millennia. *Paleoceanography* 26.

Sieron, K. and Siebe, C. 2008. Revised stratigraphy and eruption rates of Ceboruco stratovolcano and surrounding monogenetic vents (Nayarit, Mexico) from historical documents and new radiocarbon dates. *Journal of Volcanology and Geothermal Research* 176, 241-264.

Sillasoo, Ü., Väliranta, M. and Tuittila, E.S. 2011. Fire history and vegetation recovery in two raised bogs at the Baltic Sea. *J. Veg. Sci.* 22, 1084–1093.

Silvan, N., Tuittila, E.-S., Vasander, H. and Laine, J. 2004. Eriophorum vaginatum plays a major role in nutrient immobilisation in boreal peatlands, in: *Annales Botanici Fennici189*–199.

Smith, I.M. 1987. Water mites of peatlands and marshes in Canada. *Mem. Entomol. Soc. Canada* 119, 31–46.

Smith, A.J.E. 2004. *The moss flora of Britain and Ireland*. Cambridge University Press.

Smith, L.C., MacDonald, G.M., Velichko, A.A., Beilman, D.W., Borisova, O.K., Frey, K.E., Kremenetski, K. V and Sheng, Y. 2004. Siberian peatlands a net carbon sink and global methane source since the early Holocene. *Science* 303, 353–356.

Solignac, S., Seidenkrantz, M.S., Jessen, C., Kuijpers, A., Gunvald, A. K. and Olsen, J. 2011. Late-Holocene sea-surface conditions offshore Newfoundland based on dinoflagellate cysts. *The Holocene* 21, 539–552.

Spooner, I., Stolze, S., Martin, B., Robichaud, A., Herman, T., Mockford, S., Caverhill, B., Mazzucchi, D. and White, H. 2014. A 10,000-Year Record of Environmental Change from Blanding's Turtle (Emydoidea Blandingii) Habitat at Pleasant River Fen, Nova Scotia, Canada. *Wetlands* 34, 1145–1158.

Steinhilber, F., Beer, J. andFröhlich, C. 2009. Total solar irradiance during the Holocene. *Geophys. Res. Lett.* 36.

Stoneman, R. 1993. *Holocene palaeoclimates from peat stratigraphy: extending and refining the model*. PhD thesis. Univeristy of Southampton.

Struiver, M. 1961. Variations in radiocarbon concentration and sunspot activity. *J. Geophys. Res.* 66, 273–276.

Stuiver, M. and Polach, H.A. 1977. Discussion: Reporting of ^{14}C data. *Radiocarbon* 19, 355–363.

Stuiver, M., Grootes, P.M. and Braziunas, T.F. 1995. The GISP2 δ18O climate record of the past 16,500 years and the role of the sun, ocean, and volcanoes. *Quat. Res.* 44, 341–354.

Struiver, M., Reimer, P.J. and Braziunas, T.F. 1998. High-precision radiocarbon age calibration for terrestrial and marine samples. *Radiocarbon* 40, 1127-1151.

Suess, H.E. 1965. Secular variations of cosmic ray produced carbon-14 in the atmosphere and their interpretations. *J. Geophys. Res.* 70, 5937–5952.

Sullivan, M.E. andBooth, R.K. 2011. The potential influence of short-term environmental variability on the composition of testate amoeba communities in Sphagnum peatlands. *Microb. Ecol.* 62, 80–93.

Sun, C., Plunkett, G., Liu, J., Zhao, H., Sigl, M., McConnell, J.R., Pilcher, J.R., Vinther, B.M., Steffensen, J.P. and Hall, V.A. 2013 Ash from Changbaishan Millennium eruption recorded in Greenland ice: implications for determining the eruption's timing and impact. *Geophysical Research Letters* 41, 694-701.

Sutton, R.T. and Hodson, D.L.R. 2005. Atlantic Ocean forcing of North American and European summer climate. *Science* 309, 115–8.

Suzuki, T. 1996. Chemical analysis of volcanic glass by energy dispersive X-ray spectrometry with JEOL JED-2001 and JSM-5200: analytical procedures and application. *Geographical Reports of Tokyo Metropolitan Univeristy* 31, 27-26.

Swindles, G.T. and Roe, H.M. 2007. Examining the dissolution characteristics of testate amoebae (Protozoa: Rhizopoda) in low pH conditions: Implications for peatland palaeoclimate studies. *Palaeogeogr. Palaeoclimatol. Palaeoecol.* 252, 486–496.

Swindles, G.T., Plunkett, G. and Roe, H.M. 2007. A multiproxy climate record from a raised bog in County Fermanagh, Northern Ireland : a critical examination of the link between bog surface wetness and solar variability. *Journal of Quaternary Science* 22, 667–679.

Swindles, G.T., Charman, D.J., Roe, H.M. and Sansum, P. A. 2009. Environmental controls on peatland testate amoebae (Protozoa: Rhizopoda) in

the North of Ireland: Implications for Holocene palaeoclimate studies. *J. Paleolimnol.* 42, 123–140.

Swindles, G.T., De Vleeschouwer, F. and Plunkett, G. 2010. Dating peat profiles using tephra: stratigraphy, geochemistry and chronology. *Mires and Peat* 7, 1–9.

Swindles, G.T., Lawson, I.T., Savov, I.P., Connor, C.B. and Plunkett, G. 2011. A 7000 yr perspective on volcanic ash clouds affecting northern Europe. *Geology* 39, 887–890.

Swindles, G.T., Morris, P.J., Baird, A.J., Blaauw, M. and Plunkett, G. 2012a. Ecohydrological feedbacks confound peat-based climate reconstructions. *Geophys. Res. Lett.* 39.

Swindles, G.T., Blaauw, M., Blundell, A. and Turner, T.E. 2012b. Examining the uncertainties in a "tuned and stacked" peatland water table reconstruction. *Quat. Int.* 268, 58–64.

Swindles, G.T., Patterson, R.T., Roe, H.M. and Galloway, J.M. 2012c. Evaluating periodicities in peat-based climate proxy records. *Quat. Sci. Rev.* 41, 94–103.

Swindles, G.T., Lawson, I.T., Matthews, I.P., Blaauw, M., Daley, T.J., Charman, D.J., Roland, T.P., Plunkett, G., Schettler, G., Gearey, B.R., Turner, T.E., Rea, H. a., Roe, H.M., Amesbury, M.J., Chambers, F.M., Holmes, J., Mitchell, F.J.G., Blackford, J., Blundell, A., Branch, N., Holmes, J., Langdon, P., McCarroll, J., McDermott, F., Oksanen, P.O., Pritchard, O., Stastney, P., Stefanini, B., Young, D., Wheeler, J., Becker, K. and Armit, I. 2013. Centennial-scale climate change in Ireland during the Holocene. *Earth-Science Rev.* 126, 300–320.

Tappen, C.M., Webster, J.D., Mandeville, C.W. and Roderick, D. 2009. Petrology and geochemistry of ca. 2100–1000 a.B.P. magmas of Augustine volcano, Alaska, based on analysis of prehistoric pumiceous tephra. *J. Volcanol. Geotherm. Res.* 183, 42–62.

Tappen, C.M., Webster, J.D., Mandeville, C.W., Roderick, D., 2009. Petrology and geochemistry of ca. 2100-1000 a. B.P. magmas of Augustine volcano, Alaska, based on analysis of prehistoric pumiceous tephra. Journal of Volcanology and Geothermal Research 183, 42-62.

Telford, R.J. and Birks, H.J.B. 2005. The secret assumption of transfer functions: problems with spatial autocorrelation in evaluating model performance. *Quat. Sci. Rev.* 24, 2173–2179.

Telford, R.J. and Birks, H.J.B. 2009. Evaluation of transfer functions in spatially structured environments. *Quat. Sci. Rev.* 28, 1309–1316.

Telford, R.J. and Birks, H.J.B. 2011. Effect of uneven sampling along an environmental gradient on transfer-function performance. *J. Paleolimnol.* 46, 99–106.

Telford, R., Heegaard, E. and Birks, H. 2004. All age–depth models are wrong: but how badly? *Quat. Sci. Rev.* 23, 1–5.

Ter Braak, C.J.F. 1987. The analysis of vegetation-environment relationships by canonical correspondence analysis, *Theories and models in vegetation science,* 8, 69-77.

Ter Braak, C.J.F. 1995a. Non-linear methods for multivariate statistical calibration and their use in palaeoecology: a comparison of inverse (*k*- nearest neighbours, partial least squares and weighted averaging partial least squares) and classical approaches, *Chemometrics and Intelligent Laboratory Systems,* 28, 1, 165-180.

Ter Braak, C.J.F. and Verdonschot, P.F.M. 1995. Canonical correspondence analysis and related multivariate methods in aquatic ecology. *Aquat. Sci.* 57, 255–289.

Ter Braak, C. J. F. and Petr Smilauer. 1998. *CANOCO reference manual and User's guide to Canoco for windows: software for canonical community ordination (version 4.5),* Centre for Biometry, Netherlands.

Thornalley, D.J.R., Elderfield, H. and McCave, I.N. 2009. Holocene oscillations in temperature and salinity of the surface subpolar North Atlantic. *Nature* 457, 711–4.

Timmerman, A., Latif, M., Voss, R. and Grötzner, A. 1998. Northern hemispheric interdecadal variability: a coupled air-sea mode. *J. Clim.* 11, 1906–1931.

Tipping, R. 1995. Holocene evolution of a lowland Scottish landscape: Kirkpatrick Fleming. Part I, peat-and pollen-stratigraphic evidence for raised moss development and climatic change. *The Holocene* 5, 69–81.

Tokui, Y. 1989. *Volcanic Eruptions and Their Effects on Human Activity in Hokkaido, Japan After the 17th Century.* Unpublished MSc. thesis, Ochanomizu University. Reproduced In: Tokui, Y. 1995. Yumi Tokui Gyoseki Syuu (Yumi Tokui Memorial Book), Ochanomizu University, pp. 111-218 (in Japanese).

Tolonen, K. 1986. Rhizopod analysis, in: Berglund, B.E. (Ed.), *Handbook of Holocene Palaeoecology and Palaeohydrology*. John Wiley and Sons, Chichester, pp. 645–666.

Tolonen, K. and Turunen, J. 1996. Accumulation rates of carbon in mires in Finland and implications for climate change. *The Holocene* 6, 171–178.

Tolonen, K., Warner, B.G. and Vasander, H. 1992. *Ecology of testaceans (Protozoa: Rhizopoda) in mires in southern Finland*: I. Autecology. Arch. für Protistenkd. 142, 119–138.

Troels-Smith, J. 1955. *Characterisation of unconsolidated sediments*. Danmarks Geologiska Undersögelse IV, Reakke, 3, 1–73.

Trouet, V., Esper, J., Graham, N.E., Baker, A., Scourse, J.D. and Frank, D.C. 2009. Persistent positive North Atlantic oscillation mode dominated the Medieval Climate Anomaly. *Science* 324, 78–80.

Tsyganov, A.N., Nijs, I. and Beyens, L. 2011. Does climate warming stimulate or inhibit soil protist communities? A test on testate amoebae in high-arctic tundra with free-air temperature increase. *Protist* 162, 237–248.

Tuittila, E., Väliranta, M., Laine, J. and Korhola, A. 2007. Quantifying patterns and controls of mire vegetation succession in a southern boreal bog in Finland using partial ordinations. *J. Veg. Sci.* 18, 891–902.

Turetsky, M.R., Treat, C.C., Waldrop, M.P., Waddington, J.M., Harden, J.W. and McGuire, A. D. 2008. Short-term response of methane fluxes and methanogen activity to water table and soil warming manipulations in an Alaskan peatland. *J. Geophys. Res.* 113, G00A10.

Turetsky, M.R., Kane, E.S., Harden, J.W., Ottmar, R.D., Manies, K.L., Hoy, E. and Kasischke, E.S. 2011. Recent acceleration of biomass burning and carbon losses in Alaskan forests and peatlands. *Nature Geoscience* 4, 27–31.

Turner, E., Swindles, G.T. and Roucoux, K.H. 2013. Late Holocene ecohydrological and carbon dynamics of a UK raised bog: impact of human activity and climate change. *Quaternary Science Reviews* 44, 65–85.

Turner, T.E., Swindles, G.T., Charman, D.J. and Blundell, A. 2013b. Comparing regional and supra-regional transfer functions for palaeohydrological reconstruction from Holocene peatlands. *Palaeogeogr. Palaeoclimatol. Palaeoecol.* 369, 395–408.

Turney, C.S.M., Harkness, D.D. and Lowe, J.J. 1997. Rapid Communication The use of microtephra horizons to correlate Late-glacial lake sediment successions in Scotland. *Journal of Quaternary Science* 12, 525–531.

Turunen, J., Tomppo, E., Tolonen, K. and Reinikainen, A. 2002. Estimating carbon accumulation rates of undrained mires in Finland – application to boreal and subarctic regions. *The Holocene* 12, 69–80.

Usoskin, I.G. and Kovaltsov, G.A. 2008. Cosmic rays and climate of the Earth: Possible connection. *Comptes Rendus Geosci*. 340, 441–450.

Väliranta, M., Korhola, A., Seppa, H., Tuittila, E.S., Sarmaja-Korjonen, K., Laine, J. and Alm, J. 2007. High-resolution reconstruction of wetness dynamics in a southern boreal raised bog, Finland, during the late Holocene: a quantitative approach. *The Holocene* 17, 1093–1107.

Väliranta, M., Blundell, A., Charman, D.J., Karofeld, E., Korhola, A., Sillasoo, Ü., Tuittila, E.S. 2012. Reconstructing peatland water tables using transfer functions for plant macrofossils and testate amoebae: A methodological comparison. *Quat. Int*. 268, 34–43.

Van Bellen, S., Garneau, M. and Booth, R.K., 2011. Holocene carbon accumulation rates from three ombrotrophic peatlands in boreal Quebec, Canada: Impact of climate-driven ecohydrological change. *The Holocene* 21, 1217–1231.

Van Bellen, S., Garneau, M., Ali, A. A. and Bergeron, Y. 2012. Did fires drive Holocene carbon sequestration in boreal ombrotrophic peatlands of eastern Canada? *Quat. Res.* 78, 50–59.

Van Bellen, S., Mauquoy, D., Payne, R.J., Roland, T.P., Daley, T.J., Hughes, P.D.M., Loader, N.J., Street-perrot, A., Rice, E.M. and Pancotto, V.A. 2014. Testate amoebae as a proxy for reconstructing Holocene water table dynamics in southern Patagonia peat bogs. *Journal of Quaternary Science* 29, 463-474.

Van Breemen, N. 1995. How *Sphagnum* bogs down other plants. *Trends Ecol. Evol*. 10, 270-275.

Van Geel, B. and Mook, W.G. 1989. High resolution ^{14}C dating or organic deposits using natural atmospheric ^{14}C variations. *Radiocarbon* 31, 151-155.

Van den Bogaard, C., Dörfler, W., Glos, R., Nadeau, M.J., Grootes, P.M. and Erlenkeuser, H. 2002. Two Tephra Layers Bracketing Late Holocene Paleoecological Changes in Northern Germany. *Quat. Res*. 57, 314–324.

Van der Molen, P.C. andHoekstra, S.P. 1988. A palaeoecological study of a hummock-hollow complex from Engbertsdijksveen, in the Netherlands. *Rev. Palaeobot. Palynol.* 56, 213–274.

Verhoeven, J.T.A. and Toth, E. 1995, Decomposition of *Carex* and *Spahgnum* litter in fens: effects of litter quality and inhibition by living tissue homogenates, *Soil Biology and Biochemistry,* 27, 271-275.

Viau, A. E. and Gajewski, K. 2009. Reconstructing Millennial-Scale, Regional Paleoclimates of Boreal Canada during the Holocene. *J. Clim*. 22, 316–330.

Viau, A. E., Gajewski, K., Sawada, M.C. and Fines, P. 2006. Millennial-scale temperature variations in North America during the Holocene. *J. Geophys. Res*. 111, D09102.

Viau, A. E., Ladd, M. and Gajewski, K. 2012. The climate of North America during the past 2000years reconstructed from pollen data. *Glob. Planet. Change* 84-85, 75–83.

Vinther, B.M., Clausen, H.B., Johnsen, S.J., Rasmussen, S.O., Andersen, K.K., Buchardt, S.L., Dahl-Jensen, D., Seierstad, I.K., Siggaard-Andersen, M.-L.,

Steffensen, J.P., Svensson, a., Olsen, J. and Heinemeier, J. 2006. A synchronized dating of three Greenland ice cores throughout the Holocene. *J. Geophys. Res*. 111, D13102.

Virtanen, R., Oksanen, J., Oksanen, L. and Razzhivin, V.Y. 2006, Broad-scale vegetation-environment relationships in Eurasian high-latitude areas, *Journal of Vegetation Science* 17, 4, 519-528.

Volynets, O.N., Ponomareva, V.V., Braitseva, O.A., Melekestsev, I.V., and Chen, Ch.H. 1999. Holocene eruptive history of Ksudach volcanic massif, South Kamchatka: evolution of a large magmatic chamber. *Journal of Volcanology and Geothermal Research* 91, 23–42.

Waddington, J.M. and Roulet, N.T. 1996. Atmosphere-wetland carbon exchanges: Scale dependency of CO_2 and CH_4 exchange on the developmental topography of a peatland. *Global Biogeochem. Cycles* 10, 233–245.

Walker, G.T. 1924. Correlations in seasonal variations of weather. IX. *Mem Ind Meteor Dept* 24, 275–332.

Walker, G.T. and Bliss, E.W. 1932. World weather V. *Mem Roy Meteor Soc* 4, 53–84.

Walker, D. and Walker, P. 1961. Stratigraphic Evidence of Regeneration in Some Irish Bogs. *J. Ecol.* 49, 169–185.

Walker, I.R. Levesque, A.J., Cwynar, L.C. and Lotter, A.F. 1997. An expanded surface-water palaeotemperature inference model for use with fossil midges from eastern Canada, *Journal of Palaeolimnology,* 18, 165-178.

Wall, A. A. J., Gilbert, D., Magny, M. and Mitchell, E. A. D. 2009. Testate amoeba analysis of lake sediments: impact of filter size and total count on estimates of density, species richness and assemblage structure. *J. Paleolimnol.* 43, 689–704.

Wallace, B. L. 1991. L'Anse aux Meadows gateway to Vinland, the Norse of the North Atlantic. *Acta Archaeologica* 61, 166 – 197.

Wallace, B. 2003. The Norse in Newfoundland: L'Anse Aux Meadows and Vinland. *Newfoundland and Labrador Studies* 19, 5 – 43.

Wallace, J.M. 1996. Observed climate variability: Spatial structure, in: Willebrand, A. and J. (Ed.), *Decadal Variability and Climate*. Springer, Berlin, pp. 31–81.

Wanamaker, A.D., Butler, P.G., Scourse, J.D., Heinemeier, J., Eiríksson, J., Knudsen, K.L. and Richardson, C. A, 2012. Surface changes in the North Atlantic meridional overturning circulation during the last millennium. *Nat. Commun.* 3, 899.

Wanamaker, A.D., Kreutz, K.J., Schöne, B.R. and Introne, D.S. 2011. Gulf of Maine shells reveal changes in seawater temperature seasonality during the Medieval Climate Anomaly and the Little Ice Age. *Palaeogeogr. Palaeoclimatol. Palaeoecol*. 302, 43–51.

Wang, C., Deser, C., Yu, J., DiNezio, P. and Clement, A. 2012. El Niño and Southern Oscillation (ENSO): A Review, in: *Coral Reefs of the Eastern Pacific*. Springer.

Wang, X., Brown, P.M., Zhang, Y., Song, L. 2011. Imprint of the Atlantic multidecadal oscillation on tree-ring widths in northeastern Asia since 1568. *PLoS One* 6, 22740.

Wanner, M. 1999. A review on the variability of testate amoebae: Methodological approaches, environmental influences and taxonomical implications. *Acta Protozool* 38, 15–29.

Wanner, H., Holzhauser, H., Pfister, C. and Zumbühl, H. 2000. *Interannual to century scale climate variability in the European Alps* (Die Klimavariabilität im europäischen Alpenraum auf der Zeitskala von Jahren bis Jahrhunderten). Erdkunde 62–69.

Wanner, H., Beer, J., Bütikofer, J., Crowley, T.J., Cubasch, U., Flückiger, J., Goosse, H., Grosjean, M., Joos, F., Kaplan, J.O., Küttel, M., Müller, S. a., Prentice, I.C., Solomina, O., Stocker, T.F., Tarasov, P., Wagner, M. and Widmann, M. 2008. Mid- to Late Holocene climate change: an overview. *Quat. Sci. Rev*. 27, 1791–1828.

Warner, B.G. 1990. Testate amoebae (Protozoa). Methods in Quaternary ecology no. 5. *Geosci. Can.* 5, 65–74.

Warner, B.G. and Charman, D.J. 1994. Holocene changes on a peatland interpreted from testate amoebae (Protozoa) analysis. *Boreas* 23, 270–280.

Wastegard, S., 2002. Early to middle Holocene silicic tephra horizons from the Katla volcanic system, Iceland: new results from the Faroe Islands. *Journal of Quaternary Science* 17, 723-73.

Weijers, J.W.H., Schouten, S., van den Donker, J.C., Hopmans, E.C. and Damsté, J.S. 2007. Environmental controls on bacterial tetraether membrane lipid distribution in soils. Geochim. Cosmochim. *Acta* 71, 703–713.

Weijers, J.W.H., Steinmann, P., Hopmans, E.C., Schouten, S. and Damsté, J.S. 2011. Bacterial tetraether membrane lipids in peat and coal: Testing the MBT–CBT temperature proxy for climate reconstruction. *Org. Geochem.* 42, 477–486.

Whittaker, R.H. 1956. Vegetation of the Great Smoky Mountains. *Ecol. Monogr.* 26, 1-80.

Wein, R.W. 1968, *Eriophorum vaginatum* L., *Journal of Ecology,* 61, 2, 601-615.

Wieder, R.K., Scott, K.D., Kamminga, K., Vile, M. a., Vitt, D.H., Bone, T., Xu, B., Benscoter, B.W. and Bhatti, J.S. 2009. Postfire carbon balance in boreal bogs of Alberta, Canada. *Glob. Chang. Biol.* 15, 63–81.

Willard, D.A., Cronin, T.M. and Verardo, S. 2003. Late-Holocene climate and ecosystem history from Chesapeake Bay sediment cores, USA. *The Holocene* 13, 201–214.

Williams, T.G. and Flanagan, L.B. 1996. Effect of changes in water content on photosynthesis, transpiration and discrimination against $^{13}CO_2$ and $C^{18}O^{16}O$ in *Pleurozium* and *Sphagnum, Oceologia,* 108, 38-46.

Willis, K.J., Bailey, R.M., Bhagwat, S.A. and Birks, H.J.B. 2010. Biodiversity baselines, thresholds and resilience: testing predictions and assumptions using palaeoecological data. *Trends Ecol. Evol.* 25, 583–591.

Wilmshurst, J.M., Wiser, S.K. and Charman, D.J. 2003. Reconstructing Holocene water tables in New Zealand using testate amoebae: differential

preservation of tests and implications for the use of transfer functions. *The Holocene* 13, 61–72.

Wittenberg, A.T. 2009. Are historical records sufficient to constrain ENSO simulations? *Geophys. Res. Lett.* 36.

WoldeGabriel, G., Hart, W.K. and Heiken, G. 2005. Innovative tephra studies in the East African Rift System. *Eos, Trans. Am. Geophys. Union* 86, 255.

Woodland, W. A., Charman, D.J. and Sims, P.C. 1998. Quantitative estimates of water tables and soil moisture in Holocene peatlands from testate amoebae. *The Holocene* 8, 261–273.

Yamada, S. 1958. Studies on the history of volcanic eruptions of alluvium epoch in Hokkaido on the basis of depositional features of the pyroclastics. *Monogr. Assoc. Geol. Collab. Jpn.* 8 (in Japanese with English abstract).

Yamaguchi, D. 1985. Tree-ring evidence for a two-year interval between recent prehistoric explosive eruptions of Mount St. Helens. *Geology* 13 554-557.

Yamaguchi, D.K. 1983. New tree-ring dates for recent eruptions of Mount St. Helens. *Quaternary Research* 20, 554-557.

Yamaguchi, D.K. and Hoblitt, R.P. 1995. Tree-ring dating of pre-1980 volcanic flowage deposits at Mount St. Helens Washington. *Geological Society of American Bulletin* 107, 1077-1093.

Yan, H., Sun, L., Wang, Y., Huang, W., Qiu, S. and Yang, C. 2011. A record of the Southern Oscillation Index for the past 2000 years from precipitation proxies. *Nature Geoscience* 4, 611–614.

Yeloff, D. andMauquoy, D. 2006. The influence of vegetation composition on peat humification: implications for palaeoclimatic studies. *Boreas* 35, 662–673.

Yu, Z. 2011. Holocene carbon flux histories of the world's peatlands: Global carbon-cycle implications. *The Holocene* 21, 761–774.

Yu, Z. 2012. Northern peatland carbon stocks and dynamics: a review. *Biogeosciences*. 9, 4071-4085

Yu, Z., Turetsky, M., Campbell, I. and Vitt, D., 2001. Modelling long-term peatland dynamics. II. Processes and rates as inferred from litter and peat-core data. *Ecol. Modell.* 145, 159–173.

Yu, Z., Vitt, D.H., Campbell, I.D., Apps, M.J., 2003. Understanding Holocene peat accumulation pattern of continental fens in western Canada. *Can. J. Bot.* 81, 267–282.

Yu, Z., Beilman, D.W. and Jones, M.C. 2009. Sensitivity of Northern Peatland Carbon Dynamics to Holocene Climate Change In AGU Geophysical Monograph vol. 184 "*Carbon Cycling in Northern Peatlands"*, Baird A, Belyea L, Comas X, Reeve A, and Slater L (eds). Pp. 55-69.

Yu, Z., Loisel, J., Brosseau, D.P., Beilman, D.W. and Hunt, S.J. 2010. Global peatland dynamics since the Last Glacial Maximum. *Geophys. Res. Lett.* 37, L13402.

Yu, Z., Loisel, J., Charman, D.J., Beilman, D.W. and Camill, P. 2014. Holocene peatland carbon dynamics in the circum-Arctic region: An introduction. *The Holocene* 24, 1021–1027Zhang, T. 2005. Influence of the seasonal snow cover on the ground thermal regime: An overview. *Review of Geophysics* 43 RG4002.

Zielinski, G.A. and Mershon, G.R. 1997. Paleoenvironmental implications of the insoluble microparticle record in the GISP2 (Greenland) ice core during the rapidly changing climate of the Pleistocene–Holocene transition. *The Geological Society of America Bulletin* 109, 547–559.

Zielinski, G. A, Mayewski, P. a, Meeker, L.D., Whitlow, S., Twickler, M.S., Morrison, M., Meese, D. A, Gow, A.J. and Alley, R.B. 1994. Record of Volcanism Since 7000 B.C. from the GISP2 Greenland Ice Core and Implications for the Volcano-Climate System. *Science* 264, 948–52.

Zielinski, G. A., Dibb, J. E., Yang, Q., Mayewski P. A., Germani, M. S., Whitlow, S. and Twickler, M.S. 1997. Assessment of the record of the 1982 El Chichon eruption as preserved in Greenland snow. *Journal of Geophysical Research* 102, 30045 – 26640.